NOAA Technical Memorandum NMFS-AFSC-458

# Advancing Model-Based Essential Fish Habitat Descriptions for North Pacific Species in the Aleutian Islands

J. Harris, E. A. Laman, J. L. Pirtle, M. C. Siple, C. N. Rooper, T. P. Hurst, and C. L. Conrath

December 2022

U.S. DEPARTMENT OF COMMERCE

National Oceanic and Atmospheric Administration

National Marine Fisheries Service

Alaska Fisheries Science Center

The National Marine Fisheries Service's Alaska Fisheries Science Center uses the NOAA Technical Memorandum series to issue informal scientific and technical publications when complete formal review and editorial processing are not appropriate or feasible. Documents within this series reflect sound professional work and may be referenced in the formal scientific and technical literature.

The NMFS-AFSC Technical Memorandum series of the Alaska Fisheries Science Center continues the NMFS-F/NWC series established in 1970 by the Northwest Fisheries Center. The NMFS-NWFSC series is currently used by the Northwest Fisheries Science Center.

This document should be cited as follows:

Harris, J., E. A. Laman, J. L. Pirtle, M. C. Siple, C. N. Rooper, T. P. Hurst, and C. L. Conrath. 2022. Advancing model-based essential fish habitat descriptions for North Pacific species in the Aleutian Islands. U.S. Dep. Commer., NOAA Tech. Memo. NMFS-AFSC-458, 406 p.

This document is available online at:

Document available: https://repository.library.noaa.gov

Reference in this document to trade names does not imply endorsement by the National Marine Fisheries Service, NOAA.

NOAA FISHERIES

# Advancing Model-Based Essential Fish Habitat Descriptions for North Pacific Species in the Aleutian Islands

J. Harris[1], E. A. Laman[1], J. L. Pirtle[2], M. C. Siple[1], C. N. Rooper[3], T. P. Hurst[1], and C. L. Conrath[1]

[1]Resource Assessment and Conservation Engineering Division
Groundfish Assessment Program
Alaska Fisheries Science Center
7600 Sand Point Way NE
Seattle WA 98115

[2]Alaska Regional Office
709 W. 9th St.
Juneau AK 99802-1668

[3]Fisheries and Oceans Canada
3190 Hammond Bay Road
Nanaimo BC V9T 6N7

**U.S. DEPARTMENT OF COMMERCE**

National Oceanic and Atmospheric Administration
National Marine Fisheries Service
Alaska Fisheries Science Center

NOAA Technical Memorandum NOAA-TM-AFSC-458

December 2022

## ABSTRACT

Advancing model-based descriptions of essential fish habitat (EFH) for federally managed fishes and invertebrates is a key component of the 5-year review process mandated for EFH information in Fishery Management Plans. The analyses presented here demonstrate refinements and advances built on the habitat-based species distribution modeling (SDM) approach established in the previous EFH 5-year review. All of the ensemble SDMs constructed for Aleutian Island species in this present work predict EFH Level 2 information (habitat-related abundance), meeting a key objective of the EFH Research Plan for Alaska. We also met another objective of the Research Plan by introducing maps of EFH Level 3 information (habitat-related vital rates) for settled early juvenile walleye pollock in the Aleutian Islands for the first time. In the present work, we describe 53 EFH maps in the Aleutian Islands, accounting for 24 North Pacific groundfish species with up to three life stages per species as well as for two crab species and one octopus. The SDM ensemble approach achieved good predictive performance over a variety of species, and it was particularly effective for flatfish species. SDM predictions were less accurate for species with few occurrences in the trawl survey (e.g., invertebrate) or highly variable trawl catches (e.g., Atka mackerel). In general, geographic position, bottom depth and bottom currents were the most influential covariate predictors in the SDMs. The maps and descriptions presented here represent the "best available science" to form a basis for assessing anthropogenic impacts on habitats in Alaska and are extensible to other fishery management and ecosystem information needs. Recommended future research includes developing methods for combining disparate data sources to expand spatial and seasonal coverage of Alaska species distribution and abundance and increasing the scope of EFH research to address rapidly changing environmental conditions in the region.

# CONTENTS

# INTRODUCTION

The purpose of this project is to advance levels of essential fish habitat (EFH) information for federally managed groundfish and crab species in the Aleutian Islands (AI) using species distribution models (SDMs). We are guided by the Alaska EFH Research Plan (Sigler et al. 2017) Research Priority #1 near-term objectives and the Magnuson-Stevens Act (MSA) EFH requirements.

Alaska EFH Research Plan, Research Priority #1 – Characterize habitat utilization and productivity by using the best available science to accomplish the following:

Objective #1 – Develop EFH Level 1 information (distribution) for life stages and areas where missing.

Objective #2 – Raise EFH level from 1 or 2 (habitat-related densities or abundance) to Level 3 (habitat-related growth, reproduction, or survival rates).

The Final Environmental Impact Statement for EFH Identification and Conservation in Alaska[1] defines EFH as the area inhabited by 95% of a species' population (NMFS 2005). Our habitat-based modeling approach characterizes EFH for life stages of species within North Pacific Fishery Management Council (NPFMC) Fishery Management Plans (FMPs) as the area circumscribing the top 95% of the SDM-predicted abundance. To meet the research priority and objectives described above, we applied SDMs to predict the distribution and abundance of species' life stages by incorporating new and updated data sources to develop SDM EFH Level 1 and 2 maps, and we used habitat-related vital rates to map EFH Level 3 information as an adjunct to the SDM EFH Level 1 and 2 maps.

[1] https://repository.library.noaa.gov/view/noaa/17391

The MSA defines EFH as those waters and substrate necessary to fish for spawning, breeding, feeding, or growth to maturity (50 CFR 600.10). EFH regulations require that the National Marine Fisheries Service (NMFS) and Fishery Management Councils (Councils) describe and identify EFH for managed species and minimize to the extent practicable the adverse effects of anthropogenic activities (e.g., fishing, mineral and oil extraction, coastal development). As part of this requirement, EFH text descriptions and maps (EFH component 1, descriptions and identification) are necessary for each life stage of species in an FMP (50 CFR 600.815(a)(1)) with an overarching consideration that the science related to this effort meets the standards of best available science (NMFS National Standard 2 – Scientific Information 50 CFR 600.315). There are two separate and complementary FMPs for managing groundfishes[2] and crabs[3] in the Bering Sea and Aleutian Islands (BSAI) management area.

Councils and NMFS must also periodically review the EFH components of FMPs and revise or amend these components with new information at least every 5 years (50 CFR 600.815(a)(10)). In the 2017 EFH 5-year review, habitat-based SDMs incorporating Level 1 and 2 EFH information were developed for many FMP species and their life stages in the AI (Turner et al. 2017). That project, along with related projects in the Bering Sea (Laman et al. 2017, 2018) and Gulf of Alaska (Rooney et al. 2018), replaced qualitative EFH Level 1 maps that were based on adult distributions (Fisheries Leadership and Sustainability Forum 2016, Simpson et al. 2017) with SDM-based estimates for individual life stages, substantially refining Alaska groundfish and crab EFH designation and, in many cases, producing EFH Level 2 information for the first time. The EFH descriptions and maps produced

[2] http://www.fisheries.noaa.gov/alaska/sustainable-fisheries/alaska-groundfish-fisheries-management
[3] http://www.fisheries.noaa.gov/alaska/sustainable-fisheries/bering-sea-and-aleutian-islands-bsai-crab-fisheries

for the 2017 EFH 5-year Review were approved by the U.S. Secretary of Commerce as part of the EFH Omnibus Amendment package (83 FR 31340, July 5, 2018) to revise the FMPs[4].

In this EFH 5-year review, we assessed the forecasting accuracy of the 2017 SDM approach for describing EFH[5] (e.g., Laman et al. 2017, 2018), refined our modeling approach, and updated our data sources. EFH in this present work is now represented as life stage-specific and spatially-explicit population percentiles predicted from an ensemble of best-performing constituent SDMs for 24 species across up to three life stages per species of AI groundfishes, two crabs, and one octopus species. To achieve this, we expanded the SDM approach from the 2017 5-year EFH review to include up to five constituent models (three SDMs were assessed in 2017) in an ensemble and refined our methodology by using the lowest cross-validated root mean square error (RMSE) to identify the best-fitting models. We enhanced existing data sets with recent survey results (summer bottom trawl surveys 1991–2019), updated independent predictor variables (e.g., survey-dependent bottom temperature observations), and added new covariates for bathymetric position index (BPI) and rockiness. We separately modeled settled early juvenile life stages to extend consideration of EFH to critical ontogenetic habitat transitions and revised SDMs for species where maturity schedules or life stage definitions were recently updated (e.g., yellowfin sole and flathead sole; Tenbrink and Wilderbuer 2015).

[4] https://alaskafisheries.noaa.gov/portal/apps/webappviewer

[5] Pirtle et al. 2020 and our June 2020 Scientific and Statistical Committee (SSC) presentation links available at https://www.npfmc.org/efh-distribution/

## MATERIALS AND METHODS

### Study Area

The Aleutian Islands are a chain of volcanic islands stretching from southwest Alaska across the North Pacific, separating the western Gulf of Alaska (GOA) from the Bering Sea (Fig. 1). The continental shelf and upper continental slope represent a diverse mosaic of benthic habitats from Unimak Pass (165°W) in the eastern AI to Stalemate Bank in the western Aleutians (170.5°E). The Alaska Coastal Stream flows westward on the Pacific side of the Aleutians, while on the Bering Sea side, the Aleutian North Slope Current flows eastward (Stabeno et al. 1999, Stabeno et al. 2002, Ladd et al. 2005). There is extensive transport to the north through passes in the island chain from the Pacific side to the Bering Sea. In the Aleutians, there is a very narrow continental shelf that ranges in width from 20 km to greater than 200 km. The continental slope is steep and features multiple passes incising the continental shelf. The seafloor of the Aleutian Islands is diverse, with extensive rocky substrate resulting from volcanic activity dominating the continental shelf (Zimmermann et al. 2013).

### Dependent Variables: Fish and Invertebrate Data

#### Large-mesh Bottom-trawl Survey

Alaska Fisheries Science Center (AFSC) Resource Assessment and Conservation Engineering-Groundfish Assessment Program (RACE-GAP) summer bottom trawl surveys document the distribution and abundance of federally managed fish and invertebrate species (Table 1) in the Aleutian Islands archipelago from Unimak Pass to Stalemate Bank (Fig. 1). For these EFH analyses, our data set combined the AI and the Gulf of GOA surveys west of the faunal barrier represented by Unimak Pass (Stabeno et al. 2002). The two surveys have been conducted at regular intervals since 1991 and are collectively referred to in this document as the

AI survey. Triennial surveys were conducted between 1991 and 2000 in the AI and biennial surveys were conducted from 2002 to 2018 (von Szalay and Raring 2020). The western portion of the GOA survey characterizes the eastern portion of the Aleutian chain south of the archipelago and was conducted triennially from 1993 to 1999 and then biennially from 2001 to 2019 (von Szalay and Raring 2018). Both of these fishery-independent AFSC RACE-GAP surveys used a stratified random sampling design. For our analysis data set, trawlable AI survey stations located on a contiguous survey grid between Unimak Pass and Samalga Pass north of the archipelago and from Samalga Pass to Stalemate Bank north and south of the archipelago were included. Strata in the AI were based on four depth intervals (10–100 m, 101–200 m, 201–300 m, and 301–500 m) and established survey districts. The AI survey area is contained within the North Pacific Fishery Management Council's (NPFMC) BSAI management zone. For the western portion of the GOA survey appended to the AI survey area for these analyses (Unimak to Samalga Pass south of the archipelago), the survey randomly trawled stations from a continuous survey grid constrained in some years by the 700 m isobath (2011, 2013, 2017, 2019) and in other years by the 1,000 m isobath (1993, 1996, 1999, 2001, 2003, 2005, 2007, 2009, 2015). Strata in the GOA were based on up to six depth intervals (10–100 m, 101–200 m, 201–300 m, 301–500 m, 501–700 m, and 701–1,000 m) and established survey districts. Assignment of sampling effort within strata for both surveys was determined using a Neyman optimum allocation sampling strategy (Cochran 1977) which considers relative abundance and variance of commercially important groundfish species from previous surveys of the area as well as the previous year's ex-vessel price for select species. During the time period of these data collections, changes in taxonomic classifications have resulted in different effective time series for different species, and these are reflected in the analyses presented here (see Table 1). For

example, dusky and dark rockfishes were considered a single species prior to the 1996 survey, so only data since that survey were used to model these two species. All fishes and invertebrates captured by the trawl net were either identified to species or into higher-level taxonomic groups and weighed. Non-colonial taxa were also counted or estimates of total count were made. For species where length-based definitions of life stages were available, length ranges for settled early juveniles, subadults, and adults were used to partition the catch based on proportionality estimated from the random length subsample taken from each catch. These length-based definitions of ontogenetic life stages came from the extant scientific literature, web resources (e.g., the Ichthyoplankton Information System, AFSC RACE: https://access.afsc.noaa.gov/ichthyo/speciesdict.php), or length data collected in beach seines, purse seines, and small-mesh bottom-trawls and recorded in the updated Nearshore Fish Atlas (as described in Grüss et al. 2021a).

The fishing gear used on the RACE-GAP AI and GOA bottom trawl surveys consists of a Poly Nor'Eastern high-opening bottom trawl with a 27.2 m headrope, a 36.3 m footrope, and 24.2 m roller gear constructed with 36 cm rubber bobbins separated by 10 cm rubber disks (Stauffer 2004). Under fishing conditions, the average net width is 16.0 m, and average height is 6.7 m based on acoustic net mensuration equipment mounted on the wing-tips and headrope of the trawl. Each trawl was certified as conforming to measurements and dimension standards prior to its use in the survey as stipulated in the National Trawling Standards (Stauffer 2004).

## Independent Covariates: Habitat Data

The independent covariates used to parameterize SDMs (Table 2) were chosen based on their potential to influence the distribution and abundance of North Pacific groundfish and crab life stages in the regions where we sample. Some of these independent covariates (or predictor

variables) were dynamic or static habitat attributes typically collected on the bottom trawl survey (Fig. 2). Others were derived and modeled variables describing the marine environment in the study area (e.g., NEP5 ROMS; Danielson et al. 2011). They were combined into a suite of independent covariates used to parameterize the SDMs. We used variance inflation factors (VIF; Table 3) calculated using the methods in Zuur et al. (2009) to eliminate strongly collinear terms (VIF $\geq$ 5.0; Sigler et al. 2015). Independent habitat covariates from the time series (1991–2018) were interpolated on regular spatial grids ranging from 0.1–1 $km^2$ using natural neighbor interpolation (Sibson 1981), inverse distance weighting (Watson and Philip 1985), ordinary kriging (Venables and Ripley 2002) with an exponential semi-variogram, or empirical Bayesian kriging with a semi-variogram estimated using restricted maximum likelihood (REML; Diggle and Ribeiro 2002). Interpolations by inverse distance weighting and ordinary kriging were calculated on the R computing platform[6] (R Core Development Team 2020), and Bayesian kriging was generated in ESRI ArcGIS mapping software[7]. Rasters for our analyses in the AI were gridded at a resolution of 1 $km^2$. All rasters were projected in the Alaska Albers Equal Area Conic (EAC) projection (standard parallels = 55° and 65°N and center longitude = 154°W). To represent local conditions in the SDMs and to incorporate inter-annual variability in our EFH maps and descriptions, we used a mixture of observed and derived predictors extracted from these rasters at the bottom trawl stations by averaging the raster values along the towpath of each haul. These variables were used to train and identify the best-fitting SDMs. Rasterized multi-year averages of habitat covariates in each raster cell were used to represent average conditions in the

[6] R version 3.6.3 "Holding the Windsock"
[7] ESRI 2018, version 10.7

study area over time and were input into the best-fitting SDMs when predicting species distributions and abundances.

To represent local conditions in the SDMs and incorporate inter-annual variability in our EFH maps and descriptions, we utilized a mixture of observed, modeled, and derived predictors. For the RACE-GAP survey data, covariate raster values were extracted as averaged values along the towpaths at the bottom trawl stations. For species data sources supporting the settled early juvenile stage models only, covariate raster values were extracted at point locations representing the geographic location of each sampling site. In both cases, these extracted predictors were used to train and identify the best-fitting SDMs. When predicting species distribution and abundance, the complete raster of each retained covariate was used as input into the final models for a species and life stage. In the case of observed dynamic predictor variables such as bottom temperature from the RACE-GAP survey, the observed values were kriged and rasterized over the study duration (1991–2019) to represent average conditions in the study area over time.

**Bottom Depth and Temperature**

Bottom depth and temperature data were routinely collected during each trawl haul, but different instruments were used to measure these values over the survey years (Buckley et al. 2009). From 1982 to 1992, depth and temperature were recorded using expendable bathythermographs (XBTs). In 1993, the XBTs were replaced by the Brancker XL200 digital bathythermographic data logger (Richard Brancker Research, Ltd., Kanata, Ontario, Canada) mounted on the headrope of the trawl net. With the advent of continuous recording devices, the survey began reporting on-bottom depth and temperature averaged over the tow duration. Starting in 2004, the Brancker data logger was replaced by the SeaBird SBE-39 microbathythermograph (Sea-Bird Electronics, Inc., Bellevue, WA). In 1993–1995, mean gear

depth measured at the headrope was equated with bottom depth. Since 1996, mean gear depth has been added to mean net height measured during the on-bottom period of the trawl to estimate mean bottom depth.

We used two kinds of bathymetry data when formulating the SDMs used to model groundfish and crab distributions and abundances in the AI. When identifying the best-fitting constituent SDMs for the subadult and adult life stages, the bottom depth measured at each trawl station was used as a covariate predictor variable to train and test those SDMs. When predicting groundfish distribution and abundance for all life stages modeled, we used a bathymetry raster built from two sources that included data from the AI and the western GOA (Zimmermann et al. 2013, 2019). The primary sources for the bathymetry raster were depth soundings from digitized NOAA's National Ocean Service (NOS) smooth sheets from early hydrographic (Hawley 1931) and other surveys (hydrographic and non-hydrographic) that used manual soundings (e.g., lead lines), single-beam, or multi-beam acoustic echosounders. Details on the preparation and processing of the bathymetry datasets were documented in Zimmermann and Benson (2013). Point data from these compiled bathymetry datasets were gridded to the recommended resolution of 100 $m^2$ and to also create a raster surface using natural neighbor interpolation (Sibson 1981) in ArcMap. To achieve the 1 $km^2$ resolution used in our analyses, we averaged the 100 $m^2$ point data over 1 $km^2$ grid cells.

Similar to how we used depth data, we used temperatures measured at each trawl station in the AI (1991–2018) to train and identify the best-fitting SDMs and we used a raster surface of those temperatures to predict groundfish and crab distributions and abundances for the subadult and adult life stages best-fitting models. The bottom temperature raster was created by interpolating the observed temperatures at each trawl station over the study area and time series

using empirical Bayesian kriging in ArcGIS (Diggle and Ribeiro 2002) with a semi-variogram estimated using restricted maximum likelihood (REML). The raster was interpolated over a 1 $km^2$ grid of the AI study area.

**Water Movement**

Three attributes of water movement were used as habitat covariates in modeling and prediction: maximum tidal speed, bottom current speed and direction, and variability in bottom current. We estimated maximum tidal speed at each survey station over a lunar year (369 consecutive days between 1 January 2009 and 4 January 2010) using a tidal inversion program parameterized for the AI on a 1 $km^2$ grid (Egbert and Erofeeva 2002). This tidal prediction model was used to produce a series of tidal currents for spring and neap cycles at every bottom trawl survey station. The maximum of the lunar annual series of predicted tidal current was then extracted at each bottom trawl survey haul location. A 1 $km^2$ raster surface of maximum tidal current speed was kriged over the AI using an exponential semi-variogram, and values were extracted and averaged along individual trawl haul towpaths to use as input to the best-fitting SDMs when predicting distribution and abundance.

The second water movement variable was the predicted bottom water layer current speed and direction from NEP5 ROMS model runs from 1969 to 2005 (Danielson et al. 2011). These long-term current projections are available as points on a 10 $km^2$ grid. The ROMS model was based on a three-dimensional grid with 60 depth tiers for each grid cell. For example, a point at 60 m water depth would have 60 bins at 1-m intervals, while a point at 120 m depth would have 60 bins at 2-m depth intervals, etc. The bottom current speed and direction for the deepest depth bin at each point (closest to the seafloor) were used in our analyses. These regularly spaced projections were interpolated to a 100 $m^2$ raster grid covering the AI using inverse distance

weighting and then averaged over a 1 km$^2$ and across survey years (1991–2018) for our analyses. To characterize current at each bottom trawl station, ROMS current velocity components were extracted along each trawl towpath, and the mean northing and easting values were computed for each trawl haul. The interpolated bottom current raster served as covariate input to the best fitting SDMs when making spatial predictions.

Bottom current variability across summer months (May to September) was included as a third bottom current-related predictor in the SDMs. It was computed separately as the pooled standard deviation (*Pooled SD$_j$*) of the northing and easting components of bottom current at each NEP5 ROMS prediction locus through time such that

$$Pooled\ SD_j = \sqrt{\frac{\sum_{i=1}^{k}\left[(n_i-1)*s_{ij}^2\right]}{\sum_{i=1}^{k}[n_i-1]}},$$

where $j$ is the location of a prediction on the ROMS grid, $n_i$ is the number of months in year $i$, $s_{ij}^2$ is the variance at location $j$ in year $i$, and $k$ is the total number of survey years (12 in the AI). Bottom current variability can be considered a proxy for current stability near the bottom.

**Geographic Position**

Spatial modeling, such as the SDMs presented here, often includes a location variable to represent geographic position and account for spatial autocorrelation (Ciannelli et al. 2008, Politou et al. 2008, Boldt et al. 2012). To reduce the effects of spatial autocorrelation on the results, we chose to combine latitude and longitude into a smoothed bivariate geographic position term included as an independent predictor in SDM formulations. Rooper et al. (2020) demonstrated that this approach can reduce spatial autocorrelation in the modeled results. Geographic position was collected during each haul using a variety of positioning systems

through time (e.g., manual charting, long-range navigation (LORAN-C), digital global positioning system [dGPS]). Since 2006, start and end positions for the vessel during the on-bottom portion of the trawl haul were collected from a dGPS receiver mounted on the vessel. We estimated trawl position by using the recorded vessel position and estimating the distance of the trawl from the vessel based on the seafloor depth and the length of wire outassuming no catenary. We assumed that the bottom trawl was directly behind the vessel during the tow and that all bottom trawl hauls were conducted in a straight line from the beginning to the end point. The mid-point of the trawl path between the start and end positions was used as the location variable in the SDMs. The EAC projected longitude and latitude data for each haul (and all other geographical data for this study) were transformed into eastings and northings for modeling.

**Seafloor Terrain**

Several seafloor terrain metrics were derived from the bathymetry surface and describe attributes of seafloor morphology. The attributes included in the present study were slope, aspect, curvature, and bathymetric position index (BPI). Seafloor terrain metrics were derived at the original scale of the compiled bathymetry surface (100 $m^2$) using neighborhood-based analytical methods in ArcGIS 10.7 (ESRI) with the Benthic Terrain Modeler (Wright et al. 2012, Walbridge et al. 2018). All seafloor terrain metrics were derived using a 3 × 3 neighborhood of grid cells, except for BPI. Computation algorithms are provided by Walbridge et al. (2018).

Seafloor slope is the rate of change in bathymetry over a defined area. Slope is the first derivative of the bathymetry surface and was reported in degrees of incline (Horn 1981, Dolan and Lucieer 2014). Terrain slope may be a determinant of colonization since flatter areas support different substrata and communities than those found on steeper slopes (Pirtle et al. 2019).

Aspect measures the direction of the maximum gradient of slope and was expressed as angular compass direction, which is a circular variable (Horn 1981). Aspect was decomposed into sine (west-east or "eastness") and cosine (south-north or "northness") components to be used in the SDMs as continuous surfaces ranging from -1.0 to 1.0, where negative values indicate westness or southness and positive values indicate eastness or northness (e.g., Walbridge et al. 2018). Aspect eastness and northness were derived from the aspect surface. Terrain aspect is considered an indirect indicator of current velocity over and around seafloor terrain features (Mienis et al. 2007, Dolan et al. 2008).

Terrain curvature is the second derivative of the bathymetry surface and the first derivative of the slope (Zevenbergen and Thorne 1987, Schmidt et al. 2003). Curvature defines convex, concave, and linear slopes and can be used to identify seafloor features such as mounds and depressions that may be ecologically meaningful (Wilson et al. 2007). Curvature is also an indicator of how currents interact with the seafloor, either accelerating or decelerating parallel to the direction of slope and converging or diverging perpendicular to the direction of slope. We derived standard curvature as a single terrain surface, incorporating curvature in directions parallel and perpendicular to the slope (Zevenbergen and Thorne 1987, Schmidt et al. 2003). With this surface, positive values are convex slopes where currents may decelerate or diverge; negative values are concave slopes where currents may accelerate or converge, and values near zero are linear slopes where the rate and direction of flow are not expected to change.

Bathymetric position index (BPI) describes the elevation of one location relative to the mean of neighboring locations in an annulus-shaped neighborhood around a central cell or cells (Guisan et al. 1999, Weiss 2001). BPI emphasizes features shallower or deeper than the surrounding landscape area, such as ridges and valleys, and places with abrupt changes in slope,

such as the continental shelf break and the base of the continental slope. Broad-scale measures of BPI (> 1 km) have been useful in distinguishing between areas of trawlable and untrawlable seafloor encountered by the RACE-GAP bottom-trawl survey (Pirtle et al. 2015). BPI has been used as an SDM covariate describing groundfish habitat in the GOA (Pirtle et al. 2019) and other habitat analyses (Wilson et al. 2007, Howell et al. 2011). We derived BPI from AI bathymetry using a 65-cell radius neighborhood with an inner radius of 3-cells. This is equivalent to a horizontal scale of 6.5 km, representing relatively broad-scale terrain features in our study area. In the resulting surface, positive values are shallower than the surrounding area (e.g., ridges and crests), and negative values are deeper (e.g., channels and valleys). In the visualization of this covariate, we artificially stretched the scale to highlight the heterogeneity in the study area.

**Seafloor Rockiness**

A seafloor rockiness surface was developed for the AI based on a compilation of rock features and sediment attributes to represent a continuous gradient from areas with high occurrence of rocky substrate to areas with low occurrence of rocky substrate, using methods similar to Pirtle et al. (2019). The following datasets were included for the AI region: 1) sediment and substrate features from digitized smooth sheets (Zimmermann et al. 2013); 2) EBSSED-2 regional selection of samples collected from grabs and cores (Richwine et al. 2018); 3) modeled untrawlable and trawlable seafloor based on a generalized linear model of multibeam acoustic backscatter and terrain available as a 6 $m^2$ raster dataset (Pirtle et al. 2015) that was regridded to 1 $km^2$ and exported as point locations, where model predictions of untrawlable and trawlable locations are proxies for high and low occurrence of rocky substrate; and 4) RACE-GAP bottom-trawl survey historic haul locations, including hauls that incurred gear damage from seafloor contact to represent locations where untrawlable rocky features were likely encountered

and hauls with good performance to represent locations where untrawlable rocky seafloor was likely not encountered, using the corrected start positions of the on-bottom portion of tows. Compiled point location data from the four datasets were gridded using natural neighbor interpolation to produce a raster surface of 1 $km^2$ resolution (ArcGIS 10.7, ESRI).

For all of these seafloor terrain and substrate variables, values were extracted from their raster surfaces along the towpath at each trawl station and were used when training the models and identifying the best-fit SDM. The complete terrain raster was used to predict species distributions and abundances when a terrain covariate was retained in the best-fitting model.

**Biogenic Structure**

Previous studies have indicated that structure-forming invertebrates (SFI) such as sponges, corals, and Pennatulaceans (sea pens and sea whips) can form important structural habitat for temperate marine fishes (Heifetz et al. 2005, Malecha et al. 2005, Marliave and Challenger 2009, Rooper et al. 2010, Stone et al. 2011, Laman et al. 2015). The occurrence of SFIs can also be indicative of substratum type (Du Preez and Tunnicliffe 2011) because these sponges and corals attach to rocks and hard substrata, whereas sea pens and sea whips anchor into soft substrata. Therefore, we included the presence and absence of SFIs as binomial factors in the suite of habitat covariates. Rasters of these SFIs were used to predict distributions and abundances from best-fit SDMs (Rooper et al. 2014, 2016, 2017a; Sigler et al. 2015).

## Statistical Modeling

Our modeling strategy for this 5-year EFH Review has been to fit multiple environmental- and habitat-based SDMs to fish and crab abundances, skill tested among SDMs using the root-mean-square-error to indicate model performance (RMSE; Hastie et al. 2009), and has incorporated the best performing models into an ensemble in R (R Core Team 2020).

Ensemble models essentially average predictions across constituent models, making them more robust to overfitting and less sensitive to differences in predictive performance among constituents. Rooper et al. (2017b) found that ensembles performed better than the generalized linear or generalized additive models alone when predicting distributions of structure-forming invertebrates. Overall, the ensemble modeling approach provides a universal SDM application across multiple FMPs and can be easily expanded to consider additional constituent models in the future.

Previous EFH descriptions in Alaska (e.g., Turner et al. 2017) were based on habitat-related SDMs modeling species abundances from $4^{th}$-root transformed catch-per-unit-effort (CPUE; $kg \cdot ha^{-1}$) using the area swept method (Wakabayashi et al. 1985) and assuming a Gaussian distribution. However, modeling $4^{th}$-root transformed CPUE has several shortcomings with respect to our study objectives, including: 1) residuals were not informative due to the zero-inflation and overdispersion that a Gaussian distribution cannot properly address; 2) the *a priori* and *ad hoc* nature of deciding to use a $4^{th}$-root transformation relative to other equally defensible transformations; 3) the inability to interpret the scale of the output, which is in units of $4^{th}$-root CPUE and hence must be back-transformed to calculate a total predicted CPUE in any subarea; and 4) the scale-dependence of results, where the $4^{th}$-root transformation implies that density would change if the area swept in the survey changed (i.e., if sampling had occurred at a different scale). To mitigate the challenges associated with using the $4^{th}$-root transformed CPUE, we directly modeled numerical abundance with an area-swept offset to generate EFH descriptions that were less derived than those using a transformed CPUE approach as this more precisely represents fishing effort.

For this cycle, we modeled numerical abundance using five different SDMs (Table 4): a maximum entropy model (MaxEnt), a presence-absence gam (paGAM), a hurdle GAM (hGAM), and two forms of standard gam using the Poisson distribution ($GAM_P$) and the negative binomial distribution ($GAM_{nb}$). The MaxEnt and paGAM use presence or presence-absence data to estimate probabilities of occurrence (Phillips et al. 2006, Wood 2017). Using these models in conjunction with the complementary log-log (cloglog) link function allowed us to approximate abundance from the estimated probabilities (Scharf et al. 2019). Transforming these native model outputs (probability) into approximate numerical abundance yields predictions in the same units as the response variables from the other 3 SDMs, facilitating skill testing and model comparison while meeting the requirements to qualify predictions as EFH Level 2, habitat-related density or abundance. Because some models, (notably MaxEnt) produce results on different scales, a scaling factor was calculated for each model by dividing the mean of the observed abundance by the mean of the model predictions. This ensured that predictions from all models were directly comparable and could be used to construct a weighted ensemble (Fig. 3).

**Maximum Entropy Models (MaxEnt)**

Maximum entropy modeling was developed to model the probability of suitable habitat or species occurrence with presence-only data (Phillips et al. 2006) in cases of rare species and when presence-only or presence-absence data were available from multiple surveys with varied sampling designs (Guisan et al. 2007, Elith et al. 2011). This newer version of the MaxEnt model, implemented with the *maxnet* package in R (Phillips et al. 2017, R Core Team 2020), reformulates the model as an inhomogeneous Poisson process (Fithian et al. 2015), which constructs the predicted probabilities as a proportion of the product of underlying relative abundance and sampling probabilities. Because of this, it was possible to estimate the species

abundance by treating the cloglog link output of the MaxEnt model as if it were the linear predictor in a Poisson model. The relative abundance estimate was then calculated by adding an additional parameter, the entropy, to the cloglog linear predictor and exponentiating the sum.

The MaxEnt model utilized the same suite of covariates as the GAMs but it omitted geographic position (lat./long.) from the suite of predictor variables because MaxEnt does not separately distinguish spatial variation in sampling probability from spatial variation in resource density (Elith et al. 2011). The MaxEnt algorithm automatically constructed and selected terms based on several feature classes determining relationships between the species response data and covariates. The default feature set was used in this study, which includes linear, quadratic, and product interaction terms. By default, hinge features were included in models with more than 80 presence records, and threshold features were not used. As part of the fitting process, a variety of these different features were tested in different combinations. MaxEnt uses a regularization multiplier to determine the penalty applied to larger models and to help regulate overall model complexity. Here, we evaluated regularization multiplier values between 0.5 and 3.0 in intervals of 0.5, with the best value determined by the lowest RMSE after 10-fold cross-validation as described below (see subsection *Cross-Validation and Skill Testing*).

**Generalized Additive Models (GAM)**

We used three classes of GAMs in this study: the paGAM (Wood 2017), the hGAM (Cragg 1971, Barry and Welsh 2002, Potts and Elith 2006), and the standard GAM with a Poisson distribution ($GAM_P$; Hastie and Tibshirani 1990); and a negative-binomial GAM ($GAM_{nb}$; Zuur et al. 2009). All GAMs were fit using the *mgcv* package (Wood 2011) in R. The paGAM uses the binomial distribution and the cloglog link function, which allowed numerical abundance to be approximated from model predicted encounter probabilities

(Fithian et al. 2015). The hGAM models presence-absence and abundance in two stages and accounts for zero-inflation commonly seen in field-collected data (McCullagh and Nelder 1989). In the first stage of the hGAM, the probability of occurrence was predicted from presence-absence data using a paGAM and binomial distribution. In the second stage of the hGAM, a standard GAM was constructed for the positive catches using a "zero-adjusted" (Zuur et al. 2009) Poisson distribution. Finally, an abundance estimate was obtained by multiplying the predicted probability of presence from step one with the abundance estimate from step two (Barry and Welsh 2002). The $GAM_P$ estimates abundance directly using the Poisson distribution and a log link. The $GAM_{nb}$ was structurally similar to the $GAM_P$ but used a negative binomial distribution with a log link, allowing the $GAM_{nb}$ to account for overdispersion in the data (McCullagh and Nelder 1989).

For all GAMs, we used iterative backward stepwise term elimination to remove covariate terms based on minimizing the model-dependent generalized cross-validation (GCV) or unbiased risk estimator (UBRE) scores, thereby identifying the best-fitting model formulations (Weinberg and Kotwicki 2008, Zuur et al. 2009). Since the Poisson and negative-binomial GAMs were structurally very similar models, we used RMSE-based skill testing to identify and keep the best performing model (lowest RMSE) of this pair in the ensemble.

All GAMs in this study used a variety of two-dimensional smoothing terms, one-dimensional smoothing terms, and categorical variables to fit the data. To avoid overfitting in the GAMs, the basis degrees of freedom used in the smoothing function for each habitat covariate were constrained following the methods of Weinberg and Kotwicki (2008). However, attempting to extrapolate model predictions into areas with few data points requires additional consideration. In particular, the default smoother when fitting GAMs, a "thin-plate spline,"

sometimes produces exaggerated predictions in areas of sparse data (Wood 2003). To counter this behavior in one-dimensional smooth terms, we used a smoothing penalty based on the first derivative (instead of the default second derivative), which tended to push the effect curve towards zero where data were unavailable. The same method was applied for two-dimensional smooth terms, but "Duchon" splines were used instead of thin-plate or cubic splines (Duchon 1977), which improved the penalization of the smooth function in areas with sparse data. Finally, if a GAM based on thin-plate splines failed, a second version using cubic splines in the one-dimensional smooth terms was attempted. If both versions failed to converge or produced unreasonable results, that particular GAM was excluded from the final ensemble.

**Cross-Validation and Skill Testing**

Species distribution models were subjected to *k*-fold cross-validation to estimate RMSE and to assess accuracy and uncertainty. We computed the error at each cross-validation fold (*k*) by fitting an SDM to a randomly selected "in-bag" partition containing 90% of the observed abundance at trawl stations (*i*), predicting abundance at the remaining "out-of-bag" partition containing the other 10% of trawl stations, and comparing the predicted (*y*) and observed (*x*) values for the testing subset. The *k*-fold cross-validation was repeated 10 times until every point in the data set had been tested. The RMSE from the accumulated out-of-bag sample was calculated as

$$RMSE = \sqrt{\frac{\sum_{k=1}^{10}\sum_{i=1}^{n_k}(y_{ki}-x_{ki})^2}{\sum_{k=1}^{10} n_k}},$$

where $y_{ki}$ is the predicted numerical abundance in cross-validation fold $k$, $x_{ki}$ is the observed numerical abundance at trawl station $i$ in cross-validation fold $k$, and $n_k$ is the number of stations sampled in the $k$th fold. This process provides a test of prediction skill at unsampled locations

within the cross-validation and provides a measure of performance that can be used to compare models. The RMSE provides a metric of the ability of a model to predict the abundance at a series of locations accurately. The model with the lowest RMSE value was considered the best performer (Hastie et al. 2009). The cross-validation also allows for a consistent method of calculating the variance in model predictions by computing it at each location across folds.

Skill testing was used to eliminate constituent SDMs from the ensemble by identifying and dropping low-performing models with high RMSEs. Constituent SDMs retained in the ensemble were weighted by the inverse squared RMSE following the formula,

$$w_i = \frac{RMSE_i^{-2}}{\sum_{i=1}^{m} RMSE_i^{-2}} \ ,$$

where $w_i$ is the weight for model $i$, $RMSE_i$ is the cross-validated RMSE for model $i$, and $m$ is the number of constituent models. The inclusion of poor-performing models may degrade ensemble performance, so if any constituent SDM received less than a 10% relative weight, it was eliminated from the ensemble, and the weights of the remaining SDMs in the ensemble were recalculated.

The ensemble extrapolated abundance predictions into areas along the edges of the survey grid that were rarely sampled. Under these conditions, SDMs that fit most of the data quite well can still produce unacceptable predictions around the edges and in these unfrequented regions. The unacceptable predictions usually take the form of unrealistically high abundance. To address this challenge, a criterion was implemented so that any SDM generating abundance predictions > 10 times the highest observed survey abundance was excluded from the ensemble. The resulting cumulative ensemble-predicted numerical abundance, based on the combined

effects of all retained constituent SDMs, was translated into a map of the complete EFH area for each species.

**Ensemble Models and Uncertainty**

Ensemble modeling is a robust method to predict species distributions and abundances (Araujo and New 2007). Potential advantages include better estimates of uncertainty, reduced bias, and results that are less sensitive to minor changes in the underlying data (e.g., accumulating data through annual surveys; Stewart and Hicks 2018). In the present study, we combined the best-fit constituent SDMs into single-species life stage-specific ensemble predictions of habitat-related abundance to inform descriptions of EFH. In practice, this means that we first identified the best performing MaxEnt, paGAM, hGAM, and GAM SDMs. In the MaxEnt models, this entailed testing a range of regularization multipliers, while in the GAMs this involved backwards stepwise term elimination. For the standard GAM, the Poisson and negative binomial error distributions were modeled separately, and skill testing using the RMSE was employed to select the distribution that best characterized the data. The set of best SDMs from each category was then weighted by the inverse of its cross-validated RMSE, and constituent SDM weights were normalized to sum to one. Predictions from the ensemble were made by multiplying each constituent prediction by its weight and summing the weighted predictions across SDMs. The result of this exercise was a final ensemble for each species' subadult and adult life stage that predicts habitat-related abundance.

The variance of the ensemble prediction can be obtained based on a weighted combination of the variance in the predictions of each constituent model. Ten abundance prediction rasters were made for each constituent using the 10 models fit during cross-validation. The variance across these 10 folds at each location was then calculated to estimate the variance

for that constituent model. After repeating this process for all constituent models in the ensemble, we adapted the following equation from Burnham and Anderson (2002), substituting our RMSE derived weights for their AIC weights:

$$SD_j(ensemble) = \sum_{i=1}^{m} w_i \times \sqrt{var_{ij} + \left(y_j^* - y_{ij}\right)^2} \ ,$$

where $SD_j$ is the standard deviation of the ensemble at location $j$, $w_i$ is the weight for model $i$, $m$ is the number of constituent models, $var_{ij}$ is the variance for model $i$ at location $j$, $y_j^*$ is the ensemble abundance prediction at location $j$, and $y_{ij}$ is the abundance prediction for model $i$ at location $j$. Then we computed the coefficient of variation ($CV$) from the *SD (ensemble)* as:

$$CV_j = \frac{SD_j}{y_j^* + c} \ ,$$

where $CV_j$ is the coefficient of variation at location $j$, $SD_j$ is the ensemble standard deviation at location $j$, and $y^*_j$ is the ensemble prediction at location $j$. Because the term $y^*_j$ in the denominator can sometimes be zero, a small constant $c$, which was set at 1% of the max predicted abundance for that species and life stage, was added to all abundance estimates when calculating the CV.

**Species Distribution Model Performance Metrics**

In addition to the RMSE described above for skill testing among SDMs and constituent model weighting in the ensemble, we computed three commonly used metrics of SDM performance for constituent models and the ensembles. The three fit metrics that we reported were the Spearman's rank correlation coefficient ($\rho$), the area under the receiver-operator-characteristics curve (AUC; Hosmer and Lemeshow 2005), and the deviance explained based on the Poisson distribution (PDE). Each fit metric measures a different aspect of model performance and has distinct strengths and weaknesses. A model that scores poorly on one metric may still be

useful once the others are considered, and all models should be assessed with reference to the underlying biology of the species being studied.

The $\rho$ score compares predicted densities with observations for each sample and computing their rank correlation, and it measures how well a model accurately distinguished between high- and low-density areas (Best and Roberts 1975, Zar 1984). We employ the $\rho$ instead of the more familiar Pearson correlation because the $\rho$ is more appropriate to count data that do not follow a normal distribution (Legendre and Legendre 2012). Additionally, the EFH maps produced in this project are based on ranked percentiles of abundance, and $\rho$ may provide some insight to the accuracy of the EFH maps. While there is no objective standard for what constitutes a "good enough" correlation, for this project, we adopted the framework that less than 0.2 represents "poor" predictive performance, between 0.2 and 0.4 is "fair", between 0.4 and 0.6 is "good," and greater than 0.6 is "excellent." Our framework is based on our knowledge of the ecology of the species being modeled and the available data. Because $\rho$ is the rank correlation, a high value is easiest to obtain when there is a large difference between the lowest and highest abundances, such that small prediction errors do not affect the rankings. Conversely, a low value can result if the observed densities occupy a narrow range, and a small prediction error could change the rankings.

The AUC is a measure of the ability of a model to discriminate between binary outcomes, such as presence and absence. The value of the curve at any point represents the ratio of true positives to false positives at that point, and the total area under the curve represents the overall performance across the entire range of values. The AUC has a minimum value of 0.5 (i.e., random 50/50 chance) and a maximum of 1, and values under 0.7 are generally considered poor, values between 0.7 and 0.9 are average to good, and values greater than 0.9 suggest excellent

discrimination ability (Hosmer and Lemeshow 2005). The AUC provides a measure of discrimination ability that is standardized across the range of probability predictions, which makes it useful as a summary of discrimination ability. In this case, discriminating where the RACE-GAP bottom trawl survey catches individuals and where it does not. However, it can sometimes be misleading when an overwhelming majority of observations are either present or absent, and only a small portion of the probability space has been adequately sampled.

The PDE provides a generalization of "variance explained" for the constituent SDMs as well as the ensemble. We assume the Poisson distribution when computing the deviance explained for these models because count data are not normally distributed and traditional estimates of the variance explained tend to be misleading. Additionally, with the Poisson distribution, the size of errors is expected to change with the mean of the predictions. Therefore, it is common to compute the deviance explained by a model. This value is a measure of the percent reduction in the residual deviance of a model compared to a naïve null model, which contains only an intercept and no predictor terms (Pardoe 2012). Because we employ a variety of models that utilize different distributions (binomial, Poisson, negative binomial) and different underlying data types (presence-absence, count), we estimate the deviance explained in comparison to a fixed null Poisson model. Therefore, the PDE represents the percent deviance explained compared to a null Poisson model, allowing a fairer comparison of the different models. In this case, we adopt a similar metric to the correlation, where less than 0.2 indicates "poor" performance, between 0.2 and 0.4 "fair" performance, between 0.4 and 0.6 "good" performance, and greater than 0.6 is "excellent" performance. A high PDE can result when model predictions are accurate or when the observed data are highly variable, and the model represents a significant improvement over a simple null model. Similarly, a low value can

sometimes occur even when predictions are accurate if there is no improvement over the null model, indicating that a simpler method would probably be acceptable. Deviance is calculated as

$$D = 2\sum_{i=1}^{n}\left[x_i ln\left(\frac{x_i}{exp(y_i)}\right) - (x_i - exp(y_i))\right]$$

$$D_0 = 2\sum_{i=1}^{n}\left[x_i ln\left(\frac{x_i}{exp(\bar{x})}\right) - (x_i - exp(\bar{x}))\right]$$

$$PDE = \frac{D}{D_0},$$

where $D$ represents the deviance of a given model, $D_0$ is the deviance of the null model, $x_i$ represents the observed abundance for data point $i$, $\bar{x}$ represents the mean of observed abundance, and $y_i$ represents the predicted abundance for data point $i$ (Pardoe 2012).

**Essential Fish Habitat (EFH) Maps**

Maps[8] of species' habitat-related abundance predicted from the ensembles were used to describe and map EFH for this EFH 5-year Review. These maps were produced as population percentiles based on all areas where the given species and life stage was present, defined as having an encounter probability greater than or equal to 5%. To calculate the probability of encounter, we began by assuming that the ensemble predicted abundance approximately follows a Poisson distribution. Under this assumption, the probability of encounter was equal to one minus the likelihood of zero abundance, given the ensemble estimated abundance at that location. Locations with a probability of encounter below 0.05 were eliminated, and the

[8] Sean-Rohan-NOAA (2021). akgfmaps [Source Code]. https://github.com/afsc-gap-products/akgfmaps

remaining locations were ordered by increasing abundance. Four percentiles were identified from the percentiles computed above for each species' life stage and were then mapped to the areas containing the upper 95%, 75%, 50%, and 25% of locations based on the predicted numerical abundance. The 95% level corresponds to the definition of EFH area in Alaska[9] (NMFS 2005, Sigler et al. 2012). Each percentile describing subareas of the EFH area defines a more focused partition of the total EFH area. The area containing the upper 75% of ensemble abundance predictions is referred to as the principal EFH area. For the fishing effects analysis in EFH Component 2 of the 2017 EFH 5-year Review (Simpson et al. 2017), the top 50% of SDM abundance predictions were termed the "core EFH area," and we have applied this terminology to our results. We also produced a shape for the top 25% of ensemble abundance predictions which we refer to as EFH hot spots. Mapping habitat percentiles for EFH subareas like these helps demonstrate the heterogeneity of fish and crab distributions over available habitat within the larger area identified as EFH and aligns our results with those of other EFH-related projects.

**Species Complexes**

Some groundfishes in Alaska are managed as members of a stock complex (e.g., the Other Flatfish Stock Complex in the Bering Sea – Aleutian Islands). While EFH must be designated for each managed species, EFH may be designated for assemblages of species with justification or scientific rationale provided (50 CFR 600.815(a)(1)(iv)(E)). In the present study, and for the first time in an EFH 5-year review, we presented EFH descriptions of multi-species stock complexes using aggregated single-species SDMs to produce descriptions of EFH, which served as proxies for individual species in the stock complex where an SDM EFH map was not

[9] URL: http://www.npfmc.org/habitat-protections/essential-fish-habitat-efh/ [accessed 15 November 2016]

possible due to data limitations (i.e., < less than 50 catches over the study period). To achieve this, we first generated multi-species abundance maps by summing the ensemble predicted abundances at each raster cell for each species in the complex that supported an ensemble. Then, using the same method described above for single species maps, we constructed an EFH map for the stock complex. In complexes where there was a mixture of available life history information (e.g., some species with known length-based life stage definitions and some without), life stages were combined for the species mapped together from the complex. See the introductory section of each species complex chapter (*Results* section) for details about the species and life stages that were included.

### EFH Level 3 Habitat-related Vital Rates

We advanced EFH information to Level 3 (habitat-related vital rates) in the AI by integrating a temperature-dependent growth rate developed from field and laboratory studies (Laurel et al. 2016, Copeman et al. 2017) with habitat-linked SDM predictions of walleye pollock numerical abundance (EFH Level 2) to achieve a key Alaska EFH Research Plan objective for this 5-year review (Sigler et al. 2017). Laurel et al. (2016) described the temperature-dependent growth rate of early juvenile walleye pollock as:

$$GR = 0.2023 + 0.0092 * T + 0.0335 * T^2 - 0.0019 * T^3,$$

where *GR* is the growth rate expressed as the percent change in body weight per day (% body weight per day), and T is temperature in degrees Celsius. Copeman et al. (2017) describe the lipid accumulation rate (LAR) for early juvenile walleye pollock as:

$$LAR = 11.6 * \exp\left[-0.5\left(\frac{T - 14.37}{6.39}\right)^2\right],$$

where *LAR* is the lipid accumulation rate (% lipids per % body weight per day), and *T* is the temperature (°C).

We constructed these surfaces by first mapping the spatially explicit vital rates across the survey study area, using the bottom temperature covariate raster derived from the trawl-mounted temperature measurements as the temperature value in the vital rate equations. Next, we computed the product of the vital rate map and the SDM-predicted abundance map by multiplying the two rasters together. The product map was then transformed onto a relative scale, ranging from zero to one, where zero indicates areas of low abundance and low habitat-related temperature-dependent growth potential, and one indicates areas of high abundance and high habitat-related growth potential. This process was carried out twice, producing separate EFH Level 3 maps for growth and lipid accumulation rates in early juvenile walleye pollock.

Table 1. -- North Pacific groundfish and crab species from AFSC RACE-GAP summer bottom trawl surveys modeled to re-describe essential fish habitat in the AI: the years modeled were determined by taxonomic validity; life stage length ranges are fork lengths (F.L.) in mm with sources indicated ("--" indicates no length known from literature); "All" years modeled = 1991-2019, "1996"-" indicates 1996 to 2019.

| Common Names | Years Modeled | Life Stage Length Ranges | | | Source |
|---|---|---|---|---|---|
| **Flatfishes** | | **Early Juvenile** | **Subadult** | **Adult** | |
| yellowfin sole | All | 30–140 | 141–296 | > 296 | NFA[1], Doyle et al. 2019, Yeung and Cooper 2020, Tenbrink and Wilderbuer 2015 |
| northern rock sole | 1996- | 20–140 | 141–309 | > 309 | NFA, Doyle et al. 2019, Yeung and Cooper 2020, Stark 2012a |
| arrowtooth flounder | 1992- | 35–160 | 161–480 | > 480 | NFA, Debenham et al. 2019, Doyle et al. 2018, 2019, Stark 2012b |
| Dover sole | All | 30–140 | 141–439 | > 439 | Doyle et al. 2019, Abookire and Macewicz 2003 |
| flathead sole | All | 20–140 | 141–342 | > 342 | NFA, Doyle et al. 2019, Tenbrink and Wilderbuer 2015 |
| Greenland turbot | All | -- | 49–580 | > 580 | IIS, Cooper et al. 2007, Helser et al. 2019 (NPRB #1605) |
| Kamchatka flounder | 1992- | -- | 49–550 | > 550 | IIS, Stark 2012b |
| rex sole | All | 70–140 | 141–352 | > 352 | Doyle et al. 2019, Abookire 2006 |
| southern rock sole | 1996- | -- | 17–347 | > 347 | Doyle et al. 2019, Stark 2012a |
| **Roundfishes** | | | | | |
| walleye pollock | All | 40–140 | 141–381 | > 381 | Doyle et al. 2019, Pirtle et al. 2019, Stahl and Kruse 2008 |
| Pacific cod | All | 40–150 | 151–580 | > 580 | Pirtle et al. 2019, Stark 2007 |
| sablefish | All | 150–399 | 400–585 | > 585 | Sasaki 1985, D. Hanselman, AFSC-ABL, pers. comm. |
| Atka mackerel | All | -- | 49–340 | > 340 | Cooper et al. 2010 |

| Common Names | Years Modeled | Life Stage Length Ranges | | | Source |
|---|---|---|---|---|---|
| **Rockfishes** | | **Early Juvenile** | **Subadult** | **Adult** | |
| Pacific ocean perch | All | 25–200 | 201–250 | > 250 | IIS, Moser 1996, Pirtle et al. 2019, Rooper 2008 |
| northern rockfish | All | -- | 25–277 | > 277 | IIS, Moser 1996, Tenbrink and Spencer 2013 |
| rougheye rockfish | 2006- | -- | 25–450 | > 450 | IIS, Moser 1996, Conrath 2017 |
| blackspotted rockfish | 2006- | -- | 25–453 | > 453 | IIS, Moser 1996, Conrath 2017 |
| dusky rockfish | 1996- | -- | 25-365 | > 365 | Chilton 2010 |
| harlequin rockfish | All | -- | 25-188 | > 188 | Tenbrink and Helser 2021 |
| shortraker rockfish | All | -- | 25–499 | > 499 | IIS, Moser 1996, Conrath 2017 |
| shortspine thornyhead | All | -- | 20–215 | > 215 | IIS, Rooper 2008 |
| **Sharks and skates** | | | | | |
| Alaska skate | 1999- | -- | <= 930 | > 930 | Matta and Gunderson 2007 |
| Aleutian skate | 1999- | -- | <= 1320 | > 1320 | Ebert et al. 2007 |
| mud skate | 1999- | -- | <= 595 | > 595 | Ebert 2005 |
| whiteblotched skate | 1999- | -- | <=964 | >964 | Ebert 2005 |
| **Invertebrates** | | | | | |
| golden king crab | All | -- | -- | -- | |
| red king crab | All | -- | -- | -- | |
| giant octopus | All | -- | -- | -- | |

[1]NFA = Updated Nearshore Fish Atlas, NMFS Auke Bay Laboratories, Juneau, AK (as described in Grüss et al. 2021a).

[2]IIS = Ichthyoplankton Information System, Alaska Fisheries Science Center, Resource Assessment and Conservation Engineering: https://access.afsc.noaa.gov/ichthyo/speciesdict.php.

Table 2. -- Covariates used in habitat-based species distribution models (SDM) to fit (identify best-fitting formulation) and then predict distributions and abundances from the of the best -fitting models of North Pacific groundfish and crab species in Alaska and describe essential fish habitat (EFH).

| Variable | Unit | Description of Prediction Raster | Interpolation Method | Data Source and Usage |
|---|---|---|---|---|
| Bottom temperature | °C | Mean bottom temperatures measured on bottom trawls during AFSC RACE-GAP summer trawl surveys (1982–2019) | Empirical Bayesian kriging | Temperature data collected at bottom trawl hauls |
| Bottom current Northing and Easting | $m \cdot sec^{-1}$ | Seafloor ocean current components predicted from the NEP5 ROMS (Danielson et al. 2011) averaged for the bottom layer across summer years (1991–2018) | Inverse distance weighting | Training: mean towpath value<br>Prediction: raster of bottom current |
| Bottom current Northing and Easting variability | $m \cdot sec^{-1}$ | Pooled standard deviation of seafloor ocean current components predicted from the NEP5 ROMS (Danielson et al. 2011) averaged for the bottom layer across summer years (1991–2018) | Inverse distance weighting | Training: mean towpath value<br>Prediction: raster of bottom current pooled standard deviation |
| Maximum tidal current | $cm \cdot sec^{-1}$ | Predicted tidal current maximum at each bottom trawl location over a lunar year cycle (Egbert and Erofeeva 2002) | Ordinary kriging | Training: mean towpath value<br>Prediction: kriged surface of tidal maxima |
| Position | Latitude, Longitude | Midpoint of bottom trawl hauls corrected for position of the trawl net relative to the vessel in Alaska Albers Equal Area conic projection | -- | Training: position collected during bottom trawl hauls.<br>Prediction: raster of positions |
| Bottom Depth | meters (m) | Bathymetry of the seafloor based on acoustic seafloor mapping data and digitized, position corrected NOS charts | Natural neighbor | Training: mean bottom depth of trawl |

| Variable | Unit | Description of Prediction Raster | Interpolation Method | Data Source and Usage |
|---|---|---|---|---|
| | | | | Prediction: raster of bathymetry soundings data [a] |
| Slope | degrees | Maximum gradient in depth between adjacent cells, derived from bathymetry (Horn 1981) applied with Benthic Terrain Modeler in ArcGIS (Walbridge et al. 2018) | -- | Training: mean towpath value<br>Prediction: raster of slopes derived from bathymetry |
| Bathymetric Position Index | -- | Relative difference of elevation between neighboring locations, illustrates bathymetric highs and lows across the landscape, derived from bathymetry (Guisan et al. 1999) applied in ArcGIS (Walbridge et al. 2018) | -- | Training: mean towpath value<br>Prediction: raster of bathymetric position index derived from bathymetry |
| Aspect Eastness and Northness | -- | Describes concavity/convexity, as well as sloping nature, derived from bathymetry (Horn 1981) applied in ArcGIS (Walbridge et al. 2018) | -- | Training: mean towpath value<br>Prediction: raster of aspect derived from bathymetry |
| Curvature | -- | Combined plan and profile curvature to return "standard" curvature; derived from bathymetry (Schmidt et al. 2003) applied in ArcGIS (Walbridge et al. 2018) | -- | Training: mean towpath value<br>Prediction: raster of curvature derived from bathymetry |
| Rockiness | -- | Continuous surface of compiled datasets representing locations of rocky and not rocky substrate (updated from Pirtle et al. 2019) | Natural neighbor | Training: mean towpath value<br>Prediction: raster of seafloor rockiness. |
| Coral presence or absence | probability | Coral presence-absence in bottom trawl catches / model-predicted coral presence-absence (Sigler et al. 2015; Rooper et al. 2014) | -- | Training: presence-absence of corals in trawl catches<br>Prediction: Raster of model-predicted binary presence- |

| Variable | Unit | Description of Prediction Raster | Interpolation Method | Data Source and Usage |
|---|---|---|---|---|
| | | | | absence of coral (Rooper et al. 2014) |
| Sponge presence or absence | probability | Sponge presence-absence in bottom trawl catches / model-predicted sponge presence-absence (Sigler et al. 2015; Rooper et al. 2014) | -- | Training: presence-absence of sponge in trawl catches<br>Prediction: Raster of model-predicted binary presence-absence of sponge (Rooper et al. 2014) |
| Pennatulacean presence-absence | probability | Pennatulacean presence-absence in bottom trawl catches / model-predicted penn. presence-absence (Sigler et al. 2015; Rooper et al. 2014) | -- | Training: presence-absence of Pennatulaceans in trawl catches<br>Prediction: Raster of model-predicted binary presence-absence of Pennatulaceans (Rooper et al. 2014) |

a – Zimmermann et al. 2013; Zimmermann et al. 2019.

Table 3. -- Variance inflation factors (VIF) of covariates used as predictors in species distribution models (SDM) for federally managed groundfishes and invertebrates in the AI; SD = pooled standard deviation.

| **Covariate** | **VIF** |
|---|---|
| *Longitude | 3.32 |
| *Latitude | 3.05 |
| Bottom depth | 1.88 |
| Slope | 1.50 |
| Aspect Eastness | 1.07 |
| Aspect Northness | 1.28 |
| Curvature | 1.69 |
| Bottom temperature | 1.45 |
| *Bottom Current Eastings | 1.57 |
| *Bottom Current Northings | 1.64 |
| *SD bottom current Eastings | 2.24 |
| *SD bottom current Northings | 2.32 |
| Tidal maximum current | 1.32 |
| Rockiness | 1.18 |
| Bathymetric position index | 2.13 |
| Sponge presence-absence | 1.03 |
| Coral presence-absence | 1.03 |
| Pennatulacean presence-absence | 1.02 |

*represent components of covariates that form bivariate smoothed interaction terms in the generalized additive models (Longitude and Latitude = “position”, Eastings and Northings = “bottom current”, SD Eastings and SD Northings = “bottom current SD”).

Table 4. -- Species distribution models (SDMs) trained and skill tested for inclusion in an ensemble; the Maximum Entropy model (MaxEnt) uses the *maxnet*[a] package, and the generalized additive models (GAMs) use the *mgcv*[b] package.

| **Species Distribution Model (SDM)** | **Family** | **Link** | **Documentation** |
|---|---|---|---|
| Maximum Entropy (MaxEnt) | * | cloglog approx. | Phillips et al. (2017) |
| Generalized Additive Models (GAM) | | | |
| presence-absence GAM (paGAM) | binomial | cloglog | Wood (2011) |
| hurdle GAM (hGAM) | zero-adjusted Poisson | cloglog and log | Zuur et al. (2009); Wood (2011) |
| standard GAM ($GAM_P$) | Poisson | log | Wood (2011) |
| negative-binomial GAM ($GAM_{nb}$) | negative-binomial | log | Wood (2011) |

* - the distribution applied to the MaxEnt model is a heavily modified Poisson distribution representing an inhomogeneous Poisson process.

*a* - R v3.6.1; Fitting 'MaxEnt' species distribution models with 'glmnet'; *maxnet*: R package version 0.1.2.

*b* - R v3.6.1; Fast stable restricted maximum likelihood and marginal likelihood estimation of semiparametric generalized linear models; *mgcv*: R package version 1.8-29.

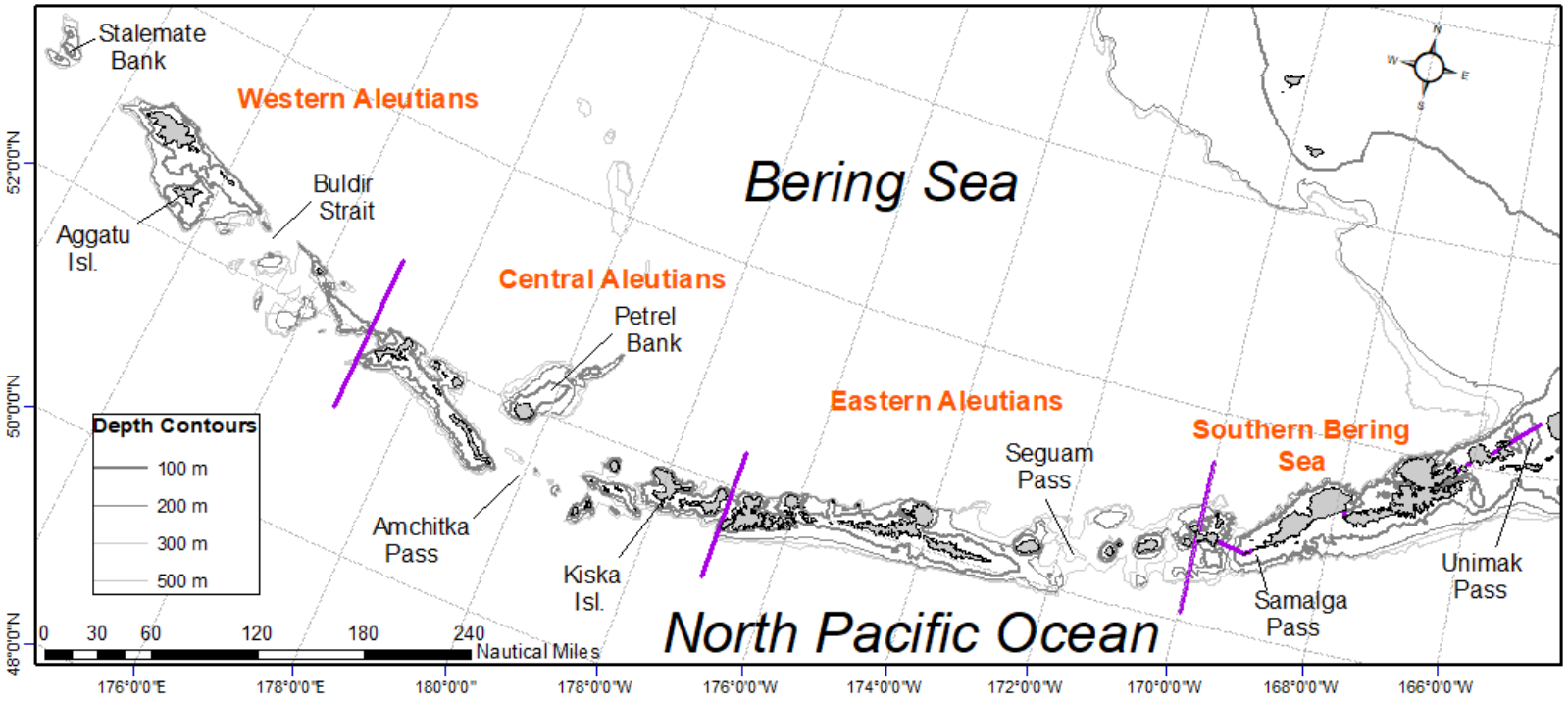


Figure 1. -- Aleutian Islands (AI) from Unimak Pass to Stalemate Bank where data for this modeling study were collected on Alaska Fisheries Science Center (AFSC), Resource Assessment and Conservation Engineering-Groundfish Assessment Program (RACE-GAP) summer bottom trawl surveys (1991-2019).

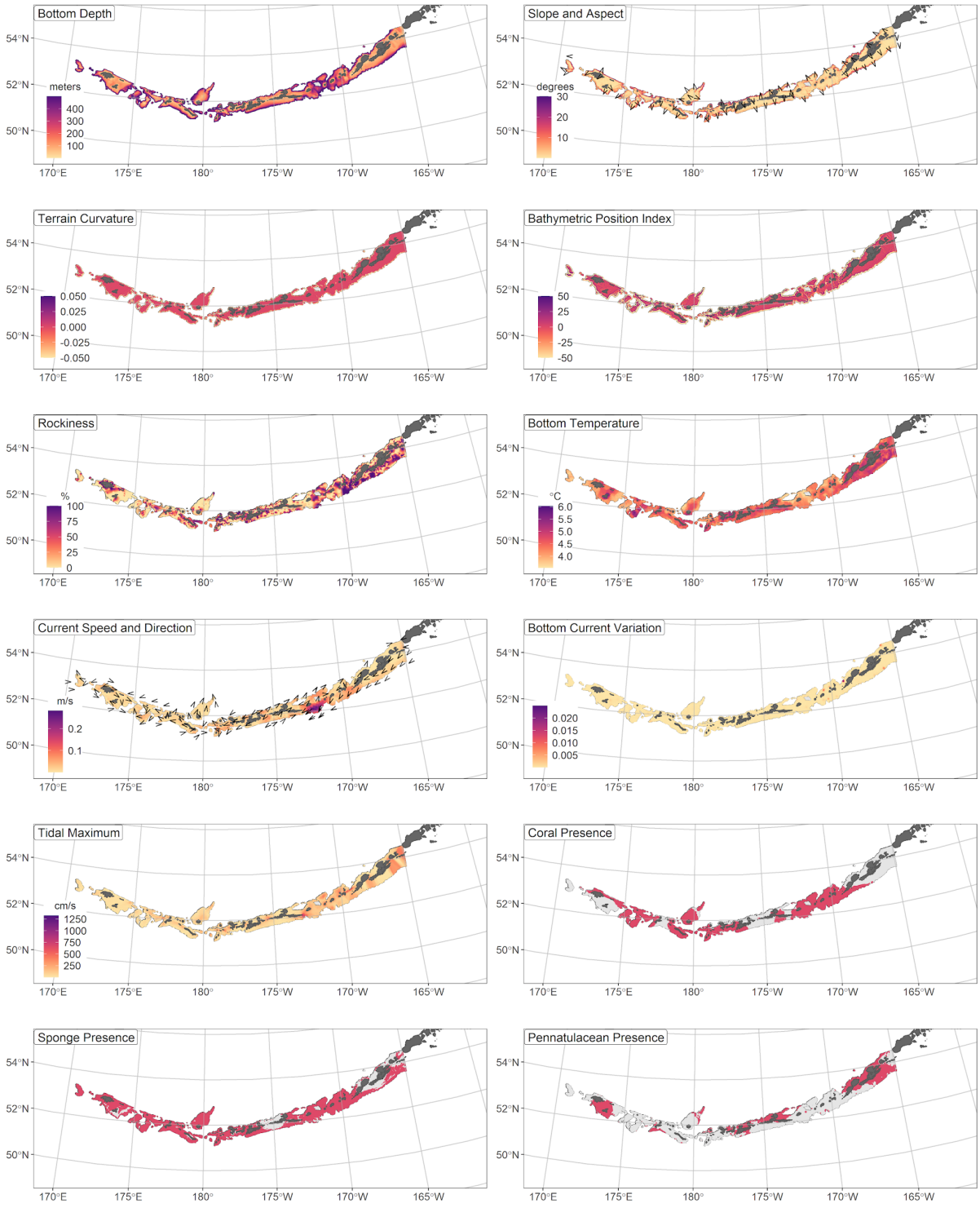


Figure 2. -- Predictor variables used to represent environmental and habitat covariates in the AI; scale of structure-forming invertebrates (SFI: corals, sponges, and pennatulacean) is light shading = absent and darker shading = present.

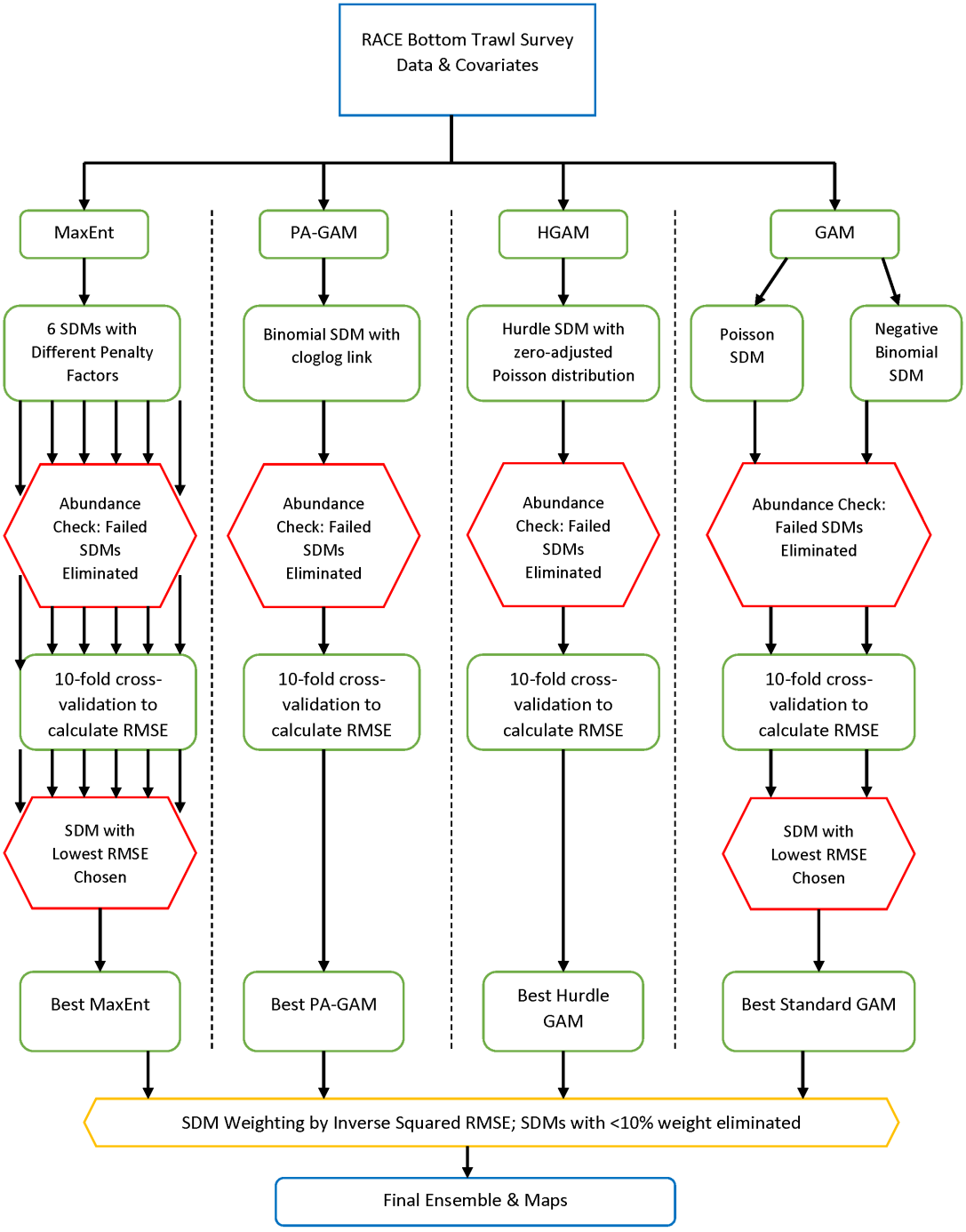


Figure 3. -- Pathways to formulation and assessment of five species distribution models (MaxEnt = maximum entropy, paGAM = presence-absence generalized additive model, hGAM = hurdle GAM, GAM = standard Poisson GAM, $GAM_{nb}$ = standard negative-binomial GAM) for inclusion in or elimination from a final ensemble predicting habitat-related distribution and abundance used to describe and map essential fish habitat (EFH) in Alaska: RMSE = root mean square error.

# RESULTS

## Flatfishes

### Arrowtooth flounder (*Atheresthes stomias*)

Arrowtooth flounder (ATF; *Atheresthes stomias*) is a large-bodied flatfish distributed from the Kuril Islands to California (Shotwell et al. 2020a). The species is morphologically similar to the less common Kamchatka flounder (*A. evermani*), and the two were not routinely distinguished in assessment surveys until 1992 (Shotwell et al. 2020a). The settled early juvenile life stage was defined as all fish between 35 mm (maximum size range of transformed pelagic early juveniles; Doyle et al. 2019) and 160 mm when ATF undergo an ontogenetic shift in habitat (Doyle et al. 2018). Female ATF have a length at 50% maturity ($L_{50}$) of 480 mm FL (Stark 2012b), and although the length at maturity is consistent across regions, the age of maturity can vary considerably (Shotwell et al. 2020a). Given its large size, this species is highly predatory and is thought to be an important part of the marine food web; in particular, it is a major predator of juvenile walleye pollock (*Gadus chalcogrammus*) (Yang and Livingston, 1986). This species was managed as a stock complex with Kamchatka flounder until 2011 when the start of a directed fishery prompted the development of separate management plans (Shotwell et al. 2020a). ATF are often captured during long-line surveys, and these may represent a useful data source in the future.

**Settled early juvenile arrowtooth flounder distribution and predicted abundance from RACE-GAP summer bottom trawl surveys in the Aleutian Islands –** Settled early juvenile ATF were relatively uncommon in the RACE-GAP summer survey of the AI compared to older life stages (Fig. 4). However, this may be an artifact of the sampling design, and smaller mesh

sampling would likely catch this life stage in greater numbers[10]. Available trawl data indicate that settled early juvenile ATF were most concentrated towards the eastern AI near Unimak Pass but they occurred in several pockets across the survey area. The final ensemble contained four SDMs with approximately equal weights and showed a fair to good performance in terms of model fit (Table 5). Specifically, the ensemble did a fair job distinguishing high and low abundance areas ($\rho = 0.35$), but it performed better in terms of deviance explained (PDE = 0.56). In conjunction with the fact that best-performing constituents were the hGAM and the $GAM_{nb}$, this pattern indicates that the ensemble is useful for predicting the patches where this life stage occurs in high numbers. Additionally, the ensemble does an excellent job of predicting presence or absence in a given haul (AUC = 0.90). Geographic position, bottom depth, tidal current maximum, and bottom currents were the most important covariates and accounted for 67.0% of the deviance explained by the model (Table 6). In general, predicted abundance was high in locations that were farther east, with shallow depths (<150 m) and with weak tides (Fig. 5). Predicted abundance was highest in shallow, sheltered inshore areas, particularly those near Unalaska Island (Fig. 5), though secondary pockets of high abundance were also predicted near Atka Island and Agattu Island. The predicted CV of abundance was higher in farther west areas of the AI, though the pattern was not strong (Fig. 2). Encounter probabilities for settled early juvenile ATF were high near the areas described above and close to zero in most places beyond the 100m depth contour (Fig. 6).

[10] A recommendation to add additional survey data types if possible to future SDM ensemble EFH mapping efforts for this species will be included as a future recommendation for research directions from the 2023 EFH 5-year review.

**Subadult arrowtooth flounder distribution and predicted abundance from RACE-GAP summer bottom trawl surveys in the Aleutian Islands –** Subadult ATF were ubiquitous within the RACE-GAP summer survey area (Fig. 7). They were present in the highest abundance in the eastern AI. The final ensemble contains three SDMs with the paGAM weighted slightly less than the others, and it demonstrated good predictive performance (Table 5). Specifically, the ensemble was excellent at identifying hauls that would have a relatively high or low density of this life stage ($\rho = 0.63$), but the lower deviance explained metric suggests that it was less effective at predicting the exact density values (PDE = 0.40). The ensemble also performed well at predicting presence and absence (AUC = 0.79). Geographic position and bottom depth were the most important covariates and accounted for 67.4% of the total deviance explained, though bottom currents and tidal maximum were also relatively important (Table 6). Like early juveniles, subadult ATF were associated with weak tidal forces and weak bottom currents. Based on the covariates, abundance should be highest in the eastern and central AI and at depths between 100 m and 300 m (Fig. 8). Overall abundance of this life stage was relatively high throughout the AI but was highest in the eastern part of the region, near Unalaska Island (Fig. 8). The predicted CV of abundance tended to be high in areas away from the areas of high abundance, reflecting the greater variability of these more marginal areas (Fig. 8). Subadult ATF are very common in the AI, and the encounter probability was near 100% across the survey area (Fig. 9).

**Adult arrowtooth flounder distribution and predicted abundance from RACE-GAP summer bottom trawl surveys in the Aleutian Islands –** Adult ATF catches were universally common throughout the RACE-GAP summer survey area in the AI (Fig. 10). High abundances were observed across the entire AI, but they were somewhat more frequent in the eastern AI. The

final ensemble contained three SDMs with the paGAM weighted slightly less than the hGAM or $GAM_P$, and the predictions generated by the ensemble had a good fit to the data (Table 5). Similar to subadults, the ensemble demonstrated good performance at identifying hauls that caught relatively high or low numbers of adult ATF ($\rho = 0.49$) but was less able to predict the density in those catches (PDE = 0.29). The ensemble displayed a fair ability to predict presence in survey catches (AUC = 0.75), though this is likely a conservative estimate, as there are almost no locations in the AI where ATF are never caught. Similar to earlier life stages, bottom depth, geographic position, current, and current variability were the most important covariates, and they accounted for a combined 78.0% of the deviance explained by the ensemble (Table 6). Adult ATF are predicted to be abundant in moderately deep waters, in the eastern AI, and at locations with weak bottom currents (Fig. 11). Adult ATF appear in somewhat lower numbers than subadults, but they are still one of the most common flatfish species throughout the AI. The highest abundance areas were in the eastern AI, near Unalaska Island and the Islands of Four Mountains, and predicted abundance was higher between 100 m and 300 m (Fig. 11). The predicted CV of abundance tended to be higher in western areas and in shallow areas (Fig. 11). Like subadults, adult ATF had a nearly 100% encounter probability in most of the survey area, with lower encounter probabilities in shallow water close to shore (Fig. 12).

**Essential fish habitat of settled early juvenile, subadult, and adult arrowtooth flounder in the Aleutian Islands –** Habitat-related abundance predictions based on RACE-GAP summer bottom trawl data (1992–2019) were translated into EFH area and additional subareas (Fig. 13). The EFH area for settled early juvenile ATF is smaller than the other life stages. Settled early juveniles had substantial EFH hot spots in the eastern AI around Unalaska Island, more centrally around Atka Island, and a third, smaller area in the far west near Agattu Island. These cases are

supported by the maps of trawl catches (Fig. 4), and hot spots in these sheltered inshore areas are consistent with positive density responses to shallow water with low currents (Fig. 5). The subadult and adult life stages had very similar EFH maps, with large hot spots around Unalaska and Atka islands, but almost the entire survey area was included in the 95% EFH area. These life stages both had an EFH area of 77,700 $km^2$ (Table 5), which was the maximum EFH area attainable using our current methods and reflected the ubiquity of this species in the AI.

Table 5. -- Constituent species distribution models (SDMs) used to construct Essential Fish Habitat (EFH) for a) settled early juvenile, b) subadult, and c) adult arrowtooth flounder: MaxEnt = Maximum entropy; paGAM = presence-absence generalized additive model; hGAM = hurdle GAM; $GAM_P$ = standard Poisson GAM; and $GAM_{nb}$ = standard negative-binomial GAM. Ensemble performance (ρ = Spearman's rank correlation coefficient), root-mean-square-error (RMSE), the area under the receiver operating characteristic (AUC), and the Poisson deviance explained (PDE) were generated from k-fold cross-validation. The "--" in a field indicates that this SDM was not included in the final ensemble.

**a) settled early juvenile arrowtooth flounder**

| Models | RMSE | Relative weight | ρ | AUC | PDE | EFH area ($km^2$) |
|---|---|---|---|---|---|---|
| MaxEnt | 1.70 | 0.24 | 0.33 | 0.88 | 0.38 | 40,900 |
| paGAM | 1.67 | 0.25 | 0.34 | 0.89 | 0.45 | 38,500 |
| hGAM | 1.68 | 0.25 | 0.34 | 0.89 | 0.46 | 31,400 |
| $GAM_P$ | 1.67 | 0.25 | 0.35 | 0.88 | 0.45 | 27,800 |
| $GAM_{nb}$ | 1.67 | 0 | 0.35 | 0.89 | 0.46 | -- |
| ensemble | 1.53 | 1 | 0.35 | 0.90 | 0.56 | 36,800 |

**b) subadult arrowtooth flounder**

| Models | RMSE | Relative weight | ρ | AUC | PDE | EFH area ($km^2$) |
|---|---|---|---|---|---|---|
| MaxEnt | 258.7 | 0 | 0.58 | 0.80 | -0.05 | -- |
| paGAM | 92.4 | 0.30 | 0.63 | 0.82 | 0.28 | 77,700 |
| hGAM | 85.3 | 0.35 | 0.60 | 0.81 | 0.37 | 77,600 |
| $GAM_P$ | 85.9 | 0.35 | 0.59 | 0.77 | 0.37 | 77,700 |
| $GAM_{nb}$ | 102.1 | 0 | 0.62 | 0.79 | 0.32 | -- |
| ensemble | 84.5 | 1 | 0.63 | 0.79 | 0.40 | 77,700 |

**c) adult arrowtooth flounder**

| Models | RMSE | Relative weight | ρ | AUC | PDE | EFH area ($km^2$) |
|---|---|---|---|---|---|---|
| MaxEnt | 186.8 | 0 | 0.50 | 0.78 | -0.29 | -- |
| paGAM | 45.2 | 0.32 | 0.52 | 0.79 | 0.13 | 77,700 |
| hGAM | 44.0 | 0.34 | 0.44 | 0.78 | 0.20 | 77,700 |

| Models | RMSE | Relative weight | ρ | AUC | PDE | EFH area ($km^2$) |
|---|---|---|---|---|---|---|
| $GAM_P$ | 43.9 | 0.34 | 0.43 | 0.72 | 0.20 | 77,700 |
| $GAM_{nb}$ | 48.2 | 0 | 0.50 | 0.76 | 0.12 | -- |
| ensemble | 42.9 | 1 | 0.49 | 0.75 | 0.29 | 77,700 |

Table 6. -- Covariates retained in the a) settled early juvenile, b) subadult, and c) adult arrowtooth flounder species distribution model (SDM) final ensembles, the percent contribution to the ensemble deviance explained by each, and the cumulative percent deviance: SD = standard deviation, and BPI = bathymetric position index.

| **arrowtooth flounder** | **Covariate** | **% Contribution** | **Cumulative % Contribution** |
|---|---|---|---|
| **a) settled early juvenile** | position | 23.6 | 23.6 |
| | tidal maximum | 16.2 | 39.8 |
| | bottom depth | 14.4 | 54.3 |
| | current | 12.7 | 67.0 |
| | aspect north | 6.6 | 73.6 |
| | BPI | 6.6 | 80.2 |
| | bottom temperature | 4.8 | 85.0 |
| | current SD | 3.9 | 88.9 |
| | aspect east | 3.1 | 92.0 |
| | rockiness | 2.5 | 94.5 |
| | slope | 2.4 | 96.9 |
| | curvature | 1.8 | 98.7 |
| | coral presence | 0.8 | 99.5 |
| | sponge presence | 0.3 | 99.8 |
| | pennatulacean presence | 0.2 | 100 |
| **b) subadult** | position | 40.9 | 40.9 |
| | bottom depth | 26.4 | 67.4 |
| | tidal maximum | 8.3 | 75.7 |
| | current | 7.4 | 83.1 |
| | current SD | 4.3 | 87.4 |
| | slope | 1.8 | 89.2 |
| | BPI | 1.8 | 91.0 |
| | sponge presence | 1.8 | 92.8 |
| | coral presence | 1.7 | 94.5 |
| | aspect north | 1.6 | 96.1 |
| | bottom temperature | 1.0 | 97.1 |
| | curvature | 0.9 | 98.0 |
| | rockiness | 0.9 | 98.9 |
| | aspect east | 0.7 | 99.6 |
| | pennatulacean presence | 0.4 | 100 |
| **c) adult** | bottom depth | 32.7 | 32.7 |
| | position | 23.8 | 56.5 |
| | current | 11.0 | 67.5 |
| | current SD | 10.5 | 78.0 |
| | aspect north | 4.4 | 82.4 |

| arrowtooth flounder | Covariate | % Contribution | Cumulative % Contribution |
|---|---|---|---|
| | bottom temperature | 4.0 | 86.4 |
| | tidal maximum | 2.8 | 89.2 |
| | rockiness | 2.8 | 92.0 |
| | aspect east | 2.7 | 94.7 |
| | sponge presence | 2.0 | 96.7 |
| | BPI | 1.1 | 97.8 |
| | slope | 0.8 | 98.6 |
| | coral presence | 0.8 | 99.4 |
| | curvature | 0.5 | 99.9 |
| | pennatulacean presence | 0.1 | 100 |

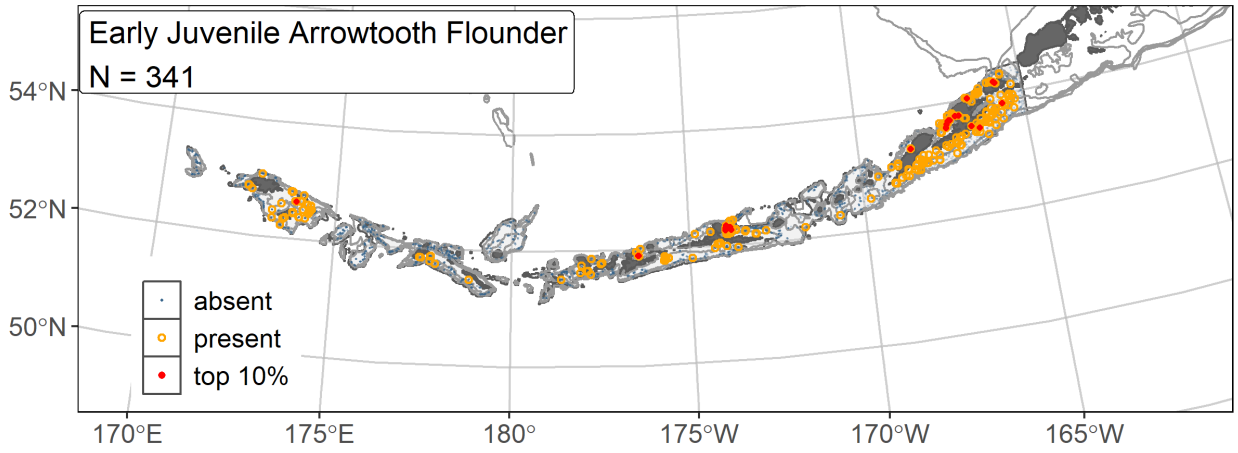


Figure 4. -- Distribution of settled early juvenile arrowtooth flounder catches (N = 347) in 1992–2019 AFSC RACE-GAP summer bottom trawl surveys of the AI with the 100 m, 300 m, and 500 m isobaths indicated; filled red circles indicate locations in top 10% of overall abundance, open orange circles indicate presence in remaining catches, and small blue dots indicate absence.

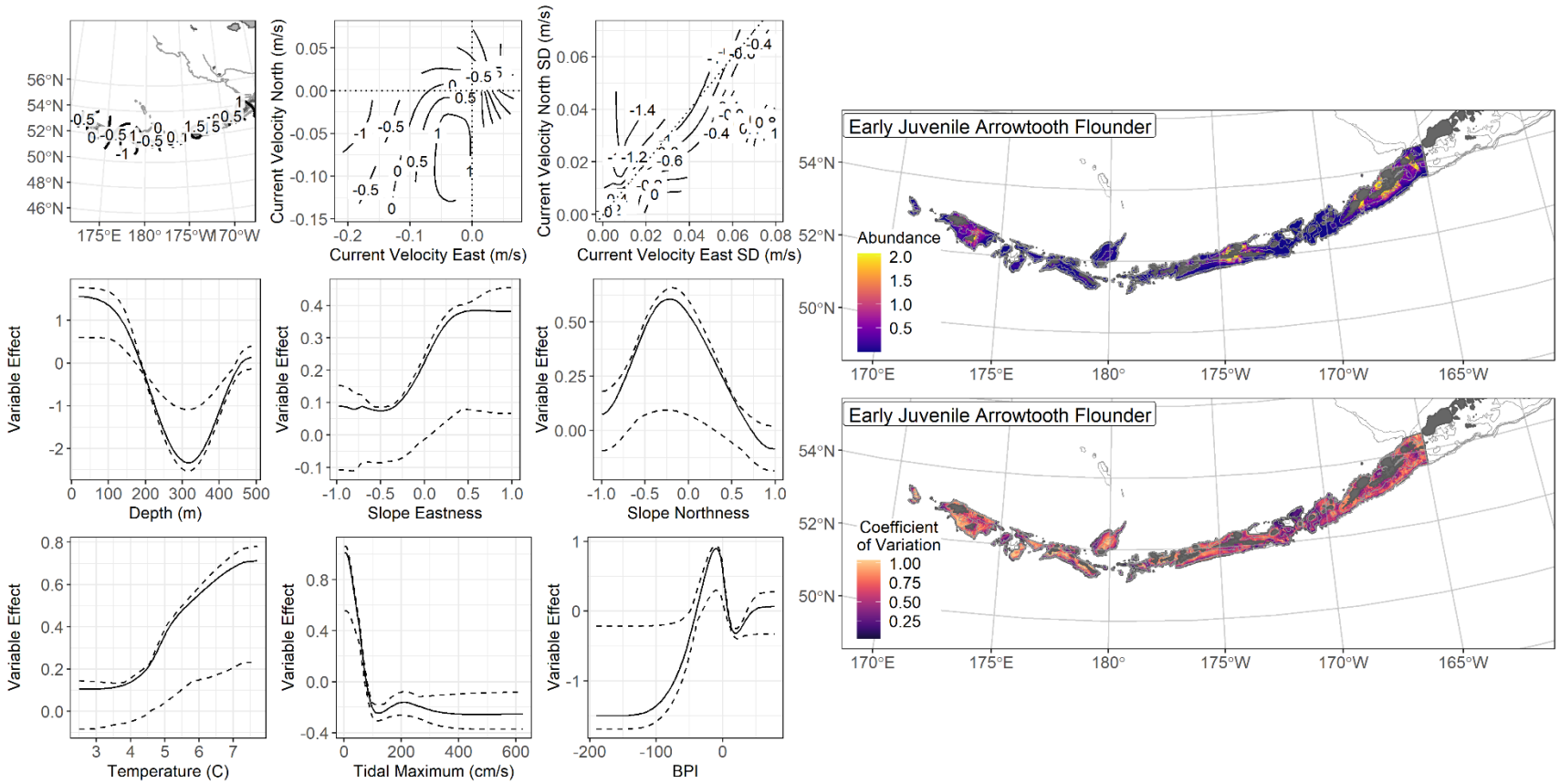


Figure 5. -- The top nine covariate effects (left panel) on ensemble-predicted settled early juvenile arrowtooth flounder numerical abundance across the AI (upper right panel) alongside the coefficient of variation of the ensemble predictions (lower right panel).

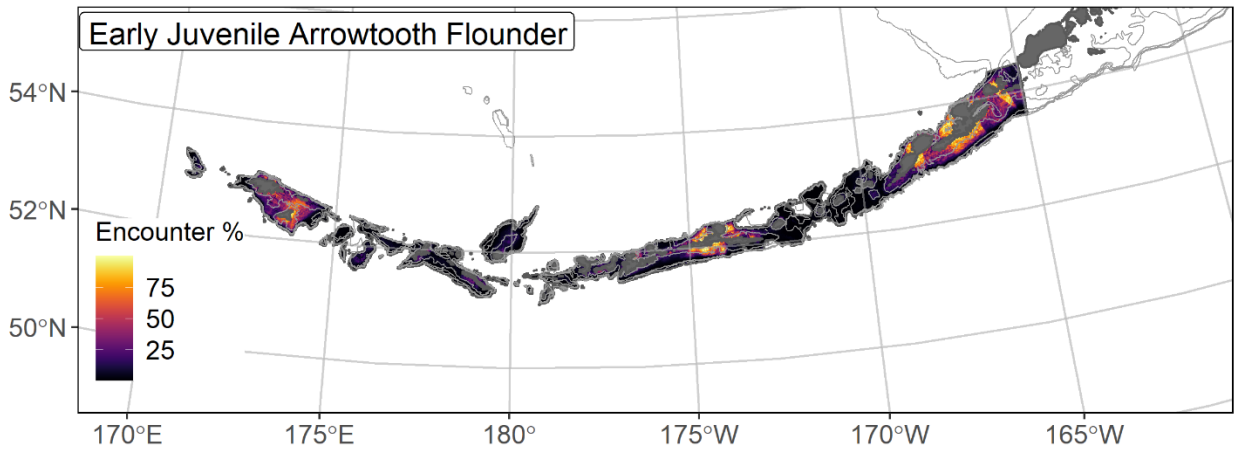


Figure 6. -- Encounter probability of settled early juvenile arrowtooth flounder from AFSC RACE-GAP summer bottom trawl surveys (1992–2019) of the AI with the 100 m, 300 m, and 500 m isobaths indicated.

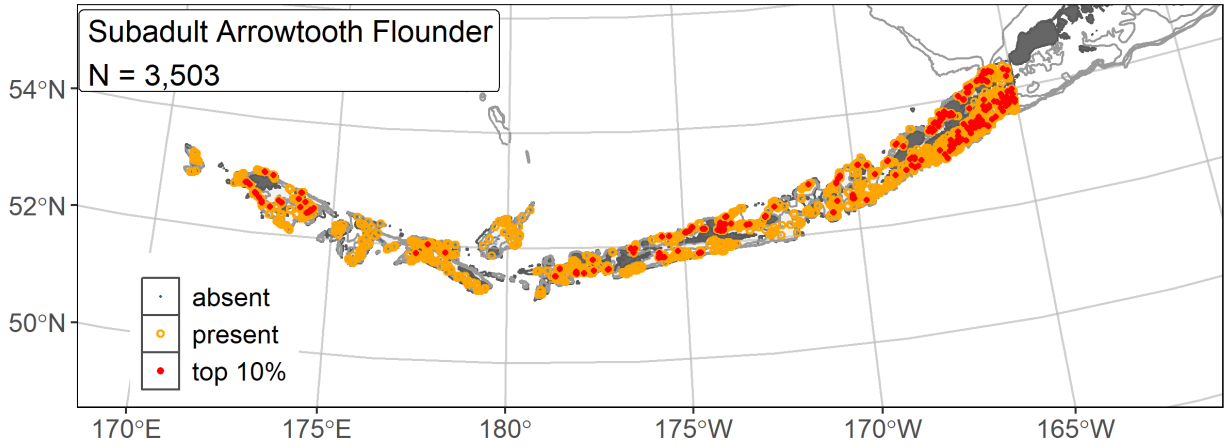


Figure 7. -- Distribution of subadult arrowtooth flounder catches (N = 3,607) in 1992–2019 AFSC RACE-GAP summer bottom trawl surveys of the AI with the 100 m, 300 m, and 500 m isobaths indicated; filled red circles indicate locations in top 10% of overall abundance, open orange circles indicate presence in remaining catches, and small blue dots indicate absence.

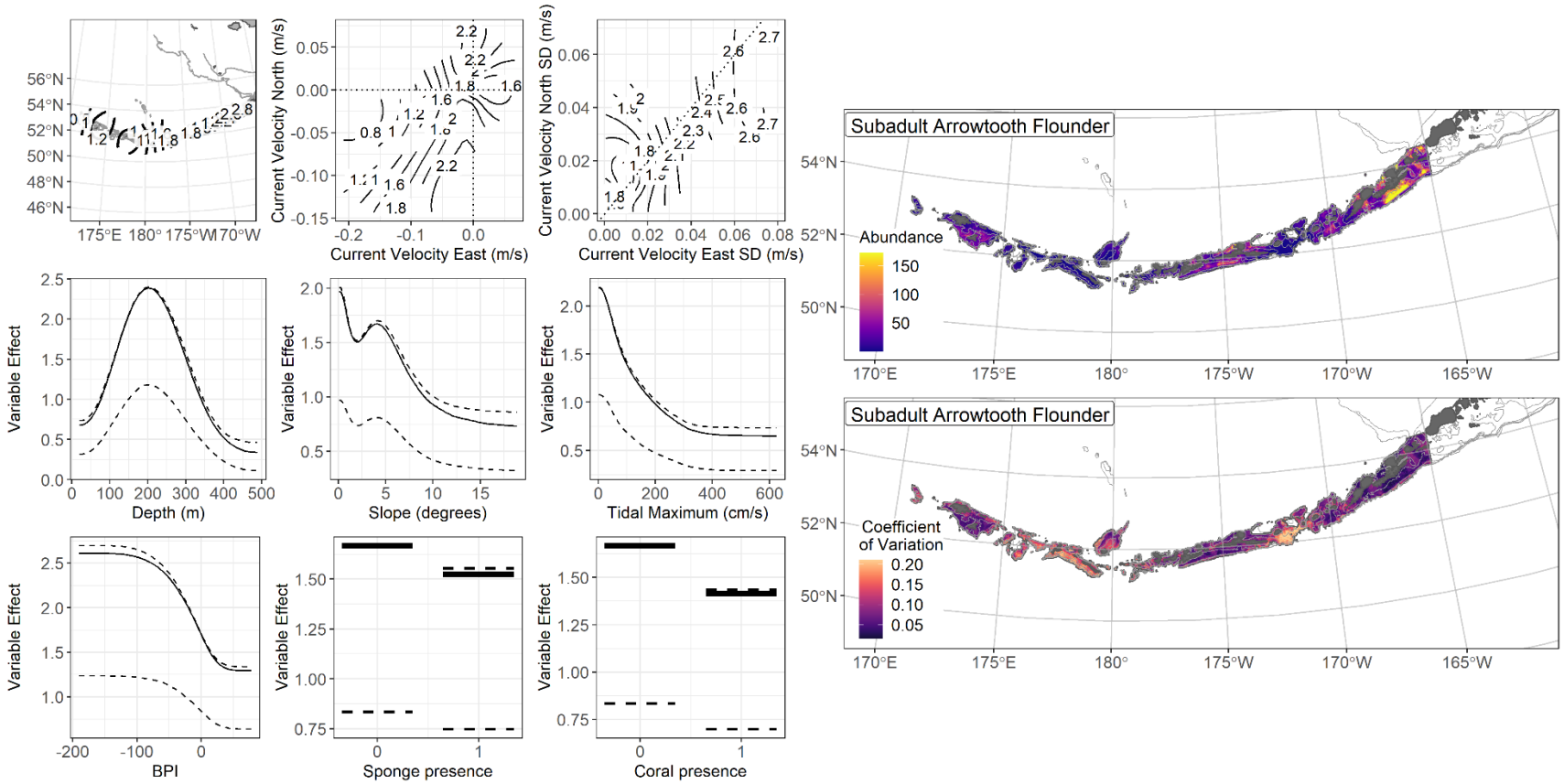


Figure 8. -- The top nine covariate effects (left panel) on ensemble-predicted subadult arrowtooth flounder numerical abundance across the AI (upper right panel) alongside the coefficient of variation of the ensemble predictions (lower right panel).

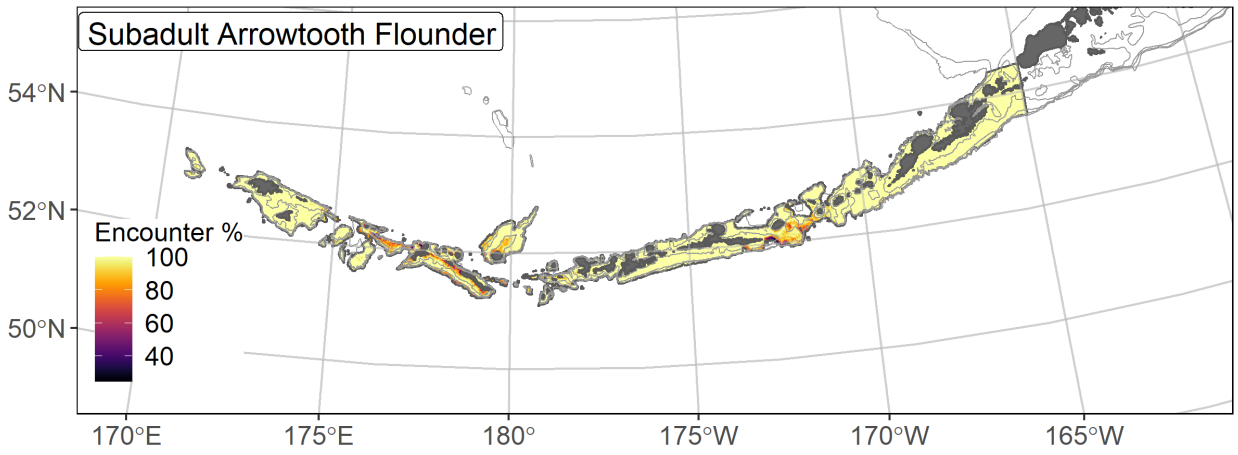


Figure 9. -- Encounter probability of subadult arrowtooth flounder from AFSC RACE-GAP summer bottom trawl surveys (1992–2019) of the AI with the 100 m, 300 m, and 500 m isobaths indicated.

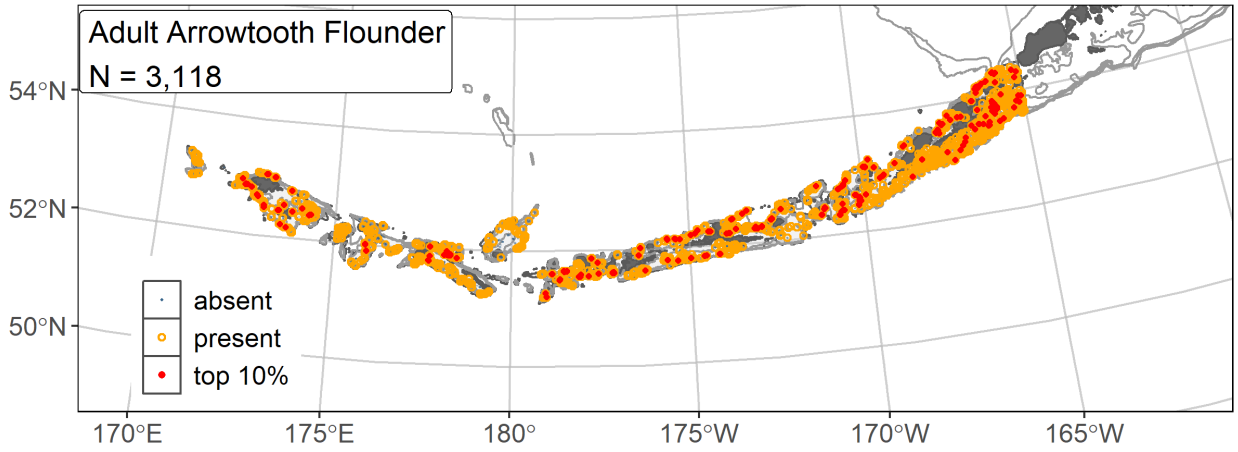


Figure 10. -- Distribution of adult arrowtooth flounder catches (N = 3,194) in 1992–2019 AFSC RACE-GAP summer bottom trawl surveys of the AI with the 100 m, 300 m, and 500 m isobaths indicated; filled red circles indicate locations in top 10% of overall abundance, open orange circles indicate presence in remaining catches, and small blue dots indicate absence.

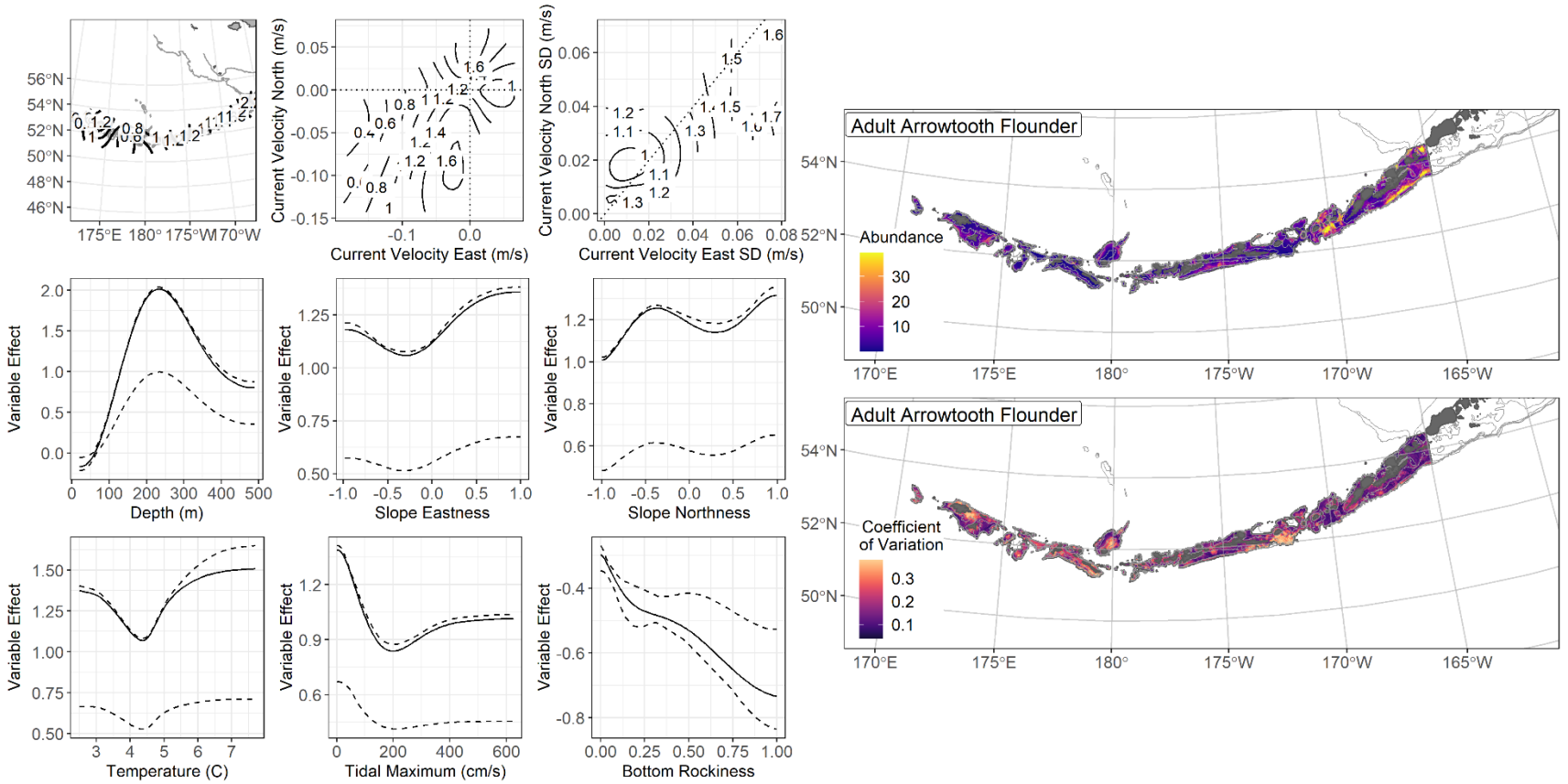


Figure 11. -- The top nine covariate effects (left panel) on ensemble-predicted adult arrowtooth flounder numerical abundance across the AI (upper right panel) alongside the coefficient of variation of the ensemble predictions (lower right panel)

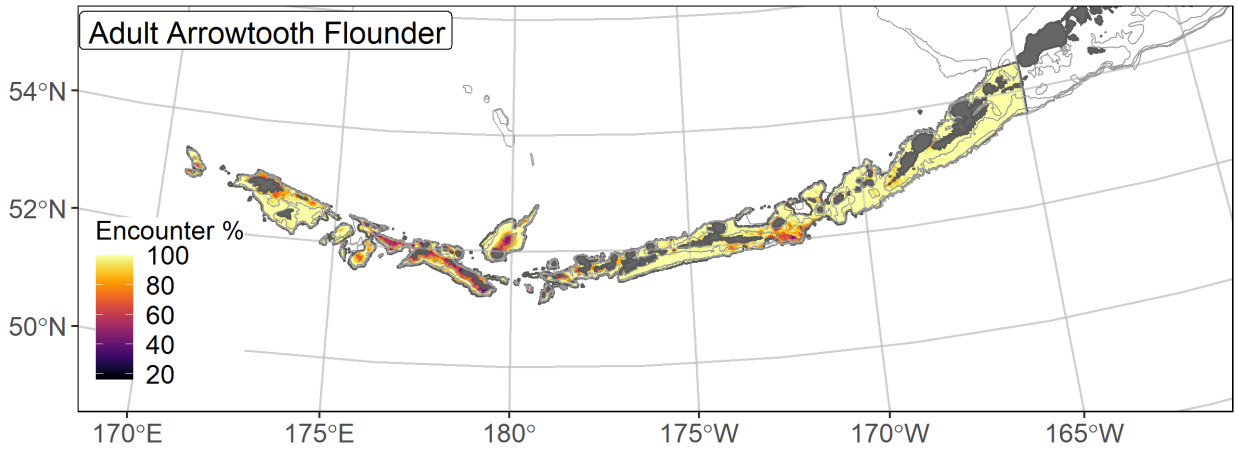


Figure 12. -- Encounter probability of adult arrowtooth flounder from AFSC RACE-GAP summer bottom trawl surveys (1992–2019) of the AI with the 100 m, 300 m, and 500 m isobaths indicated.

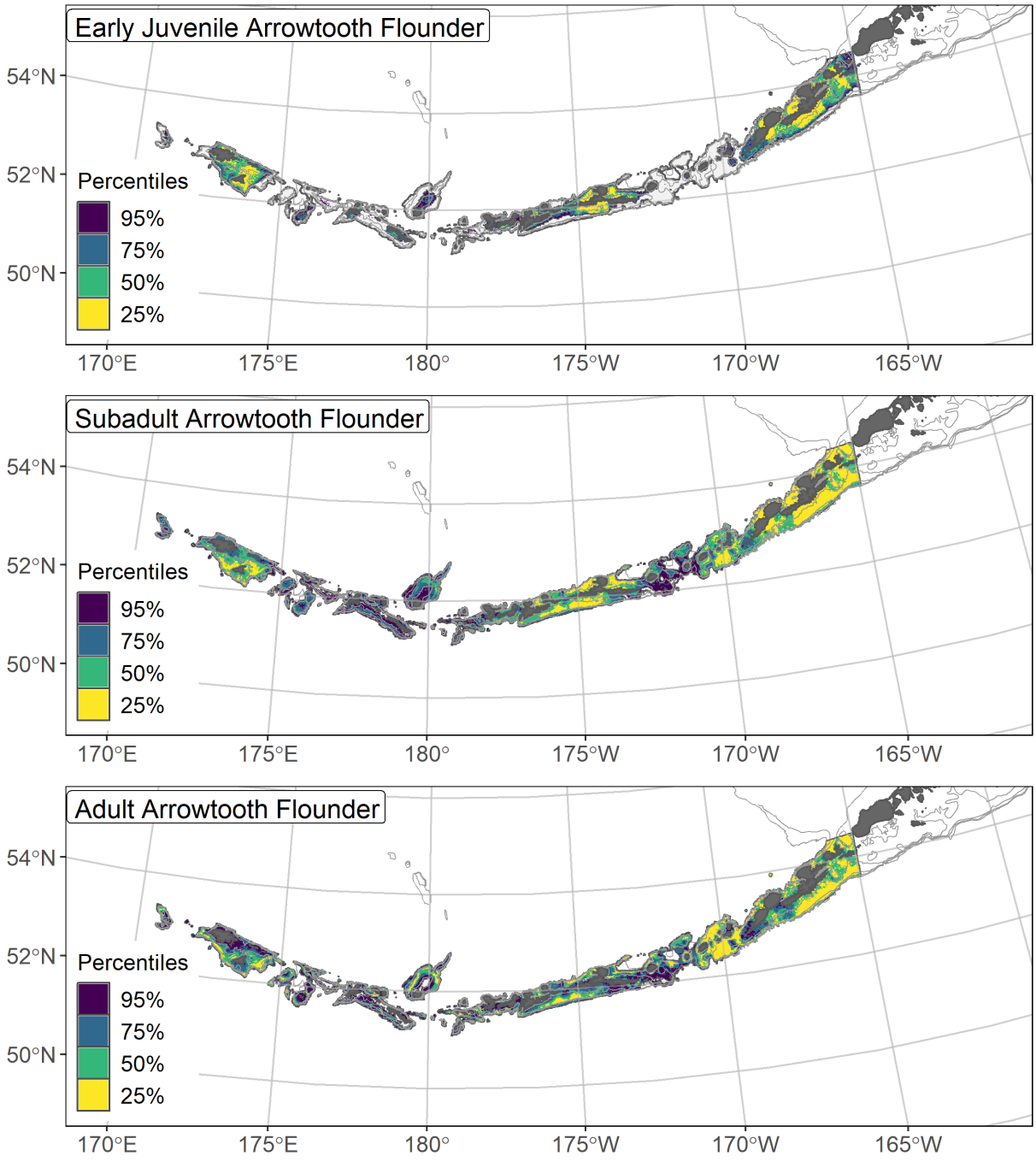


Figure 13. -- Essential fish habitat (EFH) area defined as the top 95% of numerical abundance predictions from a habitat-based ensemble model fitted to settled early juvenile (top), subadult (middle), and adult (bottom) arrowtooth flounder distribution and abundance in AFSC RACE-GAP summer bottom trawl surveys (1992–2019) with 100 m, 300 m, and 500 m isobaths indicated; internal to the EFH map are the subareas of the top 25% (EFH hot spots), top 50% (core EFH area), and top 75% (principal EFH area) of habitat-related, ensemble-predicted numerical abundance.

**Flathead sole (*Hippoglossoides elassodon*)**

Flathead sole (*Hippoglossoides elassodon*) is distributed across the north Pacific, from northern California across the AI and Bering Sea at least as far as the Kuril archipelago (Hart 1973). Spawning occurs between March and June on the continental shelf, usually in bays or other shallow habitats close to inshore nursery areas (Porter 2005). Larvae undergo transformation at 20 mm TL (Doyle et al. 2019) and remain in near shore habitats as settled early juveniles until they reach 140 mm TL (NFA). Most flathead sole reach maturity at 342 mm TL ($L_{50}$; Tenbrink and Wilderbuer 2015), and adults may grow up to 520 mm and live more than 30 years. In the BSAI region, flathead sole is managed as the dominant component (> 94%) of a mixed stock that also includes Bering flounder (*Hippoglossoides robustus*; Monnahan and Haehn, 2020), though Bering flounder are not typically caught in the AI.

**Settled early juvenile flathead sole distribution and predicted abundance from RACE-GAP summer bottom trawl surveys in the Aleutian Islands –** Settled early juvenile flathead sole were not common in the RACE-GAP summer survey of the AI compared to older life stages (Fig. 14), likely because of their small size relative to the selectivity of the trawl gear used[11]. Catches occurred near shore and in shallow water around Unalaska, Atka, or Agattu islands. The final ensemble contained three SDMs, with the MaxEnt model assigned less weight than the others, and the ensemble fit was good overall, though the fit metrics suggest a complicated picture (Table 7). The ensemble performed excellently in terms of AUC and deviance explained (AUC = 0.94; PDE = 0.81), but it scored only fair in its ability to estimate high or low abundance areas ($\rho = 0.28$). Because the Spearman's correlation is based on ranking, values this metric can

[11] A recommendation to add additional survey data types if possible to future SDM ensemble EFH mapping efforts for this species will be included as a future recommendation for research directions from the 2023 EFH 5-year review.

sometimes produce low values when many observed values are zero. By comparison, the excellent score for AUC indicates that the ensemble is quite good at estimating presence versus absence, and the high PDE suggests that it captures a majority of the variation in abundance. Finally, the map of predicted abundance (Fig. 15) agreed with the map of observed catches (Fig. 14), so this model is likely to provide accurate information. Geographic position, bottom depth, BPI, and tidal maximum were the most important covariates and explained 68.2% of the total deviance (Table 8). In general, the ensemble predicts high abundance in the far east and far west of the AI in areas of moderate to shallow depth, weak tidal currents, and a low BPI (which indicates terrain that includes troughs or valleys; Fig. 15). Predicted abundance matched the map of catches and was high in areas around Unalaska, Atka, and Agattu islands (Fig. 15). The predicted CV of abundance was moderate throughout most areas and very high in areas with high predicted abundance, reflecting uncertainty around the ensemble predictions in high abundance areas (Fig. 15). Encounter probabilities followed the same pattern with a few isolated areas of high probability (Fig. 16).

**Subadult flathead sole distribution and predicted abundance from RACE-GAP summer bottom trawl surveys in the Aleutian Islands –** In contrast to early juveniles, subadult flathead sole catches were widespread and very common in the RACE-GAP summer survey area (Fig. 17), following the same pattern as early juveniles with high abundance catches around Unalaska, Atka, and Agattu islands. The final ensemble contains four SDMs, with the hGAM given the most weight, and it demonstrated excellent predictive performance with regard to model fit (Table 7). All three fit metrics had high values ($\rho = 0.60$; AUC = 0.89; PDE = 0.72), suggesting that the ensemble predictions are accurate. Geographic position, bottom depth, tidal maximum, current speed, and current variability were the most important covariates and

accounted for 74.2% of the deviance explained by the ensemble (Table 8). In general, the ensemble model predicted high abundance in patches around the major islands, and in areas with depths between 100 and 200 m, weak tidal currents, and currents that run in north or south directions (Fig. 18). However, predicted abundance was very high overall and even predicted low-abundance areas had averages well above zero. Predicted abundance was much higher overall for the subadult life stage but was located in the same areas as settled early juveniles around Unalaska, Atka, and Agattu islands (Fig. 18). The predicted CV of abundance tended to be high around places with increased abundance (Fig. 18). These places have low average predicted abundance with occasional large catches. Predicted encounter probabilities for subadult flathead sole were high in areas shallower than 300 m, with the exception of major passes between the islands (Fig. 19).

**Adult flathead sole distribution and predicted abundance from RACE-GAP summer bottom trawl surveys in the Aleutian Islands –** Adult flathead sole catches were common in the RACE-GAP summer survey area in the AI (Fig. 20). The distribution of adult catches follows the same general pattern as subadults and settled early juveniles, with high abundance catches centered around Unalaska, Atka, and Agattu islands. The ensemble contained four equally weighted SDMs, and ensemble predictions had a good overall fit to the data (Table 7). All three fit metrics indicated a good fit ($\rho = 0.56$; AUC = 0.86; PDE = 0.48), suggesting that the ensemble provides good accuracy. Similar to earlier life stages, bottom depth, geographic position, tidal maximum, and current were the most important covariates, and they accounted for 70.0% of the deviance explained by the ensemble (Table 8). Adult flathead sole are predicted to be abundant in 100-250 m deep waters and areas with a low tidal maximum and southerly currents (Fig. 21). The estimated abundance of adults is lower overall than that of subadults but

otherwise it shows the same distribution pattern with high abundance predicted near Unalaska, Atka, and Agattu islands (Fig. 21). The predicted CV of abundance was higher overall for adults than the other life stages (Fig. 21). Encounter probabilities were predicted to be high around the larger islands in the AI and low in deeper areas and in the passes, similar to earlier life stages (Fig. 22).

**Essential fish habitat of settled early juvenile, subadult, and adult flathead sole in the Aleutian Islands –** The habitat related abundance predictions based on RACE-GAP summer bottom trawl data (1991–2019) were translated into EFH area and subareas (Fig. 23). The EFH areas for all three life stages show the same overall pattern, with hot spots around Unalaska, Atka, and Agattu islands. Although the settled early juvenile model did not perform well in terms of Spearman's ρ, high scores for AUC and PDE suggest it is still reliable for describing long-term average bottom trawl catches. Additionally, the correspondence between the early juvenile maps and the maps made by the better performing subadult and adult models suggests that the early juvenile ensemble still provides useful predictions. The settled early juvenile EFH area is much smaller than the EFH area for other life stages and is restricted to those few spots. By contrast, subadult and adult EFH descriptions extended much further and covered most areas with depths <300 m. Areas around the major passes in the islands, such as Seguam and Amchitka passes, were not EFH. Subadult and adult EFH maps were nearly identical, and overall, this species does not seem to change habitats as it grows and reaches maturity.

Table 7. – Constituent species distribution models (SDMs) used to construct Essential Fish Habitat (EFH) for a) settled early juvenile, b) subadult, and c) adult flathead sole: MaxEnt = Maximum entropy; paGAM = presence-absence generalized additive model; hGAM = hurdle GAM; $GAM_P$ = standard Poisson GAM; and $GAM_{nb}$ = standard negative-binomial GAM. Ensemble performance (ρ = Spearman's rank correlation coefficient), root-mean-square-error (RMSE), the area under the receiver operating characteristic (AUC), and the Poisson deviance explained (PDE) were generated from k-fold cross-validation. The "--" in a field indicates that this SDM was not included in the final ensemble.

**a) settled early juvenile flathead sole**

| Models | RMSE | Relative Weight | ρ | AUC | PDE | EFH area ($km^2$) |
|---|---|---|---|---|---|---|
| MaxEnt | 9.27 | 0.22 | 0.26 | 0.91 | 0.71 | 37,300 |
| paGAM | 6.89 | 0.39 | 0.28 | 0.92 | 0.68 | 29,200 |
| hGAM | -- | 0 | -- | -- | -- | -- |
| $GAM_P$ | 6.83 | 0.40 | 0.30 | 0.90 | 0.71 | 12,100 |
| $GAM_{nb}$ | -- | 0 | -- | -- | -- | -- |
| ensemble | 5.52 | 1 | 0.28 | 0.94 | 0.81 | 30,400 |

**b) subadult flathead sole**

| Models | RMSE | Relative Weight | ρ | AUC | PDE | EFH area ($km^2$) |
|---|---|---|---|---|---|---|
| MaxEnt | 97.8 | 0.23 | 0.56 | 0.87 | 0.42 | 70,400 |
| paGAM | 94.1 | 0.25 | 0.60 | 0.90 | 0.48 | 71,600 |
| hGAM | 74.9 | 0.40 | 0.55 | 0.89 | 0.71 | 49,400 |
| $GAM_P$ | -- | 0 | -- | -- | -- | -- |
| $GAM_{nb}$ | 142.1 | 0.11 | 0.60 | 0.89 | 0.59 | 42,000 |
| ensemble | 72.8 | 1 | 0.60 | 0.89 | 0.72 | 69,400 |

**c) adult flathead sole**

| Models | RMSE | Relative Weight | ρ | AUC | PDE | EFH area ($km^2$) |
|---|---|---|---|---|---|---|
| MaxEnt | 14.7 | 0.24 | 0.51 | 0.83 | 0.22 | 68,700 |
| paGAM | 14.5 | 0.25 | 0.55 | 0.86 | 0.35 | 66,100 |
| hGAM | 14.5 | 0.25 | 0.51 | 0.86 | 0.39 | 57,400 |

| Models | RMSE | Relative Weight | ρ | AUC | PDE | EFH area (km$^2$) |
|---|---|---|---|---|---|---|
| $GAM_P$ | 14.5 | 0.25 | 0.51 | 0.83 | 0.38 | 59,100 |
| $GAM_{nb}$ | 15.2 | 0 | 0.55 | 0.86 | 0.34 | -- |
| ensemble | 13.5 | 1 | 0.56 | 0.86 | 0.48 | 67,800 |

Table 8. -- Covariates retained in the a) settled early juvenile, b) subadult, and c) adult flathead sole species distribution model (SDM) final ensembles, the percent contribution to the ensemble deviance explained by each, and the cumulative percent deviance: SD = standard deviation, and BPI = bathymetric position index.

| **flathead sole** | **Covariate** | **% Contribution** | **Cumulative % Contribution** |
|---|---|---|---|
| **a) settled early juvenile** | position | 24.7 | 24.7 |
| | bottom depth | 18.8 | 43.6 |
| | BPI | 13.2 | 56.7 |
| | tidal maximum | 11.5 | 68.2 |
| | current | 8.9 | 77.1 |
| | pennatulacean presence | 4.7 | 81.8 |
| | slope | 3.8 | 85.5 |
| | current SD | 3.7 | 89.2 |
| | aspect north | 3.2 | 92.4 |
| | aspect east | 2.6 | 95.0 |
| | coral presence | 1.5 | 96.5 |
| | rockiness | 1.3 | 97.8 |
| | curvature | 1.0 | 98.8 |
| | bottom temperature | 0.8 | 99.6 |
| | sponge presence | 0.4 | 100 |
| **b) subadult** | position | 25.7 | 25.7 |
| | bottom depth | 16.9 | 42.6 |
| | tidal maximum | 15.4 | 58.1 |
| | current SD | 8.9 | 67.0 |
| | current | 7.2 | 74.2 |
| | aspect north | 4.4 | 78.6 |
| | slope | 4.1 | 82.7 |
| | BPI | 3.9 | 86.6 |
| | pennatulacean presence | 3.8 | 90.4 |
| | rockiness | 3.1 | 93.5 |
| | curvature | 1.9 | 95.4 |
| | aspect east | 1.5 | 96.9 |
| | coral presence | 1.3 | 98.2 |
| | sponge presence | 1.2 | 99.4 |
| | bottom temperature | 0.6 | 100 |
| **c) adult** | position | 31.6 | 31.6 |
| | bottom depth | 15.2 | 46.8 |
| | tidal maximum | 14.2 | 61.1 |
| | current | 8.9 | 70.0 |
| | current SD | 5.7 | 75.7 |

| flathead sole | Covariate | % Contribution | Cumulative % Contribution |
|---|---|---|---|
| | aspect east | 4.6 | 80.3 |
| | BPI | 3.5 | 83.8 |
| | pennatulacean presence | 3.2 | 87.0 |
| | aspect north | 3.1 | 90.1 |
| | slope | 2.5 | 92.6 |
| | coral presence | 2.1 | 94.7 |
| | curvature | 1.6 | 96.3 |
| | rockiness | 1.6 | 97.9 |
| | bottom temperature | 1.3 | 99.2 |
| | sponge presence | 0.8 | 100 |

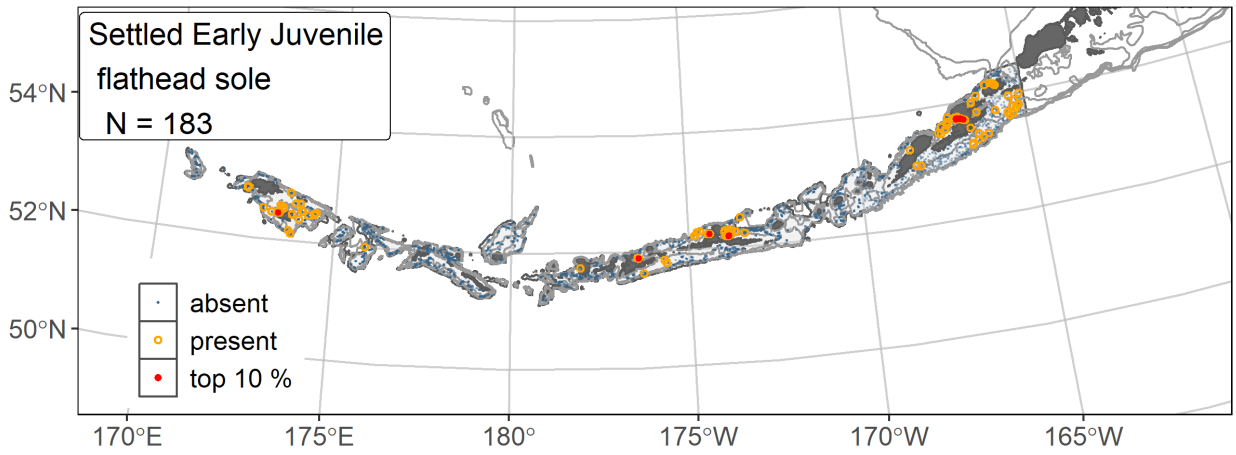


Figure 14. -- Distribution of settled early juvenile flathead sole catches (N = 183) in 1991–2019 AFSC RACE-GAP summer bottom trawl surveys of the AI with the 100 m, 300 m, and 500 m isobaths indicated; filled red circles indicate locations in top 10% of overall abundance, open orange circles indicate presence in remaining catches, and small blue dots indicate absence.

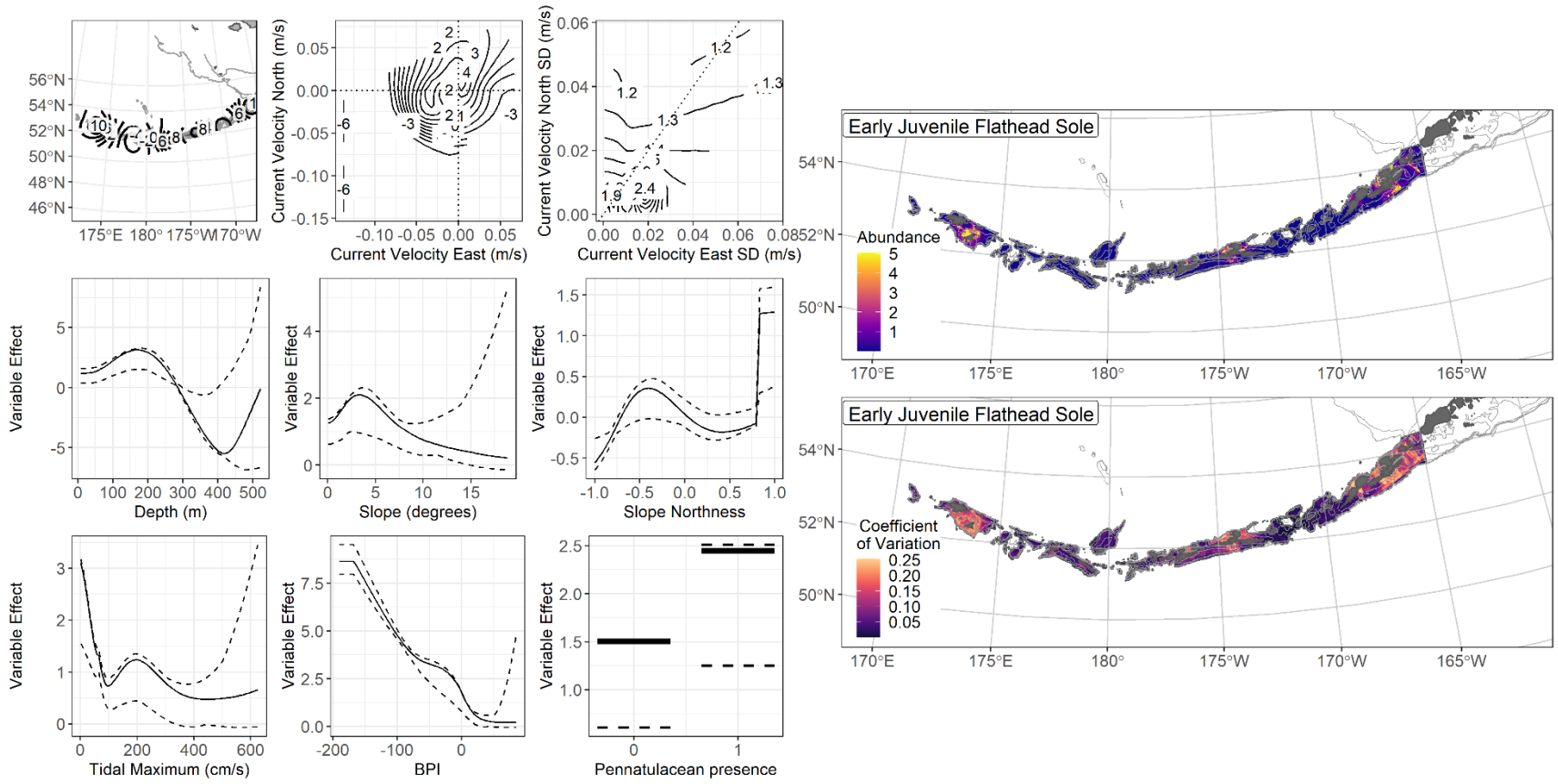


Figure 15. -- The top nine covariate effects (left panel) on ensemble-predicted settled early juvenile flathead sole numerical abundance across the AI (upper right panel) alongside the coefficient of variation of the ensemble predictions (lower right panel).

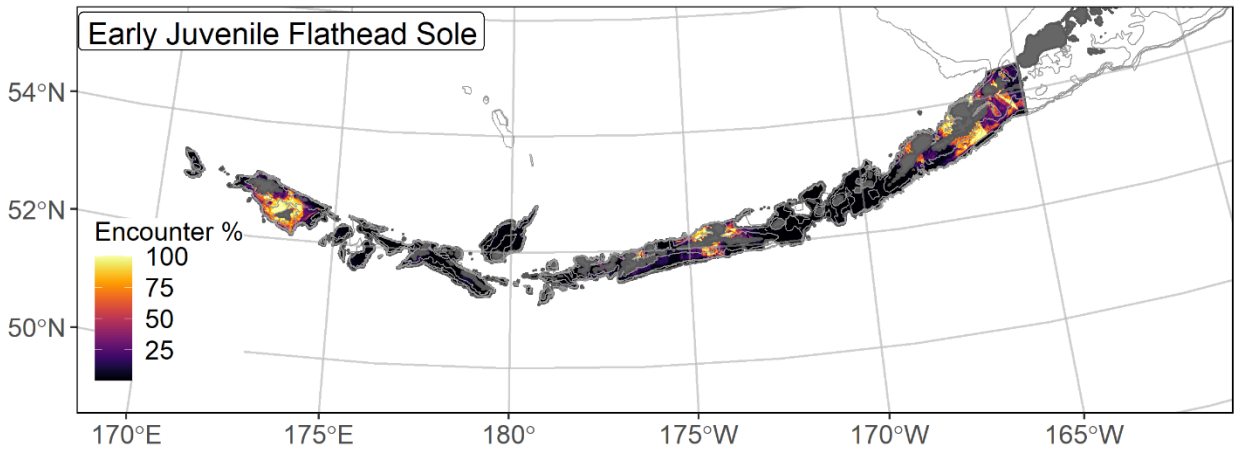


Figure 16. -- Encounter probability of settled early juvenile flathead sole from AFSC RACE-GAP summer bottom trawl surveys (1991–2019) of the AI with the 100 m, 300 m, and 500 m isobaths indicated.

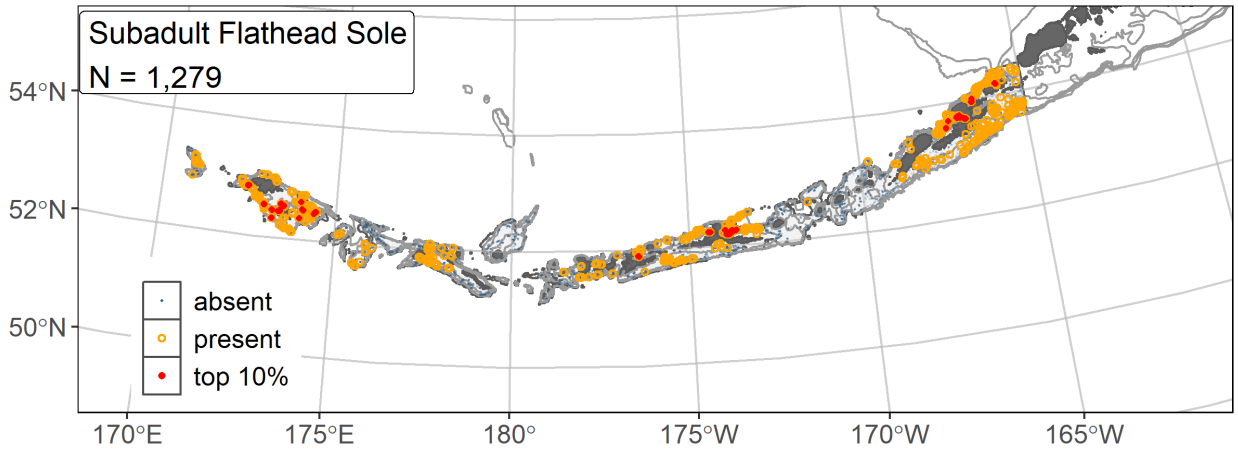


Figure 17. -- Distribution of subadult flathead sole catches (N = 1,279) in 1991–2019 AFSC RACE-GAP summer bottom trawl surveys of the AI with the 100 m, 300 m, and 500 m isobaths indicated; filled red circles indicate locations in top 10% of overall abundance, open orange circles indicate presence in remaining catches, and small blue dots indicate absence.

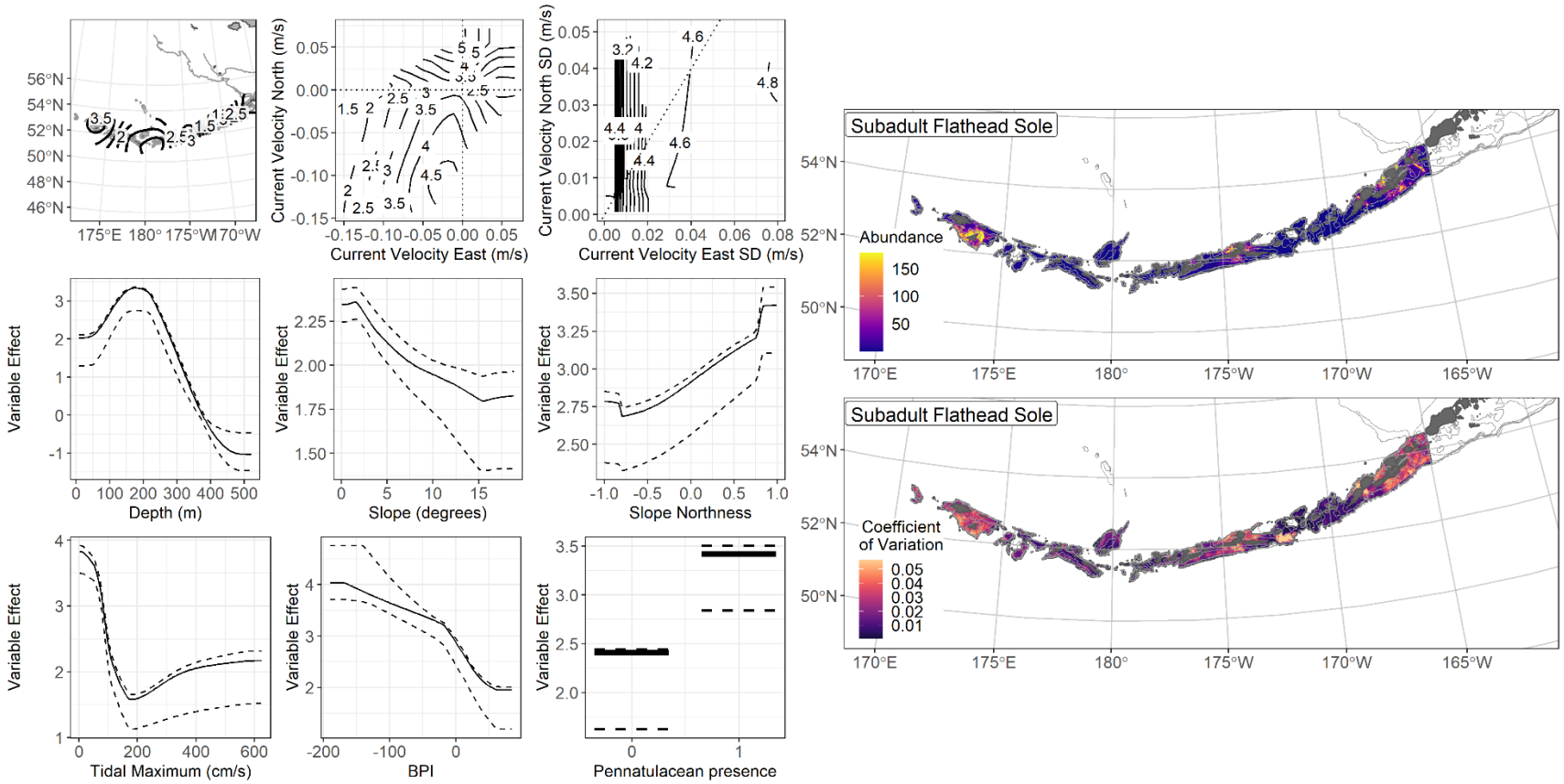


Figure 18. -- The top nine covariate effects (left panel) on ensemble-predicted subadult flathead sole numerical abundance across the AI (upper right panel) alongside the coefficient of variation of the ensemble predictions (lower right panel).

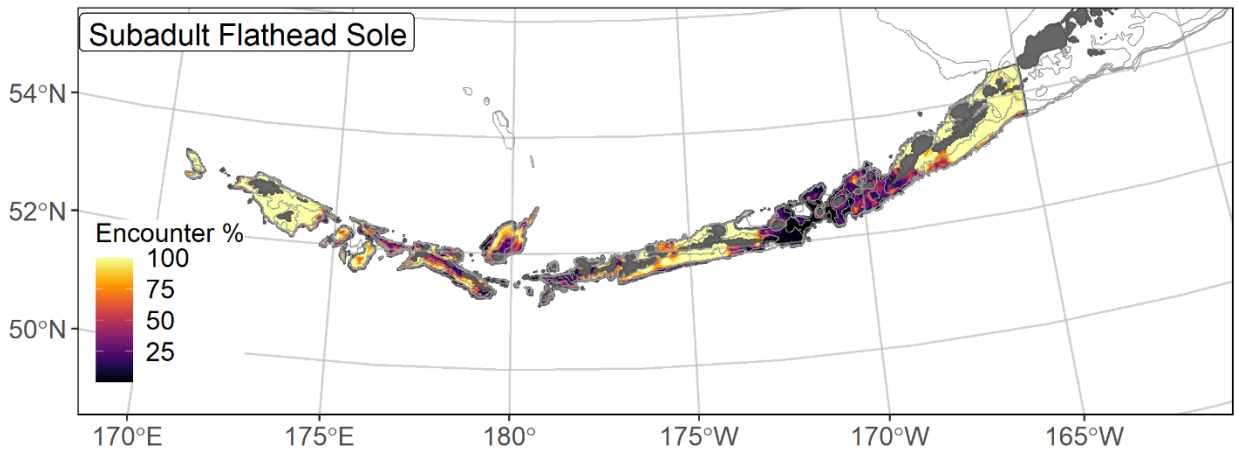


Figure 19. -- Encounter probability of subadult flathead sole from AFSC RACE-GAP summer bottom trawl surveys (1991–2019) of the AI with the 100 m, 300 m, and 500 m isobaths indicated.

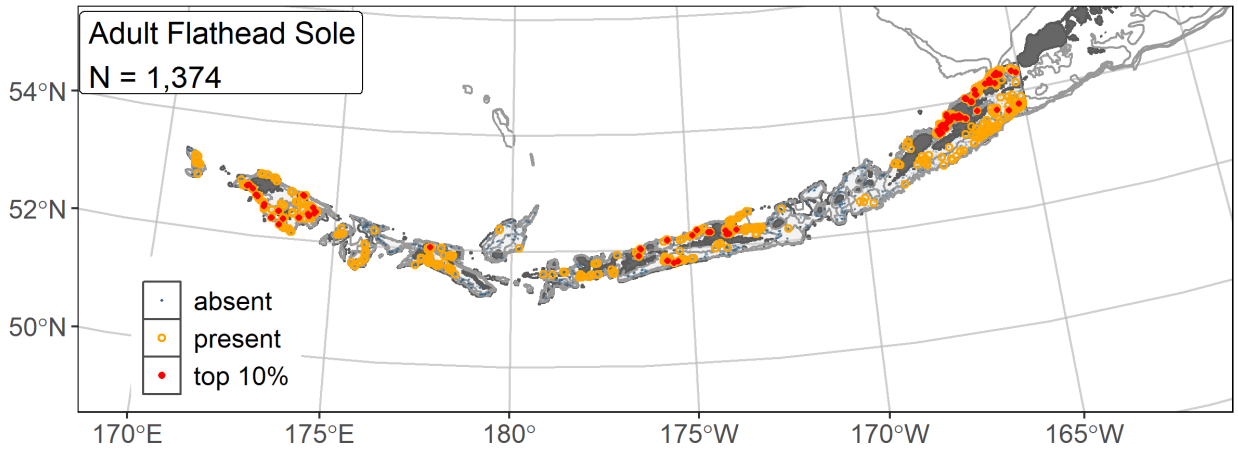


Figure 20. -- Distribution of adult flathead sole catches (N = 1,374) in 1991–2019 AFSC RACE-GAP summer bottom trawl surveys of the AI with the 100 m, 300 m, and 500 m isobaths indicated; filled red circles indicate locations in top 10% of overall abundance, open orange circles indicate presence in remaining catches, and small blue dots indicate absence.

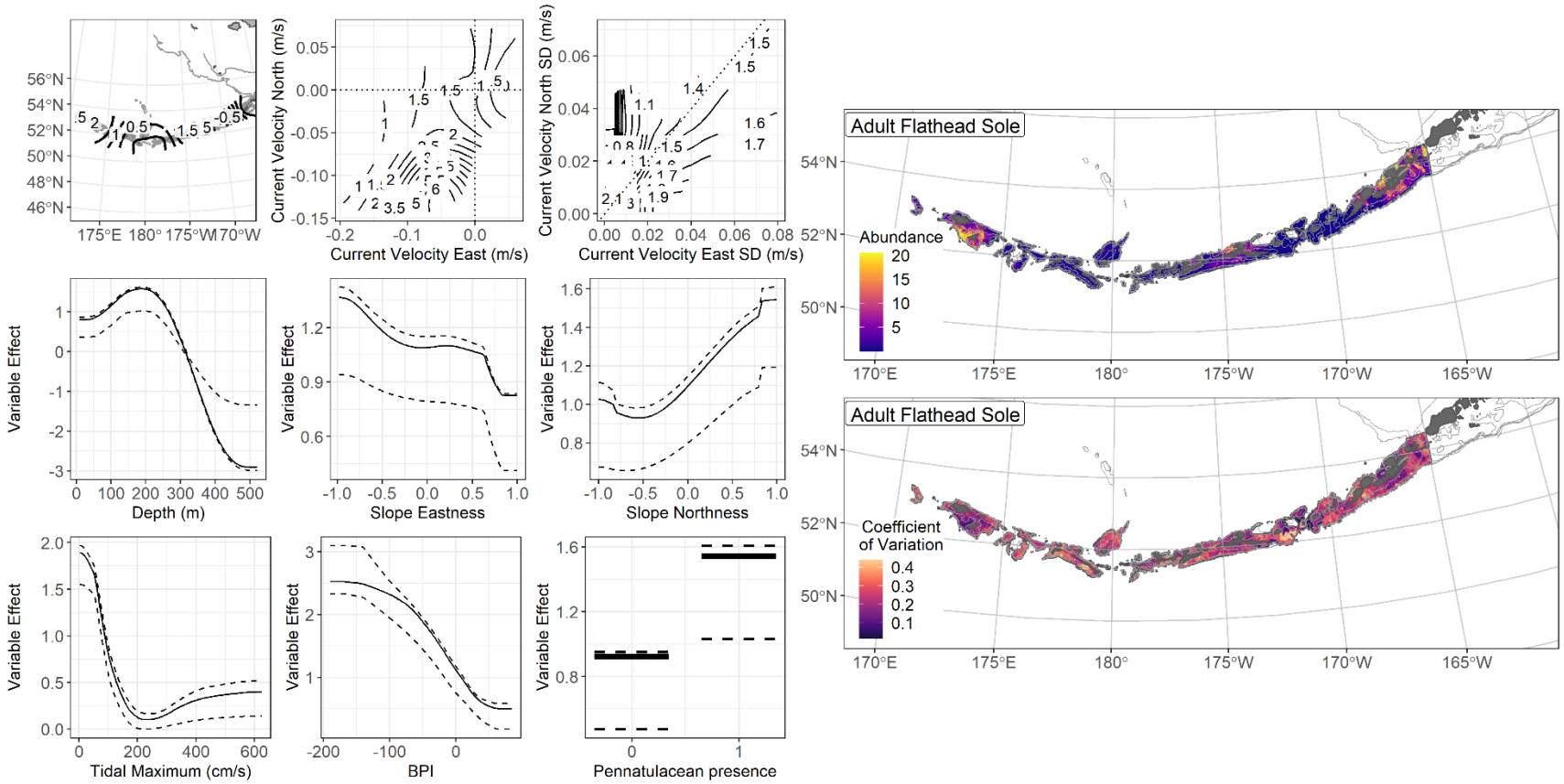


Figure 21. -- The top nine covariate effects (left panel) on ensemble-predicted adult flathead sole numerical abundance across the AI (upper right panel) alongside the coefficient of variation of the ensemble predictions (lower right panel)

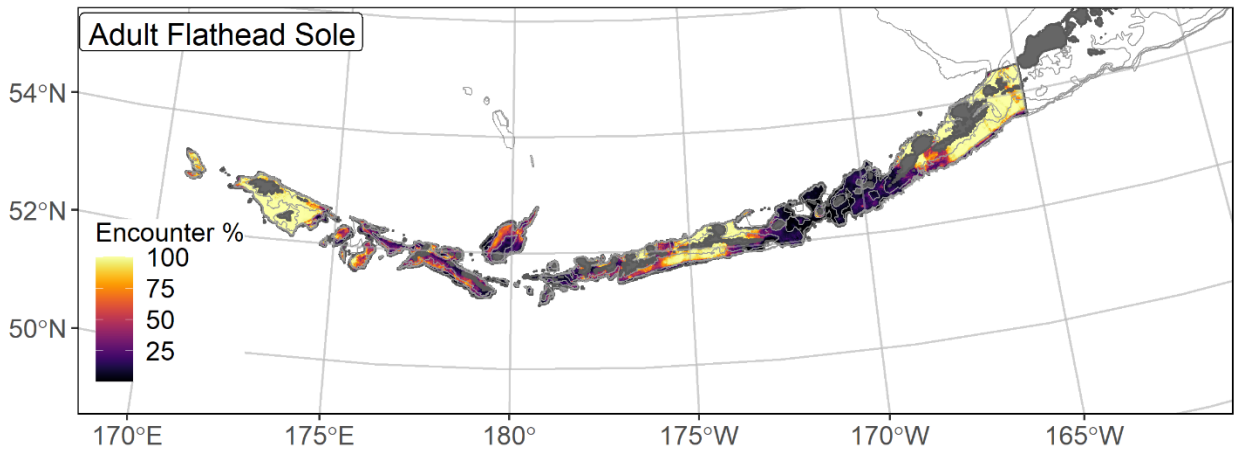


Figure 22. -- Encounter probability of adult flathead sole from AFSC RACE-GAP summer bottom trawl surveys (1991–2019) of the AI with the 100 m, 300 m, and 500 m isobaths indicated.

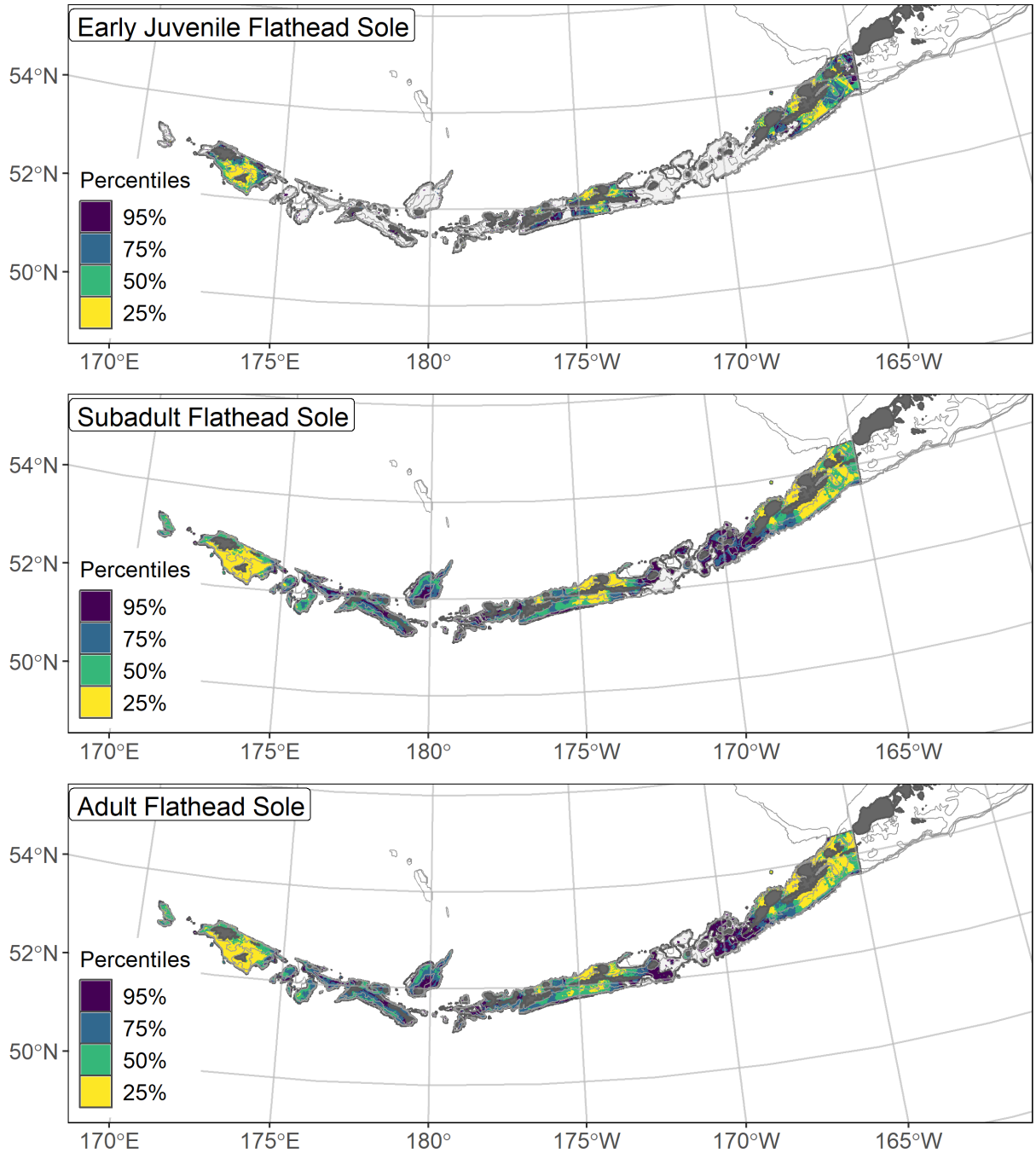


Figure 23. -- Essential fish habitat (EFH area) defined as the top 95% of numerical abundance predictions from a habitat-based ensemble fitted to settled early juvenile (top), subadult (middle), and adult (bottom) flathead sole distribution and abundance in AFSC RACE-GAP summer bottom trawl surveys (1991–2019) with 100 m, 300 m, and 500 m isobaths indicated; internal to the EFH map are the subareas of the top 25% (EFH hot spots), top 50% (core EFH area), and top 75% (principal EFH area) of habitat-related, ensemble-predicted numerical abundance.

**Greenland turbot (*Reinhardtius hippoglossoides*)**

Greenland turbot (*Reinhardtius hippoglossoides*, a.k.a. Greenland halibut) is found in both the northern Pacific and northern Atlantic Oceans, although it is mostly absent from the Arctic Ocean north of Canada and Russia (Alton et al. 1988). Adults may be over a meter long and tend to prefer deep water along the continental slope, sometimes at depths greater than 2,000 m. Spawning occurs along the continental slope and in deep canyons, with eggs and larvae typically released in deep water and gradually transported inshore (Sohn et al. 2010). Greenland turbot become sexually mature ($L_{50}$) around 580 mm FL, although they appear to have a complex spawning cycle and do not necessarily spawn in the first year of maturity (Tenbrink et al. 2021). Unlike most flatfish, this species is thought to forage primarily in the middle of the water column and is less dependent on benthic prey than other groundfish species (Alton et al. 1988). There is evidence that some individuals undertake seasonal migrations to feed in shallower water during the summer (Siwicke and Coutre 2020). In the BSAI region, Greenland turbot are managed as a single stock with a biennial assessment (Bryan et al. 2020a). Due to lack of data, only the adult life stage was modeled.

**Adult Greenland turbot distribution and predicted abundance from RACE-GAP summer bottom trawl surveys in the Aleutian Islands –** Adult Greenland turbot were occasionally caught in the RACE-GAP summer bottom trawl survey and usually found on the north side of the islands in deep water (Fig. 24). Large catches were concentrated around the Petrel Bank area and north of Atka Island. The final ensemble contained two SDMs that weighted equally, and it demonstrated an overall good to excellent fit to the data (Table 9). The ensemble showed excellent performance when predicting presence or absence (AUC = 0.96) and explained most of the deviance in the observations (PDE = 0.70). It also achieved a lower but still good score in

terms of its ability to rank catches ($\rho = 0.40$). In summary, Greenland turbot have a distinct and easily recognized distribution in the habitat, and despite only a moderate amount of data, the predictions of this ensemble fit the data well. Bottom depth was the most important covariate and accounted for 50.1% of the total deviance explained, but bottom temperature, current and geographic position also made larger than average contributions (Table 10). In general, abundance was expected to be higher in locations with high bottom depth, low temperature, weak currents, and farther west (Fig. 25). The predicted abundance map shows that almost all Greenland turbot in the AI are predicted below the 300 m depth contour, with the highest densities occurring around Petrel Bank and Seguam Pass (Fig. 25). The predicted CV of abundance was close to zero in all shallow areas where this species is always absent, and it was elevated along the slope and in the passes in the archipelago, reflecting that this species has a well-defined range but it is variable within that range (Fig. 25). The map of encounter probability shows a high chance of catching these species in most slope areas below 300 m and nearly 100% in the major passes (Fig. 26).

**Essential fish habitat of adult Greenland turbot in the Aleutian Islands –** The habitat-related abundance predictions based on RACE-GAP summer bottom trawl data (1991–2019) were translated into EFH area and subareas (Fig. 27). The adult EFH area consists of hot spots around Seguam Pass and Petrel Bank, and a thin ribbon that runs along the continental slope elsewhere. The EFH area closely follows the 300 m depth contour, and very few shallow areas qualify as EFH for this species.

Table 9. -- Constituent species distribution models (SDMs) used to construct Essential Fish Habitat (EFH) for a) adult Greenland turbot: MaxEnt = Maximum entropy; paGAM = presence-absence generalized additive model; hGAM = hurdle GAM; $GAM_P$ = standard Poisson GAM; and $GAM_{nb}$ = standard negative-binomial GAM. Ensemble performance (ρ = Spearman's rank correlation coefficient), root-mean-square-error (RMSE), the area under the receiver operating characteristic (AUC), and the Poisson deviance explained (PDE) were generated from k-fold cross-validation. The "--" in a field indicates that this SDM was not included in the final ensemble.

**a) adult Greenland turbot**

| Models | RMSE | Relative Weight | ρ | AUC | PDE | EFH area ($km^2$) |
|---|---|---|---|---|---|---|
| MaxEnt | -- | 0 | -- | -- | -- | -- |
| paGAM | 12.5 | 0.49 | 0.40 | 0.96 | 0.61 | 30,300 |
| hGAM | 29.1 | 0 | 0.40 | 0.96 | 0.50 | -- |
| $GAM_P$ | 14.9 | 0 | 0.41 | 0.94 | 0.73 | -- |
| $GAM_{nb}$ | 12.2 | 0.51 | 0.42 | 0.95 | 0.68 | 19,600 |
| ensemble | 11.6 | 1 | 0.41 | 0.96 | 0.70 | 26,600 |

Table 10. -- Covariates retained in the a) adult Greenland turbot species distribution model (SDM) final ensembles, the percent contribution to the ensemble deviance explained by each, and the cumulative percent deviance: SD = standard deviation, and BPI = bathymetric position index.

| **Greenland turbot** | **Covariate** | **% Contribution** | **Cumulative % Contribution** |
|---|---|---|---|
| **a) adult** | bottom depth | 50.1 | 50.1 |
| | bottom temperature | 11.9 | 62.0 |
| | position | 10.9 | 72.9 |
| | current | 5.9 | 78.8 |
| | BPI | 5.6 | 84.4 |
| | current SD | 5.3 | 89.7 |
| | aspect east | 3.9 | 93.6 |
| | tidal maximum | 3.3 | 96.9 |
| | aspect north | 1.9 | 98.8 |
| | slope | 0.7 | 99.5 |
| | sponge presence | 0.3 | 99.8 |
| | pennatulacean presence | 0.1 | 99.9 |
| | coral presence | 0.1 | 100 |

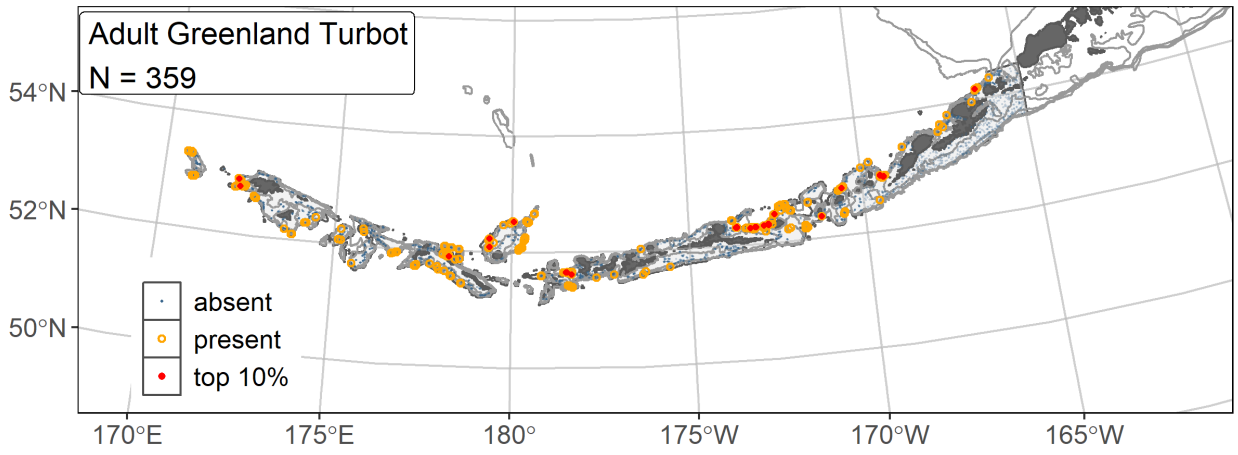


Figure 24. -- Distribution of adult Greenland turbot catches (N = 359) in 1991–2019 AFSC RACE-GAP summer bottom trawl surveys of the AI with the 100 m, 300 m, and 500 m isobaths indicated; filled red circles indicate locations in top 10% of overall abundance, open orange circles indicate presence in remaining catches, and small blue dots indicate absence.

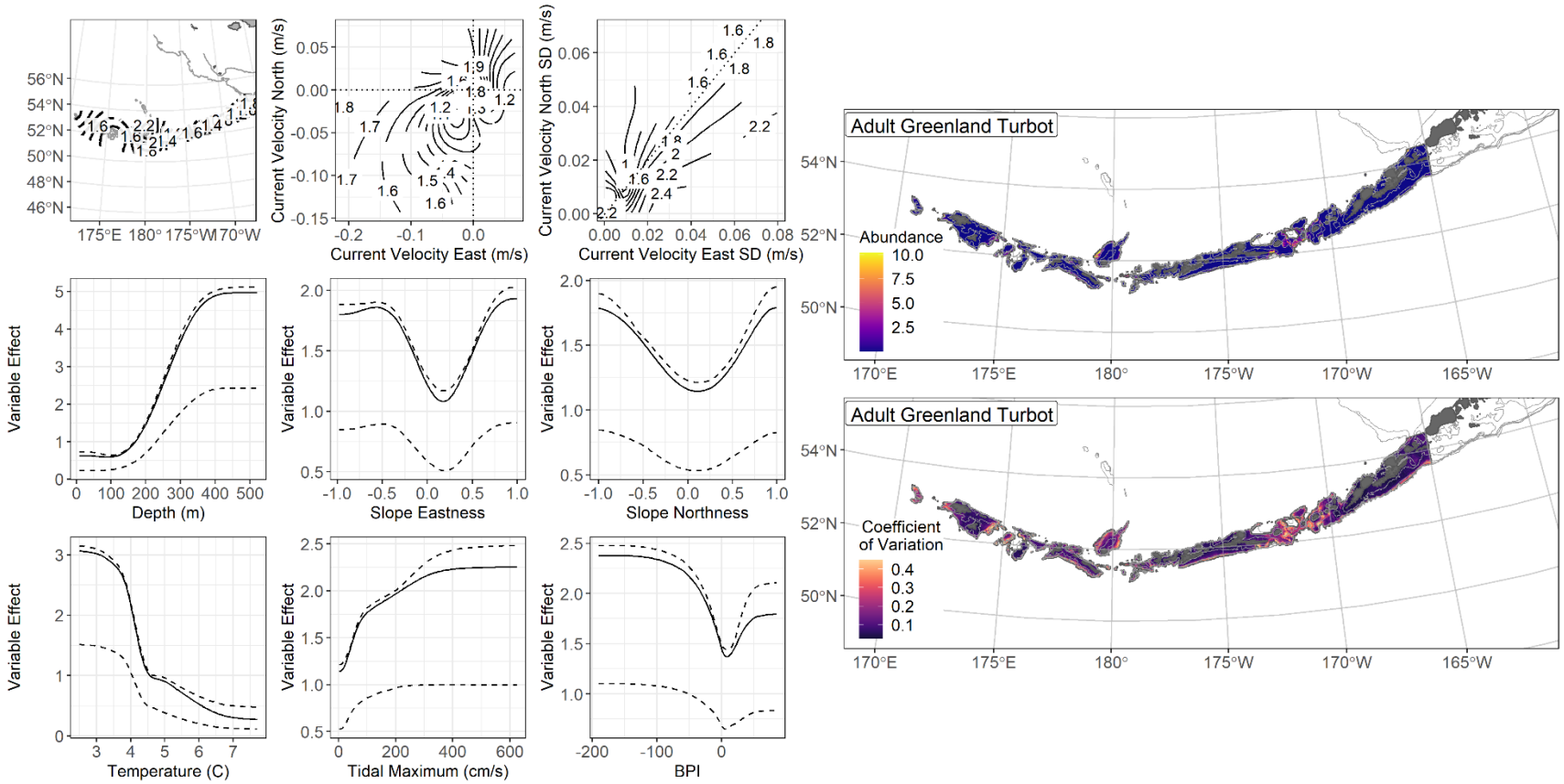


Figure 25. -- The top nine covariate effects (left panel) on ensemble-predicted adult Greenland turbot numerical abundance across the AI (upper right panel) alongside the coefficient of variation of the ensemble predictions (lower right panel).

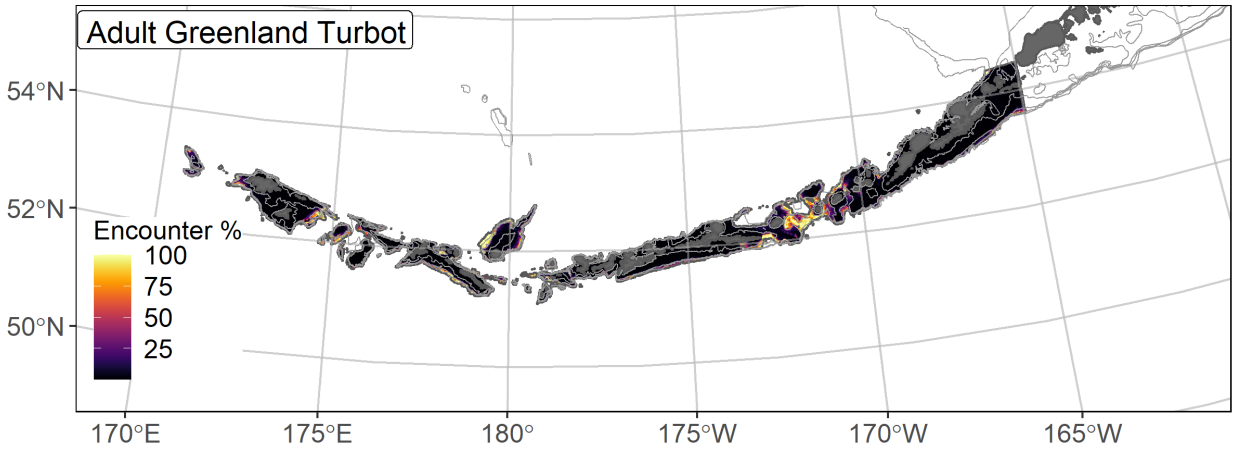


Figure 26. -- Encounter probability of adult Greenland turbot from AFSC RACE-GAP summer bottom trawl surveys (1991–2019) of the AI with the 100 m, 300 m, and 500 m isobaths indicated.

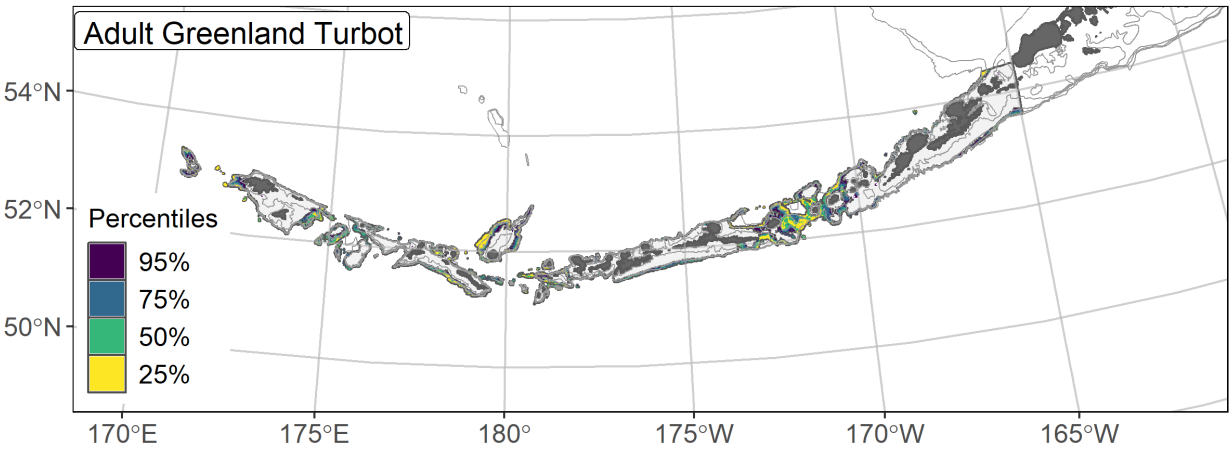


Figure 27. -- Essential fish habitat (EFH area) defined as the top 95% of numerical abundance predictions from a habitat-based ensemble fitted to adult Greenland turbot distribution and abundance in AFSC RACE-GAP summer bottom trawl surveys (1991–2019) with 100 m, 300 m, and 500 m isobaths indicated; internal to the EFH map are the subareas of the top 25% (EFH hot spots), top 50% (core EFH area), and top 75% (principal EFH area) of habitat related, ensemble-predicted numerical abundance.

**Kamchatka flounder (*Atheresthes evermani*)**

Kamchatka flounder (*Atheresthes evermani*) is large-bodied flatfish found from the Sea of Okhotsk through the Bering Sea and into the western GOA (Zimmermann and Goddard 1996). In U.S. waters, they occur in high concentrations in the western AI and in lower concentrations east of there (Bryan et al. 2020b). The species is morphologically similar to the more common arrowtooth flounder (*A. stomias*), and the two species were not routinely distinguished in assessment surveys until 1992 (Bryan et al. 2018). The majority of Kamchatka flounder become sexually mature at a relatively large size ($L_{50}$ = 550 mm FL; Stark 2012b) and can eventually grow to be 860 mm FL or more (Mecklenburg et al. 2005). Given its large size and predatory habits, this species is thought to be an important part of the marine food web and is a major predator of juvenile walleye pollock (*Gadus chalcogrammus*; Yang and Livingston 1986). This species was managed as a stock complex with arrowtooth flounder until 2011 when the start of a directed fishery for Kamchatka flounder prompted the development of separate management plans (Bryan et al. 2020b).

**Subadult Kamchatka flounder distribution and predicted abundance from RACE-GAP summer bottom trawl surveys in the Aleutian Islands –** Subadult Kamchatka flounder catches were very common throughout the RACE-GAP summer survey areas (Fig. 28), though they were less common in the eastern AI. The final ensemble contains four SDMs with the hGAM and $GAM_P$ given more weight than the others, and it demonstrated good performance across all three fit metrics (Table 11). As such, it is expected to make accurate predictions of both presence (AUC = 0.81) and abundance ($\rho$ = 0.58; PDE = 0.51). Geographic position and bottom current were the most important covariates, but bottom depth, current variability, and terrain aspect were also important (Table 12). In general, high abundance was predicted for areas farther west, with

northerly currents, and with bottom depths between 150 and 300 m (Fig. 29). Subadult Kamchatka flounder also tend to be associated with north-facing slopes. The highest densities of this life stage occurred north of Atka and Adak islands, as well as around Agattu Island (Fig. 29). Subadults showed a preference for areas on the northern side of the islands and seemed to occupy habitats where the 100 m depth contour runs close to the shore. The CV of abundance was homogenous throughout the region (Fig. 29). Predicted encounter probabilities were high in most places west of 170° W, with the exception of some shallow areas (Fig. 30).

**Adult Kamchatka flounder distribution and predicted abundance from RACE-GAP summer bottom trawl surveys in the Aleutian Islands –** Adult Kamchatka flounder in the RACE-GAP summer survey were less common than subadults, with low catches in the eastern AI (Fig. 31). The final ensemble included four SDMs with the hGAM given the most weight, and it showed good to excellent performance overall (Table 11). The ensemble demonstrated good ability to predict high-density catches ($\rho = 0.54$) but scored even better in terms of predicting presence (AUC = 0.90) and deviance explained (PDE = 0.75). Bottom depth was more important in the model for adults than for subadults and accounted for 29.7% of the total deviance explained (Table 12). Geographic position, bottom current covariates, and terrain aspect were also important to SDM predictions. High abundance was associated with increasing bottom depth, western longitudes, southerly currents, and north-facing terrain (Fig. 32). The predicted abundance map for adults was much different from the map for subadults; adults were predicted to appear in high numbers around the deep passes in the island chain, including Seguam Island, and to the east and west of the Rat Islands (Fig. 32). The majority of adult abundance was predicted to occur at depths greater than 300 m, which may indicate that some of this life stage's habitat is outside the survey area. The predicted CV of abundance was

consistently low in shallow water, where adults are usually absent, and higher in deeper water (Fig. 32). Encounter probabilities displayed the same pattern and were close to zero at most depths of less than 300 m, and 100% at depths greater than 300 m (Fig. 33).

**Essential fish habitat of subadult and adult Kamchatka flounder in the Aleutian Islands –** The habitat-related abundance predictions based on RACE-GAP summer bottom trawl data (1992–2019) were translated into EFH area and subareas (Fig. 34). Subadult Kamchatka flounder were twice as common in the trawl survey as adults, and had a larger overall EFH area. Subadult EFH hot spots occurred around Atka Island and the area between Attu and Agattu islands, as well as Petrel Bank. The eastern part of the survey area around Unalaska Island and Unimak Pass had some areas of EFH, but with lower predicted abundance. For adults, EFH hot spots are in the deep passes that cut through the AI such as Seguam Pass and Buldir Strait. Other areas of EFH occur along the edge of the continental slope. Most shallow areas, particularly in the eastern AI, do not qualify as EFH.

Table 11. -- Constituent species distribution models (SDMs) used to construct Essential Fish Habitat (EFH) for a) subadult and b) adult Kamchatka flounder: MaxEnt = Maximum entropy; paGAM = presence-absence generalized additive model; hGAM = hurdle GAM; $GAM_P$ = standard Poisson GAM; and $GAM_{nb}$ = standard negative-binomial GAM. Ensemble performance ($\rho$ = Spearman's rank correlation coefficient), root-mean-square-error (RMSE), the area under the receiver operating characteristic (AUC), and the Poisson deviance explained (PDE) were generated from k-fold cross-validation. The "--" in a field indicates that this SDM was not included in the final ensemble.

**a) subadult Kamchatka flounder**

| Models | RMSE | Relative weight | ρ | AUC | PDE | EFH area ($km^2$) |
|---|---|---|---|---|---|---|
| MaxEnt | 41.3 | 0.10 | 0.55 | 0.82 | 0.21 | 71,000 |
| paGAM | 26.7 | 0.24 | 0.58 | 0.81 | 0.28 | 77,700 |
| hGAM | 23.2 | 0.32 | 0.52 | 0.81 | 0.44 | 76,900 |
| $GAM_P$ | 22.9 | 0.33 | 0.50 | 0.76 | 0.45 | 76,400 |
| $GAM_{nb}$ | 30.1 | 0 | 0.57 | 0.80 | 0.35 | -- |
| ensemble | 22.6 | 1 | 0.58 | 0.81 | 0.51 | 77,600 |

**b) adult Kamchatka flounder**

| Models | RMSE | Relative weight | ρ | AUC | PDE | EFH area ($km^2$) |
|---|---|---|---|---|---|---|
| MaxEnt | 31.9 | 0.14 | 0.54 | 0.90 | 0.41 | 43,500 |
| paGAM | 25.2 | 0.23 | 0.55 | 0.90 | 0.46 | 65,100 |
| hGAM | 21.3 | 0.32 | 0.51 | 0.90 | 0.65 | 41,400 |
| $GAM_P$ | 22.3 | 0.30 | 0.47 | 0.84 | 0.65 | 30,600 |
| $GAM_{nb}$ | 24.5 | 0 | 0.53 | 0.89 | 0.57 | -- |
| ensemble | 19.4 | 1 | 0.54 | 0.90 | 0.75 | 51,800 |

Table 12. -- Covariates retained in the a) subadult and b) adult Kamchatka flounder species distribution model (SDM) final ensembles, the percent contribution to the ensemble deviance explained by each, and the cumulative percent deviance: SD = standard deviation, and BPI = bathymetric position index.

| Kamchatka flounder | Covariate | % Contribution | Cumulative % Contribution |
|---|---|---|---|
| **a) subadult** | current | 22.6 | 22.6 |
| | position | 18.5 | 41.1 |
| | current SD | 12.2 | 53.3 |
| | bottom depth | 12.0 | 65.3 |
| | aspect north | 9.9 | 75.2 |
| | tidal maximum | 8.1 | 83.3 |
| | BPI | 5.5 | 88.8 |
| | slope | 3.5 | 92.3 |
| | rockiness | 2.4 | 94.7 |
| | bottom temperature | 1.7 | 96.4 |
| | coral presence | 1.3 | 97.7 |
| | aspect east | 1.2 | 98.9 |
| | curvature | 0.6 | 99.5 |
| | pennatulacean presence | 0.4 | 99.9 |
| | sponge presence | 0.1 | 100 |
| **a) adult** | bottom depth | 29.7 | 29.7 |
| | position | 13.6 | 43.3 |
| | current | 11.4 | 54.7 |
| | current SD | 8.4 | 63.1 |
| | aspect east | 6.6 | 69.7 |
| | aspect north | 5.2 | 74.9 |
| | tidal maximum | 5.0 | 79.8 |
| | coral presence | 4.0 | 83.8 |
| | curvature | 3.9 | 87.7 |
| | slope | 3.4 | 91.1 |
| | BPI | 3.2 | 94.3 |
| | sponge presence | 1.6 | 95.9 |
| | bottom temperature | 1.5 | 97.4 |
| | rockiness | 1.4 | 98.8 |
| | pennatulacean presence | 1.2 | 100 |

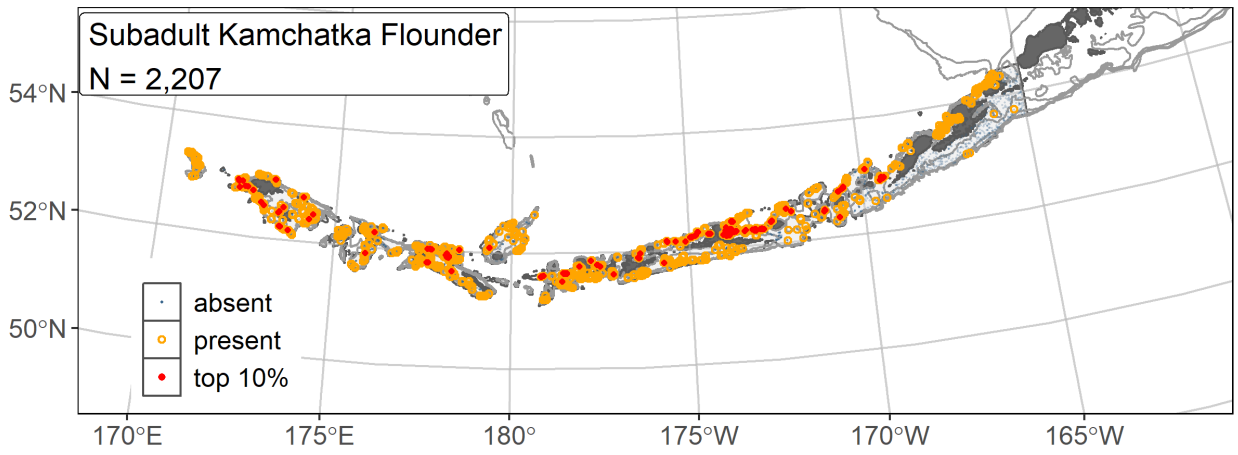


Figure 28. -- Distribution of subadult Kamchatka flounder catches (N = 2,245) in 1992–2019 AFSC RACE-GAP summer bottom trawl surveys of the AI with the 100 m, 300 m, and 500 m isobaths indicated; filled red circles indicate locations in top 10% of overall abundance, open orange circles indicate presence in remaining catches, and small blue dots indicate absence.

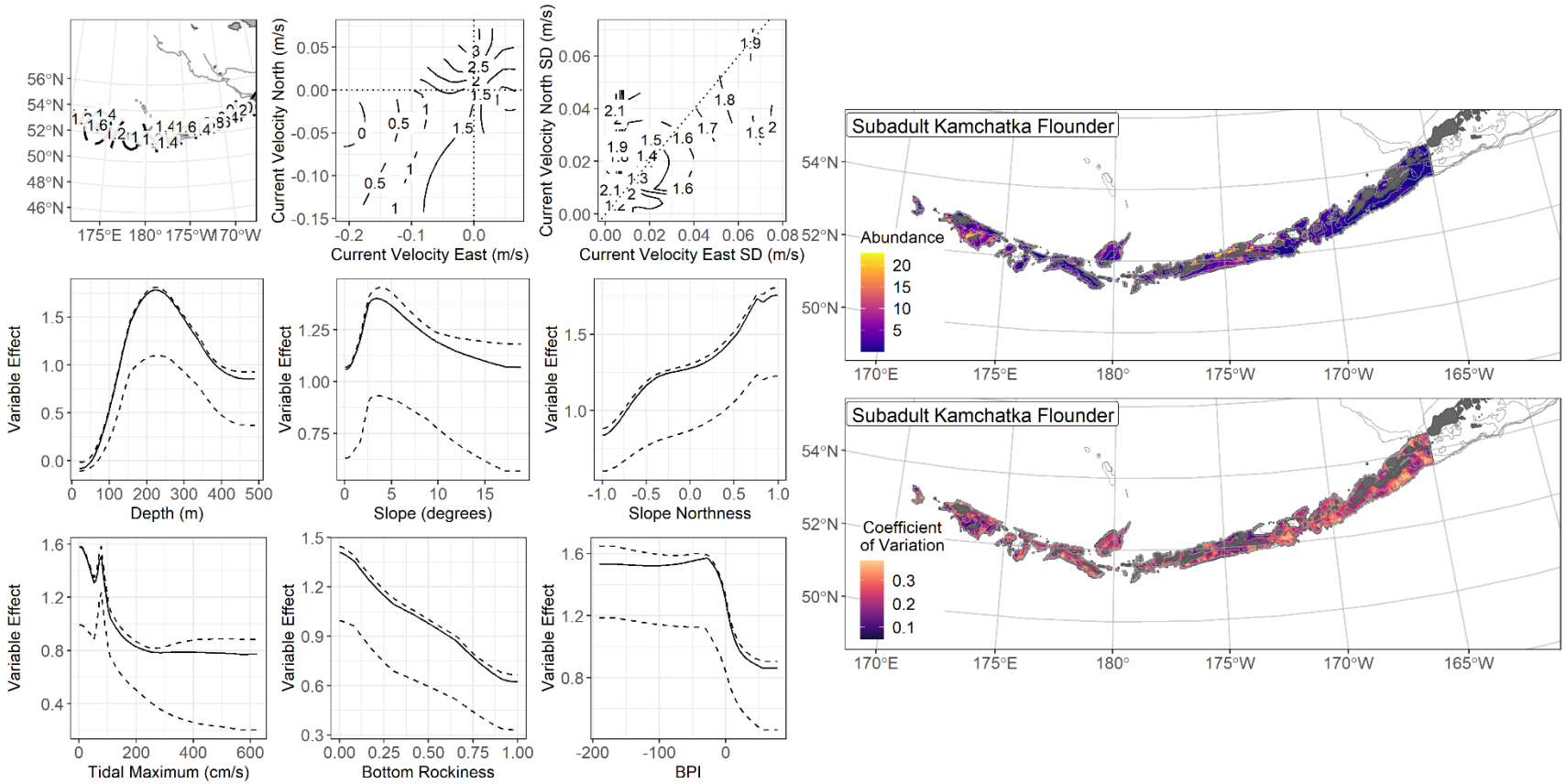


Figure 29. -- The top nine covariate effects (left panel) on ensemble-predicted subadult Kamchatka flounder numerical abundance across the AI (upper right panel) alongside the coefficient of variation of the ensemble predictions (lower right panel).

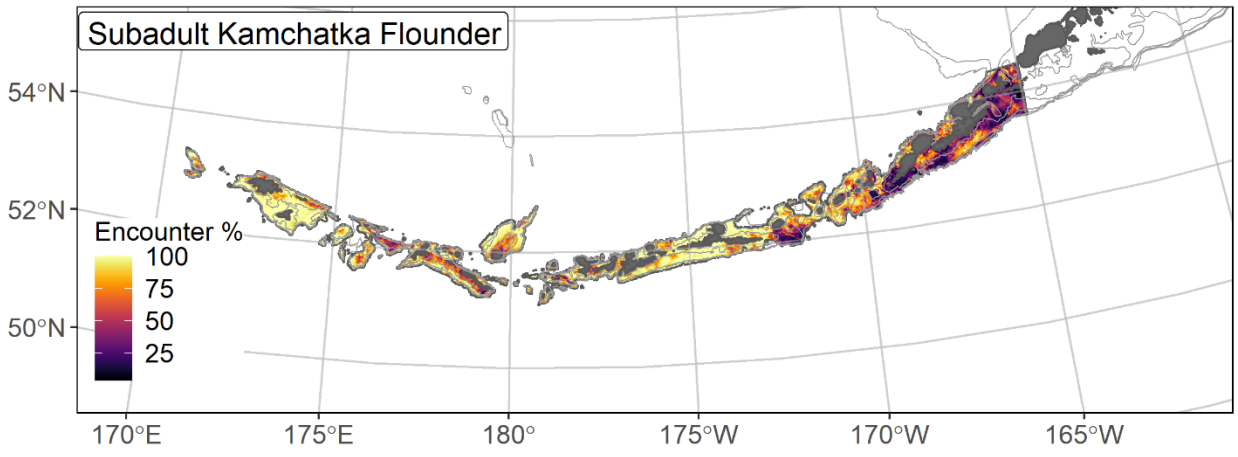


Figure 30. -- Encounter probability of subadult Kamchatka flounder from AFSC RACE-GAP summer bottom trawl surveys (1992–2019) of the AI with the 100 m, 300 m, and 500 m isobaths indicated.

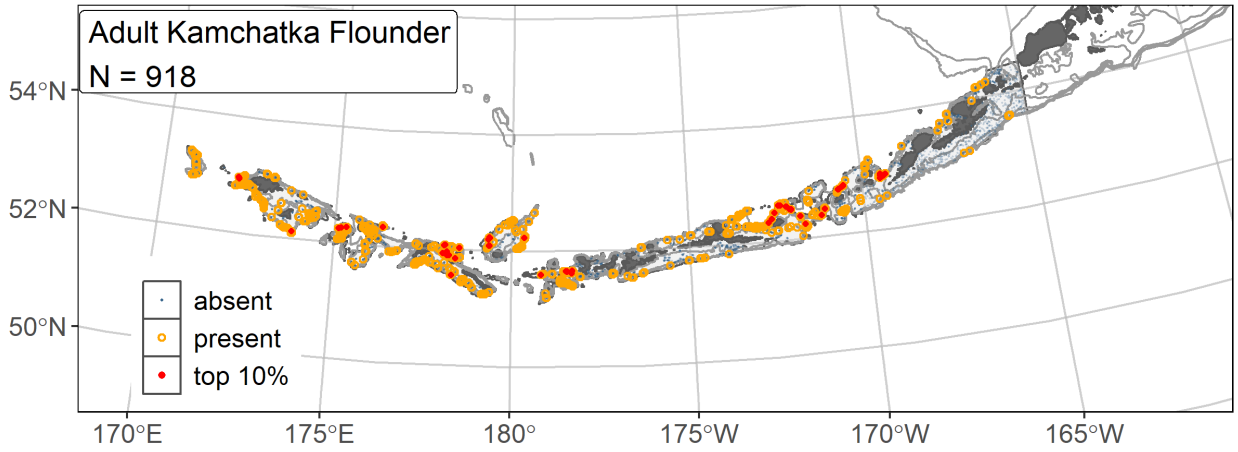


Figure 31. -- Distribution of adult Kamchatka flounder catches (N = 941) in 1992–2019 AFSC RACE-GAP summer bottom trawl surveys of the AI with the 100 m, 300 m, and 500 m isobaths indicated; filled red circles indicate locations in top 10% of overall abundance, open orange circles indicate presence in remaining catches, and small blue dots indicate absence.

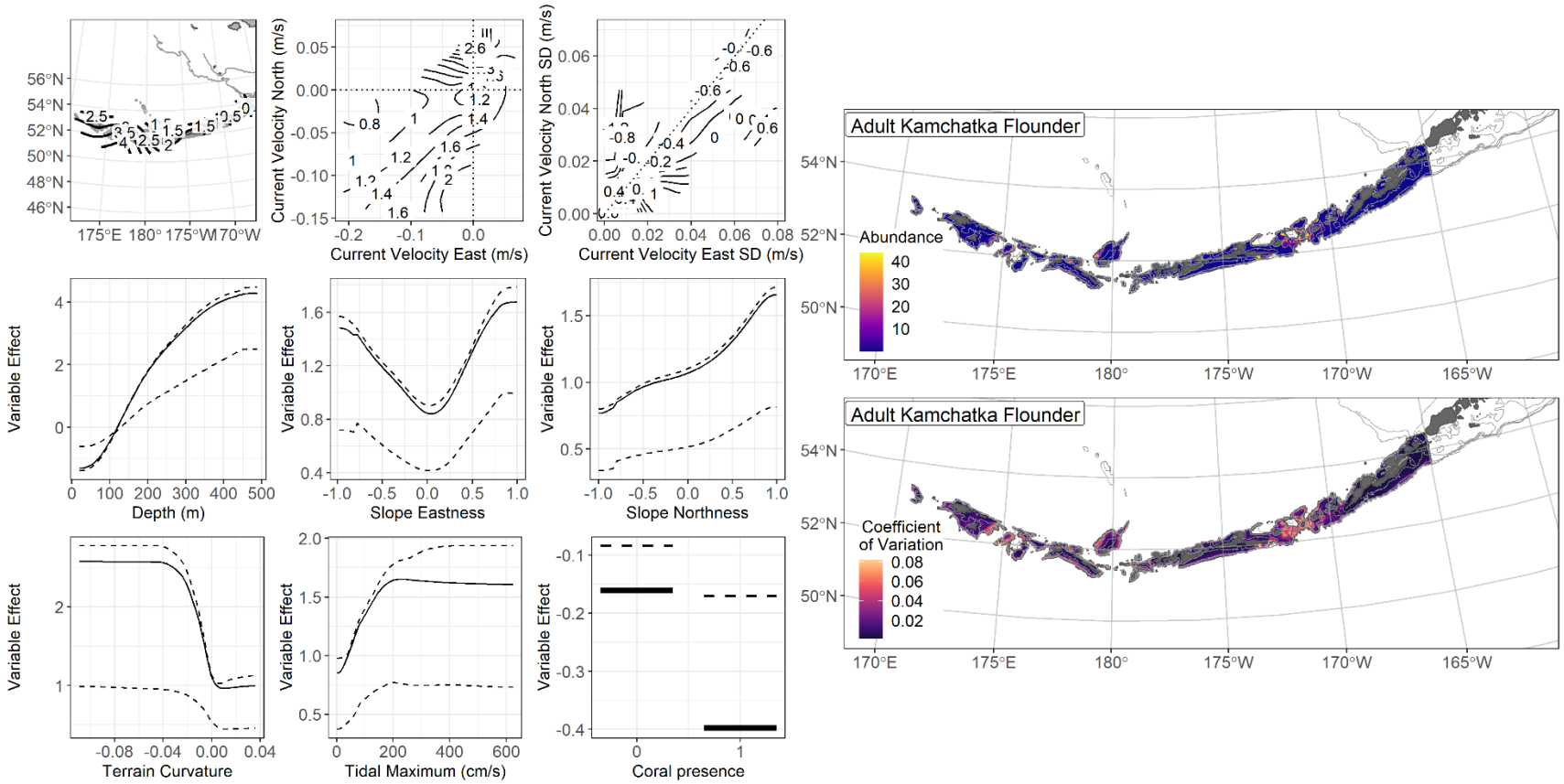


Figure 32. -- The top nine covariate effects (left panel) on ensemble-predicted adult Kamchatka flounder numerical abundance across the AI (upper right panel) alongside the coefficient of variation of the ensemble predictions (lower right panel).

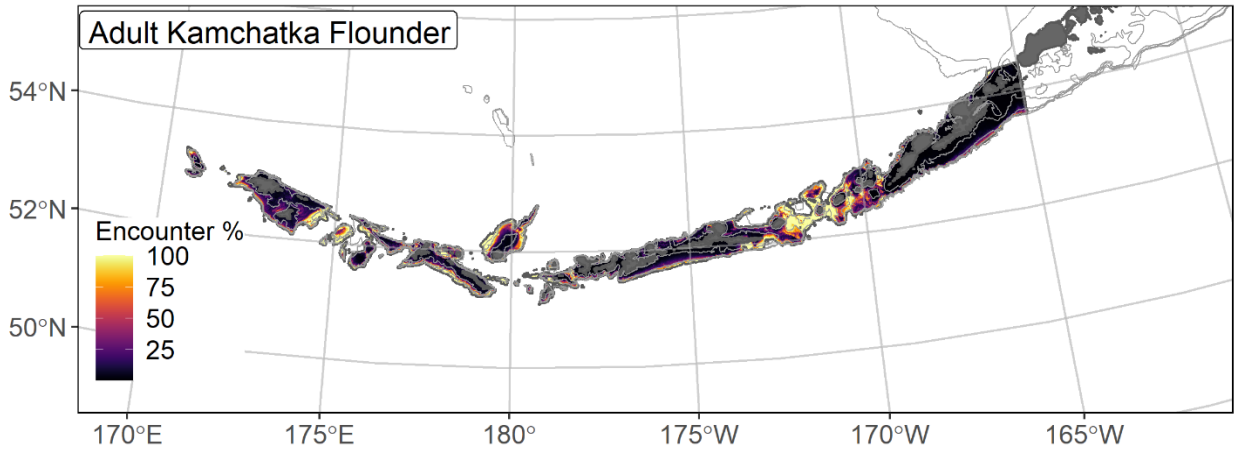


Figure 33. -- Encounter probability of adult Kamchatka flounder from AFSC RACE-GAP summer bottom trawl surveys (1992–2019) of the AI with the 100 m, 300 m, and 500 m isobaths indicated.

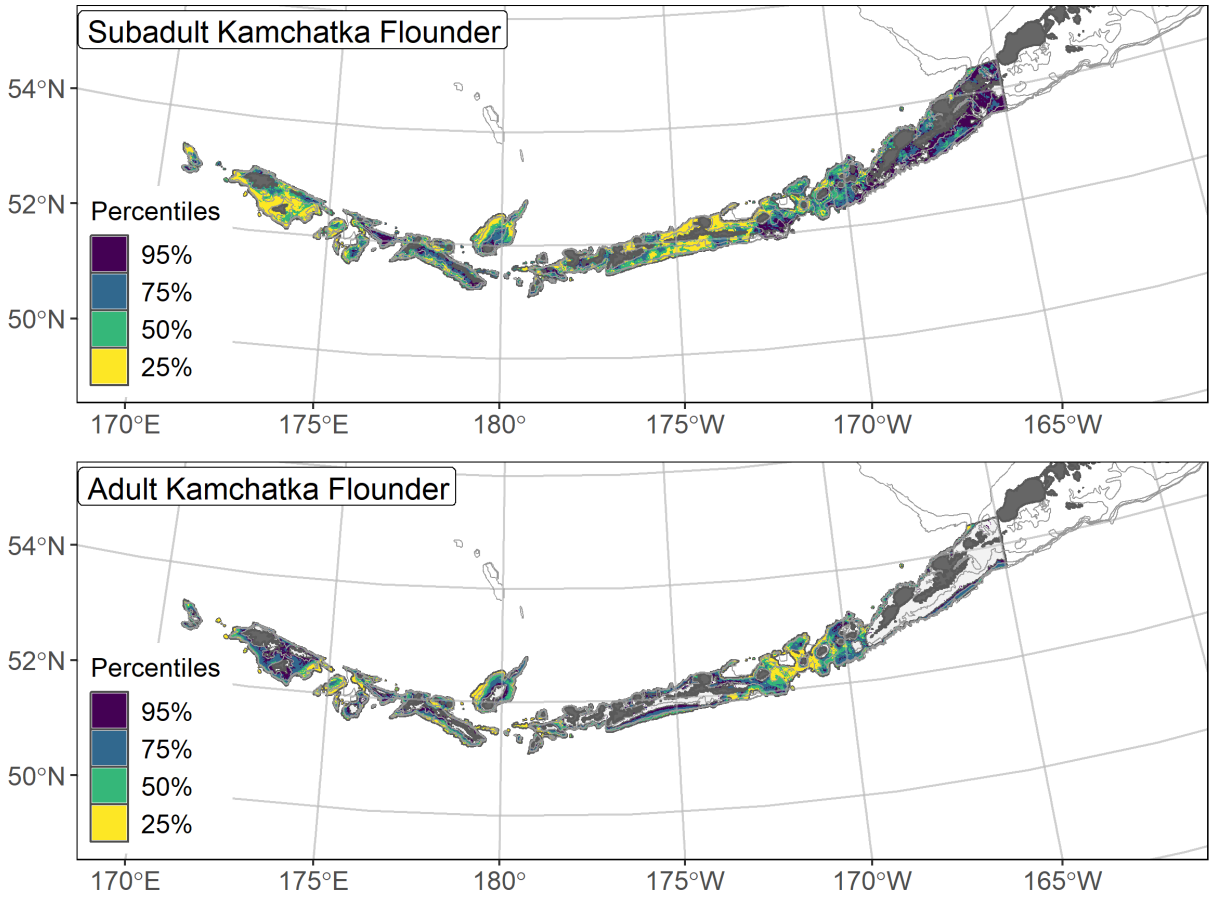


Figure 34. -- Essential fish habitat (EFH area) defined as the top 95% of numerical abundance predictions from a habitat-based ensemble fitted to subadult (top) and adult (bottom) Kamchatka flounder distribution and abundance in AFSC RACE-GAP summer bottom trawl surveys (1992–2019) with 100 m, 300 m, and 500 m isobaths indicated; internal to the EFH map are the subareas of the top 25% (EFH hot spots), top 50% (core EFH area), and top 75% (principal EFH area) of habitat related, ensemble-predicted numerical abundance.

**Northern rock sole (*Lepidopsetta polyxystra*)**

Northern rock sole (*Lepidopsetta polyxystra*) is present across the north Pacific, from Puget Sound in Washington State across the AI and Bering Sea to the Kuril Islands (Orr and Matarese 2000). The species is morphologically similar to sourthern rock sole (*L. bilineata*), and the two were not routinely distinguished in groundfish surveys until 1996. In the Bering Sea region, the vast majority of rock soles are *L. polyxystra*, though the species are often found together in the AI and GOA (Orr and Matarese 2000). Adults may grow to as much as 690 mm TL (Walters and Wilderbuer 2000). Similarly, northern rock sole in the BSAI reach maturity at a smaller size (309 mm TL) than in the GOA (328 mm TL) (Stark 2012a). Spawning begins in February and peaks in the early spring (Stark 2012a). Previous research has also defined the length interval between larval transformation at 80 mm (Doyle et al. 2019) and the transition to a sub-adult habitat at 140 mm (Yeung and Cooper 2020), so the settled early juvenile life stage is modeled here. Northern rock sole supports a valuable commercial fishery in the Bering Sea, where it is managed as a mixed stock alongside the relatively uncommon southern rock sole (McGilliard et al. 2020).

**Settled early juvenile northern rock sole distribution and predicted abundance from RACE-GAP summer bottom trawl surveys in the Aleutian Islands –** Settled early juvenile northern rock sole were relatively uncommon in the RACE-GAP summer survey of the AI compared to older life stages (Fig. 35). Within the survey area, settled early juvenile northern rock sole were distributed evenly across the AI. However, given the small size of this life stage, the gear employed during the survey may not adequately sample the population, and where

available, additional data sources should be considered[12]. The final ensemble contained four SDMs with equal weights, and it had a fair fit to the observed data (Table 13). Specifically, the ensemble performed well in predicting presence or absence (AUC = 0.89), and received a fair score in predicting high or low abundance catches ($\rho = 0.25$). The ensemble scored slightly better in terms of deviance explained (PDE = 0.38), which is not uncommon for stocks with few presences and low overall density. These metrics suggest that the ensemble can predict the areas where settled early juveniles are most likely to be caught but predicts abundance with a higher degree of uncertainty. Bottom depth was the most important covariate and accounted for 46.8% of the deviance explained by the ensemble; bottom current, terrain aspect, tidal maximum, and geographic position were also relatively important based on deviance explained (Table 14). In general, predicted abundance was high in shallow locations with southerly currents, northwest-facing terrain, and weak tides (Fig. 36). Settled early juvenile northern rock sole abundance was also weakly positively associated with the presence of structure forming invertebrates like sponges and corals. Predicted abundance was highest in shallow inshore areas, particularly near Attu Island in the west and Umnak Island in the east (Fig. 36), though still low (< 1) on average. The predicted CV of abundance was high in almost all shallow inshore areas, which reflects the fact that with such low predicted abundance, any variation is high relative to the mean (Fig. 36). Encounter probabilities for settled early juvenile northern rock sole were high near Attu and Umnak islands, moderate in shallow water, and close to zero beyond the 100 m depth contour (Fig. 37).

[12] A recommendation to add additional survey data types if possible to future SDM ensemble EFH mapping efforts for this species will be included as a future recommendation for research directions from the 2023 EFH 5-year review.

**Subadult northern rock sole distribution and predicted abundance from RACE-GAP summer bottom trawl surveys in the Aleutian Islands –** Subadult northern rock sole catches were very common across most of the RACE-GAP summer survey area (Fig. 38). They were present in especially high numbers in the western AI. The final ensemble contained four SDMs, with the MaxEnt given slightly less weight than the others. The ensemble demonstrated excellent predictive performance across all three metrics ρ = 0.73; AUC = 0.90; PDE = 0.62) (Table 13), indicating that this ensemble is expected to make accurate predictions. Bottom depth was the most important covariate and accounted for 55.6% of the deviance explained by the ensemble, though bottom currents and geographic position were also important (Table 14). Predicted abundance was highest in shallow locations, consistent south westerly currents, and locations farther west in the AI (Fig. 39). Predicted abundance of subadult northern rock sole was high in many places in the AI, particularly in the western parts, near Attu Island and the Rat Islands, and tended to be lower in the eastern AI (Fig. 39). The predicted CV of abundance tended to be highest in the eastern and central parts of the AI (Fig. 39). These places had lower average predicted abundance, but large catches of subadult northern rock sole still occurred on occasion. Subadult northern rock sole are very common in the AI, and the encounter probability is near 100% in nearly all areas shallower than 300 m, except for the area around Seguam Pass and the Islands of Four Mountains (Fig. 40).

**Adult northern rock sole distribution and predicted abundance from RACE-GAP summer bottom trawl surveys in the Aleutian Islands –** Adult northern rock sole catches were very common throughout the RACE-GAP summer survey area in the AI (Fig. 41). Large catches occurred across the entire AI area and were more frequent in the western parts of the island chain. The final ensemble included three SDMs, and the paGAM was weighted slightly less than

the hGAM or $GAM_P$ (Table 13). The predictions generated by the ensemble had a good to excellent fit to the data (Table 13). The ensemble performed excellently at predicting relatively high- or low-abundance catches ($\rho = 0.72$). It also showed a good fit in terms of AUC (0.88) and deviance explained (PDE = 0.47). The fact that $\rho$ was higher than PDE suggests that the ensemble can identify areas where larger catches are expected to occur, but it may not predict the exact abundance with the same accuracy. Similar to previous life stages, bottom depth, geographic position, current, and current variability were the most important covariates, and they accounted for a combined 74.3% of the deviance explained by the ensemble (Table 14). Adult northern rock sole were predicted to be abundant in shallow waters in the western AI and favor locations with low variability westerly bottom currents (Fig. 42). The predicted CV of abundance was relatively low in most places, and the greatest uncertainty in model predictions occurred in moderately shallow areas in the eastern AI (Fig. 42). Like subadults, adult northern rock sole had a 100% encounter probability in almost all areas shallower than 300 m, reflecting that they are common even outside the highest-abundance areas (Fig. 43).

**Essential fish habitat of settled early juvenile, subadult, and adult northern rock sole in the Aleutian Islands –** The habitat related abundance predictions based on RACE-GAP summer bottom trawl data (1996–2019) were translated into EFH area and subareas (Fig. 44). The EFH area for settled early juvenile northern rock sole is smaller than that of the other life stages. Settled early juveniles had hot spots located in the east near Umnak Island and in the west near Attu Island. However, the settled early juvenile SDMs were based on many fewer catch records and should be used conservatively. By contrast, data were plentiful for both adult and subadult life stages. These life stages have nearly identical EFH maps, and both seem to occupy nearly all

areas in the AI shallower than 300 m. Both life stages also had EFH hot spots concentrated in the central and western AI.

Table 13. -- Constituent species distribution models (SDMs) used to construct Essential Fish Habitat (EFH) for a) settled early juvenile, b) subadult, and c) adult northern rock sole: MaxEnt = Maximum entropy; paGAM = presence-absence generalized additive model; hGAM = hurdle GAM; $GAM_P$ = standard Poisson GAM; and $GAM_{nb}$ = standard negative-binomial GAM. Ensemble performance (ρ = Spearman's rank correlation coefficient), root-mean-square-error (RMSE), the area under the receiver operating characteristic (AUC), and the Poisson deviance explained (PDE) were generated from k-fold cross-validation. The "--" in a field indicates that this SDM was not included in the final ensemble.

**a) settled early juvenile northern rock sole**

| Models | RMSE | Relative Weight | ρ | AUC | PDE | EFH area ($km^2$) |
|---|---|---|---|---|---|---|
| MaxEnt | 0.59 | 0.25 | 0.23 | 0.85 | 0.27 | 31,000 |
| paGAM | 0.59 | 0.25 | 0.23 | 0.86 | 0.27 | 33,500 |
| hGAM | 0.60 | 0.25 | 0.23 | 0.87 | 0.25 | 32,700 |
| $GAM_P$ | 0.59 | 0.25 | 0.23 | 0.85 | 0.23 | 27,600 |
| $GAM_{nb}$ | 0.60 | 0 | 0.23 | 0.85 | 0.23 | -- |
| ensemble | 0.57 | 1 | 0.25 | 0.89 | 0.38 | 32,900 |

**b) subadult northern rock sole**

| Models | RMSE | Relative Weight | ρ | AUC | PDE | EFH area ($km^2$) |
|---|---|---|---|---|---|---|
| MaxEnt | 59.3 | 0.16 | 0.71 | 0.90 | 0.32 | 61,400 |
| paGAM | 46.7 | 0.25 | 0.72 | 0.91 | 0.50 | 74,300 |
| hGAM | 42.9 | 0.30 | 0.71 | 0.90 | 0.59 | 60,000 |
| $GAM_P$ | 43.1 | 0.29 | 0.70 | 0.88 | 0.59 | 59,100 |
| $GAM_{nb}$ | 50.8 | 0 | 0.73 | 0.91 | 0.53 | -- |
| ensemble | 42.3 | 1 | 0.73 | 0.90 | 0.62 | 69,500 |

**c) adult northern rock sole**

| Models | RMSE | Relative Weight | ρ | AUC | PDE | EFH area ($km^2$) |
|---|---|---|---|---|---|---|
| MaxEnt | -- | 0 | -- | -- | -- | -- |
| paGAM | 66.0 | 0.29 | 0.71 | 0.89 | 0.32 | 76,200 |
| hGAM | 59.5 | 0.36 | 0.69 | 0.89 | 0.44 | 71,900 |

| Models | RMSE | Relative Weight | ρ | AUC | PDE | EFH area (km$^2$) |
|---|---|---|---|---|---|---|
| $GAM_P$ | 60.1 | 0.35 | 0.67 | 0.86 | 0.42 | 74,000 |
| $GAM_{nb}$ | 66.3 | 0 | 0.71 | 0.88 | 0.38 | -- |
| ensemble | 58.8 | 1 | 0.72 | 0.88 | 0.47 | 74,700 |

Table 14. -- Covariates retained in the a) settled early juvenile, b) subadult, and c) adult northern rock sole species distribution model (SDM) final ensembles, the percent contribution to the ensemble deviance explained by each, and the cumulative percent deviance: SD = standard deviation, and BPI = bathymetric position index.

| **northern rock sole** | **Covariate** | **% Contribution** | **Cumulative % Contribution** |
|---|---|---|---|
| **a) settled early juvenile** | bottom depth | 46.8 | 46.8 |
| | position | 11.0 | 57.7 |
| | current | 10.3 | 68.0 |
| | aspect east | 5.5 | 73.5 |
| | tidal maximum | 5.4 | 78.9 |
| | aspect north | 3.9 | 82.8 |
| | BPI | 3.8 | 86.6 |
| | current SD | 3.4 | 90.0 |
| | coral presence | 3.3 | 93.3 |
| | sponge presence | 2.8 | 96.1 |
| | slope | 1.8 | 97.9 |
| | bottom temperature | 0.9 | 98.8 |
| | rockiness | 0.8 | 99.6 |
| | pennatulacean presence | 0.4 | 100 |
| | curvature | 0.0 | 100 |
| **b) subadult** | bottom depth | 55.6 | 55.6 |
| | position | 15.3 | 70.9 |
| | current | 7.6 | 78.5 |
| | current SD | 6.3 | 84.8 |
| | aspect north | 4.0 | 88.8 |
| | tidal maximum | 3.0 | 91.8 |
| | BPI | 1.5 | 93.3 |
| | slope | 1.4 | 94.7 |
| | aspect east | 1.4 | 96.1 |
| | curvature | 1.3 | 97.4 |
| | rockiness | 1.1 | 98.5 |
| | bottom temperature | 0.9 | 99.4 |
| | sponge presence | 0.3 | 99.7 |
| | coral presence | 0.2 | 99.9 |
| | pennatulacean presence | 0.1 | 100 |
| **c) adult** | bottom depth | 39.6 | 39.6 |
| | position | 25.1 | 64.8 |
| | current SD | 9.5 | 74.3 |
| | current | 6.5 | 80.7 |
| | aspect north | 5.4 | 86.1 |

| **northern rock sole** | **Covariate** | **% Contribution** | **Cumulative % Contribution** |
|---|---|---|---|
| | slope | 3.8 | 89.9 |
| | tidal maximum | 3.6 | 93.5 |
| | curvature | 1.9 | 95.4 |
| | aspect east | 1.1 | 96.5 |
| | coral presence | 1.1 | 97.6 |
| | rockiness | 1.0 | 98.6 |
| | BPI | 0.5 | 99.1 |
| | bottom temperature | 0.4 | 99.5 |
| | pennatulacean presence | 0.4 | 99.9 |
| | sponge presence | 0.1 | 100 |

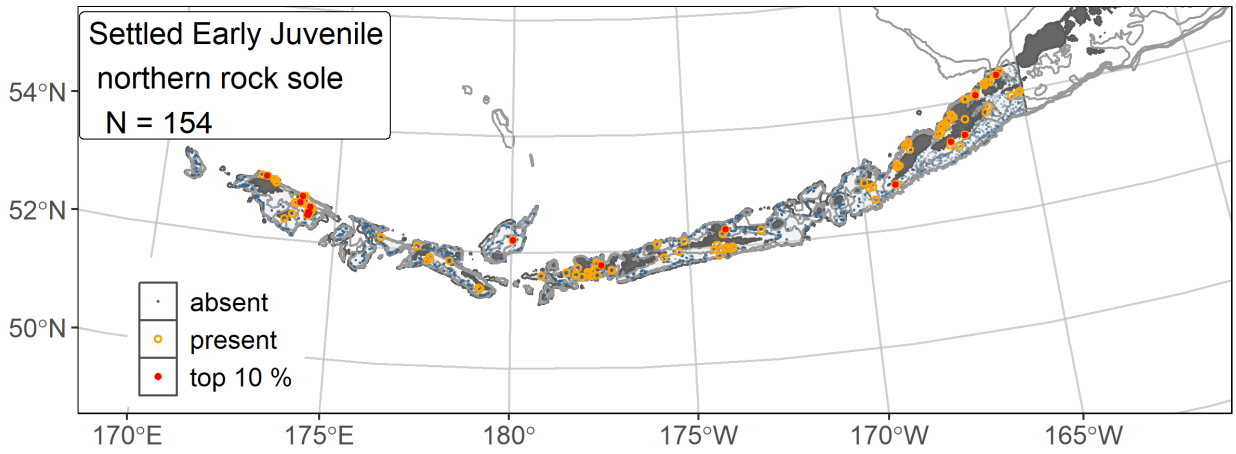


Figure 35. -- Distribution of settled early juvenile northern rock sole catches (N = 154) in 1996–2019 AFSC RACE-GAP summer bottom trawl surveys of the AI with the 100 m, 300 m, and 500 m isobaths indicated; filled red circles indicate locations in top 10% of overall abundance, open orange circles indicate presence in remaining catches, and small blue dots indicate absence.

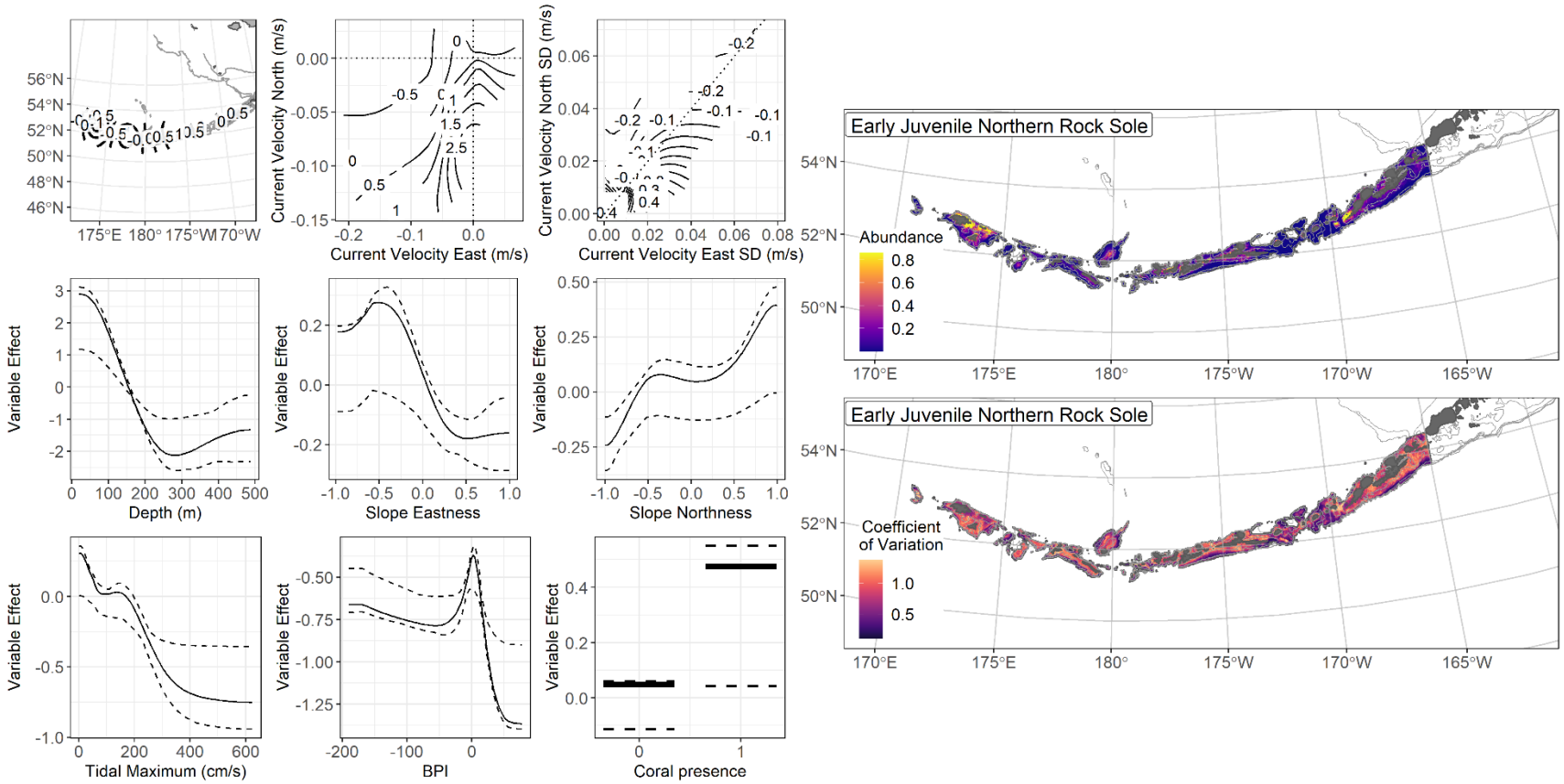


Figure 36. -- The top nine covariate effects (left panel) on ensemble-predicted settled early juvenile northern rock sole numerical abundance across the AI (upper right panel) alongside the coefficient of variation of the ensemble predictions (lower right panel).

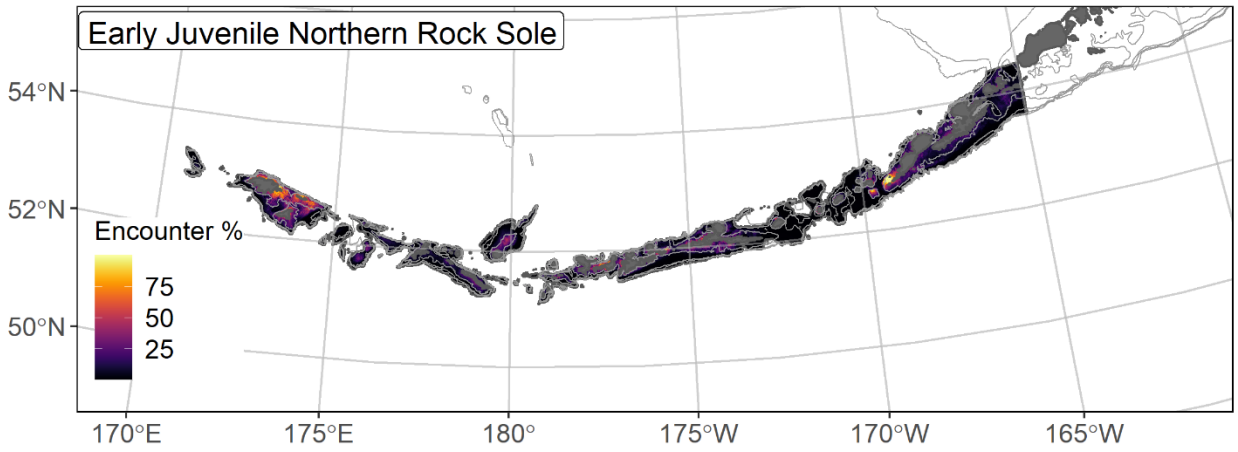


Figure 37. -- Encounter probability of settled early juvenile northern rock sole from AFSC RACE-GAP summer bottom trawl surveys (1996–2019) of the AI with the 100 m, 300 m, and 500 m isobaths indicated.

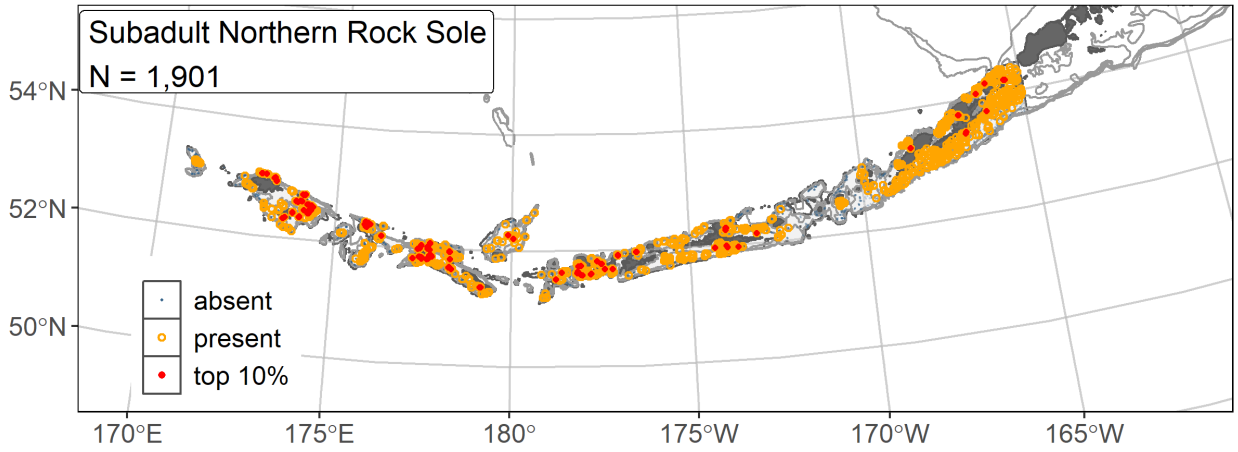


Figure 38. -- Distribution of subadult northern rock sole catches (N = 1,901) in 1996–2019 AFSC RACE-GAP summer bottom trawl surveys of the AI with the 100 m, 300 m, and 500 m isobaths indicated; filled red circles indicate locations in top 10% of overall abundance, open orange circles indicate presence in remaining catches, and small blue dots indicate absence.

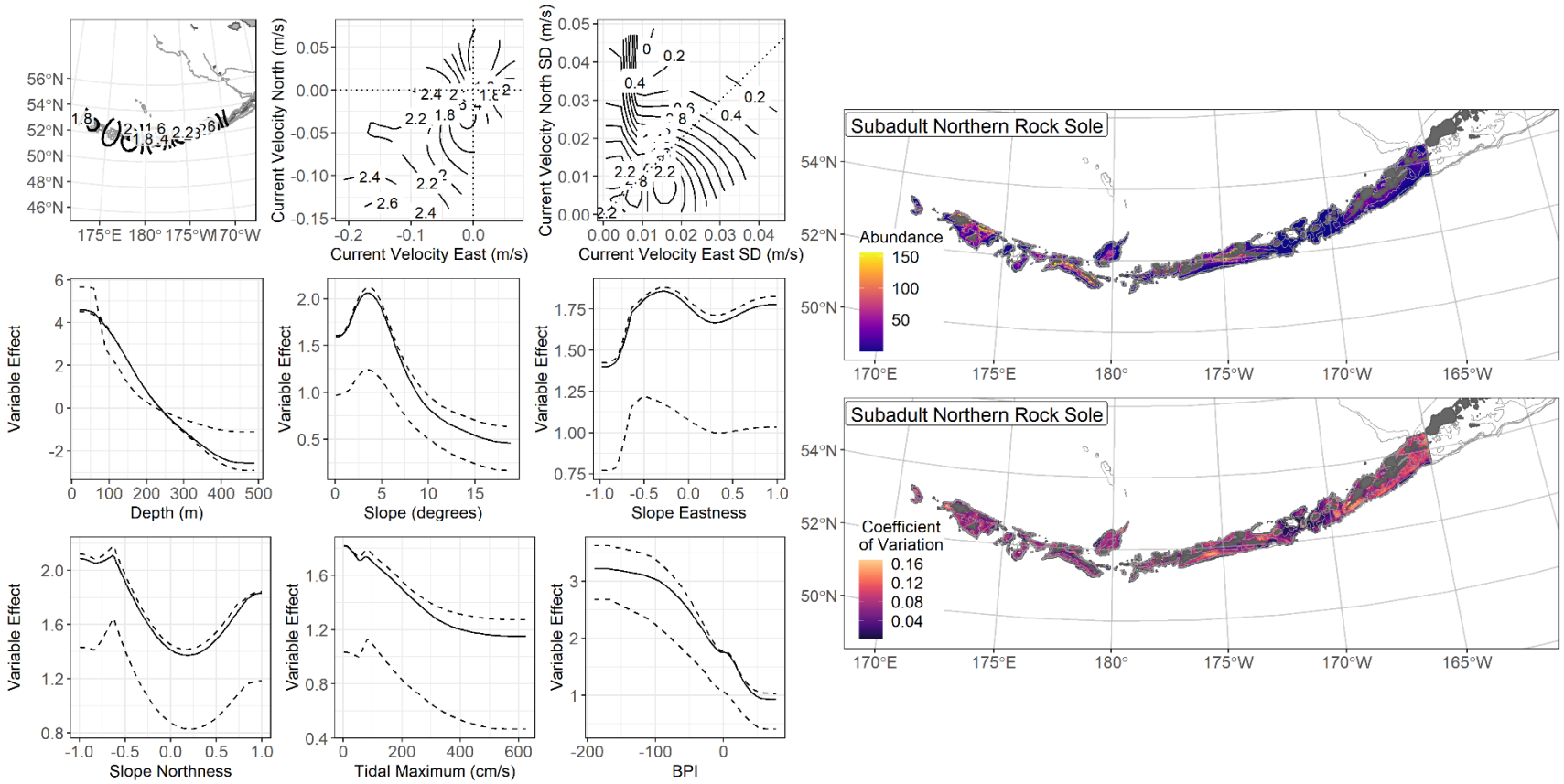


Figure 39. -- The top nine covariate effects (left panel) on ensemble-predicted subadult northern rock sole numerical abundance across the AI (upper right panel) alongside the coefficient of variation of the ensemble predictions (lower right panel).

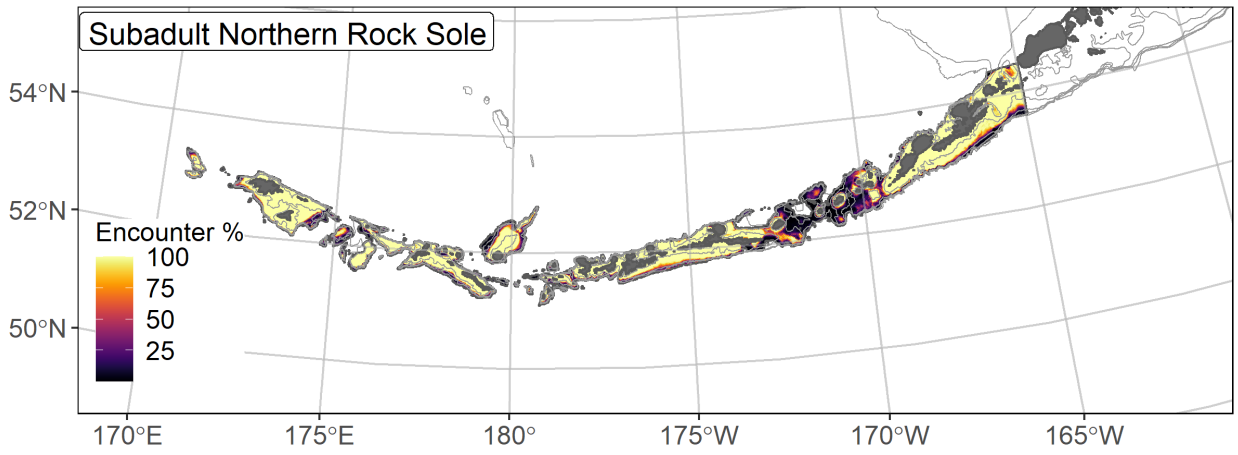


Figure 40. -- Encounter probability of subadult northern rock sole from AFSC RACE-GAP summer bottom trawl surveys (1996–2019) of the AI with the 100 m, 300 m, and 500 m isobaths indicated.

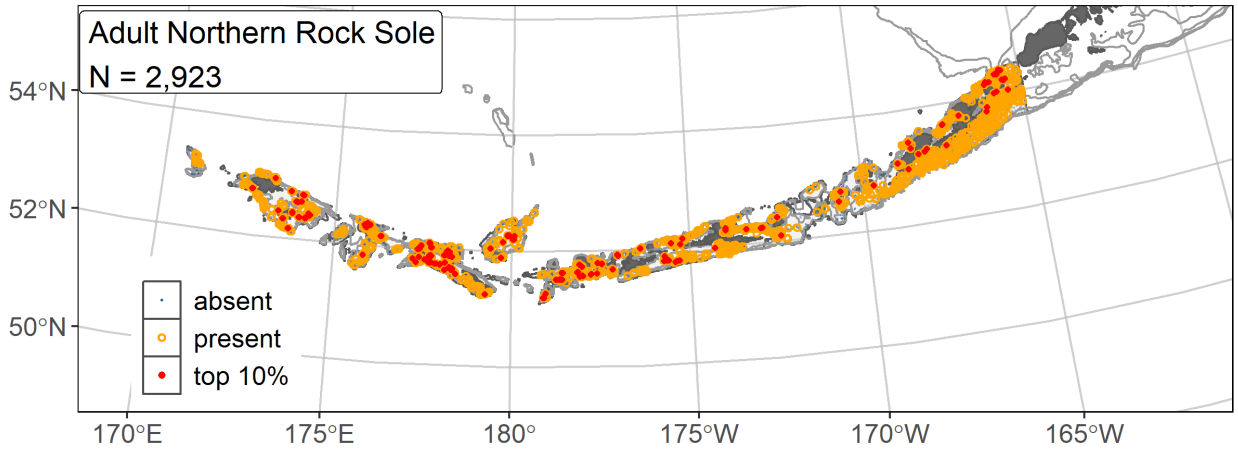


Figure 41. -- Distribution of adult northern rock sole catches (N = 2,928) in 1996–2019 AFSC RACE-GAP summer bottom trawl surveys of the AI with the 100 m, 300 m, and 500 m isobaths indicated; filled red circles indicate locations in top 10% of overall abundance, open orange circles indicate presence in remaining catches, and small blue dots indicate absence.

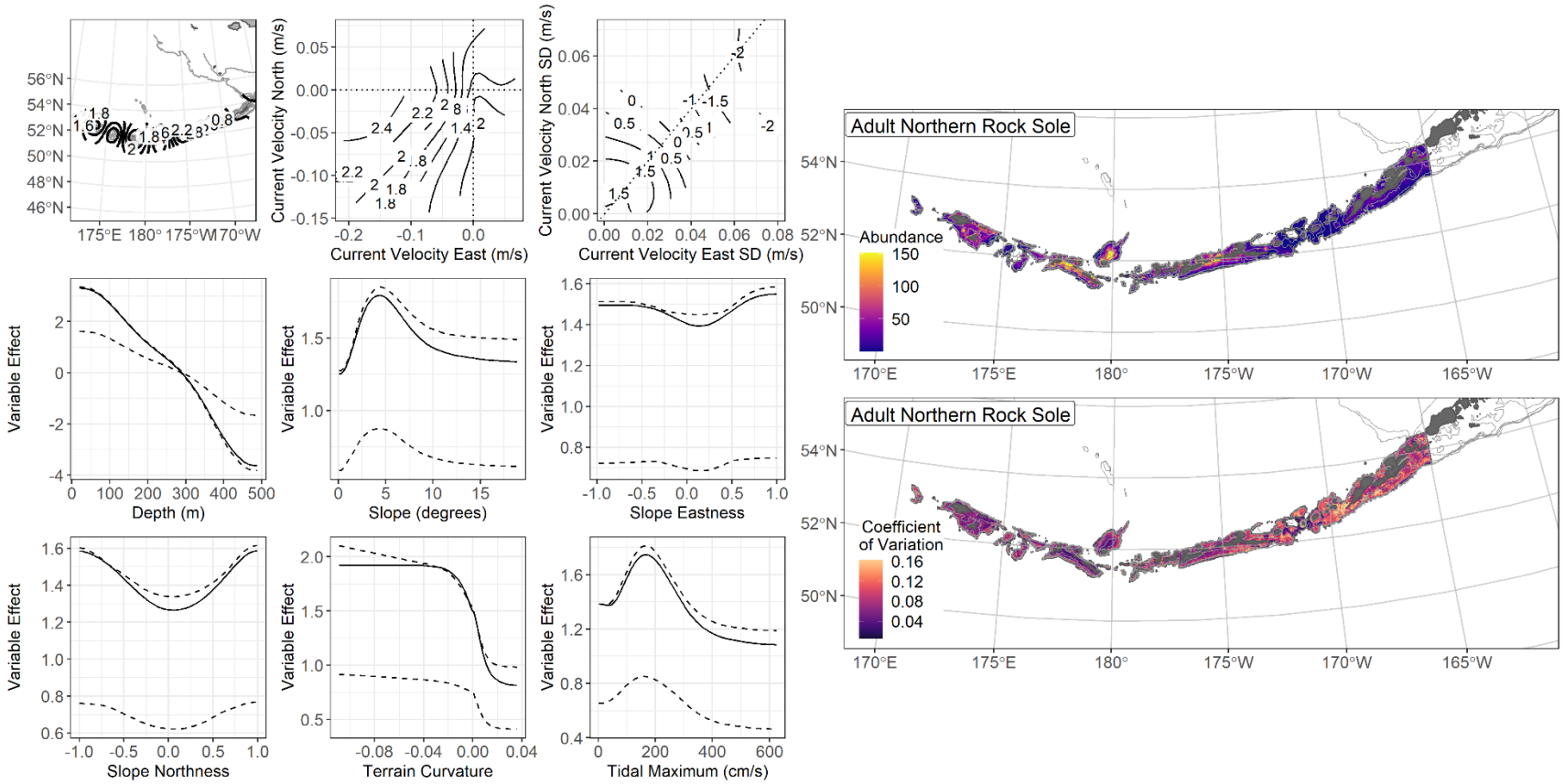


Figure 42. -- The top nine covariate effects (left panel) on ensemble-predicted adult northern rock sole numerical abundance across the AI (upper right panel) alongside the coefficient of variation of the ensemble predictions (lower right panel).

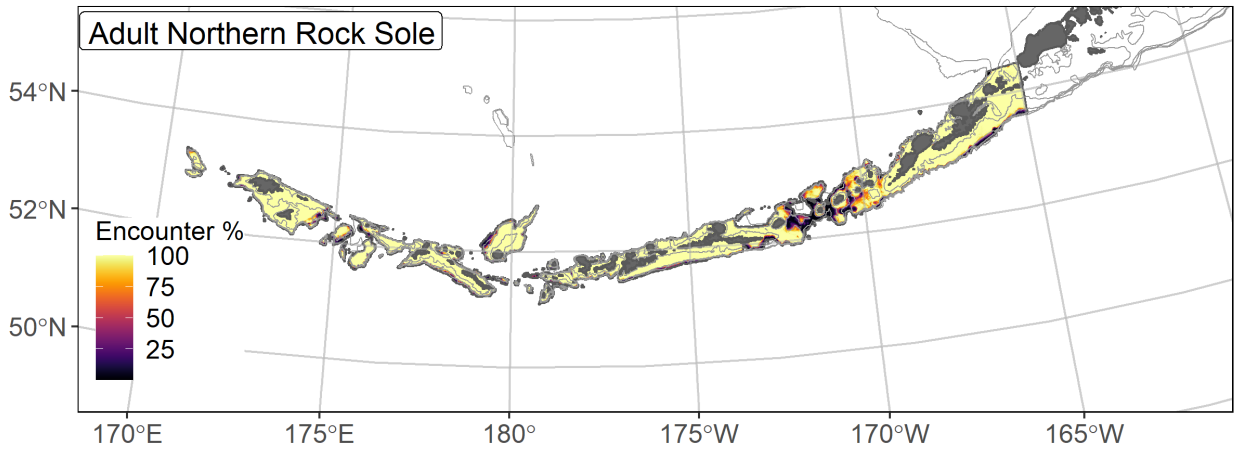


Figure 43. -- Encounter probability of adult northern rock sole from AFSC RACE-GAP summer bottom trawl surveys (1996–2019) of the AI with the 100 m, 300 m, and 500 m isobaths indicated.

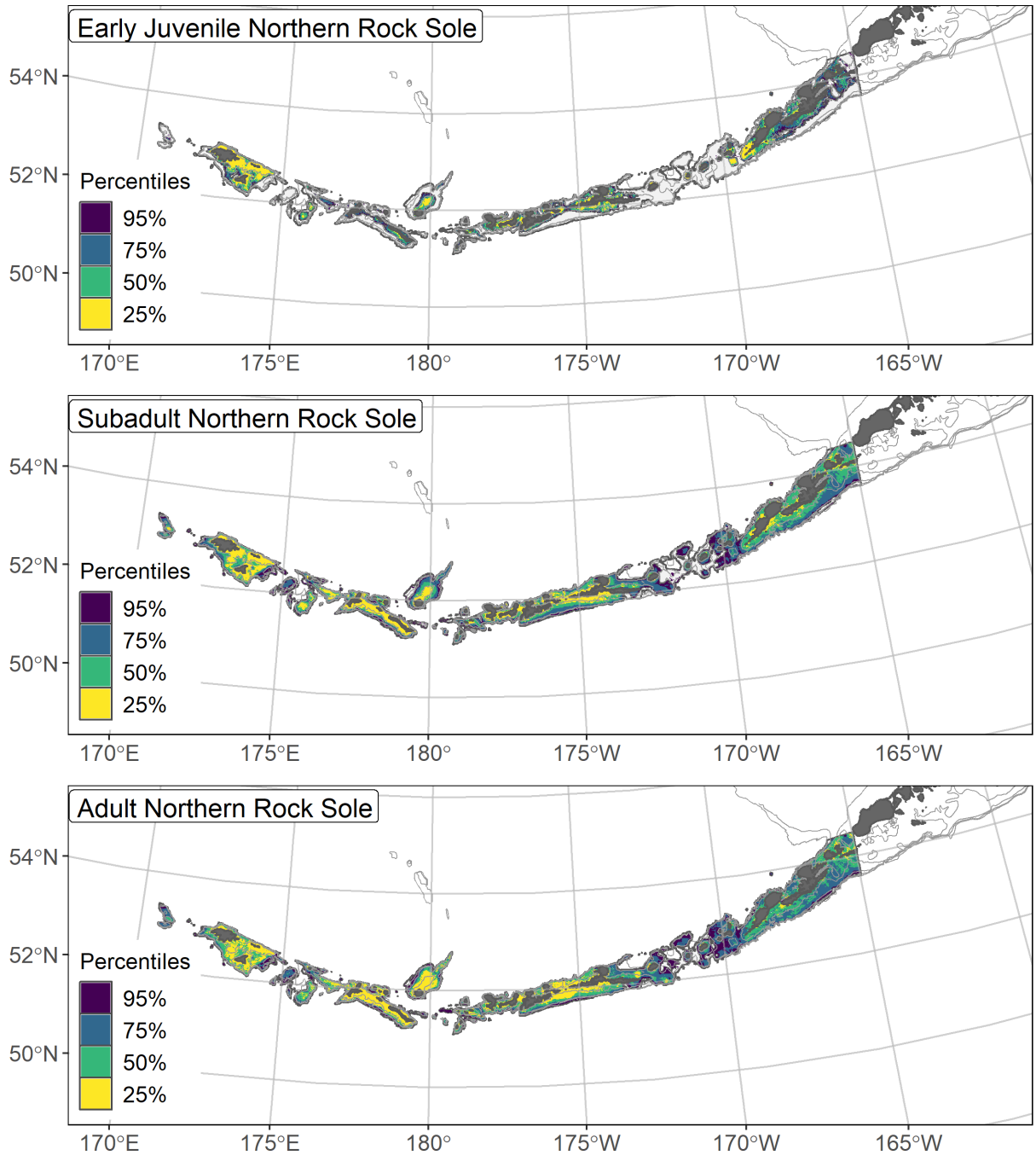


Figure 44. -- Essential fish habitat (EFH area) defined as the top 95% of numerical abundance predictions from a habitat-based ensemble fitted to settled early juvenile (top), subadult (middle), and adult (bottom) northern rock sole distribution and abundance in AFSC RACE-GAP summer bottom trawl surveys (1996–2019) with 100 m, 300 m, and 500 m isobaths indicated; internal to the EFH map are the subareas of the top 25% (EFH hot spots), top 50% (core EFH area), and top 75% (principal EFH area) of habitat-related, ensemble-predicted numerical abundance.

**Other Flatfish Stock Complex**

The Magnuson-Stevens Act mandates that EFH should be established at the lowest taxonomic level whenever possible. However, several species that lack the data necessary for a full age-structured assessment are managed as a single "other flatfish" stock complex of the BSAI region (Monnahan 2020). As a benefit to stock authors, this complex chapter includes sections for each individual species when sufficient data were available as well as a summary of the combined multi-species stock complex. Over a dozen species of flatfish are managed in this way, but only four were common enough in the RACE-GAP summer bottom trawl survey of the AI to enable the construction of an SDM: Dover sole (*Microstomus pacificus*), rex sole (*Glyptocephalus zachirus*), English sole (*Parophrys vetulus*), and southern rock sole (*Lepidopsetta bilineata*). English sole are included in the adult maps only, as there was insufficient data to construct a SDM for subadults. Rex sole is the most common species of this group in the AI, and it constitutes a majority of the "other flatfish" catch in terms of biomass. Because these species are typically managed together as a stock complex, this chapter summarizes the composite abundance, encounter probabilities, and EFH of these four species in the AI. Some caution should be used in interpreting species distribution predictions for this complex. Rex sole and southern rock sole are typically caught in the eastern AI and can appear in very high densities, whereas Dover sole is primarily caught in deeper water and farther west, and large catches are rare. The abundance and EFH maps for the complex tend to be most representative of the more numerous species' distributions.

**Subadult "Other Flatfish" Stock Complex abundance and distribution predicted from RACE-GAP summer bottom trawl surveys in the Bering Sea –** Numerical abundance predictions for Dover sole, rex sole, and southern rock sole were combined to estimate the distribution and EFH of subadults in the "other flatfish" stock complex in the AI (Fig. 45). The composite abundance map was strongly influenced by rex sole and southern rock sole, and shows high numbers of flatfish in the eastern AI and around Unalaska Island. Dover sole abundance is low relative to the other species and thus is not well represented by the EFH map. The wider distribution of all four species is more apparent in the encounter probabilities map (Fig. 45). High encounter probabilities in the eastern half of the AI are primarily due to a combination of southern rock sole and rex sole. Southern rock sole are rare west of 180°, and high-probability areas around Attu Island and Petrel Bank reflect the presence of rex sole and Dover sole. The primary EFH hot spot for subadults in the whole stock complex is in the eastern AI. Except for some deeper habitats, most of the survey area qualifies as EFH; however, this is mostly due to rex sole, which is very common throughout the region.

**Adult "Other Flatfish" Stock Complex abundance and distribution predicted from RACE-GAP summer bottom trawl surveys in the Bering Sea –** Numerical abundance predictions for adult Dover sole, rex sole, English sole and southern rock sole were combined to estimate the distribution and EFH of the "other flatfish" stock complex in the AI (Fig. 46). The abundance map for adults was very similar to that of subadults. The areas of high abundance were located in the eastern AI around Unalaska Island. Areas of high abundance close to shore consisted mostly of southern rock sole, which remain in shallow water even as adults, whereas the areas closer to the continental slope were primarily composed of rex sole, which move into deeper habitats as adults. Dover sole had a limited impact on estimated distribution of the 'other flatfishes'

complex, as they were caught less frequently and in lower numbers than the other species in the complex. The encounter probability map followed most of the same patterns. In the eastern AI, high probabilities close to shore reflected the presence of southern rock sole, and those offshore reflect the presence of rex sole. English sole overlapped with sourthern rock sole in the eastern AI, but its numbers were relatively small and did not have a strong impact on the overall map. However, southern rock sole are not present in the western AI, and many nearshore areas show a lower encounter probability. As with subadults, a large EFH hot spot for adults was located in the eastern AI, representing the area of high density of southern rock sole and rex sole. In the west, most EFH for the stock complex occurred at greater depths and mirrored the distribution of rex sole.

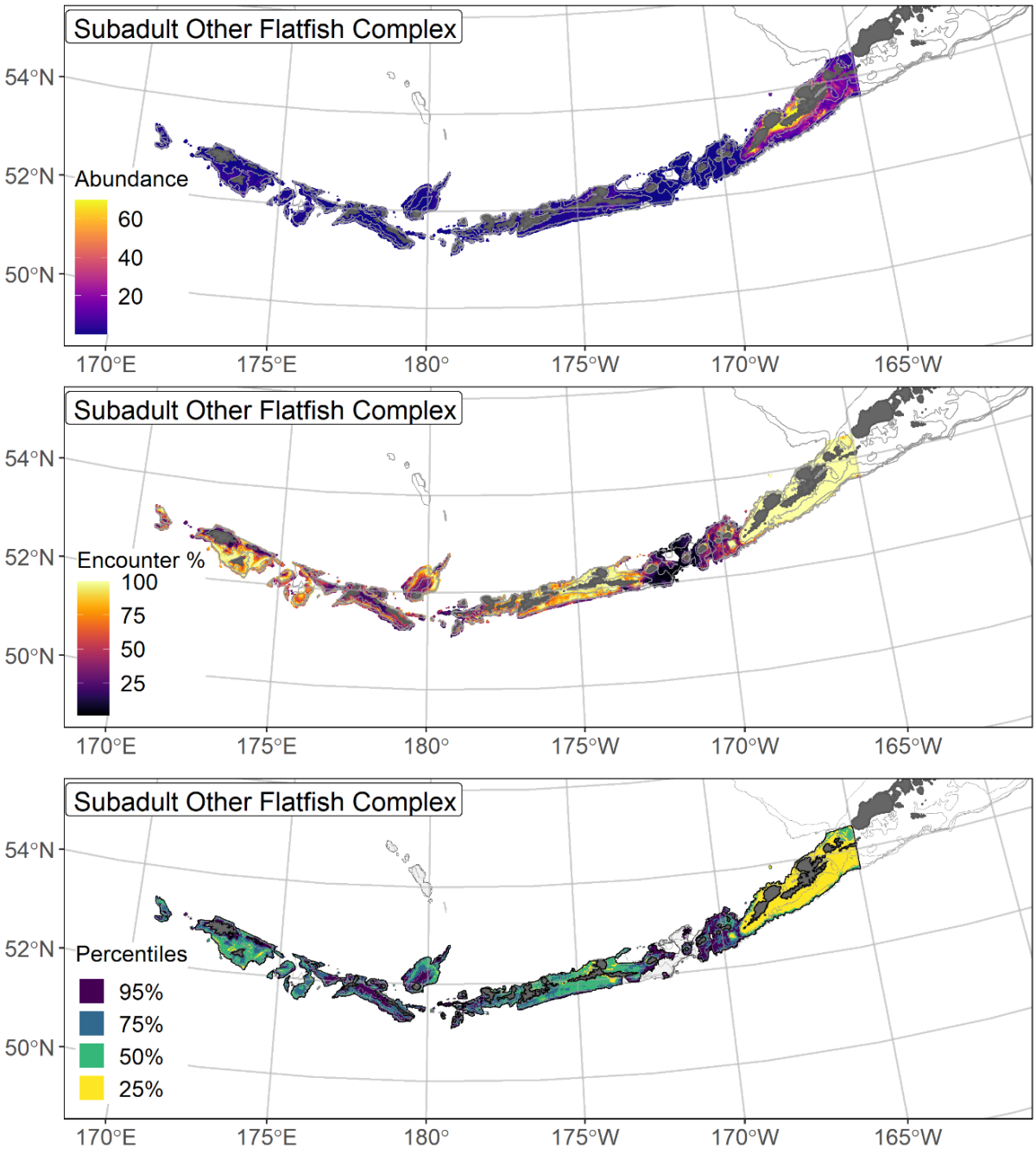


Figure 45. -- Composite predicted numerical abundance (top panel), encounter probability (middle panel), and essential fish habitat (bottom panel) of subadults from the "other flatfish" stock complex for the AI collected in AFSC RACE-GAP summer bottom trawl surveys (1991–2019) with 100 m, 300 m, and 500 m isobaths indicated; internal to the EFH map are the subareas of the top 25% (EFH hot spots), top 50% (core EFH area), and top 75% (principal EFH area) of habitat-related, ensemble-predicted numerical abundance.

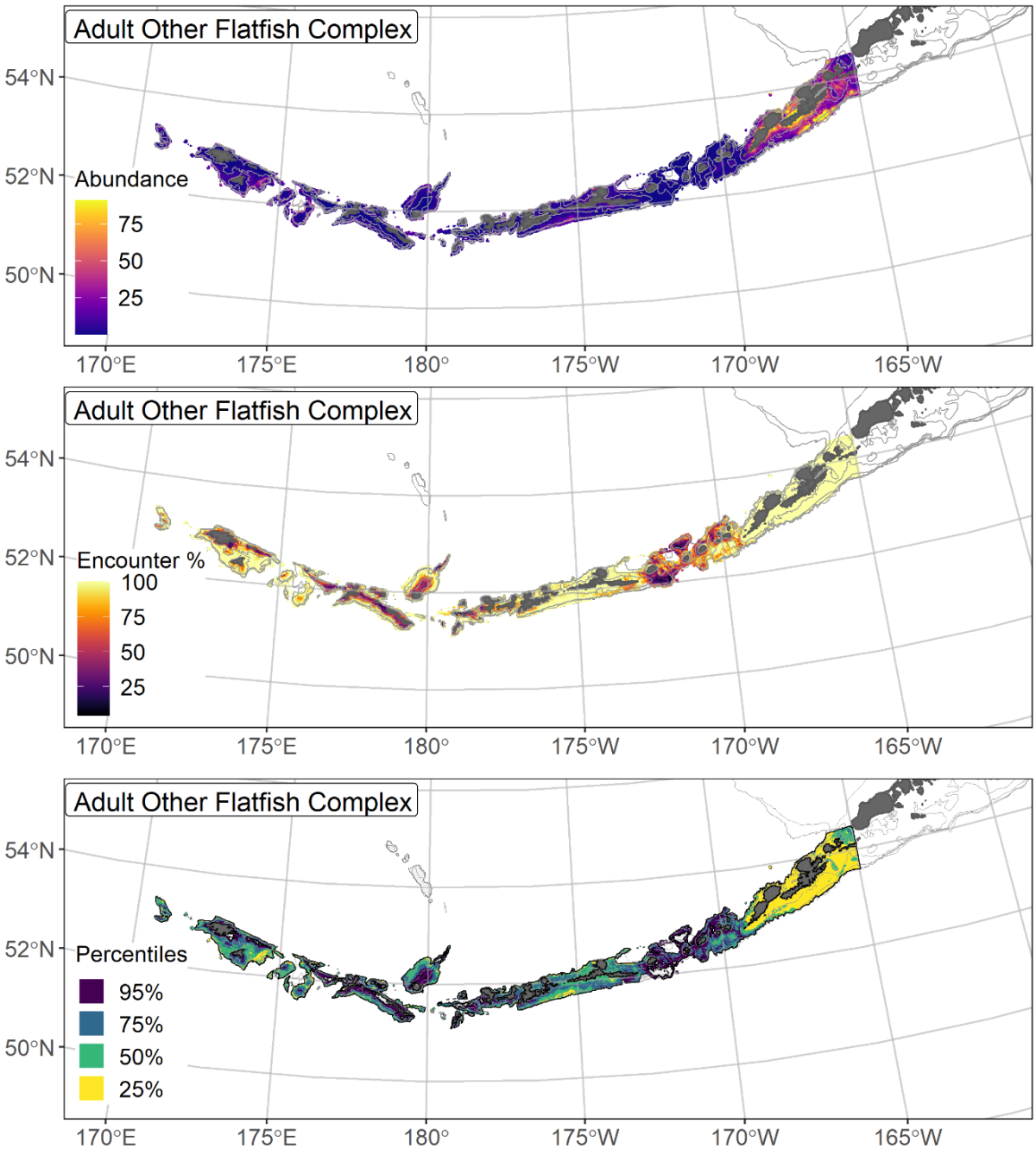


Figure 46. -- Composite predicted numerical abundance (top panel), encounter probability (middle panel), and essential fish habitat (bottom panel) of adults from the "other flatfish" stock complex for the AI collected in AFSC RACE-GAP summer bottom trawl surveys (1991–2019) with 100 m, 300 m, and 500 m isobaths; internal to the EFH map are the subareas of the top 25% (EFH hot spots), top 50% (core EFH area), and top 75% (principal EFH area) of habitat-related, ensemble-predicted numerical abundance.

**Dover sole (*Microstomus pacificus*)**

Dover sole (*Microstomus pacificus*) are distributed from Baja California to the AI and into the southeastern Bering Sea (Mecklenburg et al., 2002). $L_{50}$ in the GOA (439 mm FL; Abookire and Macewicz 2003) was used to separate subadult and adult life stages of Dover sole for these analyses. Adults attain a size of up to 660 mm FL and can be found at depths greater than 1,200 m. Spawning occurs offshore and in deeper water along the edge of the continental slope, with most juveniles occurring inshore and in shallower water. This species has a spawning period from late January to early June in the GOA (Abookire, 2006). Development in Dover sole appears to exhibit significant regional and individual variation in the timing of metamorphosis and juvenile settlement (Pearcy 1977, Bailey et al., 2008), and additional research is necessary to to address spatial and temporal variations in life history[13]. After settlement, juveniles and adults appear to migrate into deeper waters, with the oldest and largest individuals favoring greater depths. In the BSAI region, Dover sole are managed as a part of "other flatfish" stock assessment (Monnahan 2020).

**Subadult Dover sole distribution and predicted abundance from RACE-GAP summer bottom trawl surveys in the Aleutian Islands –** Subadult Dover sole catches occurred in localized patches in the RACE-GAP summer survey areas (Fig. 47). Large catches were located around Unalaksa Island, Petrel Bank, and the Rat Islands. The final ensemble contained four equally weighted SDMs showing a fair fit to the data (Table 15). Specifically, the ensemble showed good performance at predicting presence or absence in catches (AUC = 0.83) and fair accuracy in predicting abundance and deviance explained ($\rho = 0.30$; PDE = 0.35). Overall, these

[13] A request from the stock assessment author review to redefine the life stage breaks for this species based on subregional growth differences in future SDM ensemble EFH mapping efforts is included as a future research recommendation from the 2023 EFH 5-year review.

metrics suggest that the ensemble accurately describes where this species is found, but is less effective at predicting the abundance observed in trawl catches. Geographic position, bottom depth, and current vector and variability were the most important covariates for the model and accounted for 67.4% of the deviance explained by the model (Table 16). Although important in the ensemble, geographic position had an inconsistent pattern that is difficult to interpret. The other covariates show a stronger pattern, and the model predicts higher abundance in locations with weak currents, high current variability, and bottom depths between 200 and 300 m (Fig. 48). Predicted abundance was highest around Petrel Bank (Fig. 48). The predicted CV of abundance was highest near the deep passes in the island chain, such as south of Buldir Island (Fig. 48). Subadult Dover sole were not common in the AI trawl survey, and encounter probabilities were high in only a few places, including around Petrel Bank (Fig. 49).

**Adult Dover sole distribution and predicted abundance from RACE-GAP summer bottom trawl surveys in the Aleutian Islands –** Adult Dover sole catches in the RACE-GAP summer survey were not common, and the highest abundance catches were located around Petrel Bank (Fig. 50). The four SDMs in the final ensemble performed similarly and were assigned equal weights, and the ensemble provided a fair to good fit overall (Table 15). Specifically, the ensemble achieves good performance in terms of predicting presence (AUC = 0.88) and in terms of deviance explained (PDE = 0.43), but only fair ability in terms of predicting relatively high or low abundance ($\rho = 0.27$). The discrepancy between the values for $\rho$ and PDE occurred because the data have numerous observations close to zero, and this combination indicated that many of the model errors are small in absolute terms. Overall, the ensemble captured the general pattern of adult Dover sole presence and absence and demonstrated fair to good accuracy in predicting abundance. Geographic position, bottom depth, and current were the most important covariates

and accounted for 85.9% of the deviance explained (Table 16). The ensemble predicted higher abundance around Petrel Bank, and higher abundance with increasing depth and in places with variable, southerly bottom currents (Fig. 51). Predicted abundance was highest near Petrel Bank and Amchitka Pass, as well as several places along the edge of the continental slope at around 500 m depth (Fig. 51). The predicted CV of abundance was elevated along these slope areas, and while the predicted mean abundance was fairly low, these locations have a higher predicted degree of variability and may hold larger numbers of this life stage (Fig. 51). Ensemble-predicted encounter probabilities for adult Dover sole were often close to zero in depths shallower than 300 m and tended to be higher with increasing depth (Fig. 52).

**Essential fish habitat of subadult and adult Dover sole in the Aleutian Islands –** The habitat related abundance predictions based on RACE-GAP summer bottom trawl data (1991–2019) were translated into EFH area and subareas (Fig. 53). The EFH area for subadult Dover sole was larger than that of adults and showed hot spots around Petrel Bank, on the shelf south of Unalaska Island, and some areas of the far west AI. Subadult EFH included shallower, more near shore areas but was mostly located at moderately deep areas around 200–300 m. By contrast, the EFH area for adults was much smaller and showed a single main hot spot around Petrel Bank and Amchitka Pass. Additional EFH for adults is located around the deep passes through the AI chain, mostly near 500 m depth. Given this pattern and life history information about Dover sole, it is likely that much of the adult population in the AI resides in deeper areas outside of the survey area.

Table 15. -- Constituent species distribution models (SDMs) used to construct Essential Fish Habitat (EFH) for a) subadult and b) adult *Dover* sole: MaxEnt = Maximum entropy; paGAM = presence-absence generalized additive model; hGAM = hurdle GAM; $GAM_P$ = standard Poisson GAM; and $GAM_{nb}$ = standard negative-binomial GAM. Ensemble performance (ρ = Spearman's rank correlation coefficient), root-mean-square-error (RMSE), the area under the receiver operating characteristic (AUC), and the Poisson deviance explained (PDE) were generated from k-fold cross-validation. The "--" in a field indicates that this SDM was not included in the final ensemble.

**a) subadult Dover sole**

| Models | RMSE | Relative Weight | ρ | AUC | PDE | EFH area ($km^2$) |
|---|---|---|---|---|---|---|
| MaxEnt | 1.49 | 0.26 | 0.25 | 0.78 | 0.22 | 52,500 |
| paGAM | 1.49 | 0.26 | 0.27 | 0.79 | 0.26 | 43,800 |
| hGAM | 1.56 | 0.23 | 0.25 | 0.80 | 0.21 | 34,000 |
| $GAM_P$ | 1.53 | 0 | 0.26 | 0.78 | 0.26 | -- |
| $GAM_{nb}$ | 1.49 | 0.26 | 0.27 | 0.80 | 0.28 | 36,200 |
| ensemble | 1.45 | 1 | 0.30 | 0.83 | 0.35 | 44,900 |

**b) adult Dover sole**

| Models | RMSE | Relative Weight | ρ | AUC | PDE | EFH area ($km^2$) |
|---|---|---|---|---|---|---|
| MaxEnt | 1.00 | 0.23 | 0.22 | 0.82 | 0.21 | 30,400 |
| paGAM | 0.92 | 0.27 | 0.25 | 0.84 | 0.32 | 28,800 |
| hGAM | 0.98 | 0.24 | 0.24 | 0.84 | 0.28 | 24,500 |
| $GAM_P$ | 0.96 | 0.25 | 0.23 | 0.82 | 0.33 | 25,100 |
| $GAM_{nb}$ | 1.03 | 0.00 | 0.27 | 0.88 | 0.38 | -- |
| ensemble | 0.87 | 1 | 0.27 | 0.88 | 0.43 | 29,200 |

Table 16. -- Covariates retained in the a) subadult and b) adult Dover sole species distribution model (SDM) final ensembles, the percent contribution to the total deviance explained by each, and the cumulative percent deviance: SD = standard deviation, and BPI = bathymetric position index.

| Dover sole | Covariate | % Contribution | Cumulative % Contribution |
|---|---|---|---|
| **a) subadult** | position | 19.8 | 19.8 |
| | bottom depth | 18.7 | 38.5 |
| | current | 17.8 | 56.2 |
| | current SD | 11.2 | 67.4 |
| | aspect east | 6.5 | 73.9 |
| | tidal maximum | 6.3 | 80.2 |
| | aspect north | 6.2 | 86.4 |
| | BPI | 4.2 | 90.6 |
| | bottom temperature | 3.1 | 93.7 |
| | slope | 2.8 | 96.5 |
| | curvature | 1.3 | 97.8 |
| | rockiness | 0.9 | 98.7 |
| | coral presence | 0.9 | 99.6 |
| | pennatulacean presence | 0.4 | 100 |
| | sponge presence | 0.0 | 100 |
| **a) adult** | bottom depth | 26.8 | 26.8 |
| | position | 26.3 | 53.1 |
| | current | 13.9 | 67.0 |
| | current SD | 8.1 | 75.1 |
| | aspect east | 4.9 | 80.0 |
| | aspect north | 4.9 | 84.9 |
| | tidal maximum | 3.5 | 88.4 |
| | bottom temperature | 2.5 | 90.9 |
| | BPI | 2.1 | 93.0 |
| | curvature | 2.0 | 95.0 |
| | rockiness | 2.0 | 97.0 |
| | sponge presence | 1.3 | 98.3 |
| | coral presence | 0.8 | 99.1 |
| | slope | 0.5 | 99.6 |
| | pennatulacean presence | 0.4 | 100 |

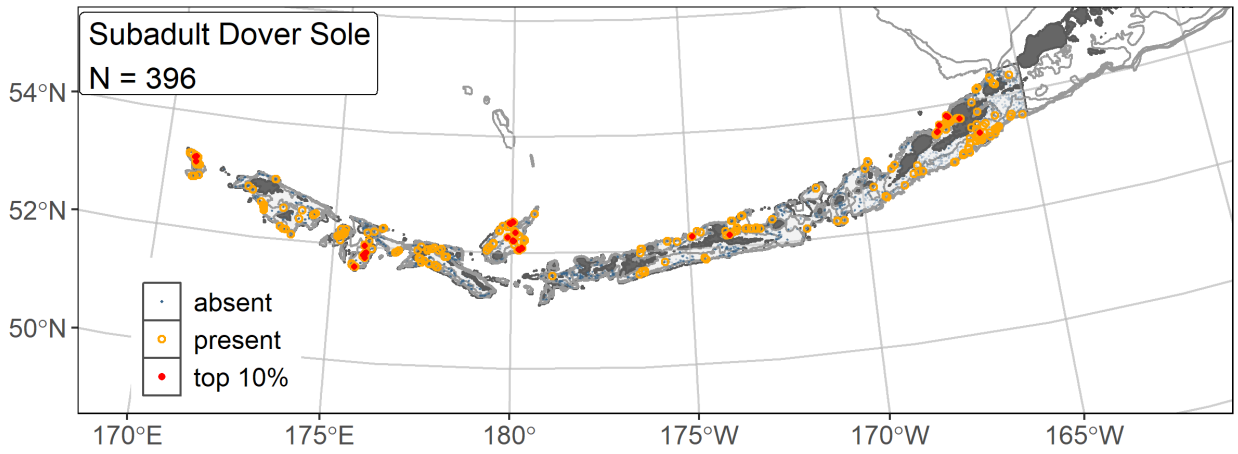


Figure 47. -- Distribution of subadult Dover sole catches (N = 396) in 1991–2019 AFSC RACE-GAP summer bottom trawl surveys of the AI with the 100 m, 300 m, and 500 m isobaths indicated; filled red circles indicate locations in top 10% of overall abundance, open orange circles indicate presence in remaining catches, and small blue dots indicate absence.

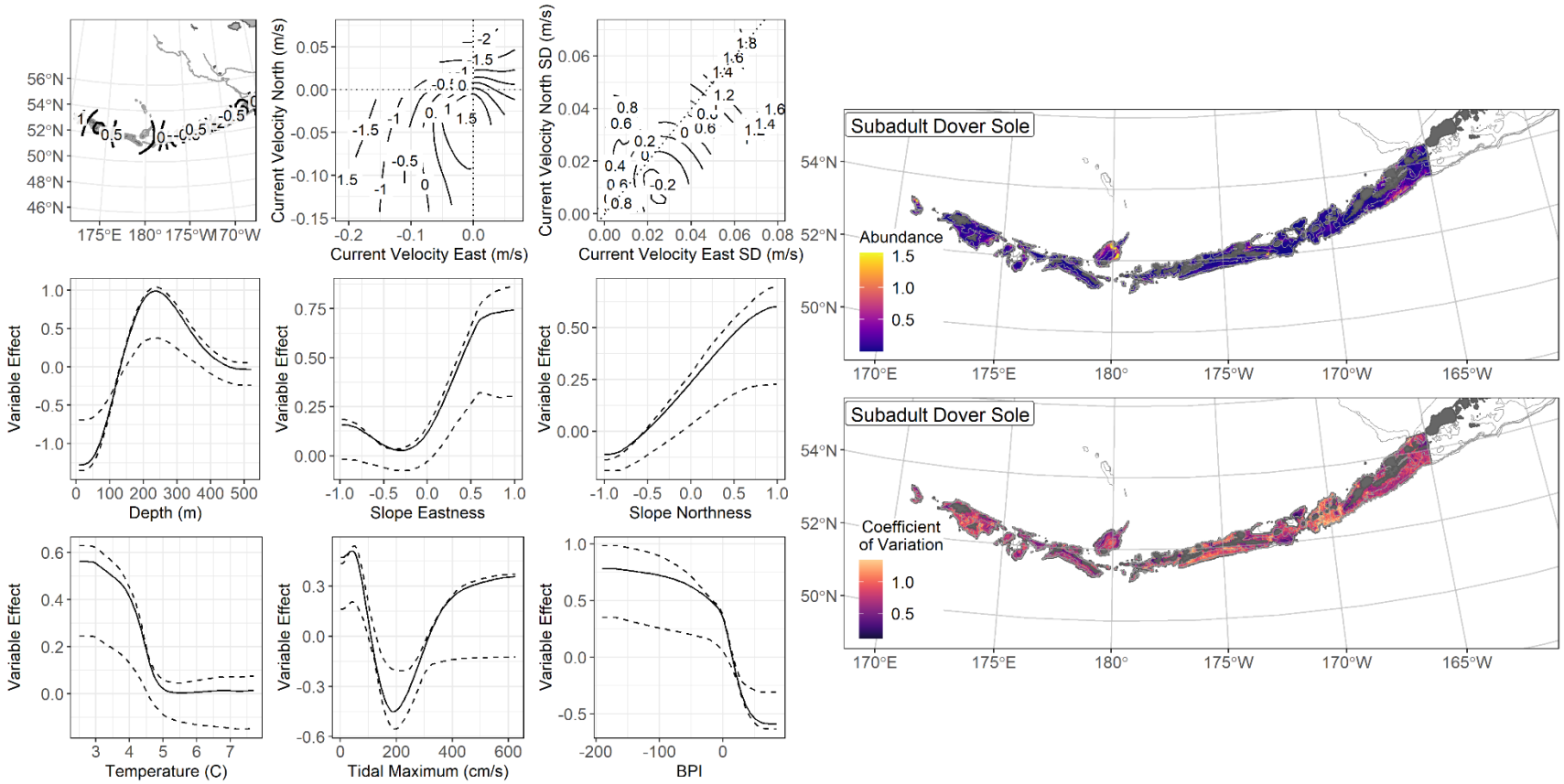


Figure 48. -- The top nine covariate effects (left panel) on ensemble-predicted subadult Dover sole numerical abundance across the AI (upper right panel) alongside the coefficient of variation of the ensemble predictions (lower right panel).

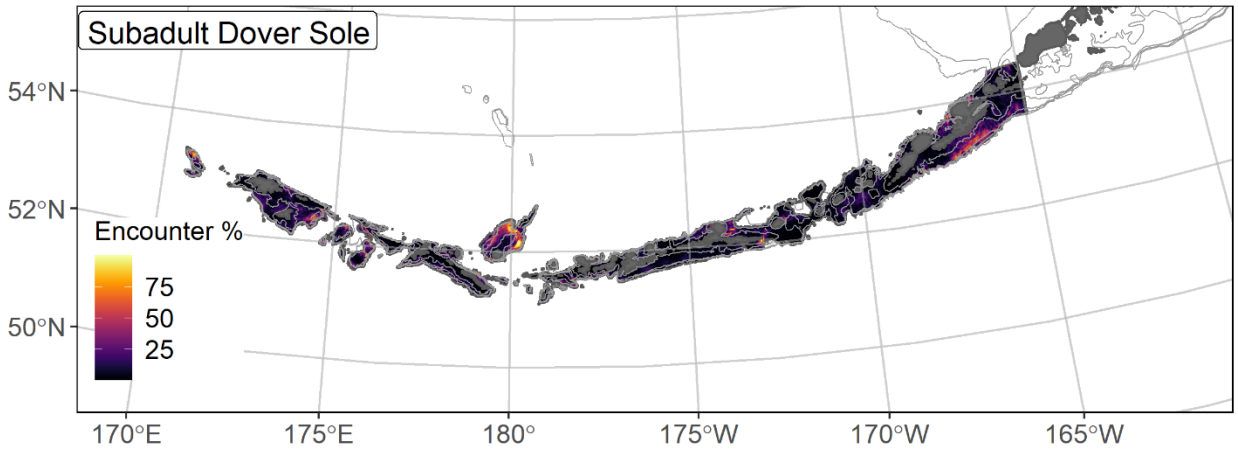


Figure 49. -- Encounter probability of subadult Dover sole from AFSC RACE-GAP summer bottom trawl surveys (1991–2019) of the AI with the 100 m, 300 m, and 500 m isobaths indicated.

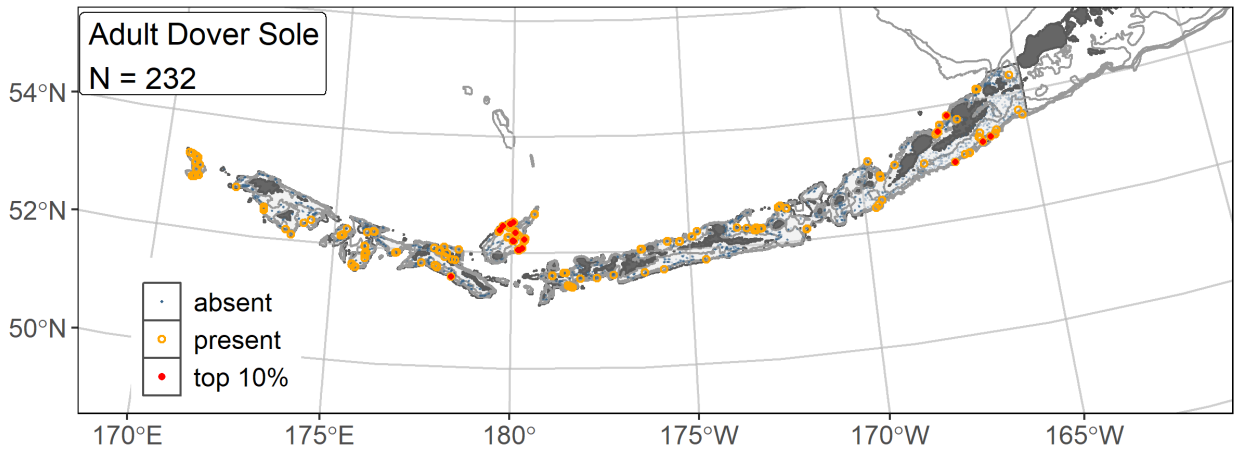


Figure 50. -- Distribution of adult Dover sole catches (N = 232) in 1991–2019 AFSC RACE-GAP summer bottom trawl surveys of the AI with the 100 m, 300 m, and 500 m isobaths indicated; filled red circles indicate locations in top 10% of overall abundance, open orange circles indicate presence in remaining catches, and small blue dots indicate absence.

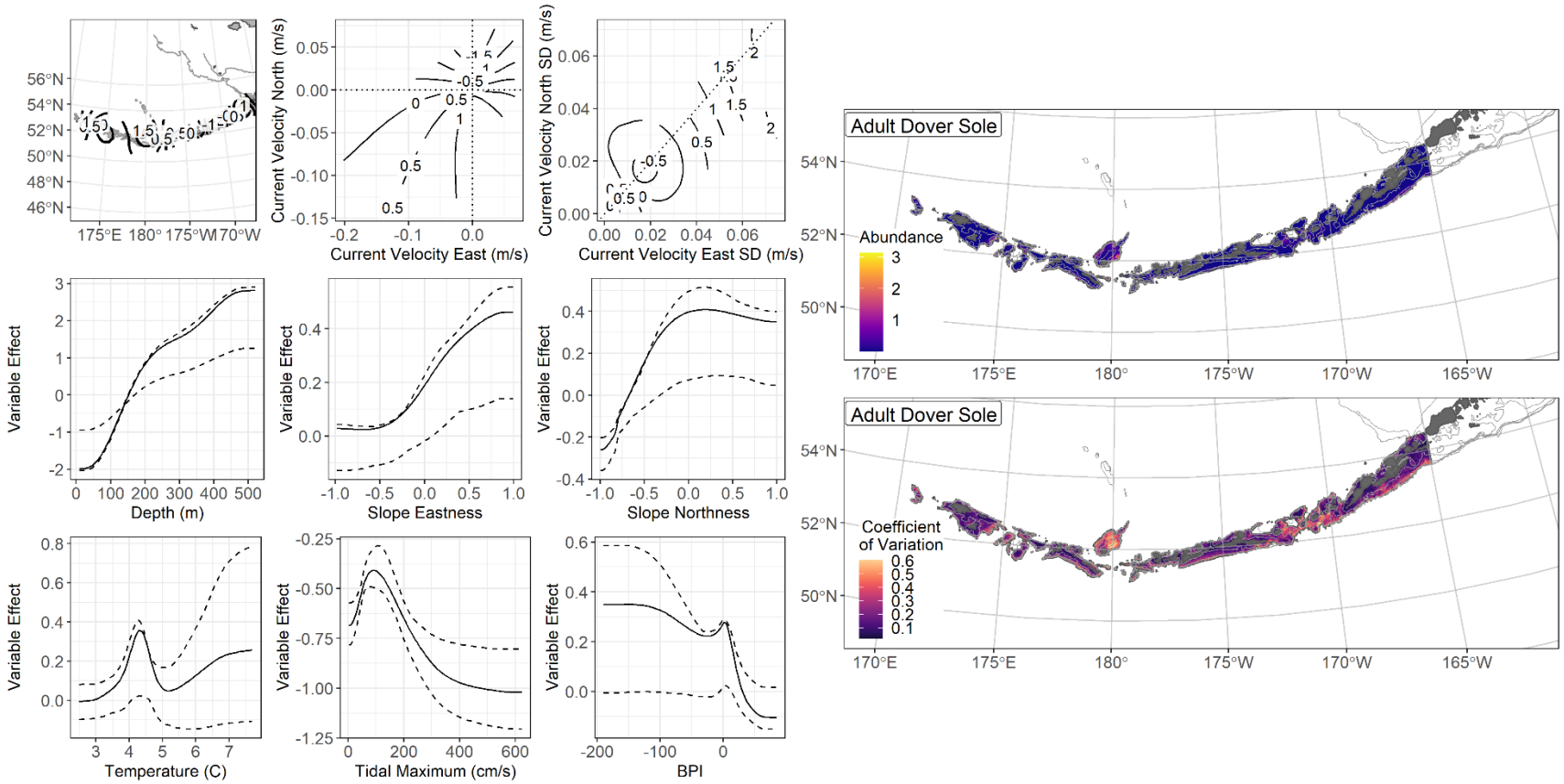


Figure 51. -- The top nine covariate effects (left panel) on ensemble-predicted adult Dover sole numerical abundance across the AI (upper right panel) alongside the coefficient of variation of the ensemble predictions (lower right panel).

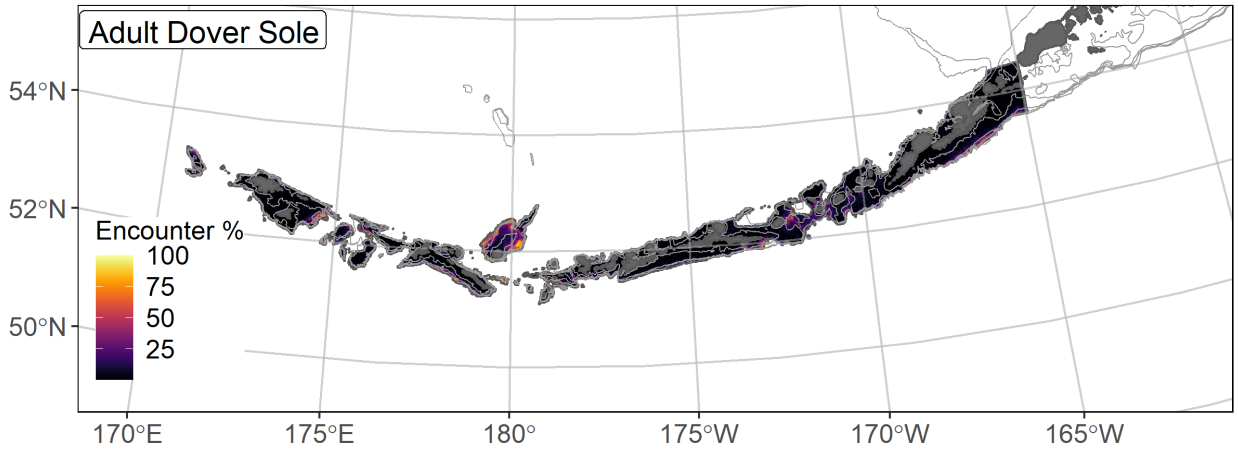


Figure 52. -- Encounter probability of adult Dover sole from AFSC RACE-GAP summer bottom trawl surveys (1991–2019) of the AI with the 100 m, 300 m, and 500 m isobaths indicated.

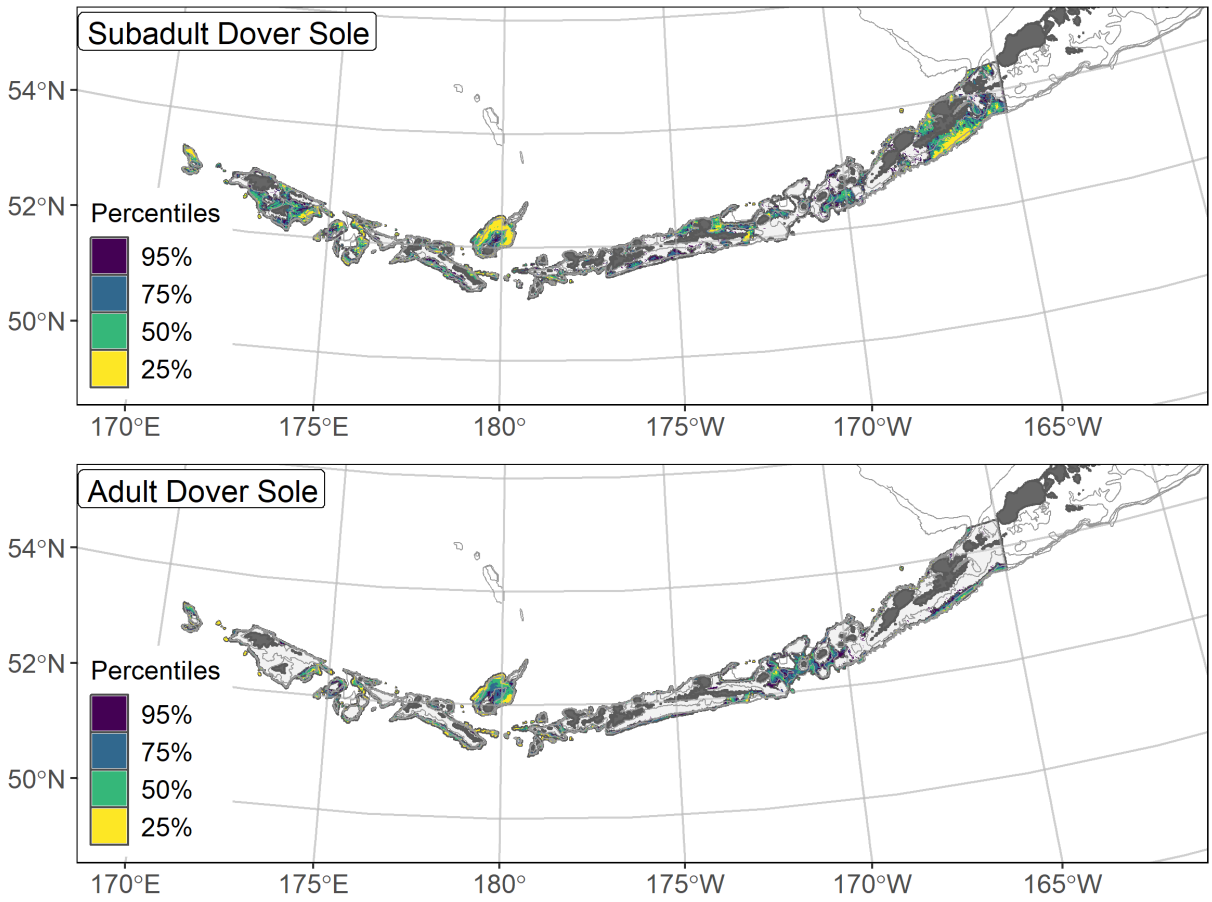


Figure 53. -- Essential fish habitat (EFH area) defined as the top 95% of numerical abundance predictions from a habitat-based ensemble fitted to subadult (top) and adult (bottom) Dover sole distribution and abundance in AFSC RACE-GAP summer bottom trawl surveys (1991–2019) with 100 m, 300 m, and 500 m isobaths indicated; internal to the EFH map are the subareas of the top 25% (EFH hot spots), top 50% (core EFH area), and top 75% (principal EFH area) of habitat-related, ensemble-predicted numerical abundance.

**English sole (*Parophrys vetulus*)**

English sole (*Parophrys vetulus*) is a moderately-sized flatfish that reaches an adult size of up to 630 mm FL in RACE-GAP bottom trawl surveys. It is found from the central AI to Baja California and in the Bering Sea (Hart 1973). Little is known about English sole life history in Alaska, but along the coasts of Oregon and Washington, the spawning season lasts from September to April (Krygier and Pearcy 1986), and juveniles spend their first year in nursery areas near estuaries before eventually spreading out along the coast (Gunderson et al. 1990). No settled early juveniles (< 140 mm FL; Yeung and Cooper 2020) and very few subadults (< 230 mm FL; $L_{50}$; Sampson and Al-Jufaily 1998) were captured in the AI bottom trawl survey, and only adults had sufficient data to construct a species distribution model. In the BSAI region, English sole are managed as part of the Other Flatfish stock complex and do not receive a species-specific fishing target (Monnahan 2020).

**Adult English sole distribution and predicted abundance from RACE-GAP summer bottom trawl surveys in the Aleutian Islands –** Adult English sole catches in the RACE-GAP summer bottom trawl survey were very rare, and almost all occurrences were near Unalaska Island (Fig. 54). In fact, only 50 positive catches of English sole were recorded in the history of the survey, a count that is considered the bare minimum amount of data to construct an SDM in this project. Because of this data limitation, findings for this species in the AI should be treated as preliminary and used with caution. The ensemble contained three SDMs with approximately equal weights, and it performed well considering the limited amount of data (Table 17). The ensemble scored well at predicting presence in trawl catches (AUC = 0.98), and the deviance explained was also excellent (PDE = 0.82). By contrast, the ensemble did not score highly in terms of predicting relative abundance ($\rho = 0.23$). These statistics should be interpreted with

caution because of the limited dataset on which they are based. On the one hand, the small number of English sole catches in the AI are almost all near shore around Unalaska Island, making presence easy to predict. On the other hand, with so few occurrences, it is hard to say if this distribution pattern should be expected to be consistent over time. Several environmental covariates were included in the ensemble for English sole catches, including tidal maximum, bottom depth, BPI, temperature, and bottom current (Table 18). English sole catches were associated with weak currents, weak tides, shallow water, and warm temperatures (Fig. 55). Predicted abundance was highest near shore around Unalaska and Umnak Islands, and low below 100 m depth (Fig. 55). The predicted CV of abundance was high in most places where this species is found, which is unsurprising given the small amount of data (Fig. 55). Predicted encounter probabilities for adult English sole were high in a few places near Unalaska Island and zero over most of the AI region (Fig. 56).

**Essential fish habitat of adult English sole in the Aleutian Islands –** The habitat-related abundance predictions based on RACE-GAP summer bottom trawl data (1991–2019) were translated into EFH area and subareas (Fig. 57). The EFH area for English sole is localized to the areas near shore around Unalaska and Umnak islands, with a smaller area near Atka Island. All EFH hot spots for English sole occur close to shore, with the overall EFH extending into deeper water up to 300 m.

Table 17. -- Constituent species distribution models (SDMs) used to construct Essential Fish Habitat (EFH) for adult English sole: MaxEnt = Maximum entropy; paGAM = presence-absence generalized additive model; hGAM = hurdle GAM; $GAM_P$ = standard Poisson GAM; and $GAM_{nb}$ = standard negative-binomial GAM. Ensemble performance (ρ = Spearman's rank correlation coefficient), root-mean-square-error (RMSE), the area under the receiver operating characteristic (AUC), and the Poisson deviance explained (PDE) were generated from k-fold cross-validation. The "--" in a field indicates that this SDM was not included in the final ensemble.

**adult English sole**

| Models | RMSE | Relative Weight | ρ | AUC | PDE | EFH area ($km^2$) |
|---|---|---|---|---|---|---|
| MaxEnt | 1.93 | 0.32 | 0.18 | 0.91 | 0.59 | 6,800 |
| paGAM | 1.88 | 0.34 | 0.17 | 0.93 | 0.63 | 12,500 |
| hGAM | -- | 0 | -- | -- | -- | -- |
| $GAM_P$ | 1.90 | 0.33 | 0.25 | 0.92 | 0.53 | 3,900 |
| $GAM_{nb}$ | 1.94 | 0 | 0.20 | 0.94 | 0.59 | -- |
| ensemble | 1.45 | 1 | 0.23 | 0.98 | 0.82 | 10,400 |

Table 18. -- Covariates retained in the adult English sole species distribution model (SDM) final ensembles, the percent contribution to the total deviance explained by each, and the cumulative percent deviance: SD = standard deviation, and BPI = bathymetric position index.

| English sole | Covariate | % Contribution | Cumulative % Contribution |
|---|---|---|---|
| **adult** | tidal maximum | 17.1 | 17.1 |
| | bottom depth | 15.3 | 32.4 |
| | BPI | 14.1 | 46.5 |
| | current SD | 11.7 | 58.2 |
| | current | 10.8 | 69.0 |
| | bottom temperature | 8.1 | 77.1 |
| | position | 6.9 | 84.0 |
| | slope | 6.7 | 90.7 |
| | rockiness | 3.0 | 93.7 |
| | aspect east | 2.3 | 96.0 |
| | pennatulacean presence | 1.3 | 97.3 |
| | aspect north | 1.1 | 98.4 |
| | curvature | 0.7 | 99.1 |
| | coral presence | 0.5 | 99.6 |
| | sponge presence | 0.4 | 100 |

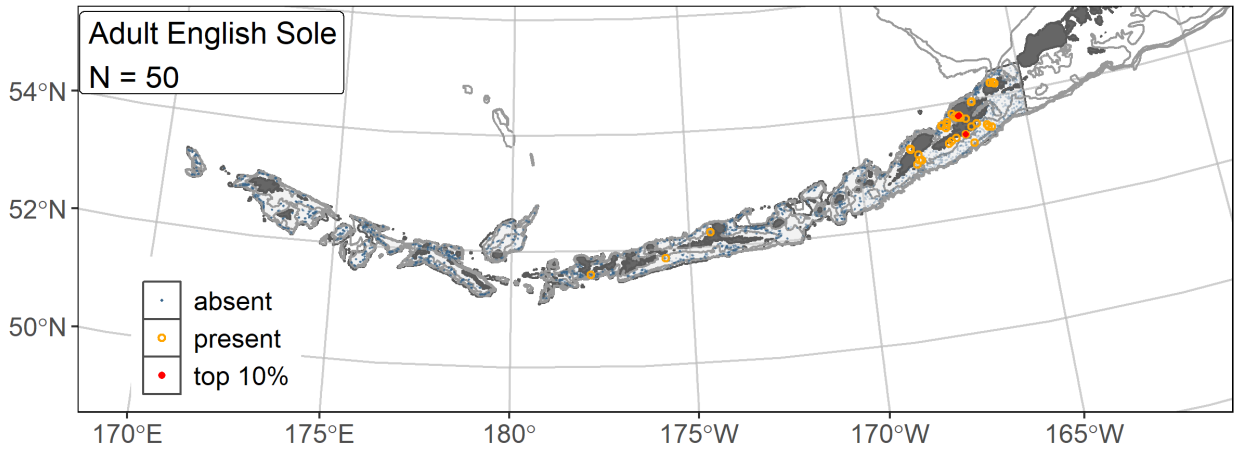


Figure 54. -- Distribution of adult English sole catches (N = 50) in 1991–2019 AFSC RACE-GAP summer bottom trawl surveys of the AI with the 100 m, 300 m, and 500 m isobaths indicated; filled red circles indicate locations in top 10% of overall abundance, open orange circles indicate presence in remaining catches, and small blue dots indicate absence.

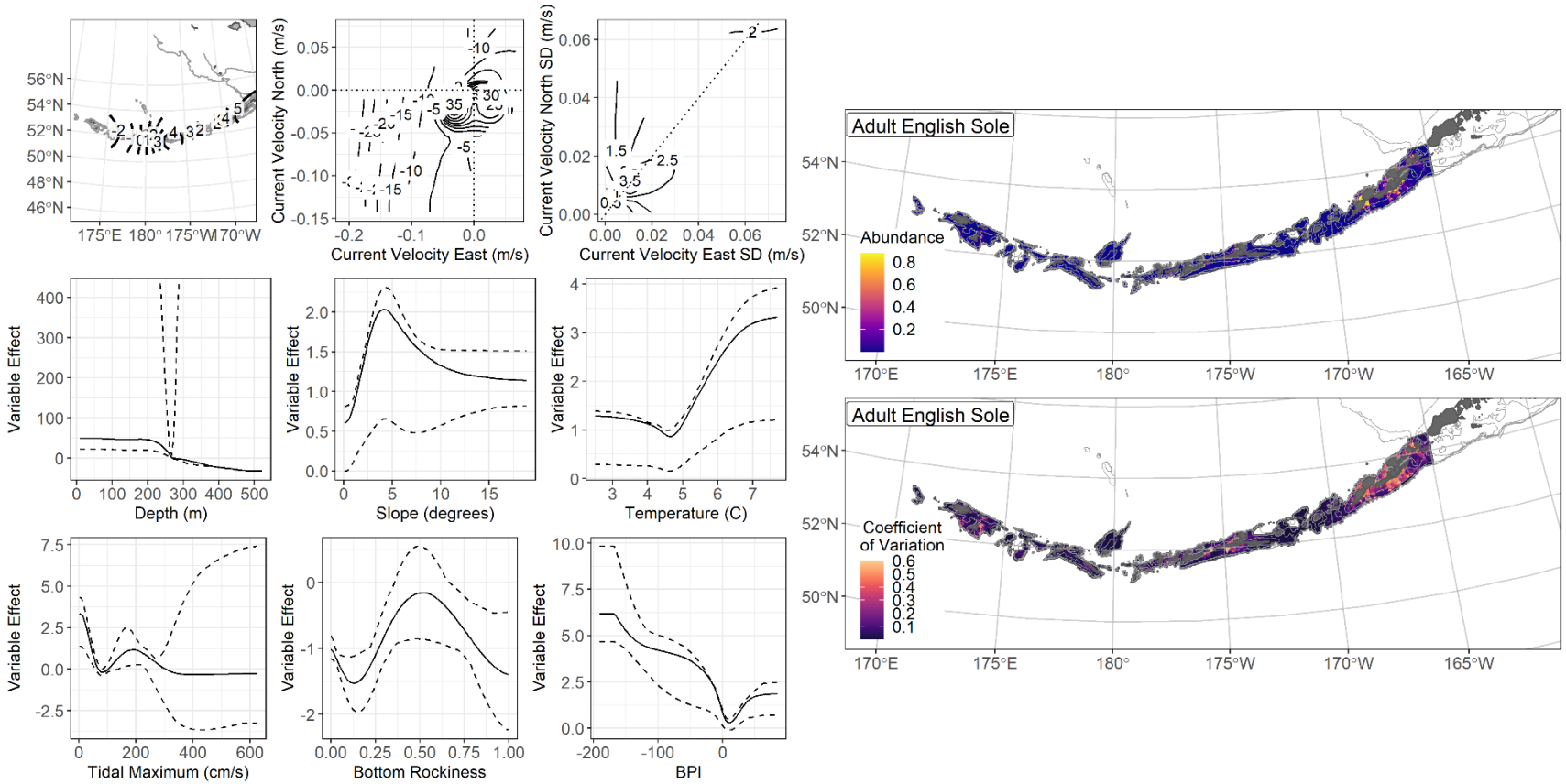


Figure 55. -- The top nine covariate effects (left panel) on ensemble-predicted adult English sole numerical abundance across the AI (upper right panel) alongside the coefficient of variation of the ensemble predictions (lower right panel).

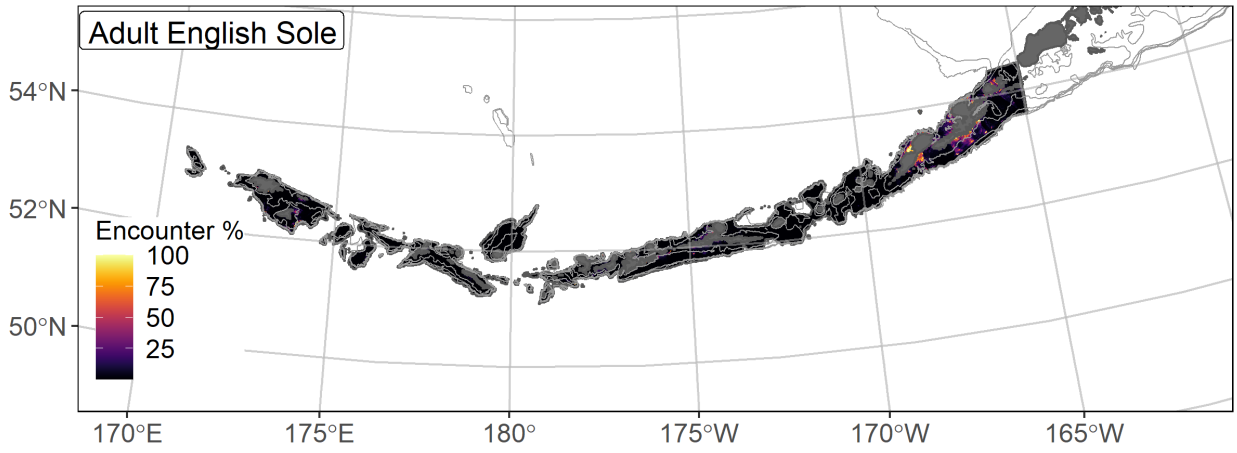


Figure 56. -- Encounter probability of adult English sole from AFSC RACE-GAP summer bottom trawl surveys (1991–2019) of the AI with the 100 m, 300 m, and 500 m isobaths indicated.

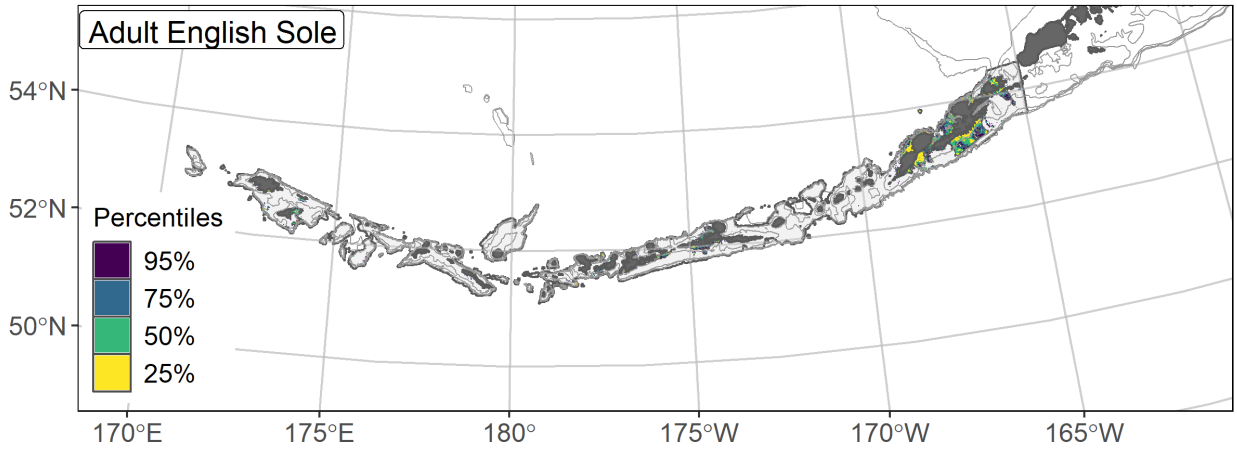


Figure 57. -- Essential fish habitat (EFH area) defined as the top 95% of numerical abundance predictions from a habitat-based ensemble fitted to adult English sole distribution and abundance in AFSC RACE-GAP summer bottom trawl surveys (1991–2019) with 100 m, 300 m, and 500 m isobaths indicated; internal to the EFH map are the subareas of the top 25% (EFH hot spots), top 50% (core EFH area), and top 75% (principal EFH area) of habitat-related, ensemble-predicted numerical abundance.

**Rex sole (*Glyptocephalus zachirus*)**

Rex sole (*Glyptocephalus zachirus*) is a widely distributed flatfish with a native range that extends from Baja California to the western Bering Sea (Mecklenburg et al. 2002). Adults may grow to 600 mm TL and are found from the surface to depths of 850 m (Abookire and Bailey 2007). Early juveniles settle between 70 and 140 mm TL (Doyle et al. 2019). The majority of rex sole reach maturity ($L_{50}$) at 352 mm (Abookire 2006). Spawning occurs offshore and in deeper water along the edge of the continental slope, with juveniles distributed inshore. This species has an estimated spawning period from October to May in the GOA (Abookire 2006) and an extended larval stage that can last from 9 months to 2 years (Abookire 2006, Pearcy et al. 1977). Significant regional differences in rex sole growth rates have been observed in the GOA and along the Oregon coast. Alaska populations have higher growth rates (Abookire 2006), but additional research will be required to address spatial or temporal differences in life history[14]. Rex sole are managed as a part of the "other flatfish" stock complex in the BSAI (Monnahan 2020).

**Subadult rex sole distribution and predicted abundance from RACE-GAP summer bottom trawl surveys in the Aleutian Islands –** Subadult rex sole catches were common throughout the RACE-GAP summer survey areas (Fig. 58) but were higher in the eastern AI. The final ensemble contained four SDMs, and the hGAM and $GAM_P$ received slightly more weight (Table 19). The ensemble performed well across all three fit metrics ($\rho = 0.48$; AUC = 0.83; PDE = 0.47; Table 19). Geographic position and bottom depth accounted for 57.9% of the deviance explained by the ensemble, though current, current variability, and tidal maximum were

[14] A request from the stock assessment author review to redefine the life stage breaks for this species based on subregional growth differences in future SDM ensemble EFH mapping efforts is included as a future research recommendation from the 2023 EFH 5-year Review.

also important (Table 20). In general, abundance was predicted to be higher at more eastern longitudes, at depths between 150 and 300 m, in weak currents, and at a low tidal maximum (Fig. 59). Predicted abundance was high in the eastern AI, particularly south of Unalaska Island and Unimak Pass, and moderate around Atka and Agattu islands (Fig. 59). The predicted CV of abundance was low in the east near Unalaska Island and somewhat higher farther west (Fig. 59). This indicates that estimates of high abundances in the eastern AI are likely to be reliable, while estimates for other locations may be more variable. Encounter probabilities for subadult rex sole were high in most areas between the 100 m and 300 m depth contours, particularly in the eastern AI, and are lower around the passes and sea mounts farther west (Fig. 60).

**Adult rex sole distribution and predicted abundance from RACE-GAP summer bottom trawl surveys in the Aleutian Islands –** Adult rex sole catches in the RACE-GAP summer survey were evenly distributed across most of the AI, though like subadults, large catches were more common in the east near Unalaska Island and Unimak Pass (Fig. 61). The final ensemble contained four SDMs, and the $GAM_P$ and hGAM performed somewhat better than the paGAM or MaxEnt and were given higher weights (Table 19). The ensemble fit the data well according to all three fit metrics ($\rho = 0.56$; AUC = 0.82; PDE = 0.43; Table 19). Geographic position and bottom depth account for a combined 49.2% of the deviance explained by the ensemble (Table 20), though current, tidal maximum, and slope aspect were also important. Like subadults, adult rex sole are predicted to be abundant in the eastern AI and are associated with areas with weak bottom currents and deeper habitats (Fig. 62). Very similar to subadults, predicted abundance of adult rex sole was highest south of Unalaska Island but occurred farther offshore and in deeper water (Fig. 62). The predicted CV of abundance was low in deeper areas and higher in moderate to shallow ones, reflecting that adult rex sole are consistently found in deeper water (Fig. 62).

Encounter probabilities for adult rex sole are high in most places except in some shallow areas close to shore (Fig. 63).

**Essential fish habitat of subadult and adult rex sole in the Aleutian Islands –** The habitat-related abundance predictions based on RACE-GAP summer bottom trawl data (1991–2019) were translated into EFH area and subareas (Fig. 64). The EFH areas for the two life stages of rex sole were similar, with large hot spots to the south of Unalaska Island. Both life stages also had smaller hot spots farther west near Atka Island and Agattu Island. Subadults were less likely to be found in waters deeper than 300 m, so areas near sea mounts or along the edge of the continental slope did not qualify as EFH. However, the greater depth range of adults allows them to occupy these areas.

Table 19. -- Constituent species distribution models (SDMs) used to construct Essential Fish Habitat (EFH) for a) subadult and b) adult rex sole: MaxEnt = Maximum entropy; paGAM = presence-absence generalized additive model; hGAM = hurdle GAM; $GAM_P$ = standard Poisson GAM; and $GAM_{nb}$ = standard negative-binomial GAM. Ensemble performance (ρ = Spearman's rank correlation coefficient), root-mean-square-error (RMSE), the area under the receiver operating characteristic (AUC), and the Poisson deviance explained (PDE) were generated from k-fold cross-validation. The "--" in a field indicates that this SDM was not included in the final ensemble.

**a) subadult rex sole**

| Models | RMSE | Relative Weight | ρ | AUC | PDE | EFH area ($km^2$) |
|---|---|---|---|---|---|---|
| MaxEnt | 9.32 | 0.23 | 0.44 | 0.80 | 0.28 | 69,400 |
| paGAM | 9.17 | 0.24 | 0.47 | 0.82 | 0.36 | 70,500 |
| hGAM | 8.53 | 0.27 | 0.43 | 0.82 | 0.41 | 60,200 |
| $GAM_P$ | 8.77 | 0.26 | 0.41 | 0.78 | 0.41 | 62,100 |
| $GAM_{nb}$ | 13.56 | 0 | 0.47 | 0.82 | 0.19 | -- |
| ensemble | 8.05 | 1 | 0.48 | 0.83 | 0.47 | 68,900 |

**b) adult rex sole**

| Models | RMSE | Relative Weight | ρ | AUC | PDE | EFH area ($km^2$) |
|---|---|---|---|---|---|---|
| MaxEnt | 26.0 | 0.22 | 0.53 | 0.81 | 0.23 | 74,400 |
| paGAM | 26.5 | 0.21 | 0.55 | 0.82 | 0.29 | 77,500 |
| hGAM | 23.0 | 0.28 | 0.51 | 0.82 | 0.39 | 73,900 |
| $GAM_P$ | 23.0 | 0.28 | 0.50 | 0.78 | 0.39 | 76,700 |
| $GAM_{nb}$ | 43.8 | 0 | 0.57 | 0.83 | 0.09 | -- |
| ensemble | 22.2 | 1 | 0.56 | 0.83 | 0.46 | 77,200 |

Table 20. -- Covariates retained in the a) subadult and b) adult rex sole species distribution model (SDM) final ensembles, the percent contribution to the ensemble deviance explained by each, and the cumulative percent deviance: SD = standard deviation, and BPI = bathymetric position index.

| rex sole | Covariate | % Contribution | Cumulative % Contribution |
|---|---|---|---|
| **a) subadult** | bottom depth | 29.5 | 29.5 |
| | position | 28.4 | 57.9 |
| | tidal maximum | 6.8 | 64.7 |
| | current | 6.7 | 71.4 |
| | aspect north | 6.2 | 77.6 |
| | current SD | 4.6 | 82.2 |
| | BPI | 3.8 | 86.0 |
| | pennatulacean presence | 3.7 | 89.7 |
| | rockiness | 3.4 | 93.1 |
| | aspect east | 2.2 | 95.3 |
| | slope | 1.9 | 97.2 |
| | bottom temperature | 1.9 | 99.1 |
| | sponge presence | 0.4 | 99.5 |
| | coral presence | 0.3 | 99.8 |
| | curvature | 0.2 | 100 |
| **a) adult** | bottom depth | 25.2 | 25.2 |
| | position | 24.0 | 49.2 |
| | aspect north | 9.9 | 59.1 |
| | current | 9.7 | 68.8 |
| | tidal maximum | 7.6 | 76.4 |
| | rockiness | 5.7 | 82.1 |
| | current SD | 5.2 | 87.3 |
| | aspect east | 4.6 | 91.9 |
| | slope | 2.4 | 94.3 |
| | BPI | 1.8 | 96.1 |
| | bottom temperature | 1.6 | 97.7 |
| | pennatulacean presence | 1.0 | 98.7 |
| | coral presence | 0.6 | 99.3 |
| | sponge presence | 0.5 | 99.8 |
| | curvature | 0.2 | 100 |

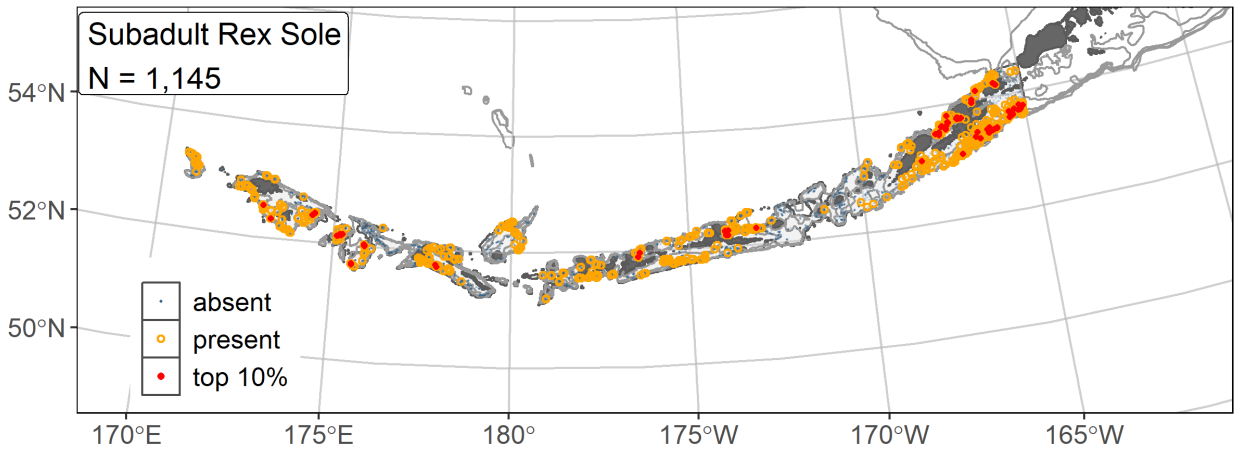


Figure 58. -- Distribution of subadult rex sole catches (N = 1,145) in 1991–2019 AFSC RACE-GAP summer bottom trawl surveys of the AI with the 100 m, 300 m, and 500 m isobaths indicated; filled red circles indicate locations in top 10% of overall abundance, open orange circles indicate presence in remaining catches, and small blue dots indicate absence.

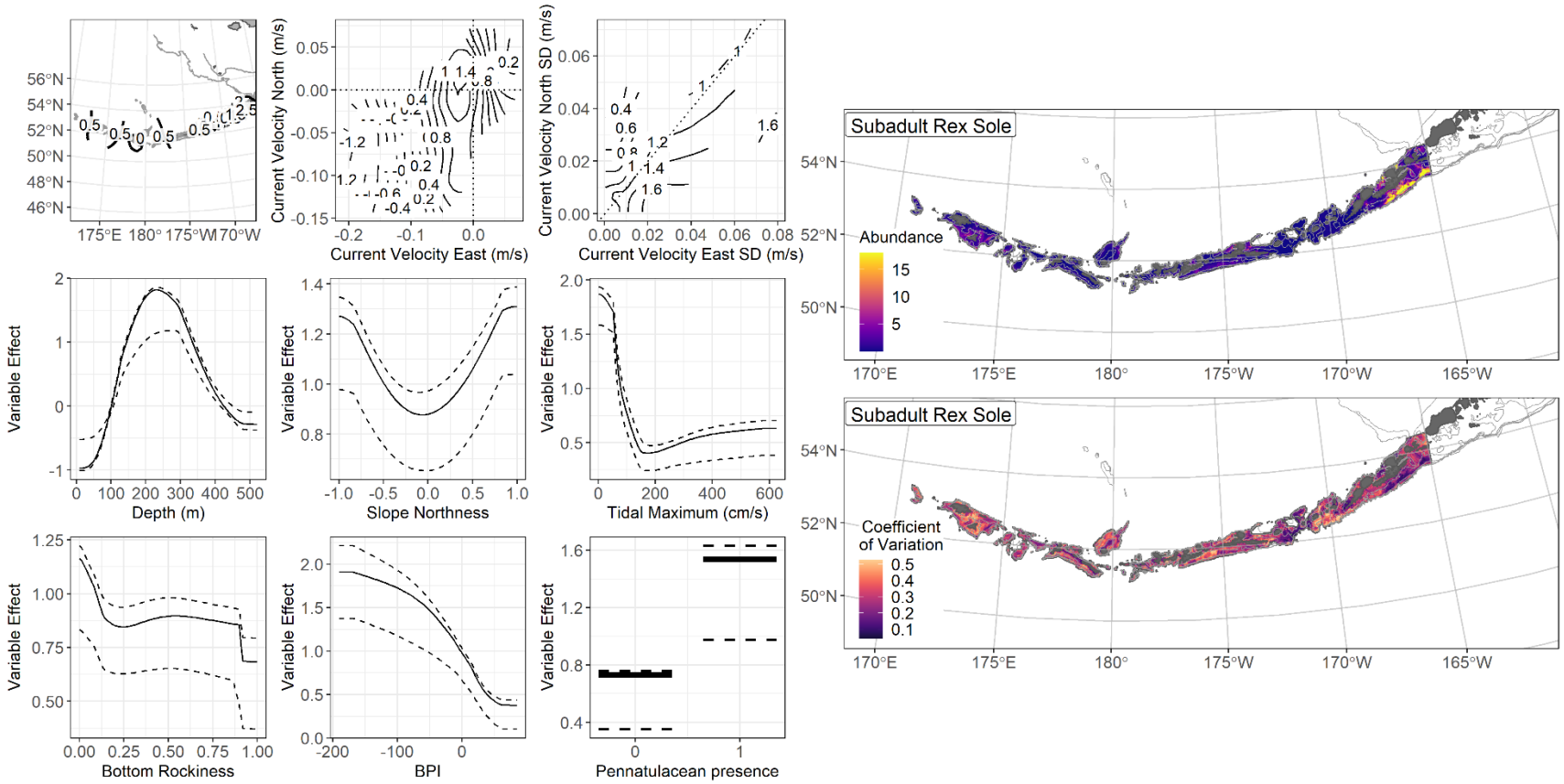


Figure 59. -- The top nine covariate effects (left panel) on ensemble-predicted subadult rex sole numerical abundance across the AI (upper right panel) alongside the coefficient of variation of the ensemble predictions (lower right panel).

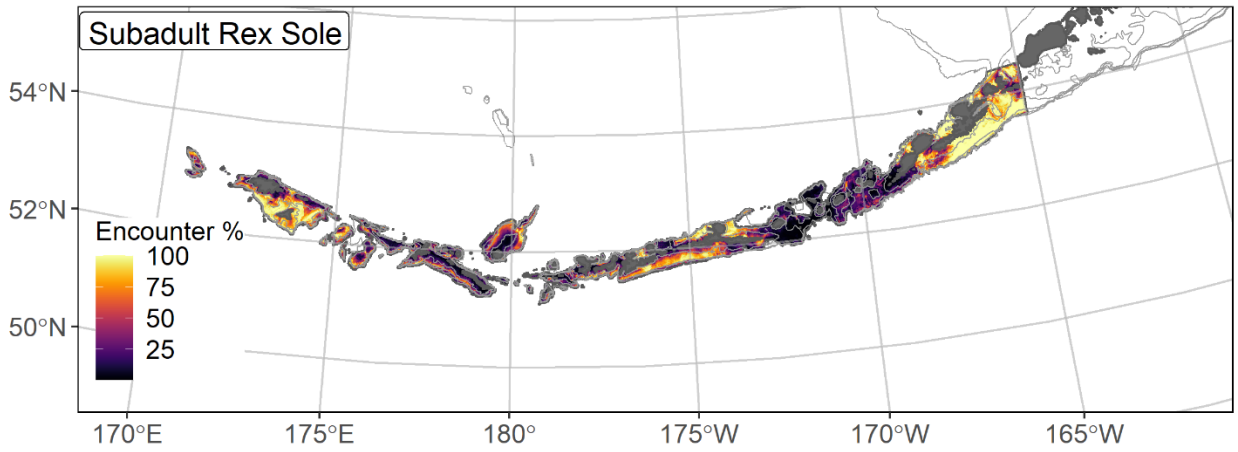


Figure 60. -- Encounter probability of subadult rex sole from AFSC RACE-GAP summer bottom trawl surveys (1991–2019) of the AI with the 100 m, 300 m, and 500 m isobaths indicated.

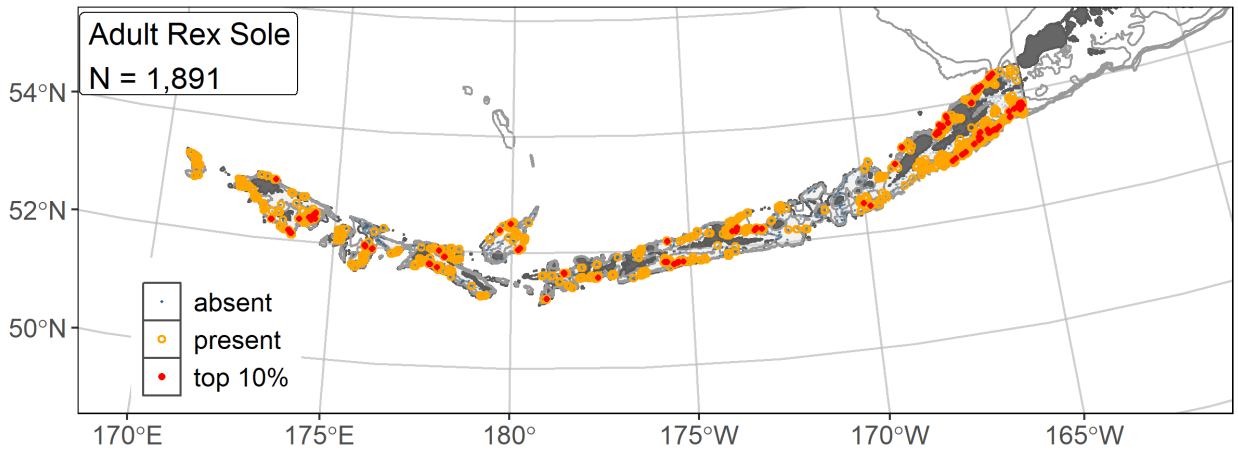


Figure 61. -- Distribution of adult rex sole catches (N = 1,891) in 1991–2019 AFSC RACE-GAP summer bottom trawl surveys of the AI with the 100 m, 300 m, and 500 m isobaths indicated; filled red circles indicate locations in top 10% of overall abundance, open orange circles indicate presence in remaining catches, and small blue dots indicate absence.

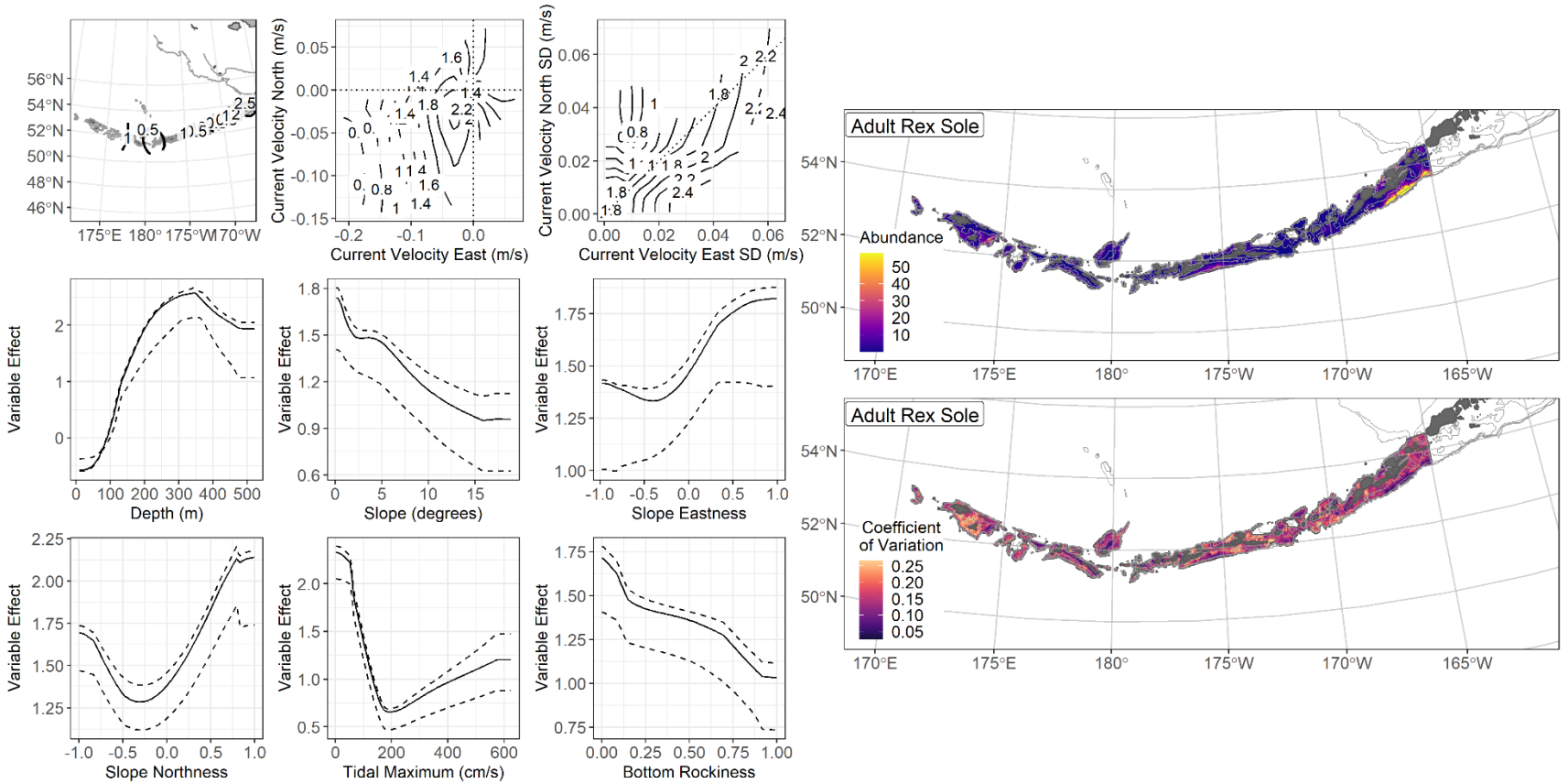


Figure 62. -- The top nine covariate effects (left panel) on ensemble-predicted adult rex sole numerical abundance across the AI (upper right panel) alongside the coefficient of variation of the ensemble predictions (lower right panel).

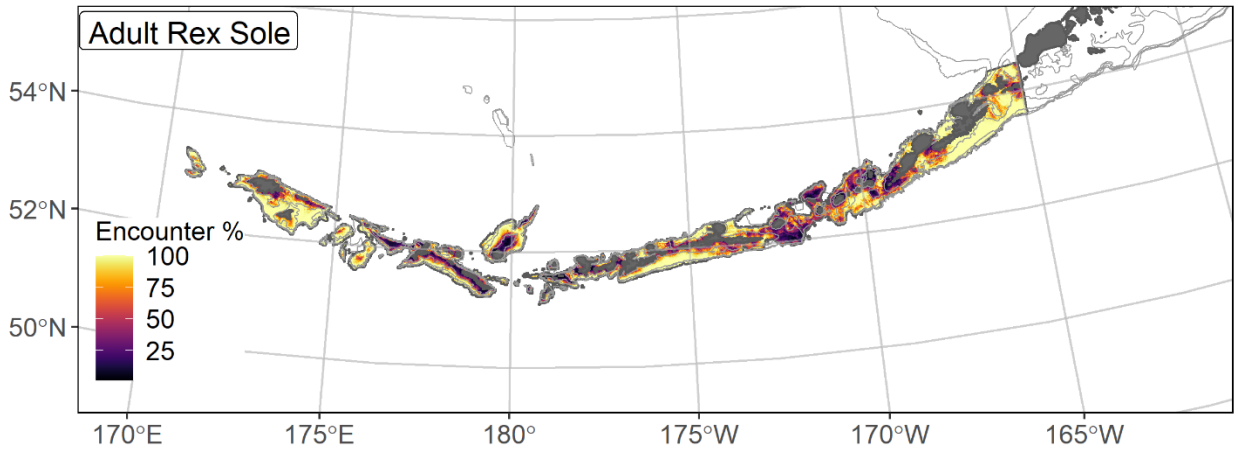


Figure 63. -- Encounter probability of adult rex sole from AFSC RACE-GAP summer bottom trawl surveys (1991–2019) of the AI with the 100 m, 300 m, and 500 m isobaths indicated.

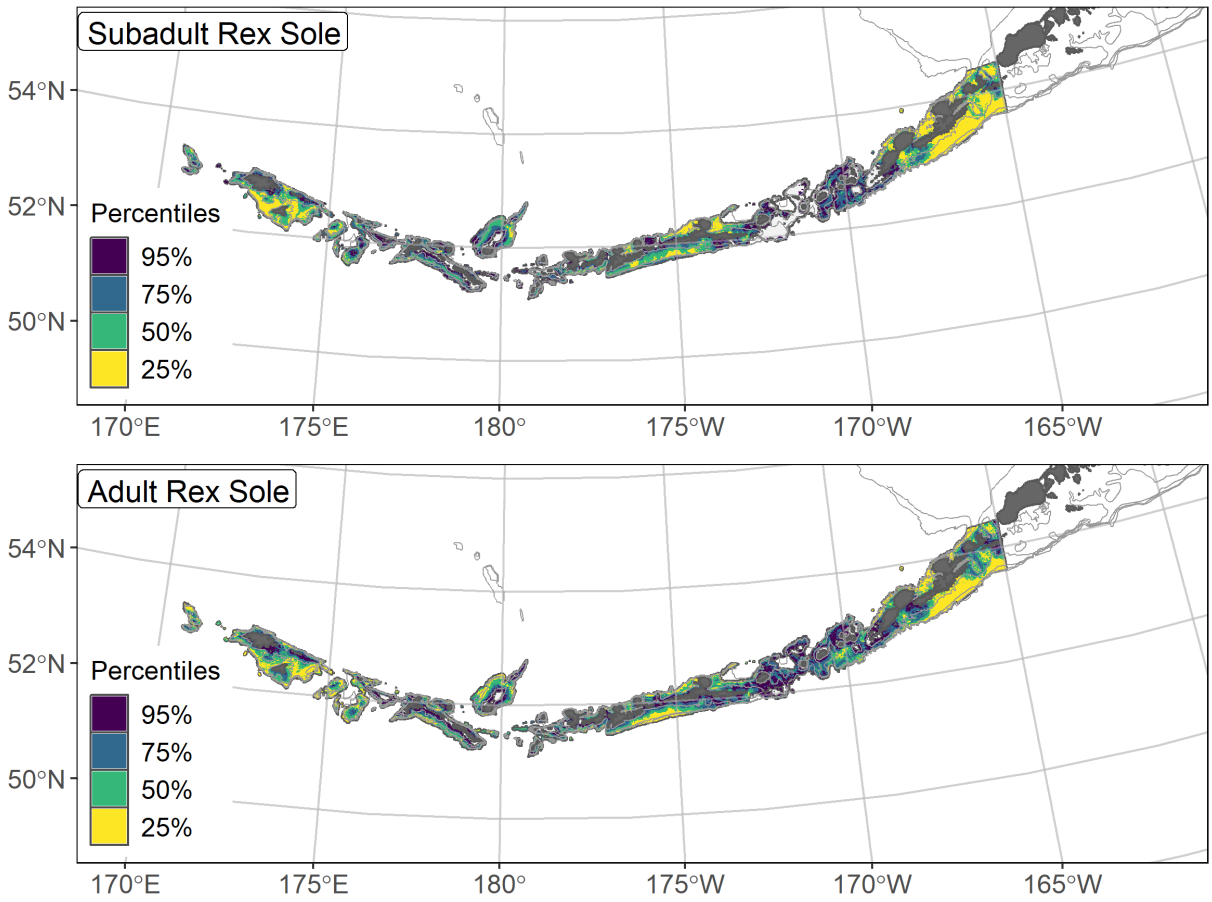


Figure 64. -- Essential fish habitat (EFH area) defined as the top 95% of numerical abundance predictions from a habitat-based ensemble fitted to subadult (top) and adult (bottom) rex sole distribution and abundance in AFSC RACE-GAP summer bottom trawl surveys (1991–2019) with 100 m, 300 m, and 500 m isobaths indicated; internal to the EFH map are the subareas of the top 25% (EFH hot spots), top 50% (core EFH area), and top 75% (principal EFH area) of habitat-related, ensemble-predicted numerical abundance.

**Southern rock sole (*Lepidopsetta bilineata*)**

Southern rock sole (*Lepidopsetta bilineata*) is found in coastal waters from the eastern AI to Baja California (Orr and Matarese 2000). The species is morphologically similar to northern rock sole (*L. polyxstra*), and the two are often confounded in older literature. They were not routinely distinguished in groundfish surveys until 1996. There is broad overlap in the two species ranges in the Gulf of Alaska and the eastern AI. Adults may grow to as much as 580 mm TL (Orr and Matarese 2000), and females become mature at approximately 347 mm TL ($L_{50}$; Stark and Somerton 2002). Female length at maturity was used to separate life stages for both sexes in this study. Compared to northern rock sole, there has been comparatively little research specific to southern rock sole. In the BSAI region, almost the entire catch of southern rock sole in the survey is from the eastern AI. It is managed in the BSAI in a mixed-stock fishery with the more abundant and commercially valuable northern rock sole stock (McGillard et al. 2020).

**Subadult southern rock sole distribution and predicted abundance from RACE-GAP summer bottom trawl surveys in the Aleutian Islands –** Subadult southern rock sole catches from the RACE-GAP summer survey were concentrated in the eastern AI (Fig. 65). Catches were less common west of 170° W. Only two equally weighted SDMs were included in the ensemble. The ensemble showed a good to excellent fit to the observed data (Table 21). Specifically, the ensemble demonstrated "good" ability to predict high vs low density catches ($\rho = 0.55$) and demonstrated "excellent" performance in terms of predicting presence and in terms of deviance explained (AUC = 0.97; PDE = 0.73). Together, these results suggested that the predictions of the ensemble were accurate and adequately described the distribution of this species. Bottom depth and geographic position accounted for 92.8% of the deviance explained by the ensemble (Table 22). In general, high abundance was predicted by shallow water, being

farther east, and weak currents (Fig. 66). Predicted abundance was highest in the eastern AI, particularly around Unalaska Island (Fig. 66). The predicted CV of abundance was high in many shallow areas across the AI, including areas where the ensemble predicted abundance (Fig. 66). Consistent with other results, the predicted encounter probability for subadult southern rock sole was high in the eastern part of the AI survey area, and in shallow water around Atka Island (Fig. 67).

**Adult southern rock sole distribution and predicted abundance from RACE-GAP summer bottom trawl surveys in the Aleutian Islands –** Similar to the subadults, adult southern rock sole catches from the RACE-GAP summer survey were concentrated in the eastern AI and southern Bering Sea (Fig. 68). All the largest catches occurred near Unalaska Island or Unimak Pass. The ensemble consisted of two SDMs, and the $GAM_P$ was weighted somewhat higher than the paGAM. The ensemble showed excellent performance across all three fit metrics (Table 21). Bottom depth and geographic position alone counted for 89.7% of the deviance explained by the ensemble (Table 22). Southern rock sole were predicted to be abundant in shallow water and in eastern longitudes (Fig. 69). As with subadults, predicted abundance for adult southern rock sole was highest in the eastern parts of the AI, particularly around Unalaska Island (Fig. 69). The predicted CV of abundance was low in most places, higher in deeper waters in the east and shallow areas in the central AI (Fig. 69). This pattern reflects that the area around Unalaska has consistently high abundance, whereas catches farther east are more variable. Encounter probabilities were uniformly high in the eastern AI, though a second area near shore around Atka Island also showed high probabilities (Fig. 70).

**Essential fish habitat of subadult and adult southern rock sole in the Aleutian Islands –** The habitat-related abundance predictions based on RACE-GAP summer bottom trawl data (1996–

2019) were translated into EFH area and subareas (Fig. 71). Overall, the EFH areas for each life stage were very similar. Both life stages had a large hot spot in the southern Bering Sea subregion centered on Unalaska Island and an area of core EFH centered on Atka Island. These regions were marked by large, shallow continental shelf habitats, and the high performance scores for the models suggested that this association is accurate. There also appeared to be a strong longitudinal cline not explained by other habitat covariates, given their low weight in the ensembles (Table 22). This indicates that other covariates not included here may explain the absence of the species from similar habitats farther west, such as Petrel Bank or the area around Attu Island.

Table 21. -- Constituent species distribution models (SDMs) used to construct Essential Fish Habitat (EFH) for a) subadult and b) adult southern rock sole: MaxEnt = Maximum entropy; paGAM = presence-absence generalized additive model; hGAM = hurdle GAM; $GAM_P$ = standard Poisson GAM; and $GAM_{nb}$ = standard negative-binomial GAM. Ensemble performance (ρ = Spearman's rank correlation coefficient), root-mean-square-error (RMSE), the area under the receiver operating characteristic (AUC), and the Poisson deviance explained (PDE) were generated from k-fold cross-validation. The "--" in a field indicates that this SDM was not included in the final ensemble.

**a) subadult southern rock sole**

| Models | RMSE | Relative Weight | ρ | AUC | PDE | EFH area ($km^2$) |
|---|---|---|---|---|---|---|
| MaxEnt | -- | 0 | -- | -- | -- | -- |
| paGAM | 13.4 | 0.50 | 0.54 | 0.97 | 0.67 | 46,200 |
| hGAM | -- | 0 | -- | -- | -- | -- |
| $GAM_P$ | 22.7 | 0 | 0.58 | 0.95 | 0.56 | -- |
| $GAM_{nb}$ | 13.4 | 0.50 | 0.58 | 0.97 | 0.73 | 30,800 |
| ensemble | 12.9 | 1 | 0.55 | 0.97 | 0.73 | 41,600 |

**b) adult southern rock sole**

| Models | RMSE | Relative Weight | ρ | AUC | PDE | EFH area ($km^2$) |
|---|---|---|---|---|---|---|
| MaxEnt | -- | 0 | -- | -- | -- | -- |
| paGAM | 12.9 | 0.43 | 0.62 | 0.97 | 0.74 | 43,900 |
| hGAM | 27.6 | 0 | 0.54 | 0.97 | 0.23 | -- |
| $GAM_P$ | 11.4 | 0.57 | 0.62 | 0.96 | 0.79 | 37,100 |
| $GAM_{nb}$ | 17.0 | 0 | 0.64 | 0.97 | 0.74 | -- |
| ensemble | 11.0 | 1 | 0.62 | 0.97 | 0.81 | 42,300 |

Table 22. -- Covariates retained in the a) subadult and b) adult southern rock sole species distribution model (SDM) final ensembles, the percent contribution to the ensemble deviance explained by each, and the cumulative percent deviance: SD = standard deviation, and BPI = bathymetric position index.

| **southern rock sole** | **Covariate** | **% Contribution** | **Cumulative % Contribution** |
|---|---|---|---|
| **a) subadult** | position | 50.4 | 50.4 |
| | bottom depth | 42.4 | 92.8 |
| | current | 4.4 | 97.2 |
| | current SD | 0.5 | 97.7 |
| | aspect north | 0.5 | 98.2 |
| | slope | 0.4 | 98.6 |
| | curvature | 0.4 | 99.0 |
| | sponge presence | 0.3 | 99.3 |
| | bottom temperature | 0.3 | 99.6 |
| | rockiness | 0.1 | 99.7 |
| | coral presence | 0.1 | 99.8 |
| | BPI | 0.1 | 99.9 |
| | pennatulacean presence | 0.1 | 100 |
| **a) adult** | position | 49.7 | 49.7 |
| | bottom depth | 40.1 | 89.7 |
| | current | 3.7 | 93.4 |
| | aspect north | 2.1 | 95.5 |
| | current SD | 1.1 | 96.6 |
| | BPI | 0.8 | 97.4 |
| | slope | 0.7 | 98.1 |
| | curvature | 0.7 | 98.8 |
| | bottom temperature | 0.4 | 99.2 |
| | tidal maximum | 0.3 | 99.5 |
| | aspect east | 0.2 | 99.7 |
| | sponge presence | 0.1 | 99.8 |
| | rockiness | 0.1 | 99.9 |
| | coral presence | 0.1 | 100 |
| | pennatulacean presence | 0 | 100 |

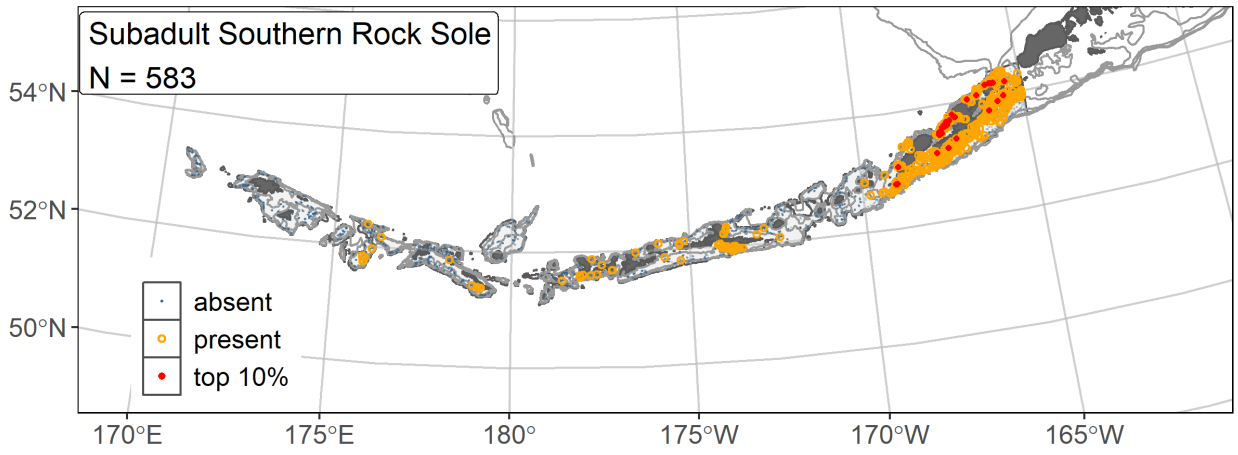


Figure 65. -- Distribution of subadult southern rock sole catches (N = 583) in 1996–2019 AFSC RACE-GAP summer bottom trawl surveys of the AI with the 100 m, 300 m, and 500 m isobaths indicated; filled red circles indicate locations in top 10% of overall abundance, open orange circles indicate presence in remaining catches, and small blue dots indicate absence.

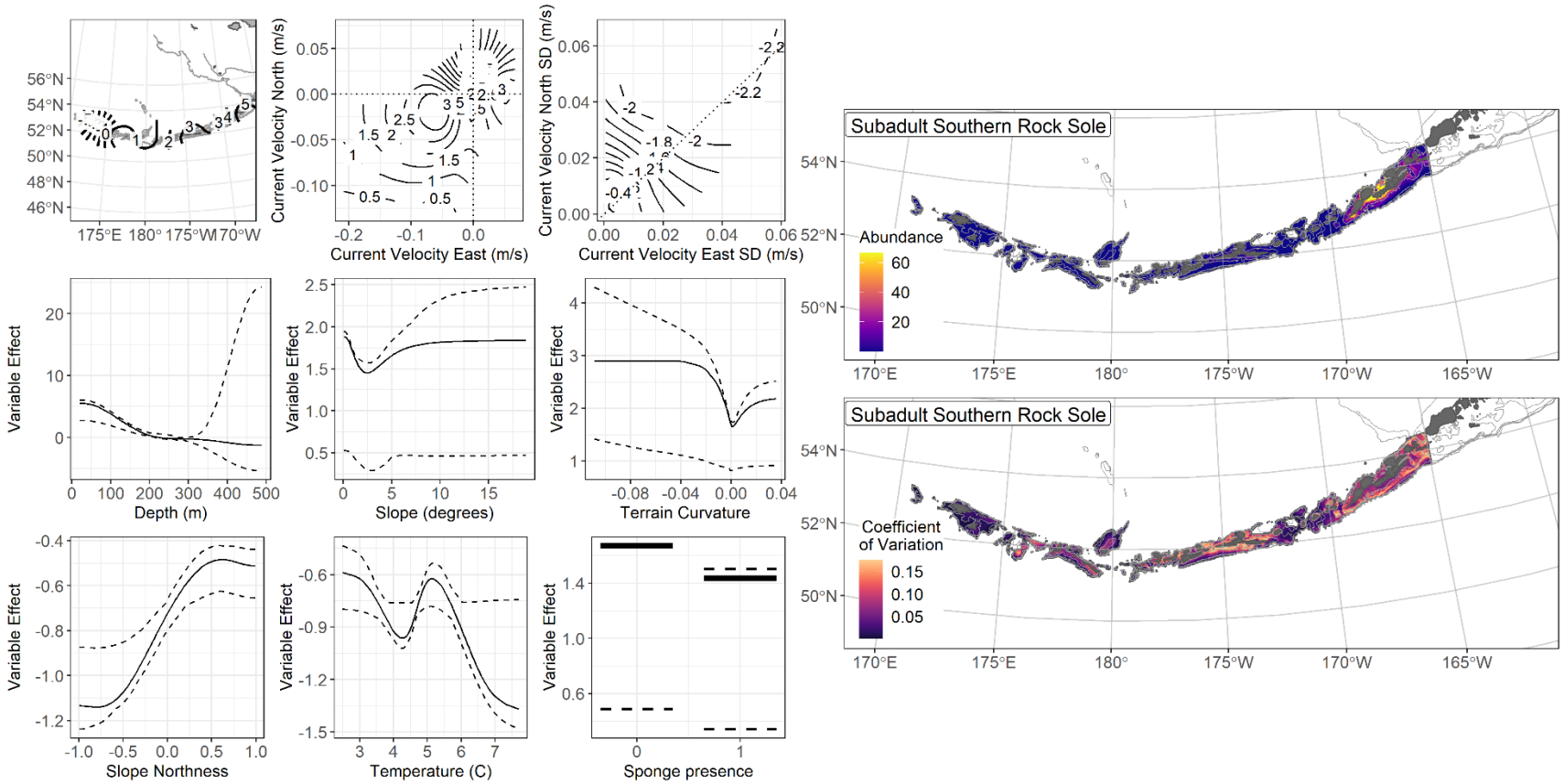


Figure 66. -- The top nine covariate effects (left panel) on ensemble-predicted subadult southern rock sole numerical abundance across the AI (upper right panel) alongside the coefficient of variation of the ensemble predictions (lower right panel).

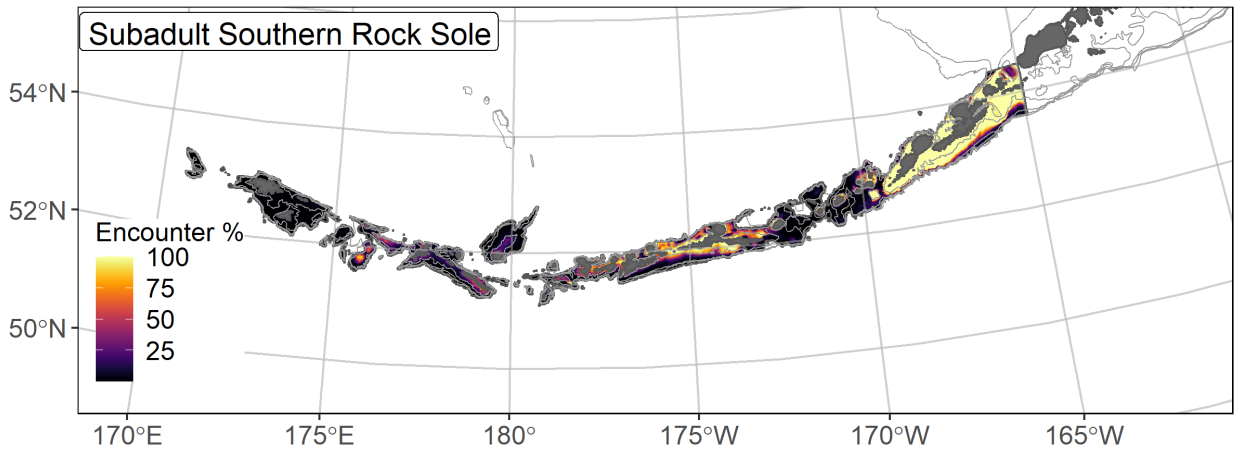


Figure 67. -- Encounter probability of subadult southern rock sole from AFSC RACE-GAP summer bottom trawl surveys (1996–2019) of the AI with the 100 m, 300 m, and 500 m isobaths indicated.

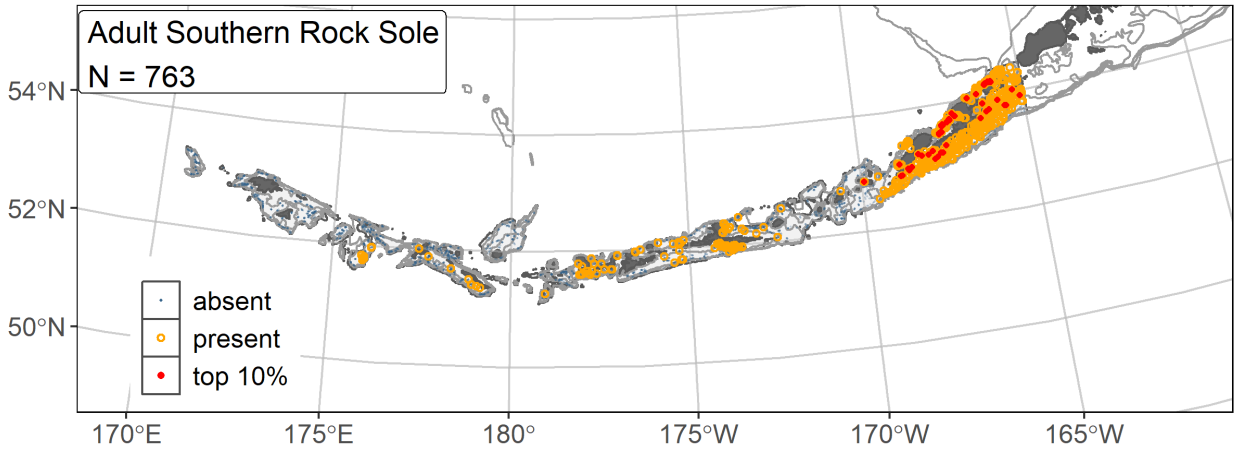


Figure 68. -- Distribution of adult southern rock sole catches (N = 763) in 1996–2019 AFSC RACE-GAP summer bottom trawl surveys of the AI with the 100 m, 300 m, and 500 m isobaths indicated; filled red circles indicate locations in top 10% of overall abundance, open orange circles indicate presence in remaining catches, and small blue dots indicate absence.

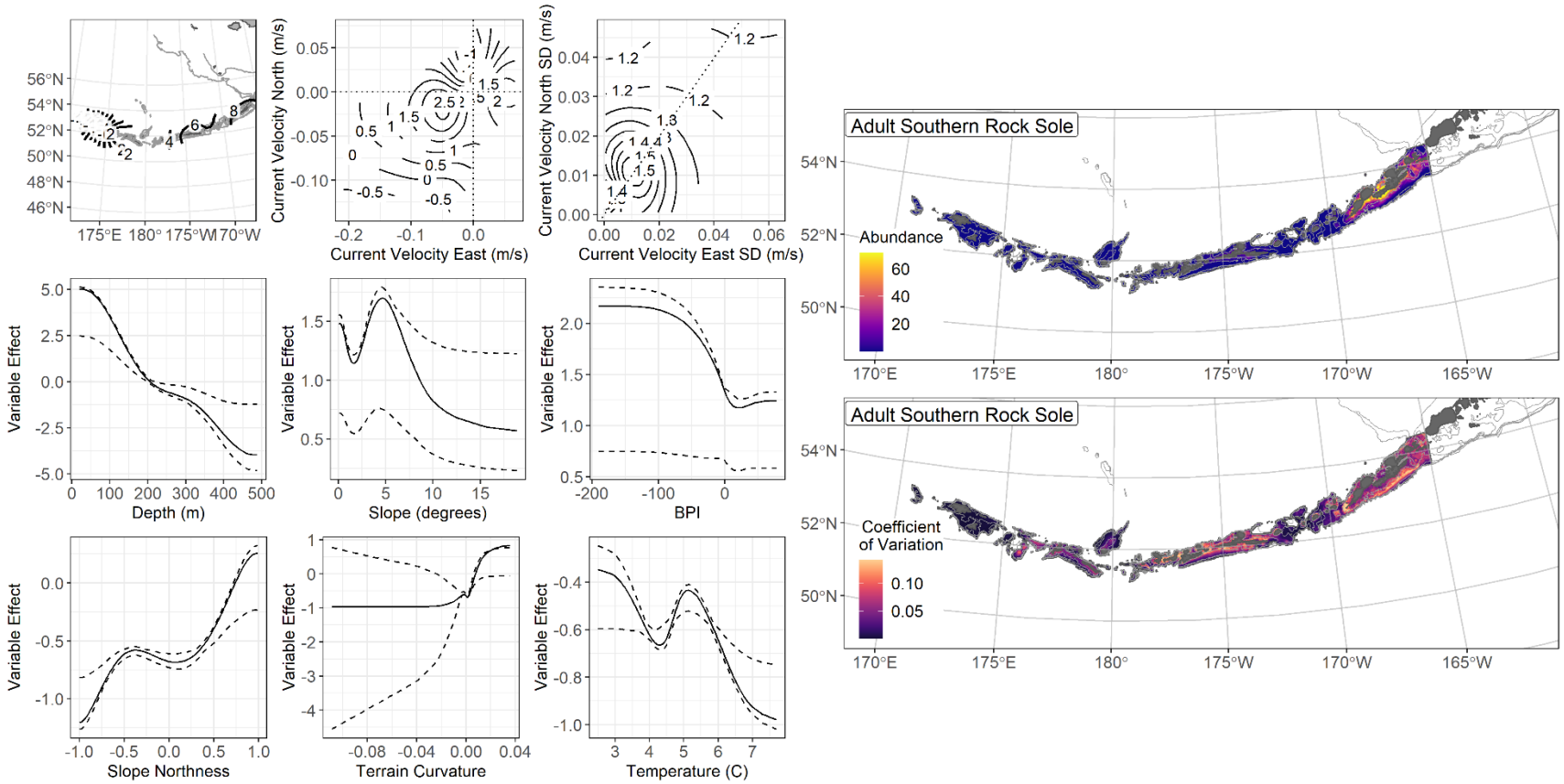


Figure 69. -- The top nine covariate effects (left panel) on ensemble-predicted adult southern rock sole numerical abundance across the AI (upper right panel) alongside the coefficient of variation of the ensemble predictions (lower right panel).

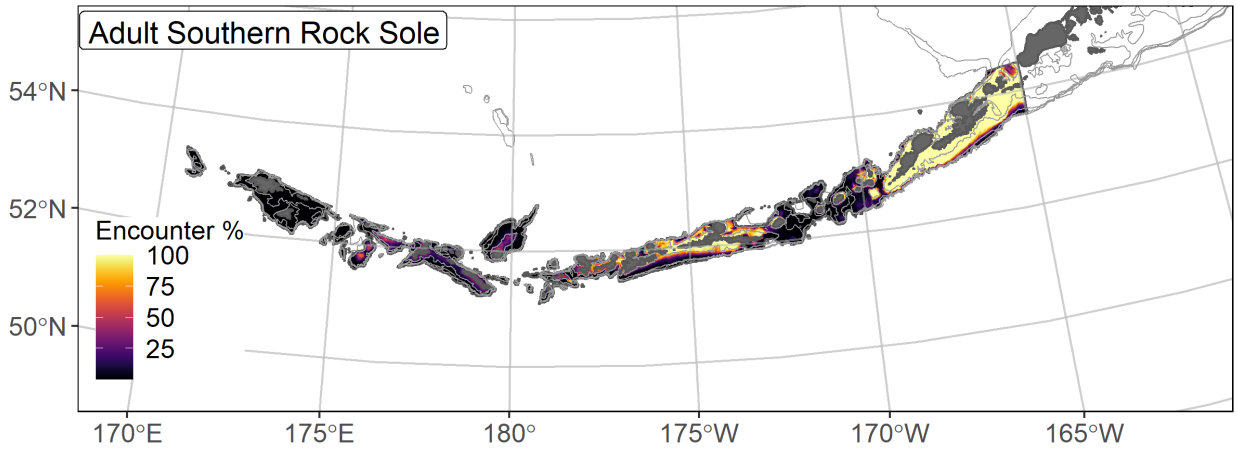


Figure 70. -- Encounter probability of adult southern rock sole from AFSC RACE-GAP summer bottom trawl surveys (1996–2019) of the AI with the 100 m, 300 m, and 500 m isobaths indicated.

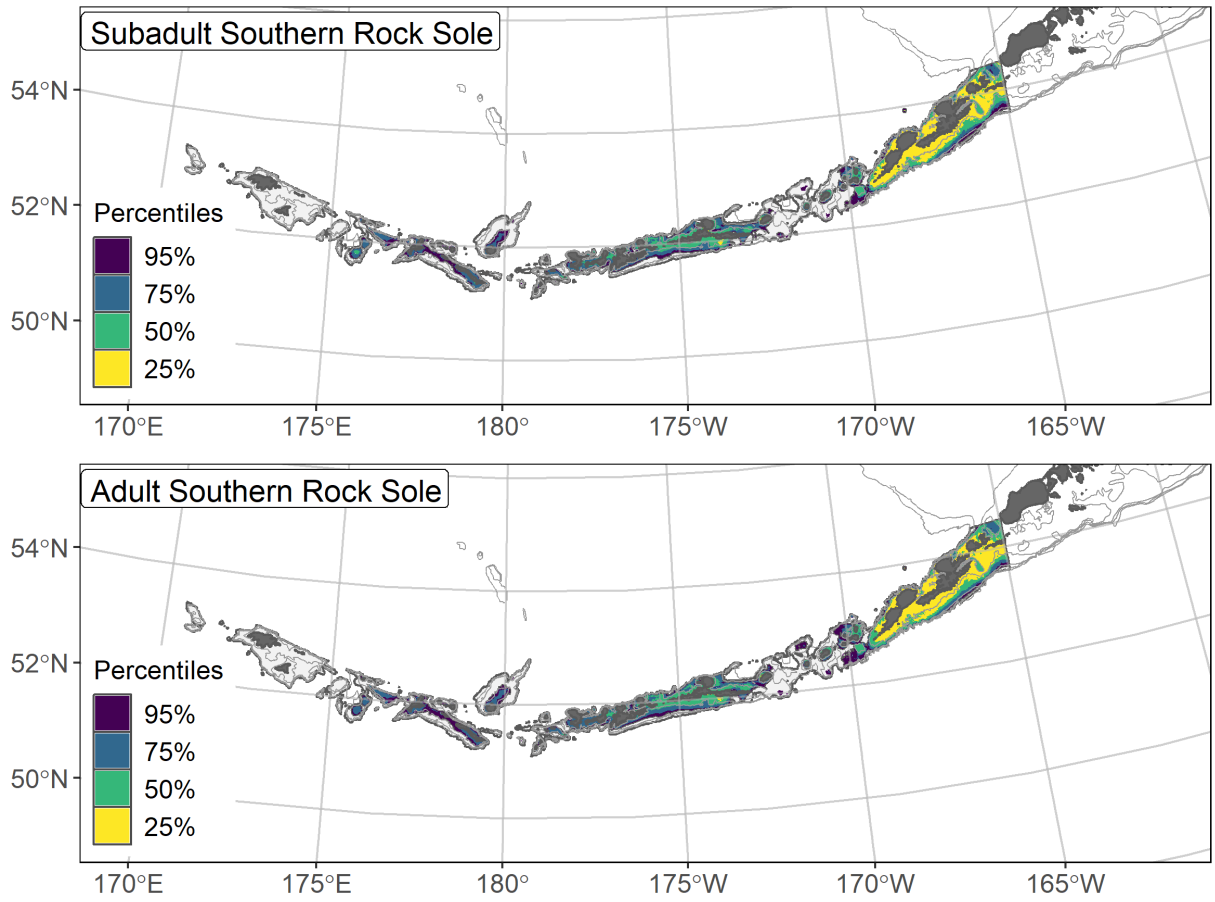


Figure 71. -- Essential fish habitat (EFH area) defined as the top 95% of numerical abundance predictions from a habitat-based ensemble fitted to subadult (top) and adult (bottom) southern rock sole distribution and abundance in AFSC RACE-GAP summer bottom trawl surveys (1996–2019) with 100 m, 300 m, and 500 m isobaths indicated; internal to the EFH map are the subareas of the top 25% (EFH hot spots), top 50% (core EFH area), and top 75% (principal EFH area) of habitat-related, ensemble-predicted numerical abundance.

## Roundfishes

### Atka mackerel (*Pleurogrammus monopterygius*)

Atka mackerel (*Pleurogrammus monopterygius*) is a member of the greenling family (Hexagrammidae) that is found across the northern Pacific Ocean from the Kuril Islands to the eastern GOA, with the largest concentrations found around Atka Island in the western AI (Lauth et al. 2007). The maturity schedule of Atka mackerel varies by region and growth conditions, though this study used an intermediate value of 344 mm FL ($L_{50}$; McDermott and Lowe 1997). Atka mackerel form nests in rocky habitat, and males guard the developing eggs for several months (Lauth et al. 2007). Adult Atka mackerel are an important component in the diets of several marine mammals, particularly Stellers sea lions (Sinclair et al. 2013) and are an important commercial stock, with most of the catch sold for export (Lowe et al. 2019).

**Subadult Atka mackerel distribution and predicted abundance from RACE-GAP summer bottom trawl surveys in the Aleutian Islands –** Subadult Atka mackerel catches from the RACE-GAP summer survey were common throughout the AI (Fig. 72). The largest catches were located in the central and western AI. The final ensemble contains three SDMs, with the $GAM_{nb}$ given slightly less weight than the others. The ensemble had a fair to good fit to the data (Table 23). Specifically, it showed a "fair" ability to predict catches where this life stage is present (AUC = 0.73) and explained a fair amount of the deviance in the data (PDE = 0.38). It performed slightly better at predicting high or low abundance catches ($\rho = 0.54$). Atka mackerel catches were extremely variable, and taken together, these metrics suggest that the model adequately predicted subadult distribution, but it was not as useful for predicting exact abundance. Geographic position and bottom depth were the most important covariates and accounted for 69.1% of the deviance explained by the ensemble (Table 24), though tidal

maximum and current variability also contributed. In general, high abundance was predicted in farther west longitudes, shallow depths, and moderate tidal currents (Fig. 73). Predicted abundance was highest in the areas around and west of the Rat Islands and was predicted to be moderate almost everywhere in the AI (Fig. 73). The ensemble predicted CV of abundance tended to be high in areas with average abundance (Fig. 73). The ensemble predicted high encounter probabilities throughout the region (Fig. 74).

**Adult Atka mackerel distribution and predicted abundance from RACE-GAP summer bottom trawl surveys in the Aleutian Islands –** Adult Atka mackerel catches from the RACE-GAP summer survey were common throughout nearly all of the AI, with the largest catches occurring in the western AI (Fig. 75). The ensemble contained four SDMs weighted almost equally and had a fair fit to the data (Table 23). The ensemble scored well in terms of predicting abundance ($\rho = 0.52$) and fair deviance explained (PDE = 0.36) but poorly in terms of predicting presence versus absence in catches (AUC = 0.65). This discrepancy is a consequence of the very patchy distribution of Atka mackerel catches. When the ensemble predicts a high average abundance at a location, it also assumes a consistent presence in trawl survey catches at that location. However, Atka mackerel can be absent from many tows before being caught in large numbers. Thus, the predictions of abundance can be accurate on average while over-predicting presence in individual hauls. Bottom depth and geographic position were the two most important covariates, accounting for 63.0% of the deviance explained by the ensemble (Table 24). Bottom current, current variability, and tidal maximum also accounted for a substantial faction of the deviance explained. Adult Atka mackerel are predicted to be abundant at shallow depths, favoring farther west areas in the AI (Fig. 76). Minor predictors of adult Atka mackerel abundance included southwesterly currents, moderate tidal currents, and warm temperatures.

Predicted abundance was highest in the areas around and west of the Rat Islands. It was also high near Atka Island (Fig. 76). The predicted CV of abundance was fairly uniform across most of the AI (Fig. 76). The ensemble predicted that the encounter probability for adult Atka mackerel was nearly 100% across the entire AI (Fig. 77). However, Atka mackerel did not conform to the assumption that high average abundance results in high encounter probability, and this species was absent from trawl catches more often than expected. While the map of predicted abundance accurately represents average trawl catches, the map of encounter probability should be used with caution.

**Essential fish habitat of subadult and adult Atka mackerel in the Aleutian Islands –**

The habitat-related abundance predictions based on RACE-GAP summer bottom trawl data (1991–2019) were translated into EFH area and subareas (Fig. 78). The EFH area for subadult and adult Atka mackerel was almost identical and encompassed nearly all of the survey area. The largest EFH hot spots for both life stages occurred along the islands in the central AI, with a second large area located east of Atka Island. Subadults have a slightly more western distribution with a larger hot spot in the far west near Attu Island, whereas adults have a slightly more eastern distribution, with a hot spot predicted along the edge of the AI survey area near Unimak Pass.

Table 23. -- Constituent species distribution models (SDMs) used to construct Essential Fish Habitat (EFH) for a) subadult and b) adult Atka mackerel: MaxEnt = Maximum entropy; paGAM = presence-absence generalized additive model; hGAM = hurdle GAM; $GAM_P$ = standard Poisson GAM; and $GAM_{nb}$ = standard negative-binomial GAM. Ensemble performance (ρ = Spearman's rank correlation coefficient), root-mean-square-error (RMSE), the area under the receiver operating characteristic (AUC), and the Poisson deviance explained (PDE) were generated from k-fold cross-validation. The "--" in a field indicates that this SDM was not included in the final ensemble.

**a) subadult Atka mackerel**

| Models | RMSE | Relative Weight | ρ | AUC | PDE | EFH area ($km^2$) |
|---|---|---|---|---|---|---|
| MaxEnt | 1,140 | 0.35 | 0.47 | 0.80 | 0.31 | 77,600 |
| paGAM | 1,147 | 0.35 | 0.52 | 0.83 | 0.30 | 77,700 |
| hGAM | -- | 0 | -- | -- | -- | -- |
| $GAM_P$ | -- | 0 | -- | -- | -- | -- |
| $GAM_{nb}$ | 1,232 | 0.30 | 0.51 | 0.83 | 0.32 | 61,200 |
| ensemble | 1,131 | 1 | 0.54 | 0.73 | 0.38 | 77,700 |

**b) adult Atka mackerel**

| Models | RMSE | Relative Weight | ρ | AUC | PDE | EFH area ($km^2$) |
|---|---|---|---|---|---|---|
| MaxEnt | 1,254 | 0.25 | 0.49 | 0.77 | 0.23 | 77,700 |
| paGAM | 1,268 | 0.24 | 0.49 | 0.77 | 0.16 | 77,700 |
| hGAM | 1,255 | 0.25 | 0.45 | 0.77 | 0.26 | 73,100 |
| $GAM_P$ | 1,222 | 0.26 | 0.46 | 0.71 | 0.31 | 60,900 |
| $GAM_{nb}$ | 1,347 | 0 | 0.47 | 0.75 | 0.18 | -- |
| ensemble | 1,190 | 1 | 0.52 | 0.65 | 0.36 | 77,700 |

Table 24. -- Covariates retained in the a) subadult and b) adult Atka mackerel species distribution model (SDM) final ensembles, the percent contribution to the ensemble deviance explained by each, and the cumulative percent deviance: SD = standard deviation, and BPI = bathymetric position index.

| Atka mackerel | Covariate | % Contribution | Cumulative % Contribution |
|---|---|---|---|
| **a) subadult** | bottom depth | 35.1 | 35.1 |
| | position | 33.9 | 69.1 |
| | tidal maximum | 7.4 | 76.4 |
| | current SD | 5.1 | 81.5 |
| | aspect north | 3.9 | 85.4 |
| | current | 2.9 | 88.3 |
| | slope | 2.9 | 91.2 |
| | aspect east | 2.3 | 93.5 |
| | bottom temperature | 1.9 | 95.4 |
| | coral presence | 1.7 | 97.1 |
| | sponge presence | 0.7 | 97.8 |
| | rockiness | 0.6 | 98.4 |
| | BPI | 0.6 | 99.0 |
| | pennatulacean presence | 0.5 | 99.5 |
| | curvature | 0.5 | 100 |
| **a) adult** | bottom depth | 37.1 | 37.1 |
| | position | 22.2 | 59.3 |
| | current | 8.3 | 67.6 |
| | tidal maximum | 5.5 | 73.1 |
| | current SD | 4.8 | 78.0 |
| | aspect east | 4.0 | 82.0 |
| | bottom temperature | 3.6 | 85.6 |
| | aspect north | 3.4 | 89.0 |
| | slope | 3.2 | 92.2 |
| | BPI | 2.6 | 94.8 |
| | sponge presence | 2.2 | 97.0 |
| | rockiness | 1.2 | 98.2 |
| | coral presence | 0.8 | 99.0 |
| | pennatulacean presence | 0.7 | 99.7 |
| | curvature | 0.3 | 100 |

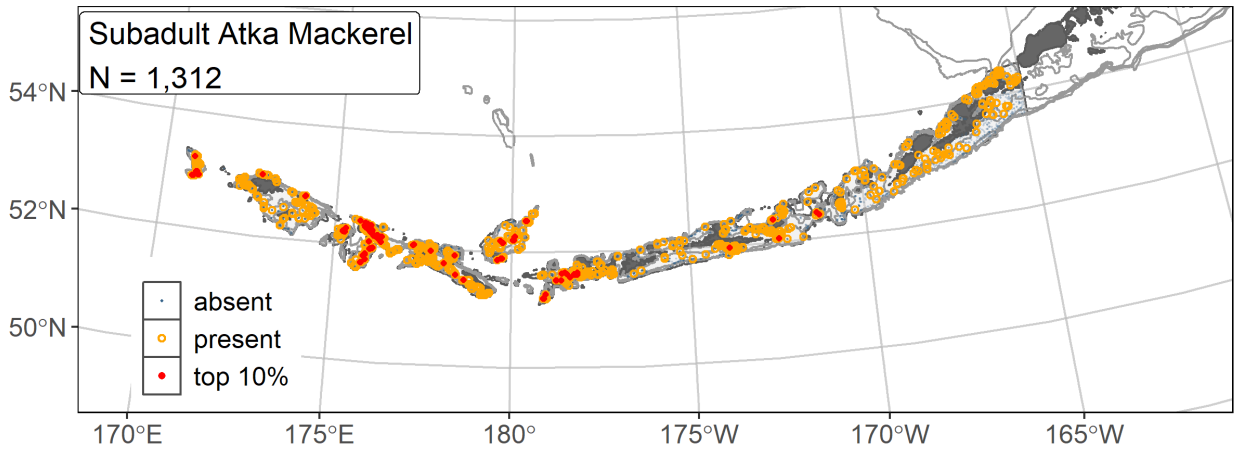


Figure 72. -- Distribution of subadult Atka mackerel catches (N = 1,312) in 1991–2019 AFSC RACE-GAP summer bottom trawl surveys of the AI with the 100 m, 300 m, and 500 m isobaths indicated; filled red circles indicate locations in top 10% of overall abundance, open orange circles indicate presence in remaining catches, and small blue dots indicate absence.

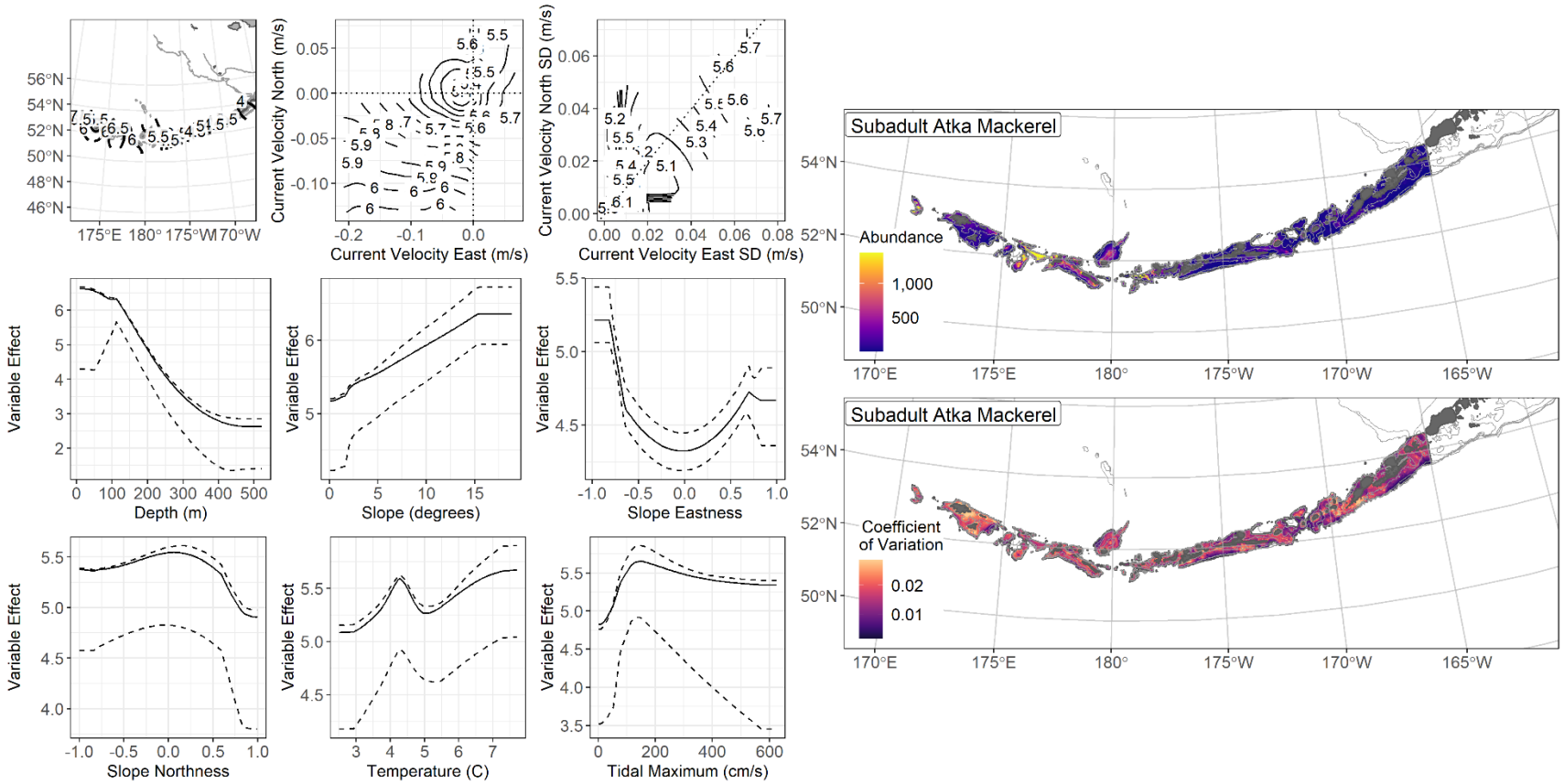


Figure 73. -- The top nine covariate effects (left panel) on ensemble-predicted subadult Atka mackerel numerical abundance across the AI (upper right panel) alongside the coefficient of variation of the ensemble predictions (lower right panel).

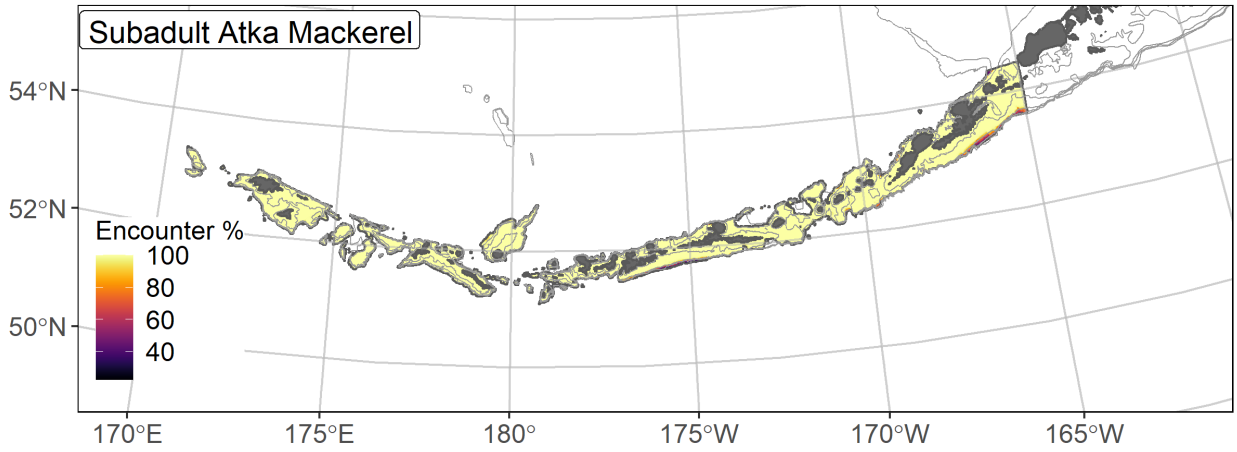


Figure 74. -- Encounter probability of subadult Atka mackerel from AFSC RACE-GAP summer bottom trawl surveys (1991–2019) of the AIwith the 100 m, 300 m, and 500 m isobaths indicated.

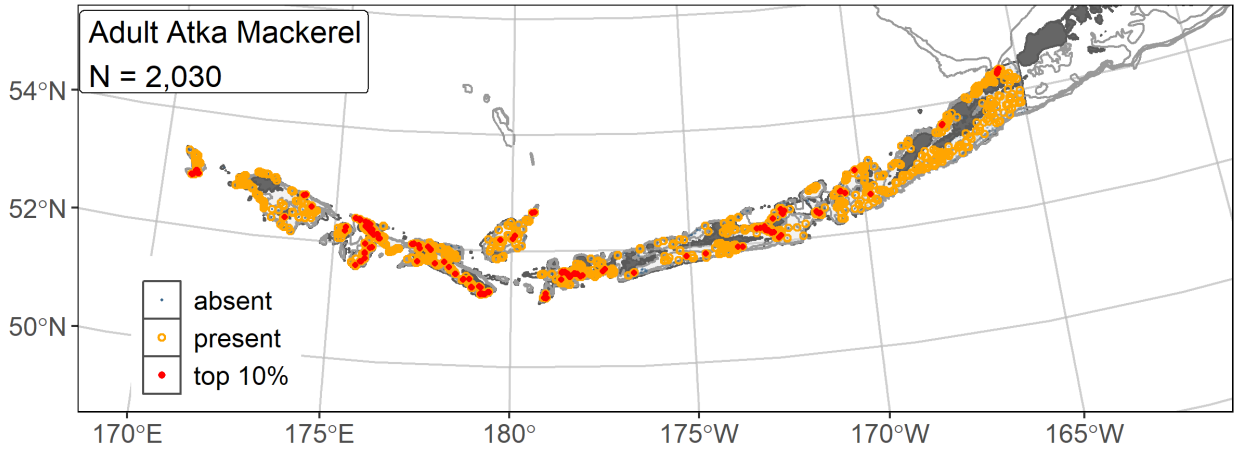


Figure 75. -- Distribution of adult Atka mackerel catches (N = 2,030) in 1991–2019 AFSC RACE-GAP summer bottom trawl surveys of the AI with the 100 m, 300 m, and 500 m isobaths indicated; filled red circles indicate locations in top 10% of overall abundance, open orange circles indicate presence in remaining catches, and small blue dots indicate absence.

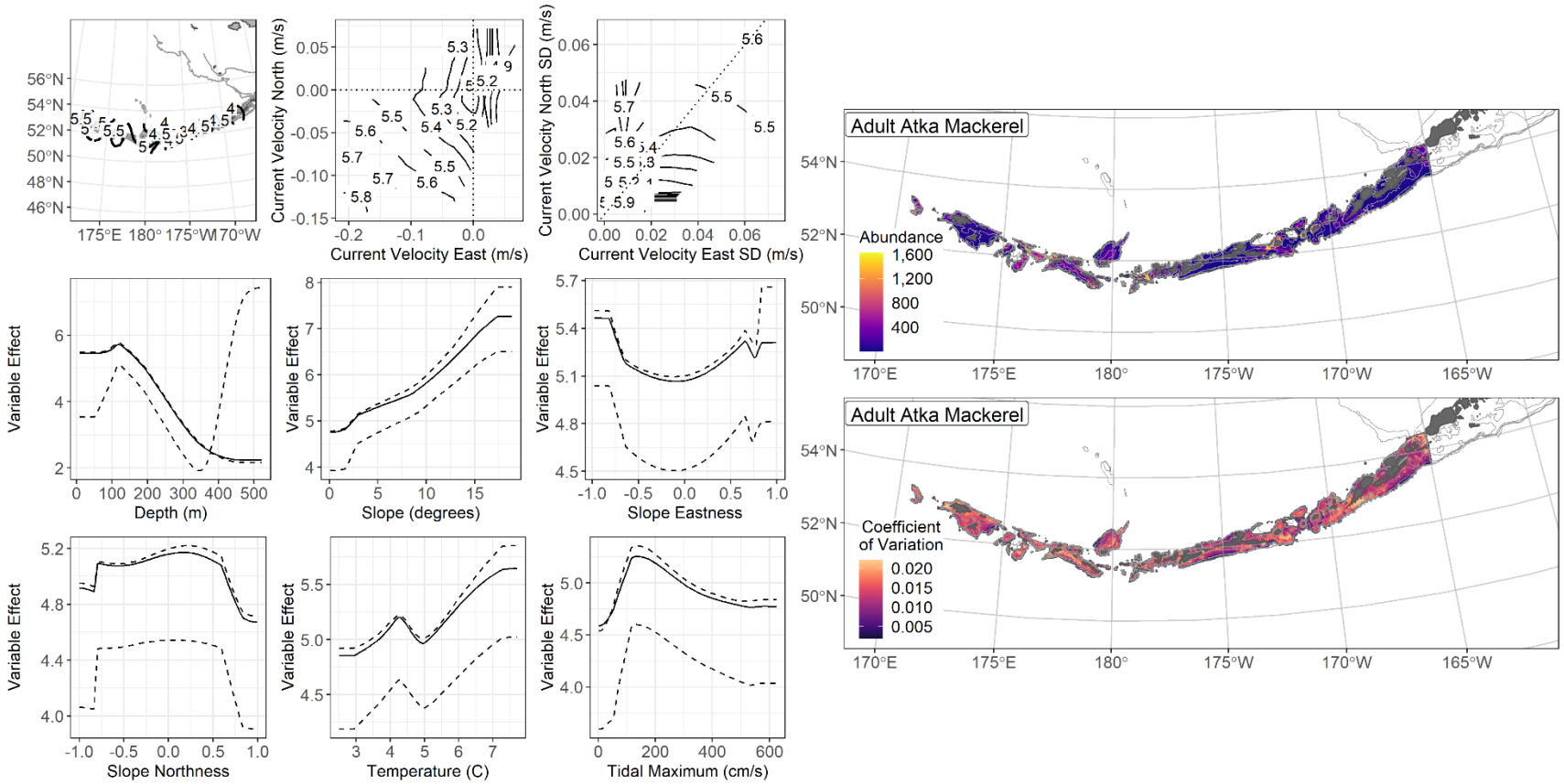


Figure 76. -- The top nine covariate effects (left panel) on ensemble-predicted adult Atka mackerel numerical abundance across the AI (upper right panel) alongside the coefficient of variation of the ensemble predictions (lower right panel).

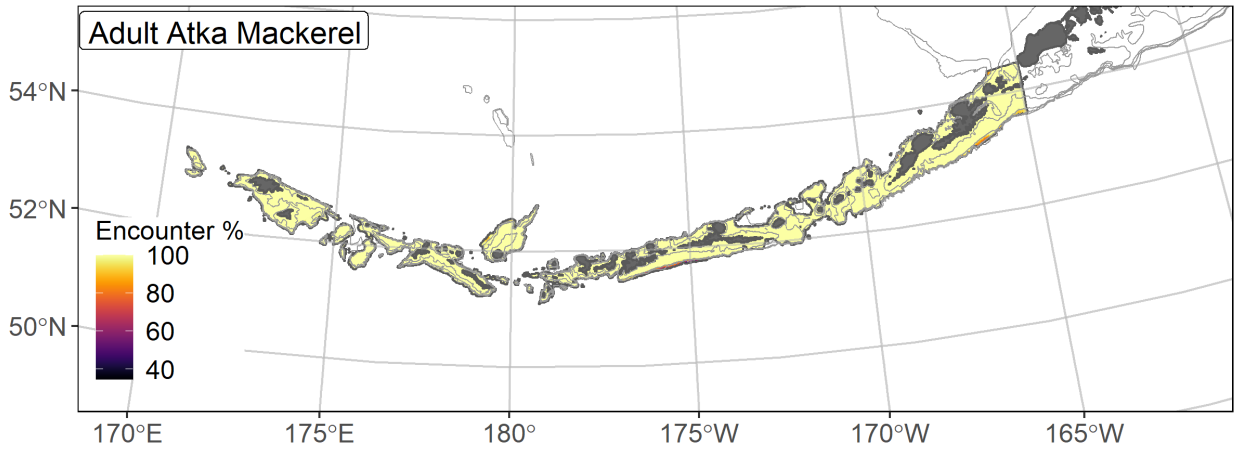


Figure 77. -- Encounter probability of adult Atka mackerel from AFSC RACE-GAP summer bottom trawl surveys (1991–2019) of the AI with the 100 m, 300 m, and 500 m isobaths indicated.

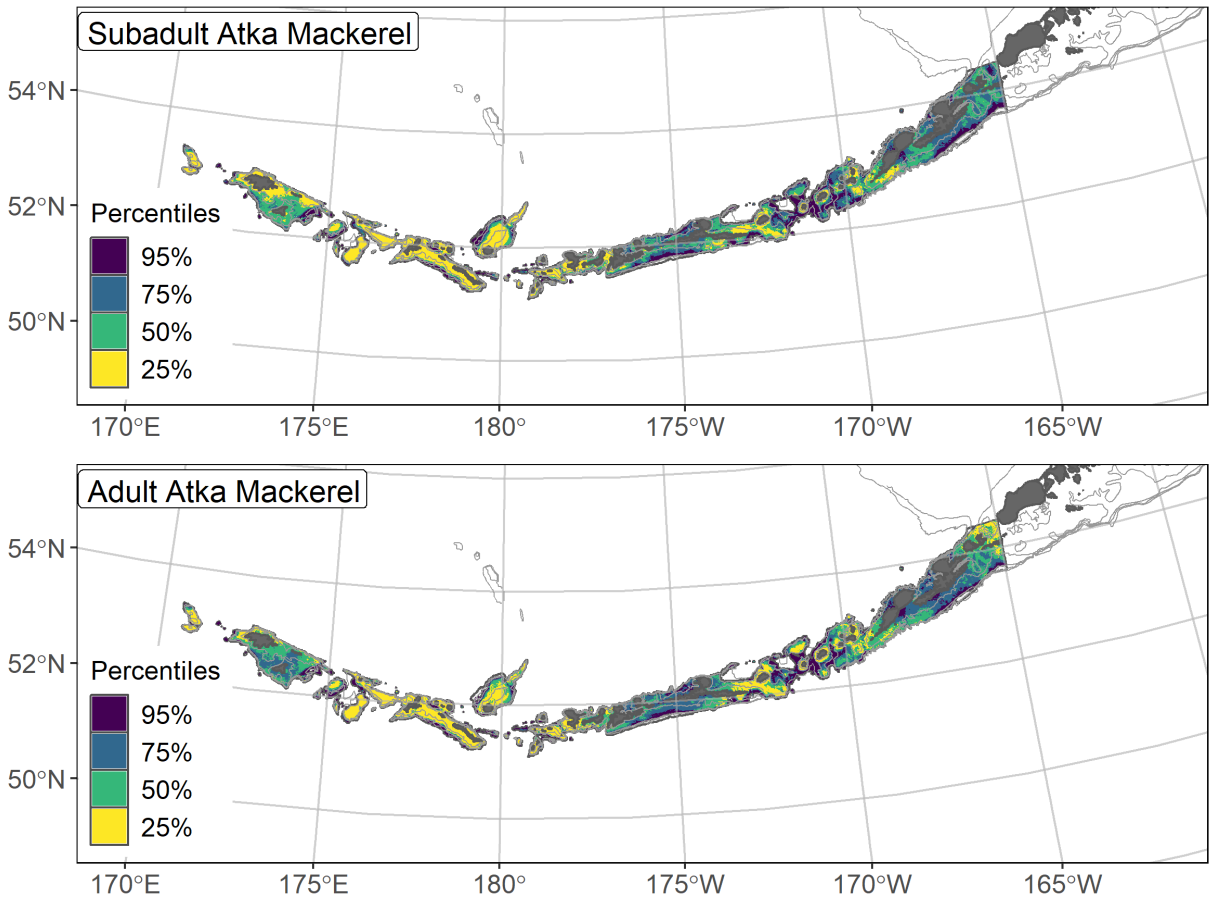


Figure 78. -- Essential fish habitat (EFH area) defined as the top 95% of numerical abundance predictions from a habitat-based ensemble fitted to subadult (top) and adult (bottom) Atka mackerel distribution and abundance in AFSC RACE-GAP summer bottom trawl surveys (1991–2019) with 100 m, 300 m, and 500 m isobaths indicated; internal to the EFH map are the subareas of the top 25% (EFH hot spots), top 50% (core EFH area), and top 75% (principal EFH area) of habitat-related, ensemble-predicted numerical abundance.

**Pacific cod (*Gadus macrocephalus*)**

Pacific cod (*Gadus macrocephalus*) occur from the shoreline to 500 m throughout the RACE-GAP study area and support an important multi-gear commercial fishery throughout Alaskan waters (Thompson et al. 2020). Tagging studies have shown that Pacific cod move between the EBS, AI, and GOA (Shimada and Kimura 1994, Bryan et al. 2021), but genetic research indicates discrete stocks in the EBS and AI (Canino et al. 2010, Spies 2012). They form aggregations during peak spawning season (Neidetcher et al. 2014) and lay demersal, adhesive eggs with a narrow thermal window for successful incubation (3–6°C). After hatching, the larvae enter an epipelagic phase and move ontogenetically toward the bottom, with early juveniles (< 150 mm FL; Laurel et al. 2009) more shallowly distributed than later life stages. Subadults settle into habitats near the bottom for several years before reaching maturity at 580 mm FL ($L_{50}$; Stark 2007). Settled early juveniles were not common in the trawl survey and there was insufficient data to construct a SDM for this life stage. Pacific cod were managed as a combined stock across the EBS and AI until 2013, but they have had separate harvest specifications in each region since 2014.

**Subadult Pacific cod distribution and predicted abundance from RACE-GAP summer bottom trawl surveys in the Aleutian Islands –** Subadult Pacific cod were common across the RACE-GAP summer survey of the AI (Fig. 79). Large catches occurred throughout the region and were absent only around the passes where deep water flows from the Pacific Ocean to the Bering Sea. The final ensemble contained four SDMs with approximately equal weights, and it showed a fair to good performance in terms of model fit (Table 25). Specifically, the ensemble demonstrated good accuracy at predicting relatively high or low density catches ($\rho = 0.47$), and it showed fair scores at measures of predicting presence or absence (AUC = 0.74) and in terms of

deviance explained (PDE = 0.28). The good score for ρ suggested that the ensemble may predict the presence or absence of subadult Pacific cod catches but may not accurately predict abundance. Bottom depth was the most important covariate in the ensemble and accounted for 47.0% of the deviance explained by the ensemble, though geographic position, current, and slope were also important (Table 26). In general, predicted abundance was high in locations less than 250 m depth, with westerly currents and a sloping bottom (Fig. 80). Although past research suggests that temperature can be an important driver of subadult Pacific cod distribution, there is relatively little variation in summer bottom temperature in the AI (Fig. 2), so temperature did not explain much of the variation in observed abundance. The predicted abundance map showed that this life stage is present across most of the AI, but the highest concentrations occurred around Atka and Adak islands, as well as in the east near Unimak Pass (Fig. 80). The predicted CV of abundance was low in most areas, reflecting that Pacific cod are consistently present in the bottom trawl catch (Fig. 80). Estimated encounter probabilities for subadult Pacific cod were near 100% in all but a few areas along the 500 m depth contour (Fig. 81).

**Adult Pacific cod distribution and predicted abundance from RACE-GAP summer bottom trawl surveys in the Aleutian Islands –** Adult Pacific cod were ubiquitous in catches from the RACE-GAP summer survey area (Fig. 82). There was no clear pattern to large catches, and large aggregations of Pacific cod occurred throughout the entirety of the AI. The final ensemble contained four SDMs with equal weights and demonstrated a fair to good fit to the observed data (Table 25). The fit metrics for adult Pacific cod were very similar to those for subadults, and the ensemble scored well in predicting the highest and lowest abundance catches (ρ = 0.50) but only fair according to other measures of fit (AUC = 0.76; PDE = 0.37). As with subadults, the values for these metrics suggest that the ensemble accurately predicts high versus low densities but it

may less accurately predict observed abundance. Bottom depth and geographic position were the most important covariates and accounted for 52.0% of the deviance explained by the ensemble, but current covariates, tidal maximum, and substrate rockiness were also important (Table 26). The model predicted high adult abundance in places with depths less than 300 m, more eastern longitudes, and areas with southwesterly currents, moderate tidal currents, and somewhat rocky substrates (Fig. 83). Adult Pacific cod occurred in most places shallower than 300 m, but the highest catches were predicted for the eastern AI around the Islands of Four Mountains and near Unimak Pass (Fig. 83). The predicted CV of abundance was elevated along the edge of the continental shelf in areas around 300 m deep, reflecting that high catches can sometimes occur outside or on the boundary of the modelled depth range (Fig. 83). Like subadults, the encounter probability for adults was near 100% across almost the entire AI region, save a few deeper locations along the continental slope (Fig. 84).

**Essential fish habitat of subadult and adult Pacific cod in the Aleutian Islands –** The habitat-related abundance predictions based on RACE-GAP summer bottom trawl data (1991–2019) were translated into EFH area and subareas (Fig. 85). Both life stages of Pacific cod were very common and had EFH areas that encompassed almost the entire survey area. Subadults had EFH hot spots predicted around Unimak Pass, the Andreanof Islands, and in the western AI near Attu Island. All areas shallower than 100 m were designated EFH, and areas deeper than 300 m were generally not EFH. Adult Pacific cod shared an EFH hot spot with subadults near Unimak Pass but they had a large hot spot around the Islands of Four Mountains that was not shared with subadults. The area around the Islands of Four Mountains has greater bottom depths and stronger currents, both associated with high adult abundance.

Table 25. -- Constituent species distribution models (SDMs) used to construct Essential Fish Habitat (EFH) for a) subadult and b) adult Pacific cod: MaxEnt = Maximum entropy; paGAM = presence-absence generalized additive model; hGAM = hurdle GAM; $GAM_P$ = standard Poisson GAM; and $GAM_{nb}$ = standard negative-binomial GAM. Ensemble performance (ρ = Spearman's rank correlation coefficient), root-mean-square-error (RMSE), the area under the receiver operating characteristic (AUC), and the Poisson deviance explained (PDE) were generated from k-fold cross-validation. The "--" in a field indicates that this SDM was not included in the final ensemble.

**a) subadult Pacific cod**

| Models | RMSE | Relative weight | ρ | AUC | PDE | EFH area ($km^2$) |
|---|---|---|---|---|---|---|
| MaxEnt | 35.3 | 0.24 | 0.39 | 0.72 | 0.09 | 76,600 |
| paGAM | 34.9 | 0.25 | 0.44 | 0.74 | 0.17 | 76,500 |
| hGAM | 34.8 | 0.25 | 0.40 | 0.74 | 0.21 | 67,400 |
| $GAM_P$ | 34.8 | 0.25 | 0.40 | 0.70 | 0.20 | 67,800 |
| $GAM_{nb}$ | 35.0 | 0 | 0.42 | 0.71 | 0.21 | -- |
| ensemble | 34.1 | 1 | 0.47 | 0.74 | 0.28 | 74,100 |

**b) adult Pacific cod**

| Models | RMSE | Relative weight | ρ | AUC | PDE | EFH area ($km^2$) |
|---|---|---|---|---|---|---|
| MaxEnt | 44.3 | 0.23 | 0.45 | 0.74 | 0.15 | 77,300 |
| paGAM | 43.4 | 0.24 | 0.49 | 0.77 | 0.19 | 77,600 |
| hGAM | 41.7 | 0.26 | 0.42 | 0.75 | 0.31 | 73,700 |
| $GAM_P$ | 41.8 | 0.26 | 0.42 | 0.71 | 0.30 | 73,500 |
| $GAM_{nb}$ | 42.9 | 0 | 0.48 | 0.75 | 0.27 | -- |
| ensemble | 40.4 | 1 | 0.50 | 0.76 | 0.37 | 77,600 |

Table 26. -- Covariates retained in the a) subadult and b) adult Pacific cod species distribution model (SDM) final ensembles, the percent contribution to the ensemble deviance explained by each, and the cumulative percent deviance: SD = standard deviation, and BPI = bathymetric position index.

| Pacific cod | Covariate | % Contribution | Cumulative % Contribution |
|---|---|---|---|
| **a) subadult** | bottom depth | 47.0 | 47.0 |
| | position | 12.1 | 59.1 |
| | current SD | 8.0 | 67.1 |
| | slope | 6.3 | 73.4 |
| | current | 5.7 | 79.1 |
| | BPI | 3.8 | 82.9 |
| | tidal maximum | 2.9 | 85.8 |
| | rockiness | 2.5 | 88.3 |
| | bottom temperature | 2.3 | 90.6 |
| | pennatulacean presence | 2.1 | 92.7 |
| | aspect east | 2.0 | 94.7 |
| | aspect north | 2.0 | 96.7 |
| | curvature | 2.0 | 98.7 |
| | sponge presence | 0.7 | 99.4 |
| | coral presence | 0.6 | 100 |
| **b) adult** | bottom depth | 39.6 | 39.6 |
| | position | 12.3 | 52.0 |
| | tidal maximum | 10.2 | 62.2 |
| | current | 7.5 | 69.7 |
| | slope | 6.7 | 76.4 |
| | rockiness | 6.7 | 83.1 |
| | current SD | 6.5 | 89.6 |
| | bottom temperature | 2.8 | 92.4 |
| | aspect east | 1.9 | 94.3 |
| | coral presence | 1.6 | 95.9 |
| | curvature | 1.4 | 97.3 |
| | aspect north | 1.1 | 98.4 |
| | BPI | 1.0 | 99.4 |
| | sponge presence | 0.4 | 99.8 |
| | pennatulacean presence | 0.2 | 100 |

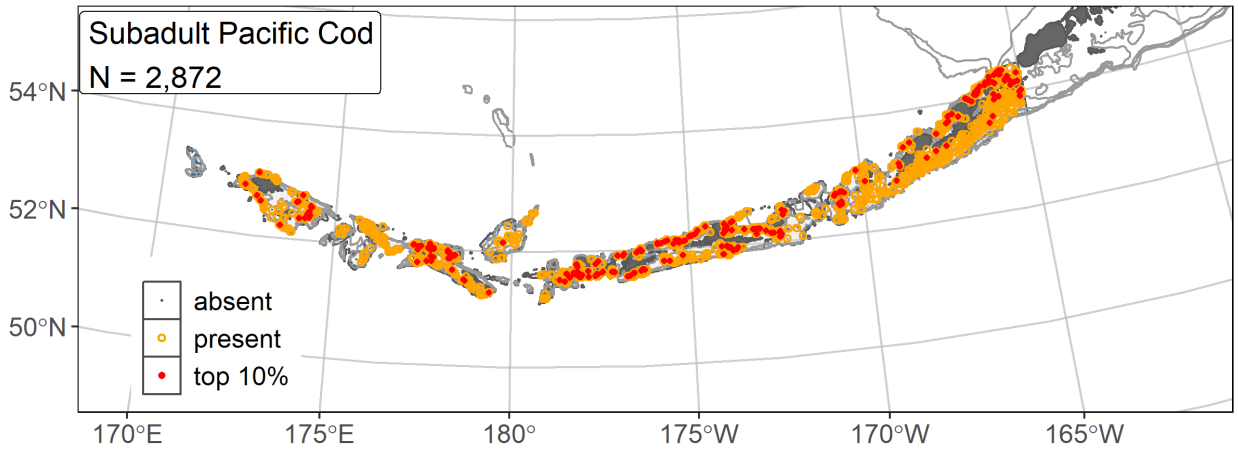


Figure 79. -- Distribution of subadult Pacific cod catches (N = 2,872) in 1991–2019 AFSC RACE-GAP summer bottom trawl surveys of the AI with the 100 m, 300 m, and 500 m isobaths indicated; filled red circles indicate locations in top 10% of overall abundance, open orange circles indicate presence in remaining catches, and small blue dots indicate absence.

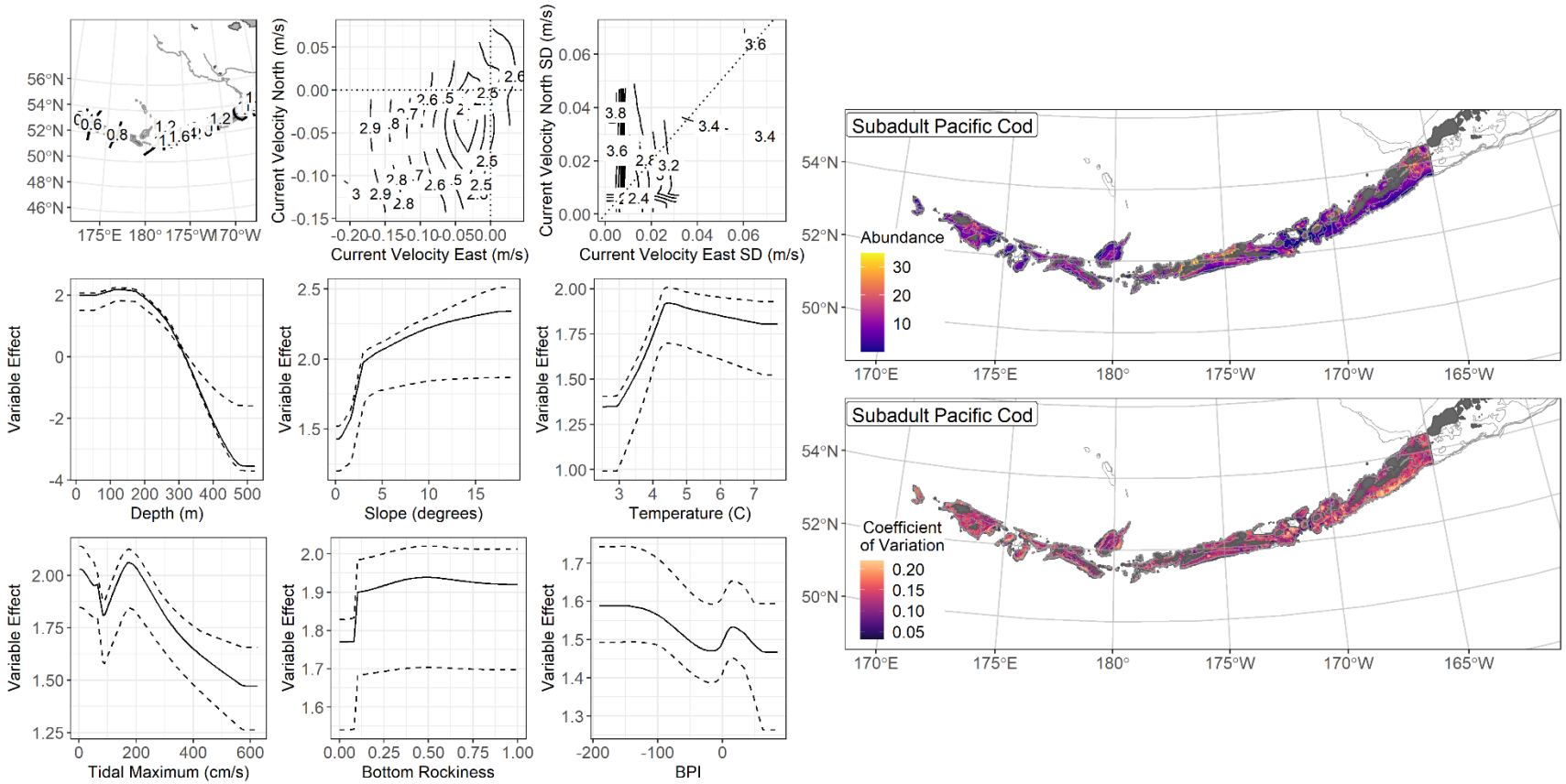


Figure 80. -- The top nine covariate effects (left panel) on ensemble-predicted subadult Pacific cod numerical abundance across the AI (upper right panel) alongside the coefficient of variation of the ensemble predictions (lower right panel).

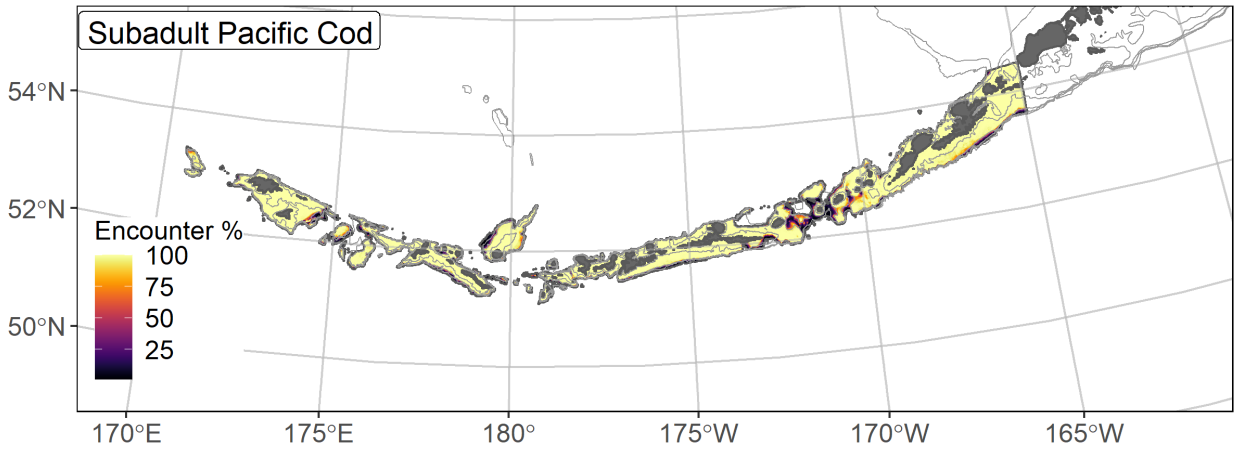


Figure 81. -- Encounter probability of subadult Pacific cod from AFSC RACE-GAP summer bottom trawl surveys (1991–2019) of the AI with the 100 m, 300 m, and 500 m isobaths indicated.

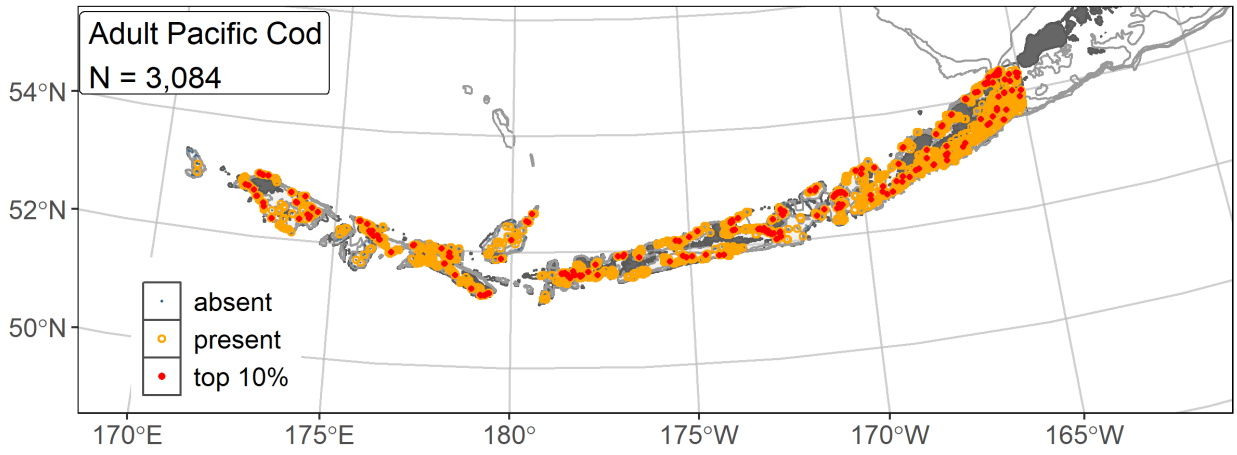


Figure 82. -- Distribution of adult Pacific cod catches (N = 3,084) in 1991–2019 AFSC RACE-GAP summer bottom trawl surveys of the AI with the 100 m, 300 m, and 500 m isobaths indicated; filled red circles indicate locations in top 10% of overall abundance, open orange circles indicate presence in remaining catches, and small blue dots indicate absence.

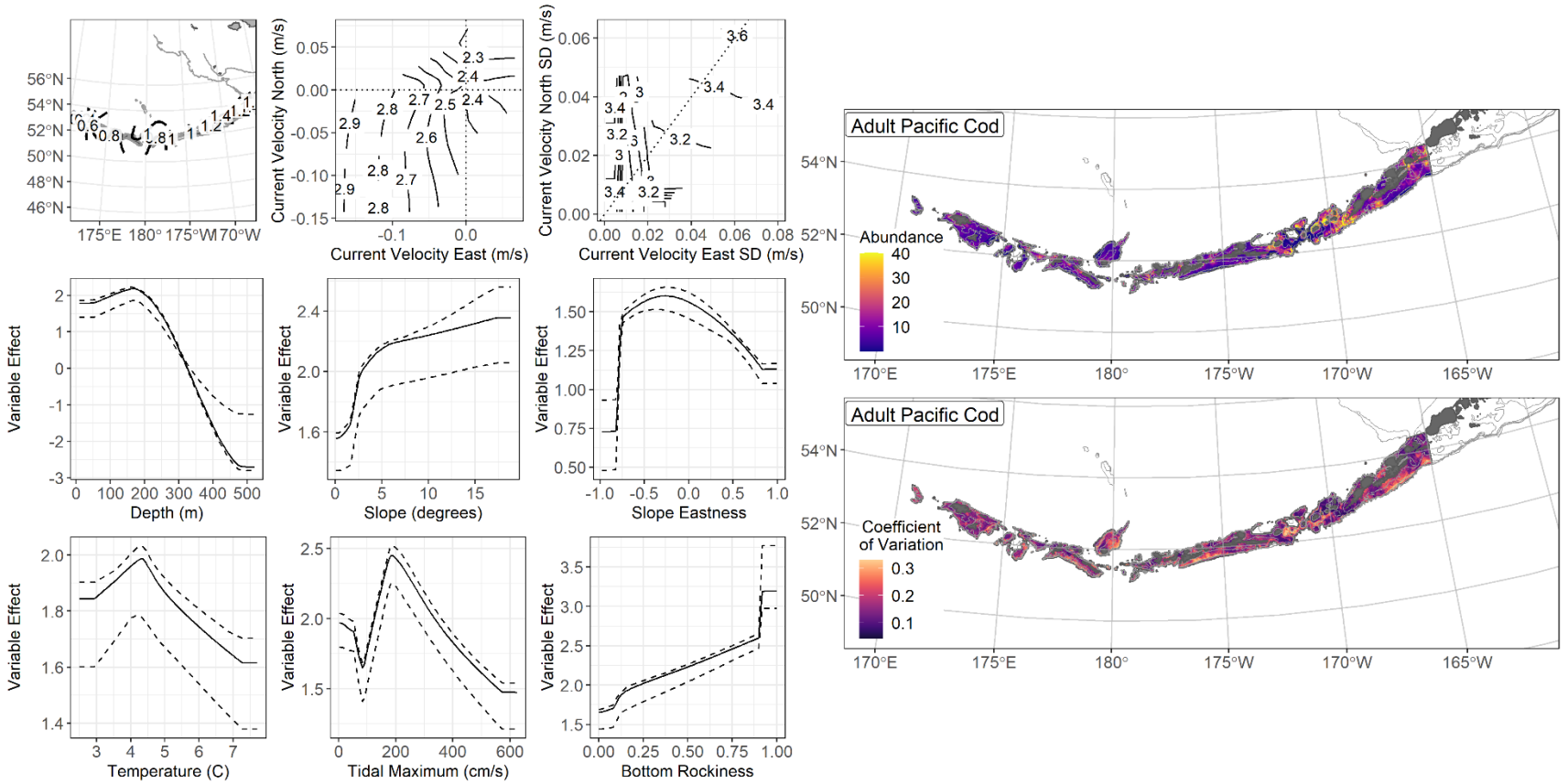


Figure 83. -- The top nine covariate effects (left panel) on ensemble-predicted adult Pacific cod numerical abundance across the AI (upper right panel) alongside the coefficient of variation of the ensemble predictions (lower right panel).

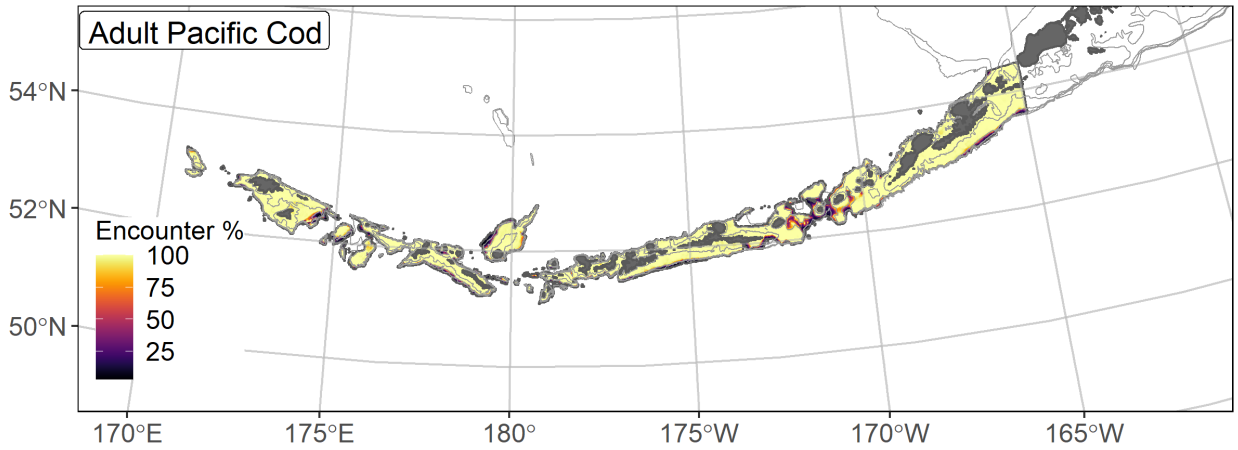


Figure 84. -- Encounter probability of adult Pacific cod from AFSC RACE-GAP summer bottom trawl surveys (1991–2019) of the AI with the 100 m, 300 m, and 500 m isobaths indicated.

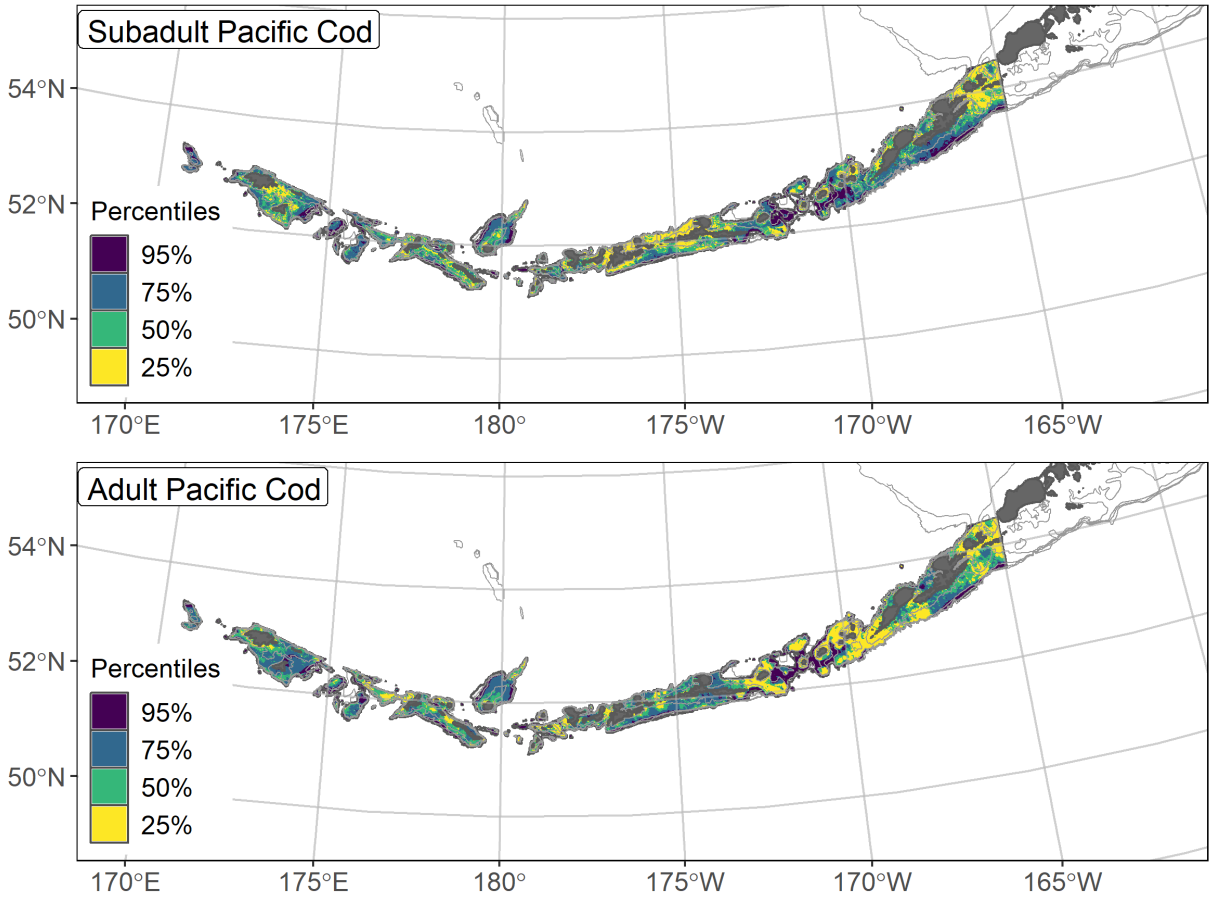


Figure 85. -- Essential fish habitat (EFH area) defined as the top 95% of numerical abundance predictions from a habitat-based ensemble fitted to subadult (top) and adult (bottom) Pacific cod distribution and abundance in AFSC RACE-GAP summer bottom trawl surveys (1991–2019) with 100 m, 300 m, and 500 m isobaths indicated; internal to the EFH map are the subareas of the top 25% (EFH hot spots), top 50% (core EFH area), and top 75% (principal EFH area) of habitat-related, ensemble-predicted numerical abundance.

**Sablefish (*Anoplopoma fimbria*)**

Sablefish (*Anoplopoma fimbria*) support an important commercial fishery in Alaska. Adults inhabit deep water (200–1,000 m) along the shelf break and upper continental slope from Baja California to Japan (Mecklenburg et al. 2002). Spawning typically occurs in deeper waters (300–500 m) near the shelf break (Mason et al. 1983) with eggs developing at depth and larvae developing near the surface (Wing 1997), and young fish typically settle in shallow coastal waters (Kendall and Matarese 1987). After overwintering in nearshore habitats, older juveniles migrate to deeper water, reaching adult habitat in three to four years (Rutecki and Varosi 1997). For the EFH descriptions in this study, we separated the settled early juvenile (150–399 mm FL; Sasaki 1985, Pirtle et al. 2019), subadult (400–585 mm FL; Rodgveller et al. 2018), and adult life stages (>585 mm FL) by length. The geographic extent of this population and the potential for large-scale movement of individuals (Heifetz and Fujioka 1991, Hanselman et al. 2015), have led to sablefish being managed as a single stock across Alaska (Goethel et al. 2020). The SDMs in the present work were parameterized with catches from the AFSC RACE-GAP summer bottom trawl survey of the AI, which typically does not sample depths below 500 m. Therefore, we recommend that AFSC longline survey data be integrated with AFSC RACE-GAP summer bottom trawl survey data into future EFH reviews[15].

**Subadult sablefish distribution and predicted abundance from RACE-GAP summer bottom trawl surveys in the Aleutian Islands –** Subadult sablefish catches in the RACE-GAP summer bottom trawl survey were common in deep water in the eastern AI, and rare west of 180° (Fig. 86). The final ensemble contained three SDMs, and the MaxEnt was weighted less

[15] A recommendation to add additional survey data types if possible to future SDM ensemble EFH mapping efforts for this species will be included as a future recommendation for research directions from the 2023 EFH 5-year Review.

than the other two (Table 27). The ensemble showed fair performance in terms of Spearman's correlation ($\rho = 0.39$), good performance according to deviance explained (PDE = 0.54), and excellent performance on the third (AUC = 0.93). The metrics suggested that the ensemble was excellent at predicting where sablefish are likely to be caught in the trawl survey, and that it is somewhat accurate at predicting the number of fish caught. However, these findings do not extend beyond the RACE-GAP survey grid, and should be considered in context with the potential limitations of bottom trawl gear. Bottom depth, geographic position, and bottom temperature were the most important covariates and accounted for a combined 76.5% of the deviance explained by the ensemble (Table 28). The ensemble predicted that abundance would be highest in areas east of 180°, with deeper depths and warmer bottom temperatures (Fig. 87). Predicted abundance was highest south of Unalaska Island at depths greater than 300 m and around the western end of the Andreanof Islands (Fig. 87). Predicted abundance was higher on the south side of the AI chain. The predicted CV of abundance was higher along the continental slope, reflecting that the catch in these locations can be quite variable (Fig. 87). Locations shallower than 200 m typically had close to zero predicted abundance with little variation. Encounter probabilities for subadult sablefish were highest along much of the continental slope on the southern side of the Aleutian Island chain and east of 180°, as well as around amidst the Islands of Four Mountains (Fig. 88).

**Adult sablefish distribution and predicted abundance from RACE-GAP summer bottom trawl surveys in the Aleutian Islands –** Adult sablefish catches in the RACE-GAP summer survey were distributed similarly to the subadults; they were common along the continental slope areas east of 180° (Fig. 89). The three models in the final ensemble were assigned close to equal weights, and the ensemble did a good job of fitting the data (Table 27). Specifically, the

ensemble scored excellently at predicting presence or absence (AUC = 0.95) and explaining deviance (PDE = 0.66), but only fair in terms of ranking the catches by abundance ($\rho = 0.40$). Given the values of these metrics, the ensemble predictions accurately describe the distribution and much of the observed abundance of adult sablefish. As with subadults, caution should be used in interpreting these predictions, as they do not account for portions of the population below 500 m depth and reflect only the catch from bottom trawl gear. Bottom depth and geographic position were the most important covariates and accounted for 56.4% of the deviance explained by the ensemble (Table 28), though current and terrain curvature were also important covariates. Like subadults, adult sablefish were predicted to be abundant in the eastern AI and in deep water (Fig. 90). Unlike subadults, temperature was not a strong predictor of survey catches; instead, the model predicted high adult abundance in places with northeastern or southwestern currents and along terrain with a concave surface. Predicted abundance was highest in several places along the continental slope east of 180° (Fig. 90). Compared to subadults, adults tended to be located farther west and were less abundant south of Unalaska Island. The predicted CV of abundance was highest around many of the slope areas where adults were predicted to be abundant (Fig. 90). Encounter probabilities for adult sablefish followed the same pattern and were high along continental slope areas and low in shallow water (Fig. 91).

**Essential fish habitat of subadult and adult sablefish in the Aleutian Islands –**

The habitat-related abundance predictions based on RACE-GAP summer bottom trawl data (1991–2019) were translated into EFH area and subareas (Fig. 92). The EFH areas for the two life stages of sablefish were almost identical. Both show EFH hot spots along most of the continental slope east of 180°, particularly south of the AI chain. The areas at the west end of the Andreanof Islands and the Islands of Four Mountains were also included in the core EFH.

Subadults differ from adults in that their EFH area is more likely to extend into shallow water, particularly in the eastern AI south of Unalaska Island. It is well-established that much of the sablefish population, especially adults, is found below 500 m and thus is not accessible to the bottom trawl survey. The addition of data from longline surveys would allow EFH for this species to be defined across its entire habitat.

Table 27. – Constituent species distribution models (SDMs) used to construct Essential Fish Habitat (EFH) for a) subadult and b) adult sablefish: MaxEnt = Maximum entropy; paGAM = presence-absence generalized additive model; hGAM = hurdle GAM; $GAM_P$ = standard Poisson GAM; and $GAM_{nb}$ = standard negative-binomial GAM. Ensemble performance (ρ = Spearman's rank correlation coefficient), root-mean-square-error (RMSE), the area under the receiver operating characteristic (AUC), and the Poisson deviance explained (PDE) were generated from k-fold cross-validation. The "--" in a field indicates that this SDM was not included in the final ensemble.

**a) subadult sablefish**

| Models | RMSE | Relative Weight | ρ | AUC | PDE | EFH area ($km^2$) |
|---|---|---|---|---|---|---|
| MaxEnt | 13.0 | 0.24 | 0.39 | 0.90 | 0.22 | 39,700 |
| paGAM | 10.4 | 0.38 | 0.43 | 0.93 | 0.42 | 43,800 |
| hGAM | 19.9 | 0 | 0.08 | 0.93 | -2.73 | -- |
| $GAM_P$ | 10.5 | 0.37 | 0.40 | 0.90 | 0.40 | 29,800 |
| $GAM_{nb}$ | 11.9 | 0 | 0.44 | 0.93 | 0.37 | -- |
| ensemble | 9.7 | 1 | 0.43 | 0.93 | 0.54 | 41,400 |

**b) adult sablefish**

| Models | RMSE | Relative Weight | ρ | AUC | PDE | EFH area ($km^2$) |
|---|---|---|---|---|---|---|
| MaxEnt | -- | 0 | -- | -- | -- | -- |
| paGAM | 9.65 | 0.36 | 0.40 | 0.95 | 0.43 | 32,600 |
| hGAM | 10.17 | 0.32 | 0.38 | 0.95 | 0.32 | 33,600 |
| $GAM_P$ | 10.29 | 0.32 | 0.38 | 0.92 | 0.28 | 24,000 |
| $GAM_{nb}$ | 11.41 | 0 | 0.42 | 0.95 | 0.43 | -- |
| ensemble | 8.11 | 1 | 0.40 | 0.95 | 0.66 | 33,100 |

Table 28. -- Covariates retained in the a) subadult and b) adult sablefish species distribution model (SDM) final ensembles, the percent contribution to the ensemble deviance explained by each, and the cumulative percent deviance: SD = standard deviation, and BPI = bathymetric position index.

| sablefish | Covariate | % Contribution | Cumulative % Contribution |
|---|---|---|---|
| **a) subadult** | bottom depth | 35.6 | 35.6 |
| | position | 30.1 | 65.8 |
| | bottom temperature | 10.7 | 76.5 |
| | current | 5.3 | 81.8 |
| | tidal maximum | 4.6 | 86.4 |
| | current SD | 3.2 | 89.6 |
| | aspect north | 3.2 | 92.8 |
| | aspect east | 2.4 | 95.2 |
| | rockiness | 1.7 | 96.9 |
| | slope | 1.1 | 98.0 |
| | pennatulacean presence | 0.8 | 98.8 |
| | sponge presence | 0.4 | 99.2 |
| | curvature | 0.3 | 99.5 |
| | BPI | 0.3 | 99.8 |
| | coral presence | 0.2 | 100 |
| **a) adult** | bottom depth | 29.2 | 29.2 |
| | position | 27.1 | 56.4 |
| | curvature | 13.0 | 69.4 |
| | current | 8.1 | 77.5 |
| | slope | 5.9 | 83.4 |
| | tidal maximum | 4.3 | 87.7 |
| | BPI | 2.6 | 90.3 |
| | coral presence | 2.4 | 92.7 |
| | current SD | 1.6 | 94.3 |
| | aspect east | 1.3 | 95.6 |
| | sponge presence | 1.3 | 96.9 |
| | bottom temperature | 1.0 | 97.9 |
| | pennatulacean presence | 0.8 | 98.7 |
| | aspect north | 0.8 | 99.5 |
| | rockiness | 0.5 | 100 |

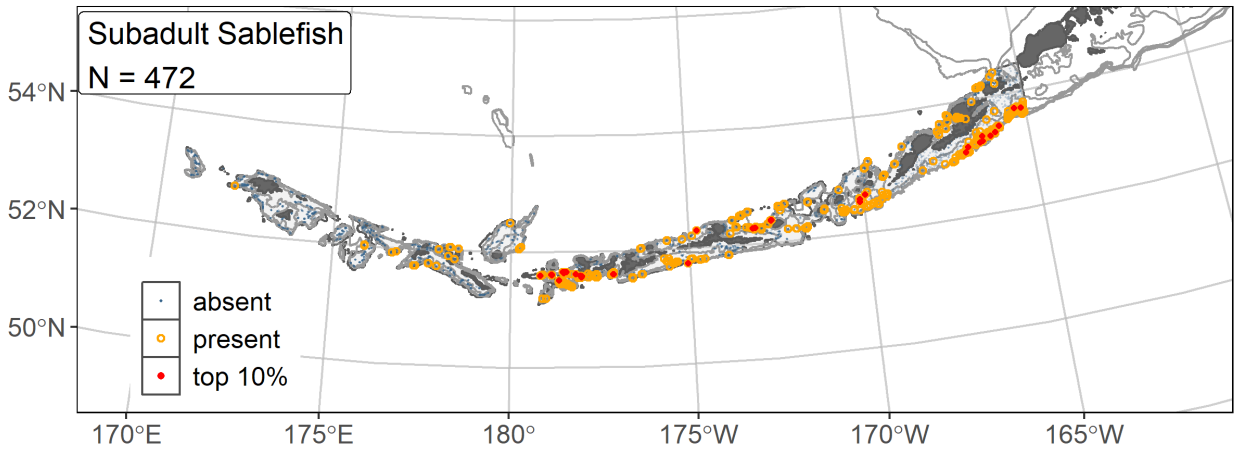


Figure 86. -- Distribution of subadult sablefish catches (N = 472) in 1991–2019 AFSC RACE-GAP summer bottom trawl surveys of the AI with the 100 m, 300 m, and 500 m isobaths indicated; filled red circles indicate locations in top 10% of overall abundance, open orange circles indicate presence in remaining catches.

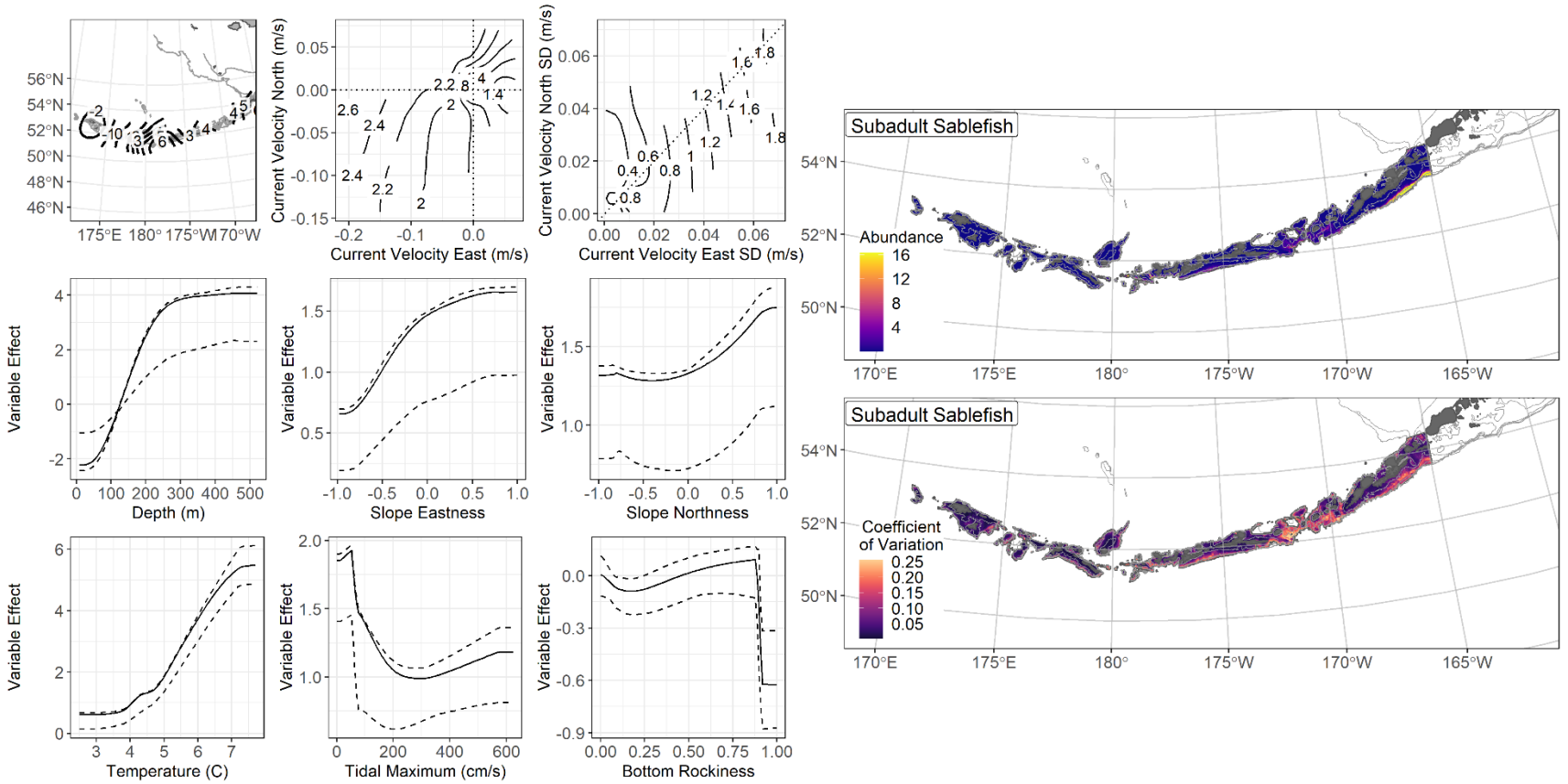


Figure 87. -- The top nine covariate effects (left panel) on ensemble-predicted subadult sablefish numerical abundance across the AI (upper right panel) alongside the coefficient of variation of the ensemble predictions (lower right panel).

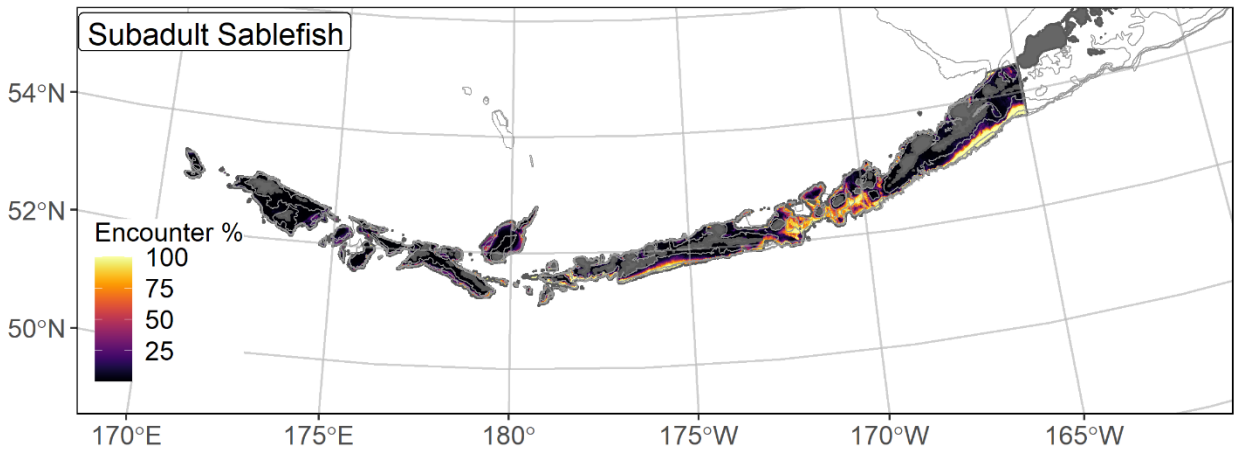


Figure 88. -- Encounter probability of subadult sablefish from AFSC RACE-GAP summer bottom trawl surveys (1991–2019) of the AI with the 100 m, 300 m, and 500 m isobaths indicated.

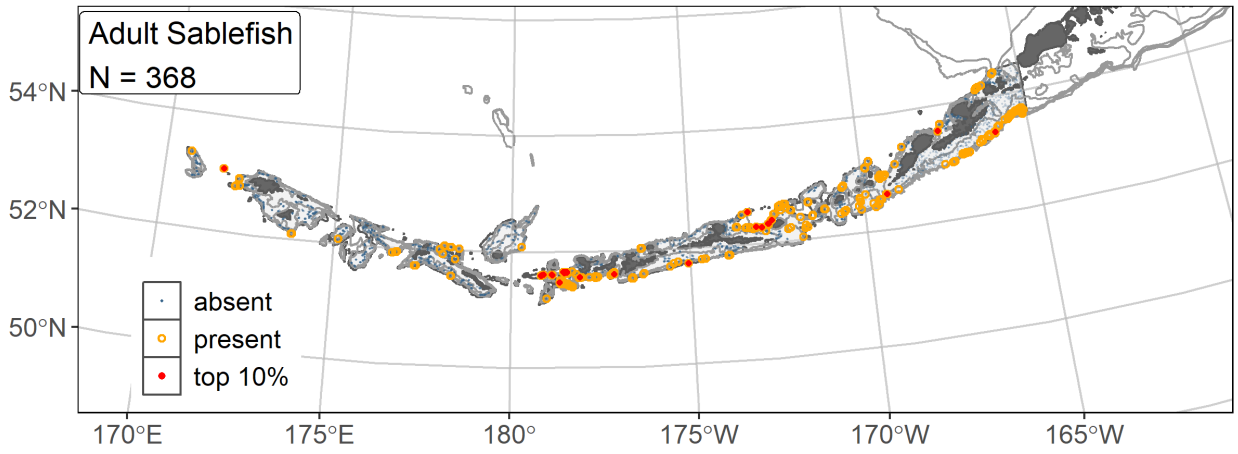


Figure 89. -- Distribution of adult sablefish catches (N = 368) in 1991–2019 AFSC RACE-GAP summer bottom trawl surveys of the AI with the 100 m, 300 m, and 500 m isobaths indicated; filled red circles indicate locations in top 10% of overall abundance, open orange circles indicate presence in remaining catches.

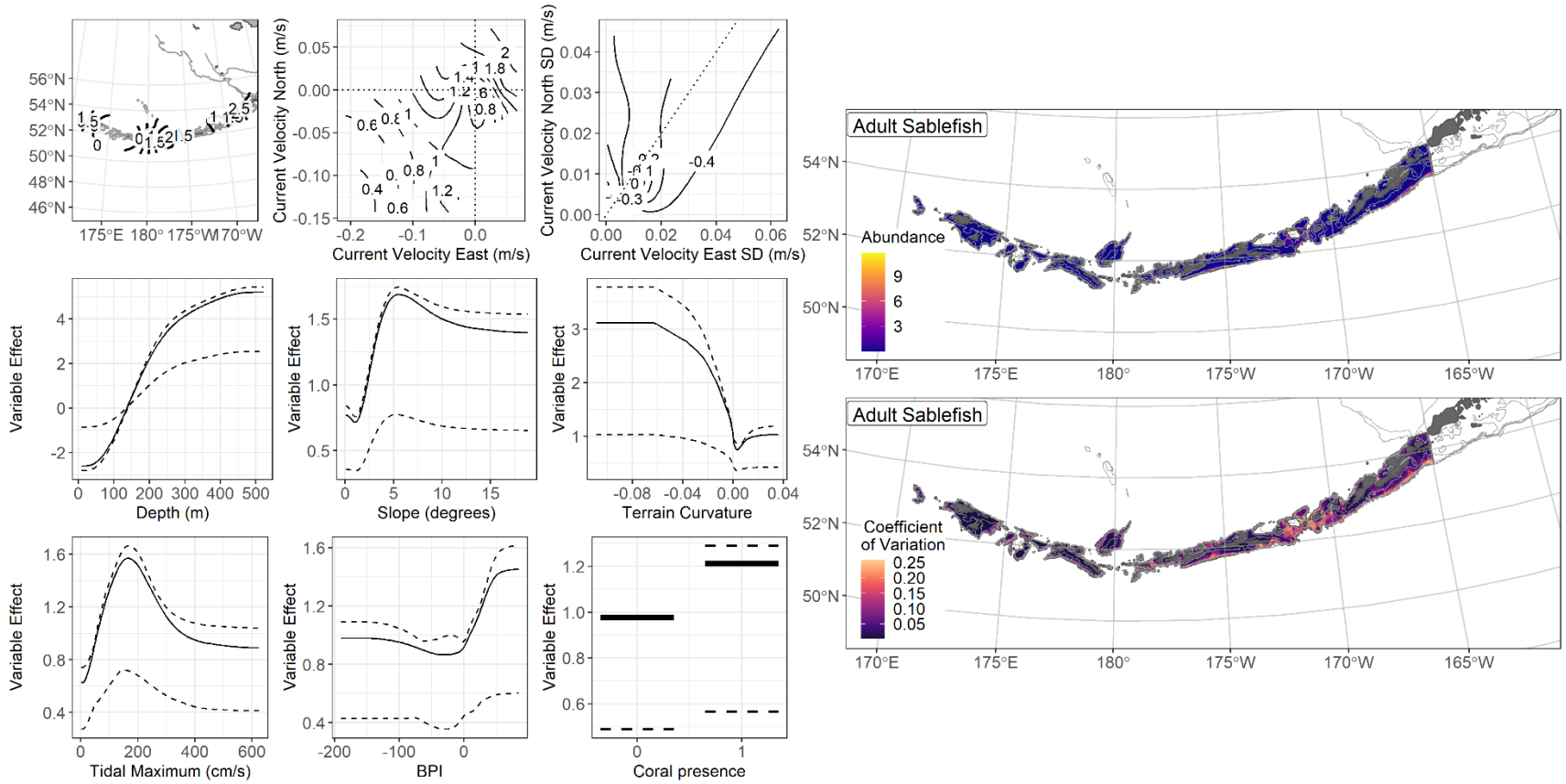


Figure 90. -- The top nine covariate effects (left panel) on ensemble-predicted adult sablefish numerical abundance across the AI(upper right panel) alongside the coefficient of variation of the ensemble predictions (lower right panel).

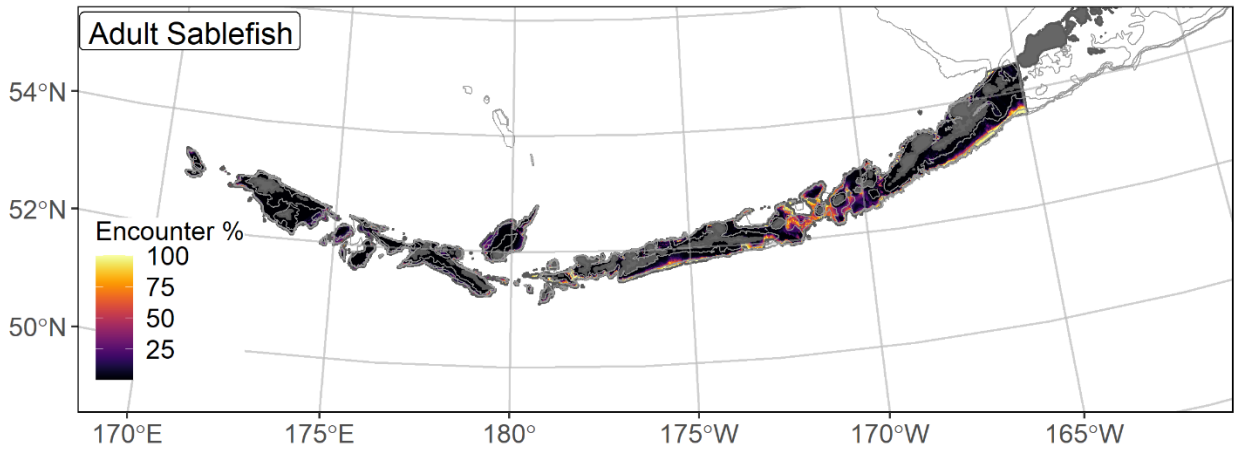


Figure 91. -- Encounter probability of adult sablefish from AFSC RACE-GAP summer bottom trawl surveys (1991–2019) of the AI with the 100 m, 300 m, and 500 m isobaths indicated.

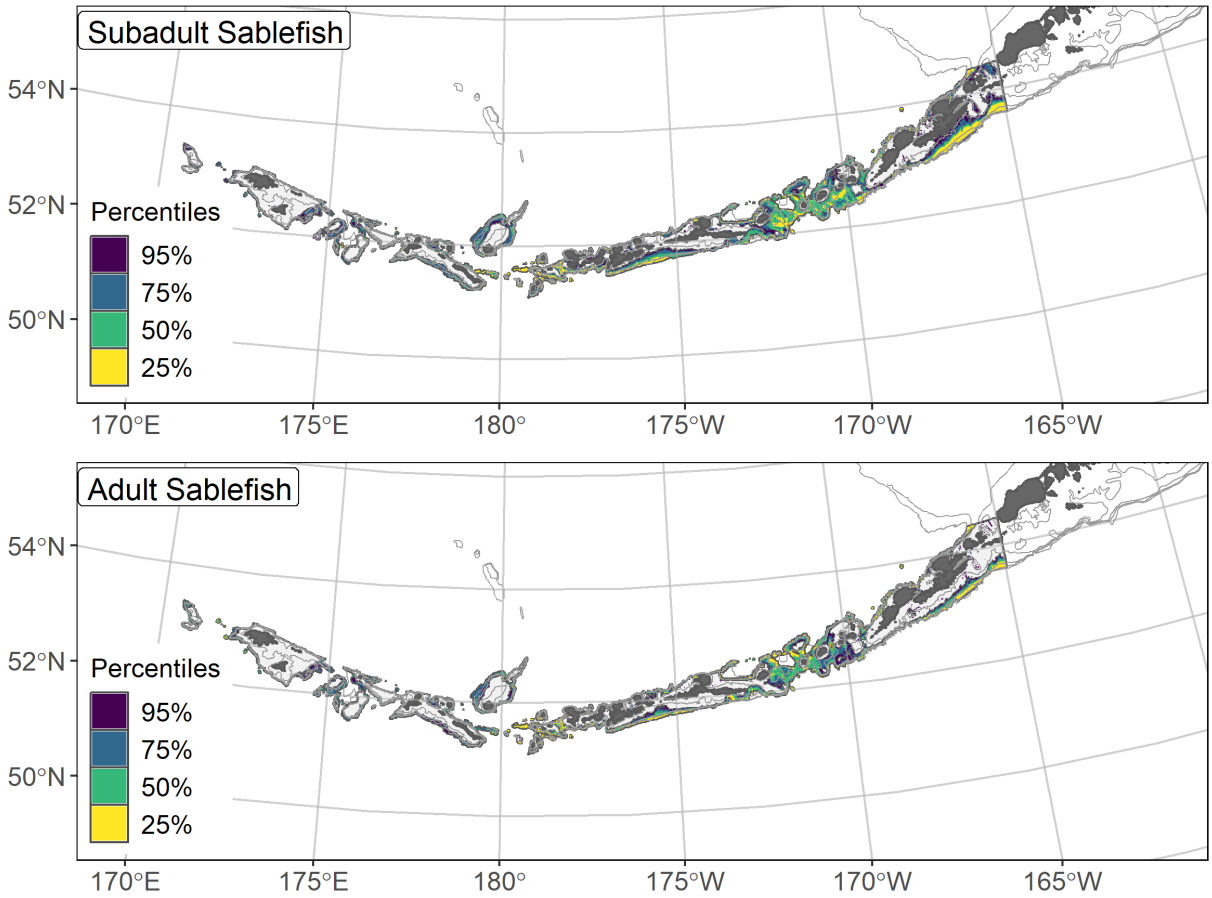


Figure 92. -- Essential fish habitat (EFH area) defined as the top 95% of numerical abundance predictions from a habitat-based ensemble fitted to subadult (top) and adult (bottom) sablefish distribution and abundance in AFSC RACE-GAP summer bottom trawl surveys (1991–2019) with 100 m, 300 m, and 500 m isobaths indicated; internal to the EFH map are the subareas of the top 25% (EFH hot spots), top 50% (core EFH area), and top 75% (principal EFH area) of habitat-related, ensemble-predicted numerical abundance.

**Walleye pollock (*Gadus chalcogrammus*)**

Bering Sea-Aleutian Islands walleye pollock are ecologically important and support one of the world's largest commercial fisheries in the BSAI (Fissel et al. 2019). They spawn in March–May (Bailey 2000), with earlier spawning near shore north of Unimak Island in March and April and spawning in the Pribilof Islands later in the season (Bacheler et al. 2010); females can spawn up to 10 batches of eggs per year. Young-of-the-year pollock feed on plankton (Ciannelli et al. 2004) and provide forage for piscivores (Yang and Livingston 1986, Barnes et al. 2020). Two- to three-year-old pollock are rarely collected in bottom trawls but are detected by mid-water acoustic summer surveys (e.g., McCarthy et al. 2020). Younger pollock are more common in the northern portions of the RACE-GAP bottom trawl survey area, and a pattern of movement to the southeast Bering Sea as they age has been noted (Buckley et al. 2009, Thorson et al. 2017). Length ranges were used to define ontogenetic stages for walleye pollock. Settled early juvenile walleye pollock lengths range from 40 mm FL at the end of the transformation stage (Doyle et al. 2018) to 140 mm FL (Pirtle et al. 2019). Subadults (141–381 mm FL) were assigned based on $L_{50}$ reported by Stahl and Kruse (2008) for EBS pollock; the adult life stage was defined as fish with lengths greater than 381 mm FL.

**Settled early juvenile walleye pollock distribution and predicted abundance from RACE-GAP summer bottom trawl surveys in the Aleutian Islands –** Settled early juvenile walleye pollock were relatively uncommon in the RACE-GAP summer bottom trawl survey of the AI compared to older life stages (Fig. 93). They occurred throughout the survey area and were most concentrated towards the eastern AI around Unalaska Island. The final ensemble contains three SDMs with approximately equal weights. The ensemble showed fair performance overall in terms of model fit (Table 29). Specifically, the model had an AUC of 0.86, which indicates a

strong ability to discriminate presence from non-presence areas. However, the lower scores for ρ and PDE (0.23 and 0.37, respectively) suggest that this model may not accurately predict abundance in all cases. These metrics suggested that the model provides a somewhat accurate description of the areas where settled early juvenile pollock can be found, though it does not provide an accurate estimate of their abundance. The inclusion of small mesh trawls or similar methods in the future might provide better data and allow for better predictions[16]. No single covariate had a particularly large effect on model predictions of settled early juvenile pollock abundance, but bottom depth, geographic position, terrain aspect, current, and bottom temperature were the most important covariates and accounted for 77.7% of the deviance explained by the ensemble (Table 30). In general, the ensemble predicted that high abundance in shallow areas in the eastern AI and areas with cool temperatures, weak currents, and south-facing terrain (Fig. 94). Predicted abundance was highest in the eastern AI, near-shore to Unalaska Island, with additional pockets of high abundance around Atka and Attu islands (Fig. 94). The predicted CV of abundance was high throughout most of the region, with the highest values occurring close to shore (Fig. 94). This reflects that the catch of early juveniles is often quite variable, even inside their usual habitat. Encounter probabilities for settled early juvenile walleye pollock were high near the areas described above and close to zero in most places with depth greater than 200 m (Fig. 95).

[16] A recommendation to add additional survey data types if possible to future SDM ensemble EFH mapping efforts for this species will be included as a future recommendation for research directions from the 2023 EFH 5-year review.

**Subadult walleye pollock distribution and predicted abundance from RACE-GAP summer bottom trawl surveys in the Aleutian Islands –** Subadult walleye pollock catches were very common within the RACE-GAP summer survey area (Fig. 96). Large catches were distributed evenly across the AI. The final ensemble contained four SDMs with equal weights and demonstrated fair to good predictive performance ($\rho = 0.41$, Table 29). The AUC of 0.75 suggests a fair ability to identify where subadults will be caught, and the PDE of 0.40 shows that the model explains a fair amount of the observed deviance. Considering that subadult walleye pollock catches are quite variable, these metrics show that the ensemble predictions capture the general distribution of pollock in trawl catches but may not be precise. Bottom depth was the most important covariate and accounted for 40.8% of the deviance explained by the model, but geographic position, tidal maximum, rockiness, current variables, and temperature also contributed (Table 30). Based on the covariates, subadult walleye pollock are more likely to be found in water 100-200 m in depth, locations in the western AI, weaker tides, rocky terrain, and warmer temperatures (Fig. 97). The estimated abundance of the subadult life stage was high in the far west around Attu Island and in the east around Unalaska Island, with lower abundance predicted in between. As with early juveniles, predicted subadult abundance is highest in shallow areas, and almost all subadults are predicted to occur above the 300 m depth contour (Fig. 97). The predicted CV of abundance was uniformly high throughout the entire region (Fig. 97). Subadult walleye pollock are very common in the AI, and the estimated encounter probability was near 100% in almost all areas, except in deeper water at the edge of the continental slope (Fig. 98).

**Adult walleye pollock distribution and predicted abundance from RACE-GAP summer bottom trawl surveys in the Aleutian Islands –** Adult walleye pollock catches were ubiquitous throughout the RACE-GAP summer survey area in the AI (Fig. 99). Large catches occurred across the entire AI and tended to occur farther from shore compared to earlier life stages. The four SDMs included in the ensemble were assigned approximately equal weights, and the predictions generated by the ensemble model had a good fit to the data ($\rho = 0.50$, Table 29). The AUC of 0.71 was only "fair," but this may be influenced by the fact that there were almost no areas in the AI where adult walleye pollock were consistently absent. The PDE was somewhat lower at 0.28, corresponding to a "fair" amount of the deviance. Overall, the abundance of adult walleye pollock in the AI was highly variable, and the fit metrics for the model ensemble suggest that predictions about distribution were accurate, but abundance estimates were less accurate. Bottom depth, geographic position, and current were the most important covariates and explained 74.2% of the deviance explained by the ensemble (Table 30). The ensemble predicted that adult walleye pollock were more abundant in the eastern AIand preferred areas from 200 to 300 m in depth with southerly currents (Fig. 100). Adult walleye pollock appear in greater numbers than the other life stages and were predicted to occur in especially high densities near Unimak Pass and in the eastern AI (Fig. 100). However, even in the western AI, where adult abundance was comparatively lower, average catches of 50-100 pollock per haul could still be expected in many areas. Despite the very high abundance predicted in the east, the CV of abundance there is not higher than average, conveying that the eastern AI had reliably high abundance, whereas predictions for the other areas were more variable (Fig. 100). The lowest predicted encounter probability for walleye pollock of any location in the AI summer bottom

trawl survey was 84%, demonstrating that this species was common throughout the region (Fig. 101).

**Essential fish habitat of settled early juvenile, subadult, and adult walleye pollock in the Aleutian Islands –** The habitat-related abundance predictions based on RACE-GAP summer bottom trawl data (1991–2019) were translated into EFH area and subareas (Fig. 102). The EFH area for settled early juvenile walleye pollock is smaller than that of the other life stages. The most extensive section of EFH for this life stage was centered around Unalaska Island, though additional hot spots were predicted near Atka Island and Attu Island. Most of the EFH for this life stage occurred in relatively shallow water was absent from areas with greater than 300 m depth. Both the subadult and adult life stages included nearly the whole survey area as EFH, but the details of their respective maps differ in some important ways. Subadult EFH showed a similar pattern to the early juveniles, with notable hot spots occurring near the same islands described above. However, subadults showed an increased depth range, with some parts of the EFH extending out towards the continental slope and deeper water. By contrast, the adult EFH map showed hot spots and core EFH areas concentrated in the east near Unalaska Island and Unimak Pass and in deeper water along the slope. Shallow near-shore areas were generally not predicted to be part of the core EFH (50%) or hot spots. Given the similarity of the early juvenile and subadult EFH maps, it is curious that the adult population does not have a similar hot spot in the western AI. It is possible that adults in that region migrate elsewhere in the island chain, or descend into waters deeper than 500 m, thereby avoiding the survey. The ensembles for settled early juveniles showed marginal predictive performance and should be interpreted with caution, but the agreement between subadult and early juvenile maps suggested that the ensemble did not make unreasonable predictions.

**Settled early juvenile walleye pollock Level 3 Essential Fish Habitat Information – Habitat-Related Vital Rates**

Laboratory-reared early juvenile walleye pollock displayed temperature-dependent growth following the below equation (Laurel et al. 2016):

$$GR = 0.2023 + 0.0092 * T + 0.0335 * T^2 - 0.0019 * T^3,$$

where *GR* is the growth rate (% body weight (g) per day (d)), and *T* is the temperature. The raster product of early juvenile walleye pollock predicted abundance, and their spatially explicit temperature-dependent growth resulted in an EFH Level 3 map of habitat-related population (abundance) growth potential. The growth rate of early juvenile walleye pollock had a theoretical maximum around 11°C (Laurel et al. 2016). However, the summer bottom temperature in the AI had a more limited range than other regions, from around 3 to 7 °C (Fig. 2). In the resulting map of temperature dependent growth, the highest growth areas were about 40% higher than the lowest growth areas (Fig. 103). Notably, some areas with the highest temperature dependent growth rate occurred in the eastern AI, which is a major EFH hot spot. This was observed in the map of growth potential and abundance, which showed that only a few locations have both high growth potential and high predicted abundance (Fig. 103). Some areas with high temperatures and hence high potential growth rates were not accompanied by high settled juvenile abundance, suggesting that temperature is not the only driver of walleye pollock distribution. However, the higher growth potential predicted in the eastern AI suggests that this section of EFH may be of greater importance to the overall health of the walleye pollock population compared to other EFH areas farther west in the islands.

A second vital rate, summer lipid accumulation rate (LAR), was determined from laboratory reared early juvenile walleye pollock according to the below equation (Copeman et al. 2017):

$$LAR = 11.6 * \exp\left[-0.5\left(\frac{T-14.37}{6.39}\right)^2\right],$$

where *LAR* is the lipid accumulation rate (% lipids per % body weight per day), and *T* is the temperature (°C). The map of temperature-dependent LAR (Fig. 104) was nearly identical to that of the temperature-dependent growth rate (Fig. 104). This is unsurprising since both are based on temperature. While Copeman et al. (2017) found that the optimal temperature for lipid accumulation (13-14 °C) was higher than the optimal growth rate temperature of 11°C (Laurel et al. 2016), both temperatures are much higher than are routinely found in the AI region, and this difference has little impact.

Table 29. -- Constituent species distribution models (SDMs) used to construct Essential Fish Habitat (EFH) for a) settled early juvenile, b) subadult, and c) adult walleye pollock: MaxEnt = Maximum entropy; paGAM = presence-absence generalized additive model; hGAM = hurdle GAM; $GAM_P$ = standard Poisson GAM; and $GAM_{nb}$ = standard negative-binomial GAM. Ensemble performance ($\rho$ = Spearman's rank correlation coefficient), root-mean-square-error (RMSE), the area under the receiver operating characteristic (AUC), and the Poisson deviance explained (PDE) were generated from k-fold cross-validation. The "--" in a field indicates that this SDM was not included in the final ensemble.

**a) settled early juvenile walleye pollock**

| Models | RMSE | Relative Weight | ρ | AUC | PDE | EFH area (km$^2$) |
|---|---|---|---|---|---|---|
| MaxEnt | 4.81 | 0.33 | 0.18 | 0.78 | 0.20 | 58,500 |
| paGAM | 4.80 | 0.34 | 0.21 | 0.82 | 0.28 | 52,800 |
| hGAM | -- | 0 | -- | -- | -- | -- |
| $GAM_P$ | 5.22 | 0 | 0.21 | 0.80 | 0.18 | -- |
| $GAM_{nb}$ | 4.84 | 0.33 | 0.21 | 0.82 | 0.24 | 38,100 |
| ensemble | 4.75 | 1 | 0.23 | 0.86 | 0.37 | 54,300 |

**b) subadult walleye pollock**

| Models | RMSE | Relative Weight | ρ | AUC | PDE | EFH area (km$^2$) |
|---|---|---|---|---|---|---|
| MaxEnt | 336.9 | 0.25 | 0.39 | 0.75 | 0.01 | 77,600 |
| paGAM | 336.7 | 0.25 | 0.42 | 0.76 | 0.07 | 77,700 |
| hGAM | 344.2 | 0.24 | 0.32 | 0.76 | 0.01 | 65,700 |
| $GAM_P$ | 342.5 | 0 | 0.32 | 0.70 | -0.03 | -- |
| $GAM_{nb}$ | 337.3 | 0.25 | 0.36 | 0.72 | 0.10 | 69,800 |
| ensemble | 324.2 | 1 | 0.41 | 0.75 | 0.40 | 77,700 |

**c) adult walleye pollock**

| Models | RMSE | Relative Weight | ρ | AUC | PDE | EFH area (km$^2$) |
|---|---|---|---|---|---|---|
| MaxEnt | 476.4 | 0.24 | 0.48 | 0.77 | -0.13 | 77,700 |
| paGAM | 469.0 | 0.24 | 0.53 | 0.79 | 0.06 | 77,700 |
| hGAM | 453.7 | 0.26 | 0.31 | 0.78 | 0.22 | 77,700 |

| Models | RMSE | Relative Weight | ρ | AUC | PDE | EFH area (km$^2$) |
|---|---|---|---|---|---|---|
| $GAM_P$ | 450.3 | 0.26 | 0.30 | 0.63 | 0.23 | 77,600 |
| $GAM_{nb}$ | 954.9 | 0 | 0.49 | 0.75 | -0.14 | -- |
| ensemble | 446.7 | 1 | 0.50 | 0.71 | 0.28 | 77,700 |

Table 30. – Covariates retained in the a) settled early juvenile, b) subadult, and c) adult walleye pollock species distribution model (SDM) final ensembles, the percent contribution to the ensemble deviance explained by each, and the cumulative percent deviance: SD = standard deviation, and BPI = bathymetric position index.

| walleye pollock | Covariate | % Contribution | Cumulative % Contribution |
|---|---|---|---|
| **a) settled early juvenile** | bottom depth | 21.0 | 21.0 |
| | position | 20.7 | 41.7 |
| | aspect north | 14.0 | 55.8 |
| | current | 12.0 | 67.8 |
| | bottom temperature | 9.9 | 77.7 |
| | rockiness | 5.4 | 83.1 |
| | current SD | 4.8 | 87.9 |
| | BPI | 3.9 | 91.8 |
| | aspect east | 2.6 | 94.4 |
| | tidal maximum | 2.0 | 96.4 |
| | pennatulacean presence | 1.3 | 97.7 |
| | coral presence | 0.9 | 98.6 |
| | curvature | 0.7 | 99.3 |
| | sponge presence | 0.5 | 99.8 |
| | slope | 0.2 | 100 |
| **b) subadult** | bottom depth | 40.8 | 40.8 |
| | position | 14.7 | 55.5 |
| | rockiness | 7.1 | 62.6 |
| | bottom temperature | 6.4 | 69.0 |
| | tidal maximum | 5.9 | 74.9 |
| | current SD | 5.4 | 80.3 |
| | BPI | 4.7 | 85.0 |
| | slope | 3.7 | 88.7 |
| | current | 3.4 | 92.1 |
| | pennatulacean presence | 2.1 | 94.2 |
| | aspect east | 1.6 | 95.8 |
| | aspect north | 1.5 | 97.3 |
| | curvature | 1.5 | 98.8 |
| | coral presence | 1.0 | 99.8 |
| | sponge presence | 0.2 | 100 |
| **c) adult** | bottom depth | 36.4 | 36.4 |
| | position | 26.6 | 62.9 |
| | current | 11.3 | 74.2 |
| | aspect north | 4.9 | 79.1 |
| | tidal maximum | 4.4 | 83.5 |

| walleye pollock | Covariate | % Contribution | Cumulative % Contribution |
|---|---|---|---|
| | bottom temperature | 3.0 | 86.5 |
| | current SD | 2.8 | 89.3 |
| | rockiness | 2.4 | 91.7 |
| | sponge presence | 2.2 | 93.9 |
| | aspect east | 1.9 | 95.8 |
| | slope | 1.4 | 97.2 |
| | coral presence | 1.0 | 98.2 |
| | BPI | 0.9 | 99.1 |
| | curvature | 0.6 | 99.7 |
| | pennatulacean presence | 0.3 | 100 |

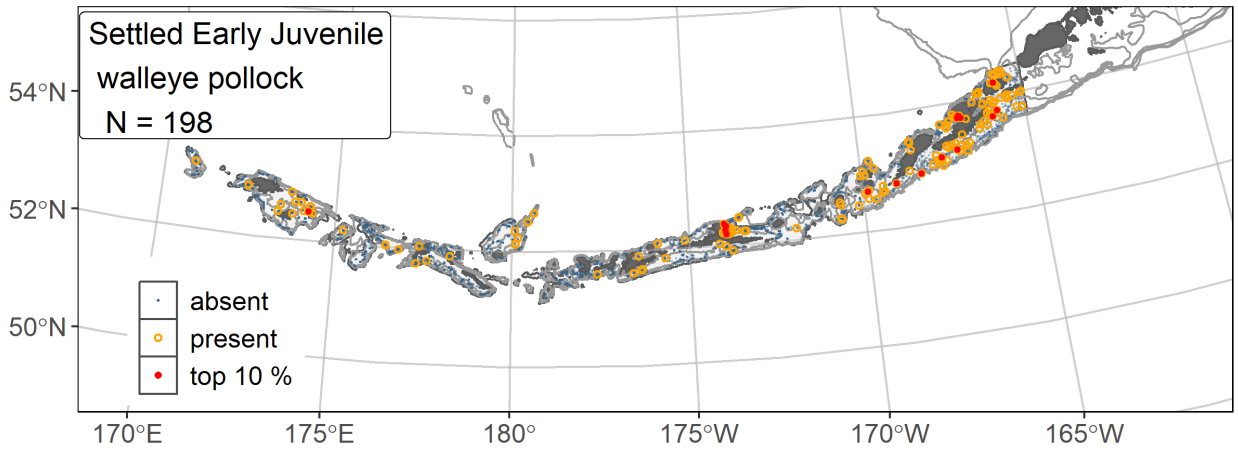


Figure 93. -- Distribution of settled early juvenile walleye pollock catches (N = 198) in 1991–2019 AFSC RACE-GAP summer bottom trawl surveys of the AI with the 100 m, 300 m, and 500 m isobaths indicated; filled red circles indicate locations in top 10% of overall abundance, open orange circles indicate presence in remaining catches, and small blue dots indicate absence.

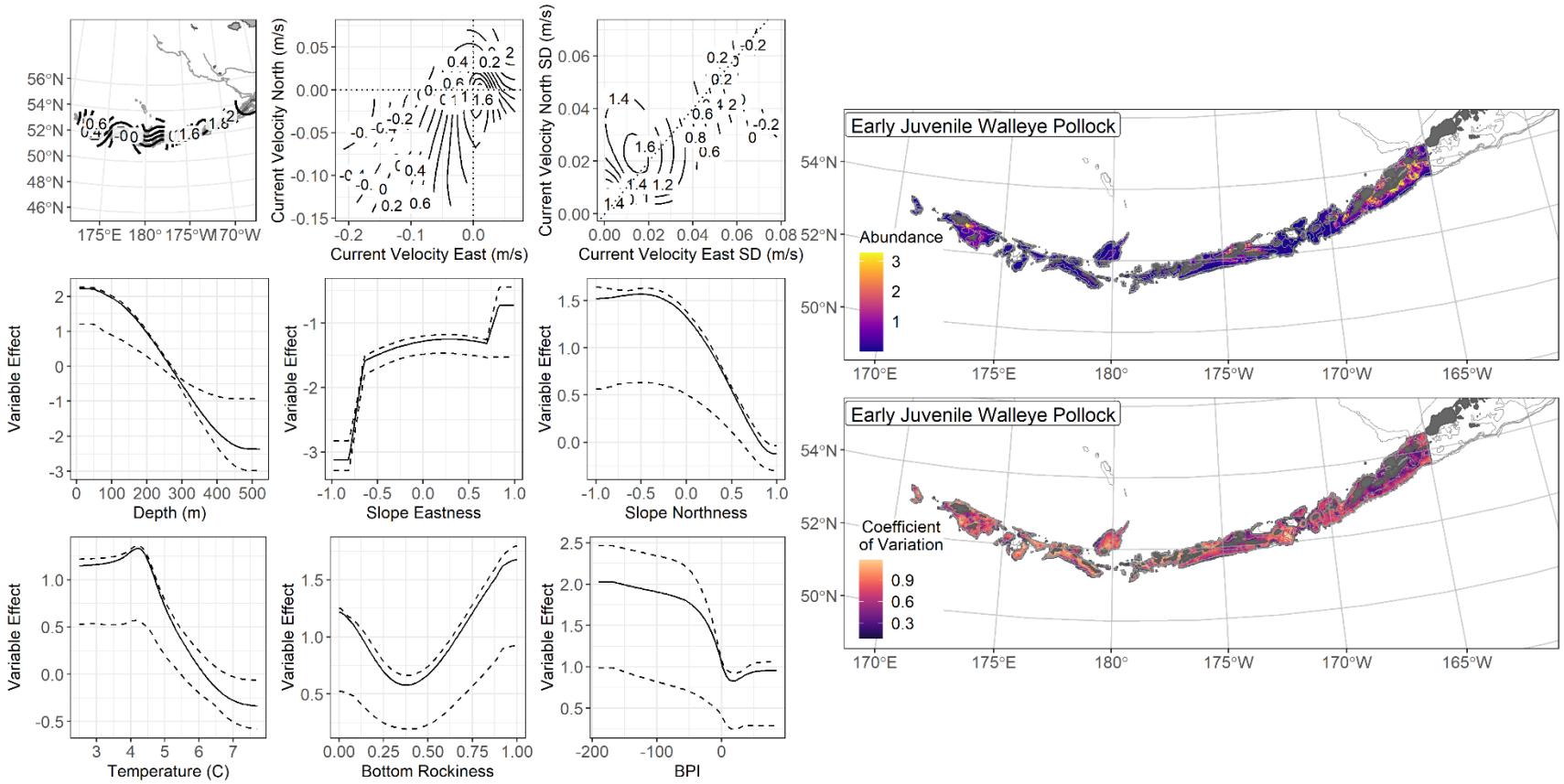


Figure 94. -- The top nine covariate effects (left panel) on ensemble-predicted settled early juvenile walleye pollock numerical abundance across the AI (upper right panel) alongside the coefficient of variation of the ensemble predictions (lower right panel).

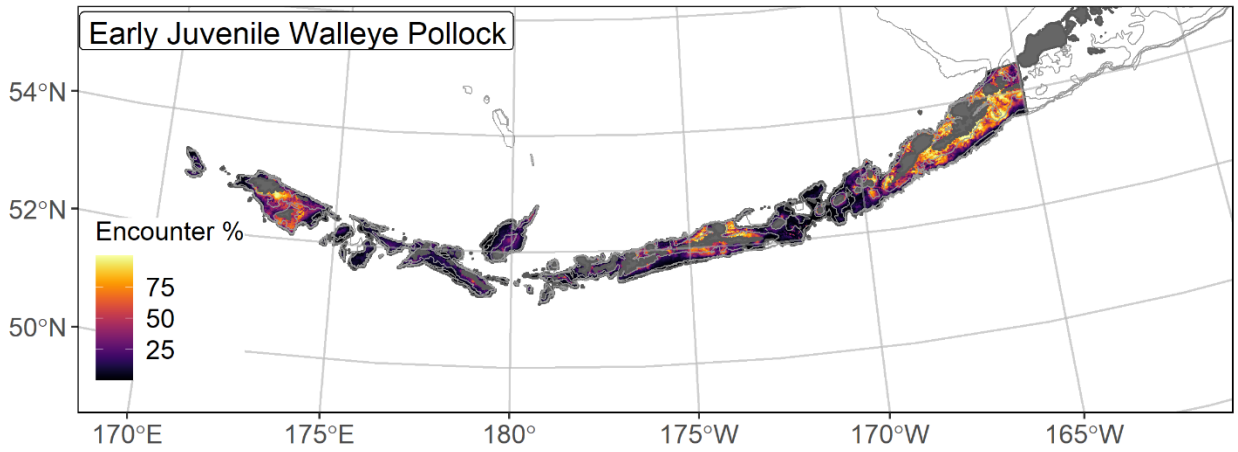


Figure 95. -- Encounter probability of settled early juvenile walleye pollock from AFSC RACE-GAP summer bottom trawl surveys (1991–2019) of the AI with the 100 m, 300 m, and 500 m isobaths indicated.

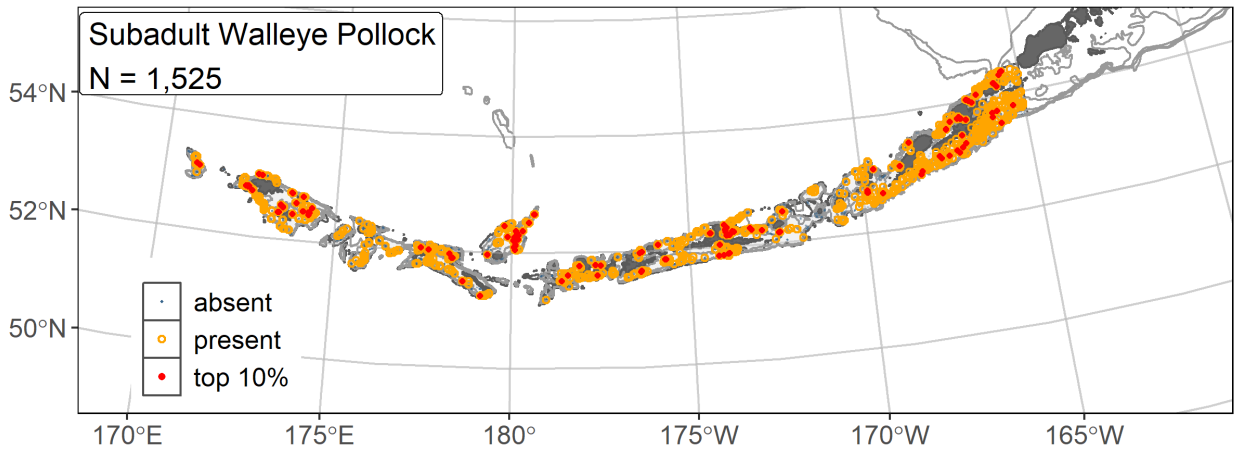


Figure 96. -- Distribution of subadult walleye pollock catches (N = 1,525) in 1991–2019 AFSC RACE-GAP summer bottom trawl surveys of the AI with the 100 m, 300 m, and 500 m isobaths indicated; filled red circles indicate locations in top 10% of overall abundance, open orange circles indicate presence in remaining catches, and small blue dots indicate absence.

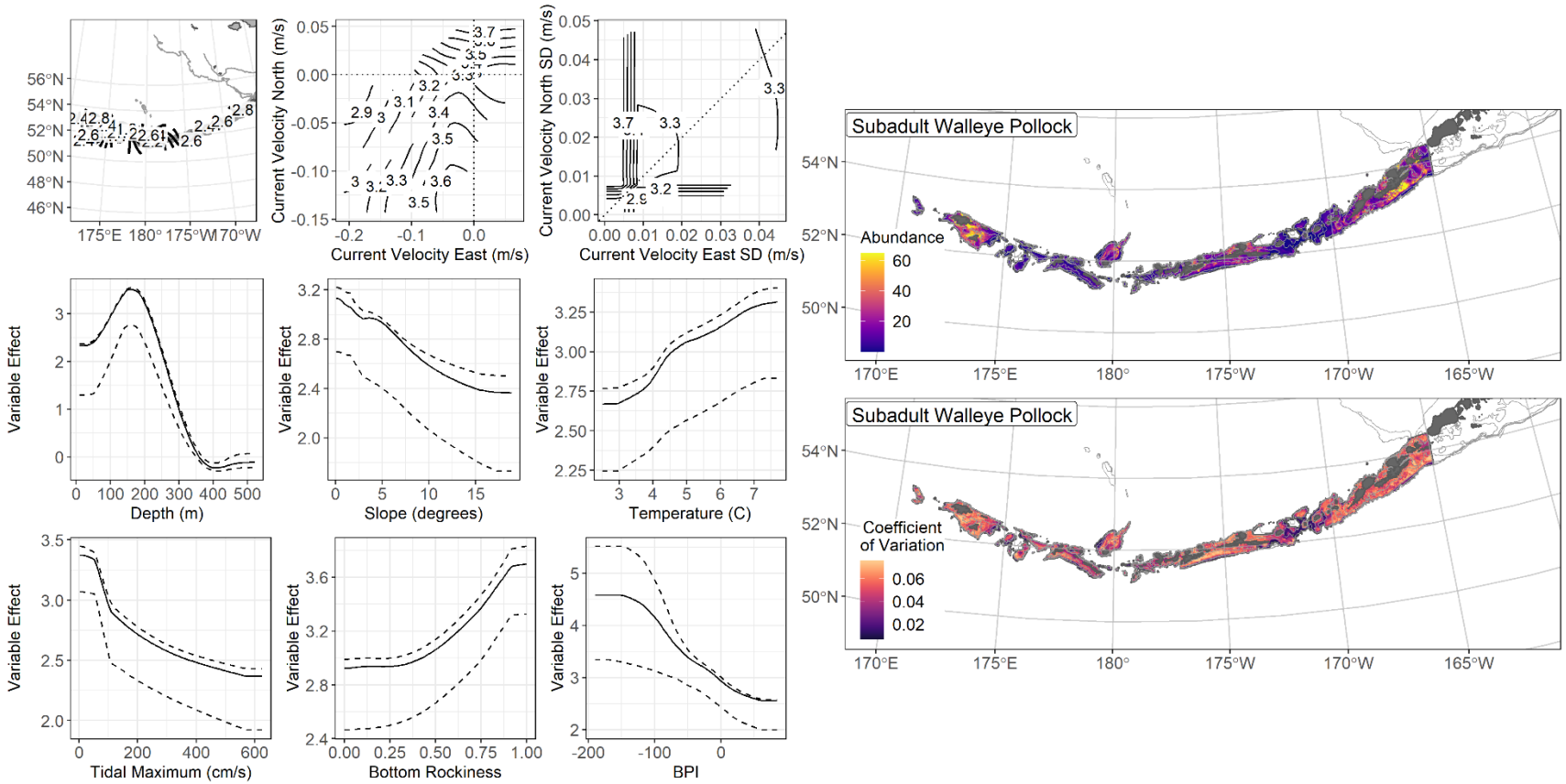


Figure 97. -- The top nine covariate effects (left panel) on ensemble-predicted subadult walleye pollock numerical abundance across the AI (upper right panel) alongside the coefficient of variation of the ensemble predictions (lower right panel).

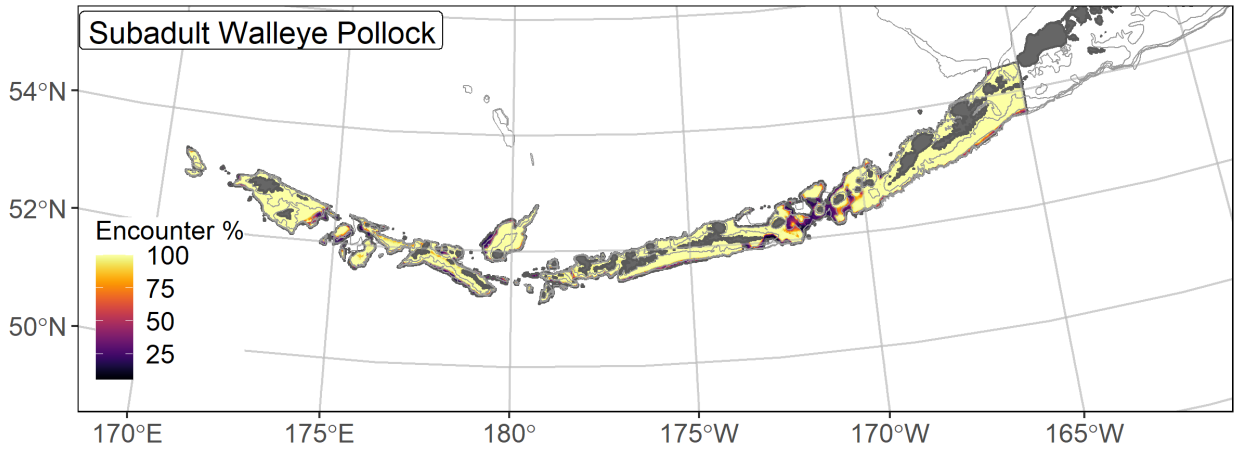


Figure 98. -- Encounter probability of subadult walleye pollock from AFSC RACE-GAP summer bottom trawl surveys (1991–2019) of the AI with the 100 m, 300 m, and 500 m isobaths indicated.

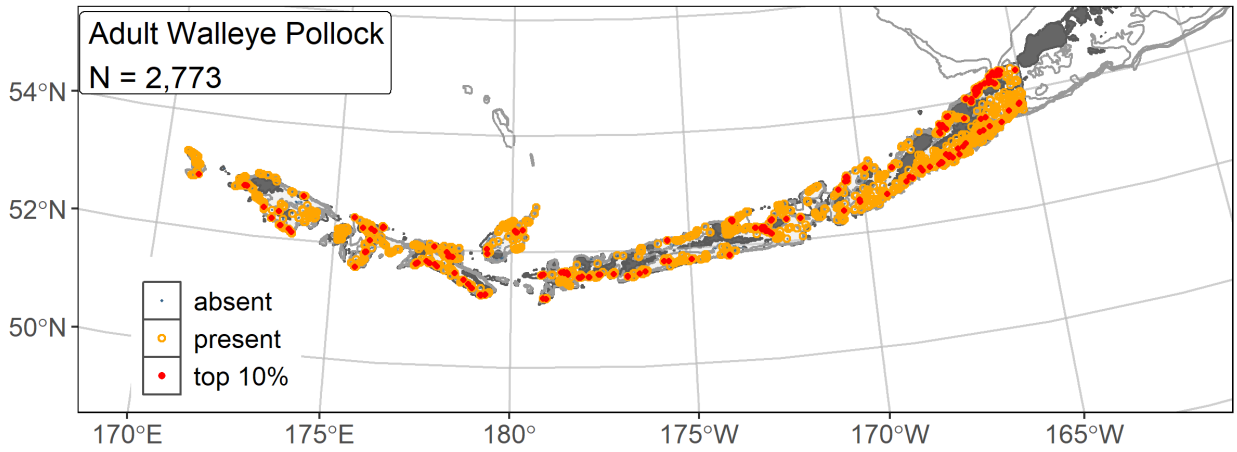


Figure 99. -- Distribution of adult walleye pollock catches (N = 2,773) in 1991–2019 AFSC RACE-GAP summer bottom trawl surveys of the AI with the 100 m, 300 m, and 500 m isobaths indicated; filled red circles indicate locations in top 10% of overall abundance, open orange circles indicate presence in remaining catches, and small blue dots indicate absence.

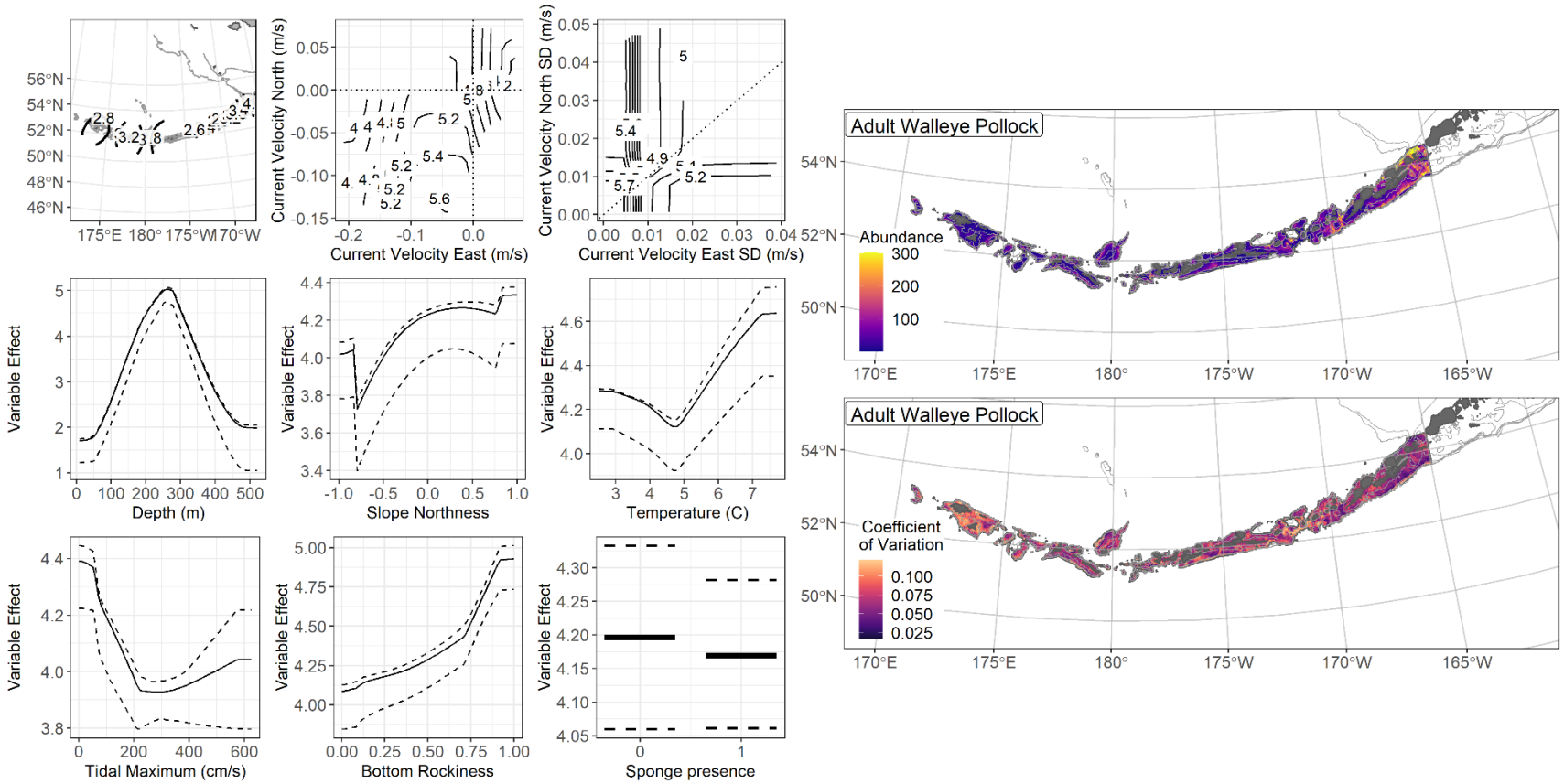


Figure 100. -- The top nine covariate effects (left panel) on ensemble-predicted adult walleye pollock numerical abundance across the AI (upper right panel) alongside the coefficient of variation of the ensemble predictions (lower right panel).

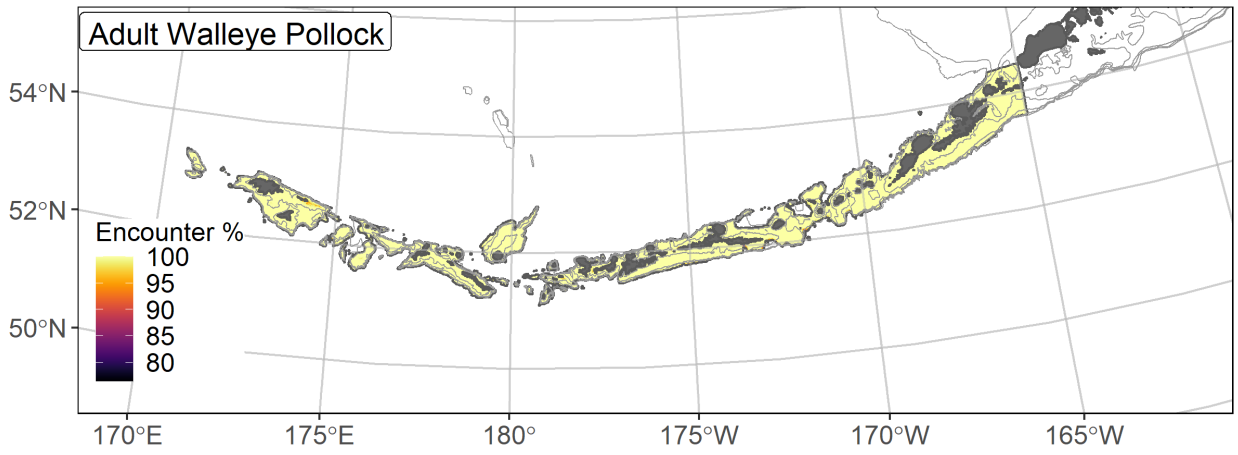


Figure 101. -- Encounter probability of adult walleye pollock from AFSC RACE-GAP summer bottom trawl surveys (1991–2019) of the AI with the 100 m, 300 m, and 500 m isobaths indicated.

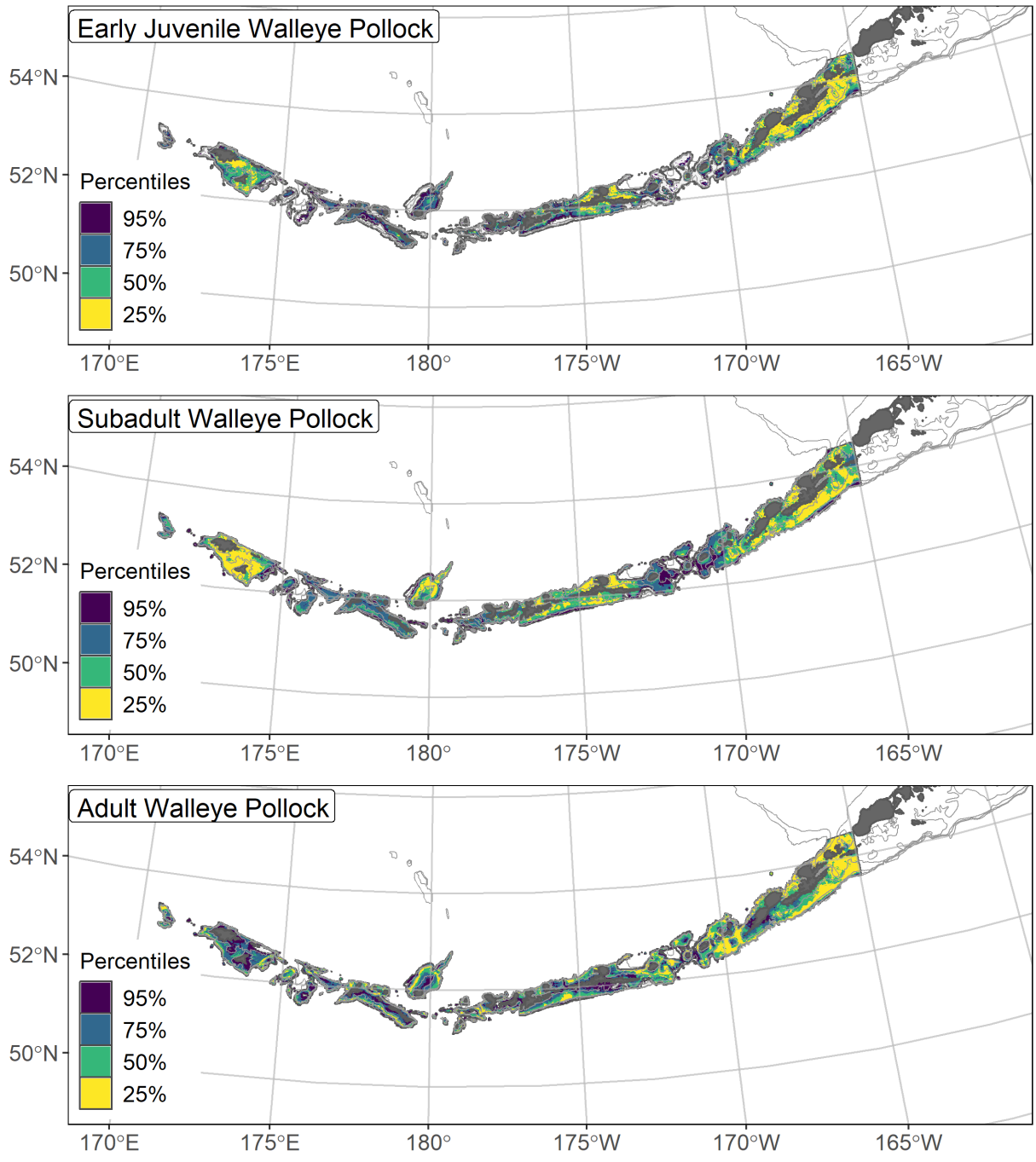


Figure 102. -- Essential fish habitat (EFH area) defined as the top 95% of numerical abundance predictions from a habitat-based ensemble fitted to settled early juvenile (top), subadult (middle), and adult (bottom) walleye pollock distribution and abundance in AFSC RACE-GAP summer bottom trawl surveys (1991–2019) with 100 m, 300 m, and 500 m isobaths indicated; internal to the EFH map are the subareas of the top 25% (EFH hot spots), top 50% (core EFH area), and top 75% (principal EFH area) of habitat related, ensemble-predicted numerical abundance.

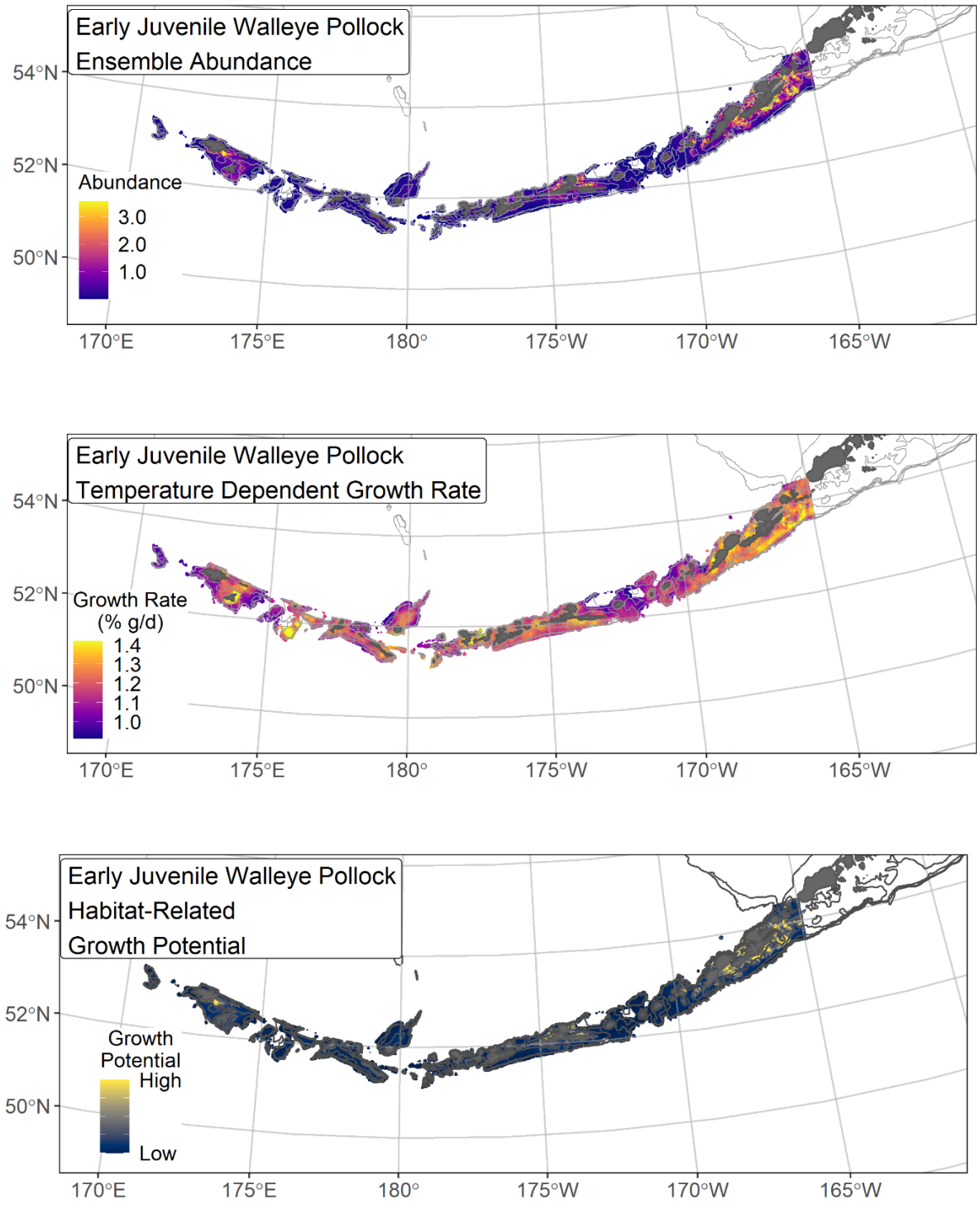


Figure 103. -- Early juvenile walleye pollock ensemble-predicted abundance from RACE-GAP summer bottom trawl surveys of the AI (1991–2019; top panel), temperature-dependent growth rate (% body weight (g) per day; center panel), and habitat-related growth potential (bottom panel; this is the raster product of ensemble-predicted abundance and spatially-explicit, temperature-dependent growth rate).

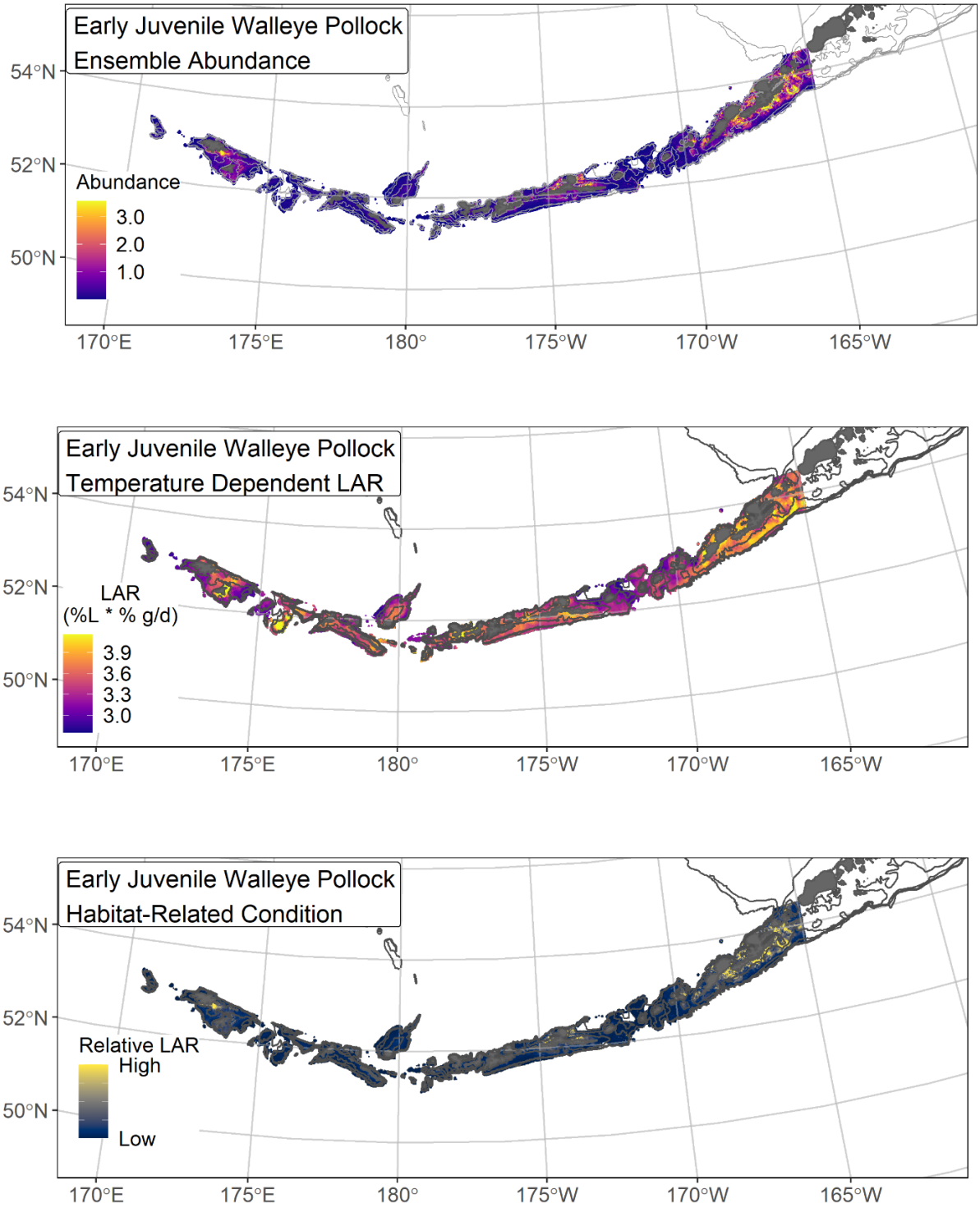


Figure 104. -- Early juvenile walleye pollock ensemble-predicted abundance from RACE-GAP summer bottom trawl surveys of the AI (1991–2019; top panel), temperature-dependent lipid accumulation rate (LAR; % lipids per % body weight (g) per day; center panel), and habitat-related lipid condition (bottom panel; the raster product of ensemble-predicted abundance and temperature-dependent growth rate).

## Rockfishes

### Northern rockfish (*Sebastes polyspinis*)

Northern rockfish (*Sebastes polyspinis*) are common in Alaska waters from British Columbia to the Kuril Islands and Kamchatka Peninsula (Clausen and Heifetz 2002). They are the second most common rockfish species in the BSAI and are most abundant along the shelf break. Like other members of the genus *Sebastes*, northern rockfish are long-lived, ovoviviparous, and may skip mating during years with unfavorable conditions (Conrath 2019). Northern rockfish in the AI reach maturity at 277 mm FL ($L_{50}$; Tenbrink and Spencer 2013), which is somewhat smaller than in the GOA. Catches of northern rockfish in the BSAI have historically occurred as bycatch in other fisheries (i.e., Pacific ocean perch, Atka mackerel), but in recent years targeted fishing of northern rockfish has increased (Spencer and Ianelli 2019).

**Subadult northern rockfish distribution and predicted abundance from RACE-GAP summer bottom trawl surveys in the Aleutian Islands –** Subadult northern rockfish catches were common across the area covered by the RACE-GAP summer bottom trawl survey (Fig. 105). Large catches occurred mostly in the western AI and consisted of thousands of northern rockfish per tow. The final ensemble contained three equally weighted SDMs, and its predictions demonstrated good performance (Table 31). The ensemble scored well across all three metrics ($\rho = 0.43$; AUC = 0.82; PDE = 0.50), indicating that its predictions are accurate. Geographic position, bottom depth, and current accounted for 75.3% of the deviance explained by the ensemble (Table 32). Predicted, abundance increased farther west in the AI and in shallow depths and southerly currents (Fig. 106). Predicted abundance was increased in the western AI and was particularly high around Attu Island, the sea mounts near Buldir Strait, and Stalemate Bank (Fig. 106). The CV of abundance was homogenous across the entire survey area (Fig. 106).

This species and life stage were common across the AI survey area, and a high encounter probability was predicted everywhere except in some habitats deeper than 300 m (Fig. 107).

**Adult northern rockfish distribution and predicted abundance from RACE-GAP summer bottom trawl surveys in the Aleutian Islands –** Adult northern rockfish catches in the RACE-GAP summer survey were very common in all parts of the AI (Fig. 108). Like subadults, the highest density catches were concentrated in the western AI. The four SDMs in the final ensemble were assigned equal weights, and the resulting model showed mixed predictive performance (Table 31). Specifically, the ensemble achieved good scores at predicting abundance ($\rho = 0.56$; PDE = 0.42) but performed poorly in terms of predicting presence and absence (AUC = 0.67). The wide-ranging magnitude of adult northern rockfish catches (from 0 to thousands) resulted in high average abundances which the ensemble assumed to be locations with consistent presence. However, this assumption did not hold in this case, and the ensemble over-predicted observed presence in trawl catches. The most important covariates were geographic position and bottom depth, which explained 67.9% of the deviance explained in the ensemble (Table 32). According to the model, abundance is expected to increase from east to west, in depths between 100 and 200 m, and with strong but variable southerly currents (Fig. 109). Predicted abundance was high overall, particularly around sea mounts in Buldir Strait and Stalemate Bank (Fig. 109), but areas with relatively low abundance still averaged a hundred or more fish per haul. The predicted CV of abundance was elevated in many deeper areas near locations with high abundance, reflecting some uncertainty as to whether high abundance is driven mainly by geographic location or by depth (Fig. 109). Adult northern rockfish were ubiquitous in the AI, and the nearly 100% encounter probability predicted in most places was consistent with their high numbers and wide distribution (Fig. 110).

**Essential fish habitat of subadult and adult northern rockfish in the Aleutian Islands –** The habitat-related abundance predictions based on RACE-GAP summer bottom trawl data (1991–2019) were translated into EFH area and subareas (Fig. 111). Both life stages of northern rockfish were very common throughout the AI. The EFH maps for the two life stages were nearly identicalcovering almost the entire region. In the EFH hot spots around Buldir Strait and Stalemate Bank, a single haul often encountered several thousand northern rockfish, and in areas of lower abundance it was common to catch dozens per tow. Most EFH hot spots were located at shallow depths in the western AI, and lower abundance EFH areas were usually in deeper water along the continental slope.

Table 31. -- Constituent species distribution models (SDMs) used to construct Essential Fish Habitat (EFH) for a) subadult and b) adult northern rockfish: MaxEnt = Maximum entropy; paGAM = presence-absence generalized additive model; hGAM = hurdle GAM; $GAM_P$ = standard Poisson GAM; and $GAM_{nb}$ = standard negative-binomial GAM. Ensemble performance (ρ = Spearman's rank correlation coefficient), root-mean-square-error (RMSE), the area under the receiver operating characteristic (AUC), and the Poisson deviance explained (PDE) were generated from k-fold cross-validation. The "--" in a field indicates that this SDM was not included in the final ensemble.

**a) subadult northern rockfish**

| Models | RMSE | Relative Weight | ρ | AUC | PDE | EFH area ($km^2$) |
|---|---|---|---|---|---|---|
| MaxEnt | 297.9 | 0.30 | 0.39 | 0.80 | 0.27 | 74,600 |
| paGAM | 277.9 | 0.35 | 0.41 | 0.82 | 0.38 | 76,300 |
| hGAM | -- | 0 | -- | -- | -- | -- |
| $GAM_P$ | -- | 0 | -- | -- | -- | -- |
| $GAM_{nb}$ | 276.2 | 0.35 | 0.39 | 0.80 | 0.54 | 52,900 |
| ensemble | 270.9 | 1 | 0.43 | 0.82 | 0.50 | 75,200 |

**b) adult northern rockfish**

| Models | RMSE | Relative Weight | ρ | AUC | PDE | EFH area ($km^2$) |
|---|---|---|---|---|---|---|
| MaxEnt | 828.5 | 0.25 | 0.49 | 0.77 | 0.20 | 77,700 |
| paGAM | 836.3 | 0.25 | 0.53 | 0.79 | 0.20 | 77,700 |
| hGAM | 831.1 | 0.25 | 0.44 | 0.79 | 0.33 | 71,200 |
| $GAM_P$ | 821.2 | 0.25 | 0.44 | 0.67 | 0.37 | 58,000 |
| $GAM_{nb}$ | 960.9 | 0 | 0.50 | 0.75 | 0.28 | -- |
| ensemble | 779.4 | 1 | 0.56 | 0.67 | 0.42 | 77,700 |

Table 32. -- Covariates retained in the a) subadult and b) adult northern rockfish species distribution model (SDM) final ensembles, the percent contribution to the ensemble deviance explained by each, and the cumulative percent deviance: SD = standard deviation, and BPI = bathymetric position index.

| northern rockfish | Covariate | % Contribution | Cumulative % Contribution |
|---|---|---|---|
| **a) subadult** | bottom depth | 42.6 | 42.6 |
| | position | 26.7 | 69.2 |
| | current | 6.0 | 75.3 |
| | current SD | 4.3 | 79.6 |
| | tidal maximum | 4.0 | 83.6 |
| | coral presence | 3.2 | 86.8 |
| | rockiness | 2.9 | 89.7 |
| | slope | 2.6 | 92.3 |
| | aspect east | 2.6 | 94.9 |
| | aspect north | 2.3 | 97.2 |
| | sponge presence | 1.5 | 98.7 |
| | bottom temperature | 1.2 | 99.9 |
| | pennatulacean presence | 0.1 | 100 |
| | curvature | 0 | 100 |
| **a) adult** | bottom depth | 38.9 | 38.9 |
| | position | 29.1 | 67.9 |
| | current SD | 5.7 | 73.6 |
| | current | 5.5 | 79.2 |
| | rockiness | 3.1 | 82.3 |
| | aspect east | 2.5 | 84.8 |
| | slope | 2.4 | 87.2 |
| | tidal maximum | 2.4 | 89.6 |
| | coral presence | 2.4 | 92.0 |
| | bottom temperature | 2.3 | 94.3 |
| | BPI | 2.0 | 96.3 |
| | aspect north | 1.6 | 97.9 |
| | sponge presence | 1.2 | 99.1 |
| | curvature | 0.6 | 99.7 |
| | pennatulacean presence | 0.3 | 100 |

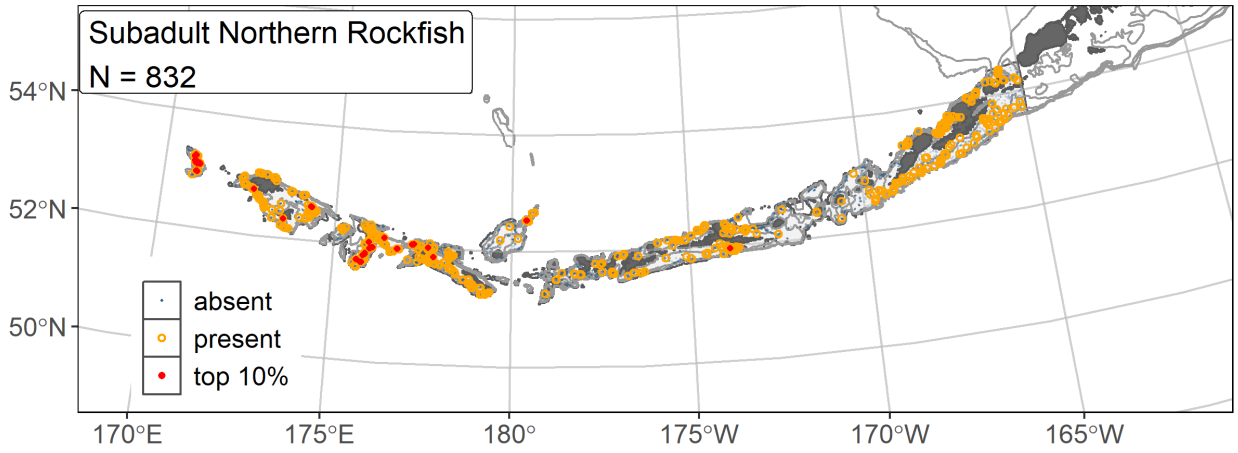


Figure 105. -- Distribution of subadult northern rockfish catches (N = 832) in 1991–2019 AFSC RACE-GAP summer bottom trawl surveys of the AI with the 100 m, 300 m, and 500 m isobaths indicated; filled red circles indicate locations in top 10% of overall abundance, open orange circles indicate presence in remaining catches, and small blue dots indicate absence.

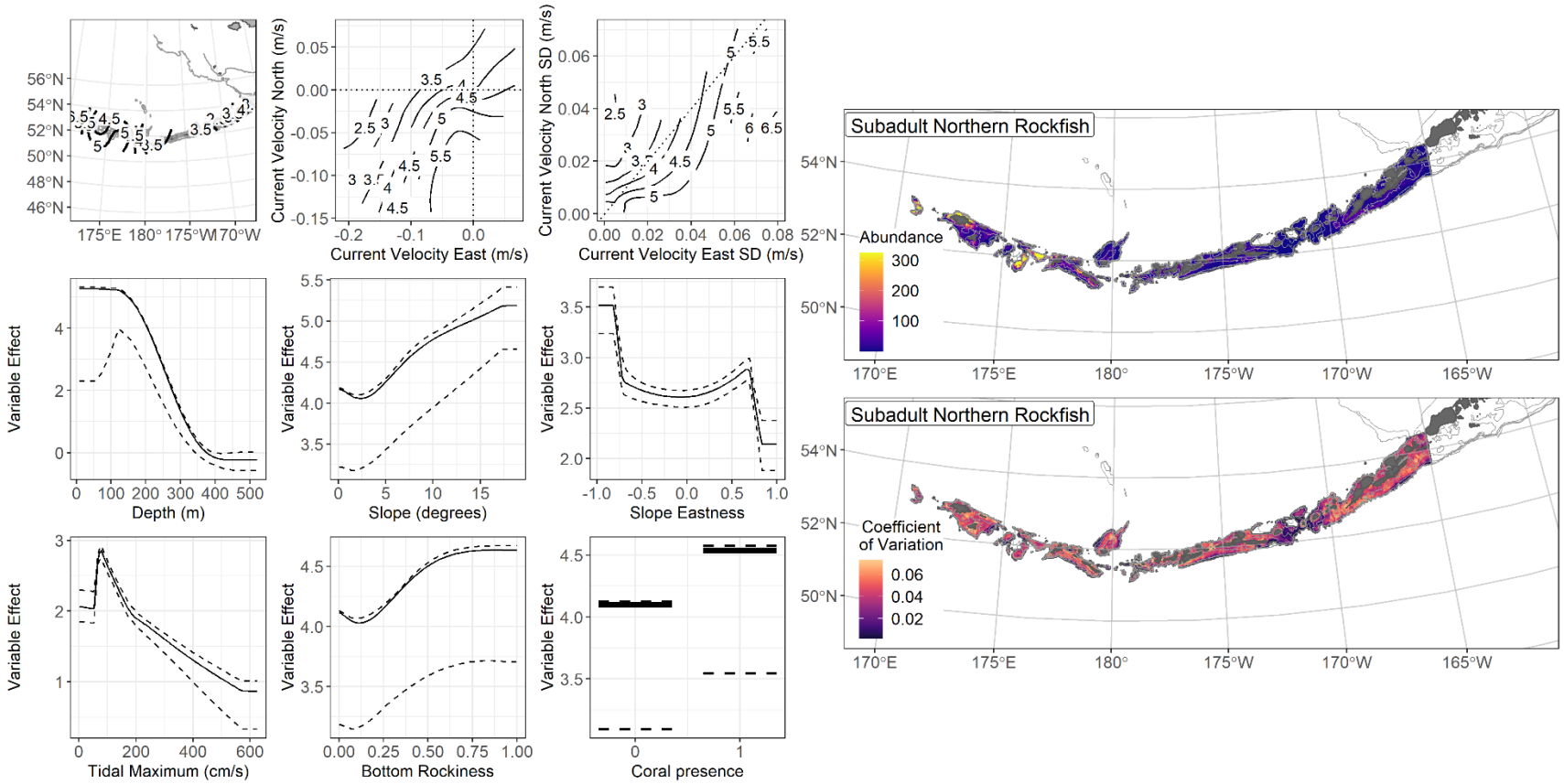


Figure 106. -- The top nine covariate effects (left panel) on ensemble-predicted subadult northern rockfish numerical abundance across the AI (upper right panel) alongside the coefficient of variation of the ensemble predictions (lower right panel).

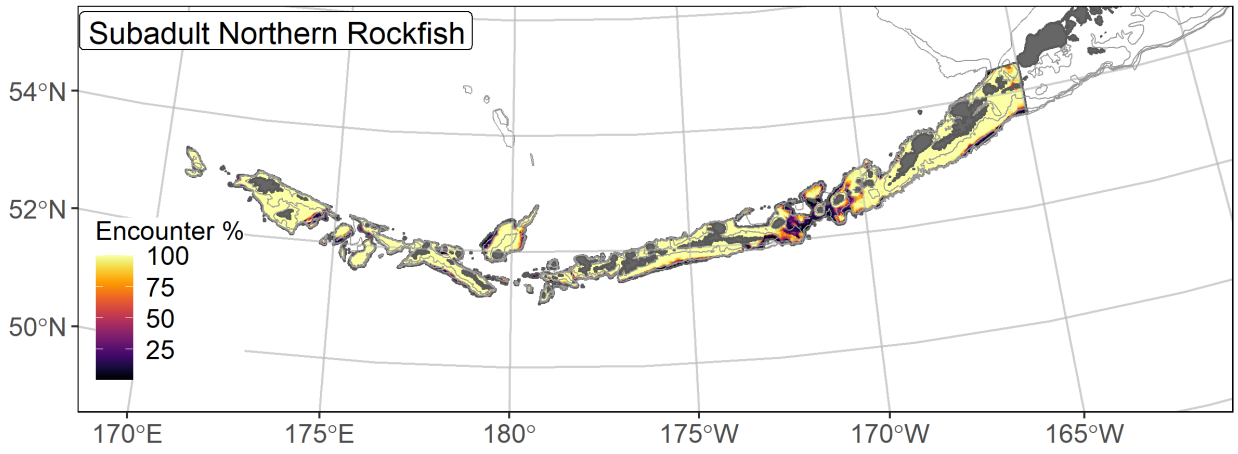


Figure 107. -- Encounter probability of subadult northern rockfish from AFSC RACE-GAP summer bottom trawl surveys (1991–2019) of the AI with the 100 m, 300 m, and 500 m isobaths indicated.

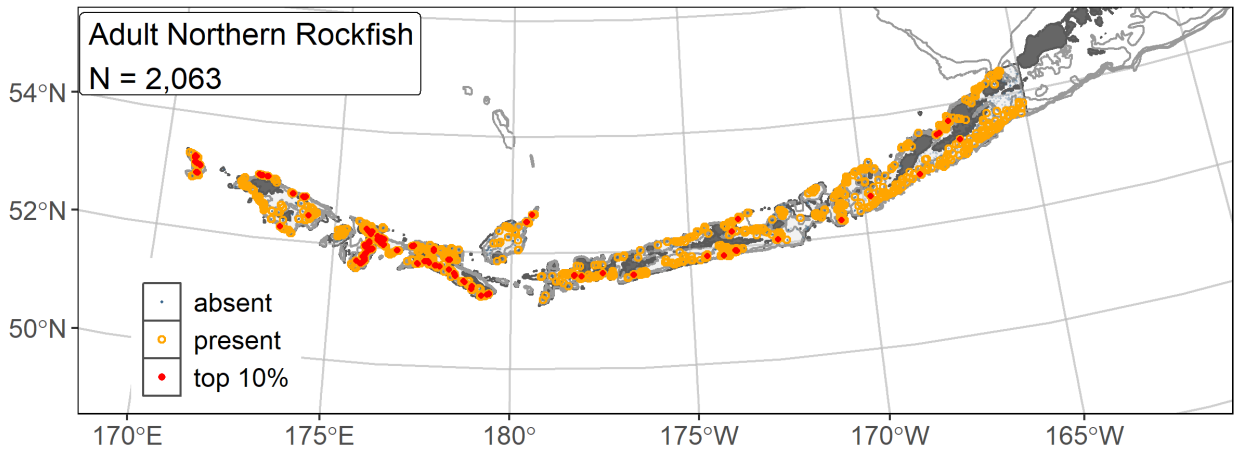


Figure 108. -- Distribution of adult northern rockfish catches (N = 2,063) in 1991–2019 AFSC RACE-GAP summer bottom trawl surveys of the AI with the 100 m, 300 m, and 500 m isobaths indicated; filled red circles indicate locations in top 10% of overall abundance, open orange circles indicate presence in remaining catches, and small blue dots indicate absence.

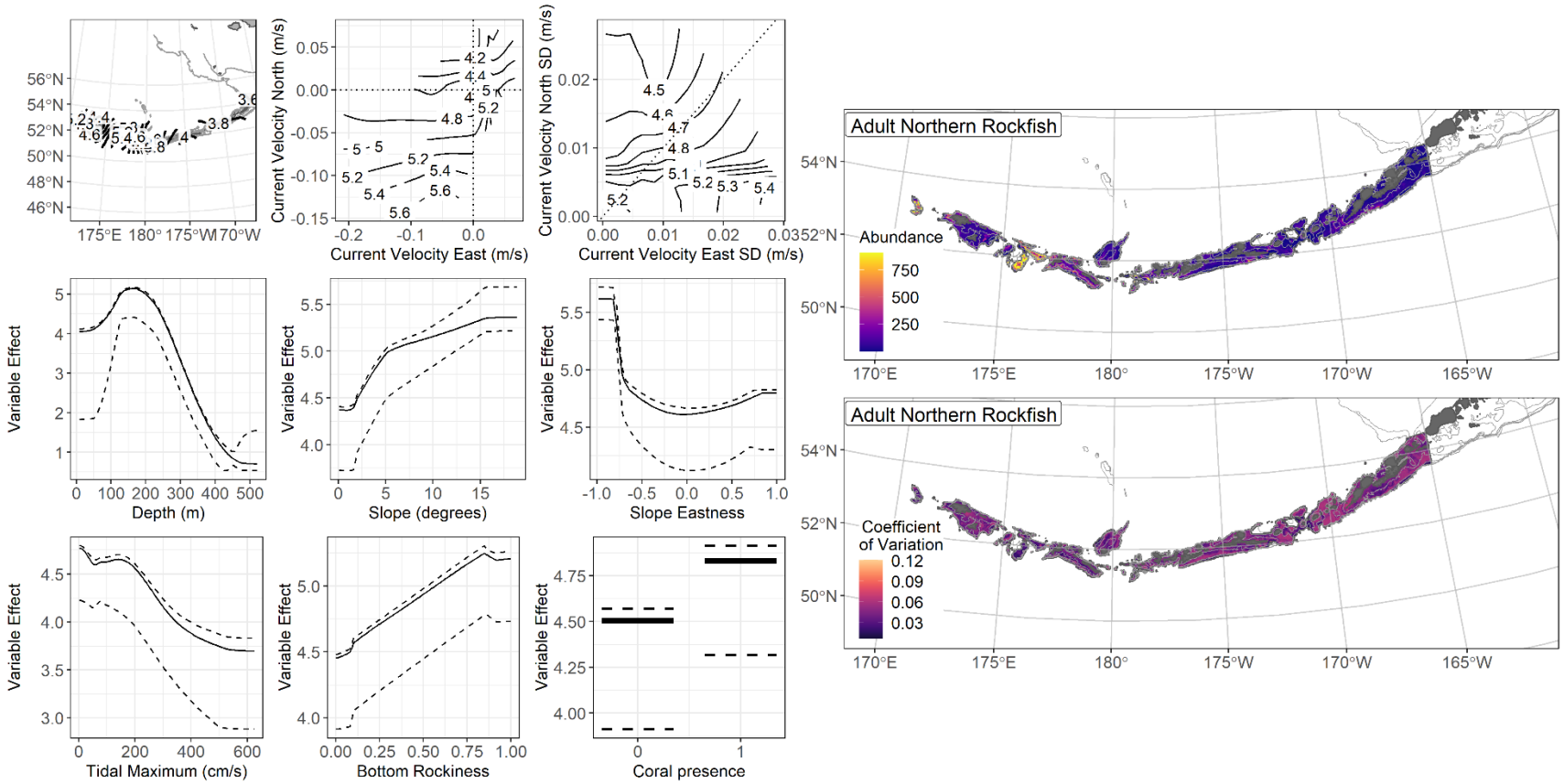


Figure 109. -- The top nine covariate effects (left panel) on ensemble-predicted adult northern rockfish numerical abundance across the AI (upper right panel) alongside the coefficient of variation of the ensemble predictions (lower right panel).

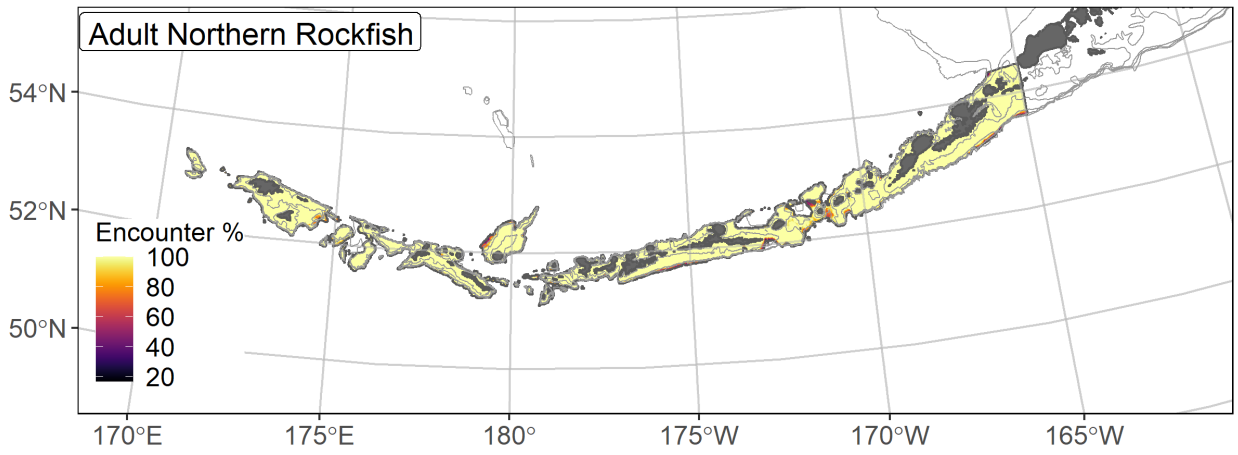


Figure 110. -- Encounter probability of adult northern rockfish from AFSC RACE-GAP summer bottom trawl surveys (1991–2019) of the AI with the 100 m, 300 m, and 500 m isobaths indicated.

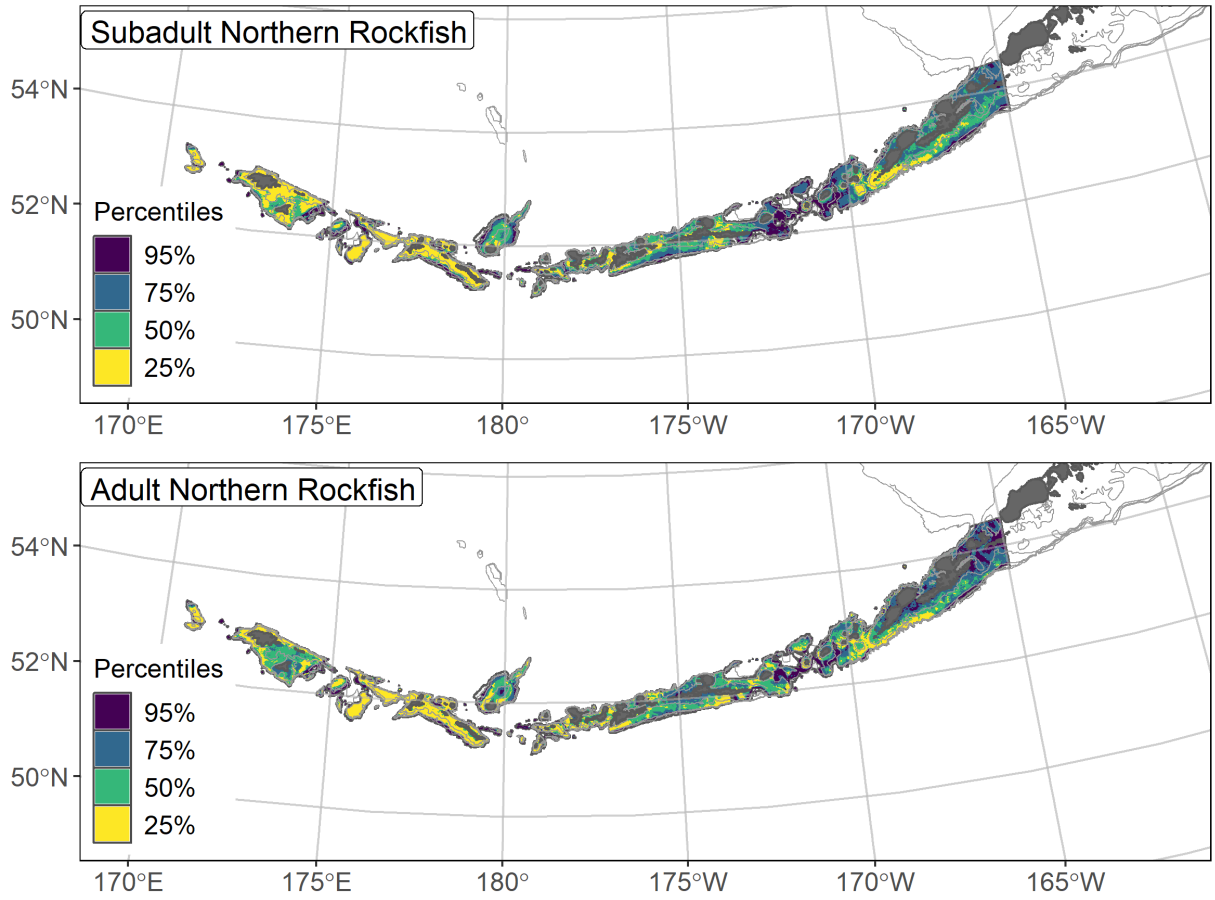


Figure 111. -- Essential fish habitat (EFH area) defined as the top 95% of numerical abundance predictions from a habitat-based ensemble fitted to subadult (top) and adult (bottom) northern rockfish distribution and abundance in AFSC RACE-GAP summer bottom trawl surveys (1991–2019) with 100 m, 300 m, and 500 m isobaths indicated; internal to the EFH map are the subareas of the top 25% (EFH hot spots), top 50% (core EFH area), and top 75% (principal EFH area) of habitat-related, ensemble-predicted numerical abundance.

**Pacific ocean perch (*Sebastes alutus*)**

Pacific ocean perch (*Sebastes alutus*, POP) are distributed across the North Pacific, including the Bering Sea ranging from Baja California to Japan, and are the most common and commercially important rockfish species in the BSAI region (Mecklenburg et al. 2002). Seasonal differences in depth distributions were noted by Love et al. (2002) and compare favorably with the depths where POP are typically encountered on RACE-GAP summer bottom trawl surveys of the EBS (150–300 m). Adults inhabit deeper waters (300–420 m) in fall and winter before migrating in May. Juveniles have been found in shallow (37 m) inshore waters, gradually moving to deeper habitats with age (Carlson and Straty 1981). These rockfish display pronounced diel vertical movements (Brodeur 2001) and often form dense, localized schools off bottom (Hanselman et al. 2001, Hulson et al. 2017). Species in the genus *Sebastes* are ovoviviparous, with internal fertilization and the release of live young. After birthing, early juvenile POP (50–200 mm FL) settle into nursery habitat until they grow large enough to occupy their primary habitat (Pirtle et al. 2019). At approximately 250 mm, subadults become sexually mature and are thought to undertake another habitat transition towards deeper waters (Carlson and Straty 1981, Rooper et al. 2007, Rooper 2008).

**Settled early juvenile Pacific ocean perch distribution and predicted abundance from RACE-GAP summer bottom trawl surveys in the Aleutian Islands –** Settled early juvenile POP were common across most areas covered in the RACE-GAP summer survey of the AI (Fig. 112). Large catches were less common in the eastern AI, but were evenly distributed otherwise. POP do not transition to a subadult lifestyle until the relatively large size of 200 mm, and the bottom trawl survey was able to sample a large number of them. However, it is possible that the current data missed smaller individuals, and additional data sources might be useful for

this life stage[17]. The final ensemble contained four SDMs with approximately equal weights, which showed fair performance compared to the data (Table 33). Specifically, the ensemble showed good ability at predicting presence and absence (AUC = 0.80), and it had fair accuracy at predicting abundance and accounting for variation (ρ = 0.37; PDE = 0.38). Overall, this indicates that the ensemble is able to identify the areas POP are most likely to be found but may not accurately predict the number caught. Considering that POP catches are highly variable and can involve a small handful of individuals or a school of thousands, some uncertainty in numbers is to be expected and these predictions should still provide useful information. Geographic position, bottom depth, and bottom currents were the most important covariates and accounted for 55.0% of the deviance explained in the ensemble (Table 34). This shows that a wide range of variables influenced predictions of settled early juvenile distribution. In general, predicted abundance was high in locations farther west, in 100–300 m depths, with westerly currents, and with corals and sponges (Fig. 113). Predicted abundance was highest in areas of moderate depth, like Seguam Pass and Stalemate Bank (Fig. 113). The predicted CV of abundance was higher near areas of high abundance, which reflected the high variation found in large POP catches (Fig. 113). Encounter probabilities for settled early juvenile POP were high in most places shallower than 300 m and tended to be somewhat lower in the eastern AI (Fig. 114).

**Subadult Pacific ocean perch distribution and predicted abundance from RACE-GAP summer bottom trawl surveys in the Aleutian Islands –** Subadult POP catches were common and evenly distributed within the RACE-GAP summer survey area (Fig. 115). They were present in high density in many places in the eastern AI. The final ensemble contains four SDMs with

[17] A recommendation to add additional survey data types if possible to future SDM ensemble EFH mapping efforts for this species will be included as a future recommendation for research directions from the 2023 EFH 5-year review.

equal weights, and it demonstrated a fair fit to the observed data as measured by all three metrics ($\rho = 0.40$; AUC = 0.78; PDE = 0.39; Table 33). Taken together, this suggested that this ensemble was fairly accurate, but some errors should be expected. Geographic position and bottom depth were the most important covariates but accounted for only 47.3% of the deviance explained, and a variety of other covariates were also important to ensemble predictions (Table 34). Like the early juveniles, moderate depths and rocky substrates had a strong positive effect on model predictions (Fig. 116). Overall abundance of this life stage was predicted to be lowest in the eastern AI and highest around the sea mounts near Seguam Pass, Buldir Strait, and Stalemate Bank (Fig. 116). The predicted coefficient of variation was fairly low in most places and did not display any obvious pattern (Fig. 116). Subadult POP are very common in the AI, and the encounter probability was near 100% in almost all surveyed areas, except the deepest locations along the edge of the continental slope (Fig. 117).

**Adult Pacific ocean perch distribution and predicted abundance from RACE-GAP summer bottom trawl surveys in the Aleutian Islands –** Adult Pacific ocean perch catches were universally common throughout the RACE-GAP summer survey area in the AI (Fig. 118). Large catches occurred across the entire AI area but were somewhat more frequent in the western parts of the island chain. The final ensemble included three SDMs with equal weights, and the predictions showed a good fit, though the metrics suggested some complications (Table 33). Specifically, the ensemble performed well in terms of deviance explained (PDE = 0.46) and excellently in predicting areas of relatively high or low abundance ($\rho = 0.71$). However, it showed poor ability at predicting catches where POP would be present (AUC = 0.68), which likely reflects a failure to predict the minority of catches where POP were absent. In summary, this ensemble performed well at predicting abundance on average, and very well at identifying

the highest abundance catches, but it underestimated the frequency of absences in catches. Bottom depth alone accounted for 68.9% of the deviance explained by the ensemble, while geographic position, slope, and bottom current made smaller contributions (Table 34). The model predicted high abundance in places with moderate depth (200–300 m) and a high slope (Fig. 119). POP were concentrated along the upper edge of the continental slope, usually just above the 300 m depth contour (Fig. 119). The predicted CV of abundance was highest in areas of high abundance along the edge of the continental slope, reflecting that schools of POP vary greatly in size (Fig. 119). The lowest encounter probability predicted by the ensemble was 97%, illustrating that adult POP can be found everywhere in the AI, although not always in large aggregations (Fig. 120).

**Essential fish habitat of settled early juvenile, subadult, and adult Pacific ocean perch in the Aleutian Islands –** The habitat-related abundance predictions based on RACE-GAP summer bottom trawl data (1991–2019) were translated into EFH area and subareas (Fig. 121). The EFH areas for all three life stages encompassed nearly the entire survey area, reflecting that POP were very common in the AI region. Settled early juveniles had EFH hot spots east of Atka Island and around sea mounts in many areas. The EFH areas for subadults were similar but were farther offshore. Adult EFH followed a distinct pattern compared to the other life stages. The EFH hot spots for adults occurred farther offshore and closely tracked the 300 m depth contour.

Table 33. -- Constituent species distribution models (SDMs) used to construct Essential Fish Habitat (EFH) for a) settled early juvenile, b) subadult, and c) adult Pacific ocean perch: MaxEnt = Maximum entropy; paGAM = presence-absence generalized additive model; hGAM = hurdle GAM; $GAM_P$ = standard Poisson GAM; and $GAM_{nb}$ = standard negative-binomial GAM. Ensemble performance (ρ = Spearman's rank correlation coefficient), root-mean-square-error (RMSE), the area under the receiver operating characteristic (AUC), and the Poisson deviance explained (PDE) were generated from k-fold cross-validation. The "--" in a field indicates that this SDM was not included in the final ensemble.

**a) settled early juvenile Pacific ocean perch**

| Models | RMSE | Relative weight | ρ | AUC | PDE | EFH area ($km^2$) |
|---|---|---|---|---|---|---|
| MaxEnt | 71.7 | 0.25 | 0.37 | 0.81 | 0.17 | 65,500 |
| paGAM | 71.9 | 0.25 | 0.35 | 0.80 | 0.14 | 75,600 |
| hGAM | 72.9 | 0.25 | 0.26 | 0.79 | 0.10 | 58,700 |
| $GAM_P$ | 72.8 | 0.25 | 0.26 | 0.72 | 0.06 | 52,500 |
| $GAM_{nb}$ | 76.0 | 0 | 0.34 | 0.79 | 0.21 | -- |
| ensemble | 68.8 | 1 | 0.37 | 0.80 | 0.38 | 69,600 |

**b) subadult Pacific ocean perch**

| Models | RMSE | Relative weight | ρ | AUC | PDE | EFH area ($km^2$) |
|---|---|---|---|---|---|---|
| MaxEnt | 185.6 | 0.25 | 0.40 | 0.79 | 0.17 | 73,900 |
| paGAM | 184.7 | 0.25 | 0.40 | 0.79 | 0.17 | 77,600 |
| hGAM | 184.7 | 0.25 | 0.28 | 0.79 | 0.21 | 73,500 |
| $GAM_P$ | 185.4 | 0.25 | 0.30 | 0.71 | 0.22 | 66,200 |
| $GAM_{nb}$ | 212.6 | 0 | 0.37 | 0.77 | 0.19 | -- |
| ensemble | 174.5 | 1 | 0.40 | 0.78 | 0.39 | 77,500 |

**c) adult Pacific ocean perch**

| Models | RMSE | Relative weight | ρ | AUC | PDE | EFH area ($km^2$) |
|---|---|---|---|---|---|---|
| MaxEnt | -- | 0 | -- | -- | -- | -- |
| paGAM | 1,734 | 0.32 | 0.69 | 0.87 | 0.28 | 77,700 |
| hGAM | 1,668 | 0.34 | 0.66 | 0.87 | 0.44 | 77,700 |
| $GAM_P$ | 1,668 | 0.34 | 0.65 | 0.70 | 0.45 | 77,500 |
| $GAM_{nb}$ | 2,018 | 0 | 0.69 | 0.84 | 0.35 | -- |

| Models | RMSE | Relative weight | ρ | AUC | PDE | EFH area ($km^2$) |
|---|---|---|---|---|---|---|
| ensemble | 1,568 | 1 | 0.71 | 0.68 | 0.46 | 77,700 |

Table 34. -- Covariates retained in the a) settled early juvenile, b) subadult, and c) adult Pacific ocean perch species distribution model (SDM) final ensembles, the percent contribution to the ensemble deviance explained by each, and the cumulative percent deviance: SD = standard deviation, and BPI = bathymetric position index.

| Pacific ocean perch | Covariate | % Contribution | Cumulative % Contribution |
|---|---|---|---|
| **a) settled early juvenile** | bottom depth | 22.0 | 22.0 |
| | position | 18.1 | 40.1 |
| | current | 13.8 | 53.9 |
| | sponge presence | 5.9 | 59.8 |
| | current SD | 5.8 | 65.6 |
| | aspect north | 5.3 | 70.9 |
| | coral presence | 5.3 | 76.2 |
| | bottom temperature | 5.0 | 81.2 |
| | rockiness | 4.7 | 85.9 |
| | aspect east | 4.4 | 90.3 |
| | tidal maximum | 3.8 | 94.1 |
| | BPI | 3.2 | 97.3 |
| | slope | 1.7 | 99.0 |
| | curvature | 0.9 | 99.9 |
| | pennatulacean presence | 0.1 | 100 |
| **b) subadult** | bottom depth | 29.3 | 29.3 |
| | position | 18.0 | 47.3 |
| | aspect east | 7.5 | 54.8 |
| | current SD | 7.4 | 62.2 |
| | rockiness | 6.8 | 69.0 |
| | sponge presence | 5.6 | 74.6 |
| | current | 4.9 | 79.5 |
| | BPI | 4.8 | 84.3 |
| | coral presence | 3.5 | 87.8 |
| | tidal maximum | 3.2 | 91.0 |
| | aspect north | 2.9 | 93.9 |
| | bottom temperature | 2.4 | 96.3 |
| | slope | 1.9 | 98.2 |
| | curvature | 1.8 | 100 |
| | pennatulacean presence | 0 | 100 |
| **c) adult** | bottom depth | 68.9 | 68.9 |
| | position | 9.7 | 78.6 |
| | current | 7.1 | 85.7 |
| | slope | 4.2 | 90.0 |
| | BPI | 2.9 | 92.9 |

| Pacific ocean perch | Covariate | % Contribution | Cumulative % Contribution |
|---|---|---|---|
| | sponge presence | 1.5 | 94.4 |
| | current SD | 1.2 | 95.6 |
| | rockiness | 0.9 | 96.5 |
| | aspect east | 0.8 | 97.3 |
| | coral presence | 0.8 | 98.0 |
| | aspect north | 0.8 | 98.8 |
| | bottom temperature | 0.6 | 99.4 |
| | tidal maximum | 0.3 | 99.7 |
| | pennatulacean presence | 0.2 | 99.8 |
| | curvature | 0.2 | 100 |

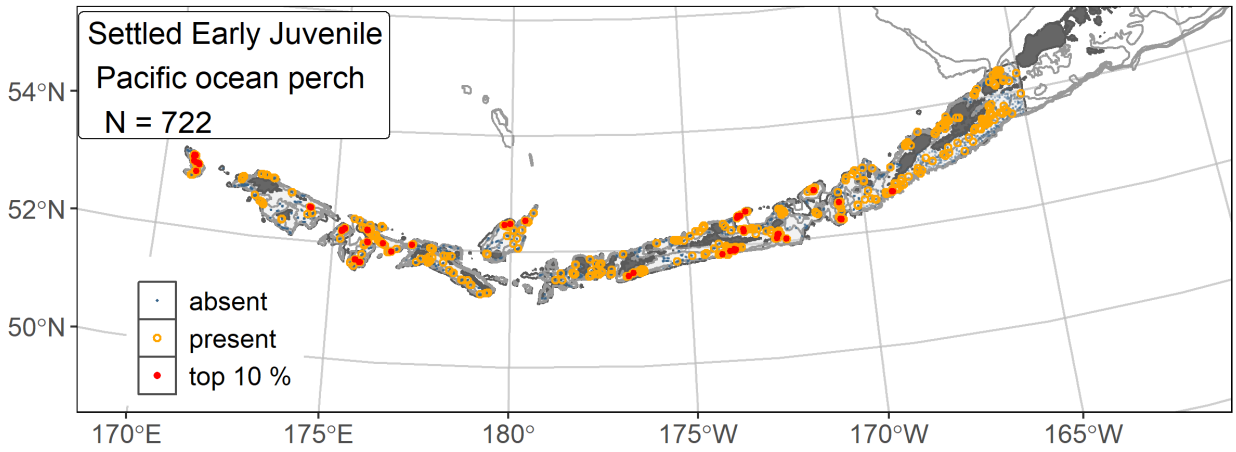


Figure 112. -- Distribution of settled early juvenile Pacific ocean perch catches (N = 722) in 1991–2019 AFSC RACE-GAP summer bottom trawl surveys of the AI with the 100 m, 300 m, and 500 m isobaths indicated; filled red circles indicate locations in top 10% of overall abundance, open orange circles indicate presence in remaining catches, and small blue dots indicate absence.

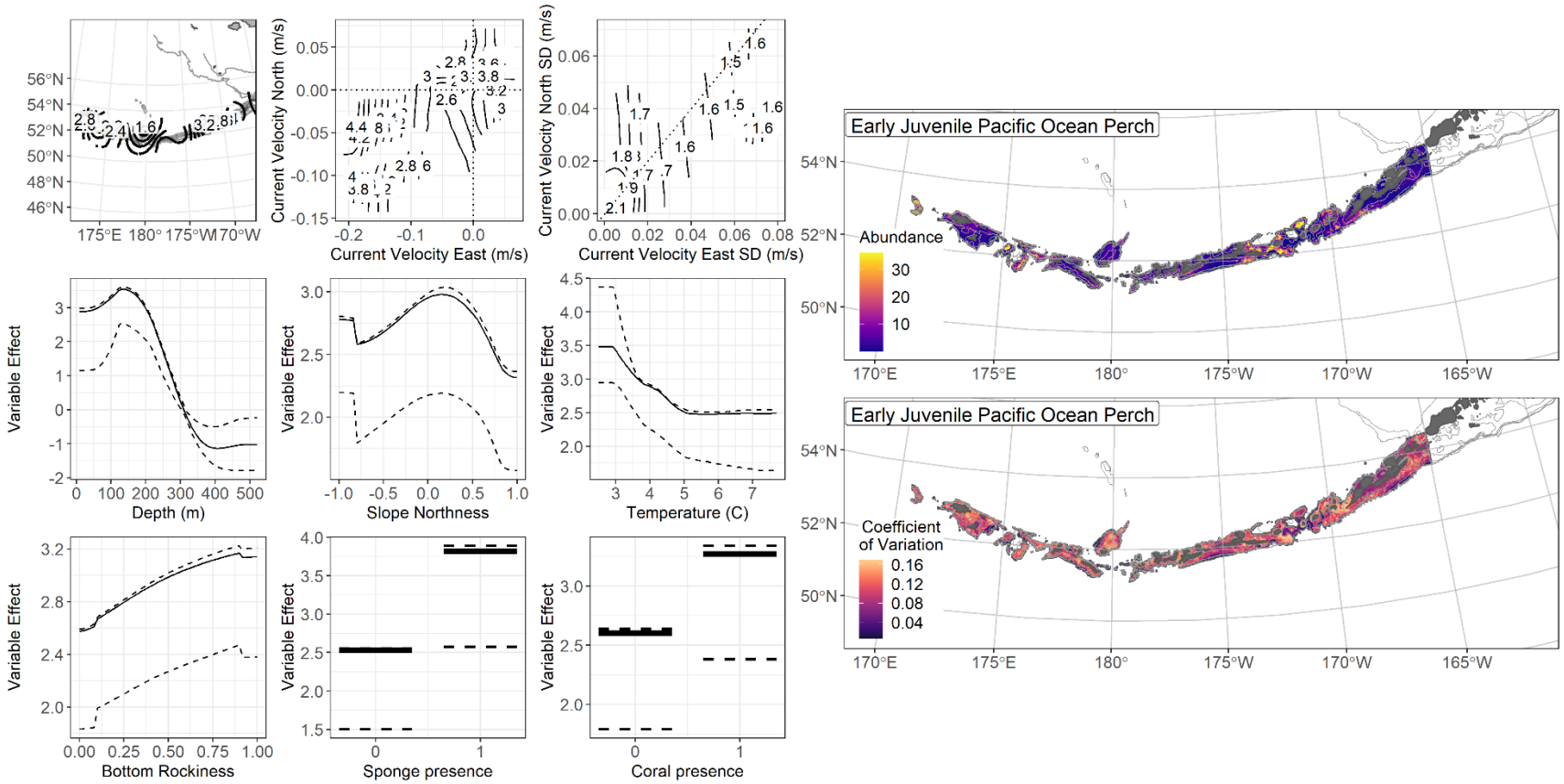


Figure 113. -- The top nine covariate effects (left panel) on ensemble-predicted settled early juvenile Pacific ocean perch numerical abundance across the AI (upper right panel) alongside the coefficient of variation of the ensemble predictions (lower right panel).

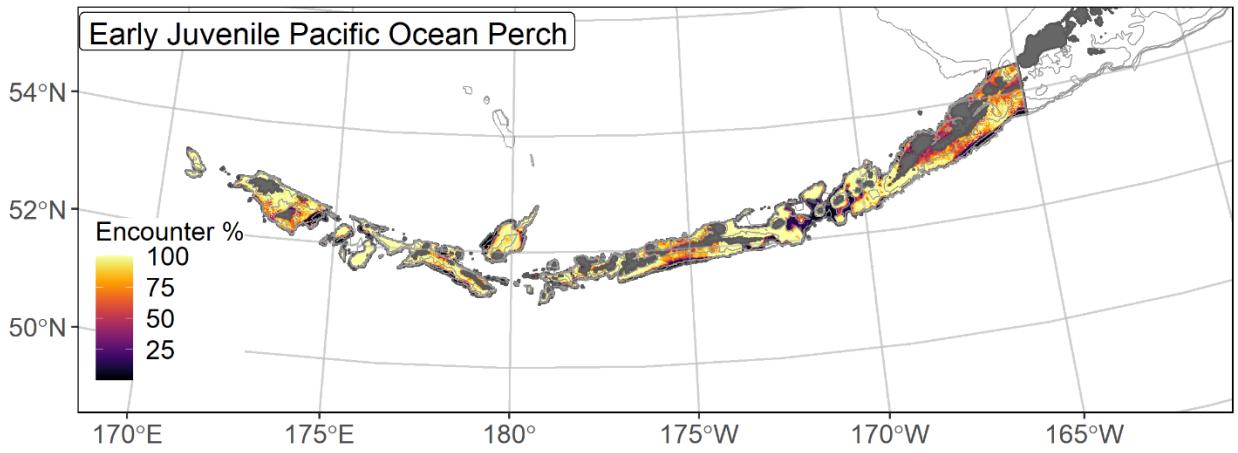


Figure 114. -- Encounter probability of settled early juvenile Pacific ocean perch from AFSC RACE-GAP summer bottom trawl surveys (1991–2019) of the AI with the 100 m, 300 m, and 500 m isobaths indicated.

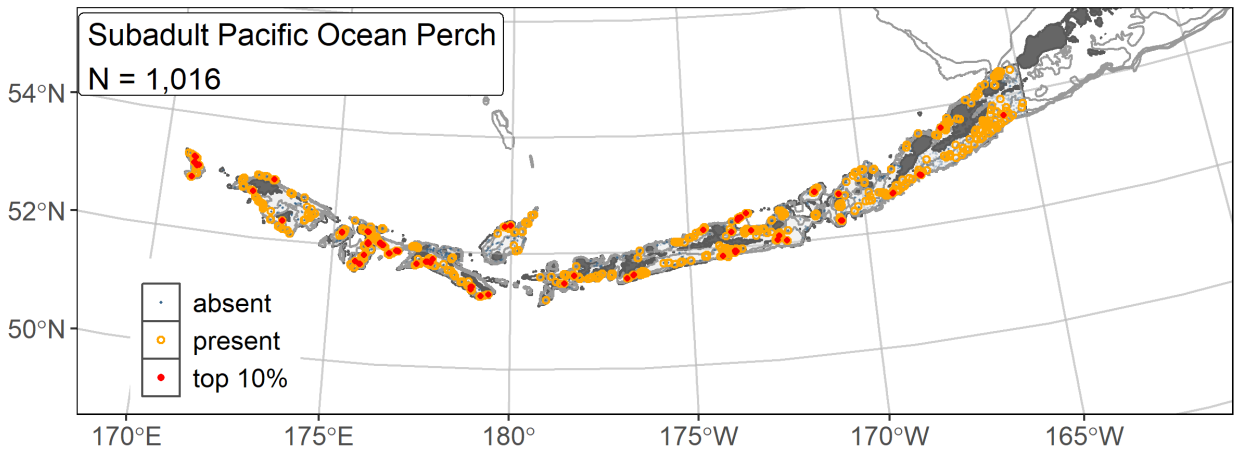


Figure 115. -- Distribution of subadult Pacific ocean perch catches (N = 1,016) in 1991–2019 AFSC RACE-GAP summer bottom trawl surveys of the AI with the 100 m, 300 m, and 500 m isobaths indicated; filled red circles indicate locations in top 10% of overall abundance, open orange circles indicate presence in remaining catches, and small blue dots indicate absence.

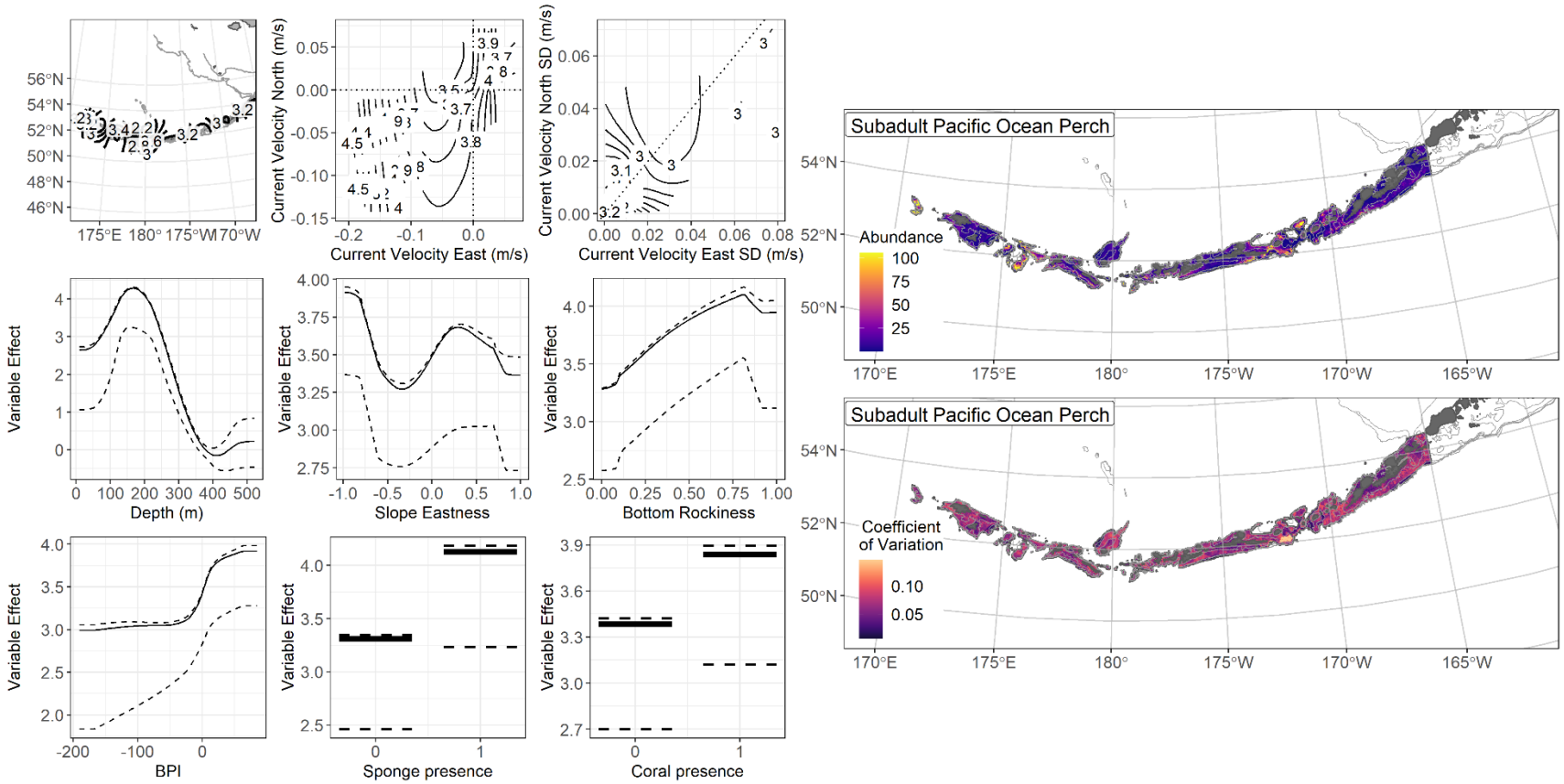


Figure 116. -- The top nine covariate effects (left panel) on ensemble-predicted subadult Pacific ocean perch numerical abundance across the AI (upper right panel) alongside the coefficient of variation of the ensemble predictions (lower right panel).

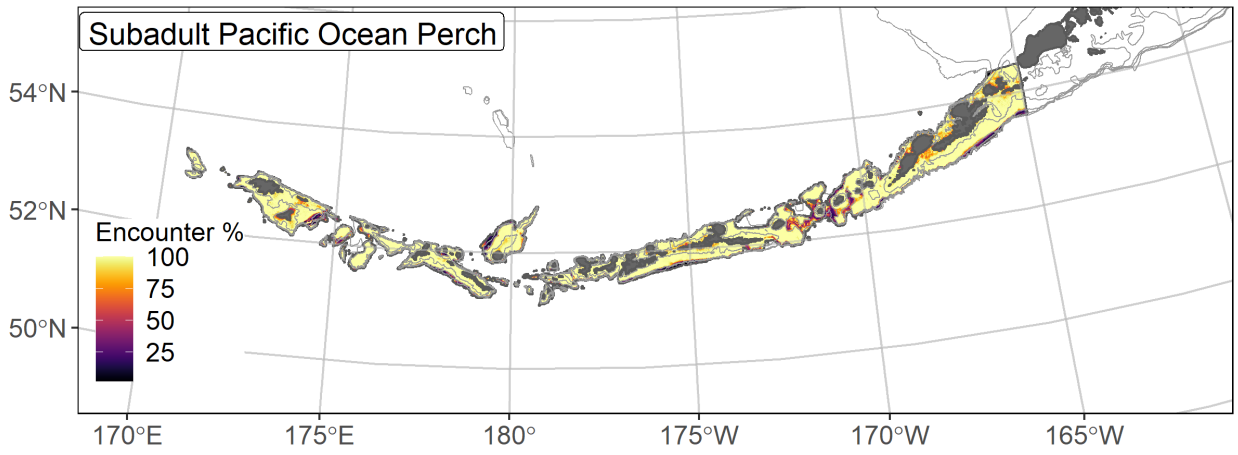


Figure 117. -- Encounter probability of subadult Pacific ocean perch from AFSC RACE-GAP summer bottom trawl surveys (1991–2019) of the AI with the 100 m, 300 m, and 500 m isobaths indicated.

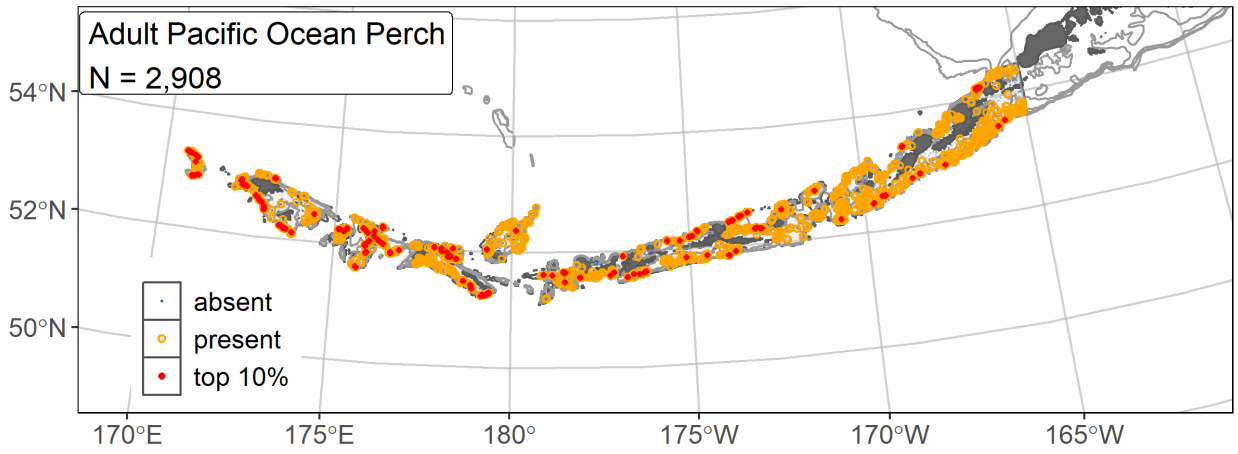


Figure 118. -- Distribution of adult Pacific ocean perch catches (N = 2,908) in 1991–2019 AFSC RACE-GAP summer bottom trawl surveys of the AI with the 100 m, 300 m, and 500 m isobaths indicated; filled red circles indicate locations in top 10% of overall abundance, open orange circles indicate presence in remaining catches, and small blue dots indicate absence.

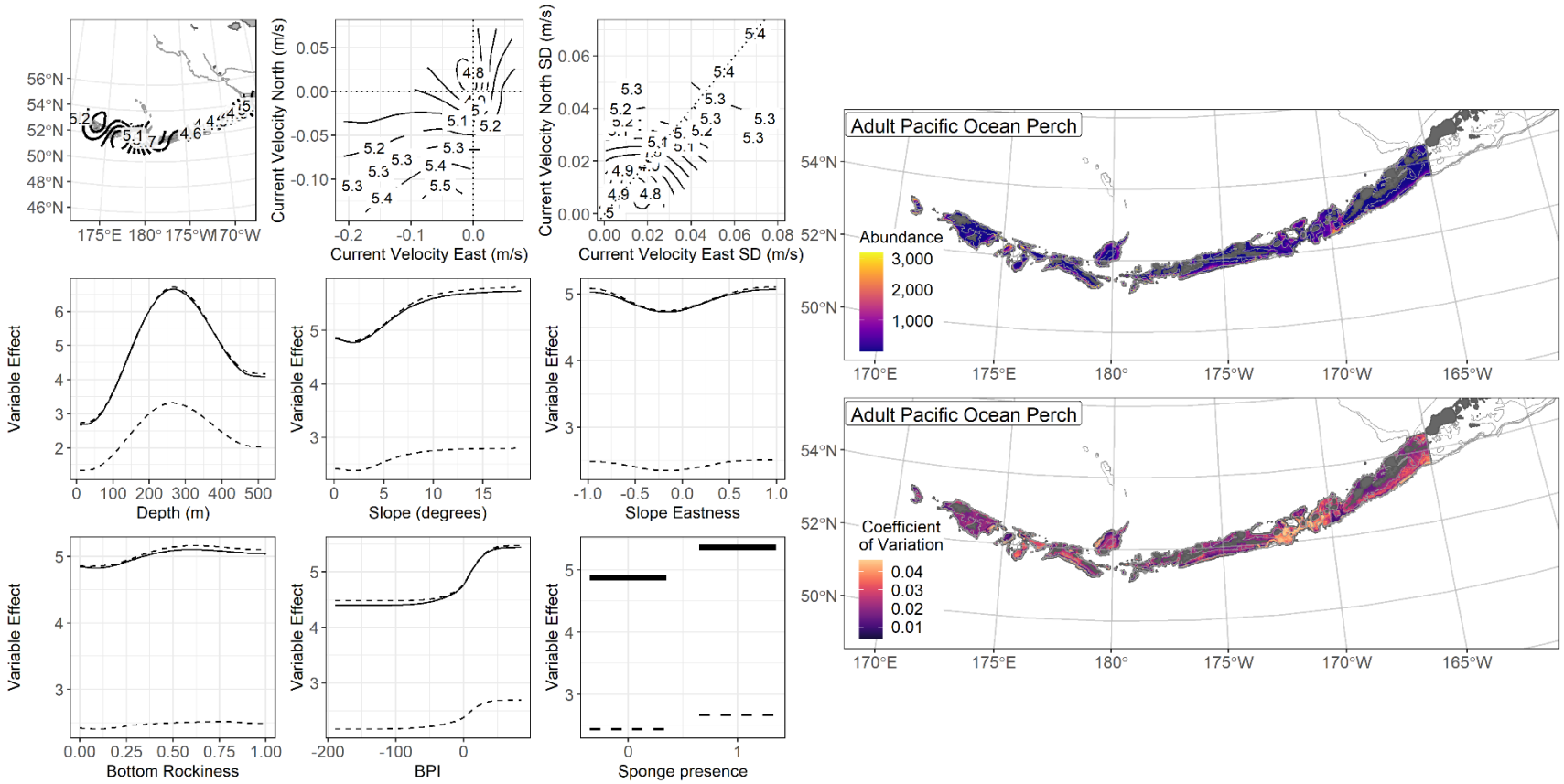


Figure 119. -- The top nine covariate effects (left panel) on ensemble-predicted adult Pacific ocean perch numerical abundance across the AI (upper right panel) alongside the coefficient of variation of the ensemble predictions (lower right panel)

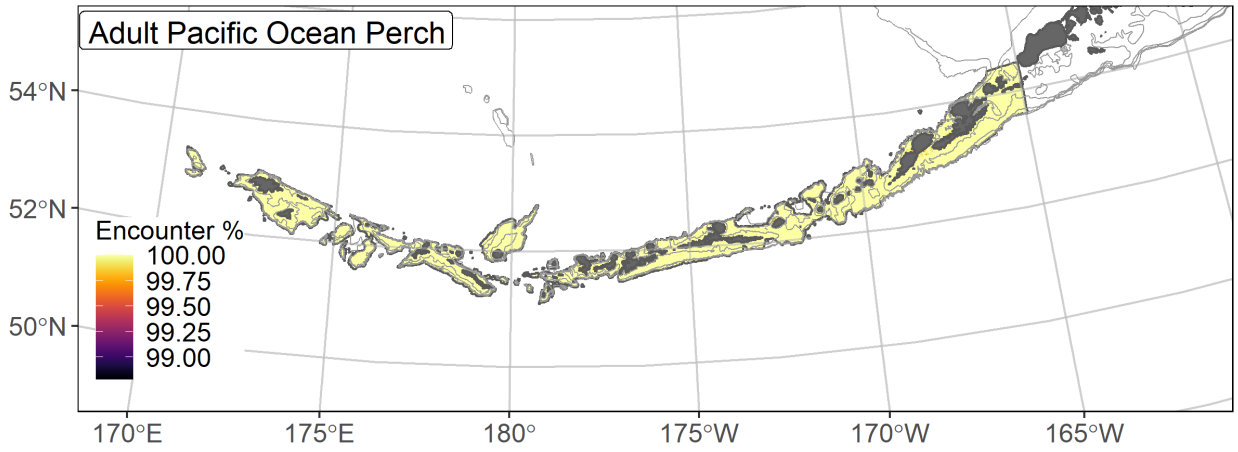


Figure 120. -- Encounter probability of adult Pacific ocean perch from AFSC RACE-GAP summer bottom trawl surveys (1991–2019) of the AI with the 100 m, 300 m, and 500 m isobaths indicated.

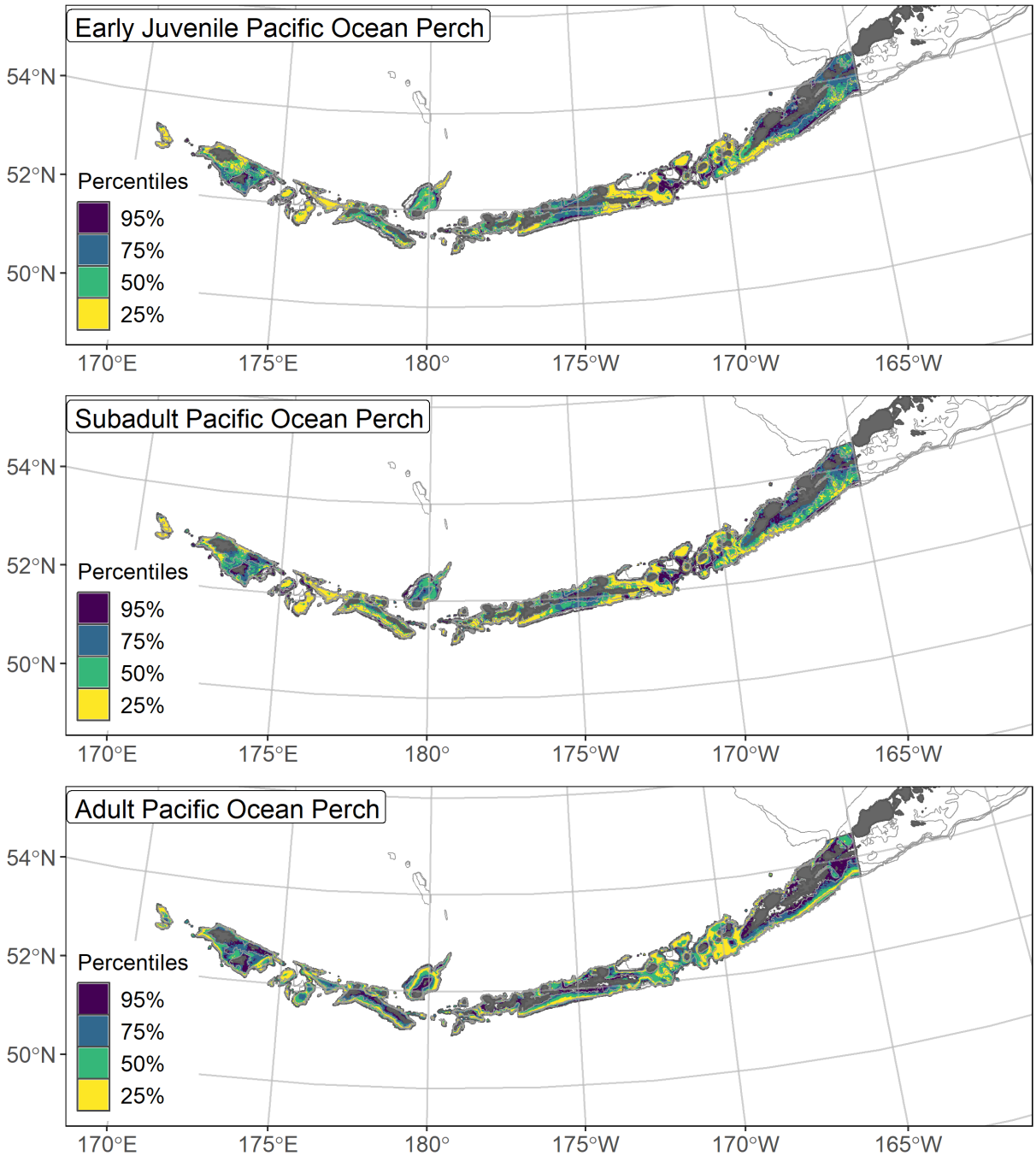


Figure 121. -- Essential fish habitat (EFH area) defined as the top 95% of numerical abundance predictions from a habitat-based ensemble fitted to settled early juvenile (top), subadult (middle), and adult (bottom) Pacific ocean perch distribution and abundance in AFSC RACE-GAP summer bottom trawl surveys (1991–2019) with 100 m, 300 m, and 500 m isobaths indicated; internal to the EFH map are the subareas of the top 25% (EFH hot spots), top 50% (core EFH area), and top 75% (principal EFH area) of habitat-related, ensemble-predicted numerical abundance.

**Shortraker rockfish (*Sebastes borealis*)**

Shortraker rockfish (*Sebastes borealis*) range from Japan to California, including the Bering Sea (Mecklenburg et al. 2002). With a maximum size of 1,130 mm, this is the largest species of rockfish encountered in the Alaska trawl surveys, and ageing studies suggest they can live up to 157 years, making them one of the oldest animal species on earth. They are most abundant on the continental slope at depths between 300 and 500 m (Rooper 2008) though they range from 25 to 1,200 m. Shortraker rockfish become mature at a length of 499 mm FL (Conrath 2017), and like other species in the genus, they show internal fertilization and egg development, leading to the release of live larvae. Shortraker rockfish are seasonal synchronous spawners, with the onset of egg development occurring later in the summer and parturition taking place from March through May (Conrath 2017). Although not as commercially important as species like Pacific ocean perch (*S. alutus*), the slow development and late maturity of shortraker rockfish make them potentially vulnerable to overfishing and they have received a separate assessment in the BSAI region since 2004 (Shotwell et al. 2020b).

**Subadult shortraker rockfish distribution and predicted abundance from RACE-GAP summer bottom trawl surveys in the Aleutian Islands –** Subadult shortraker rockfish were common along many of the continental slope areas covered in the RACE-GAP summer survey of the AI (Fig. 122). All large catches occurred in deep water around the 300 m depth contour and were more common on the south side of the island chain. The final ensemble contains three SDMs with the paGAM given less weight than the others, and it demonstrated good to excellent accuracy when compared to the observed data (Table 35). In particular, the ensemble performed excellently at predicting presence/absence (AUC = 0.98) and explained most of the deviance (0.86). The ensemble scored less well according to its Spearman correlation, which scored in the

range considered good (ρ = 0.47). The high PDE and AUC scores suggest that the model is very accurate at predicting bottom trawl catches. Bottom depth was the most important covariate in the ensemble and accounted for 50.6% of the deviance explained, though geographic position, current, and slope were also somewhat important (Table 36). Predicted abundance was generally high in locations with more than 350 m depth, with weak or southwesterly currents, and with a sloping bottom (Fig. 123). Most shortraker rockfish were predicted deeper than 300 m, with the highest abundance occurring in scattered patches along the 500 m depth contour (Fig. 123). The predicted CV of abundance mirrored the abundance map, with more variation in deep water and zero in shallow areas where the species almost never occurs (Fig. 123). Encounter probabilities for subadults were high in most places below the 300 m depth contour and very low in shallower areas (Fig. 124).

**Adult shortraker rockfish distribution and predicted abundance from RACE-GAP summer bottom trawl surveys in the Aleutian Islands –** Adult shortraker rockfish catches from the RACE-GAP summer survey followed the same pattern as subadults and were restricted to areas deeper than 300 m along the continental slope (Fig. 125). The final ensemble contained three SDMs with equal weight and demonstrated a good to excellent fit to the observed data (Table 35). The pattern observed in the adult metrics was similar to that of subadults; the ensemble scored excellently at predicting presence/absence (AUC = 0.96) and on measures of deviance explained (PDE = 0.76), and it achieved a good rating in terms of Spearman correlation (ρ = 0.48). Overall, this suggested that the ensemble predictions are accurate both in predicting which catches will contain shortraker rockfish and roughly how many will be caught. Like subadults, bottom depth, geographic position, bottom currents, and slope were the most important covariates (Table 36). Similar to subadults, the ensemble predicted that adult

abundance will be high in locations with deeper water, southwesterly currents, and a sloped bottom (Fig. 126). The predicted abundance map showed that adults mostly occupy habitats below the 300 m depth contour, with the highest densities found even deeper, particularly around Amchitka Pass (Fig. 126). The predicted CV of abundance was highest just above the 300 m depth contour where this life stage is sometimes absent (Fig. 126). Similar to the abundance map, the map of encounter probability showed a fairly high chance of catching shortraker rockfish below 300 m and a very low chance above that (Fig. 127).

**Essential fish habitat of subadult and adult shortraker rockfish in the Aleutian Islands –** The habitat-related abundance predictions based on RACE-GAP summer bottom trawl data (1991–2019) were translated into EFH area and subareas (Fig. 128). Both life stages displayed the same pattern in their abundance and EFH, and it is difficult to point to any differences between them. The EFH encompassed most of the area between the 300 m and 500 m depth contours, with intermittent hot spots along the continental slope south of the AI and around the deeper passes between the islands. Given its depth preferences and other observations of this species, it seems likely that much of its essential habitat exists in depths beyond what is covered in the bottom trawl survey. While this project has produced high quality models for both life stages, additional sources of data (i.e., longline surveys) could help extend these findings for of shortraker rockfish[18].

[18] A recommendation to add additional survey data types if possible to future SDM ensemble EFH mapping efforts for this species will be included as a future recommendation for research directions from the 2023 EFH 5-year review.

Table 35. -- Constituent species distribution models (SDMs) used to construct Essential Fish Habitat (EFH) for a) subadult and b) adult shortraker rockfish: MaxEnt = Maximum entropy; paGAM = presence-absence generalized additive model; hGAM = hurdle GAM; $GAM_P$ = standard Poisson GAM; and $GAM_{nb}$ = standard negative-binomial GAM. Ensemble performance (ρ = Spearman's rank correlation coefficient), root-mean-square-error (RMSE), the area under the receiver operating characteristic (AUC), and the Poisson deviance explained (PDE) were generated from k-fold cross-validation. The "--" in a field indicates that this SDM was not included in the final ensemble.

**a) subadult shortraker rockfish**

| Models | RMSE | Relative weight | ρ | AUC | PDE | EFH area ($km^2$) |
|---|---|---|---|---|---|---|
| MaxEnt | -- | 0 | -- | -- | -- | -- |
| paGAM | 13.6 | 0.27 | 0.45 | 0.98 | 0.71 | 26,200 |
| hGAM | 11.4 | 0.38 | 0.50 | 0.98 | 0.77 | 21,600 |
| $GAM_P$ | 11.9 | 0.35 | 0.50 | 0.96 | 0.76 | 21,100 |
| $GAM_{nb}$ | 15.4 | 0 | 0.51 | 0.97 | 0.71 | -- |
| ensemble | 8.4 | 1 | 0.47 | 0.98 | 0.86 | 23,300 |

**b) adult shortraker rockfish**

| Models | RMSE | Relative weight | ρ | AUC | PDE | EFH area ($km^2$) |
|---|---|---|---|---|---|---|
| MaxEnt | -- | 0 | -- | -- | -- | -- |
| paGAM | 9.53 | 0.28 | 0.47 | 0.96 | 0.55 | 29,500 |
| hGAM | 8.54 | 0.34 | 0.48 | 0.96 | 0.66 | 26,100 |
| $GAM_P$ | 8.10 | 0.38 | 0.49 | 0.95 | 0.66 | 25,500 |
| $GAM_{nb}$ | 9.68 | 0 | 0.51 | 0.96 | 0.58 | -- |
| ensemble | 6.14 | 1 | 0.48 | 0.96 | 0.76 | 27,400 |

Table 36. -- Covariates retained in the a) subadult and b) adult shortraker rockfish species distribution model (SDM) final ensembles, the percent contribution to the ensemble deviance explained by each, and the cumulative percent deviance: SD = standard deviation, and BPI = bathymetric position index.

| Shortraker rockfish | Covariate | % Contribution | Cumulative % Contribution |
|---|---|---|---|
| **a) subadult** | bottom depth | 50.6 | 50.6 |
| | position | 19.5 | 70.1 |
| | current | 10.5 | 80.5 |
| | slope | 6.4 | 86.9 |
| | rockiness | 3.8 | 90.7 |
| | current SD | 2.7 | 93.4 |
| | BPI | 1.3 | 94.7 |
| | aspect east | 1.2 | 95.9 |
| | aspect north | 1.1 | 97.0 |
| | curvature | 1.0 | 98.0 |
| | tidal maximum | 0.7 | 98.7 |
| | coral presence | 0.5 | 99.2 |
| | sponge presence | 0.4 | 99.6 |
| | bottom temperature | 0.2 | 99.8 |
| | pennatulacean presence | 0.2 | 100 |
| **b) adult** | bottom depth | 36.7 | 36.7 |
| | position | 22.6 | 59.3 |
| | current SD | 8.5 | 67.8 |
| | current | 6.5 | 74.3 |
| | aspect east | 6.3 | 80.6 |
| | slope | 4.7 | 85.3 |
| | rockiness | 3.3 | 88.6 |
| | BPI | 3.0 | 91.6 |
| | aspect north | 2.8 | 94.4 |
| | tidal maximum | 1.5 | 95.9 |
| | bottom temperature | 1.3 | 97.2 |
| | sponge presence | 1.3 | 98.5 |
| | coral presence | 0.7 | 99.2 |
| | curvature | 0.7 | 99.9 |
| | pennatulacean presence | 0.1 | 100 |

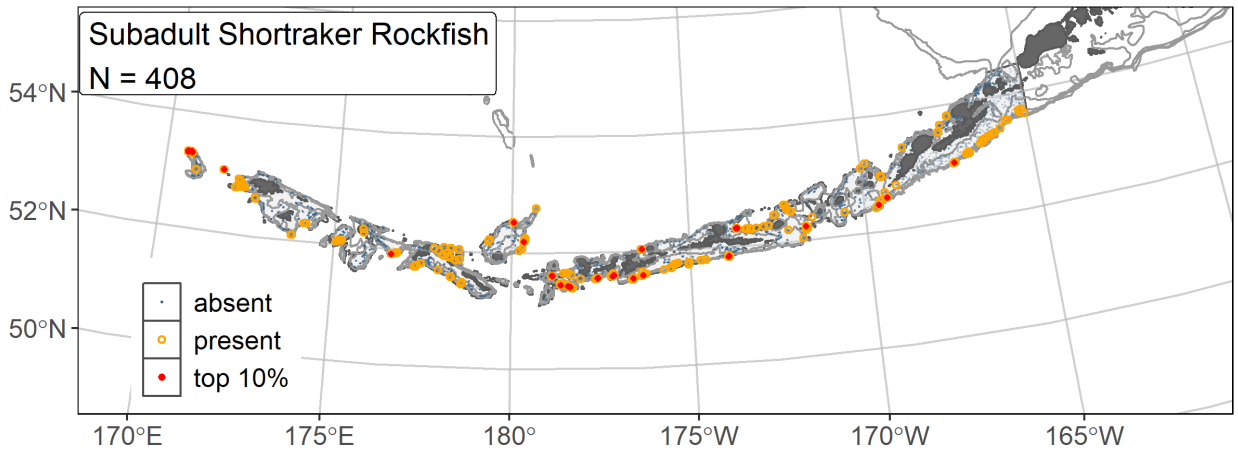


Figure 122. -- Distribution of subadult shortraker rockfish catches (N = 408) in 1991–2019 AFSC RACE-GAP summer bottom trawl surveys of the AI with the 100 m, 300 m, and 500 m isobaths indicated; filled red circles indicate locations in top 10% of overall abundance, open orange circles indicate presence in remaining catches, and small blue dots indicate absence.

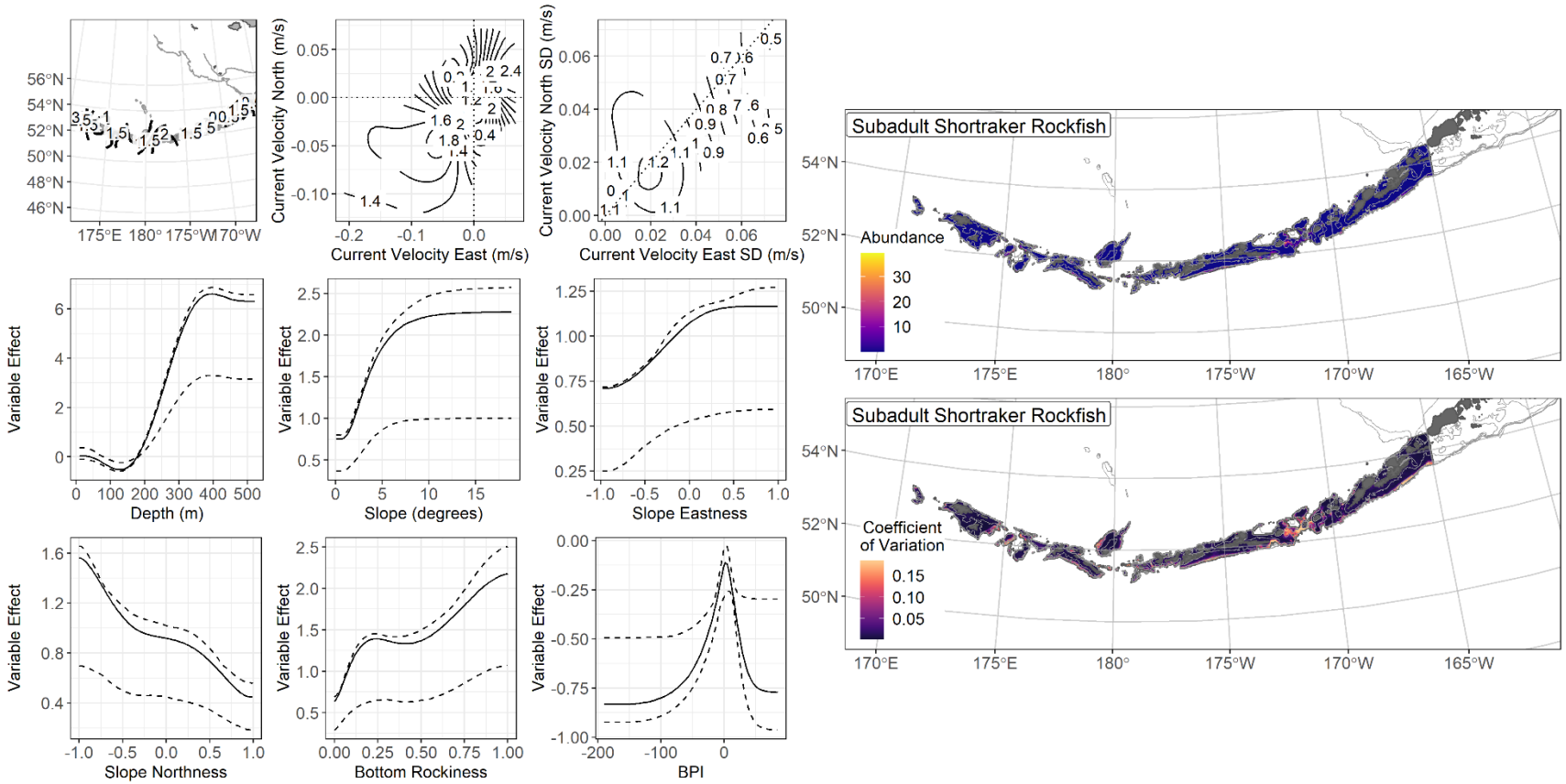


Figure 123. -- The top nine covariate effects (left panel) on ensemble-predicted subadult shortraker rockfish numerical abundance across the AI (upper right panel) alongside the coefficient of variation of the ensemble predictions (lower right panel).

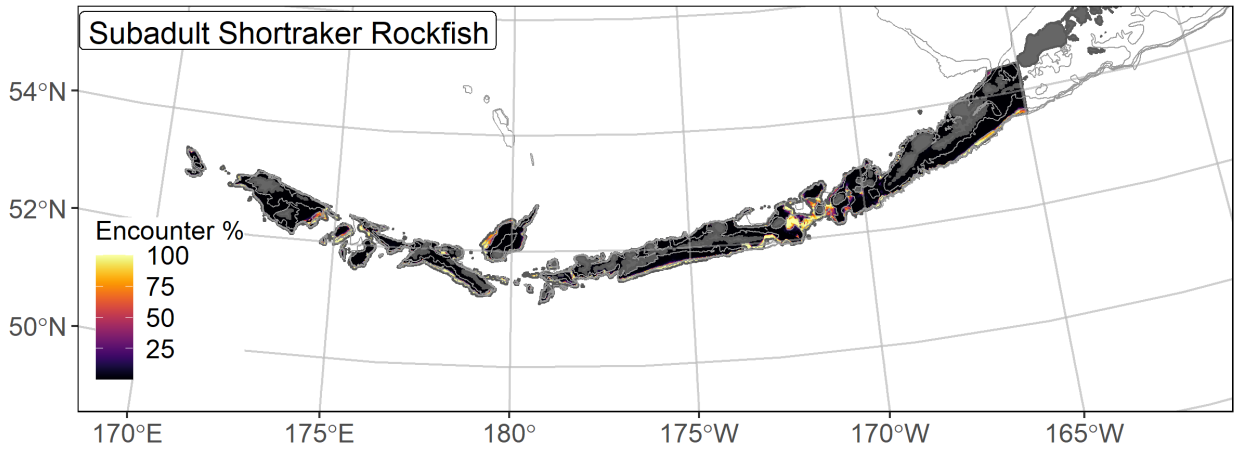


Figure 124. -- Encounter probability of subadult shortraker rockfish from AFSC RACE-GAP summer bottom trawl surveys (1991–2019) of the AI with the 100 m, 300 m, and 500 m isobaths indicated.

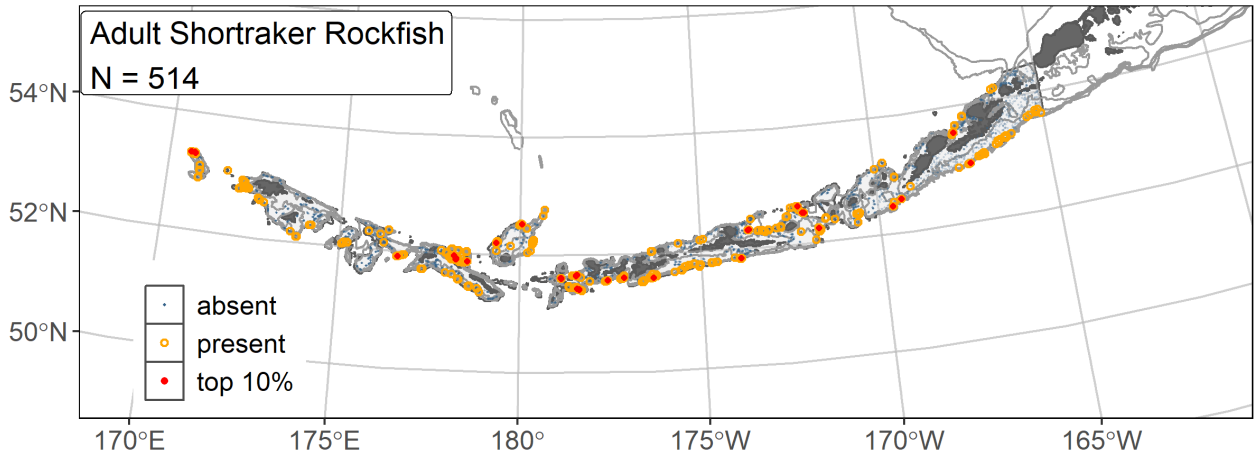


Figure 125. -- Distribution of adult shortraker rockfish catches (N = 514) in 1991–2019 AFSC RACE-GAP summer bottom trawl surveys of the AI with the 100 m, 300 m, and 500 m isobaths indicated; filled red circles indicate locations in top 10% of overall abundance, open orange circles indicate presence in remaining catches, and small blue dots indicate absence.

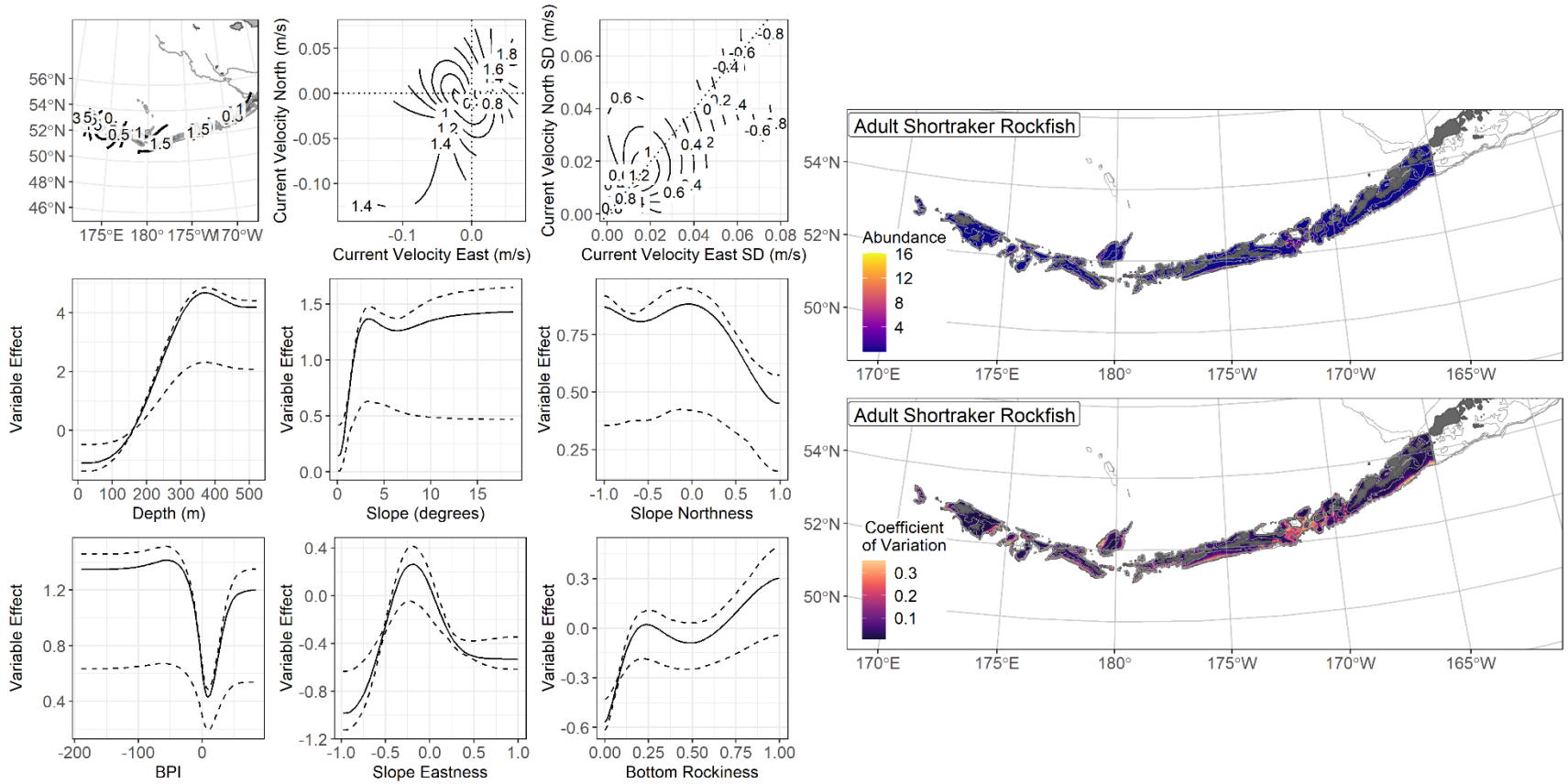


Figure 126. -- The top nine covariate effects (left panel) on ensemble-predicted adult shortraker rockfish numerical abundance across the AI (upper right panel) alongside the coefficient of variation of the ensemble predictions (lower right panel).

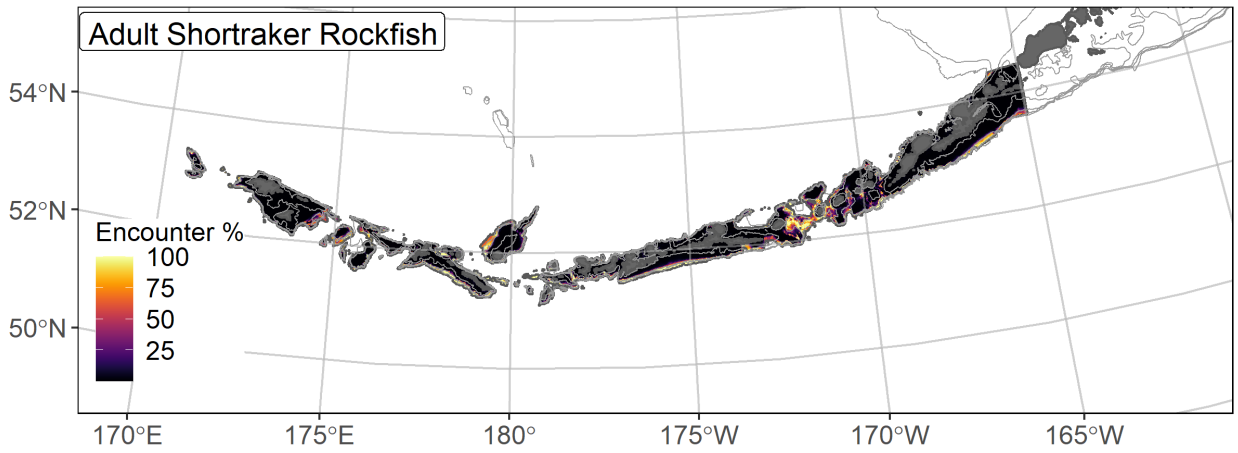


Figure 127. -- Encounter probability of adult shortraker rockfish from AFSC RACE-GAP summer bottom trawl surveys (1991–2019) of the AI with the 100 m, 300 m, and 500 m isobaths indicated.

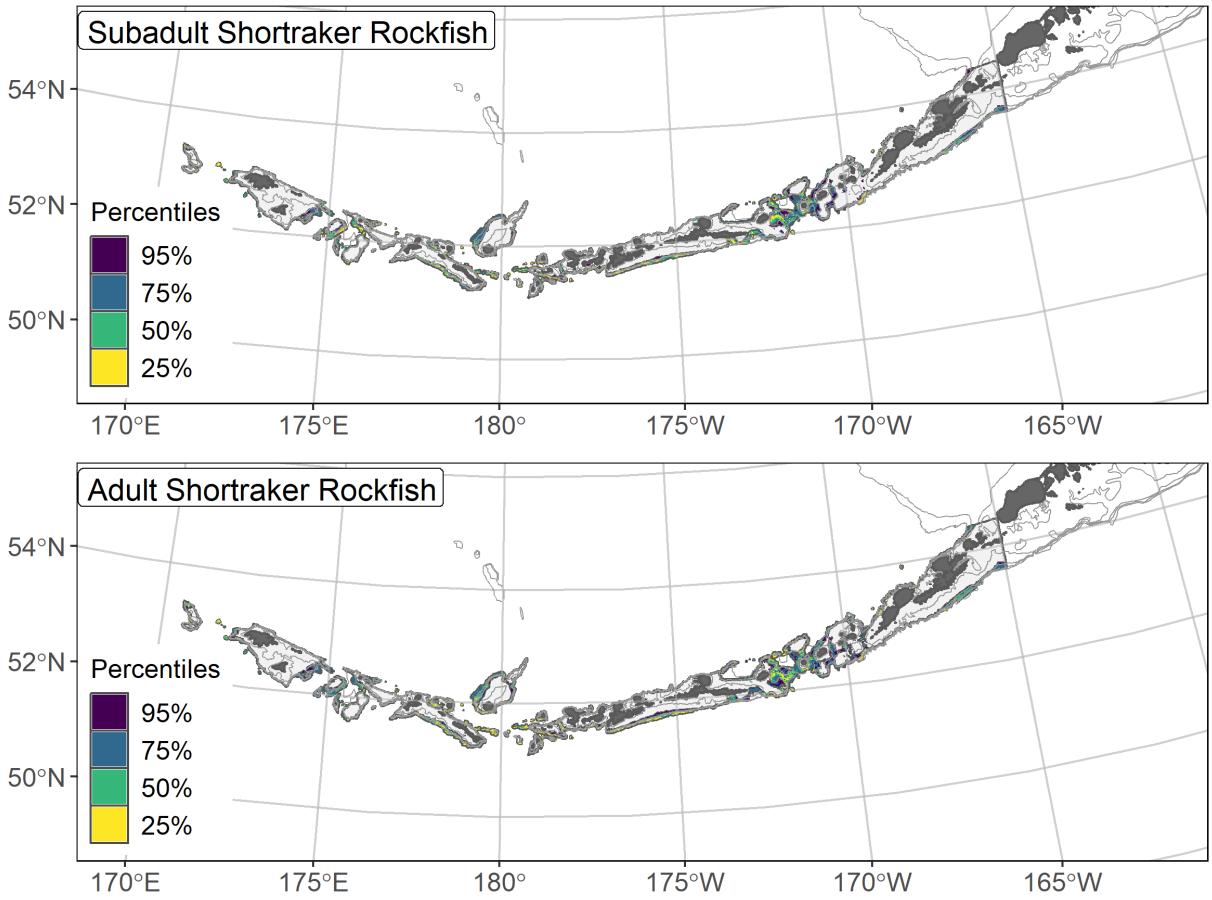


Figure 128. -- Essential fish habitat (EFH area) defined as the top 95% of numerical abundance predictions from a habitat-based ensemble fitted to subadult (top) and adult (bottom) shortraker rockfish distribution and abundance in AFSC RACE-GAP summer bottom trawl surveys (1991–2019) with 100 m, 300 m, and 500 m isobaths indicated; internal to the EFH map are the subareas of the top 25% (EFH hot spots), top 50% (core EFH area), and top 75% (principal EFH area) of habitat-related, ensemble-predicted numerical abundance.

**Complex: Rougheye/Blackspotted rockfish (*Sebastes aleutianus/Sebastes melanostictus*)**

Rougheye rockfish (*Sebastes aleutianus*) and blackspotted rockfish (*S. melanostictus*) are distributed along the outer continental shelf and upper continental slope of the northeastern Pacific and across the North Pacific from Japan to Point Conception, California, including the Bering Sea (Kramer and O'Connell 1988). They are some of the largest rockfish species and both reach maximum lengths over 700 mm. The two species co-occur throughout their range and overlap extensively (Gharrett et al. 2005) though blackspotted rockfish extend farther into the western AI and towards Russia and Japan (Orr and Hawkins 2008). Blackspotted rockfish also tend to occupy deeper water than rougheye rockfish, but they frequently co-occur between 300 and 500 m along the upper continental slope in the GOA (Ito 1999). While the two species reach maturity at approximately the same length (blackspotted $L_{50}$ = 453 mm FL, rougheye $L_{50}$ = 450 mm FL), rougheye rockfish exhibit faster growth and reach this length at a younger age (Conrath 2017). Due to high field misidentification rates, these two species are presently managed as a complex in the BSAI and GOA regions (Spencer et al. 2020), and this project models them with a single ensemble.

**Subadult rougheye/blackspotted rockfish distribution and predicted abundance from RACE-GAP summer bottom trawl surveys in the Aleutian Islands –** Subadult rougheye/blackspotted rockfish were common in many areas covered in the RACE-GAP summer survey of the AI, with most catches occurring at depths greater than 300 m (Fig. 129). The final ensemble contained three SDMs with approximately equal weights, and it performed well with respect to the observed data (Table 37). All three fit metrics scored in the range that is considered "good" ($\rho$ = 0.53; AUC = 0.88; PDE = 0.51), indicating that this ensemble is reliable and makes accurate predictions. Bottom depth, geographic position, current, and current variability were the

most important covariates and accounted for 75.9% of the deviance explained by the ensemble (Table 38). Predicted abundance was generally high in locations around 300 m depth, with weak but variable currents (Fig. 130). The abundance map predicted that most rougheye and blackspotted rockfishes will be found along the edge of the continental slope, between the 300 m and 500 m depth contours (Fig. 130). The highest abundance occurred in scattered patches that are near the passes through the island chain. The predicted CV of abundance mirrored the abundance map, with more variation in deep water and zero in shallow areas where the species almost never occurred (Fig. 130). Encounter probabilities for subadults were high in most places below the 300 m depth contour, particularly on the south side of the AI and in the passes, and were very low in shallower areas (Fig. 131).

**Adult rougheye/blackspotted rockfish distribution and predicted abundance from RACE-GAP summer bottom trawl surveys in the Aleutian Islands –** Adult rougheye/blackspotted rockfish catches from the RACE-GAP summer survey followed the same pattern as subadults and were most common at around 300 m depth along the continental slope (Fig. 132). Large catches were scattered across the AI, but a notable cluster occurred north of the Rat Islands. The final ensemble contained four SDMs with the MaxEnt given less weight and demonstrated a good to excellent fit to the observed data (Table 37). Specifically, it scored excellently in terms of predicting presence (AUC = 0.94) and deviance explained (PDE = 0.76) and performed well at predicting relative abundance ($\rho = 0.52$). Overall, this suggests that these predictions are accurate and accounted for a majority of the variation in observed catches. Bottom depth, geographic position, current variability, and bottom temperature were the most important covariates and accounted for 75.6% of the deviance explained by the ensemble (Table 38). Similar to subadults, the ensemble predicted an ideal bottom depth of around 300 m, but the

confidence interval is much wider in adults, suggesting a more uncertain relationship with depth (Fig. 133). Also, adults are associated with colder water, while bottom temperature was not an important predictor of subadult abundance. The predicted abundance map showed that rougheye/blackspotted rockfishes occupied habitats below the 300 m depth contour, with the highest densities found around Seguam Pass and the Rat Islands (Fig. 133). The predicted CV of abundance was similar to the map of abundance, demonstrating that most of the variation in catch is confined to those slope areas where this species was common (Fig. 133). The map of encounter probability showed a high chance of catching these species below 300 m and around the various passes that cut through the archipelago (Fig. 134).

**Essential fish habitat of subadult and adult rougheye/blackspotted rockfish in the Aleutian Islands –** The habitat-related abundance predictions based on RACE-GAP summer bottom trawl data (1991–2019) were translated into EFH area and subareas (Fig. 135). The subadult EFH map encompassed nearly twice the overall area of the adult map, primarily because the subadult EFH included shallower water. While all EFH hot spots for subadults occurred in water from about 250-500 m deep, the EFH area extended into some shallower areas in the eastern AI. By contrast, the EFH for adults was strictly confined to deeper water and did not extend shallower than 300 m. This pattern would be consistent with many other species in this region that tend to migrate towards deeper habitats as they grow larger. It seems likely that much of the EFH for adults and possibly subadults is below 500 m, and additional data from other sources, such as the long-line survey may help extend these findings[19].

[19] A recommendation to add additional survey data types if possible to future SDM ensemble EFH mapping efforts for this species will be included as a future recommendation for research directions from the 2023 EFH 5-year review.

Table 37. -- Constituent species distribution models (SDMs) used to construct Essential Fish Habitat (EFH) for a) subadult and b) adult rougheye/blackspotted rockfish: MaxEnt = Maximum entropy; paGAM = presence-absence generalized additive model; hGAM = hurdle GAM; $GAM_P$ = standard Poisson GAM; and $GAM_{nb}$ = standard negative-binomial GAM. Ensemble performance (ρ = Spearman's rank correlation coefficient), root-mean-square-error (RMSE), the area under the receiver operating characteristic (AUC), and the Poisson deviance explained (PDE) were generated from k-fold cross-validation. The "--" in a field indicates that this SDM was not included in the final ensemble.

**a) subadult rougheye/blackspotted rockfish**

| Models | RMSE | Relative Weight | ρ | AUC | PDE | EFH area ($km^2$) |
|---|---|---|---|---|---|---|
| MaxEnt | -- | 0 | -- | -- | -- | -- |
| paGAM | 11.5 | 0.33 | 0.54 | 0.89 | 0.43 | 70,600 |
| hGAM | 11.6 | 0.32 | 0.49 | 0.88 | 0.43 | 59,400 |
| $GAM_P$ | 11.3 | 0.34 | 0.49 | 0.85 | 0.45 | 60,000 |
| $GAM_{nb}$ | 12.1 | 0 | 0.52 | 0.87 | 0.40 | -- |
| ensemble | 10.9 | 1 | 0.53 | 0.88 | 0.51 | 65,600 |

**b) adult rougheye/blackspotted rockfish**

| Models | RMSE | Relative Weight | ρ | AUC | PDE | EFH area ($km^2$) |
|---|---|---|---|---|---|---|
| MaxEnt | 32.1 | 0.17 | 0.51 | 0.93 | 0.24 | 33,500 |
| paGAM | 26.8 | 0.24 | 0.51 | 0.93 | 0.45 | 54,400 |
| hGAM | 24.6 | 0.29 | 0.50 | 0.93 | 0.62 | 28,800 |
| $GAM_P$ | 24.0 | 0.30 | 0.50 | 0.91 | 0.64 | 25,700 |
| $GAM_{nb}$ | 25.9 | 0 | 0.51 | 0.92 | 0.60 | -- |
| ensemble | 19.4 | 1 | 0.52 | 0.94 | 0.76 | 34,800 |

Table 38. -- Covariates retained in the a) subadult and b) adult rougheye/blackspotted rockfish species distribution model (SDM) final ensembles, the percent contribution to the ensemble deviance explained by each, and the cumulative percent deviance: SD = standard deviation, and BPI = bathymetric position index.

| rougheye/ blackspotted rockfish | Covariate | % Contribution | Cumulative % Contribution |
|---|---|---|---|
| **a) subadult** | bottom depth | 43.1 | 43.1 |
| | position | 16.6 | 59.8 |
| | current | 9.0 | 68.8 |
| | current SD | 7.1 | 75.9 |
| | aspect east | 5.6 | 81.5 |
| | aspect north | 4.6 | 86.2 |
| | BPI | 3.3 | 89.5 |
| | curvature | 2.1 | 91.6 |
| | tidal maximum | 2.0 | 93.6 |
| | rockiness | 1.8 | 95.4 |
| | slope | 1.5 | 96.9 |
| | coral presence | 1.5 | 98.4 |
| | sponge presence | 1.1 | 99.5 |
| | bottom temperature | 0.5 | 100 |
| | pennatulacean presence | 0 | 100 |
| **b) adult** | bottom depth | 48.3 | 48.3 |
| | position | 12.9 | 61.3 |
| | current SD | 8.2 | 69.5 |
| | bottom temperature | 6.1 | 75.6 |
| | current | 4.6 | 80.2 |
| | BPI | 4.1 | 84.3 |
| | slope | 4.0 | 88.3 |
| | aspect east | 3.9 | 92.2 |
| | aspect north | 2.9 | 95.1 |
| | rockiness | 1.8 | 96.9 |
| | sponge presence | 1.7 | 98.6 |
| | coral presence | 0.6 | 99.2 |
| | curvature | 0.5 | 99.7 |
| | tidal maximum | 0.2 | 99.9 |
| | pennatulacean presence | 0.1 | 100 |

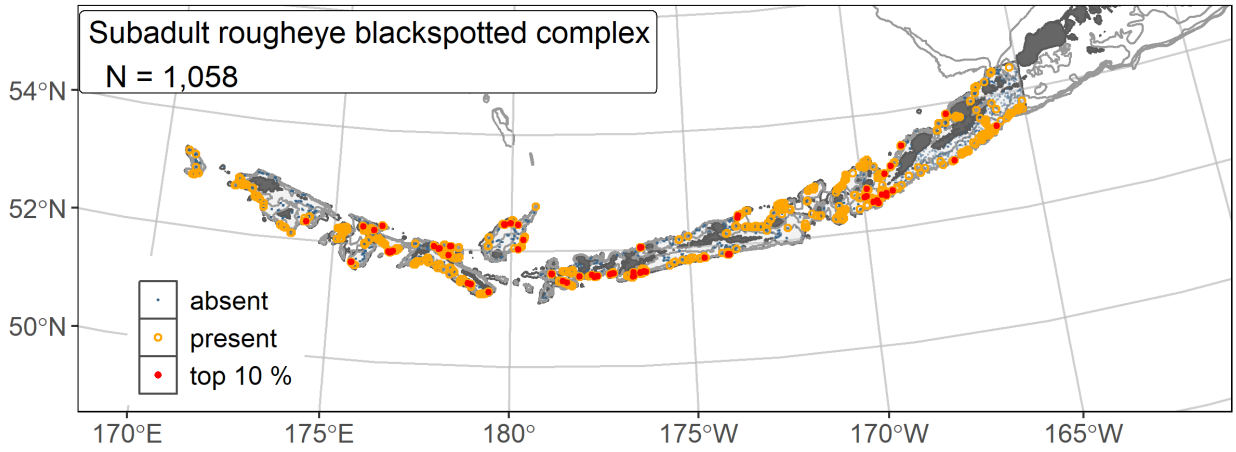


Figure 129. -- Distribution of subadult rougheye/blackspotted rockfish catches (N = 1,058) in 1991–2019 AFSC RACE-GAP summer bottom trawl surveys of the AI with the 100 m, 300 m, and 500 m isobaths indicated; filled red circles indicate locations in top 10% of overall abundance, open orange circles indicate presence in remaining catches, and small blue dots indicate absence.

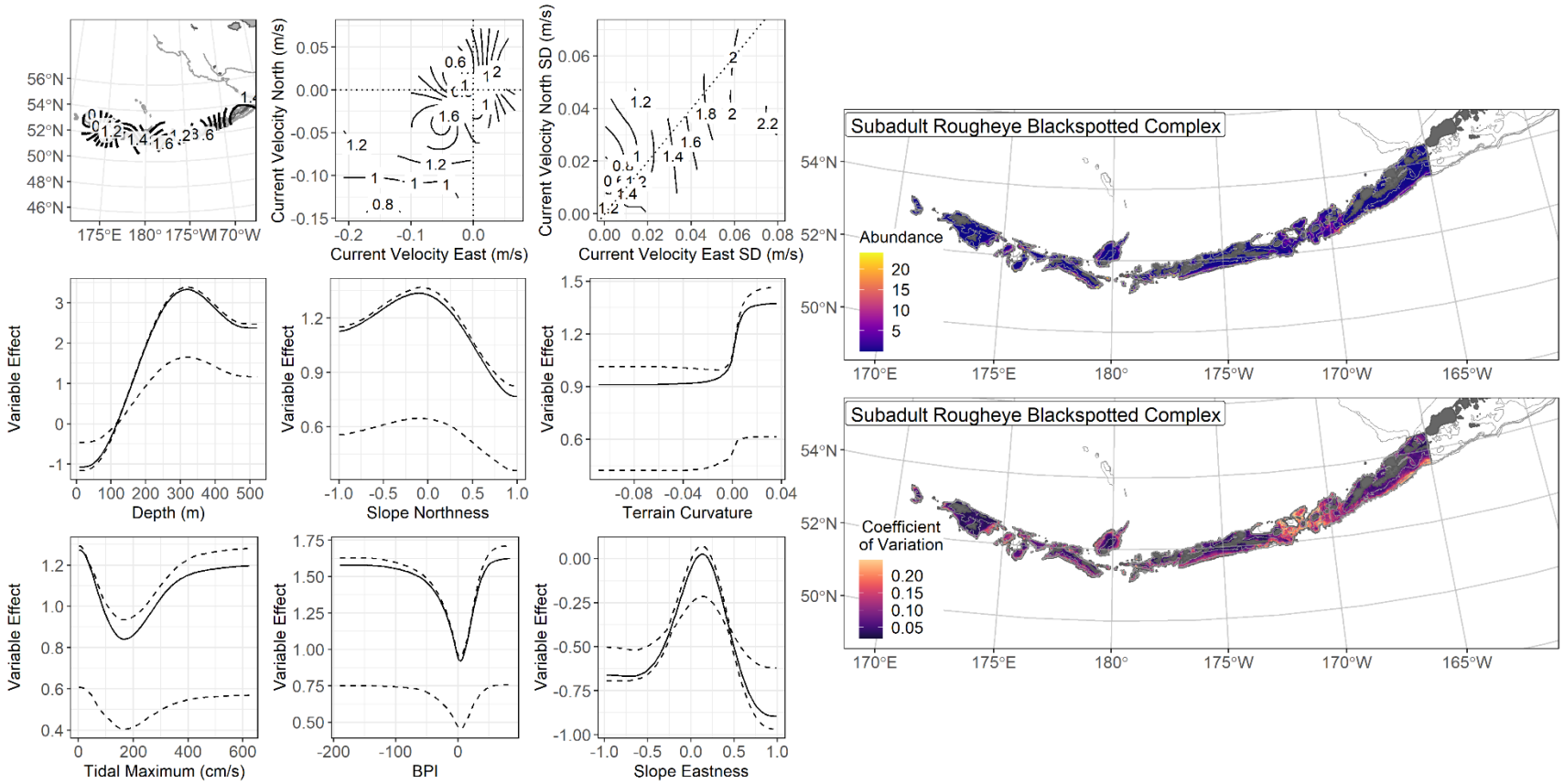


Figure 130. -- The top nine covariate effects (left panel) on ensemble-predicted subadult rougheye/blackspotted rockfish numerical abundance across the AI (upper right panel) alongside the coefficient of variation of the ensemble predictions (lower right panel).

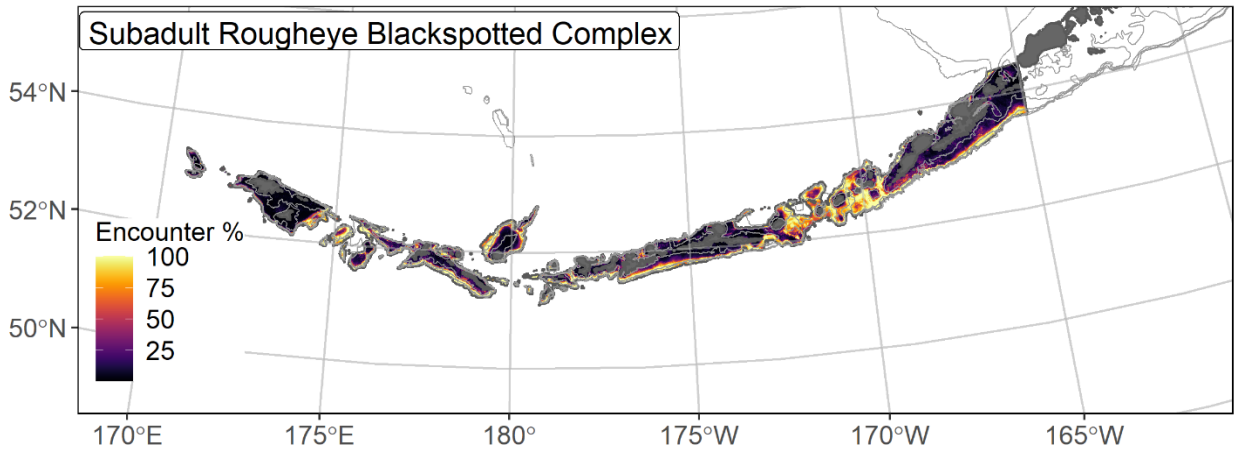


Figure 131. -- Encounter probability of subadult rougheye/blackspotted rockfish from AFSC RACE-GAP summer bottom trawl surveys (1991–2019) of the AI with the 100 m, 300 m, and 500 m isobaths indicated.

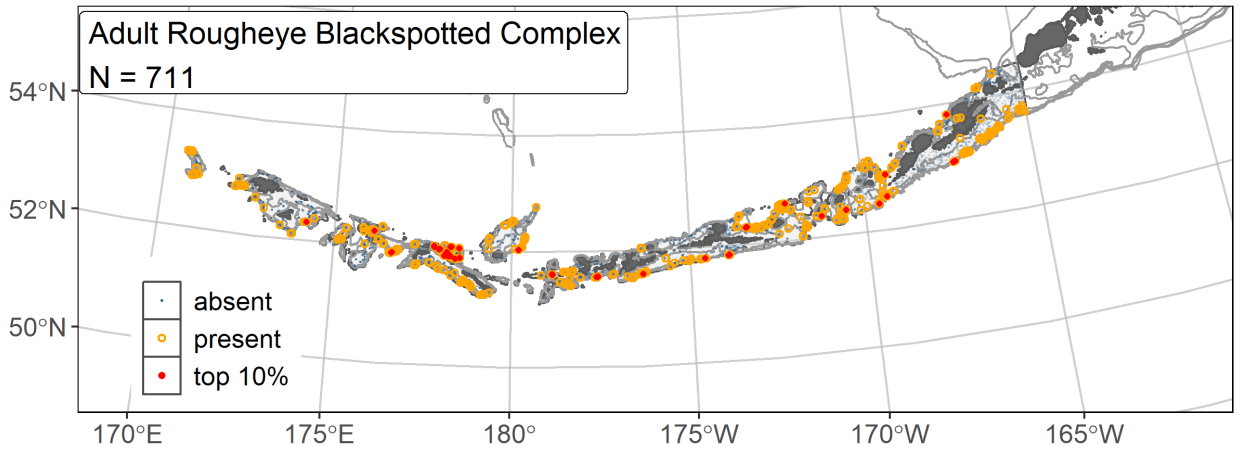


Figure 132. -- Distribution of adult rougheye/blackspotted rockfish catches (N = 711) in 1991–2019 AFSC RACE-GAP summer bottom trawl surveys of the AI with the 100 m, 300 m, and 500 m isobaths indicated; filled red circles indicate locations in top 10% of overall abundance, open orange circles indicate presence in remaining catches, and small blue dots indicate absence.

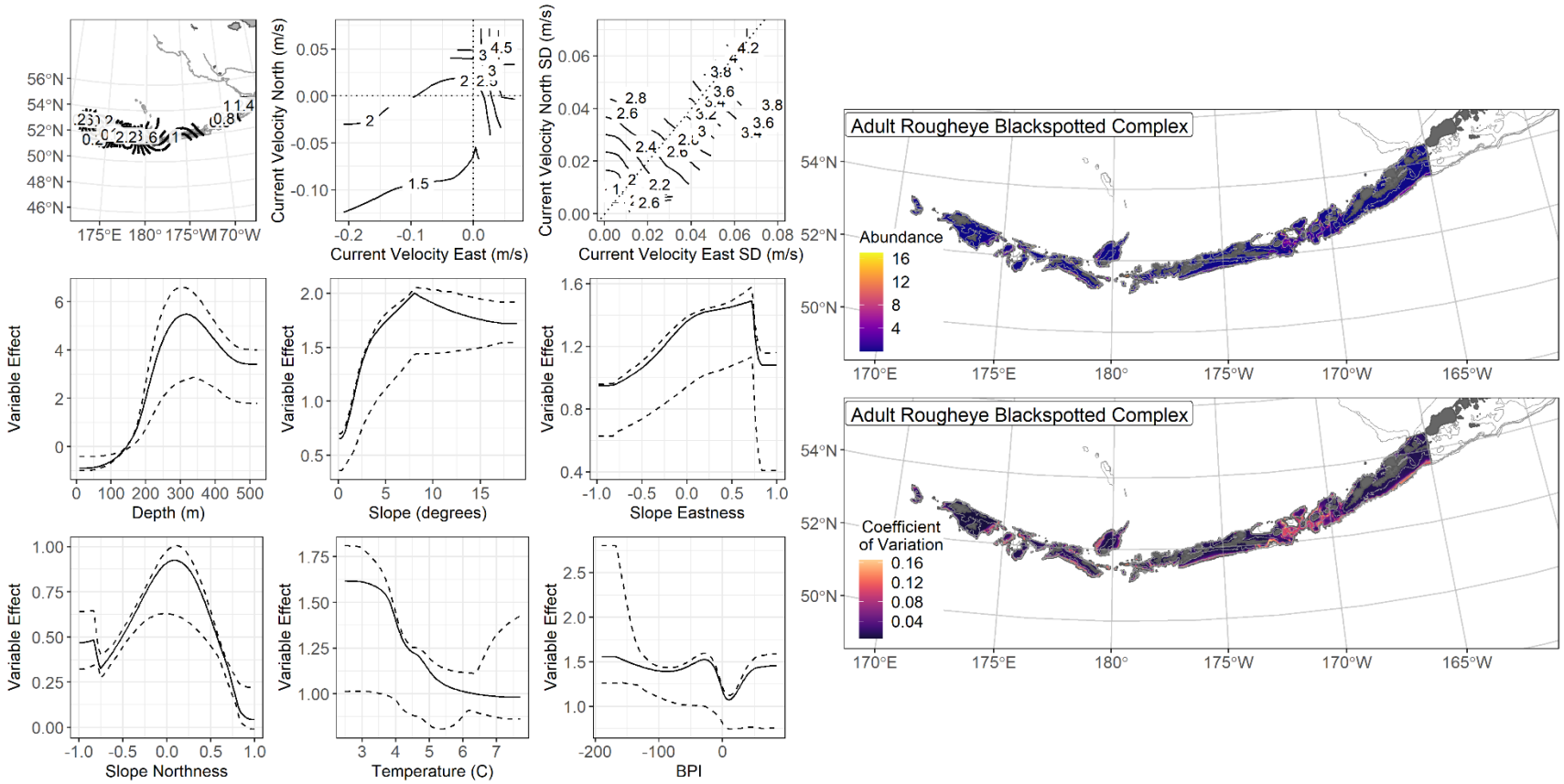


Figure 133. -- The top nine covariate effects (left panel) on ensemble-predicted adult rougheye/blackspotted rockfish numerical abundance across the AI (upper right panel) alongside the coefficient of variation of the ensemble predictions (lower right panel).

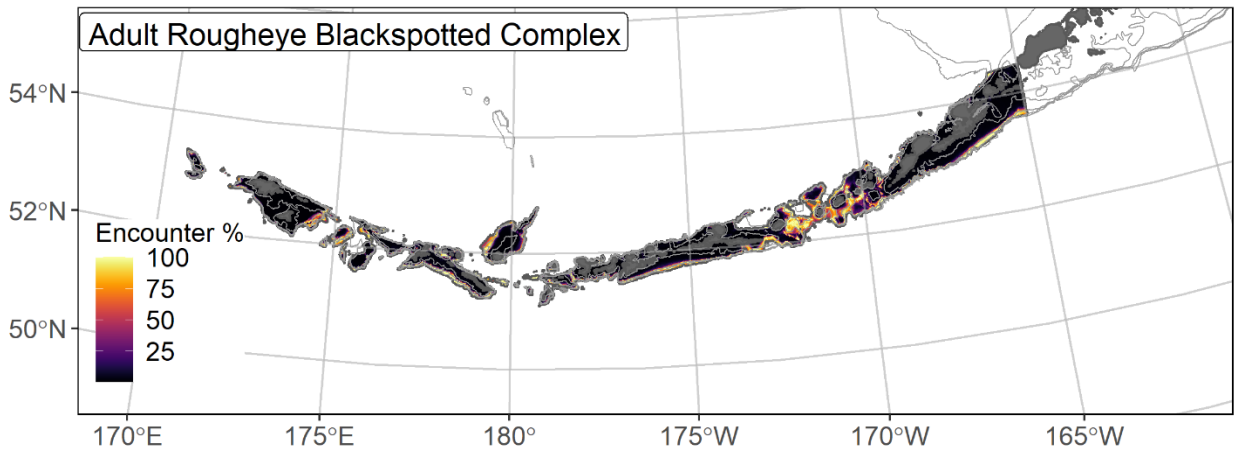


Figure 134. -- Encounter probability of adult rougheye/blackspotted rockfish from AFSC RACE-GAP summer bottom trawl surveys (1991–2019) of the AI with the 100 m, 300 m, and 500 m isobaths indicated.

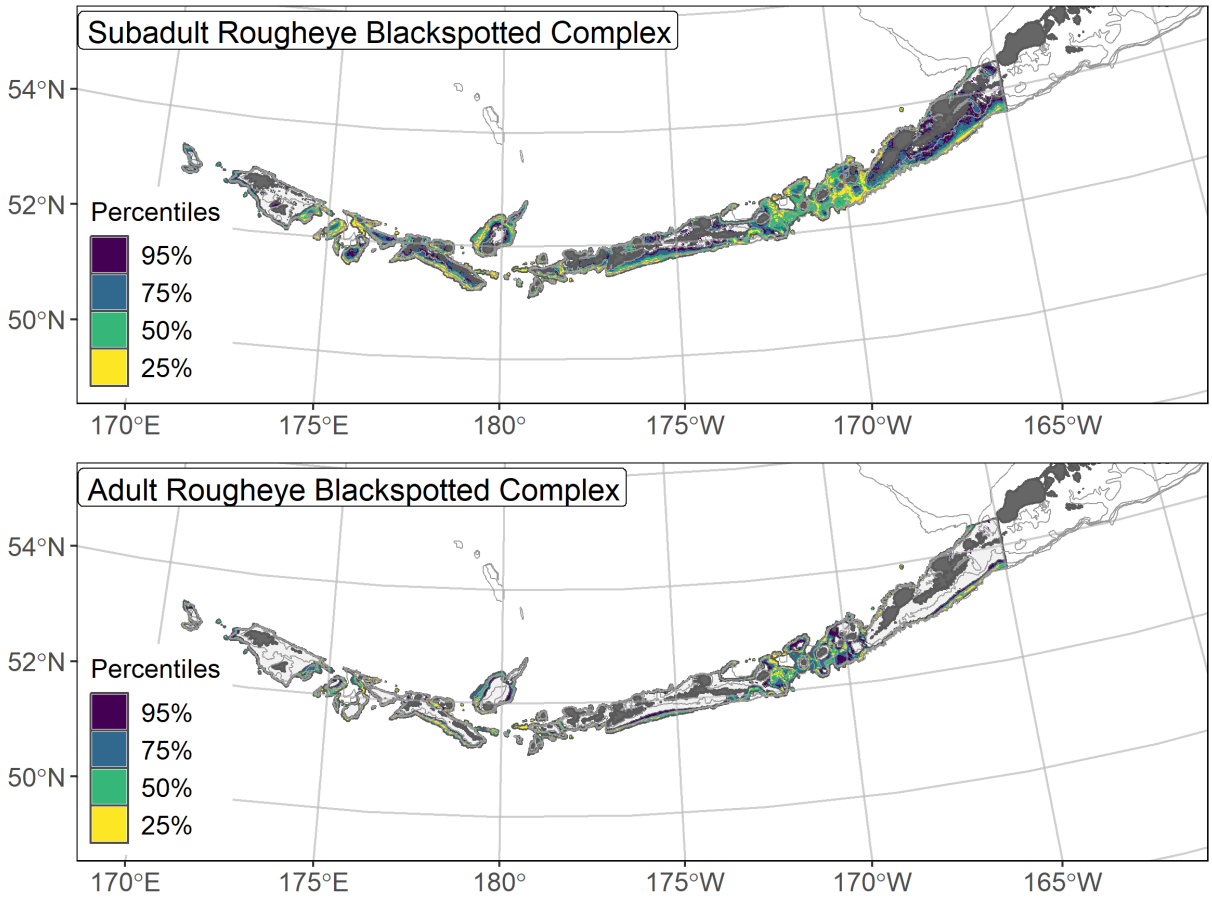


Figure 135. -- Essential fish habitat (EFH area) defined as the top 95% of numerical abundance predictions from a habitat-based ensemble fitted to subadult (top) and adult (bottom) rougheye/blackspotted rockfish distribution and abundance in AFSC RACE-GAP summer bottom trawl surveys (1991–2019) with 100 m, 300 m, and 500 m isobaths indicated; internal to the EFH map are the subareas of the top 25% (EFH hot spots), top 50% (core EFH area), and top 75% (principal EFH area) of habitat-related, ensemble-predicted numerical abundance.

**Stock Complex: Other Rockfishes**

Several species that lack the data necessary for a full age structured assessment are managed under the "other rockfish" stock complex of the BSAI region (Sullivan et al 2020). In practice, this consists of data from seven rockfish species that occur often enough in the fishery to be of concern, but only three were common enough in the RACE-GAP summer bottom trawl survey of the AI to enable the construction of an SDM: dusky rockfish (*Sebastes variabilis*), harlequin rockfish (*Sebastes variegatus*), and shortspine thornyhead (*Sebastolobus alascanus*). Additionally, insufficient data were available to construct a model for subadult harlequin rockfish, so both adult and subadult life stages were combined to make a single set of maps for the "other rockfish" stock complex. In the AI, shortspine thornyhead (SST) accounted for 90% of the survey catch of species in this complex, and the resulting maps are somewhat biased towards areas with high abundance of this species. However, as all three species occupied similar environments, this imbalance is unlikely to have an adverse effect on EFH predictions. Of more significant concern is that because adults are much more common than subadults, the resulting maps may not adequately reflect the habitats necessary for the young life stages of these rockfish species.

**"Other Rockfish" Stock Complex abundance and distribution predicted from RACE-GAP summer bottom trawl surveys in the Bering Sea –** Numerical abundance predictions for three rockfish species were combined to estimate the abundance and EFH of the "other rockfish" stock complex in the AI (Fig. 136). SST strongly influenced the composite abundance map, and the resulting map shows high numbers of rockfishes predicted along the continental slope south of Unalaska Island. This was slightly different from the main areas of abundance for adult dusky and harlequin rockfishes, which occurred a little farther west along the slope. Additionally,

subadult and adult dusky rockfish were sometimes found in shallower water closer to shore, which was not apparent from the map. While the abundance map was strongly weighted towards SST, the encounter probability map was less influenced by a single high-density species. Notably, this map showed high encounter probabilities in many shallower areas in the eastern AI, which better reflected the distribution of dusky rockfish. The EFH map for the complex predicted hot spots along most of the continental slope throughout the region. This was consistent with the distributions of adults from all three species and subadult shortspine thornyhead. Many inshore areas in the eastern AI were part of the core EFH area, which reflected data from subadult dusky rockfish. As subadult dusky rockfish were less common in the western AI, most shallow areas in the west were not part of the EFH area.

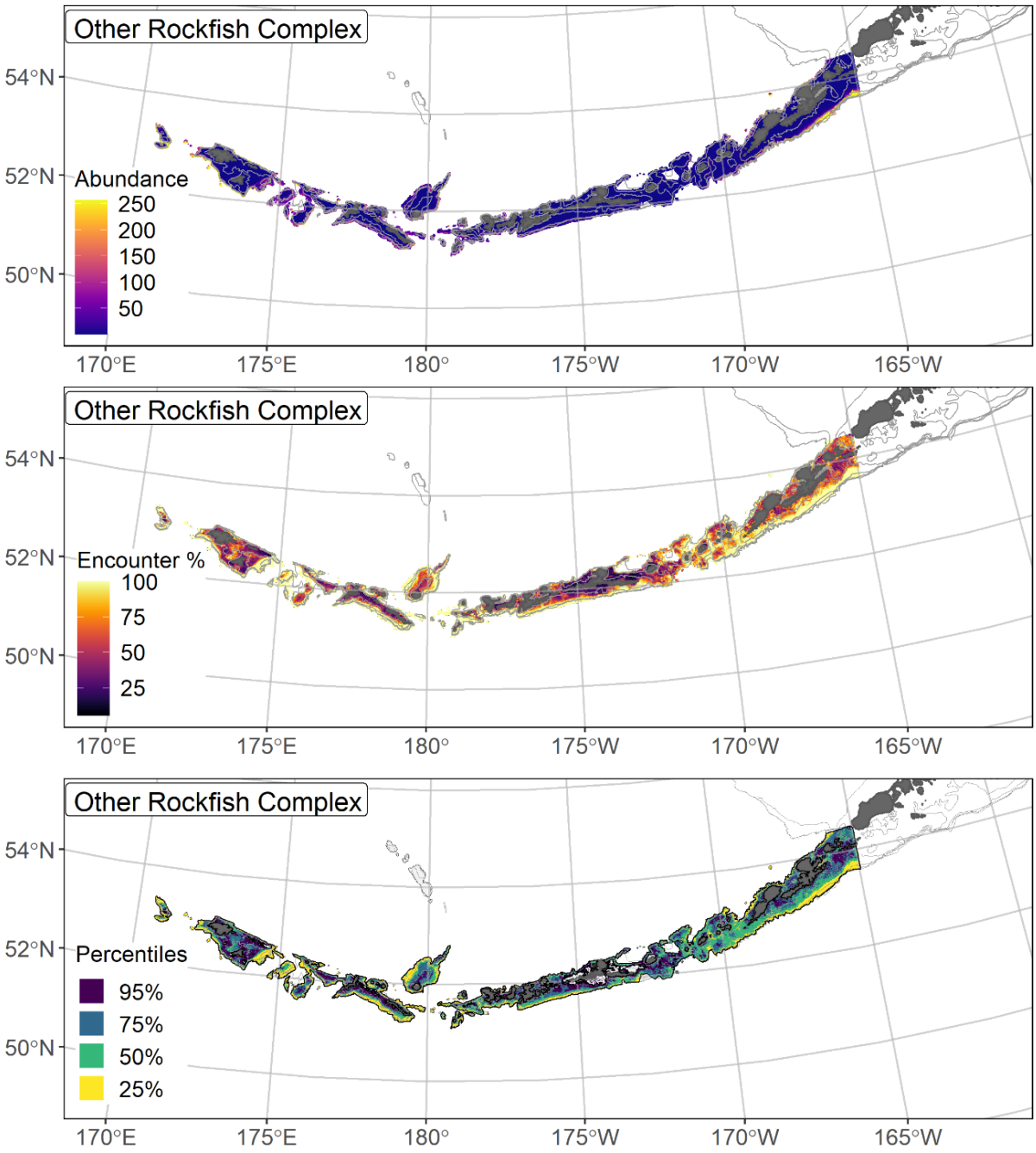


Figure 136. -- Composite predicted numerical abundance (top panel), encounter probability (middle panel), and essential fish habitat (bottom panel) for the "other rockfish" stock complex in the AI collected in the AFSC RACE-GAP summer bottom trawl surveys (1991–2019) with 100 m, 300 m, and 500 m isobaths indicated. EFH is defined as the top 95% of numerical abundance predictions above a presence threshold, and integral to the EFH map are the top 25% (EFH hot spots), top 50% (core EFH area), and top 75% (principal EFH area) of habitat-related, ensemble-predicted numerical abundance.

**Dusky rockfish (*Sebastes variabilis*)**

Dusky rockfish (*Sebastes variabilis*) is a moderately large (up to 590 mm) rockfish that is found from the Oregon coast across the AI, and as far as Hokkaido Japan (Orr and Blackburn 2004). It is one of the more common rockfish species in the BSAI region, though it is primarily found in the AI and GOA, and only rarely in the Bering Sea (Sullivan et al. 2020). Like other members of the genus *Sebastes*, dusky rockfish are long-lived and may skip spawning during years with unfavorable conditions (Conrath 2019). Dusky rockfish become mature ($L_{50}$) beginning around 365 mm FL, and display traits such as internal fertilization and live birth that are common to other members of the genus *Sebastes* (Chilton 2010). Prior to 1996, this species was often mixed with catches of the dark rockfish (*S. ciliatus*), which is similar in morphology but darker in coloration. For a time, catches of these species were recorded as "light dusky" or "dark dusky," which allowed for the true species to be retroactively determined from the RACE-GAP survey data after the species were officially described by Orr and Blackburn (2004). In the BSAI region, dusky rockfish are managed as the second most abundant species in the "other rockfish complex" (Sullivan et al. 2020).

**Subadult dusky rockfish distribution and predicted abundance from RACE-GAP summer bottom trawl surveys in the Aleutian Islands –** Subadult dusky rockfish catches were somewhat common in the eastern AI near Unimak Pass and Unalaska Island, but were less common farther west (Fig. 137). The final ensemble contained three SDMs that received equal weights (Table 5). The ensemble showed fair performance when compared with observed data (Table 39). Specifically, the ensemble scored well in predicting presence or absence in catches (AUC = 0.88), but scored only fair at predicting abundance ($\rho = 0.20$) and in terms of deviance explained (PDE = 0.32). Taken together, this suggested that predictions about presence or

absence are likely to be accurate, but that predictions of abundance were more uncertain. This is partly explained by the limited amount of data available (108 positive records), and so the ensemble outputs should be used with caution. Geographic position, bottom depth, and bottom currents were the most important covariates and accounted for 70.9% of the deviance explained by the ensemble (Table 40). Ensemble predictions showed high abundance in the eastern AI, shallower depths, and places with south to southeasterly currents, but the confidence intervals around many of the covariates were very wide and do not support strong conclusions (Fig. 138). Predicted abundance was highest around Unalaksa Island, though localized areas of high abundance are also predicted near Umnak and Amchitka Islands (Fig. 138). This pattern is supported by the survey catch records, which show some high-density catches in those areas (Fig. 138). The map of the predicted CV of abundance was difficult to interpret but was consistent with the high uncertainty around the estimated covariate effects (Fig. 138). Encounter probabilities for subadult dusky rockfish were low in most places across the AI, but they were common near shore around Unalaska Island, in pockets around the Fox Islands and Amchitka Island (Fig. 139).

**Adult dusky rockfish distribution and predicted abundance from RACE-GAP summer bottom trawl surveys in the Aleutian Islands –** Adult dusky rockfish catches in the RACE-GAP summer survey were distributed throughout the AI, but were most concentrated in the east near Unalaska Island (Fig. 140). The four SDMs retained in the final ensemble were equally weighted and performed slightly better than the subadult ensemble when compared to the data (Table 39). Two metrics scored in the range considered fair ($\rho = 0.27$; AUC = 0.78) while the estimate of deviance explained was somewhat better (PDE = 0.45). They suggest that the ensemble's predictions were somewhat accurate, but caution is still advised when using the

following maps. Geographic position, bottom depth, bottom currents, and slope were responsible for 63.1% of the deviance explained by the ensemble (Table 40), though current variability, temperature, and rocky terrain also made minor contributions. The model predicted high abundance in locations farther east with bottom depths between 100-200 m, a slope of at least 5°, and strong southerly currents (Fig. 141). The predicted abundance map for adults was similar to subadults in that it predicted areas of high abundance south of Unalaska Island and Umnak Island. However, the areas of high abundance were farther offshore and the overall abundance of adults in the survey was much higher than that of subadults (Fig. 141). The predicted CV of abundance was highest in the eastern AI around locations of high abundance (Fig. 141). Encounter probabilities for adult ducky rockfish were high in the eastern AI and in a few other places where the preferred depth and other conditions were present (Fig. 142).

**Essential fish habitat of subadult and adult dusky rockfish in the Aleutian Islands –** The habitat-related abundance predictions based on RACE-GAP summer bottom trawl data (1996–2019) were translated into EFH area and subareas (Fig. 143). The EFH area for subadults was much smaller than that of adults and was concentrated east of 170° W. Smaller pockets of EFH were present around the inshore areas of other islands farther west in the chain, such as Amchitka Island. The adult EFH was much larger, though its primary hot spot also occurred in the eastern AI, east of 170° W. The adult EFH extended into areas with greater depths and covered much of the area around the Islands of Four Mountains and Andreanof Islands before becoming sparser farther west.

Table 39. -- Constituent species distribution models (SDMs) used to construct Essential Fish Habitat (EFH) for a) subadult and b) adult dusky rockfish: MaxEnt = Maximum entropy; paGAM = presence-absence generalized additive model; hGAM = hurdle GAM; $GAM_P$ = standard Poisson GAM; and $GAM_{nb}$ = standard negative-binomial GAM. Ensemble performance (ρ = Spearman's rank correlation coefficient), root-mean-square-error (RMSE), the area under the receiver operating characteristic (AUC), and the Poisson deviance explained (PDE) were generated from k-fold cross-validation. The "--" in a field indicates that this SDM was not included in the final ensemble.

**a) subadult dusky rockfish**

| Models | RMSE | Relative Weight | ρ | AUC | PDE | EFH area ($km^2$) |
|---|---|---|---|---|---|---|
| MaxEnt | 1.39 | 0.33 | 0.16 | 0.79 | 0.15 | 42,300 |
| paGAM | 1.38 | 0.34 | 0.18 | 0.85 | 0.22 | 29,600 |
| hGAM | -- | 0 | -- | -- | -- | -- |
| $GAM_P$ | 1.44 | 0 | 0.18 | 0.81 | -0.06 | -- |
| $GAM_{nb}$ | 1.39 | 0.33 | 0.19 | 0.84 | 0.22 | 23,500 |
| ensemble | 1.37 | 1 | 0.20 | 0.88 | 0.32 | 36,800 |

**b) adult dusky rockfish**

| Models | RMSE | Relative Weight | ρ | AUC | PDE | EFH area ($km^2$) |
|---|---|---|---|---|---|---|
| MaxEnt | 9.71 | 0.26 | 0.22 | 0.73 | 0.17 | 66,600 |
| paGAM | 9.71 | 0.26 | 0.24 | 0.75 | 0.16 | 68,200 |
| hGAM | 10.21 | 0.23 | 0.20 | 0.75 | 0.01 | 44,100 |
| $GAM_P$ | 9.96 | 0.25 | 0.16 | 0.67 | 0.06 | 38,300 |
| $GAM_{nb}$ | 10.78 | 0.00 | 0.25 | 0.75 | 0.33 | -- |
| ensemble | 9.17 | 1 | 0.27 | 0.78 | 0.45 | 64,700 |

Table 40. -- Covariates retained in the a) subadult and b) adult dusky rockfish species distribution model (SDM) final ensembles, the percent contribution to the ensemble deviance explained by each, and the cumulative percent deviance: SD = standard deviation, and BPI = bathymetric position index.

| dusky rockfish | Covariate | % Contribution | Cumulative % Contribution |
|---|---|---|---|
| **a) subadult** | bottom depth | 29.5 | 29.5 |
| | position | 22.3 | 51.8 |
| | current | 19.2 | 70.9 |
| | aspect east | 5.5 | 76.4 |
| | slope | 5.3 | 81.7 |
| | sponge presence | 4.4 | 86.2 |
| | current SD | 4.3 | 90.5 |
| | tidal maximum | 3.7 | 94.2 |
| | aspect north | 3.0 | 97.2 |
| | bottom temperature | 1.0 | 98.2 |
| | BPI | 0.9 | 99.1 |
| | rockiness | 0.4 | 99.5 |
| | coral presence | 0.3 | 99.8 |
| | curvature | 0.2 | 100 |
| **a) adult** | position | 19.4 | 19.4 |
| | current | 16.9 | 36.3 |
| | bottom depth | 14.9 | 51.2 |
| | slope | 11.9 | 63.1 |
| | current SD | 8.5 | 71.6 |
| | BPI | 5.6 | 77.2 |
| | bottom temperature | 4.6 | 81.8 |
| | rockiness | 4.3 | 86.1 |
| | tidal maximum | 4.1 | 90.2 |
| | aspect east | 3.3 | 93.5 |
| | aspect north | 3.2 | 96.7 |
| | curvature | 1.9 | 98.6 |
| | coral presence | 0.7 | 99.3 |
| | sponge presence | 0.4 | 99.7 |
| | pennatulacean presence | 0.3 | 100 |

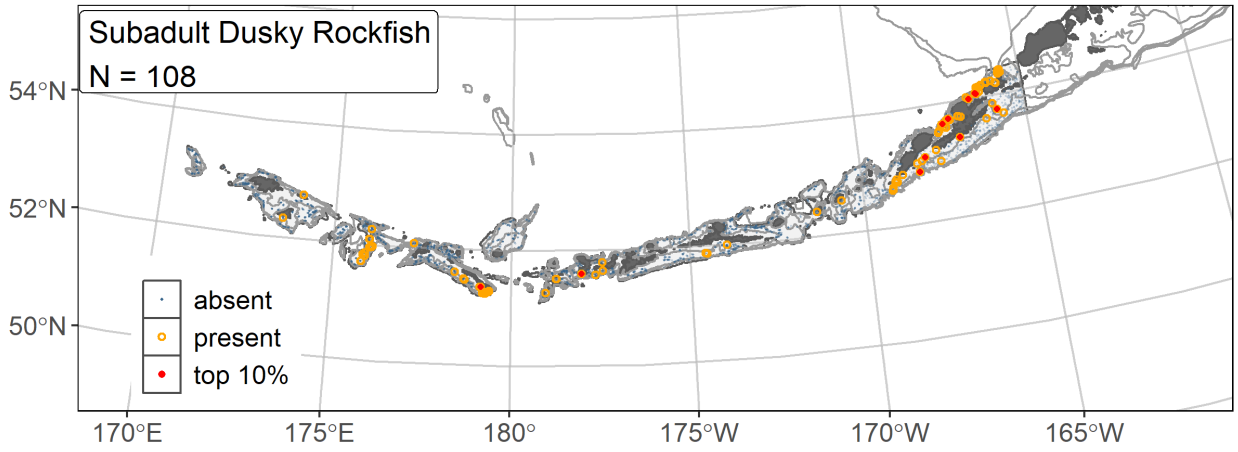


Figure 137. -- Distribution of subadult dusky rockfish catches (N = 108) in 1996–2019 AFSC RACE-GAP summer bottom trawl surveys of the AI with the 100 m, 300 m, and 500 m isobaths indicated; filled red circles indicate locations in top 10% of overall abundance, open orange circles indicate presence in remaining catches, and small blue dots indicate absence.

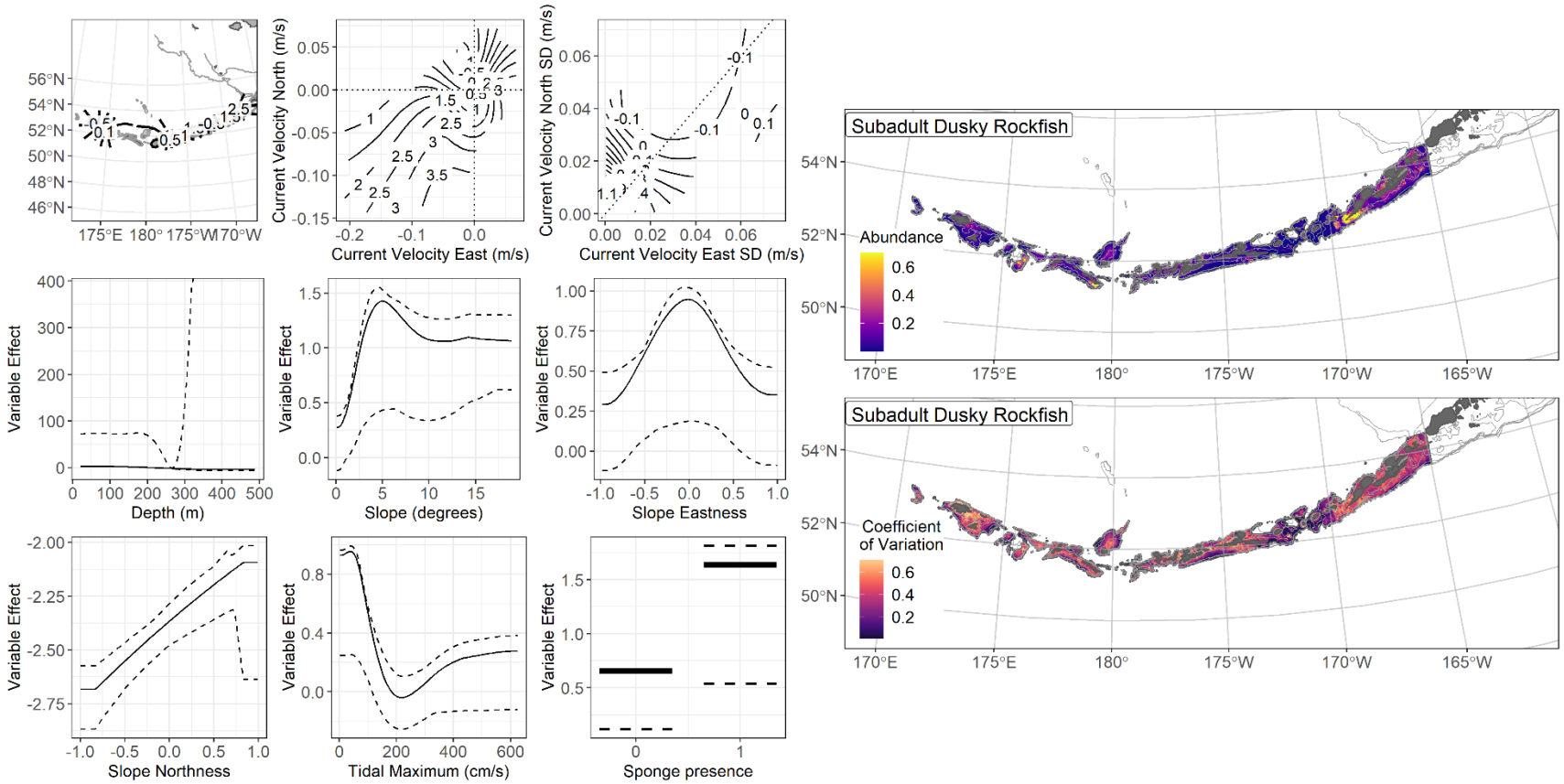


Figure 138. -- The top nine covariate effects (left panel) on ensemble-predicted subadult dusky rockfish numerical abundance across the AI (upper right panel) alongside the coefficient of variation of the ensemble predictions (lower right panel).

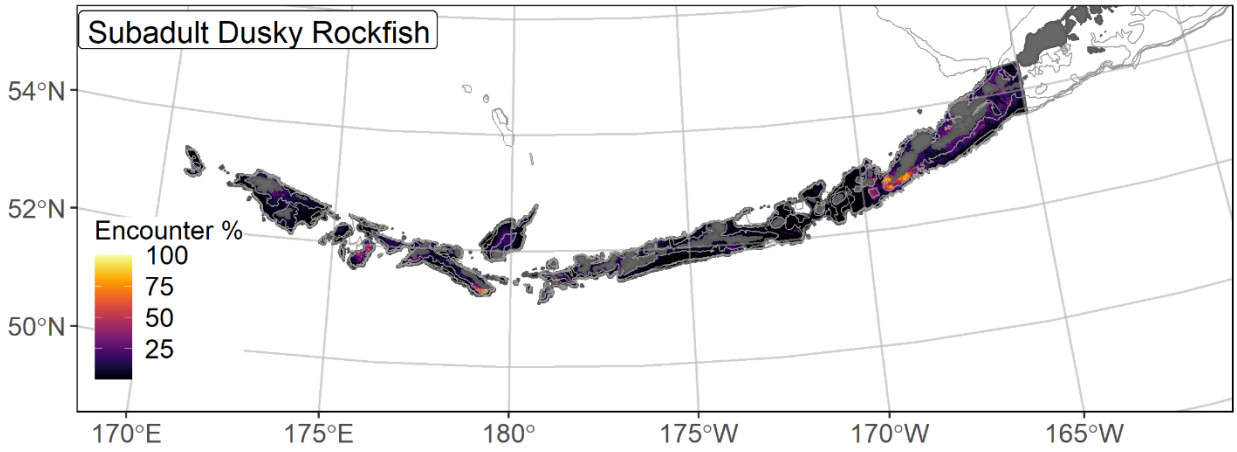


Figure 139. -- Encounter probability of subadult dusky rockfish from AFSC RACE-GAP summer bottom trawl surveys (1996–2019) of the AI with the 100 m, 300 m, and 500 m isobaths indicated.

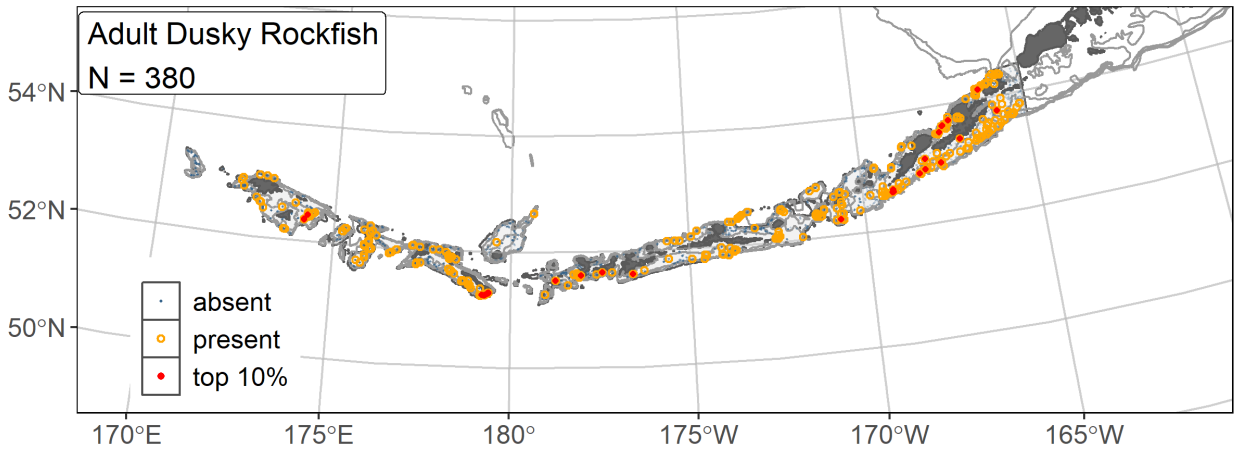


Figure 140. -- Distribution of adult dusky rockfish catches (N = 221) in 1996–2019 AFSC RACE-GAP summer bottom trawl surveys of the AI with the 100 m, 300 m, and 500 m isobaths indicated; filled red circles indicate locations in top 10% of overall abundance, open orange circles indicate presence in remaining catches, and small blue dots indicate absence.

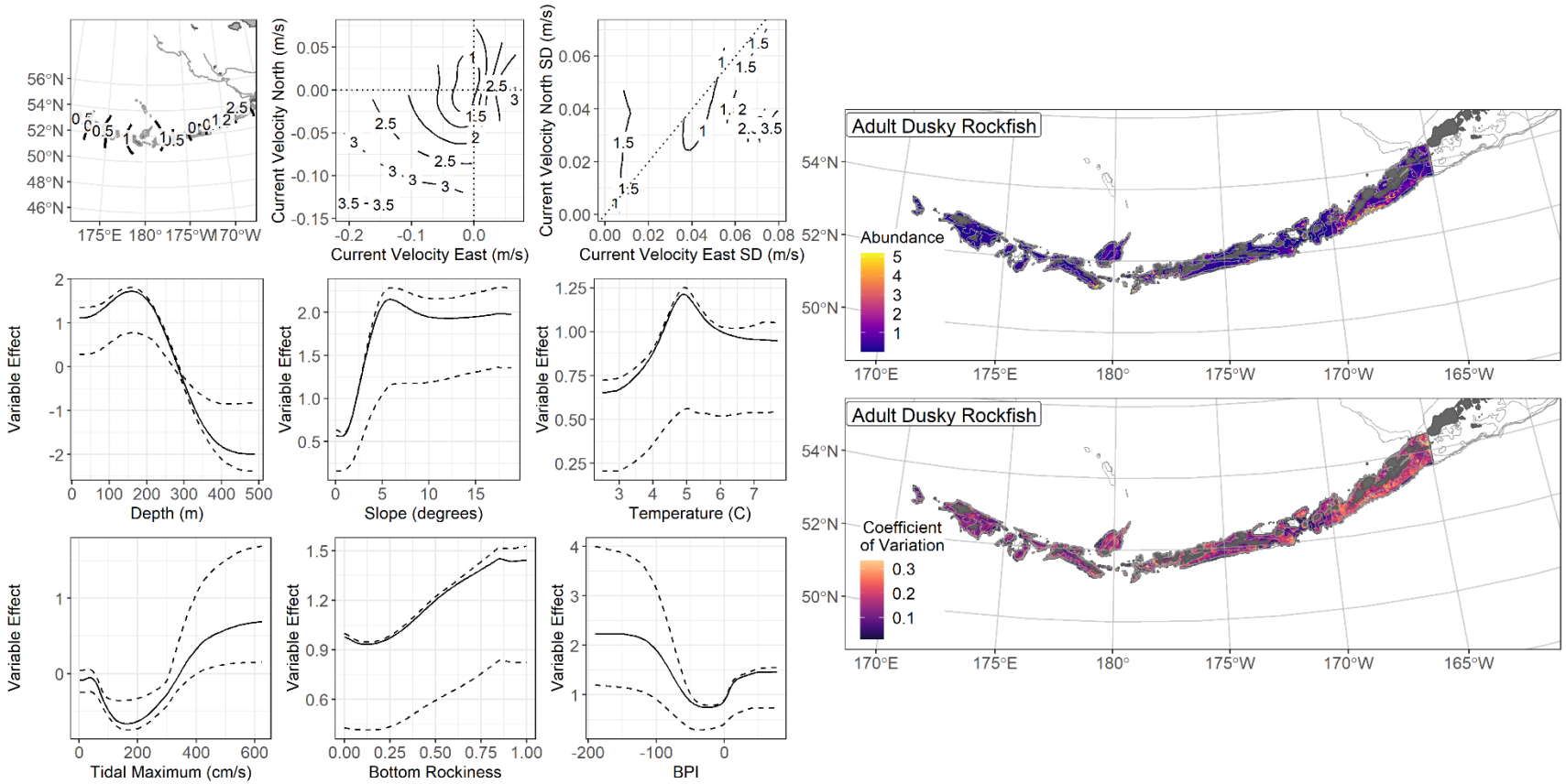


Figure 141. -- The top nine covariate effects (left panel) on ensemble-predicted adult dusky rockfish numerical abundance across the AI (upper right panel) alongside the coefficient of variation of the ensemble predictions (lower right panel).

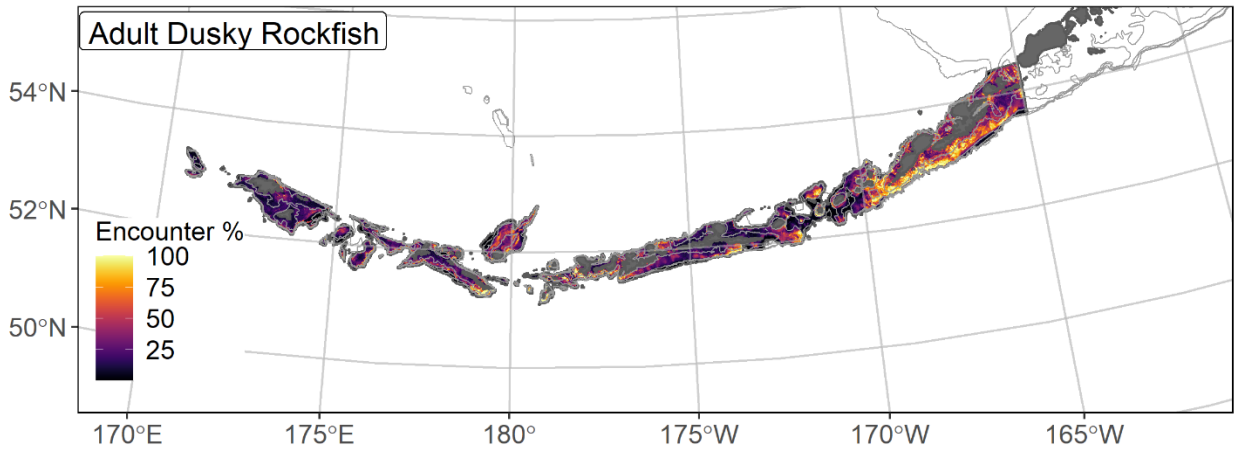


Figure 142. -- Encounter probability of adult dusky rockfish from AFSC RACE-GAP summer bottom trawl surveys (1996–2019) of the AI with the 100 m, 300 m, and 500 m isobaths indicated.

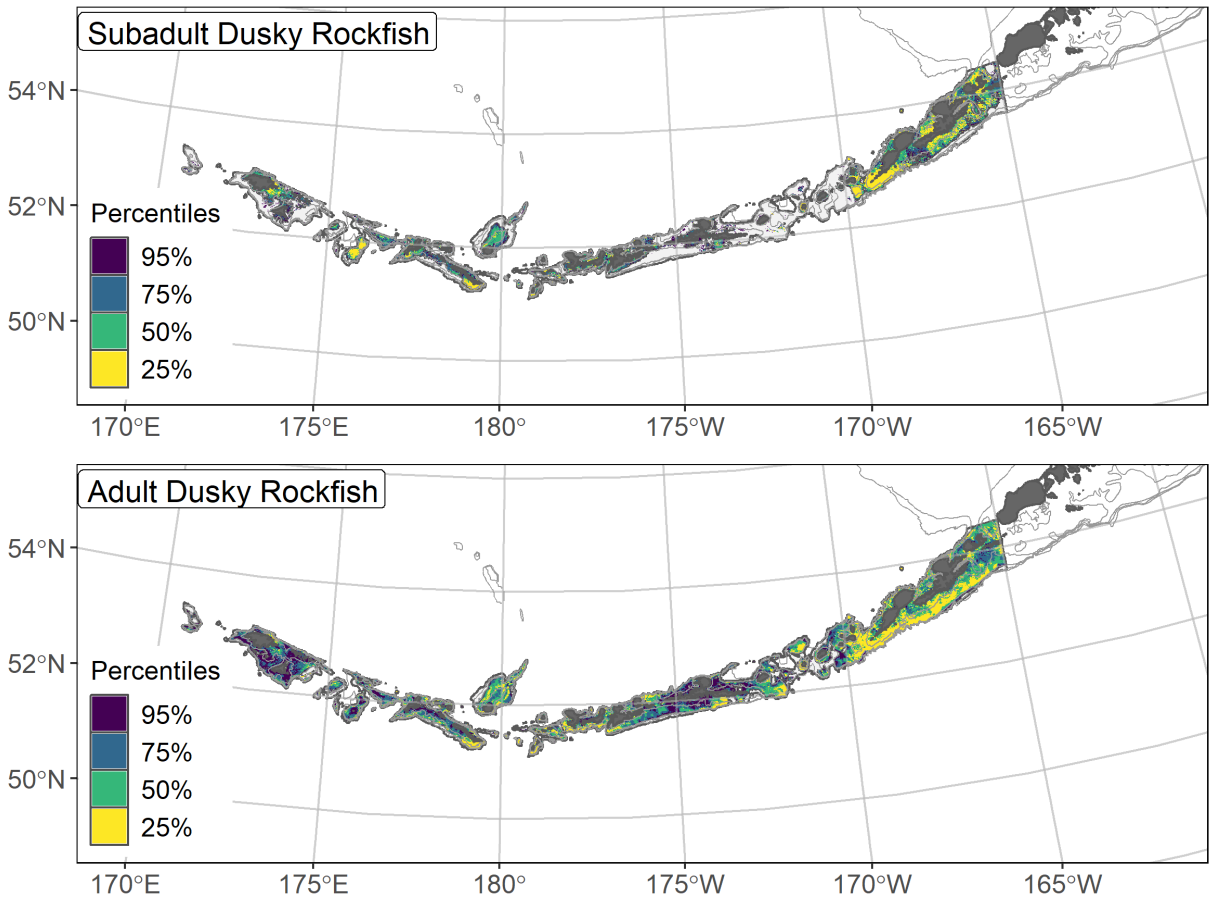


Figure 143. -- Essential fish habitat (EFH area) defined as the top 95% of numerical abundance predictions from a habitat-based ensemble fitted to subadult (top) and adult (bottom) dusky rockfish distribution and abundance in AFSC RACE-GAP summer bottom trawl surveys (1996–2019) with 100 m, 300 m, and 500 m isobaths indicated; internal to the EFH map are the subareas of the top 25% (EFH hot spots), top 50% (core EFH area), and top 75% (principal EFH area) of habitat-related, ensemble-predicted numerical abundance.

**Harlequin rockfish (*Sebastes variegatus*)**

Harlequin rockfish (*Sebastes variegatus*) is found from the Oregon coast to the western AI (Love et al. 2002). Harlequin rockfish is one of the smaller species of rockfish, and females become mature at a length of 188 mm FL ($L_{50}$; Tenbrink and Helser 2021) and achieve a maximum length of 420 mm FL (Rooper 2008). This species becomes mature at a relatively young age for sebastid rockfishes (4.5 years) but can still live as long as 75 years (Kastelle et al. 2020). One complication for the assessment of this species is that it is often associated with habitat that is untrawlable using standard RACE-GAP survey gear, including areas that are rocky or have a high density of structure forming invertebrates such as corals (Conrath et al. 2019). In multiple studies, harlequin rockfish were found to be closely associated with the bottom or amidst rocks (Johnson et al. 2003, Jones et al. 2012). Harlequin rockfish is managed as part of the "other rockfish" stock complex in both the BSAI and GOA regions, though the species is poorly sampled by the trawl survey in the AI and is uncommon in the Bering Sea (Sullivan et al. 2020). In the GOA, it is the most common species in the "other rockfish" stock by survey catch (Tribuzio and Echave 2019). The subadult life stage was present in fewer than 50 hauls in the RACE-GAP AI trawl survey and therefore, results are only available for the adult life stage.

**Adult harlequin rockfish distribution and predicted abundance from RACE-GAP summer bottom trawl surveys in the Aleutian Islands –** Adult harlequin rockfish from the RACE-GAP summer survey were sparsely distributed across the AI, with no particular area showing higher catches (Fig. 144). Catches occurred primarily in shallow water around 100 m deep. The final ensemble contained three equally weighted SDMs that showed a poor to fair fit to the data (Table 41). Specifically, the ensemble scored well on predicting presence or absence

(AUC = 0.86) and explained a fair amount of the deviance in the data (PDE = 0.39). However, it scored poorly on measures of its ability to predict relatively high or low abundance catches ($\rho = 0.18$). This pattern in the fit metrics can sometimes occur in species with limited data (111 positive catches 1991-2019) and many observations near zero. The high score on AUC suggested that this ensemble was capable of identifying the most likely locations adult harlequin rockfish would be found. However, the combination of limited data, low value for $\rho$, and the preference of this species for untrawlable areas (Johnson et al. 2012) suggests that these predictions should be used with caution. There was no dominant covariate that influenced model predictions. Geographic position, bottom depth, bottom currents, BPI, slope angle, and slope aspect accounted for 84.2% of the deviance explained (Table 42). In general, high abundance was predicted in either the eastern or western AI (but not the center), at bottom depths from 100 to 300 m, where there were high variability currents and with steep, south-facing slopes. (Fig. 145). A positive BPI, which describes locations relatively higher than their surroundings, such as along the slope/shelf transition, was also correlated with increased abundance. Predicted abundance was highest along the edge of the continental slope, particularly south of Unalaska and Umnak islands (Fig. 145). The CV of abundance for the predictions was high along the edge of the continental slope and was zero in shallower water, where the species was rarely found (Fig. 145). Predicted encounter probability was high only around those areas described above as having high abundance (Fig. 146). However, these probabilities reflect the likelihood of encounter in a trawl survey, which is likely to underestimate their density in complex, rocky habitats.

**Essential fish habitat of adult harlequin rockfish in the Aleutian Islands –** The habitat-related abundance predictions based on RACE-GAP summer bottom trawl data (1991–2019) were translated into EFH area and subareas (Fig. 147). Despite the relatively uncommon presence of harlequin rockfish in trawl catches, the EFH area covered approximately 75% of the AI. Most of the area south of the archipelago along the edge of the continental slope was designated as EFH hot spots for harlequin rockfish. Shallow, inshore areas were typically not EFH. The constituent SDMs disagreed about the size of the EFH area, and the $GAM_{nb}$ predicted an area that is only a quarter of the size of the others (Table 41), which suggests that the EFH for this species should be interpreted with some caution.

Table 41. -- Constituent species distribution models (SDMs) used to construct Essential Fish Habitat (EFH) for adult harlequin rockfish: MaxEnt = Maximum entropy; paGAM = presence-absence generalized additive model; hGAM = hurdle GAM; $GAM_P$ = standard Poisson GAM; and $GAM_{nb}$ = standard negative-binomial GAM. Ensemble performance (ρ = Spearman's rank correlation coefficient), root-mean-square-error (RMSE), the area under the receiver operating characteristic (AUC), and the Poisson deviance explained (PDE) were generated from k-fold cross-validation. The "--" in a field indicates that this SDM was not included in the final ensemble.

| Models | RMSE | Relative Weight | ρ | AUC | PDE | EFH area ($km^2$) |
|---|---|---|---|---|---|---|
| MaxEnt | 23.6 | 0.33 | 0.16 | 0.81 | 0.14 | 60,100 |
| paGAM | 23.6 | 0.33 | 0.13 | 0.78 | 0.20 | 66,200 |
| hGAM | -- | 0 | -- | -- | -- | -- |
| $GAM_P$ | -- | 0 | -- | -- | -- | -- |
| $GAM_{nb}$ | 23.6 | 0.33 | 0.14 | 0.78 | 0.23 | 14,700 |
| ensemble | 23.4 | 1 | 0.18 | 0.86 | 0.39 | 62,000 |

Table 42. -- Covariates retained in the adult harlequin rockfish species distribution model (SDM) final ensemble, the percent contribution to the ensemble deviance explained by each, and the cumulative percent deviance: BPI = bathymetric position index.

| harlequin rockfish a) adults | Covariate | % Contribution | Cumulative % Contribution |
|---|---|---|---|
| | position | 16.5 | 16.5 |
| | current | 15.6 | 32.2 |
| | bottom depth | 11.6 | 43.8 |
| | BPI | 11.6 | 55.4 |
| | aspect north | 10.8 | 66.2 |
| | slope | 9.4 | 75.7 |
| | current SD | 8.5 | 84.2 |
| | rockiness | 3.3 | 87.5 |
| | aspect east | 2.9 | 90.4 |
| | coral presence | 2.7 | 93.1 |
| | bottom temperature | 2.0 | 95.1 |
| | tidal maximum | 1.7 | 96.8 |
| | sponge presence | 1.7 | 98.5 |
| | curvature | 1.5 | 100 |
| | pennatulacean presence | 0.0 | 100 |

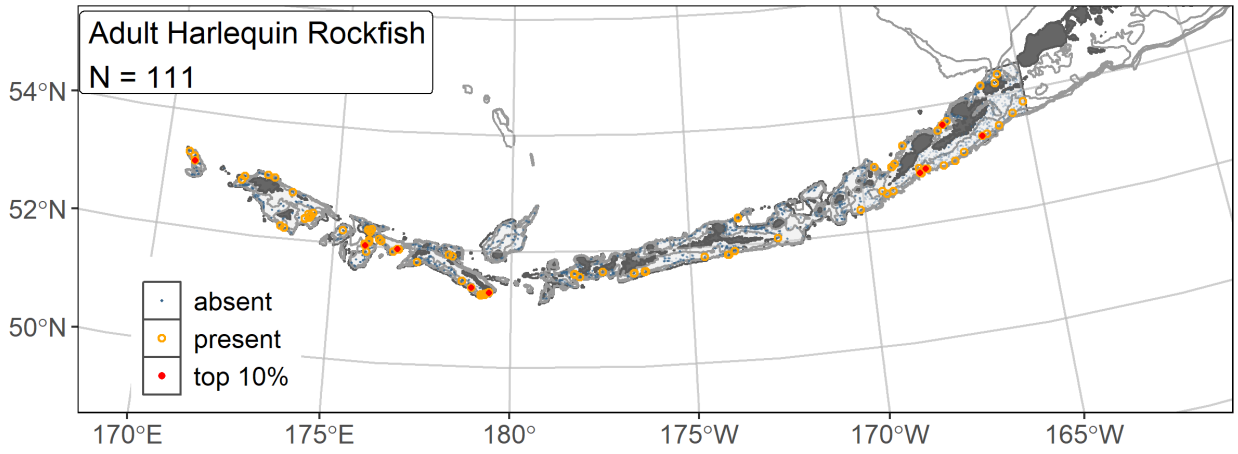


Figure 144. -- Distribution of adult harlequin rockfish catches (N = 111) in 1991–2019 AFSC RACE-GAP summer bottom trawl surveys of the AI with the 100 m, 300 m, and 500 m isobaths indicated; filled red circles indicate locations in top 10% of overall abundance, open orange circles indicate presence in remaining catches, and small blue dots indicate absence.

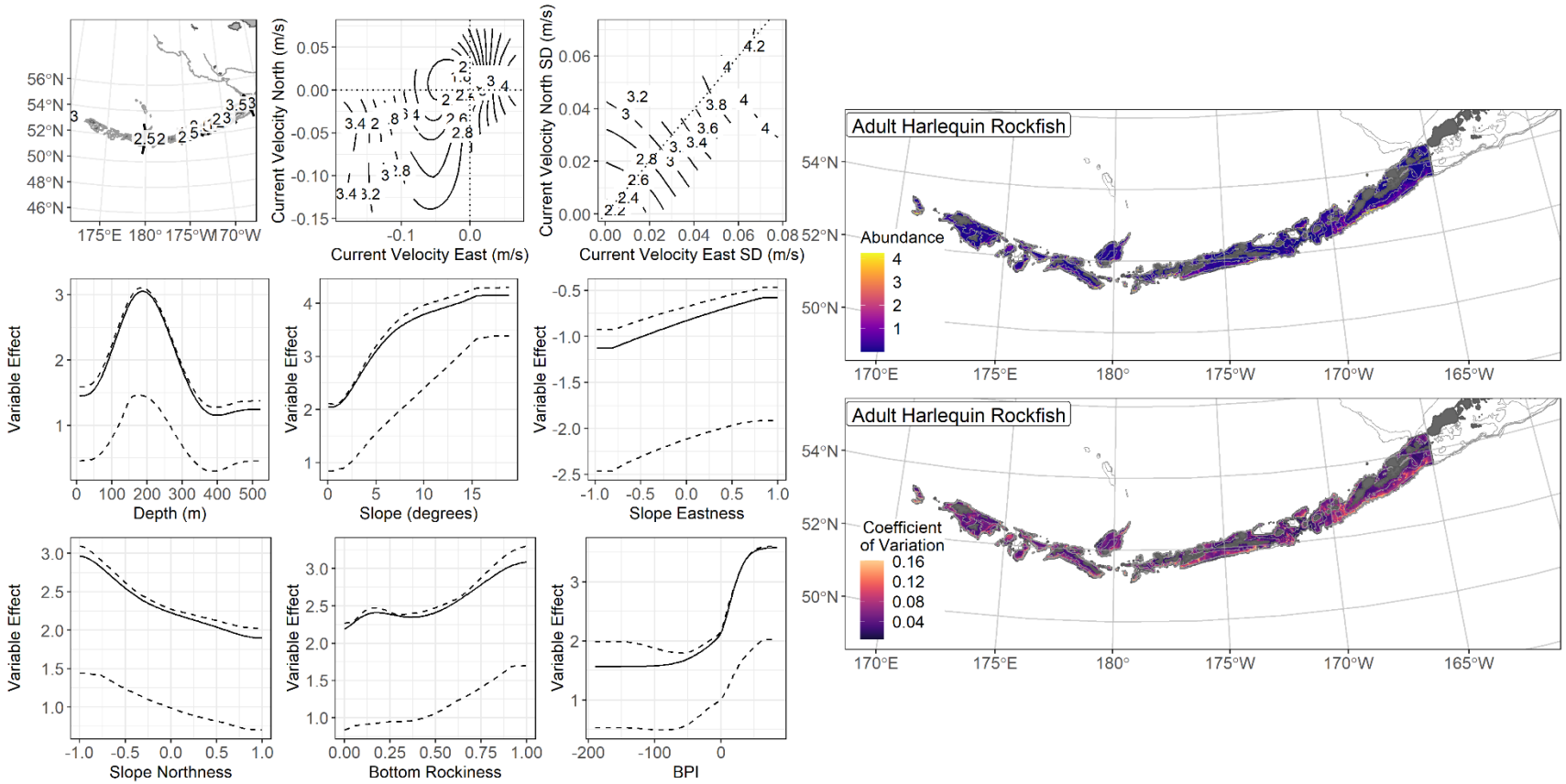


Figure 145. -- The top nine covariate effects (left panel) on ensemble-predicted adult harlequin rockfish numerical abundance across the AI (upper right panel) alongside the coefficient of variation of the ensemble predictions (lower right panel).

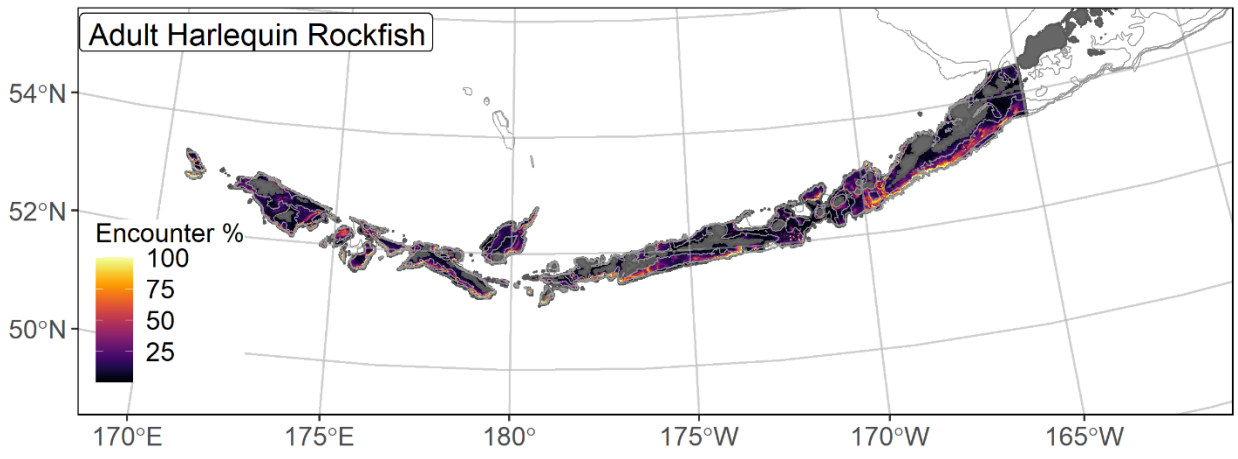


Figure 146. -- Encounter probability of adult harlequin rockfish from AFSC RACE-GAP summer bottom trawl surveys (1991–2019) of the AI with the 100 m, 300 m, and 500 m isobaths indicated.

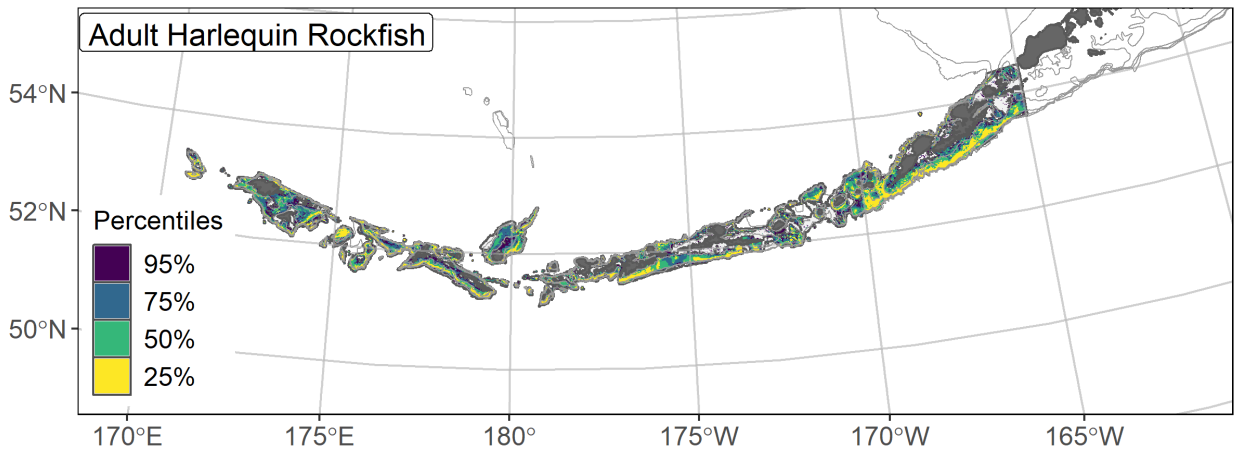


Figure 147. -- Essential fish habitat (EFH area) defined as the top 95% of numerical abundance predictions from a habitat-based ensemble fitted to adult harlequin rockfish distribution and abundance in AFSC RACE-GAP summer bottom trawl surveys (1991–2019) with 100 m, 300 m, and 500 m isobaths indicated; internal to the EFH map are the subareas of the top 25% (EFH hot spots), top 50% (core EFH area), and top 75% (principal EFH area) of habitat-related, ensemble-predicted numerical abundance.

### Shortspine thornyhead (*Sebastolobus alascanus*)

Shortspine thornyhead (*Sebastolobus alascanus*; SST) are encountered from Russia and Japan to the northern Bering Sea (Navarin Canyon) and through the AI to Baja California (Love et al. 2002, Mecklenburg et al. 2002). They inhabit a wide range of depths (20–1,500 m) but are most abundant in Alaska between 150 and 500 m. Although related to sebastid rockfishes, thornyheads lack a swim bladder and release pelagic eggs as opposed to live young (Pearson and Gunderson 2003). Shortspine thornyheads can grow to a maximum length of 750 mm and live up to 100 years (Kastelle et al. 2000). Larvae have a prolonged pelagic phase of up to 15 months, and juveniles are often found over mud bottoms 100–600 m before migrating into deeper depths as they mature. The $L_{50}$ for both sexes has been reported as 215 mm FL (Pearson and Gunderson 2003), and we used this length to separate subadult and adult SST for this study. In the BSAI region, SST is managed as part of the "other rockfish" stock complex, where it is typically one of the top two components (Sullivan et al. 2020).

**Subadult shortspine thornyhead distribution and predicted abundance from RACE-GAP summer bottom trawl surveys in the Aleutian Islands –** Subadult SST catches in the RACE-GAP summer trawl survey were split between the slope areas south of Unalaska Island in the east, and several deep water sites in the western AI (Fig. 148). The final ensemble only contained two SDMs, and the $GAM_P$ received about twice as much weight as the paGAM. The ensemble displayed good to excellent predictive performance (Table 43). Specifically, the ensemble received excellent scores for predictions of presence/absence (AUC = 0.98) and deviance explained (PDE = 0.76), and it performed well, though not excellently, at predicting relative abundance ($\rho = 0.46$). Given the near-perfect score on AUC and the high portion of the deviance explained, this ensemble appeared to make very accurate predictions. Bottom depth was the most

important covariate and accounted for 40.0% of the deviance explained by the ensemble (Table 44). Geographic position, current, and slope aspect also made substantial contributions. The model predicted higher subadult abundance at greater depths, in areas with weak bottom currents, and on the southern side of the island chain (Fig. 149). Predicted abundance was highest in the east, along the slope south of Unalaska Island, though localized areas of high abundance were predicted farther west (Fig. 149). Invariably, high abundance occurred along the continental slope, often at the edge of the survey area. The map of the predicted CV of abundance showed high variation in most deep slope areas (Fig. 149). Encounter probabilities for subadult SST demonstrated the same pattern, with high probabilities in many slope areas (Fig. 150).

**Adult shortspine thornyhead distribution and predicted abundance from RACE-GAP summer bottom trawl surveys in the Aleutian Islands –** Adult SST catches in the RACE-GAP summer survey were more common than subadults. The geographic distribution of adult catches was similar to subadults with most catches taken from 300 to 500 m (Fig. 151). The final ensemble combined the three SDMs, with the paGAM given about half the weight of the others, and showed an excellent fit to the data (Table 43). All three fit metrics were rated as excellent ($\rho = 0.61$; AUC = 0.93; PDE = 0.74), suggesting that this ensemble was very effective at predicting the presence and abundance of adult SST in bottom trawl catches. Geographic position and bottom depth were the most important covariates and accounted for 72.0% of the deviance explained by the ensemble (Table 44). In general, the model predicted that abundance would be higher in places with deeper bottom depths and in locations that were either in the eastern or western AI (Fig. 152). Adult SST abundance was predicted to be highest along the continental slope south of Unalaska Island, and in general was often quite high within limited

geographic patches (Fig. 152). The predicted CV of abundance was highest along the slope near the 500 m depth contour (Fig. 152). Encounter probabilities were high along most of the slope areas of sufficient depth (Fig. 153).

**Essential fish habitat of subadult and adult shortspine thornyhead in the Aleutian Islands –** The habitat-related abundance predictions based on RACE-GAP summer bottom trawl data (1991–2019) were translated into EFH area and subareas (Fig. 154). The EFH of both life stages was located in deep water along the continental slope, particularly south of Unalaska Island. Almost all of the EFH area for subadults was located in waters more than 300 m deep. The EFH for adults was considerably larger than that of subadults, but followed the same general patterns. Around Unalaska Island and Attu Island, the EFH for adults extended into shallow water closer to shore. Given the observed and predicted depth distribution of this species, it seems likely that much of the habitat for SST is deeper than 500 m and hence outside the range of the RACE-GAP survey. Additional data sources, such as from longline surveys, might characterize this species' habitat[20] more effectively.

[20] A recommendation to add additional survey data types if possible to future SDM ensemble EFH mapping efforts for this species will be included as a future recommendation for research directions from the 2023 EFH 5-year review.

Table 43. -- Constituent species distribution models (SDMs) used to construct Essential Fish Habitat (EFH) for a) subadult and b) adult shortspine thornyhead: MaxEnt = Maximum entropy; paGAM = presence-absence generalized additive model; hGAM = hurdle GAM; $GAM_P$ = standard Poisson GAM; and $GAM_{nb}$ = standard negative-binomial GAM. Ensemble performance ($\rho$ = Spearman's rank correlation coefficient), root-mean-square-error (RMSE), the area under the receiver operating characteristic (AUC), and the Poisson deviance explained (PDE) were generated from k-fold cross-validation. The "--" in a field indicates that this SDM was not included in the final ensemble.

**a) subadult shortspine thornyhead**

| Models | RMSE | Relative Weight | ρ | AUC | PDE | EFH area ($km^2$) |
|---|---|---|---|---|---|---|
| MaxEnt | -- | 0 | -- | -- | -- | -- |
| paGAM | 14.34 | 0.31 | 0.45 | 0.98 | 0.61 | 22,300 |
| hGAM | -- | 0 | -- | -- | -- | -- |
| $GAM_P$ | 9.59 | 0.69 | 0.47 | 0.97 | 0.66 | 22,500 |
| $GAM_{nb}$ | 17.71 | 0 | 0.52 | 0.98 | 0.55 | -- |
| ensemble | 8.08 | 1 | 0.46 | 0.98 | 0.76 | 23,200 |

**b) adult shortspine thornyhead**

| Models | RMSE | Relative Weight | ρ | AUC | PDE | EFH area ($km^2$) |
|---|---|---|---|---|---|---|
| MaxEnt | -- | 0 | -- | -- | -- | -- |
| paGAM | 36.7 | 0.23 | 0.62 | 0.94 | 0.63 | 59,500 |
| hGAM | 27.9 | 0.39 | 0.60 | 0.94 | 0.71 | 46,400 |
| $GAM_P$ | 28.0 | 0.39 | 0.60 | 0.92 | 0.70 | 56,400 |
| $GAM_{nb}$ | -- | 0 | -- | -- | -- | -- |
| ensemble | 26.1 | 1 | 0.61 | 0.93 | 0.74 | 54,800 |

Table 44. -- Covariates retained in the a) subadult and b) adult shortspine thornyhead species distribution model (SDM) final ensembles, the percent contribution to the ensemble deviance explained by each, and the cumulative percent deviance: SD = standard deviation, and BPI = bathymetric position index.

| Shortspine thornyhead | Covariate | % Contribution | Cumulative % Contribution |
|---|---|---|---|
| **a) subadult** | bottom depth | 40.0 | 40.0 |
| | position | 24.7 | 64.6 |
| | current | 9.3 | 73.9 |
| | aspect north | 8.2 | 82.1 |
| | current SD | 4.3 | 86.4 |
| | BPI | 3.5 | 89.9 |
| | curvature | 2.1 | 92.0 |
| | rockiness | 1.7 | 93.7 |
| | aspect east | 1.6 | 95.3 |
| | slope | 1.6 | 96.9 |
| | tidal maximum | 1.3 | 98.2 |
| | pennatulacean presence | 0.9 | 99.1 |
| | sponge presence | 0.6 | 99.7 |
| | bottom temperature | 0.3 | 100 |
| **a) adult** | bottom depth | 36.6 | 36.6 |
| | position | 35.5 | 72.0 |
| | aspect north | 10.1 | 82.1 |
| | current | 5.3 | 87.4 |
| | current SD | 2.9 | 90.3 |
| | bottom temperature | 2.9 | 93.2 |
| | aspect east | 2.0 | 95.2 |
| | slope | 1.9 | 97.1 |
| | curvature | 0.7 | 97.8 |
| | tidal maximum | 0.6 | 98.4 |
| | sponge presence | 0.6 | 99.0 |
| | rockiness | 0.4 | 99.4 |
| | BPI | 0.4 | 99.8 |
| | pennatulacean presence | 0.2 | 100 |

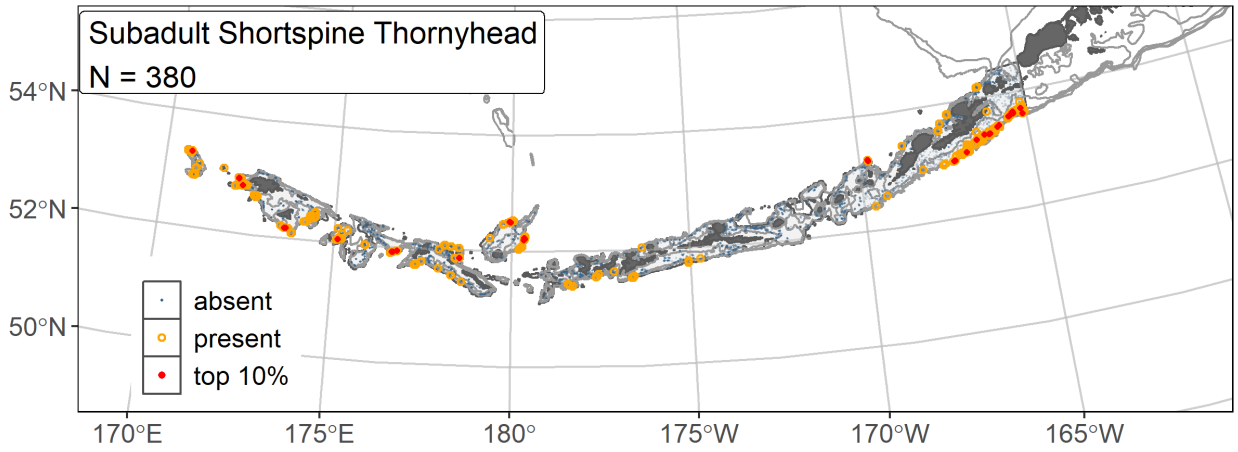


Figure 148. -- Distribution of subadult shortspine thornyhead catches (N = 380) in 1991–2019 AFSC RACE-GAP summer bottom trawl surveys of the AI with the 100 m, 300 m, and 500 m isobaths indicated; filled red circles indicate locations in top 10% of overall abundance, open orange circles indicate presence in remaining catches.

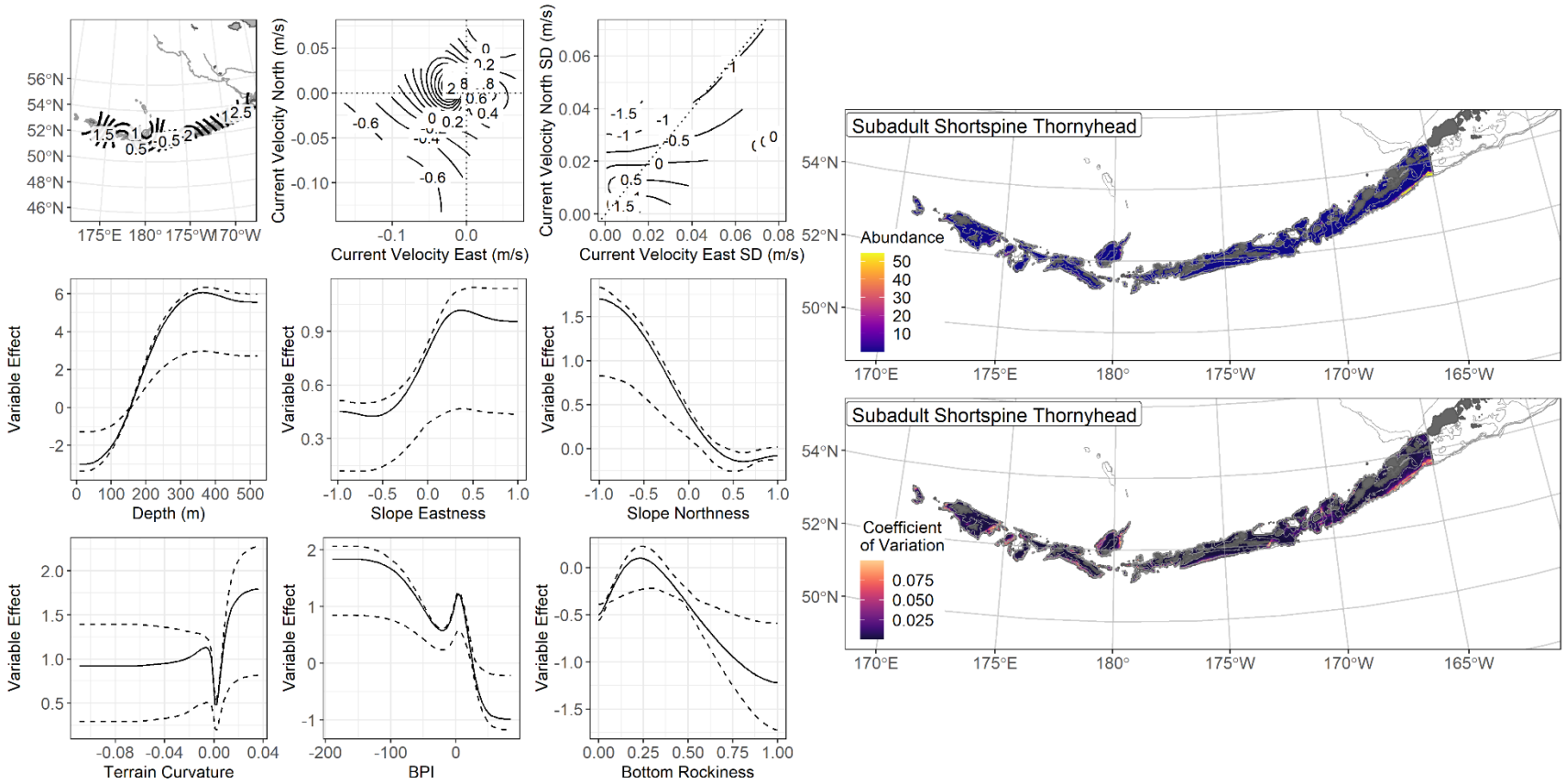


Figure 149. -- The top nine covariate effects (left panel) on ensemble-predicted subadult shortspine thornyhead numerical abundance across the AI (upper right panel) alongside the coefficient of variation of the ensemble predictions (lower right panel).

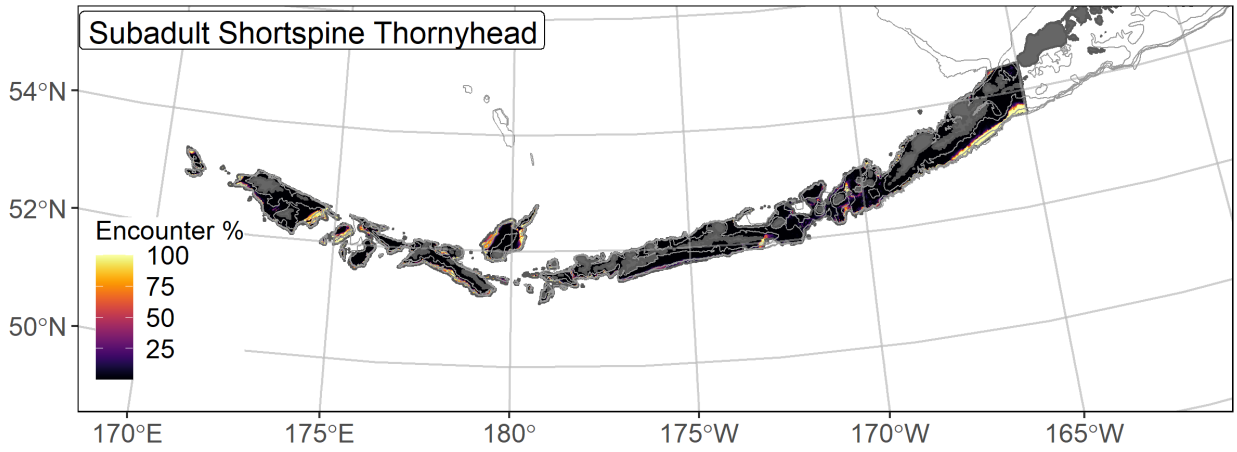


Figure 150. -- Encounter probability of subadult shortspine thornyhead from AFSC RACE-GAP summer bottom trawl surveys (1991–2019) of the AI with the 100 m, 300 m, and 500 m isobaths indicated.

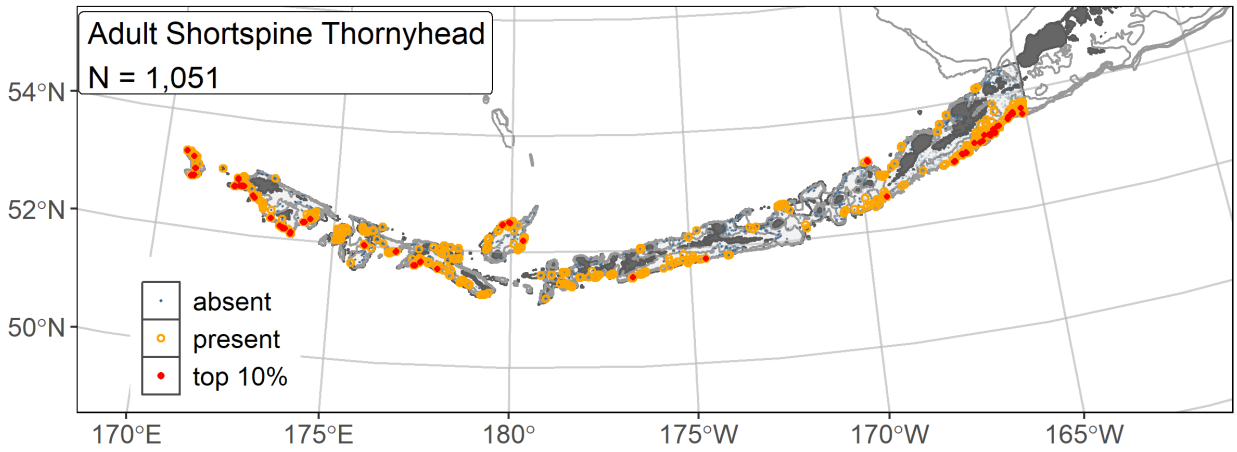


Figure 151. -- Distribution of adult shortspine thornyhead catches (N = 1,051) in 1991–2019 AFSC RACE-GAP summer bottom trawl surveys of the AI with the 100 m, 300 m, and 500 m isobaths indicated; filled red circles indicate locations in top 10% of overall abundance, open orange circles indicate presence in remaining catches.

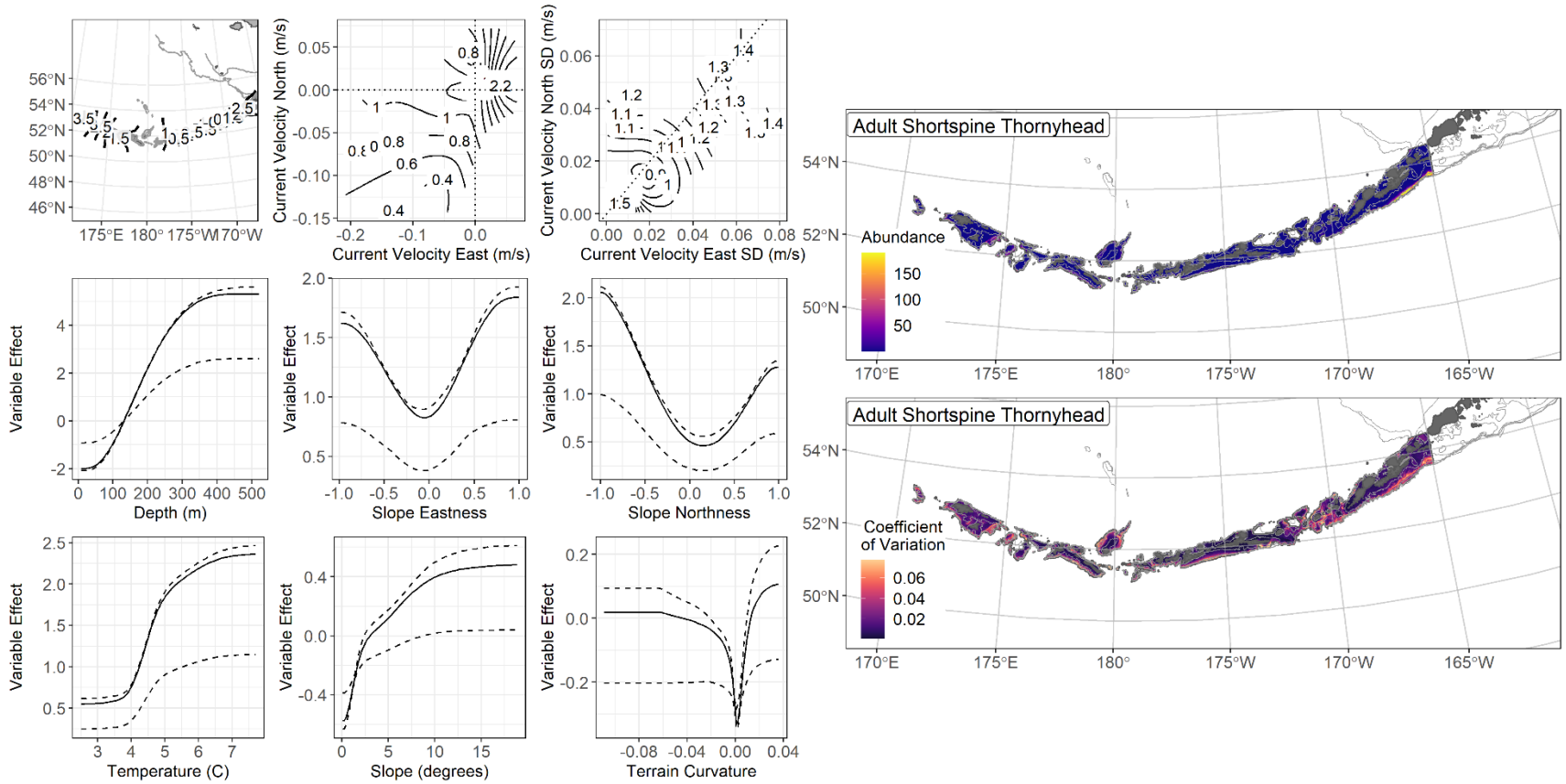


Figure 152. -- The top nine covariate effects (left panel) on ensemble-predicted adult shortspine thornyhead numerical abundance across the AI (upper right panel) alongside the coefficient of variation of the ensemble predictions (lower right panel).

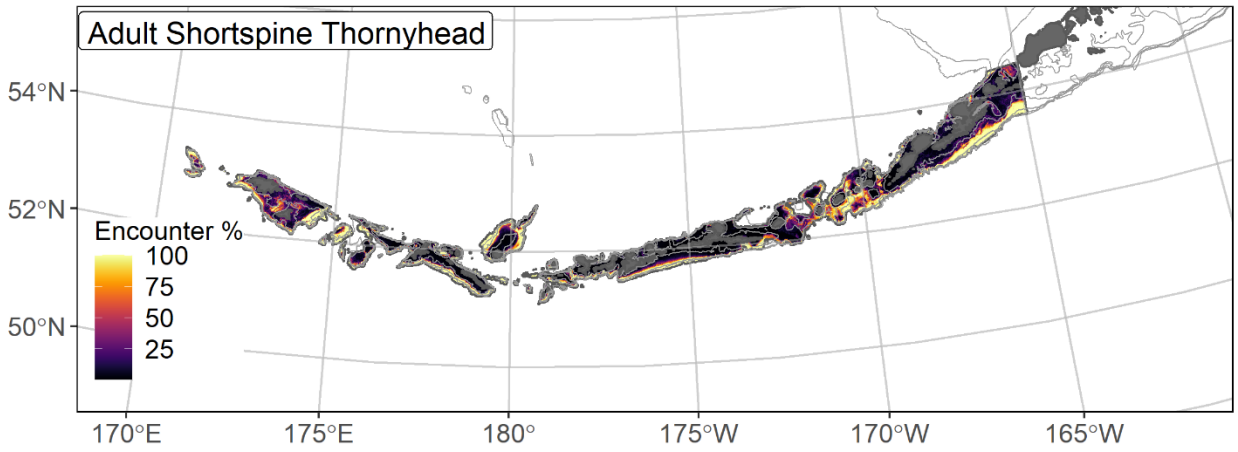


Figure 153. -- Encounter probability of adult shortspine thornyhead from AFSC RACE-GAP summer bottom trawl surveys (1991–2019) of the AI with the 100 m, 300 m, and 500 m isobaths indicated.

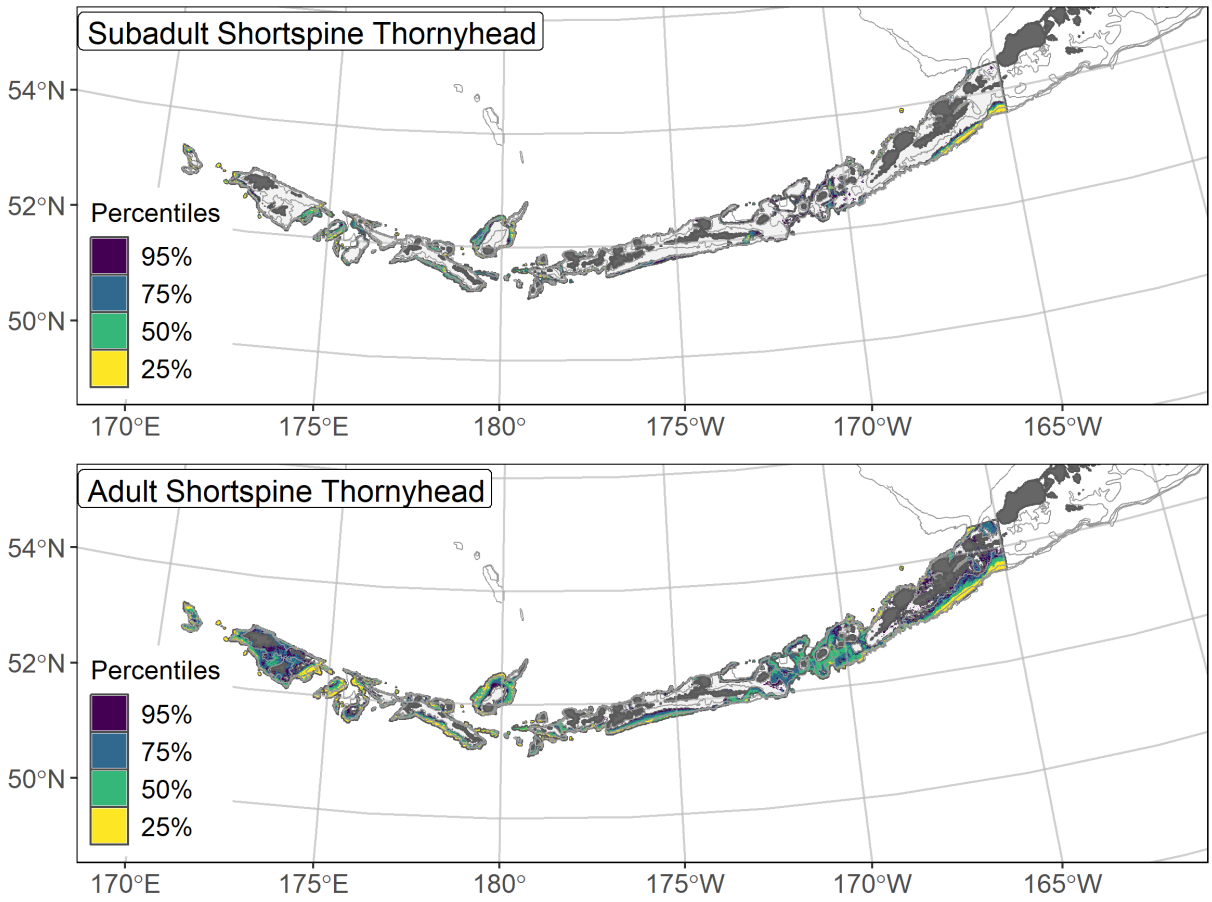


Figure 154. -- Essential fish habitat (EFH area) defined as the top 95% of numerical abundance predictions from a habitat-based ensemble fitted to subadult (top) and adult (bottom) shortspine thornyhead distribution and abundance in AFSC RACE-GAP summer bottom trawl surveys (1991–2019) with 100 m, 300 m, and 500 m isobaths indicated; internal to the EFH map are the subareas of the top 25% (EFH hot spots), top 50% (core EFH area), and top 75% (principal EFH area) of habitat-related, ensemble-predicted numerical abundance.

## Skates - Stock Complex

Aleutian Islands skates are managed in aggregate as part of the skate stock complex of the BSAI region (Ormseth 2020). In the Bering Sea, Alaska skate (*Bathyraja parmifera*) is the dominant species, but it is less abundant in the AI. For the BSAI management region, Alaska skate receives a separate assessment, although harvest specifications are made for the complex as a whole. For this project, four species of skates were prevalent enough in the RACE-GAP summer bottom trawl surveys to allow for the development of SDMs: Alaska skate, Aleutian skate (*B. aleutica*), mud skate (*B. taranetzi*), and whiteblotched skate (*B. maculata*). A fifth species, the leopard skate (*B. panthera*), likely has sufficient data to develop a SDM and will be investigated during the 2027 EFH cycle. All four of the species currently included were modeled with both subadult and adult life stages. Because these species are typically managed together as a stock complex, this chapter summarizes the composite abundance, encounter probabilities, and EFH of these four species in the AI as a single complex. Stock assessments have identified whiteblotched skate as the dominant species in the AI, representing over 50% of the total skate biomass (Ormseth 2020), which is apparent in the complex maps below.

**Subadult Skate Stock Complex abundance and distribution predicted from RACE-GAP summer bottom trawl surveys in the Bering Sea –**

Numerical abundance predictions for four species of subadult skates were combined to estimate the abundance and EFH of the subadult skate stock complex in the AI (Fig. 155). The composite abundance map was strongly influenced by whiteblotched and mud skates, and the resulting map showed high numbers of skates around Seguam Pass and the Islands of Four Mountains. Amchitka Pass and Stalemate Bank were predicted to have moderately high skate abundance, and Amchitka Pass contained EFH hot spots for all four species. Some areas of high

abundance also occurred along the continental slope south of Adak Island, which was important habitat for mud skates and Aleutian skates. Subadult Alaska skate were rarely encountered in the AI and made a minimal contribution to the complex map. Encounter probabilities for subadults in the skate complex were high in the areas described above and generally tended to be high in most areas with a moderate depth. The EFH areas for subadults in this complex followed the same pattern, with most of the core EFH and EFH hot spot subareas located farther from shore along the continental slope.

**Adult Skate Stock Complex abundance and distribution predicted from RACE-GAP summer bottom trawl surveys in the Bering Sea –** Numerical abundance predictions for four species of adult skates were combined to estimate the abundance and EFH of the adult skate stock complex in the AI (Fig. 156). The map for the adult skate complex in the AI was very similar to the map for subadults. This map was consistent with the SDMs for the individual species, which also predicted only minor differences in habitat usage between adults and subadults. The composite abundance map was dominated by whiteblotched skates, and the resulting complex map was very similar to the map of whiteblotched skate abundance (Fig. 182). Notably, this included the area around Seguam Pass and to the east. Some areas of high abundance also occurred farther to the west along the slope. Alaska skate abundance was more influential in the adult skate complex map, as it was more likely to be found in shallower water as an adult, unlike Aleutian and mud skates. Encounter probabilities for adults in the skate complex were high in Seguam Pass, as well as some areas around Petrel Bank, Amchitka Pass, and Stalemate Bank. Unlike subadults, adult encounter probability was not notably higher in the deeper water along the continental slope. This was likely an effect of the species included in the complex, as older Alaska and whiteblotched skates were more common in these shallower

habitats, whereas adult Aleutian skate and mud skate were common in deeper waters but were less abundant in the survey. The EFH map for adults in this complex reflected the areas of high abundance described above.

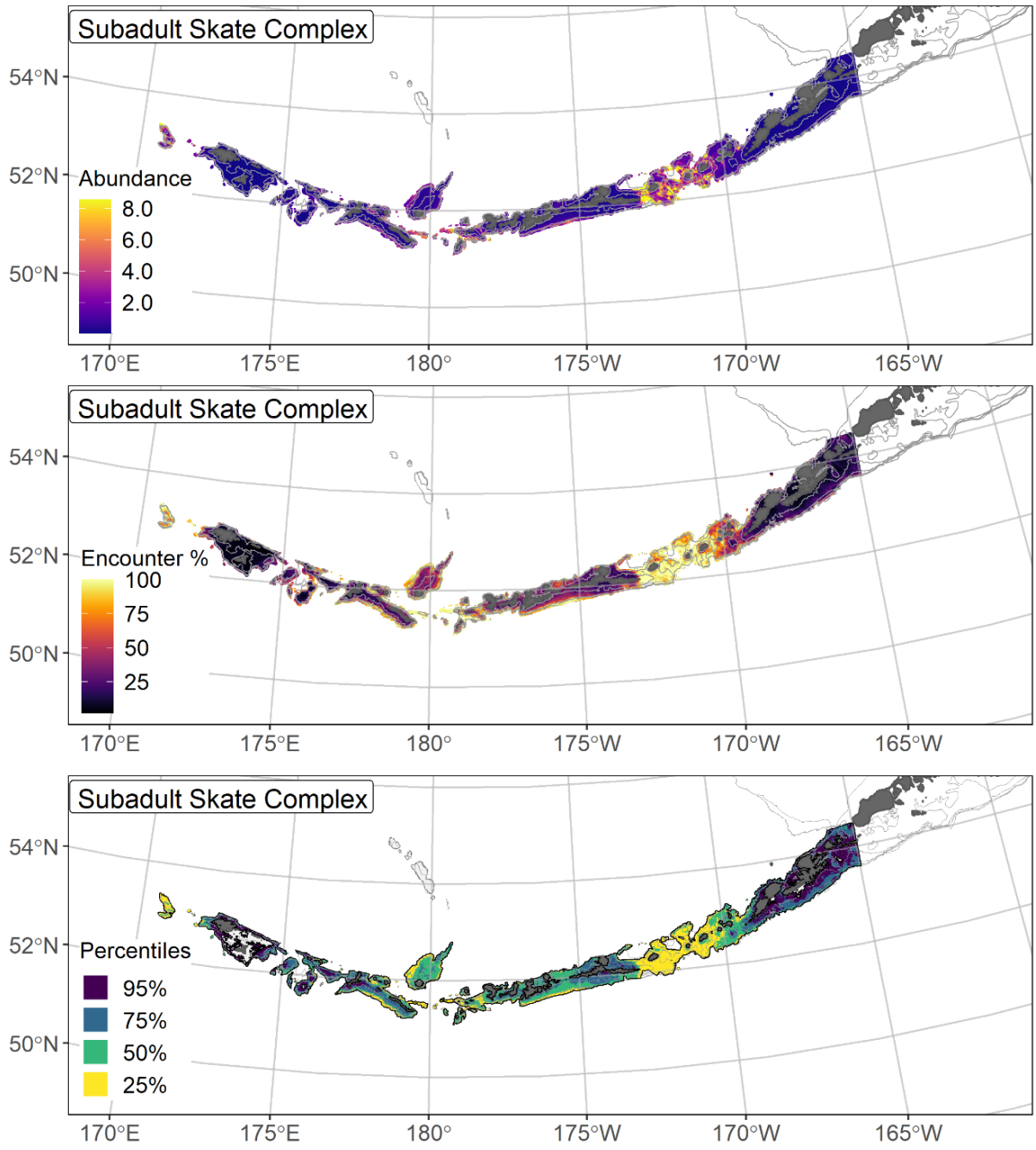


Figure 155. -- Composite predicted numerical abundance (top panel), encounter probability (middle panel), and essential fish habitat (bottom panel) of subadult skates from the AI collected in AFSC RACE-GAP summer bottom trawl surveys (1991–2019) with 100 m, 300 m, and 500 m isobaths indicated. EFH defined as the top 95% of numerical abundance predictions above a presence threshold, and integral to the EFH map are the shapes of the top 25% (EFH hot spots), top 50% (core EFH area), and top 75% (principal EFH area) of habitat-related, ensemble-predicted numerical abundance.

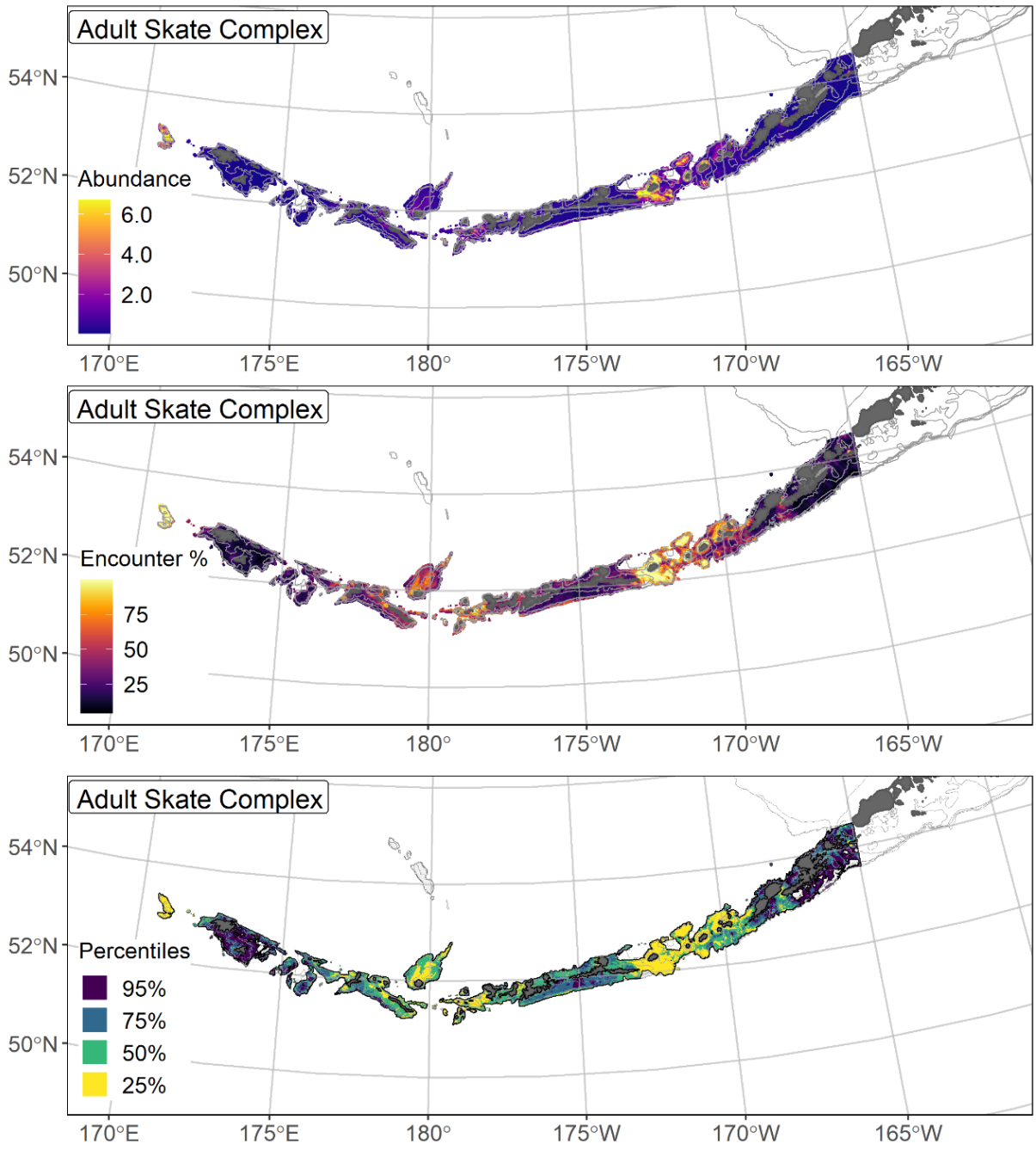


Figure 156. -- Composite predicted numerical abundance (top panel), encounter probability (middle panel), and essential fish habitat (bottom panel) of adult skates from AI collected in AFSC RACE-GAP summer bottom trawl surveys (1991–2019) with 100 m, 300 m, and 500 m isobaths indicated. EFH defined as the top 95% of numerical abundance predictions above a presence threshold, and integral to the EFH map are the shapes of the top 25% (EFH hot spots), top 50% (core EFH area), and top 75% (principal EFH area) of habitat-related, ensemble-predicted numerical abundance.

**Alaska skate (*Bathyraja parmifera*)**

The Alaska skate (*Bathyraja parmifera*) is a large, shallow water skate (Ebert 2005, Stevenson et al. 2007) that is common throughout shallow to moderate depths in the AI RACE-GAP summer bottom trawl surveys. Hoff (2008) determined that reproductive activity for this species in the EBS occurs primarily in several defined nursery areas. Similar locations have not been located in the AI region, but this species prefers areas between 150 m and 300 m in depth near the slope/shelf interface in the EBS. The Alaska skate grows to fairly large sizes and attains a maximum length of at least 1350 mm (Stevenson et al. 2007). Subadults (≤ 930 mm TL) were distinguished from adults (> 930 mm TL) based on $L_{50}$ (Matta and Gunderson 2007). The AI are also home to the endemic leopard skate (*Bathyraja panthera*), which is similar in appearance to Alaska skate. Prior to 2006, the survey data reflects a mix of these two species, and therefore only data for Alaska skate from 2006 to 2019 are modeled here. Alaska skate are managed in a complex with several other species, and while they are the dominant species in the BSAI, they are a smaller component of the more diverse skate assemblage found in the AI (Ormseth 2020).

**Subadult Alaska skate distribution and predicted abundance from RACE-GAP summer bottom trawl surveys in the Aleutian Islands –** Subadult Alaska skate catches from the RACE-GAP summer survey of the AI were somewhat rare (N = 102, Fig. 157). The highest density catches were located in the central AI. The final ensemble contained three SDMs with approximately equal weights, demonstrating poor to fair performance overall (Table 45). The ensemble performed well at discriminating presence and absence (AUC = 0.80), but had a poor fit to the abundance data ($\rho$ = 0. 20) and explained only a fair amount of the deviance (PDE = 0.25). The ability of the SDMs to fit the data was probably impaired by the relatively small amount of data available since records before 2006 are confounded with *B. panthera*.

Geographic position, bottom depth, bottom current, and slope aspect were the most important covariates and accounted for 86.1% of the deviance explained by the ensemble (Table 46). In general, high abundance was predicted by being located in the central part of the AI, in shallow depths, with weak bottom currents and steep terrain oriented towards the northeast (Fig. 158). Predicted abundance was low overall but was highest in the central part of the islands, between Atka and Adak islands, and tended to be higher on the northern side of the islands facing the Bering Sea. The CV of abundance for ensemble predictions was highest in the east near Unalaska Island and Unimak Pass. Predicted encounter probability was generally low except around the central AI (Fig. 159).

**Adult Alaska skate distribution and predicted abundance from RACE-GAP summer bottom trawl surveys in the Aleutian Islands –** Adult Alaska skate catches from the RACE-GAP summer survey were uncommon throughout much of the Aleutian Islands, with the highest density catches located in the central AI (Fig. 160). The final ensemble contained four SDMS, which were weighted about equally and displayed fair predictive ability overall (Table 45). More specifically, the ensemble was a good predictor of the presence of adult Alaska skate in a catch (AUC = 0.82), showed a fair fit to the observed abundance data ($\rho = 0.25$), and provided a fair reduction in the overall deviance (PDE = 0.27). Together, these metrics indicated that the ensemble can provide general predictions about the presence of adults, but they may not accurately estimate abundance. Due to taxonomic issues with Alaska and leopard skates, only seven survey years of data were available, and these findings should be considered temporary until additional data are available. A variety of covariates were important to the model, including geographic position, bottom depth, current, current variability, slope, and BPI (Table 46). Adult Alaska skates were predicted to be abundant at shallow depths near 180° longitude (Fig. 161).

The ensemble also predicted high abundance in areas with variable northerly currents and terrain with valleys or similar features. Predicted abundance was highest in the central AI and above the 100 m depth contour. The predicted CV of abundance was mostly uniform. Adult Alaska skates encounter probability was usually highest close to shore and close to zero in most places greater than 300 m depth (Fig. 162).

**Essential fish habitat of subadult and adult Alaska skate in the Aleutian Islands –** The habitat-related abundance predictions based on RACE-GAP summer bottom trawl data (2006–2019) were translated into EFH area and subareas (Fig. 163). The EFH area for subadult Alaska skate encompassed most shallow areas between 174° W and 179° E. EFH hot spots occurred around Petrel Bank and the Andreanof Islands. The adult EFH area was larger and included all the areas of the subadult life stage, as well as the regions around Attu Island and Unalaska Island. In summary, while both life stages showed a strong association with shallow water, subadults are confined to a subset of the suitable terrain, whereas adults appear to occupy almost all areas less than 200 m deep.

Table 45. -- Constituent species distribution models (SDMs) used to construct Essential Fish Habitat (EFH) for a) subadult and b) adult Alaska skate: MaxEnt = Maximum entropy; paGAM = presence-absence generalized additive model; hGAM = hurdle GAM; $GAM_P$ = standard Poisson GAM; and $GAM_{nb}$ = standard negative-binomial GAM. Ensemble performance (ρ = Spearman's rank correlation coefficient), root-mean-square-error (RMSE), the area under the receiver operating characteristic (AUC), and the Poisson deviance explained (PDE) were generated from k-fold cross-validation. The "--" in a field indicates that this SDM was not included in the final ensemble.

**a) subadult Alaska skate**

| Models | RMSE | Relative weight | ρ | AUC | PDE | EFH area ($km^2$) |
|---|---|---|---|---|---|---|
| MaxEnt | -- | 0 | -- | -- | -- | -- |
| paGAM | 0.43 | 0.34 | 0.16 | 0.74 | 0.14 | 25,500 |
| hGAM | 0.43 | 0.33 | 0.16 | 0.74 | 0.12 | 23,500 |
| $GAM_P$ | 0.43 | 0 | 0.15 | 0.73 | 0.11 | -- |
| $GAM_{nb}$ | 0.43 | 0.34 | 0.16 | 0.74 | 0.15 | 27,300 |
| ensemble | 0.42 | 1 | 0.20 | 0.80 | 0.25 | 25,700 |

**b) adult Alaska skate**

| Models | RMSE | Relative weight | ρ | AUC | PDE | EFH area ($km^2$) |
|---|---|---|---|---|---|---|
| MaxEnt | 0.66 | 0.26 | 0.20 | 0.76 | 0.17 | 44,600 |
| paGAM | 0.66 | 0.26 | 0.19 | 0.74 | 0.15 | 48,700 |
| hGAM | 0.70 | 0.23 | 0.18 | 0.75 | 0.08 | 42,500 |
| $GAM_P$ | 0.67 | 0 | 0.20 | 0.75 | 0.10 | -- |
| $GAM_{nb}$ | 0.67 | 0.25 | 0.19 | 0.74 | 0.14 | 45,300 |
| ensemble | 0.65 | 1 | 0.25 | 0.82 | 0.27 | 48,600 |

Table 46. -- Covariates retained in the a) subadult and b) adult Alaska skate species distribution model (SDM) final ensembles, the percent contribution to the ensemble deviance explained by each, and the cumulative percent deviance: SD = standard deviation, and BPI = bathymetric position index.

| Alaska skate | Covariate | % Contribution | Cumulative % Contribution |
|---|---|---|---|
| **a) subadult** | position | 33.2 | 33.2 |
| | bottom depth | 20.0 | 53.1 |
| | aspect east | 13.1 | 66.2 |
| | aspect north | 10.5 | 76.7 |
| | current | 9.4 | 86.1 |
| | slope | 3.5 | 89.6 |
| | BPI | 3.4 | 93.0 |
| | coral presence | 2.4 | 95.4 |
| | bottom temperature | 1.5 | 96.9 |
| | pennatulacean presence | 1.5 | 98.4 |
| | sponge presence | 0.9 | 99.3 |
| | current SD | 0.7 | 100 |
| | tidal maximum | 0.0 | 100 |
| **a) adult** | bottom depth | 31.3 | 31.3 |
| | position | 12.3 | 43.6 |
| | current SD | 7.8 | 51.4 |
| | current | 7.5 | 58.9 |
| | BPI | 7.2 | 66.1 |
| | tidal maximum | 6.2 | 72.3 |
| | slope | 5.5 | 77.7 |
| | coral presence | 4.4 | 82.1 |
| | curvature | 3.6 | 85.7 |
| | aspect east | 3.3 | 89.0 |
| | aspect north | 3.1 | 92.1 |
| | rockiness | 2.7 | 94.8 |
| | pennatulacean presence | 2.7 | 97.5 |
| | bottom temperature | 1.9 | 99.4 |
| | sponge presence | 0.6 | 100 |

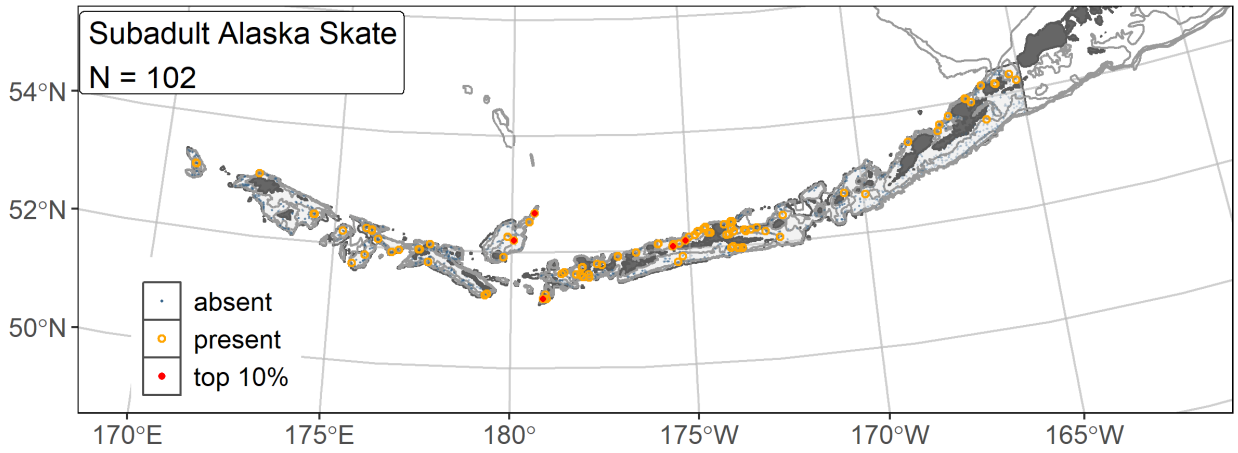


Figure 157. -- Distribution of subadult Alaska skate catches (N = 102) in 2006–2019 AFSC RACE-GAP summer bottom trawl surveys of the AI with the 100 m, 300 m, and 500 m isobaths indicated; filled red circles indicate catches in top 10% of overall abundance, open orange circles indicate presence in remaining catches, and small blue dots indicate absence.

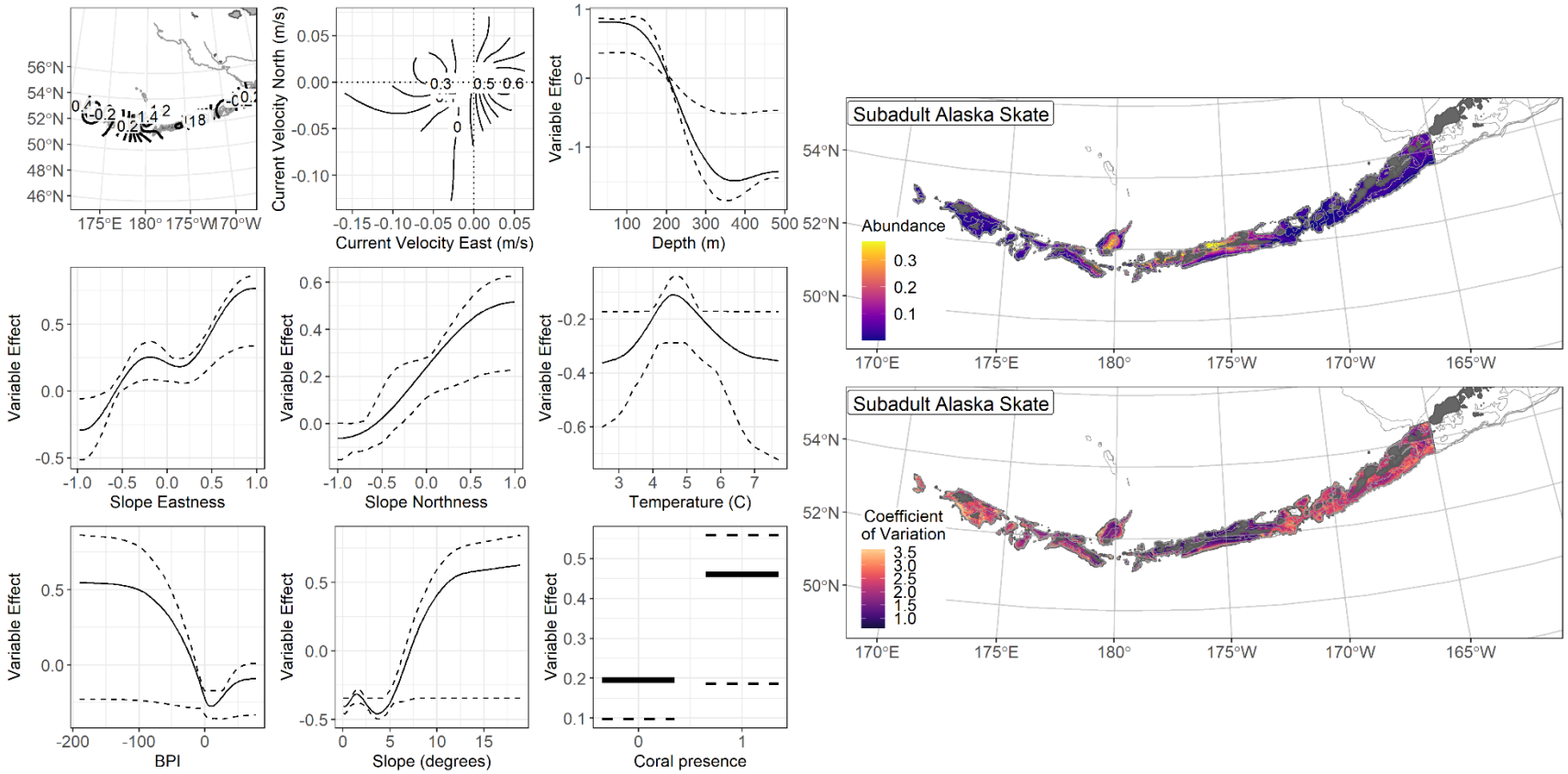


Figure 158. -- The top nine covariate effects (left panel) on ensemble-predicted subadult Alaska skate numerical abundance across the AI (upper right panel) alongside the coefficient of variation of the ensemble predictions (lower right panel).

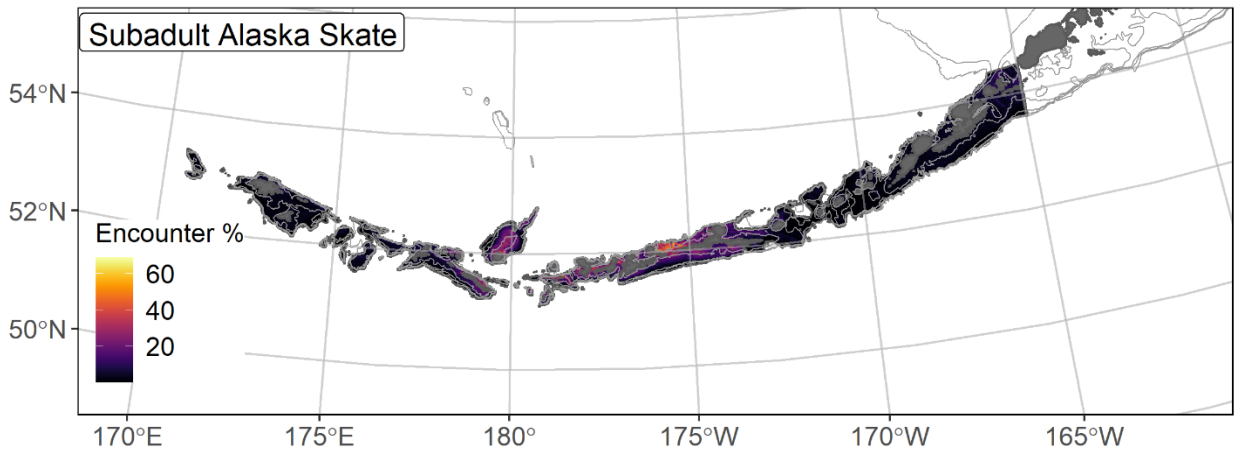


Figure 159. -- Encounter probability of subadult Alaska skate from AFSC RACE-GAP summer bottom trawl surveys (2006–2019) of the AI with the 100 m, 300 m, and 500 m isobaths indicated.

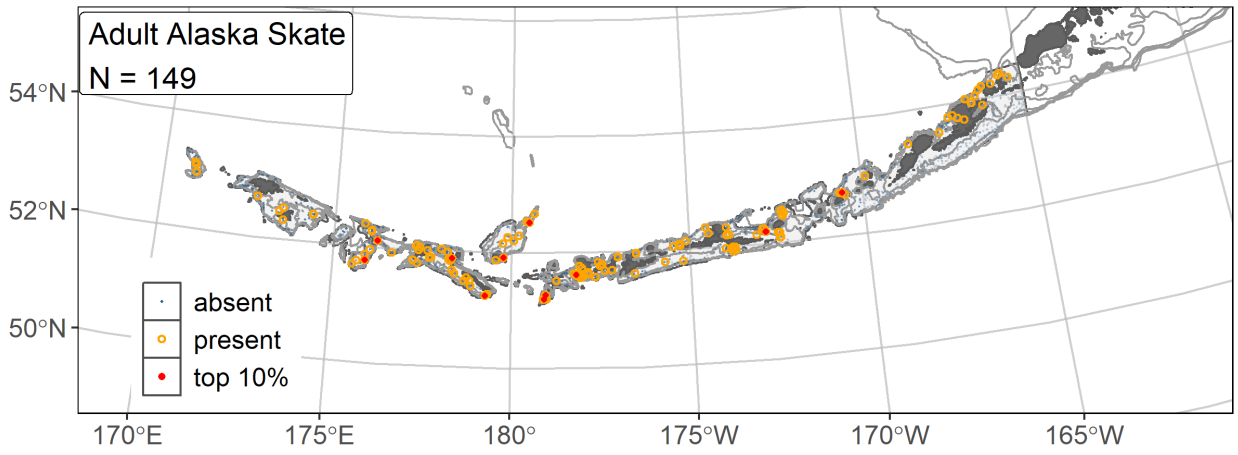


Figure 160. -- Distribution of adult Alaska skate catches (N = 149) in 2006–2019 AFSC RACE-GAP summer bottom trawl surveys of the AI with the 100 m, 300 m, and 500 m isobaths indicated; filled red circles indicate catches in top 10% of overall abundance, open orange circles indicate presence in remaining catches, and small blue dots indicate absence.

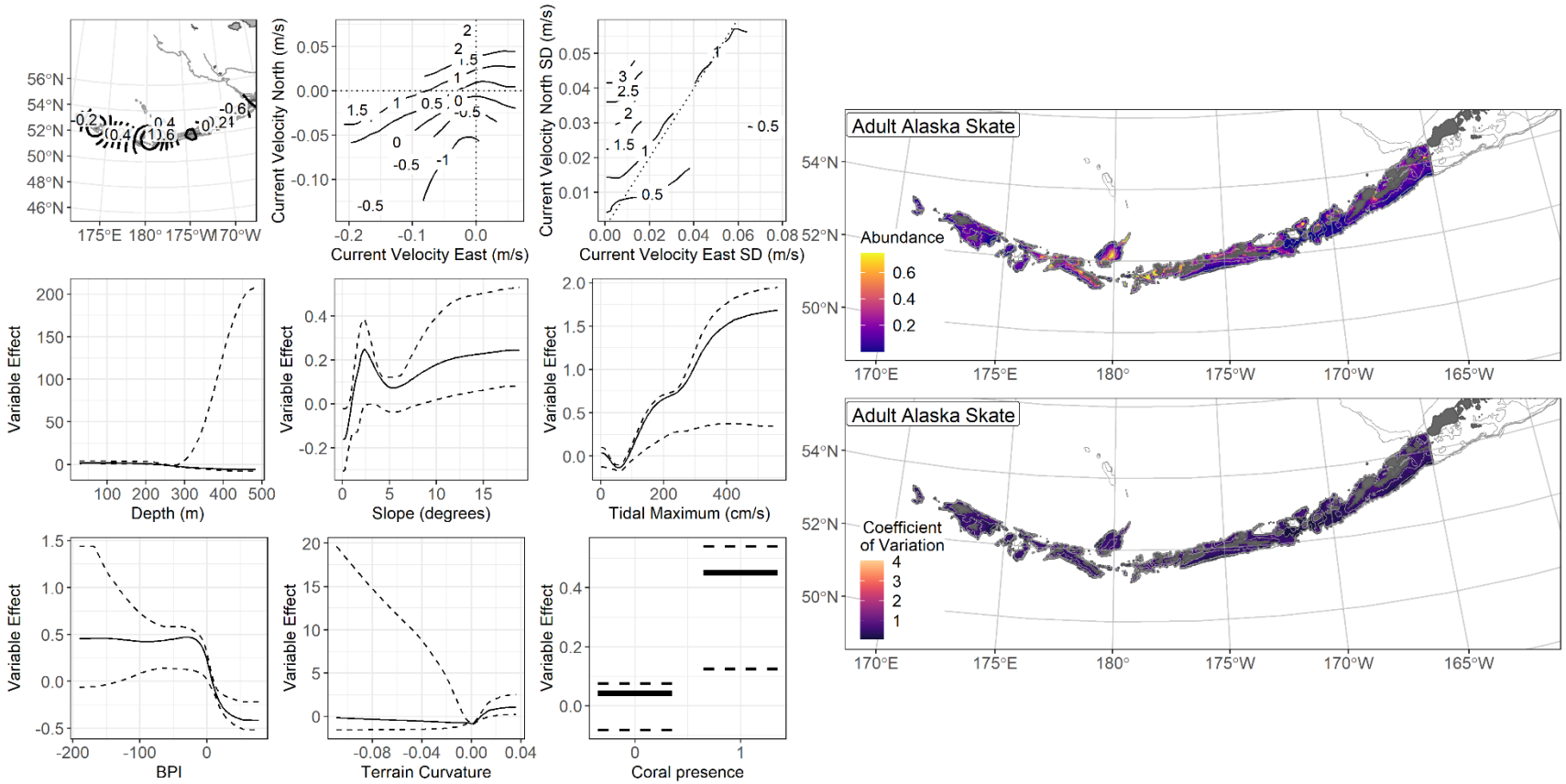


Figure 161. -- The top nine covariate effects (left panel) on ensemble-predicted adult Alaska skate numerical abundance across the AI (upper right panel) alongside the coefficient of variation of the ensemble predictions (lower right panel).

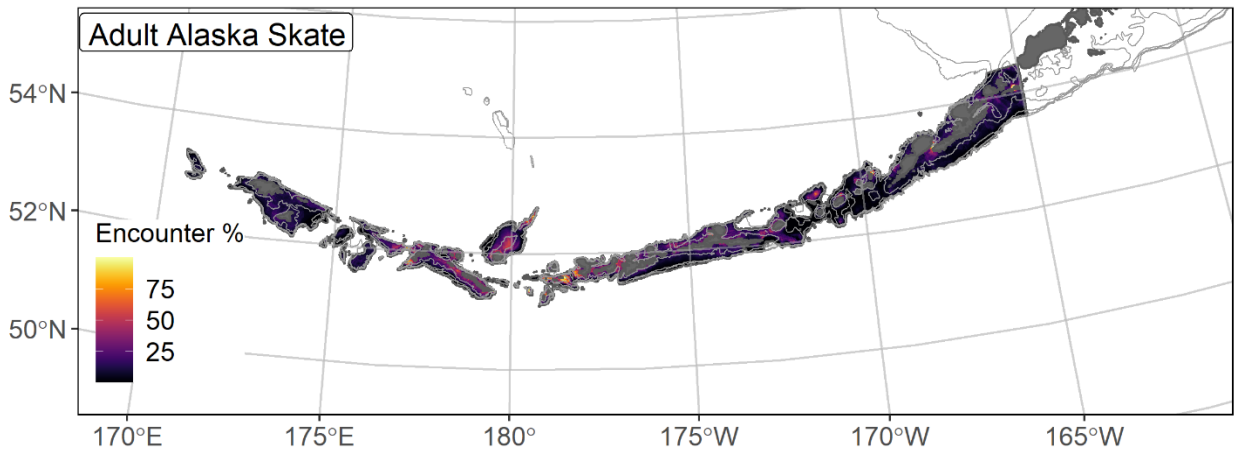


Figure 162. -- Encounter probability of adult Alaska skate from AFSC RACE-GAP summer bottom trawl surveys (2006–2019) of the AI with the 100 m, 300 m, and 500 m isobaths indicated.

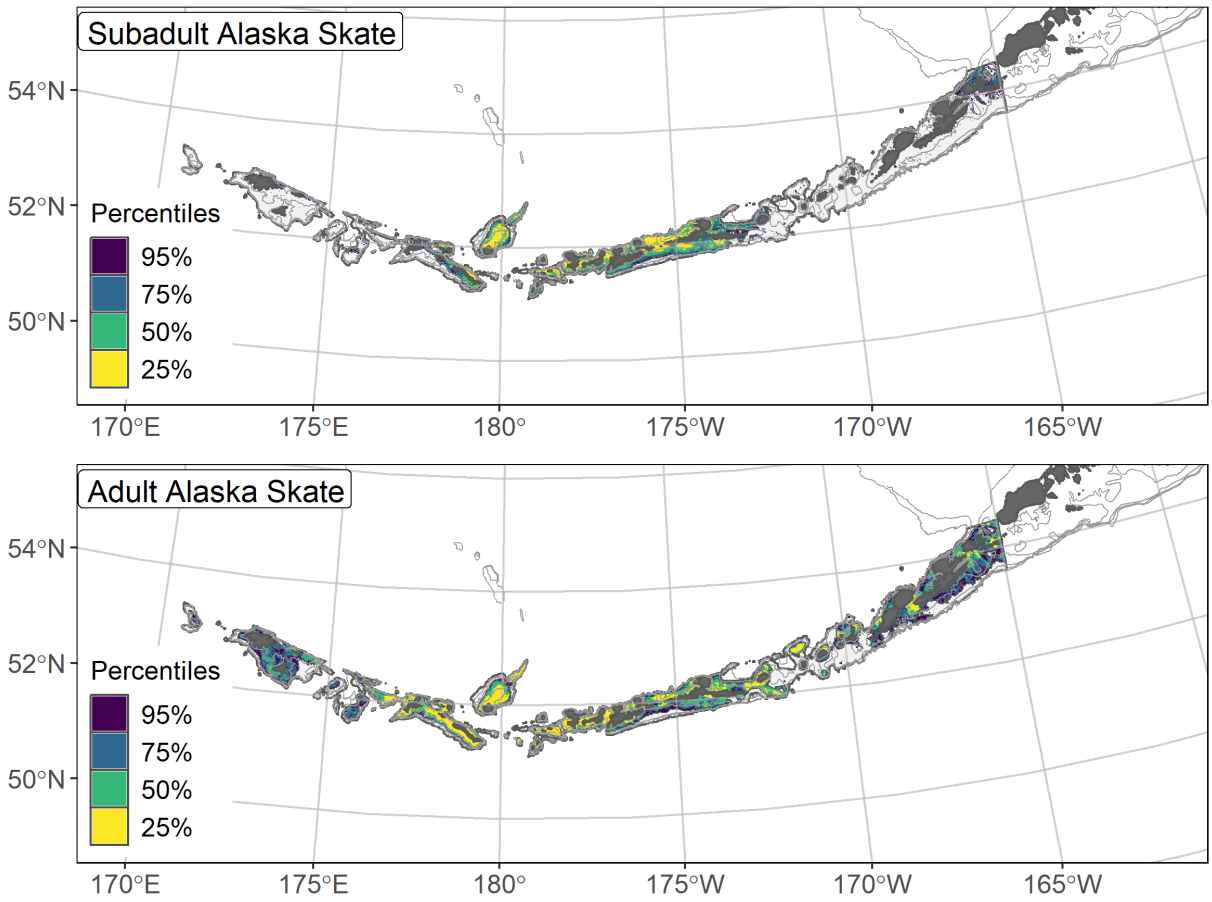


Figure 163. -- Essential fish habitat (EFH area) defined as the top 95% of numerical abundance predictions from a habitat-based ensemble fitted to subadult (top) and adult (bottom) Alaska skate distribution and abundance in AFSC RACE-GAP summer bottom trawl surveys (2006–2019) with 100 m, 300 m, and 500 m isobaths indicated; internal to the EFH map are the subareas of the top 25% (EFH hot spots), top 50% (core EFH area), and top 75% (principal EFH area) of habitat-related, ensemble-predicted numerical abundance.

**Aleutian skate (*Bathyraja aleutica*)**

The Aleutian skate (*Bathyraja aleutica*) is a large (161 cm TL maximum length) species that ranges from the GOA and AI into the Bering Sea. This species is found over a wide range of depths (29–950 m; Stevenson et al. 2007), and in the RACE-GAP bottom trawl surveys of the AI, they are found at moderate depths in most of the island chain (Hoff 2009). Aleutian skates mature slowly and do not reproduce until attaining a large size (> 1,320 mm TL), depositing their egg sacs in distinct nursery grounds (Ebert et al. 2007, Haas et al. 2016). Aleutian skates are among the most abundant skates in RACE-GAP AI bottom trawl surveys and are managed in aggregate as part of the skate complex across the BSAI region (Ormseth 2020). Aleutian skates were not routinely identified to species until 1999, so these models exclude data collected before that year.

**Subadult Aleutian skate distribution and predicted abundance from RACE-GAP summer bottom trawl surveys in the Aleutian Islands –** Subadult Aleutian skate catches were somewhat common and evenly distributed across the RACE-GAP summer survey areas (Fig. 164). There was no particular spatial pattern to large catches, and the majority of hauls in which the species was present contained a single individual. The final ensemble contained four SDMs with equal weights, and it demonstrated poor to fair performance (Table 47). The ensemble showed fair performance in two of the three metrics ($\rho = 0.26$, AUC = 0.76) but displayed poor performance in terms of deviance explained (PDE = 0.19). Taken together, this suggests that the ensemble could only predict some general patterns in the presence and abundance of subadult Aleutian skates, and it did not explain much of the variation in observed abundance. Geographic position and bottom depth were the most important covariates and accounted for 46.5% of the deviance explained (Table 48), though current covariates and bottom

temperature also contributed. In general, higher abundance was predicted in deeper water and with warmer temperatures (Fig. 165). Though important to the models, geographic position and current did not show a clear trend. Predicted abundance was highest in the areas west and south of Adak Island, though subadult Aleutian skates were predicted in lesser abundance along most slope areas (Fig. 165). The predicted CV of abundance was fairly uniform across most of the AI (Fig. 165). Although not rare, encounter probabilities for Aleutian skate were fairly low, except in the region near Adak Island, reflecting that this species was not caught in large numbers (Fig. 166).

**Adult Aleutian skate distribution and predicted abundance from RACE-GAP summer bottom trawl surveys in the Aleutian Islands –** Adult Aleutian skate catches were somewhat common and evenly distributed across the RACE-GAP summer survey areas (Fig. 167). The slopes around Attu Island produced several large catches, but other areas in the AI region showed no obvious pattern. The final ensemble consisted of three SDMs with equal weights but showed a poor fit to the data (Table 47). The ensemble managed to produce fair estimates of presence and relative abundance (AUC = 0.76, $\rho = 0.21$), but performed poorly with respect to deviance explained (PDE = 0.18). Overall, this model provided a preliminary picture of Aleutian skate distribution, but it should be used with caution until more data and better predictions are available. Aleutian skates are known to inhabit deep water environments (Hoff 2009), but the RACE-GAP survey of the AI only covered depths up to 500 m, meaning that a portion of this population might not have been adequately sampled in the current dataset. Bottom depth, current, geographic position, and tidal maximum were the most important covariates, accounting for 78.1% of the deviance explained in the ensemble (Table 48). Aleutian skates were predicted to be abundant in moderate and deeper water at various locations, and with easterly currents and a

low tidal maximum (Fig. 168). Predicted abundance was highest around Attu Island, though several pockets of above-average abundance existed elsewhere (Fig. 168). The predicted CV of abundance was uniform across most of the AI (Fig. 168). Encounter probabilities for Aleutian skate were fairly low throughout the region (Fig. 169).

**Essential fish habitat of subadult and adult Aleutian skate in the Aleutian Islands –** The habitat related abundance predictions based on RACE-GAP summer bottom trawl data (1999–2019) were translated into EFH area and subareas (Fig. 170). The EFH area for subadult Aleutian skate was larger than that of adults, and had a large continuous hot spot along the continental slope south of Adak Island. Subadults were also distinguished by having a large section of EFH core habitat near Unimak Pass. By contrast, the EFH for adults was discontinuous, with several patches scattered around the AI. Some areas were EFH for both life stages, such as the area around Attu Island. Both life stages showed a bimodal relationship with bottom depth with a peak in predicted abundance at the edge of the sampled depth range (Figs. 165 and 168). It is possible that a portion of the population for each life stage is located deeper than 500 m and is not sampled by the RACE-GAP bottom trawl survey.

Table 47. -- Constituent species distribution models (SDMs) used to construct Essential Fish Habitat (EFH) for a) subadult and b) adult Aleutian skate: MaxEnt = Maximum entropy; paGAM = presence-absence generalized additive model; hGAM = hurdle GAM; $GAM_P$ = standard Poisson GAM; and $GAM_{nb}$ = standard negative-binomial GAM. Ensemble performance (ρ = Spearman's rank correlation coefficient), root-mean-square-error (RMSE), the area under the receiver operating characteristic (AUC), and the Poisson deviance explained (PDE) were generated from k-fold cross-validation. The "--" in a field indicates that this SDM was not included in the final ensemble.

**a) subadult Aleutian skate**

| Models | RMSE | Relative Weight | ρ | AUC | PDE | EFH area ($km^2$) |
|---|---|---|---|---|---|---|
| MaxEnt | 0.63 | 0.25 | 0.16 | 0.66 | 0.06 | 56,800 |
| paGAM | 0.63 | 0.25 | 0.22 | 0.72 | 0.11 | 55,900 |
| hGAM | 0.62 | 0.25 | 0.20 | 0.71 | 0.12 | 54,800 |
| $GAM_P$ | 0.63 | 0.25 | 0.20 | 0.70 | 0.12 | 47,100 |
| $GAM_{nb}$ | 0.63 | 0 | 0.21 | 0.71 | 0.12 | -- |
| ensemble | 0.61 | 1 | 0.26 | 0.76 | 0.19 | 56,000 |

**b) adult Aleutian skate**

| Models | RMSE | Relative Weight | ρ | AUC | PDE | EFH area ($km^2$) |
|---|---|---|---|---|---|---|
| MaxEnt | 0.36 | 0.33 | 0.14 | 0.68 | 0.07 | 24,300 |
| paGAM | 0.36 | 0.33 | 0.14 | 0.68 | 0.09 | 22,000 |
| hGAM | -- | 0 | -- | -- | -- | -- |
| $GAM_P$ | 0.36 | 0.34 | 0.14 | 0.68 | 0.09 | 21,000 |
| $GAM_{nb}$ | 0.36 | 0 | 0.14 | 0.68 | 0.09 | -- |
| ensemble | 0.35 | 1 | 0.21 | 0.76 | 0.18 | 23,400 |

Table 48. -- Covariates retained in the a) subadult and b) adult Aleutian skate species distribution model (SDM) final ensembles, the percent contribution to the ensemble deviance explained by each, and the cumulative percent deviance: SD = standard deviation, and BPI = bathymetric position index.

| Aleutian skate | Covariate | % Contribution | Cumulative % Contribution |
|---|---|---|---|
| **a) subadult** | position | 24.0 | 24.0 |
| | bottom depth | 22.5 | 46.5 |
| | current | 12.5 | 59.0 |
| | current SD | 9.7 | 68.7 |
| | bottom temperature | 5.0 | 73.7 |
| | aspect north | 4.1 | 77.8 |
| | aspect east | 4.0 | 81.8 |
| | curvature | 4.0 | 85.8 |
| | BPI | 4.0 | 89.8 |
| | slope | 3.0 | 92.8 |
| | tidal maximum | 2.9 | 95.7 |
| | rockiness | 2.6 | 98.3 |
| | coral presence | 1.2 | 99.5 |
| | sponge presence | 0.4 | 99.9 |
| | pennatulacean presence | 0.1 | 100 |
| **a) adult** | bottom depth | 24.8 | 24.8 |
| | current | 24.5 | 49.3 |
| | position | 19.0 | 68.3 |
| | tidal maximum | 9.8 | 78.1 |
| | current SD | 6.1 | 84.2 |
| | rockiness | 4.9 | 89.1 |
| | aspect north | 2.7 | 91.8 |
| | aspect east | 1.8 | 93.6 |
| | curvature | 1.7 | 95.3 |
| | BPI | 1.5 | 96.8 |
| | bottom temperature | 1.2 | 98.0 |
| | slope | 1.0 | 99.0 |
| | pennatulacean presence | 0.8 | 99.8 |
| | coral presence | 0.2 | 100 |

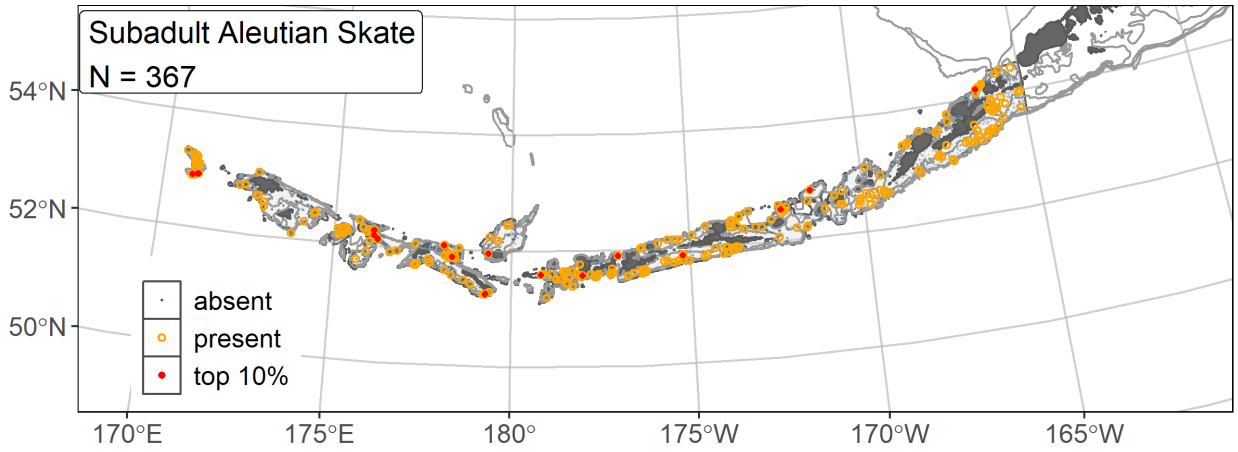


Figure 164. -- Distribution of subadult Aleutian skate catches (N = 367) in 1999–2019 AFSC RACE-GAP summer bottom trawl surveys of the AI with the 100 m, 300 m, and 500 m isobaths indicated; filled red circles indicate locations in top 10% of overall abundance, open orange circles indicate presence in remaining catches, and small blue dots indicate absence.

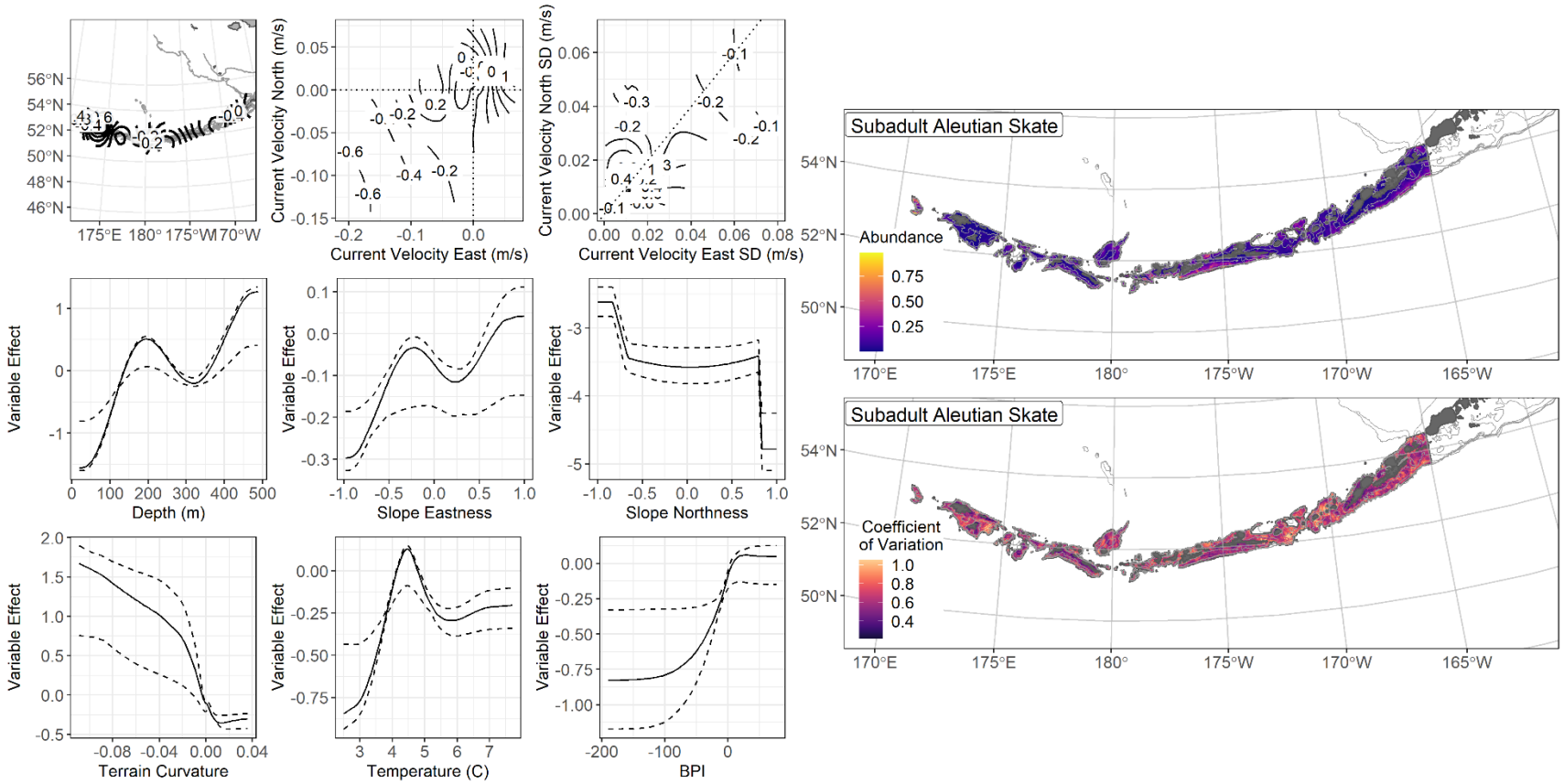


Figure 165. -- The top nine covariate effects (left panel) on ensemble-predicted subadult Aleutian skate numerical abundance across the AI (upper right panel) alongside the coefficient of variation of the ensemble predictions (lower right panel).

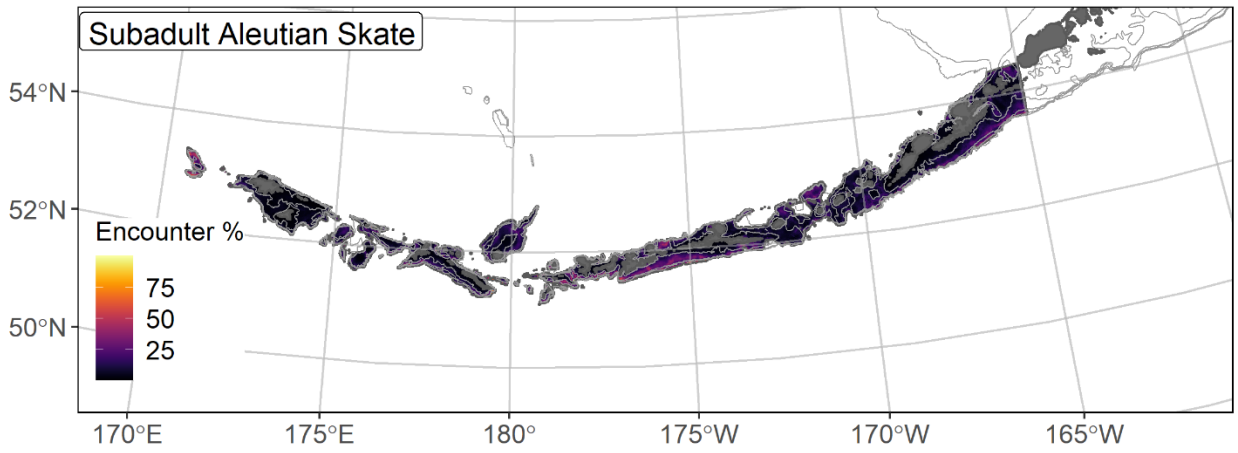


Figure 166. -- Encounter probability of subadult Aleutian skate from AFSC RACE-GAP summer bottom trawl surveys (1999–2019) of the AI with the 100 m, 300 m, and 500 m isobaths indicated.

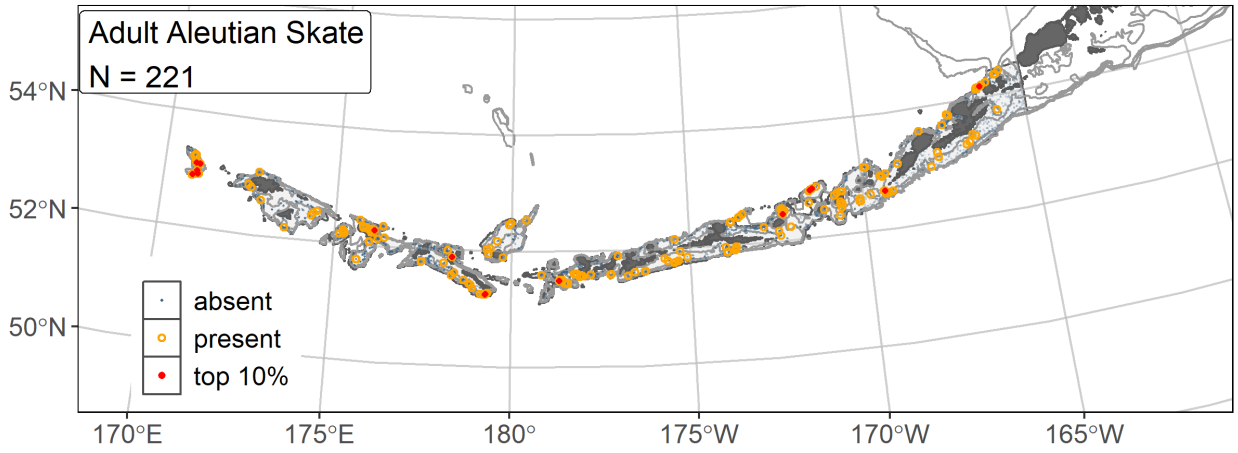


Figure 167. -- Distribution of adult Aleutian skate catches (N = 221) in 1999–2019 AFSC RACE-GAP summer bottom trawl surveys of the AI with the 100 m, 300 m, and 500 m isobaths indicated; filled red circles indicate locations in top 10% of overall abundance, open orange circles indicate presence in remaining catches, and small blue dots indicate absence.

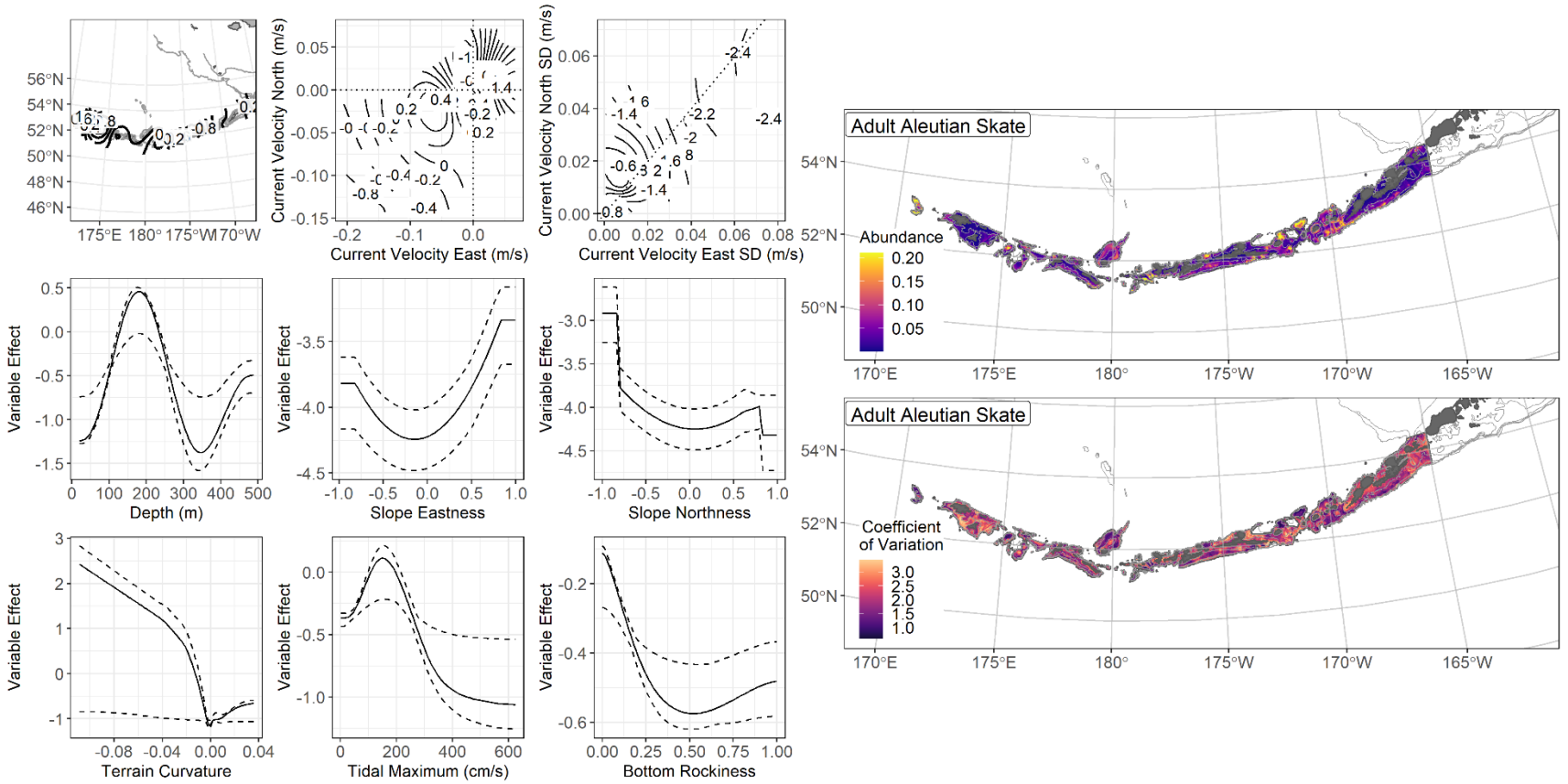


Figure 168. -- The top nine covariate effects (left panel) on ensemble-predicted adult Aleutian skate numerical abundance across the AI (upper right panel) alongside the coefficient of variation of the ensemble predictions (lower right panel).

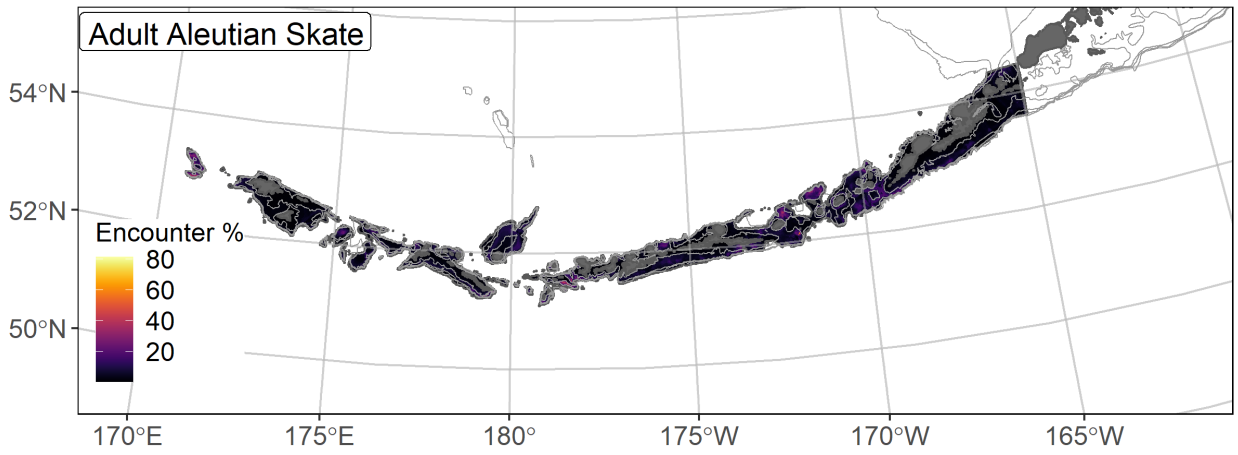


Figure 169. -- Encounter probability of adult Aleutian skate from AFSC RACE-GAP summer bottom trawl surveys (1999–2019) of the AI with the 100 m, 300 m, and 500 m isobaths indicated.

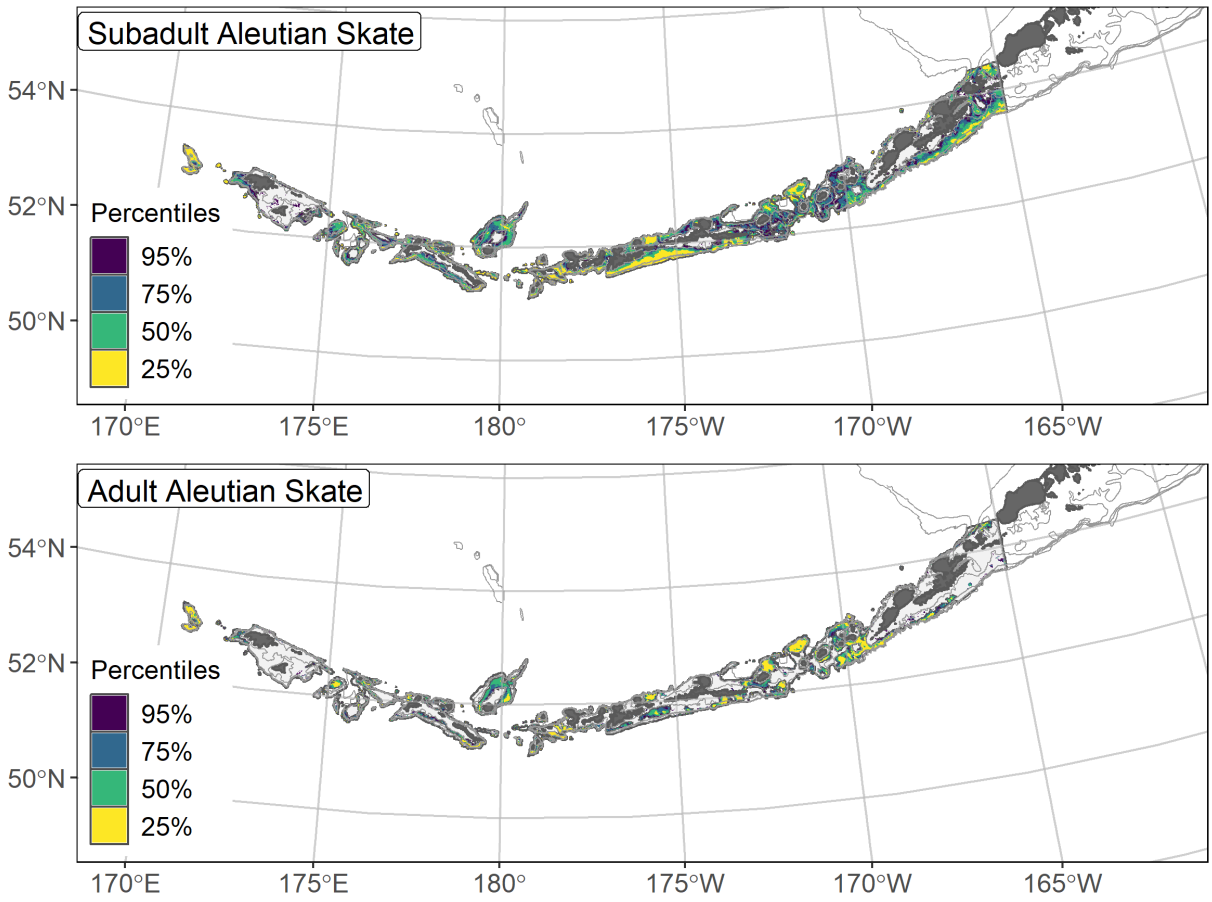


Figure 170. -- Essential fish habitat (EFH area) defined as the top 95% of numerical abundance predictions from a habitat-based ensemble fitted to subadult (top) and adult (bottom) Aleutian skate distribution and abundance in AFSC RACE-GAP summer bottom trawl surveys (1999–2019) with 100 m, 300 m, and 500 m isobaths indicated; internal to the EFH map are the subareas of the top 25% (EFH hot spots), top 50% (core EFH area), and top 75% (principal EFH area) of habitat-related, ensemble-predicted numerical abundance.

**Mud skate (*Bathyraja taranetzi*)**

The mud skate (*Bathyraja taranetzi*) is the smallest species of skate commonly found in Alaska waters, with a maximum TL of 700 mm (Ebert 2005). This species is widely distributed across the north Pacific and ranges from the western GOA to the Kuril Islands (Stevenson et al. 2007). In RACE-GAP summer bottom trawl survey catches from the AI, mud skate ranks sixth in skate biomass (Ormseth 2020). Mud skate reach maturity around 595 mm TL (Ebert 2005), and Balanov et al. (2021) report the presence of a mud skate nursery area similar to those located for Alaska skate (*B. parmifera*; Hoff 2008), though no such locations have been identified in U.S. waters. The preferred habitat for this species is primarily along the continental slope at depths greater than 200 m (Stevenson et al. 2007). Mud skates are managed in aggregate as part of the skate complex across the BSAI region (Ormseth 2020). Most skates of the genus *Bathyraja* were not routinely identified to species until 1999, so these models exclude data collected before that year.

**Subadult mud skate distribution and predicted abundance from RACE-GAP Summer bottom trawl surveys in the Aleutian Islands –** Subadult mud skates catches were common across the RACE-GAP summer survey areas, with the largest catches being found in the central AI, approximately between 180° and 170° W (Fig. 171). The final ensemble contained three SDMs with approximately equal weights, and it showed good to excellent performance when compared to the data (Table 49). Specifically, the ensemble demonstrated good performance at predicting catches with high versus low abundance ($\rho = 0.46$) and excellent performance with respect to predicting presence-absence (AUC = 0.90) and deviance explained (PDE = 0.63). The discrepancy between the values for $\rho$ and PDE suggested that many of the errors in ensemble predictions were minor and that the ensemble predictions are accurate considering the non-

normal distribution of count data. Geographic position and bottom depthwere the most important covariates and accounted for 67.7% of the deviance explained, though bottom current variables and substrate rockiness also contributed (Table 50). High abundance was generally predicted by proximity to the central AI, greater bottom depth, and moderate south to southwesterly currents (Fig. 172). Cooler temperatures and a less rocky substrate were also associated with high abundance. Predicted abundance was highest in the eastern and central AI, particularly around Seguam Pass, Amchitka Pass, and along the continental slope south of Atka Island (Fig. 172). The predicted CV of abundance was high along slope areas near centers of higher abundance, reflecting variation in high abundance areas (Fig. 172). Encounter probabilities for mud skate were low near shore and high along continental slope areas described above (Fig. 173).

**Adult mud skate distribution and predicted abundance from RACE-GAP summer bottom trawl surveys in the Aleutian Islands –** Adult mud skate catches were much less common than subadults in the RACE-GAP summer survey in the AI (Fig. 174). Despite being encountered less frequently, the geographic distribution of adults was very similar to that of subadults, and the greatest number and largest catches occurred in the eastern and central AI. The final ensemble consisted of four SDMs that were weighted about equally, and they had a fair fit to the data overall (Table 49). Specifically, the ensemble performed well at discriminating presence or absence in trawl catches (AUC = 0.82) and showed fair ability to distinguish between high and low catches and explain ensemble deviance ($\rho = 0.28$; PDE = 0.26). The predictions of this ensemble provided a good description of mud skate occurrences in the AI, but predictions of abundance are likely to contain errors. Bottom depth, geographic position, and slope aspect were the most important covariates, accounting for 59.1% of the ensemble deviance explained (Table 50), though bottom current variability, slope angle, and bottom temperature also

contributed. Adult mud skates were predicted to be abundant in deeper waters in the central AI, and were often found on slopes that ascend in a northerly direction, such as those on the south side of the AI (Fig. 175). Like subadults, adult mud skate were not predicted over rocky substrates, but unlike subadults, they were associated with areas without strong bottom currents. Predicted abundance was highest in the central part of the Aleutians, particularly around Amchitka Pass and along the continental slope south of Adak Island (Fig. 175). The predicted CV of abundance was lowest along the continental slope where adult mud skates were frequently encountered and higher near shore (Fig. 175). Encounter probabilities for adult mud skate were fairly low throughout the AI region, except in a few places near Adak Island, as described above (Fig. 176). Given the association between adult mud skates and deep water and the continental slope, some of the population may be located outside of the survey area.

**Essential fish habitat of subadult and adult mud skate in the Aleutian Islands –** The habitat-related abundance predictions based on RACE-GAP summer bottom trawl data (1999–2019) were translated into EFH area and subareas (Fig. 177). The EFH areas for subadult and adult mud skates were similar, and both life stages have EFH hot spots around Seguam Pass, Amchitka Pass, and south of Adak Island. Generally, subadult EFH included areas in the eastern and central AI that are deeper than 100 m and along the continental slope. While the EFH maps for the two life stages were very similar, adults showed a stronger association with greater bottom depths. Like other species in this genus, it is possible that part of the population was located to deep for the RACE-GAP bottom trawl survey to observe.

Table 49. -- Constituent species distribution models (SDMs) used to construct Essential Fish Habitat (EFH) for a) subadult and b) adult mud skate: MaxEnt = Maximum entropy; paGAM = presence-absence generalized additive model; hGAM = hurdle GAM; $GAM_P$ = standard Poisson GAM; and $GAM_{nb}$ = standard negative-binomial GAM. Ensemble performance (ρ = Spearman's rank correlation coefficient), root-mean-square-error (RMSE), the area under the receiver operating characteristic (AUC), and the Poisson deviance explained (PDE) were generated from k-fold cross-validation. The "--" in a field indicates that this SDM was not included in the final ensemble.

**a) subadult mud skate**

| Models | RMSE | Relative Weight | ρ | AUC | PDE | EFH area ($km^2$) |
|---|---|---|---|---|---|---|
| MaxEnt | -- | 0 | -- | -- | -- | -- |
| paGAM | 2.47 | 0.31 | 0.45 | 0.90 | 0.50 | 39,400 |
| hGAM | 2.35 | 0.34 | 0.45 | 0.90 | 0.55 | 31,200 |
| $GAM_P$ | 2.33 | 0.35 | 0.44 | 0.89 | 0.54 | 30,400 |
| $GAM_{nb}$ | 2.45 | 0 | 0.45 | 0.90 | 0.53 | -- |
| ensemble | 2.06 | 1 | 0.46 | 0.90 | 0.63 | 34,200 |

**b) adult mud skate**

| Models | RMSE | Relative Weight | ρ | AUC | PDE | EFH area ($km^2$) |
|---|---|---|---|---|---|---|
| MaxEnt | 0.43 | 0.25 | 0.22 | 0.75 | 0.15 | 35,900 |
| paGAM | 0.43 | 0.25 | 0.25 | 0.78 | 0.19 | 38,600 |
| hGAM | 0.43 | 0.25 | 0.25 | 0.78 | 0.19 | 35,700 |
| $GAM_P$ | 0.43 | 0.25 | 0.25 | 0.78 | 0.19 | 32,400 |
| $GAM_{nb}$ | 0.43 | 0 | 0.25 | 0.79 | 0.19 | -- |
| ensemble | 0.41 | 1 | 0.28 | 0.82 | 0.26 | 36,600 |

Table 50. -- Covariates retained in the a) subadult and b) adult mud skate species distribution model (SDM) final ensembles, the percent contribution to the ensemble deviance explained by each, and the cumulative percent deviance: SD = standard deviation, and BPI = bathymetric position index.

| mud skate | Covariate | % Contribution | Cumulative % Contribution |
|---|---|---|---|
| **a) subadult** | bottom depth | 36.9 | 36.9 |
| | position | 30.7 | 67.7 |
| | rockiness | 8.1 | 75.8 |
| | current | 6.9 | 82.7 |
| | slope | 5.4 | 88.1 |
| | current SD | 2.0 | 90.1 |
| | bottom temperature | 2.0 | 92.1 |
| | aspect north | 1.8 | 93.9 |
| | curvature | 1.7 | 95.6 |
| | aspect east | 1.5 | 97.1 |
| | BPI | 1.2 | 98.3 |
| | sponge presence | 0.6 | 98.9 |
| | pennatulacean presence | 0.6 | 99.5 |
| | tidal maximum | 0.3 | 99.8 |
| | coral presence | 0.2 | 100 |
| **a) adult** | bottom depth | 23.3 | 23.3 |
| | aspect north | 19.4 | 42.6 |
| | position | 17.4 | 60.0 |
| | current SD | 9.5 | 69.5 |
| | bottom temperature | 6.4 | 75.8 |
| | current | 5.9 | 81.7 |
| | slope | 5.4 | 87.1 |
| | rockiness | 4.0 | 91.1 |
| | BPI | 2.8 | 93.9 |
| | aspect east | 1.9 | 95.8 |
| | sponge presence | 1.5 | 97.3 |
| | curvature | 1.2 | 98.5 |
| | tidal maximum | 1.1 | 99.6 |
| | pennatulacean presence | 0.3 | 99.9 |
| | coral presence | 0.1 | 100 |

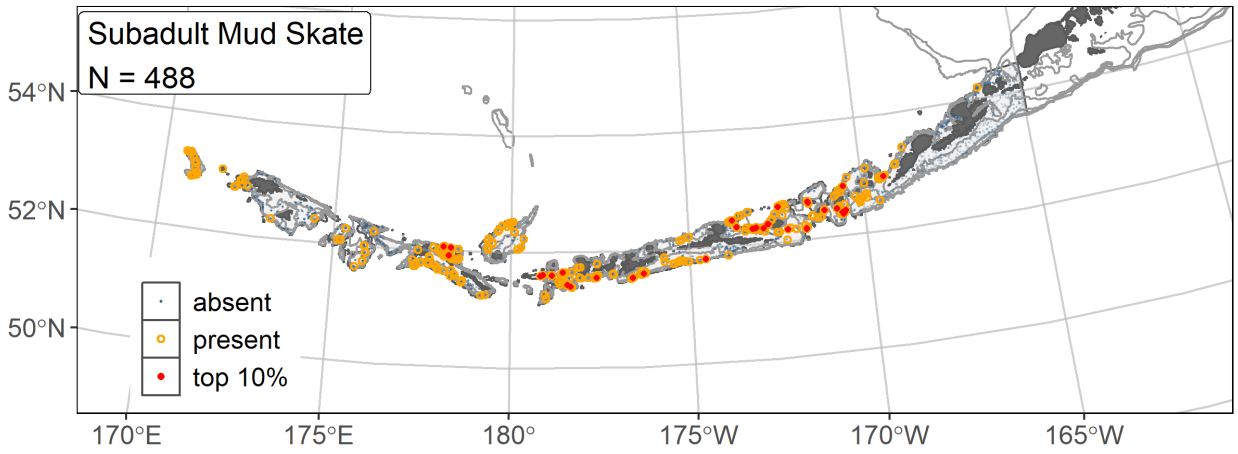


Figure 171. -- Distribution of subadult mud skate catches (N = 488) in 1999–2019 AFSC RACE-GAP summer bottom trawl surveys of the AI with the 100 m, 300 m, and 500 m isobaths indicated; filled red circles indicate locations in top 10% of overall abundance, open orange circles indicate presence in remaining catches, and small blue dots indicate absence.

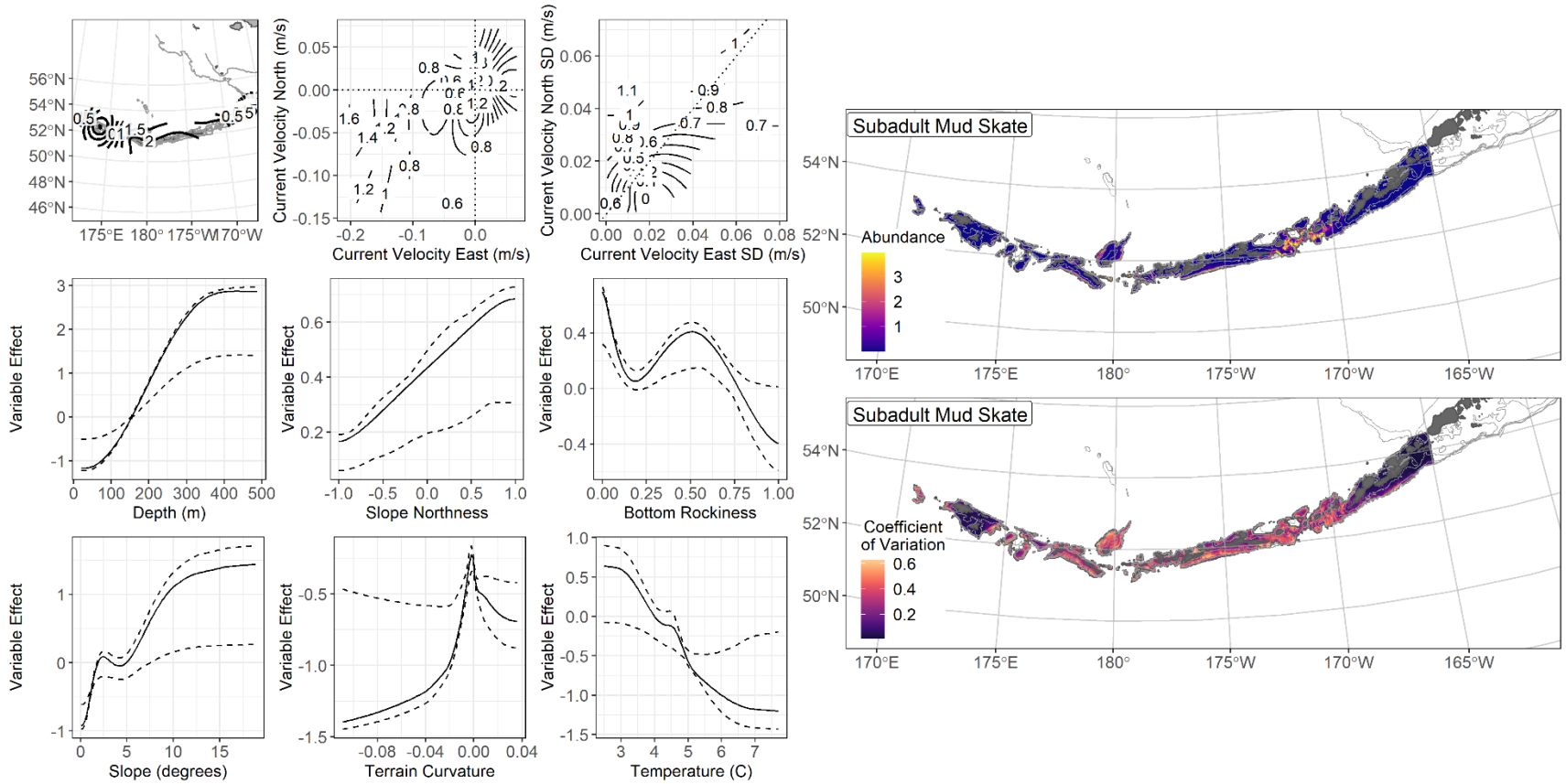


Figure 172. -- The top nine covariate effects (left panel) on ensemble-predicted subadult mud skate numerical abundance across the AI (upper right panel) alongside the coefficient of variation of the ensemble predictions (lower right panel).

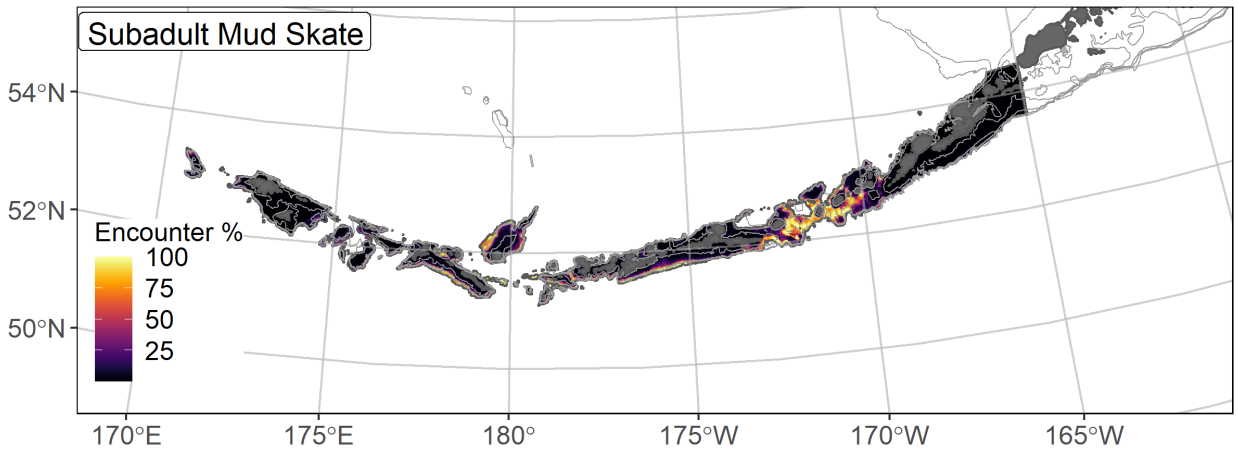


Figure 173. -- Encounter probability of subadult mud skate from AFSC RACE-GAP summer bottom trawl surveys (1999–2019) of the AI with the 100 m, 300 m, and 500 m isobaths indicated.

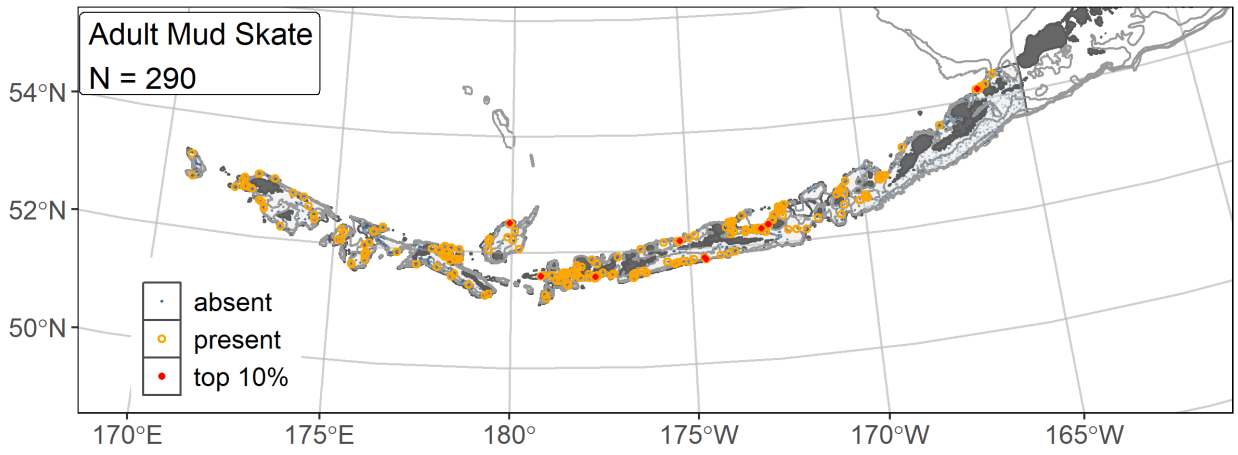


Figure 174. -- Distribution of adult mud skate catches (N = 290) in 1999–2019 AFSC RACE-GAP summer bottom trawl surveys of the AI with the 100 m, 300 m, and 500 m isobaths indicated; filled red circles indicate locations in top 10% of overall abundance, open orange circles indicate presence in remaining catches, and small blue dots indicate absence.

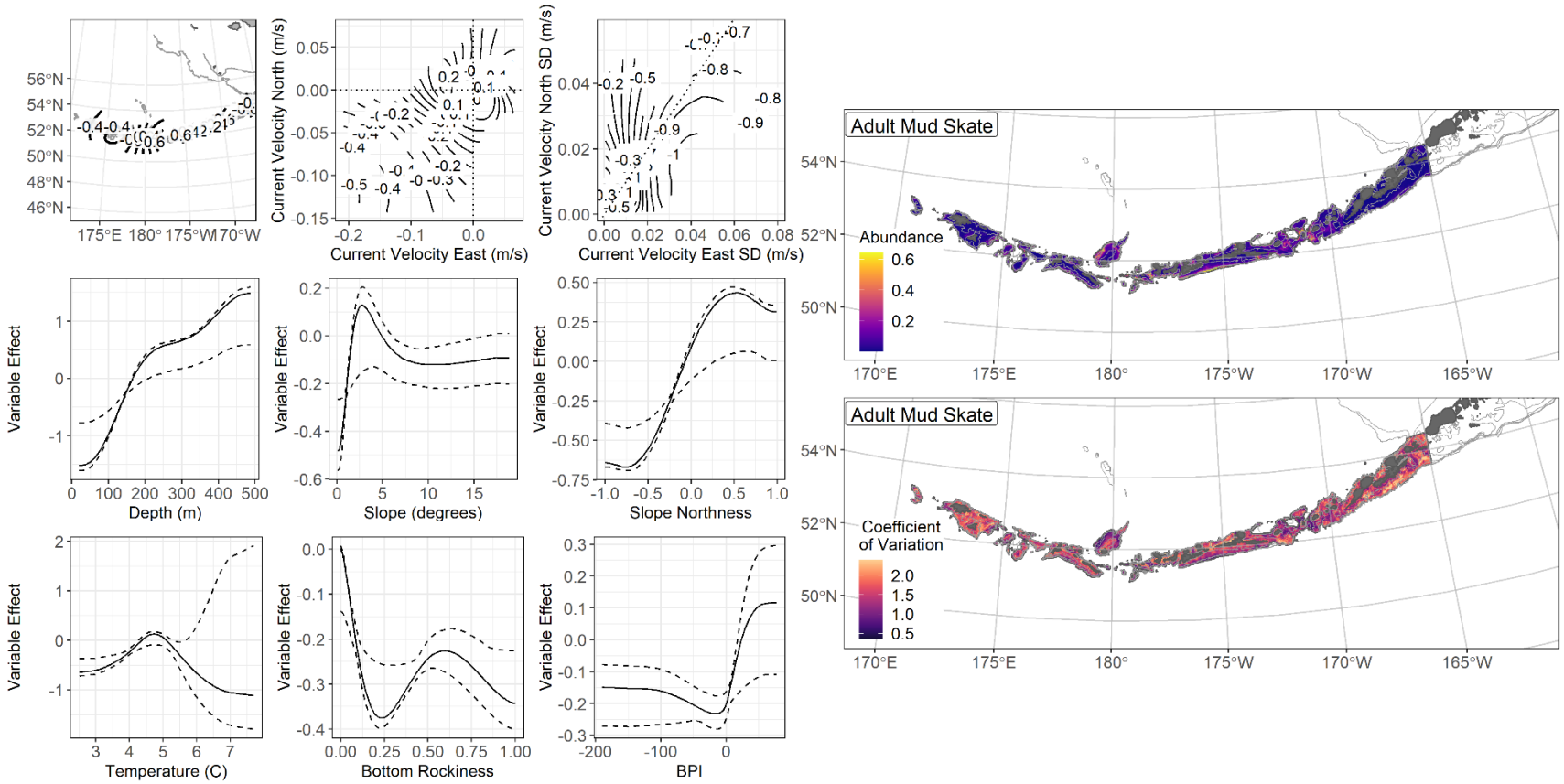


Figure 175. -- The top nine covariate effects (left panel) on ensemble-predicted adult mud skate numerical abundance across the AI (upper right panel) alongside the coefficient of variation of the ensemble predictions (lower right panel).

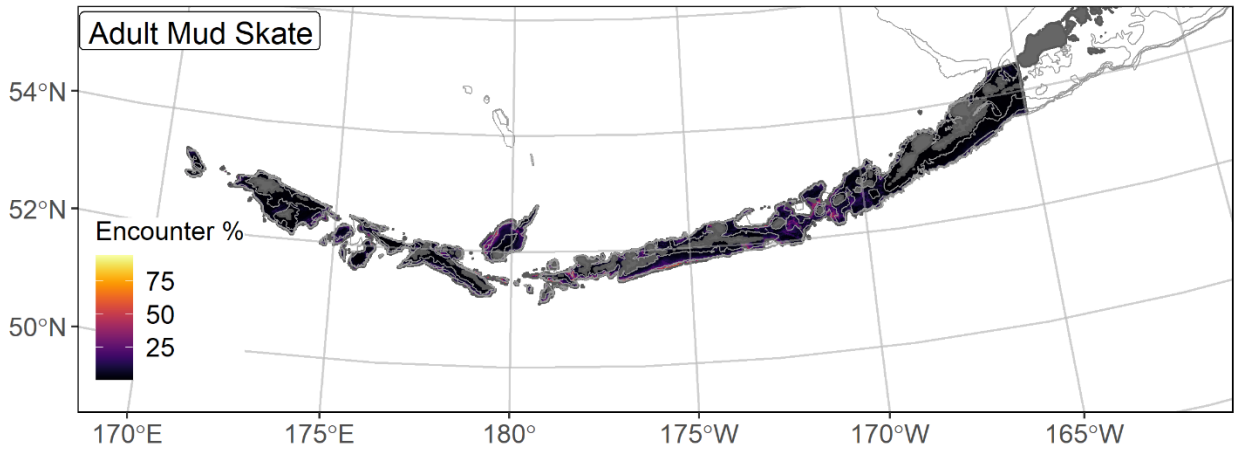


Figure 176. -- Encounter probability of adult mud skate from AFSC RACE-GAP summer bottom trawl surveys (1999–2019) of the AI with the 100 m, 300 m, and 500 m isobaths indicated.

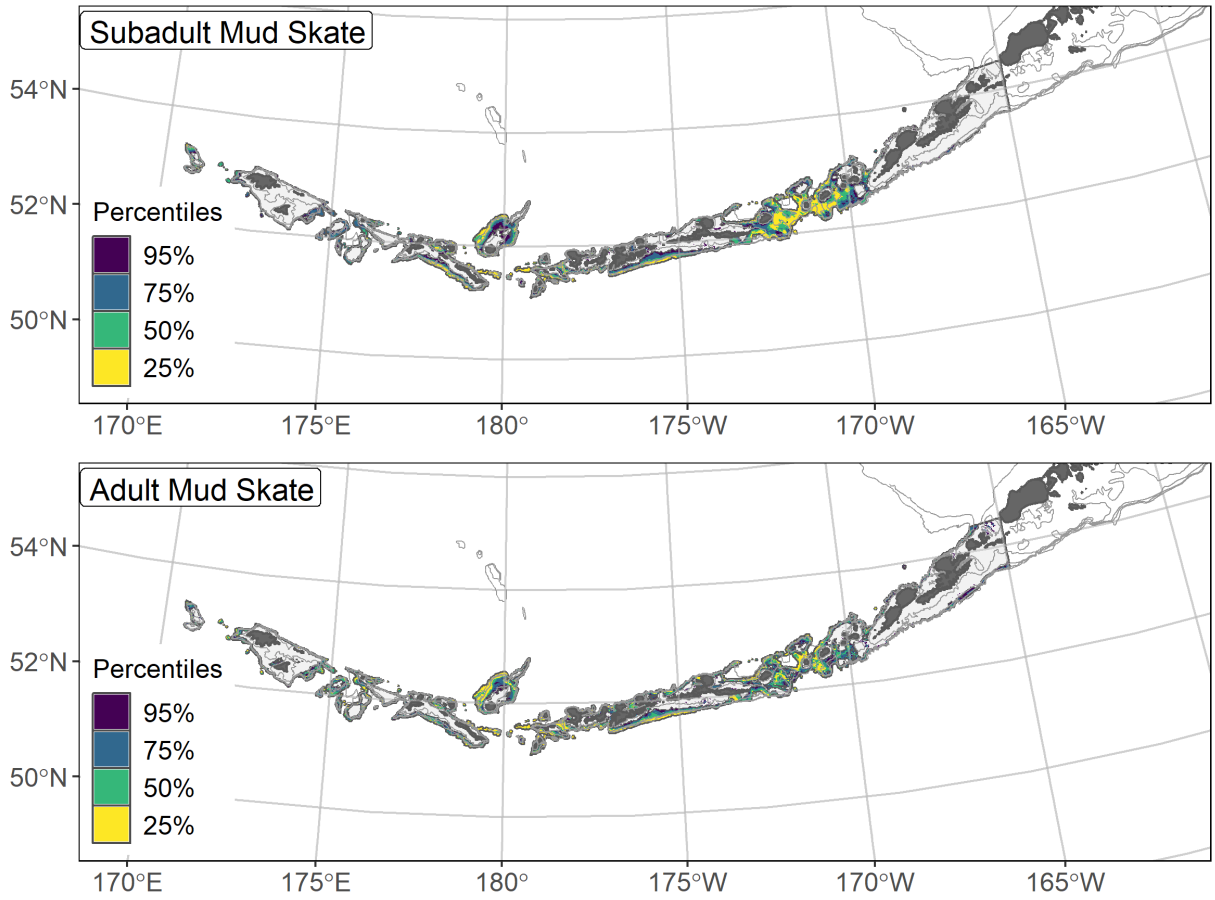


Figure 177. -- Essential fish habitat (EFH area) defined as the top 95% of numerical abundance predictions from a habitat-based ensemble fitted to subadult (top) and adult (bottom) mud skate distribution and abundance in AFSC RACE-GAP summer bottom trawl surveys (1999–2019) with 100 m, 300 m, and 500 m isobaths indicated; internal to the EFH map are the subareas of the top 25% (EFH hot spots), top 50% (core EFH area), and top 75% (principal EFH area) of habitat-related, ensemble-predicted numerical abundance.

**Whiteblotched skate (*Bathyraja maculata*)**

Whiteblotched skate (*Bathyraja maculata*) is a moderately large skate found from the western GOA to the Kuril Islands (Stevenson 2007). Whiteblotched skate is the dominant species of skate in the AI, representing over 50% of total skate biomass in the region (Ormseth 2018). Like many species in the genus *Bathyraja*, it is predominantly found along the continental slope, or near the interface between slope and shelf areas. It can reach an adult length of 1200 mm TL (Mecklenburg et al. 2002), and like many skates, has a long juvenile phase with an average $L_{50}$ of 964 mm TL across both sexes (Ebert 2005). As an adult, this species is a major predator in the region and derives a significant amount of its diet from important commercial fish species like Atka mackerel and walleye pollock (Yang 2007). Skates from the genus *Bathyraja* were not commonly identified to species in RACE-GAP trawl surveys until 1999, so data on whiteblotched skate before then is lacking. There is no directed fishery for skates, and all skates in the BSAI region are managed as part of a single multi-species complex (Ormseth 2018).

**Subadult whiteblotched skate distribution and predicted abundance from RACE-GAP summer bottom trawl surveys in the Aleutian Islands –** Subadult whiteblotched skate catches were common in some areas covered by the RACE-GAP summer survey (Fig. 178). Notably, they were prevalent in Seguam and Amchitka passes, and around Stalemate Bank. The final ensemble contained three SDMs with approximately equal weights, and it showed good to excellent performance when compared to the data (Table 51). Specifically, the ensemble demonstrated good performance at distinguishing areas of high and low abundance ($\rho = 0.48$) and excellent performance with respect to predicting presence-absence (AUC = 0.94) and explaining deviance explained (PDE = 0.67). Geographic position alone accounted for 48.7% of the deviance explained by the ensemble, though current, current variability, bottom temperature,

and tidal maximum were also relatively important (Table 52). In general, the ensemble predicted high abundance in the eastern AI, in areas with strong northerly to northeasterly currents, and areas with strong tides (Fig. 179). Predicted abundance was highest around Seguam Pass, though an additional area of high abundance occurred in the far west at Stalemate Bank (Fig. 179). The predicted CV of abundance was highest around the passes through the island chain and low elsewhere (Fig. 179). Encounter probabilities for subadult whiteblotched skate were high around Seguam Pass and Stalemate Bank, moderate around Amchitka Pass, and low elsewhere (Fig. 180).

**Adult whiteblotched skate distribution and predicted abundance from RACE-GAP summer bottom trawl surveys in the Aleutian Islands –** Adult whiteblotched skate catches in the RACE-GAP summer survey were distributed similarly to subadults; they were common around Seguam Pass, Amchitka Pass, and Stalemate Bank (Fig. 181). The final ensemble contained three SDMs, and the $GAM_P$ and hGAM performed somewhat better than the paGAM and were weighted slightly higher (Table 51). Overall, the ensemble showed good to excellent predictive skill across the fit metrics (Table 51). Specifically, the ensemble demonstrated good performance at distinguishing areas of high versus low abundance ($\rho = 0.49$) and was excellent at predicting presence or absence (AUC = 0.92) and deviance explained (PDE = 0.72). The particularly high value for the deviance explained suggested that most of the variation in adult whiteblotched skate catches was accounted for in the ensemble. Geographic position was responsible for the majority of the deviance explained in the ensemble (65.1%; Table 52), though bottom depth, current conditions, and tidal maximum made minor contributions. Like subadults, adult whiteblotched skates were predicted to be abundant around the passes in the AI and occupied a distinct set of areas, consistent with the high value placed on geographic position in

the model (Fig. 182). Predicted abundance was highest in and around Seguam Pass and Stalemate Bank, with more moderate abundances predicted in Amchitka Pass (Fig. 182). The predicted CV of abundance was highest around the passes through the island chain and low elsewhere (Fig. 182). Encounter probabilities for adult whiteblotched skate followed the same pattern as abundance, with encounters likely in Seguam Pass, Stalemate Bank, and Amchitka Pass, and unlikely in other places (Fig. 183).

**Essential fish habitat of subadult and adult whiteblotched skate in the Aleutian Islands –** The habitat-related abundance predictions based on RACE-GAP summer bottom trawl data (1999–2019) were translated into EFH area and subareas (Fig. 184). The EFH areas for the two life stages of whiteblotched skate were almost identical. The largest hot spot for both life stages was in Seguam Pass, with smaller hot spots at Stalemate Bank and Amchitka Pass. The ensembles for both life stages assigned a large portion of the deviance explained to latitude and longitude, and it is difficult to say which habitat covariates drove the association between this species and these locations.

Table 51. -- Constituent species distribution models (SDMs) used to construct Essential Fish Habitat (EFH) for a) subadult and b) adult whiteblotched skate: MaxEnt = Maximum entropy; paGAM = presence-absence generalized additive model; hGAM = hurdle GAM; $GAM_P$ = standard Poisson GAM; and $GAM_{nb}$ = standard negative-binomial GAM. Ensemble performance (ρ = Spearman's rank correlation coefficient), root-mean-square-error (RMSE), the area under the receiver operating characteristic (AUC), and the Poisson deviance explained (PDE) were generated from k-fold cross-validation. The "--" in a field indicates that this SDM was not included in the final ensemble.

**a) subadult whiteblotched skate**

| Models | RMSE | Relative Weight | ρ | AUC | PDE | EFH area ($km^2$) |
|---|---|---|---|---|---|---|
| MaxEnt | -- | 0 | -- | -- | -- | -- |
| paGAM | 2.86 | 0.33 | 0.47 | 0.93 | 0.54 | 40,400 |
| hGAM | 2.83 | 0.34 | 0.47 | 0.93 | 0.58 | 32,100 |
| $GAM_P$ | 2.86 | 0.33 | 0.48 | 0.92 | 0.59 | 27,800 |
| $GAM_{nb}$ | 4.33 | 0 | 0.50 | 0.94 | 0.52 | -- |
| ensemble | 2.50 | 1 | 0.48 | 0.94 | 0.67 | 35,800 |

**b) adult whiteblotched skate**

| Models | RMSE | Relative Weight | ρ | AUC | PDE | EFH area ($km^2$) |
|---|---|---|---|---|---|---|
| MaxEnt | -- | 0 | -- | -- | -- | -- |
| paGAM | 2.62 | 0.27 | 0.49 | 0.91 | 0.59 | 41,300 |
| hGAM | 2.26 | 0.36 | 0.48 | 0.91 | 0.68 | 35,500 |
| $GAM_P$ | 2.22 | 0.37 | 0.48 | 0.90 | 0.68 | 31,600 |
| $GAM_{nb}$ | 2.44 | 0 | 0.49 | 0.91 | 0.66 | -- |
| ensemble | 2.05 | 1 | 0.49 | 0.92 | 0.72 | 37,000 |

Table 52. -- Covariates retained in the a) subadult and b) adult whiteblotched skate species distribution model (SDM) final ensembles, the percent contribution to the ensemble deviance explained by each, and the cumulative percent deviance: SD = standard deviation, and BPI = bathymetric position index.

| whiteblotched skate | Covariate | % Contribution | Cumulative % Contribution |
|---|---|---|---|
| **a) subadult** | position | 48.7 | 48.7 |
| | current | 15.8 | 64.5 |
| | tidal maximum | 9.3 | 73.8 |
| | current SD | 7.4 | 81.3 |
| | bottom temperature | 5.5 | 86.8 |
| | slope | 3.5 | 90.3 |
| | aspect east | 3.4 | 93.7 |
| | aspect north | 2.4 | 96.1 |
| | bottom depth | 1.5 | 97.6 |
| | sponge presence | 1.1 | 98.7 |
| | BPI | 0.5 | 99.2 |
| | coral presence | 0.4 | 99.6 |
| | rockiness | 0.3 | 99.9 |
| | curvature | 0.1 | 100 |
| **a) adult** | position | 65.1 | 65.1 |
| | tidal maximum | 7.4 | 72.5 |
| | bottom depth | 7.2 | 79.7 |
| | current SD | 5.7 | 85.5 |
| | current | 3.7 | 89.2 |
| | aspect north | 3.4 | 92.6 |
| | bottom temperature | 2.6 | 95.2 |
| | slope | 1.8 | 97.0 |
| | aspect east | 1.5 | 98.5 |
| | BPI | 0.6 | 99.1 |
| | coral presence | 0.3 | 99.4 |
| | pennatulacean presence | 0.3 | 99.7 |
| | rockiness | 0.2 | 99.9 |
| | curvature | 0.1 | 100 |
| | sponge presence | 0 | 100 |

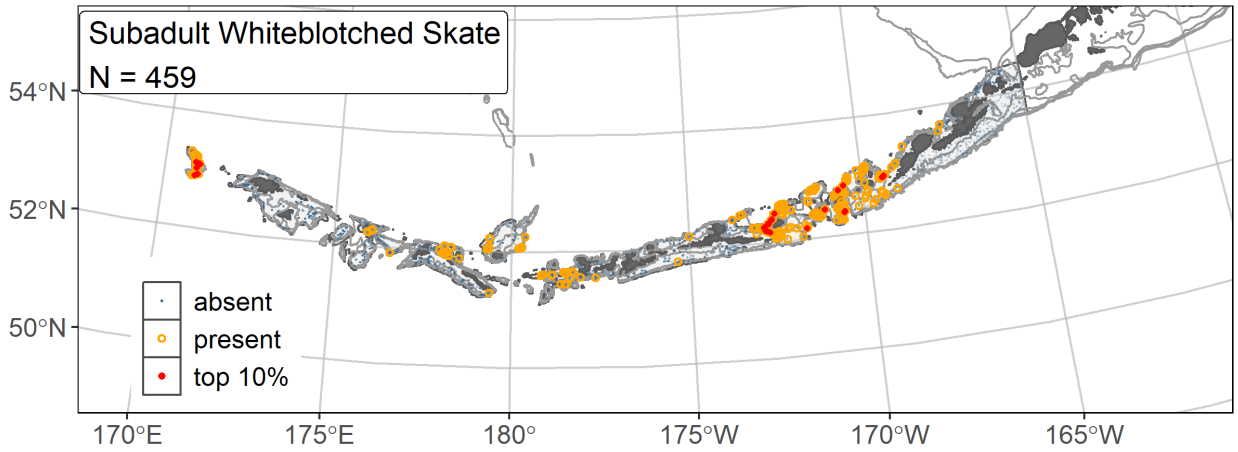


Figure 178. -- Distribution of subadult whiteblotched skate catches (N = 459) in 1999–2019 AFSC RACE-GAP summer bottom trawl surveys of the AI with the 100 m, 300 m, and 500 m isobaths indicated; filled red circles indicate locations in top 10% of overall abundance, open orange circles indicate presence in remaining catches, and small blue dots indicate absence.

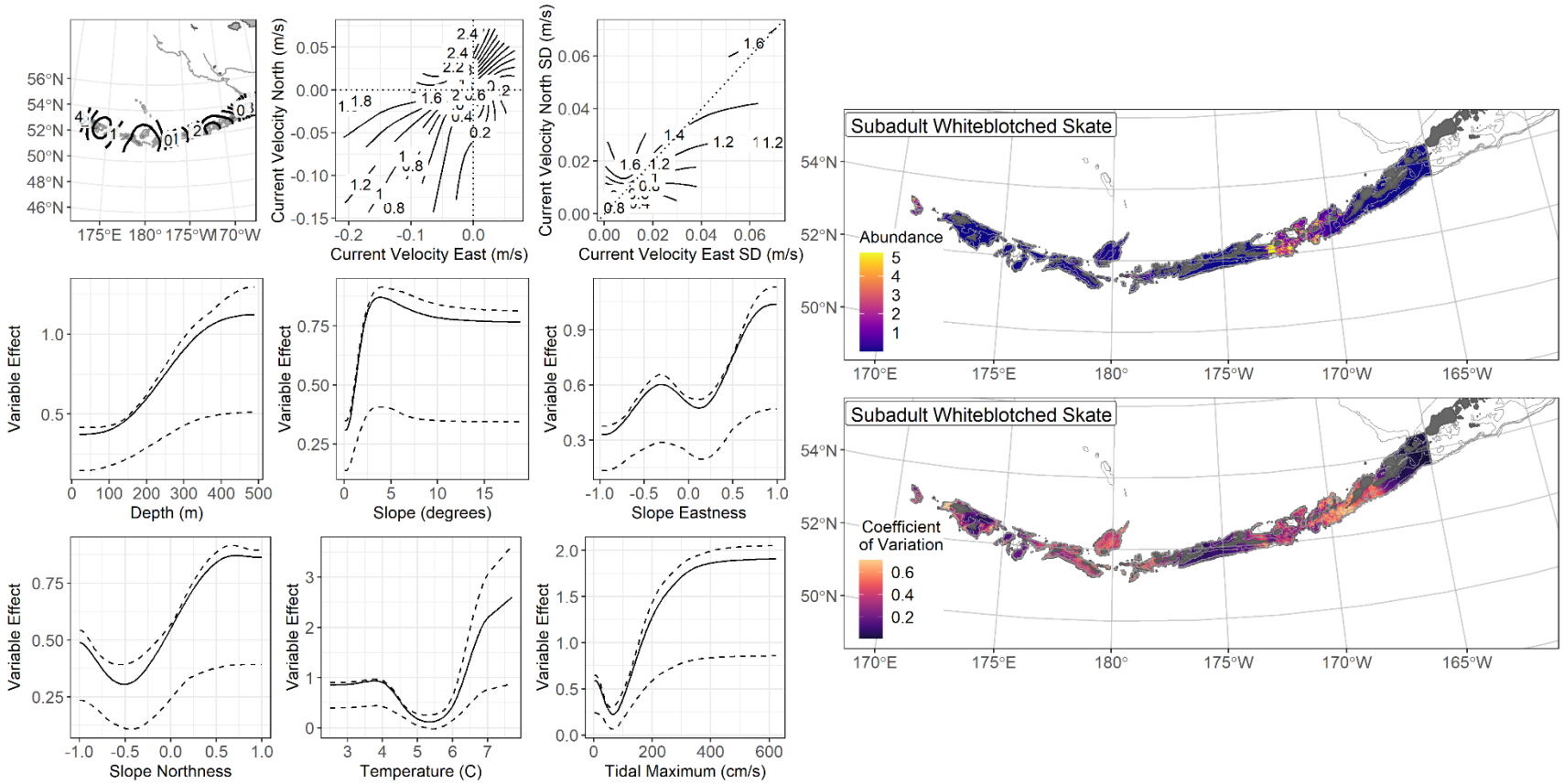


Figure 179. -- The top nine covariate effects (left panel) on ensemble-predicted subadult whiteblotched skate numerical abundance across the AI (upper right panel) alongside the coefficient of variation of the ensemble predictions (lower right panel).

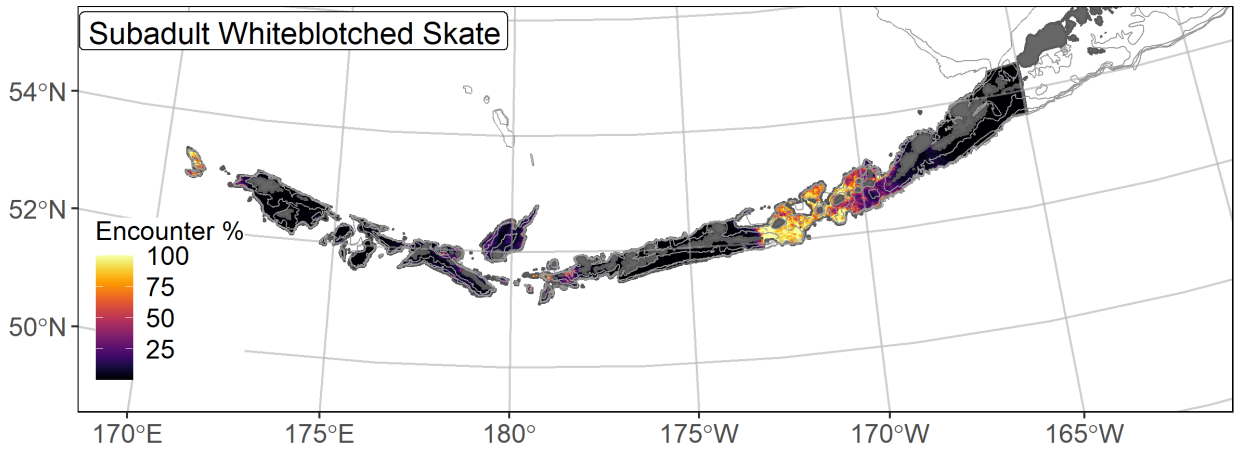


Figure 180. -- Encounter probability of subadult whiteblotched skate from AFSC RACE-GAP summer bottom trawl surveys (1999–2019) of the AI with the 100 m, 300 m, and 500 m isobaths indicated.

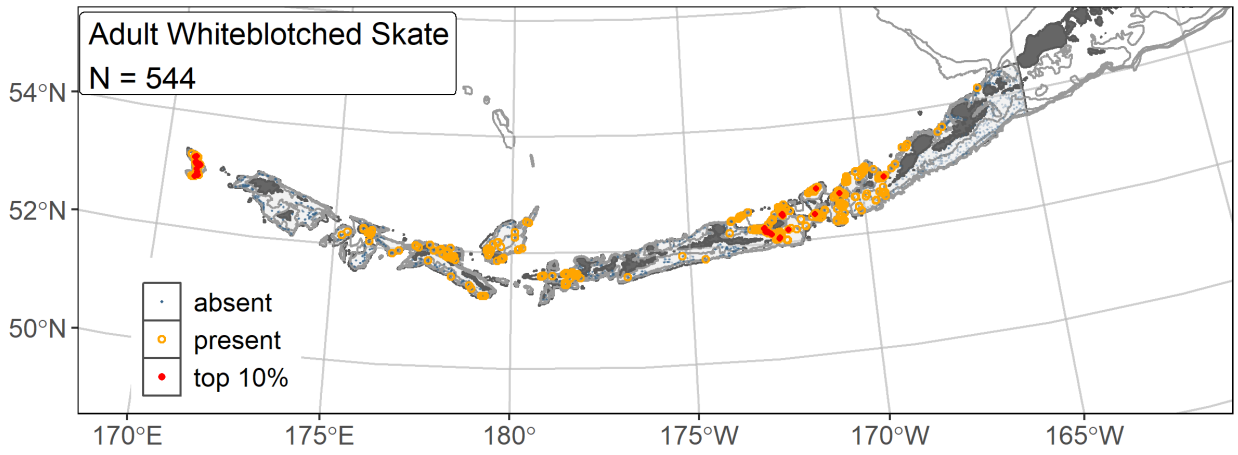


Figure 181. -- Distribution of adult whiteblotched skate catches (N = 544) in 1999–2019 AFSC RACE-GAP summer bottom trawl surveys of the AI with the 100 m, 300 m, and 500 m isobaths indicated; filled red circles indicate locations in top 10% of overall abundance, open orange circles indicate presence in remaining catches, and small blue dots indicate absence.

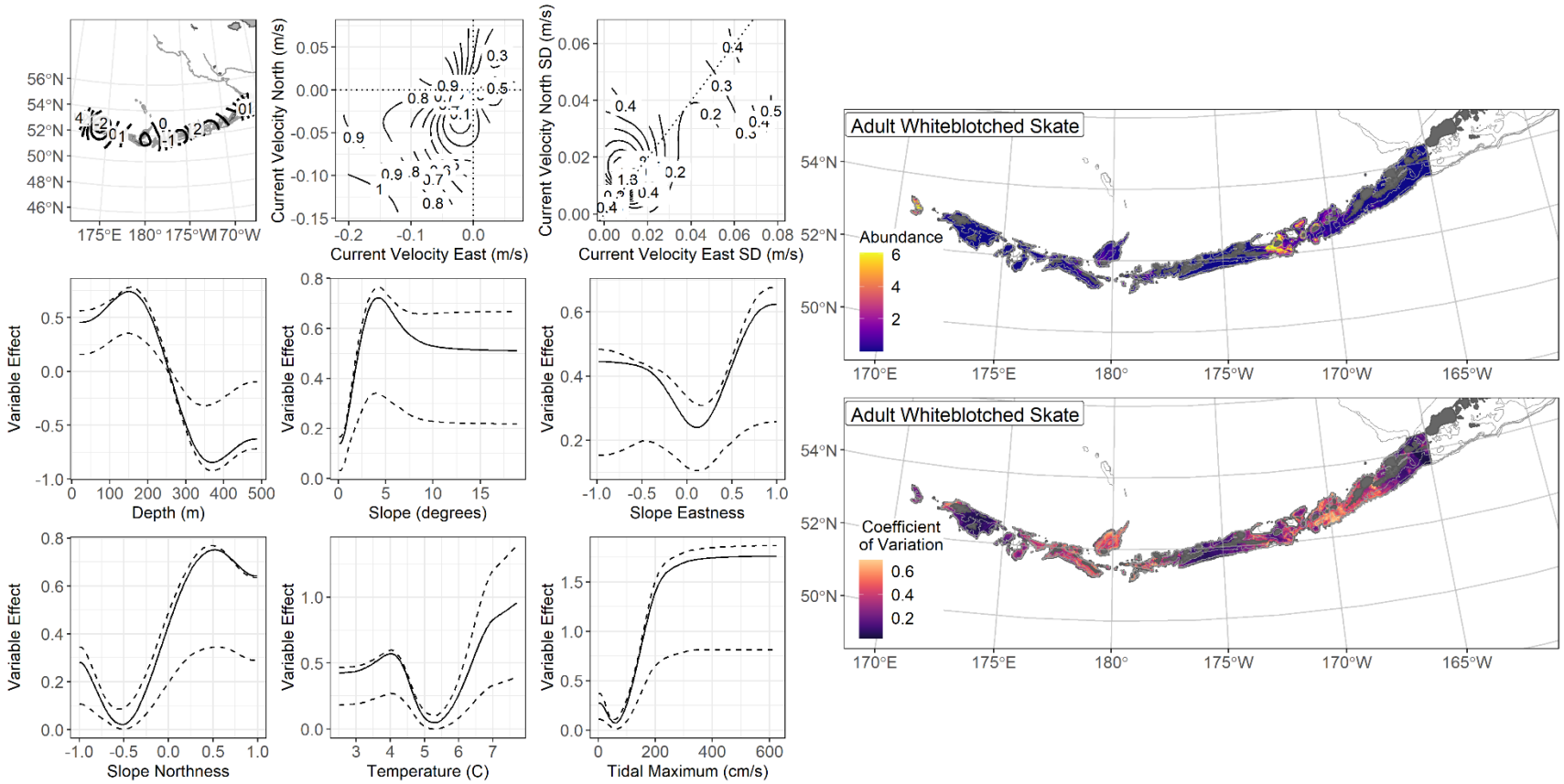


Figure 182. -- The top nine covariate effects (left panel) on ensemble-predicted adult whiteblotched skate numerical abundance across the AI (upper right panel) alongside the coefficient of variation of the ensemble predictions (lower right panel).

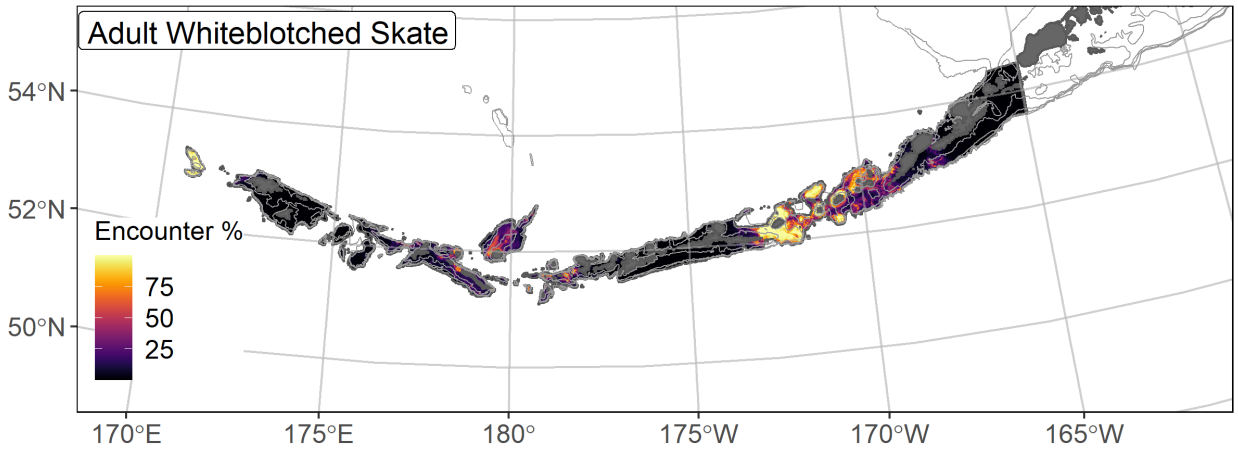


Figure 183. -- Encounter probability of adult whiteblotched skate from AFSC RACE-GAP summer bottom trawl surveys (1999–2019) of the AI with the 100 m, 300 m, and 500 m isobaths indicated.

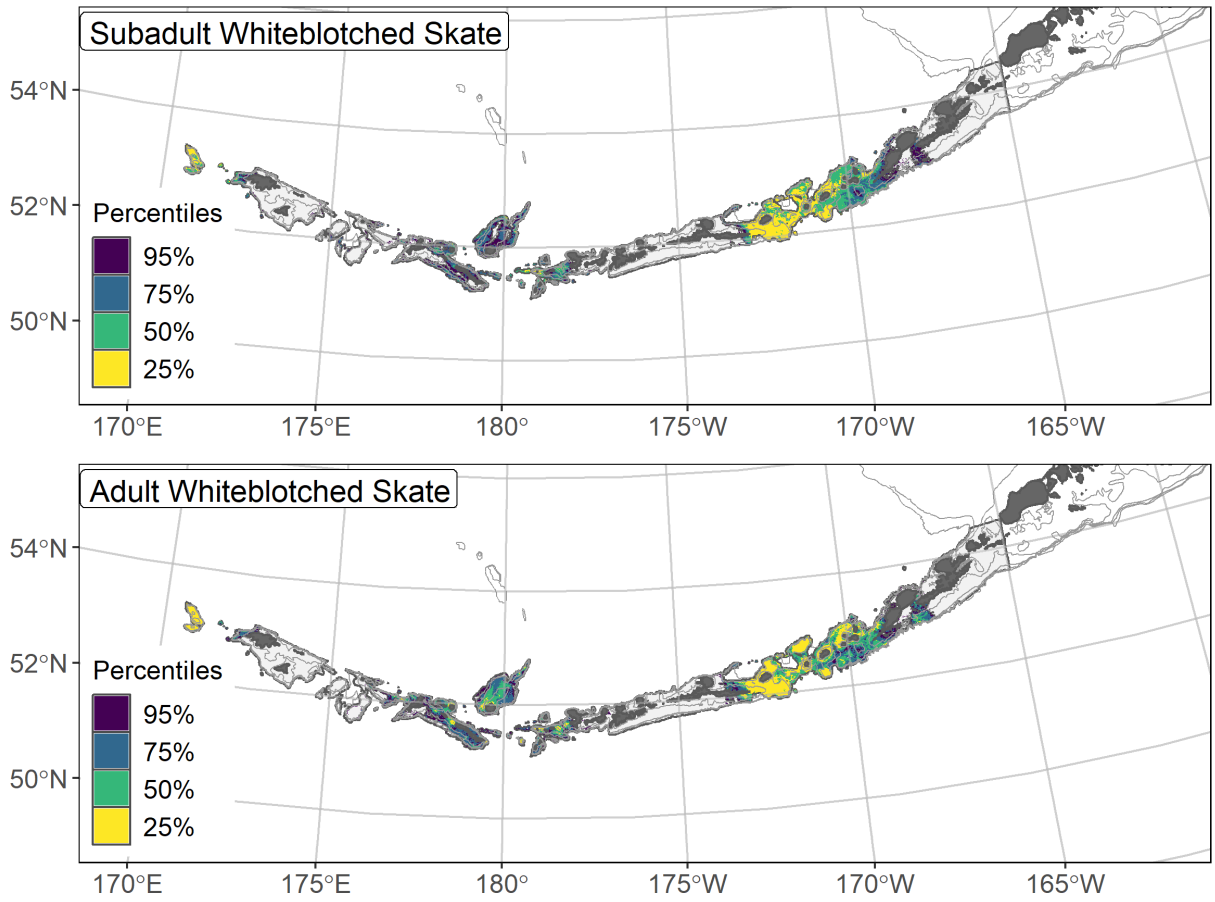


Figure 184. -- Essential fish habitat (EFH area) is the top 95% of numerical abundance predictions from a habitat-based ensemble fitted to subadult (top) and adult (bottom) whiteblotched skate distribution and abundance in AFSC RACE-GAP summer bottom trawl surveys (1999–2019) with 100 m, 300 m, and 500 m isobaths indicated; internal to the EFH map are the subareas of the top 25% (EFH hot spots), top 50% (core EFH area), and top 75% (principal EFH area) of habitat-related, ensemble-predicted numerical abundance.

## Invertebrates

### Golden king crab (*Lithodes aequispinus*)

Golden king crab (*Lithodes aequispinus*) are found from the coast of British Columbia across the North Pacific to Japan. For management purposes, the AI population is divided into two sub-stocks separated at the 174° W meridian (Siddeck et al. 2019). Golden king crab are typically found in deep water (>300 m; Somerton and Otto 1981) and often prefer high-relief rocky or coral habitats. These characteristics make this species more difficult to harvest by trawl gear, and prior to the mid-1980s, the fishery for golden king crab was limited. However, declines in other king crab species have resulted in increased interest in this species and prompted advances in its management (Olsen et al. 2018). The reproductive cycle is thought to last approximately 24 months, and at any time of year, ovigerous females can be found carrying egg clutches in highly disparate developmental states (Otto and Cummiskey 1985). Eggs are relatively large compared to other king crab species and appear to be carried by the females for an extended period before hatching. Larvae do not appear to remain at depth, and owing to their large yolk reserves, they can develop into juveniles without additional feeding (Shirley and Zhou, 1997). Long molting cycles also contribute to difficulty in assigning ages to this species. These life-history complexities and the lack of a fishery-independent crab survey have made golden king crab populations difficult to assess using standard age-based stock assessment tools (Sideek et al. 2019).

**Golden king crab (all life stages combined) distribution and predicted abundance from RACE-GAP summer bottom trawl surveys in the Aleutian Islands –** Golden king crab from the RACE-GAP summer survey were distributed across the AI beginning at 169° W and extending across the archipelago (Fig. 185). Catches occurred primarily along the continental

slope and were highest around Seguam Pass. The final ensemble contained four SDMs with approximately equal weights and achieved a good fit to the data (Table 53). The ensemble was generally able to predict relatively high or low abundance areas ($\rho = 0.56$), distinguish between presence and absence locations (AUC = 0.89), and was able to account for a good portion of the observed deviance (PDE = 0.48). Bottom depth, geographic position, and bottom current were the most important covariates and accounted for 55.9% of the deviance explained in the ensemble, but other covariates such as maximum tidal current, temperature, rockiness, and slope aspect were also important (Table 54). In general, higher abundance was predicted with increasing depth, northeasterly currents, strong tidal movement, low temperatures, and rocky terrain (Fig. 186). Predicted abundance was highest in the area between Atka and Unalaska Islands, with pockets of high density predicted farther to the west (Fig. 186). The CV of abundance was high near areas where predicted abundance was high, which reflected uncertainty in the numbers caught in high abundance areas (Fig. 186). Encounter probability was high in the passes through the island chain, consistent with the modeled covariate effects for deep water and stronger currents (Fig. 187).

**Essential fish habitat of golden king crab in the Aleutian Islands –** The habitat-related abundance predictions based on RACE-GAP summer bottom trawl data (1991–2019) were translated into EFH area and subareas (Fig. 188). The EFH area encompassed most of the survey area along the continental slope at depths greater than 300 m. Hot spots occurred at Seguam Pass, Amchitka Pass, and Buldir Strait. The RACE-GAP summer bottom trawl surveys used trawl gear that is not ideally suited for surveying crab species, so this EFH description should be used with caution. However, the ensemble showed good performance across multiple metrics, so

this map should be a useful resource until additional data sources can be incorporated into the EFH process.

Table 53. -- Constituent species distribution models (SDMs) used to construct Essential Fish Habitat (EFH) for golden king crab: MaxEnt = Maximum entropy; paGAM = presence-absence generalized additive model; hGAM = hurdle GAM; $GAM_P$ = standard Poisson GAM; and $GAM_{nb}$ = standard negative-binomial GAM. Ensemble performance (ρ = Spearman's rank correlation coefficient), root-mean-square-error (RMSE), the area under the receiver operating characteristic (AUC), and the Poisson deviance explained (PDE) were generated from k-fold cross-validation. The "--" in a field indicates that this SDM was not included in the final ensemble.

| Models | RMSE | Relative Weight | ρ | AUC | PDE | EFH area ($km^2$) |
|---|---|---|---|---|---|---|
| MaxEnt | 6.95 | 0.23 | 0.55 | 0.89 | 0.17 | 40,900 |
| paGAM | 6.60 | 0.26 | 0.56 | 0.89 | 0.25 | 47,400 |
| hGAM | 6.64 | 0.26 | 0.53 | 0.89 | 0.26 | 49,500 |
| $GAM_P$ | 6.69 | 0.25 | 0.51 | 0.85 | 0.23 | 53,100 |
| $GAM_{nb}$ | 6.75 | 0 | 0.55 | 0.88 | 0.24 | -- |
| ensemble | 6.13 | 1 | 0.56 | 0.89 | 0.48 | 51,400 |

Table 54. -- Covariates retained in the golden king crab species distribution model (SDM) final ensemble, the percent contribution to the ensemble deviance explained by each, and the cumulative percent deviance: SD = standard deviation, and BPI = bathymetric position index.

| Golden king crab | Covariate | % Contribution | Cumulative % Contribution |
|---|---|---|---|
| **a) all life stages** | bottom depth | 29.5 | 29.5 |
| | current | 14.8 | 44.3 |
| | position | 11.5 | 55.9 |
| | tidal maximum | 7.2 | 63.1 |
| | bottom temperature | 6.2 | 69.3 |
| | aspect north | 5.0 | 74.3 |
| | current SD | 4.6 | 78.9 |
| | rockiness | 4.6 | 83.5 |
| | aspect east | 4.1 | 87.6 |
| | coral presence | 3.3 | 90.9 |
| | sponge presence | 3.1 | 94.0 |
| | slope | 2.3 | 96.3 |
| | curvature | 2.2 | 98.5 |
| | BPI | 1.5 | 100 |
| | pennatulacean presence | 0.0 | 100 |

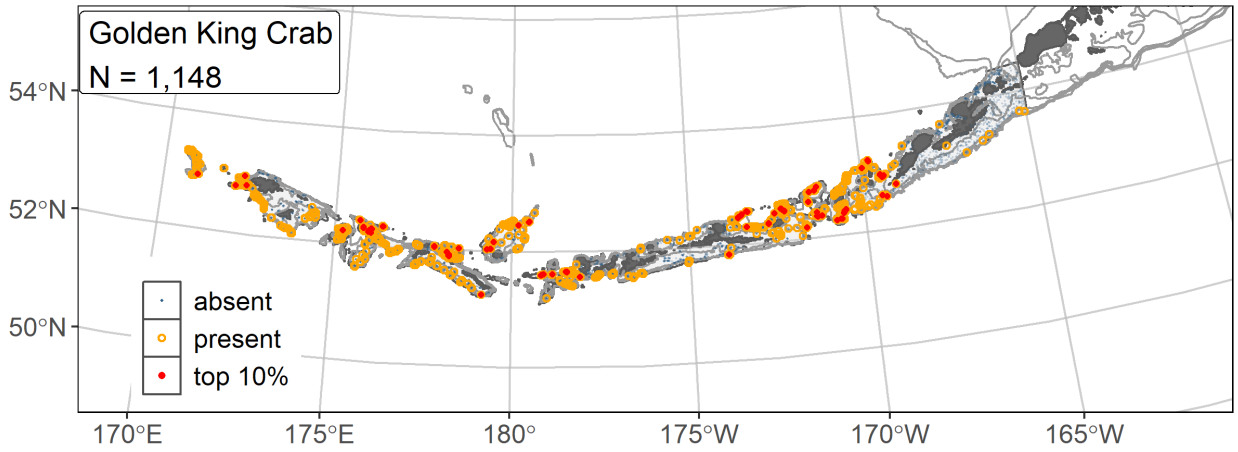


Figure 185. -- Distribution of golden king crab catches (N = 1,148) in 1991–2019 AFSC RACE-GAP summer bottom trawl surveys of the AI with the 100 m, 300 m, and 500 m isobaths indicated; filled red circles indicate locations in top 10% of overall abundance, open orange circles indicate presence in remaining catches, and small blue dots indicate absence.

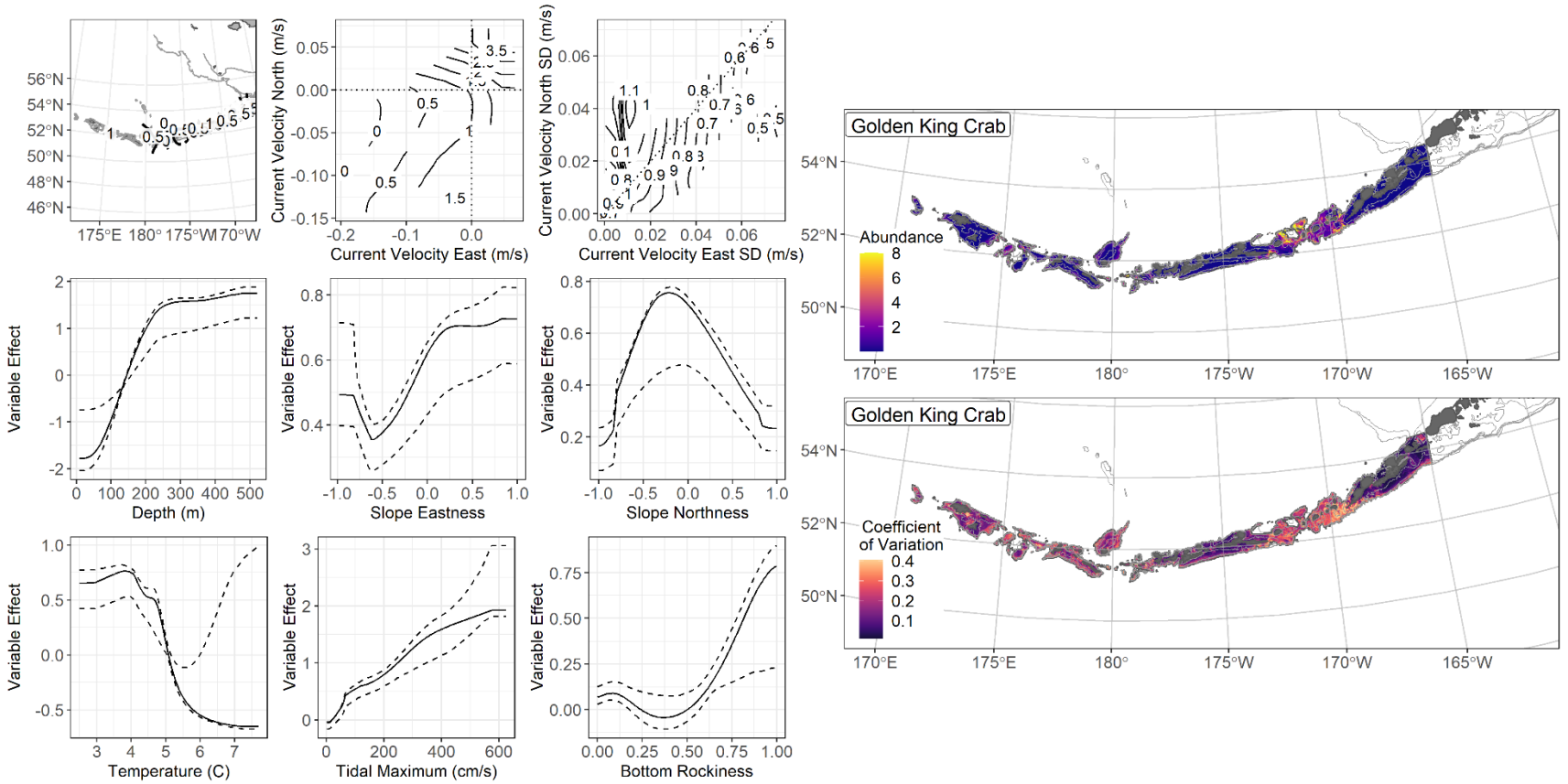


Figure 186. -- The top nine covariate effects (left panel) on ensemble-predicted golden king crab numerical abundance across the AI (upper right panel) alongside the coefficient of variation (CV) of the ensemble predictions (lower right panel).

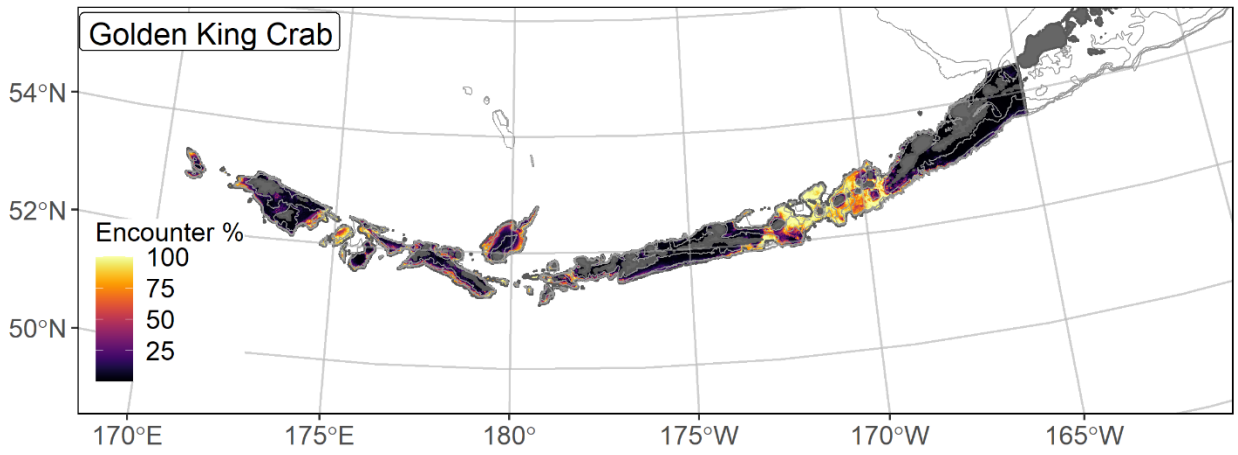


Figure 187. -- Encounter probability of golden king crab from AFSC RACE-GAP summer bottom trawl surveys (1991–2019) of the AI with the 100 m, 300 m, and 500 m isobaths indicated.

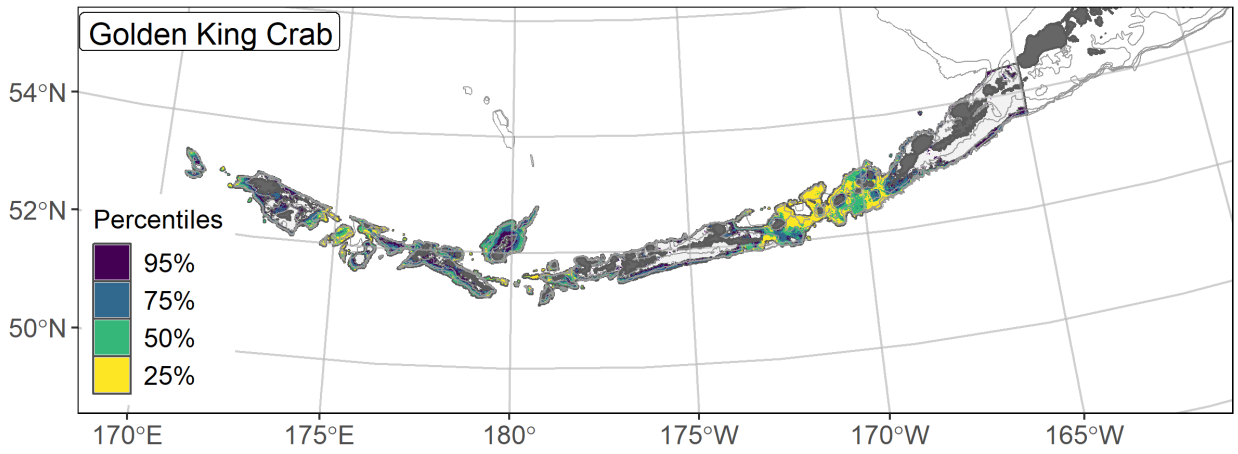


Figure 188. -- Essential fish habitat (EFH area) defined as the top 95% of numerical abundance predictions from a habitat-based ensemble fitted to golden king crab distribution and abundance in AFSC RACE-GAP summer bottom trawl surveys (1991–2019) with 100 m, 300 m, and 500 m isobaths indicated; internal to the EFH map are the subareas of the top 25% (EFH hot spots), top 50% (core EFH area), and top 75% (principal EFH area) of habitat-related, ensemble-predicted numerical abundance.

**Red king crab (*Paralithodes camtschaticus*)**

Red king crab (*Paralithodes camtschaticus*) are found from the coast of British Columbia across the North Pacific to Japan (Zheng and Siddeek 2019). In the AI, they are primarily found in the west, with the largest concentrations found in the shallow waters of Petrel Bank (Daly 2020). Red king crab growth rates are strongly influenced by temperature, and they can take over 9 years to reach maturity after larval settlement, depending on the stock (Loher et al. 2001). Concern has been raised about the potential response of red king crab (and other crustaceans) to potential ocean acidification, as a significant reduction in pH had a strong negative effect on larval survival in a laboratory study (Long et al. 2013). The red king crab fishery in the AI has been closed since the 2003/2004 season due to uncertainty on the status of pre-recruit legal males and low catch rates during cooperative industry-ADFG surveys (Daly 2020). For this study, we did not separate red king crabs into life stages and modeled all crabs caught in AI RACE-GAP bottom trawls as a single, composite life stage.

**Red king crab (all life stages combined) distribution and predicted abundance from RACE-GAP summer bottom trawl surveys in the Aleutian Islands –** Red king crab from the RACE-GAP summer survey were sparsely distributed across the eastern AI and were more concentrated near Petrel Bank and farther to the west (Fig. 189). Catches occurred primarily in shallow water around 100 m deep. The final ensemble contained three SDMs with approximately equal weights and achieved a poor to fair fit to the observed data (Table 55), potentially due to the scarcity of red king crab in the survey (only 83 catches from 1991–2019). While the model showed a fair ability to discriminate catches where this species was present or absent (AUC = 0.85), and similarly explained a fair amount of the deviance (PDE = 0.27), it showed a poor ability to predict high or low abundance catches ($\rho = 0.15$). These scores, along with the

small number of positive catches, suggest that this model should be used with caution. Geographic position, bottom depth, tidal current, and bottom currents were the most important covariates and accounted for 66.7% of the deviance explained (Table 56). In general, high abundance was predicted farther west, in shallow depths, with a low tidal maximum, and southwesterly ocean currents (Fig. 190). Predicted abundance was highest around Petrel Bank, with additional pockets of high abundance predicted around the Rat Islands and near Unalaska Island (Fig. 190). The predicted CV of abundance was high in shallow areas such as between Adak and Atka, where environmental conditions suggested suitable habitat exists but where there were few observed catches (Fig. 190). Predicted encounter probability was high only around those pockets described above, reflecting the fairly limited distribution of red king crab in the AI region (Fig. 191).

**Essential fish habitat of red king crab in the Aleutian Islands –** The habitat-related abundance predictions based on RACE-GAP summer bottom trawl data (1991–2019) were translated into EFH area and subareas (Fig. 192). The EFH area encompassed most of the survey area around Petrel Bank and shallow areas farther west. A second area of EFH is located near Unalaska. Given the poor scores from the fit metrics, the low amount of data, and the difficulty in sampling crabs using trawl gear, this EFH description should be used with caution.

Table 55. -- Constituent species distribution models (SDMs) used to construct Essential Fish Habitat (EFH) for red king crab: MaxEnt = Maximum entropy; paGAM = presence-absence generalized additive model; hGAM = hurdle GAM; $GAM_P$ = standard Poisson GAM; and $GAM_{nb}$ = standard negative-binomial GAM. Ensemble performance (ρ = Spearman's rank correlation coefficient), root-mean-square-error (RMSE), the area under the receiver operating characteristic (AUC), and the Poisson deviance explained (PDE) were generated from k-fold cross-validation. The "--" in a field indicates that this SDM was not included in the final ensemble.

| Models | RMSE | Relative Weight | ρ | AUC | PDE | EFH area ($km^2$) |
|---|---|---|---|---|---|---|
| MaxEnt | 1.55 | 0.33 | 0.09 | 0.71 | 0.12 | 26,700 |
| paGAM | 1.55 | 0.34 | 0.11 | 0.75 | 0.15 | 34,800 |
| hGAM | -- | 0 | -- | -- | -- | -- |
| $GAM_P$ | 1.69 | 0 | 0.10 | 0.71 | -0.19 | -- |
| $GAM_{nb}$ | 1.56 | 0.33 | 0.10 | 0.74 | 0.11 | 20,700 |
| ensemble | 1.55 | 1 | 0.15 | 0.85 | 0.27 | 29,900 |

Table 56. -- Covariates retained in the red king crab species distribution model (SDM) final ensemble, the percent contribution to the ensemble deviance explained by each, and the cumulative percent deviance: BPI = bathymetric position index.

| Red king crab a) all life stages | Covariate | % Contribution | Cumulative % Contribution |
|---|---|---|---|
| | position | 30.4 | 30.4 |
| | bottom depth | 13.9 | 44.3 |
| | tidal maximum | 11.4 | 55.7 |
| | current | 11.0 | 66.7 |
| | rockiness | 7.5 | 74.2 |
| | current SD | 6.2 | 80.5 |
| | BPI | 4.8 | 85.3 |
| | bottom temperature | 3.8 | 89.1 |
| | slope | 3.4 | 92.5 |
| | aspect north | 2.9 | 95.4 |
| | aspect east | 2.5 | 97.9 |
| | pennatulacean presence | 0.9 | 98.8 |
| | curvature | 0.8 | 99.6 |
| | coral presence | 0.2 | 99.8 |
| | sponge presence | 0.2 | 100 |

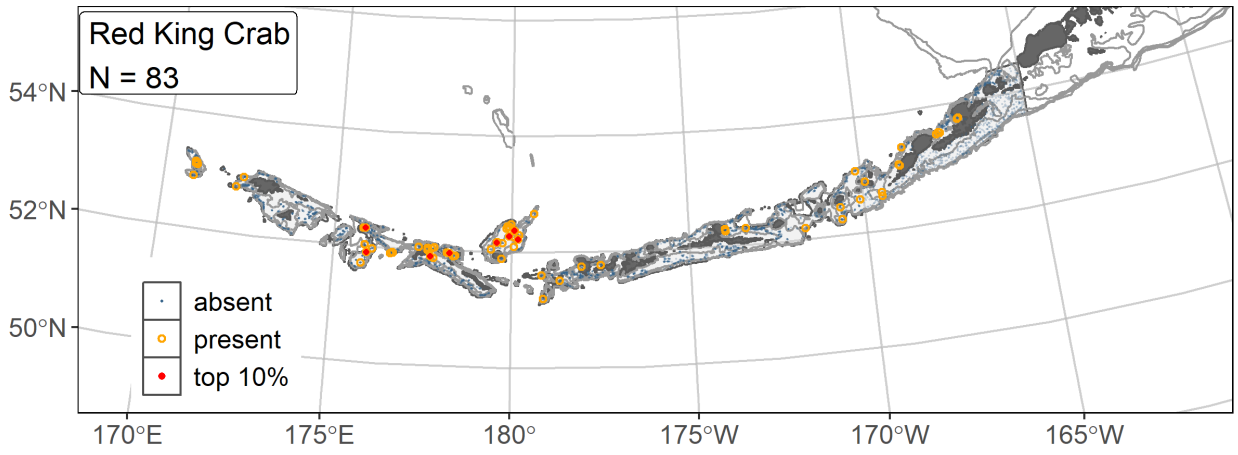


Figure 189. -- Distribution of red king crab catches (N = 83) in 1991–2019 AFSC RACE-GAP summer bottom trawl surveys of the AI with the 100 m, 300 m, and 500 m isobaths indicated; filled red circles indicate catches in top 10% of overall abundance, open orange circles indicate presence in remaining catches, .

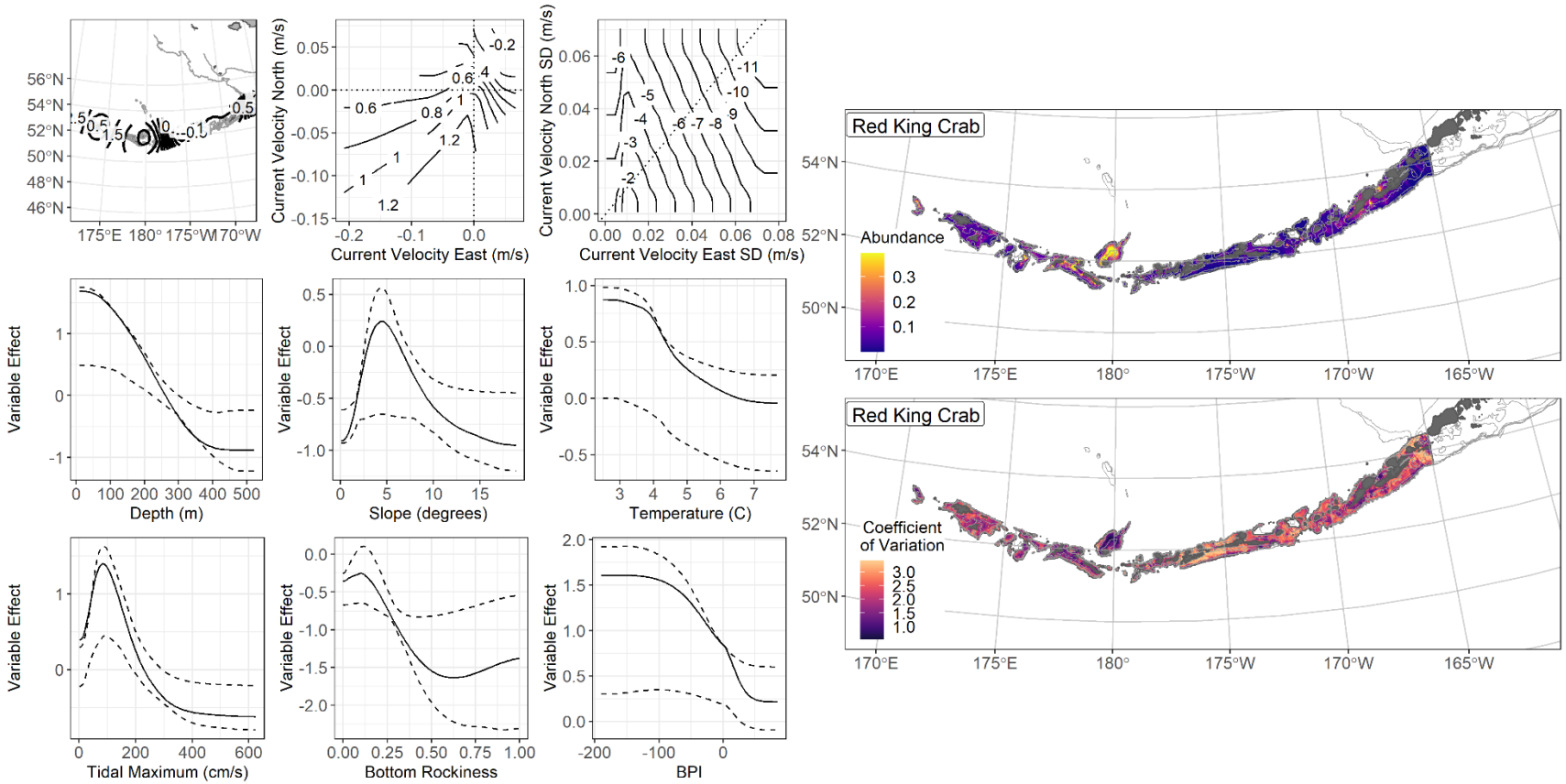


Figure 190. -- The top nine covariate effects (left panel) on ensemble-predicted red king crab numerical abundance across the AI (upper right panel) alongside the coefficient of variation of the ensemble predictions (lower right panel).

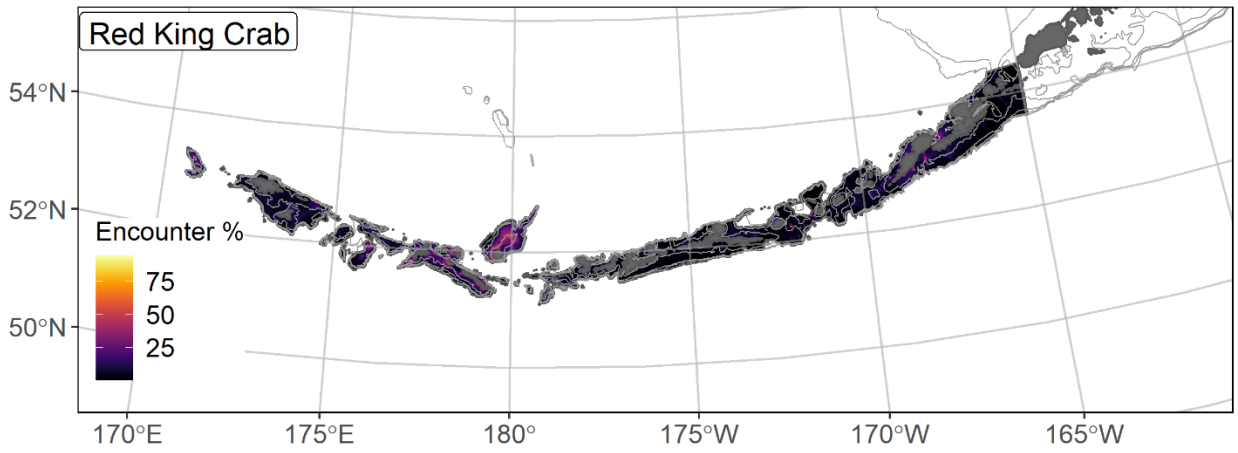


Figure 191. -- Encounter probability of red king crab from AFSC RACE-GAP summer bottom trawl surveys (1991–2019) of the AI with the 100 m, 300 m, and 500 m isobaths indicated.

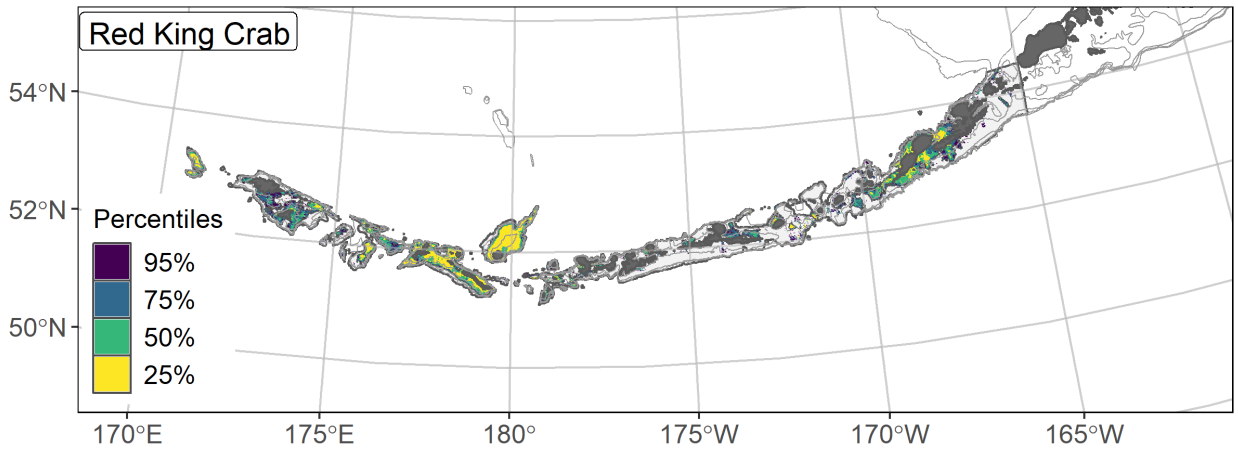


Figure 192. -- Essential fish habitat (EFH area) is the top 95% of numerical abundance predictions from a habitat-based ensemble fitted to red king crab distribution and abundance in AFSC RACE-GAP summer bottom trawl surveys (1991–2019) with 100 m, 300 m, and 500 m isobaths indicated; internal to the EFH map are the subareas of the top 25% (EFH hot spots), top 50% (core EFH area), and top 75% (principal EFH area) of habitat-related, ensemble-predicted numerical abundance.

**Octopus (*Enteroctopus dofleini*)**

The giant Pacific octopus (*Enteroctopus dofleini*) is the most common octopod encountered in the RACE-GAP summer bottom trawl survey of the AI (Ormseth et al. 2018). True to its name, this species is the largest species of octopus in the world and can be over two meters long. Giant Pacific octopus are terminal spawners that die after mating (males) and the hatching of eggs (females; Jorgensen 2009). Peak spawning occurs in the winter and early spring (Brewer 2016), and females release between 40,000 to 240,000 eggs (Conrath and Conners 2014). While weight at 50% maturity is available for this species (Brewer and Norcross 2012), all life stages are combined for this project. Data on sex-specific octopus weights are not regularly collected in either the commercial fisheries or the RACE-GAP bottom trawl surveys, and estimates of octopus biomass are considered unreliable at this time (Ormseth et al. 2018). In 2011, FMPs were amended to provide for separate management of the sharks, skates, sculpins, and octopuses that previously comprised the "other species" complex managed in BSAI through 2010 (Ormseth et al. 2018).

**Giant Pacific octopus (all life stages combined) distribution and predicted abundance from RACE-GAP summer bottom trawl surveys in the Aleutian Islands –** Giant Pacific octopus catches from the RACE-GAP summer survey were common throughout the AI (Fig. 193). Most catches occurred at moderate depths from 100-300 m and were slightly more common farther west. The final ensemble contained four equally weighted SDMs that fitted the data poorly (Table 57) and should be used with some caution. While the ensemble achieved a fair degree of accuracy in predicting catches with relatively low or high density ($\rho = 0.20$), it performed poorly by other metrics (AUC = 0.67; PDE = 0.09). It is unclear why the ensemble did not perform better, but stock managers have also reported difficulty estimating octopus population numbers

and biomass. As this species typically hides in the substrate and rocky areas, it is possible that trawl gear is not an efficient method of sampling for octopods. The most important covariate in the ensemble was the presence of sponges, though this accounted for only 24.9% of the explained deviance, and a variety of covariates such as bottom depth, geographic position, bottom temperature, currents, and tidal maximum are required to account for the rest (Table 58). Octopus abundance was predicted to be high in places where sponges were present, bottom temperatures were warm, and the depth was approximately 150 m (Fig. 194). Predicted abundance was high in areas with moderate depth and in patches near Atka, Adak, and the Rat islands (Fig. 194). These patches are similar to the distribution of sponges in the AI. The predicted CV of abundance did not display any clear patterns, and was high throughout (Fig. 194). The predicted encounter probability map showed a few places with high values but many places where the encounter probability is 20-40% (Fig. 195). This reflected that octopus are rarely caught in large numbers. Given the issues discussed above, it is difficult to determine if this indicates the actual population density of the species is usually low or if they are difficult to sample using trawl gear.

**Essential fish habitat of giant Pacific octopus (all life stages combined) in the Aleutian Islands –** The habitat-related abundance predictions based on RACE-GAP summer bottom trawl data (1991–2019) were translated into EFH area and subareas (Fig. 196). Despite the low overall abundance of giant Pacific octopus in the survey, they were present in many areas of the AI, and the predicted EFH area was large. EFH hot spots were located in the central and western AI and correspond to locations where sponges are likely to be present. The ensemble predicted a very close association between this species and sponges, which would seem to be a promising target

for future research. However, given the poor model fit and the sampling issues inherent to this species, this EFH map should be treated with some caution.

Table 57. -- Constituent species distribution models (SDMs) used to construct Essential Fish Habitat (EFH) for giant Pacific octopus: MaxEnt = Maximum entropy; paGAM = presence-absence generalized additive model; hGAM = hurdle GAM; $GAM_P$ = standard Poisson GAM; and $GAM_{nb}$ = standard negative-binomial GAM. Ensemble performance (ρ = Spearman's rank correlation coefficient), root-mean-square-error (RMSE), the area under the receiver operating characteristic (AUC), and the Poisson deviance explained (PDE) were generated from k-fold cross-validation. The "--" in a field indicates that this SDM was not included in the final ensemble.

| **Models** | **RMSE** | **Relative Weight** | **ρ** | **AUC** | **PDE** | **EFH area ($km^2$)** |
|---|---|---|---|---|---|---|
| MaxEnt | 0.82 | 0.25 | 0.18 | 0.66 | 0.06 | 71,000 |
| paGAM | 0.82 | 0.25 | 0.16 | 0.64 | 0.05 | 73,500 |
| hGAM | 0.83 | 0.24 | 0.15 | 0.63 | 0.03 | 68,600 |
| $GAM_P$ | 0.82 | 0 | 0.16 | 0.64 | 0.04 | -- |
| $GAM_{nb}$ | 0.82 | 0.25 | 0.16 | 0.63 | 0.04 | 67,200 |
| ensemble | 0.81 | 1 | 0.20 | 0.67 | 0.09 | 72,000 |

Table 58. -- Covariates retained in the giant Pacific octopus species distribution model (SDM) final ensemble, the percent contribution to the ensemble deviance explained by each, and the cumulative percent deviance: BPI = bathymetric position index.

| Giant Pacific octopus a) all life stages | Covariate | % Contribution | Cumulative % Contribution |
|---|---|---|---|
| | sponge presence | 24.9 | 24.9 |
| | bottom temperature | 10.9 | 35.8 |
| | bottom depth | 9.7 | 45.5 |
| | current SD | 8.3 | 53.8 |
| | tidal maximum | 7.8 | 61.6 |
| | current | 7.5 | 69.1 |
| | position | 7.1 | 76.2 |
| | aspect east | 5.7 | 81.9 |
| | aspect north | 5.5 | 87.4 |
| | curvature | 3.2 | 90.6 |
| | coral presence | 2.4 | 93.0 |
| | BPI | 2.3 | 95.3 |
| | pennatulacean presence | 1.9 | 97.2 |
| | rockiness | 1.8 | 99.0 |
| | slope | 1.0 | 100 |

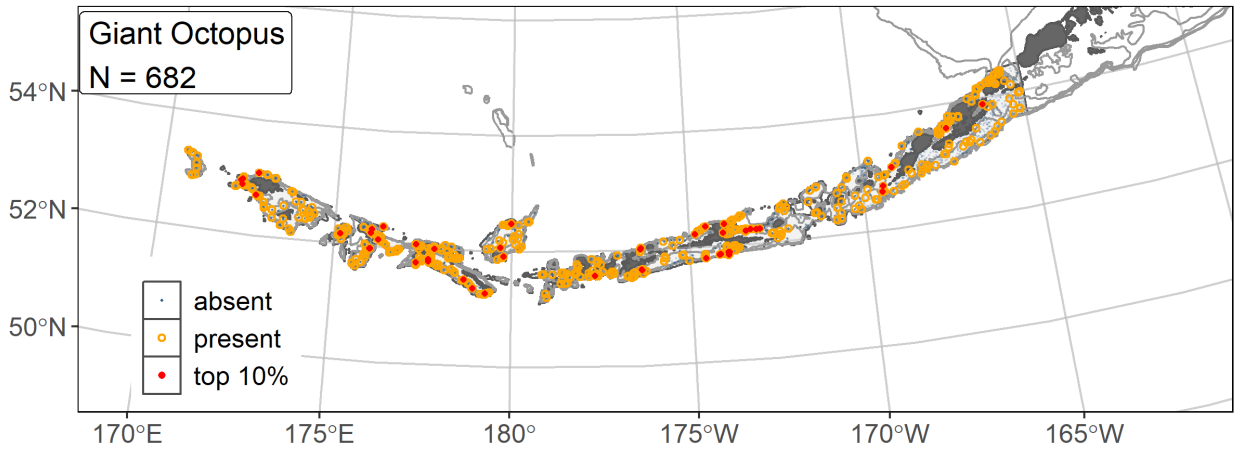


Figure 193. -- Distribution of giant Pacific octopus catches (N = 682) in 1991–2019 AFSC RACE-GAP summer bottom trawl surveys of the AI with the 100 m, 300 m, and 500 m isobaths indicated; filled red circles indicate locations in top 10% of overall abundance, open orange circles indicate presence in remaining catches, and small blue dots indicate absence.

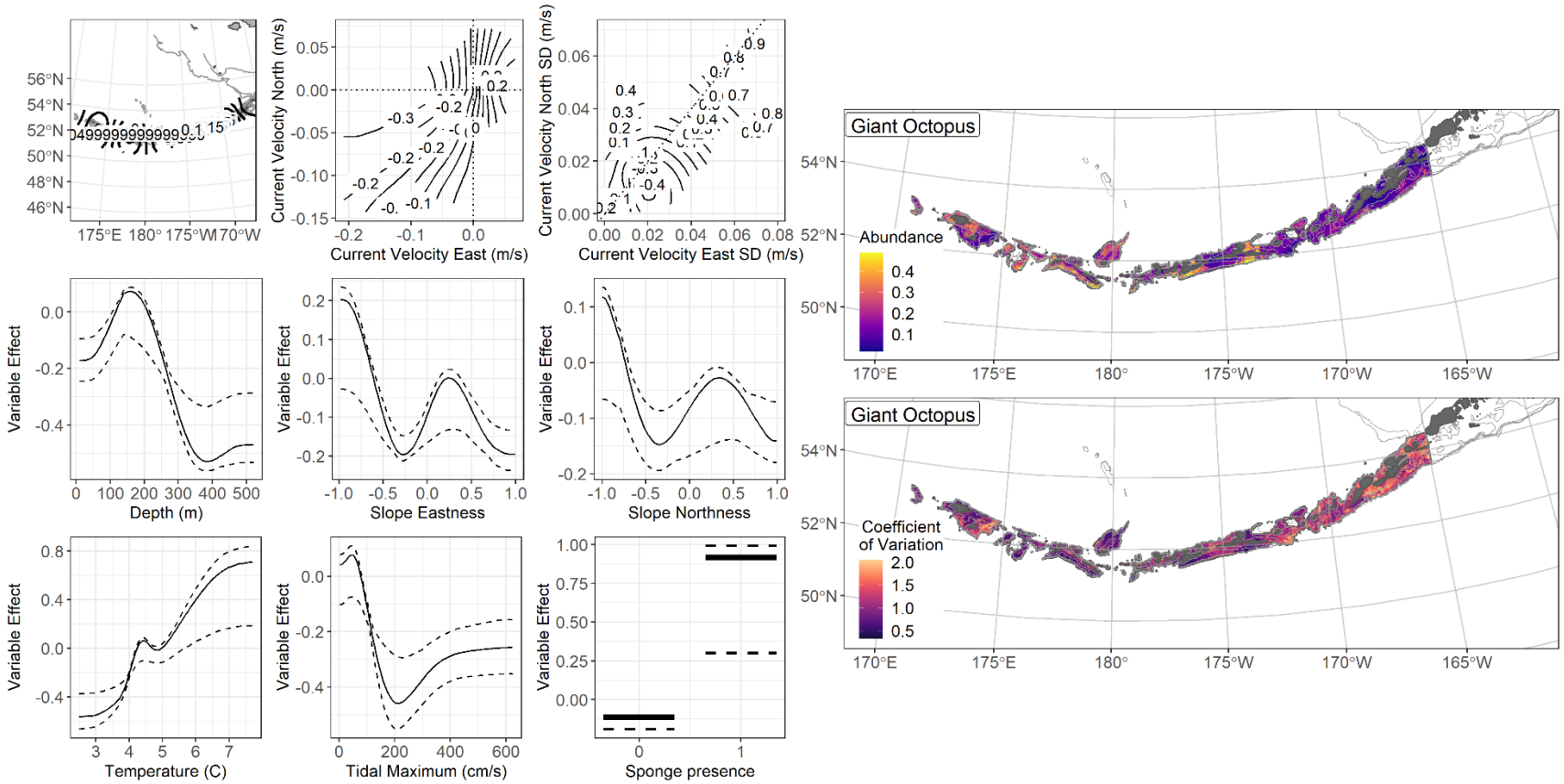


Figure 194. -- The top nine covariate effects (left panel) on ensemble-predicted giant Pacific octopus numerical abundance across the AI (upper right panel) alongside the coefficient of variation of the ensemble predictions (lower right panel).

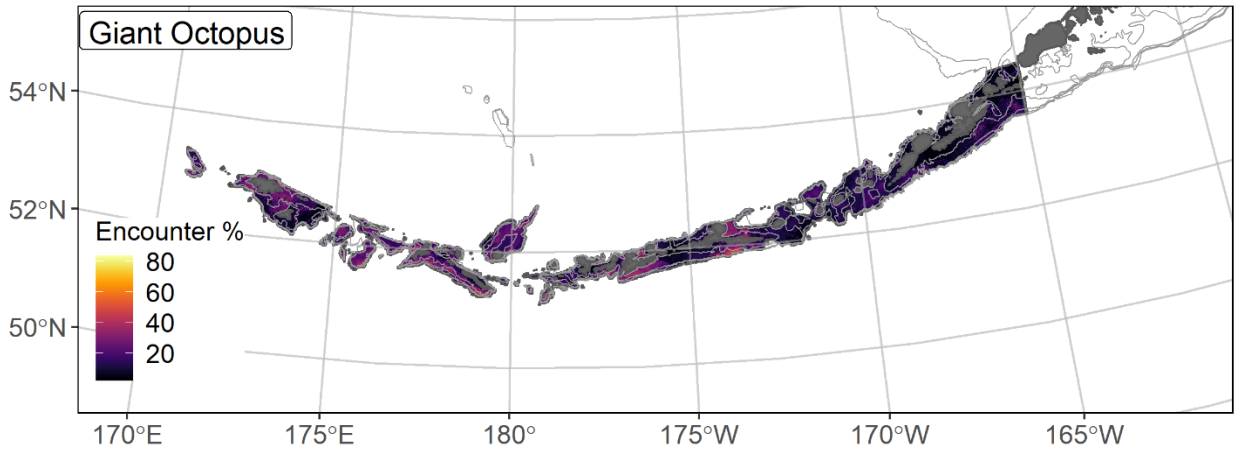


Figure 195. -- Encounter probability of giant Pacific octopus from AFSC RACE-GAP summer bottom trawl surveys (1991–2019) of the AI with the 100 m, 300 m, and 500 m isobaths indicated.

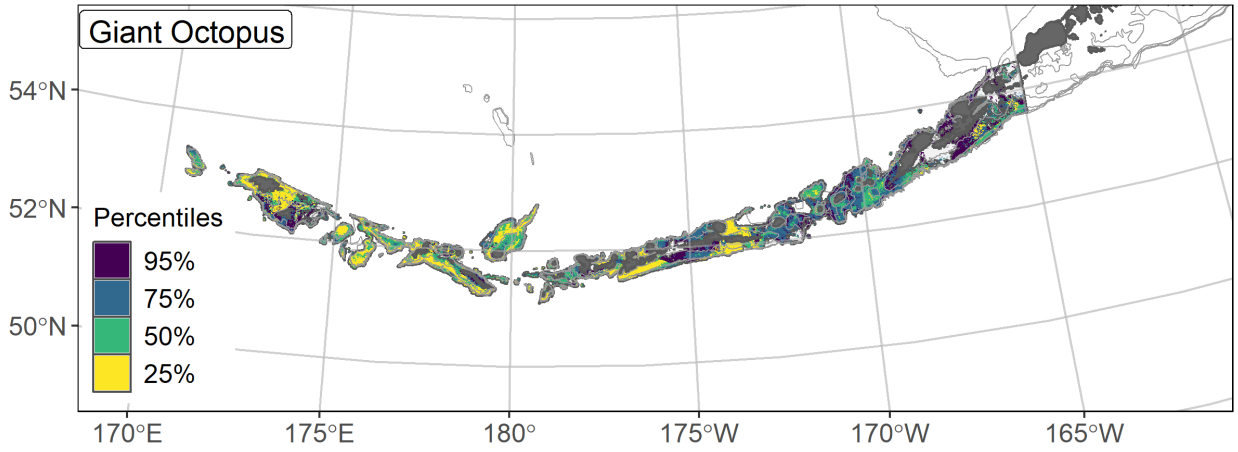


Figure 196. -- Essential fish habitat (EFH area) defined as the top 95% of numerical abundance predictions from a habitat-based ensemble fitted to giant Pacific octopus distribution and abundance in AFSC RACE-GAP summer bottom trawl surveys (1991–2019) with 100 m, 300 m, and 500 m isobaths indicated; internal to the EFH map are the subareas of the top 25% (EFH hot spots), top 50% (core EFH area), and top 75% (principal EFH area) of habitat-related, ensemble-predicted numerical abundance.

## FUTURE RECOMMENDATIONS

The EFH Final Rule requires that Fishery Management Councils and NMFS must periodically review the EFH components of FMPs and revise or amend these components with respect to new information at least every 5 years (50 CFR 600.815(a)(10)) with an overarching consideration that the science related to this effort meets the standards of best available science (NMFS National Standard 2 – Scientific Information 50 CFR 600.315). In the present work, we have adhered to these mandates as we have described and mapped EFH for FMP species in Alaska, using species distribution models (SDMs); incorporating modeling refinements and additional data sources where appropriate. While completing this work, and through conversation and review with stock assessment authors, other species experts, Plan Team members, the SSC, and additional stakeholders, we have also identified future refinements and recommendations that could be considered for future EFH 5-year Reviews. These recommendations fall into three areas: prioritizing and improving EFH for select species, increasing the scope and applicability of EFH research, and improving process.

### Prioritize and improve EFH for select species

The existing methodology for describing EFH works well for most species. However, for others, approaches need to be modified in order to better capture drivers of density and generate habitat descriptions. These approaches may involve incorporating new datasets (for fish distribution, environmental covariates, or life history parameters), or the development of modeling approaches that are amenable to their distributions (e.g., modeling at a broader spatial scale). For some of these species, the need for model improvements has been discussed in the results chapters for the current EFH Review cycle; in the future, it is important to have processes in place (both modeling approaches and communication approaches) for these species. These

may include agreed-upon differences in the modeling approach depending on the data needs and model ensemble performance in previous cycles.

**Leverage existing species distribution data**

Data for species and life stages that are not well-sampled in the RACE-GAP summer bottom trawl surveys may need to be augmented with data from other sources. In this study, we combined additional surveys and data sources inshore of the RACE-GAP survey area in a single, presence-only SDM (MaxEnt) to more comprehensively describe and map the EFH for the settled early juvenile life stage of 11 groundfish species. Data sets for EFH species, particularly the settled early juvenile life stage of groundfishes and crabs in nearshore areas, should be further developed to improve EFH descriptions and maps for species in nursery habitats and to improve our understanding of how management decisions for nearshore and coastal nursery habitats may affect fishery productivity (e.g., Thorson et al. 2021).

Data other than the RACE-GAP summer bottom trawl survey that could be included in EFH descriptions include data from the North Pacific Observer program, the AFSC and IPHC longline surveys, and Midwater Assessment and Conservation Engineering (MACE) acoustic surveys (e.g., McGowan et al. 2019, Monnahan et al. 2021). In these and other instances, it is important, at a minimum, to estimate fishing-power corrections between gears, and in some cases might be helpful to identify differences in vertical availability or selectivity ratios (Kotwicki et al. 2017, 2018; Monnahan et al. 2021; see "Develop methodology for combining disparate datasets" section below). The stock assessment author review of the EFH descriptions and identification (maps) (component 1) for the 2023 EFH 5-year Review suggested that the addition of longline survey data may be particularly helpful for arrowtooth flounder, blackspotted and rougheye

rockfishes, shortraker rockfish, shortspine thornyhead, sablefish, and Pacific sleeper sharks. In addition, tagging studies and genetic data may be helpful and most useful for fitting process models, which can, in turn, inform SDMs for EFH species (Thorson et al. 2021). These data sources are summarized in Table 59. SDMs that take advantage of multiple data sources may improve the resolution and reliability of existing EFH descriptions.

Incorporating existing datasets into future EFH descriptions and maps may also expand the spatial scope of EFH areas. For example, in the present work, we combined nearshore surveys with offshore surveys in the GOA to develop more comprehensive coverage of EFH species and life stages in nearshore areas (see above). There is also a potential for a multiscale approach to EFH that includes paired maps of nearshore and offshore areas, where nearshore maps could be of finer spatial resolution than the offshore maps depending on available data (e.g., Grüss et al. 2021b). With enough detailed information from other surveys, it may also be possible to identify biological processes occurring at a subregional scale, such as differences in growth or reproductive output. Dover sole (McGilliard et al. 2019) and rex sole (McGilliard and Palsson 2017) in the GOA are other examples of species where additional survey data may help better distinguish subregional growth differences. Additional information can not only improve Level 3 EFH information, but is useful for stock assessments, especially for species with spatial management (e.g., sablefish; Hanselman et al. 2019). The spatial scope of EFH descriptions and maps will also expand with surveys of untrawlable habitats, including camera surveys.

Combining data between the RACE-GAP bottom trawl surveys and other sources in the SDM ensemble framework presented by this study will require additional research and some collaborative guidelines for deciding on criteria for survey and data source inclusion (including non-standard surveys). These criteria may result in the elimination of some datasets from the

current RACE-GAP summer bottom trawl survey collection. For example, the Eastern Bering Sea slope survey was only conducted in 2002, 2004, 2008, 2010, 2012, and 2016 and may not improve the EFH definitions for Bering Sea species. It will take some modeling effort to determine parameters like gear efficiency ratios that can be used for combining data in SDMs.

Some species have distributions that occupy a narrow subarea within the trawl survey area or have limited data, and thus likely require alternative SDM approaches. For these species, it may be sensible to adopt species-specific modeling approaches where possible to accommodate some of these idiosyncrasies. Species like sablefish and shortraker rockfish in the EBS have “long and skinny distributions”, which result in poor model fits; species with limited data in a particular region have relatively low ensemble performance compared to other species modeled in the present study, and would benefit from additional survey data to improve ensemble outcomes. In the case of some species at the edge of their distribution, expanding the spatial scope of the modeled area may yield better EFH information (e.g., Atka mackerel EFH in the EBS might be improved by modeling the Bering Sea and Aleutian Islands together); in other cases additional survey data from the same location may be needed (e.g., EBS sablefish from longline surveys).

Table 59. -- Data sources to consider incorporating for species distribution.

| Data source | Type of data (presence/absence, density, etc) | Species for which these data are important | Path to SDMs |
|---|---|---|---|
| North Pacific Observer Program | Presence/absence (PA), density, age, and length distributions | Commercially targeted species (e.g., pollock, cod, sablefish, yellowfin sole, etc.) | PA and density data can be used directly; age and length distributions can inform IBMs |
| IPHC longline surveys | PA, density, age, and length distributions | Arrowtooth flounder, blackspotted and rougheye rockfishes, shortraker rockfish, shortspine thornyhead, sablefish, and Pacific sleeper shark, skates | PA and density data can be used directly; age and length distributions can inform IBMs |
| AFSC longline surveys | PA, density, age, and length distributions | Arrowtooth flounder, blackspotted and rougheye rockfishes, shortraker rockfish, shortspine thornyhead, sablefish, and Pacific sleeper shark, skates | PA and density data can be used directly; age and length distributions can inform IBMs |
| MACE acoustic surveys | PA, density | Prey species, groundfish with more midwater distributions (e.g., pollock) | Include directly in SDMs after estimating gear efficiency ratios |
| Tagging studies | Movement parameters and nonlocal effects | Sablefish, Pacific cod, arrowtooth flounder, Pacific ocean perch | Parameterize IBMs to inform species distribution models |
| Genetic data | PA, density | Blackspotted rockfish, Atka mackerel | Include directly in SDMs after estimating gear efficiency ratios and/or spatial sampling precision |

**Leverage environmental data**

The suite of habitat-related covariates used to parameterize SDMs in the present work was extensive, covering static and dynamic metrics ranging from bathymetry and seafloor terrain features to long-term averaged, observed bottom temperatures, and modeled tidal and bottom currents. Ongoing work is exploring the utility of fitting bottom temperature or other covariates

over annual time scales, which may provide insight as to how well models with long-term averaged covariates explain historical species distributions (e.g., Barnes et al. *in review*). Covariates from climatological models (e.g., Bering10K ROMS or GOA 3K ROMS NPZ) can be used for hindcasting and forecasting population responses over a variety of climate scenarios and time scales (Thorson et al. 2020b; Rooper et al. 2021, Barnes et al. 2022). In addition, covariates utilized in the present work should be evaluated *post hoc* to determine if some of the present suite of predictors could be eliminated in the next EFH Review.

As of this EFH report, environmental habitat covariates have included geographic position, bottom temperature, depth, bathymetry-derived terrain metrics, tidal and bottom currents, sediment grain size, seafloor rockiness, and the presence of structure-forming invertebrates. Several other covariates may impact groundfish and crab distributions, including including (1) irradiance (spatially interpolated from net sensors); ; (2) average (across years and/or seasons) surface chlorophyll (from satellites),, perhaps broken into size or functional groups; (3) average storm frequency (as a proxy for turbulent mixing); ; (4) average mixed layer depth or other stratification variables; (5) spatially interpolated empirical data or modeled values for secondary producers (copepods and euphausiids) from RPP/MACE/EMA programs and ROMS. Surface chlorophyll covariates were produced for the 2017 EFH report. These data were used for pelagic early life stages in 2017 and could be adapted to future SDMs for pelagic and demersal life stages.

New dynamic covariates can also be explored for inclusion in the SDMs in the future (e.g., prey fields, remote sensing data sets, the Cold Pool or El Niño Southern Oscillation indices, etc.). Many of the covariates in the current report are fixed characteristics of the physical habitat, including substrate and depth. However, for more mobile and/or more pelagic species,

important physical habitat may also include areas with high productivity, prey density, and temperature. We recommend the careful consideration and inclusion of important covariates as they are available in future EFH Reviews. Many of these data are currently available, though some work will be required to properly prepare them for use in SDMs (Table 60). We encourage further evaluation of SDMs with dynamic covariates to leverage high-resolution temporal and spatiotemporal data and improve the accuracy of EFH information. In these cases, we would likely need to average predictions of density across some larger number of years.

Existing data should be updated based on ongoing work, including covariate data and species distribution data. For example, bathymetry for the EBS has been updated and should be included in the next EFH report. Some datasets (e.g., trawl data from the Northern Bering Sea prior to 2010) may be used to extend the temporal scope of EFH. Summarizing and communicating data limitations will help prioritize data gaps to fill. Existing data may be used in new ways to inform ecological differences between regions; for example, covariate effects may vary across regions and this information could be useful for stock assessments and regional management.

**Leverage life history information and process studies**

The data necessary for using SDMs to describe and map EFH are species-specific response variables (i.e., presence-absence or abundance) and habitat-related predictors (covariates) such as bottom depth or bottom temperature. Because the MSA EFH Regulations specify that EFH descriptions are both species- and life stage-specific, life history updates are an integral part of incorporating new data and applying best available science to the EFH

components of FMPs. Striving to improve life history data and EFH information for ecologically distinct and underrepresented life stages is an ongoing priority.

This report employed species-specific length-based life stage definitions to separate settled early juveniles from subadult stages and subadults from adult stages. We recommend that future EFH work leverages existing data sources and process studies, including novel approaches, to continually improve the available life history information. For example, stock assessment author review during this cycle led to a recommendation that life stage breaks for rex sole and Dover sole be revised in the future based on subregional growth differences. The next EFH 5-year Review should apply the crab maturity data regularly collected on Bering Sea RACE-GAP bottom trawl surveys to inform life stage-specific SDMs for these ecologically important species in the BSAI King and Tanner Crabs FMP. This effort should involve collaboration with scientists from the AFSC Kodiak Laboratory and the Alaska Department of Fish and Game (ADFG), both of which have crab size measurements and maturity data. These data could be used to apportion crab catches to mature and immature life stages in the EBS and to describe and map those life stages for the next EFH 5-year Review.

Existing process studies on species physiology, behavior, and diets can be used to improve the selection of habitat covariates, inform life history and behavioral parameters, generally improve SDMs, and inform mechanistic models that can be used to link environment drivers and ecosystem processes. For example, process studies may inform which life stage of a given species is most likely to be influenced by a given environmental process. Life stage-specific parameters can be integrated to obtain growth parameters at the population level. They can also inform IBMs that account for life stage-specific habitat needs and behaviors (e.g., foraging, water column position, movement between areas). In 2020, the SSC recommended

several pathways by which IBMs could be used to improve habitat information, including mapping pelagic early life stage habitat (EFH), incorporating of ecosystem model outputs in IBMs, and the use of IBMs to estimate the value of different spawning locations. IBMs can also be used to integrate life stage information, and better assess the impacts of human activities (e.g., fishing) at the population scale. Process modeling studies can also incorporate existing IBMs (e.g., Daly et al. 2020, red king crab; Gibson et al. 2019, sablefish; Hinckley et al. 2019, Pacific cod), where life history and behavioral parameters can be updated with new process studies from the laboratory and field and advancements to the modeling environment (e.g., ROMS).

Structural equation models (SEMs) can help better identify environmental drivers and link them mechanistically to population impacts (Thorson et al. 2021). Spatial demographic models accounting for movement rates among areas can help address issues of non-local habitat impacts, impacts of management decisions on non-surveyed age classes, and provide another way to evaluate the combined effects of fishing and habitat impacts at the population scale. Process-based approaches are helpful to describe and map EFH, inform ecosystem-based fisheries management (EBFM) (e.g., Goldstein et al. 2020), and determine the population-level impacts of management decisions (e.g., Thorson et al. 2021).

**Combine disparate datasets**

In the present studies, our primary response variable was numerical abundance generated from the fishery-independent RACE-GAP summer bottom trawl surveys. We also modeled settled early juvenile life stage distribution from a variety of inshore and offshore fishery-independent surveys utilizing various sampling modes (e.g., RACE-GAP large mesh bottom trawls, ADFG small-mesh bottom trawls, and beach seines) employing MaxEnt modeling of

presence as a vehicle to combine these disparate data sources in analyses. There is a growing body of research that could be harnessed in the future to better quantitatively combine data from disparate data sources and fishery-dependent collections, thereby expanding the scope and seasonal availability of species response variables to the SDMs. We recommend that combining disparate data sources be a priority area of research development for future EFH Reviews.

One of the refinements we implemented in the present work was to move away from single models for species-specific SDMs to an ensemble modeling approach. Ensemble models have been shown to improve performance (better model fits; Rooper et al., 2017b). Of the five constituent models estimated and considered for the final ensembles in the present work, four were GAMs, and the fifth was a MaxEnt model describing the probability of the presence of suitable habitat for each species in a given location. One recommendation for future EFH Reviews is to expand the variety and types of models considered in the ensemble approach (e.g., random forest or spatio-temporal models) to expand the range of fitting capabilities across the wide array of distribution patterns encountered in our data sets. As mentioned above, taking a modeling approach that facilitates combining data from disparate data sources should also be considered since it would expand the number and types of response variables available to the EFH descriptions in both space and time.

There are several datasets that could be used to either improve existing EFH information within the survey areas or to expand the spatial and temporal extent over which we provide EFH information (e.g., North Pacific Observer data, AFSC longline survey, ADFG small-mesh bottom trawl survey, etc.). Additional work is needed to be able to combine these disparate datasets in the same SDMs, including the estimation of sampling efficiency ratios for surveys with different gear efficiencies (e.g., O'Leary et al. 2021).

### Consider diverse constituent models

SDM approaches are still under development and should be reviewed regularly. As of the present report, MaxEnt models do not directly model absences (Phillips and Dudík 2008) and may overpredict occupancy based on covariates in the detection areas into areas where a species was not detected. GAM approaches explicitly account for presence/absence and do so in a more ecologically realistic way by modeling presence and absence as a binomial process. In this EFH Review, we presented presence-absence GAMs, hurdle GAMs, standard GAMs using the Poisson distribution, and GAMs using the negative binomial distribution to account for overdispersion. In the future, we propose to explore alternatives for modeling distributions. For species with limited data, random forests, boosted regression trees, and other approaches may be more appropriate to include in model ensembles. Our current ensemble framework can be readily expanded to test and incorporate additional constituent SDMs.

### Increase scope and applicability of EFH research

Ongoing discussions with the SSC and stock assessment authors have identified conceptual frameworks that should be considered in the future for developing, evaluating, and utilizing EFH descriptions and maps. Considering how EFH is defined in terms of scale and ecological function could improve the utility of this concept for management. The current working definition of EFH equates the area containing 95% of the total estimated occupied habitat with EFH (NMFS 2005), and core habitat as the area containing 50% of occupied habitat. In the present work, occupancy was defined as areas with >5% probability of an encounter based on the RACE-GAP bottom trawl survey data. However, this definition may not be as ecologically meaningful for highly mobile species or those with a high degree of uncertainty in the estimate of their population density. For example, the distribution of highly mobile predators

might be more strongly impacted by prey availability than by environmental conditions. It may also not be a useful metric if a shrinking proportion of their population is available to the bottom trawl survey, as is the case for species with poleward-shifting distributions. As models describing and predicting species distribution and abundance (density or biomass) become more tightly and realistically linked to habitat and environmental change, there may be opportunity to reconsider how EFH is defined, potentially arriving at a more objective and constrained (less open to interpretation) definition that could be universally applicable across species and regions.

**Describe prey species habitat**

Many groundfish species are predators of smaller forage species and likely respond to changes in the density of euphausiids and other prey species. They may also be adequate samplers not only of available forage for predators, but also of prey biomass (Ng et al. 2021). Approaching groundfish density from the perspective of prey availability aligns with EFH component 7 in the FMPs (Prey Species: "FMPs should list the major prey species for the species in the fishery management unit and discuss the location of prey species' habitat"; 50 CFR 600.815(a)(7)), which includes predator-prey dynamics. Several data sources are available for capturing predator-prey interactions spatially, including data on forage density from midwater acoustic surveys done by the Midwater Assessment and Conservation Engineering (MACE) division and stomach content data from Resource Ecology and Ecosystem Modeling (REEM). For midwater predators especially, data from midwater acoustic surveys may provide useful information on prey fields and therefore distribution. As prey fields shift on short time scales, the appropriate modeling approach will likely be dynamic as opposed to the static EFH maps drawn based on temporal averages.

Stomach contents, behavioral studies, genetics, and other datasets can be used to identify areas of prey abundance, and diet proportions can be analyzed to provide new SDM predictors (Thorson et al. 2021, Grüss et al. 2020, Grüss et al. 2021b). In addition, predator stomach contents can be fit with environmental covariates, providing a more mechanistic approach for modeling trophic interactions. We recommend that future studies further explore the potential for predator diets to serve as indices of prey abundance and distribution, including through an SDM framework to develop maps of prey habitat (i.e., EFH component 7 - "location of prey species habitat"). This effort may, in turn, help identify areas of importance for their EFH species predators.

**Expand to EFH Levels 3 and 4 where appropriate**

In the present EFH Review, growth, lipid accumulation, and energy loss are the vital rate parameters included to explore Level 3 EFH (habitat-related vital rates). In the future, we recommend adding other vital rates such as lipid consumption or fecundity, and Level 4 rates like habitat-related productivity or recruitment. Currently, we have Level 2 EFH information for crab species in the EBS and AI; Level 3 information for crab species could be obtained with growth rate information from surveys carried out by ADFG and the AFSC Kodiak Laboratory (see the "Add life stages" section above).

**Continue to advance and apply dynamic SDM methods**

Ongoing research indicates that dynamic models that capture interannual shifts in density and habitat covariates describe historical habitat better than static models (Barnes et al. 2022). Other work shows that many biological processes affecting fish distributions occur on a seasonal or weekly timescale (e.g., Thorson et al. 2020a). In 2020, the SSC asked about the implications

of higher or lower sampling frequency for EFH descriptions; considering more dynamic models in the model ensemble would help address this. Continuing to evaluate the impacts of model complexity (including time-varying covariates) on model fit will be necessary to ensure that EFH maps capture relevant processes.

Many of the habitat covariates identified for further exploration are dynamic and require a modeling approach that accounts for this. For example, areas of high productivity or high prey density may be important for higher trophic levels, but their location will shift over time in response to environmental drivers, including currents, light, and the timing of ice retreat. Therefore, dynamic SDMs applied over shorter time spans should be considered as an option for presenting dynamic maps alongside static SDM EFH maps (based on long-term averages) in the next EFH Review. Pairing temporally dynamic and static (long-term) approaches to describe and map EFH will improve understanding of how species habitat availability and spatial stock structure shift in space and time, which is needed to improve climate-responsive approaches to EBFM.

Table 60. -- Existing environmental datasets to explore as covariates in future EFH analysis.

| Covariate | Source | Current status | Future direction | Data processing needed |
|---|---|---|---|---|
| Light levels (irradiance) | Bering Sea ROMS model. Vertical profiles of light levels (PAR) available from RPA (EcoFOCI PMEL, EMA) data. Contacts: Jeanette Gann, Phyllis Stabeno. | Water column irradiance could be calculated from ROMS light attenuation and other variables but is not currently a diagnostic output of the ROMS model. In Access database for EMA Bering surveys (2003-present); PMEL mooring survey data also available. | Use light fields to define suitable habitat for visual predators. | If it is to be used as a covariate, irradiance will have to be added as a diagnostic output to future versions of the Bering Sea ROMS model. Then it can be used to calculate other values. |
| Bottom light levels (optical depth) | Net sensors on bottom trawls (vertical profiles and on bottom in situ irradiance-RACE GAP); vertical profiles of light levels (PAR) available from RPA (EcoFOCI PMEL, EMA) data. Contacts: Jeanette Gann, Phyllis Stabeno. | Available for recent years (EBS: 2004-present, NBS: 2010-present, GOA: 2005-present, AI: 2006-present) (Rohan et al. 2020; Rohan et al. 2021) | Use light fields to define suitable habitat for visual predators. Optical depth (depth × diffuse attenuation coefficient) can be used to identify areas where predators can find prey | Data may require additional kriging; interpolation for years/areas where data are absent |
| Surface total chlorophyll estimates (satellite) | Satellite data (when cloud cover and sea ice are not interfering). Contact: Jens Nielsen (CICOES). | Includes all phytoplankton together. Data have been organized for including as covariates as of 2017 EFH report. | Test phytoplankton as covariate in SDMs | No further processing needed. |
| Surface total chlorophyll estimates (discrete/ in situ) | CTD cast data from discrete sampling stations; includes fluorometer for chl a from RPA cruises. Contacts: Jeanette Gann, Colleen Harpold. | Bering Sea data stored in Access; GOA and AI data may not be available yet. | Use as coarser measure of productivity | Unknown |
| Ice algae | Not available yet | Not yet available | Likely related to sea ice; food resource for crabs and other benthic invertebrates | Unknown |
| Size-fractionated surface chlorophyll (discrete / in situ) | Taxonomic data collection in progress. Contacts: Lisa Eisner; Jeanette Gann | Bering Sea data stored in Access; GOA and AI data may not be available yet (PI: Lisa Eisner; contact Jeanette Gann with database inquiries) | Larger phytoplankton may be better food (e.g., diatoms) so size fractions might better indicate food availability / quality. There will be a seasonal shift to smaller sizes but persistent hotspots probably have many sizes. | Unknown |
| Size-fractionated surface chlorophyll (satellite) | Contact: Jens Nielsen | Satellite algorithm still in development. Included in ESR for Eastern Bering Sea. | Larger phytoplankton may be better food (e.g., diatoms) so size fractions might better indicate food availability / quality. | Additional interpolation may be necessary. |

| Covariate | Source | Current status | Future direction | Data processing needed |
|---|---|---|---|---|
| Size-fractionated and size-specific or vertically integrated chlorophyll samples (spring and fall) | Contacts: Lisa Eisner, PhD student Jeanette Gann | TBD following collaboration discussion. In Access database for EMA Bering surveys (2003-present); PMEL mooring survey data also available. | Larger phytoplankton may be better food (e.g., diatoms) so size fractions might better indicate food availability / quality. | Additional interpolation may be necessary. |
| Storm frequency (proxy for turbulent mixing) | May be available from wind speeds (Contact: Pelland) or in ESRs. | Unknown | Turbulent mixing may influence food availability and productivity. | Unknown |
| Timing and size of spring bloom | Derived from variables described above | Nielsen in ESR for Eastern Bering Sea | For a spatially-varying response, an annual index can still generate interesting differences in distribution among years (Thorson 2019) | Annual indices ready to use for EBS; may be available for other regions. |
| Average mixed layer depth | PMEL moorings (seasonal coverage) and oceanographic surveys (PMEL, RPA). Contact: Jeanette Gann, Jens Nielsen, Phyllis Stabeno. | In Access database for EMA Bering surveys (2003-present); PMEL mooring survey data also available. | Mixed layer depth may impact food availability and productivity; may be useful for Component 1 descriptions. | Unknown |
| Cold Pool Index (CPI) | Net sensors on bottom trawls. CTD data from RPA ecosystem and mooring surveys. Also ROMS model output. Contact: Kearney. | CPI is fairly standard (O'Leary et al. 2020) but has not been used in EFH so far. Data ready for use. | Use CPI as covariate to improve EFH Component 1 descriptions. | May require additional interpolation. |
| Secondary producers (other forage including copepods and euphausiids) | RPP/MACE/EMA surveys-zooplankton water column net tows (Contact: Dave Kimmel) and diets in forage fish (Contacts: Dave Kimmel, Alex Andrews).<br>Gut contents from stomach sampling on trawl surveys.<br>ROMS modeled values (e.g., GOA NPZ 3K ROMS small and large copepod fields; Contact: K Coyle) | Data available | Use prey data to develop prey habitat descriptions for Component 7. | May require additional interpolation and/or diet data to determine important taxa or sizes. |
| Secondary producers: euphausiids | MACE product from midwater acoustic survey (Contact: Patrick Ressler) | Used annually for Ecosystem Status Reports. | Use prey survey data to explore EFH for predators, e.g., euphausiid data can be used as covariate for midwater foragers like walleye pollock | May require additional interpolation. Acoustic data may need additional manipulation. |
| Secondary producers: stomach contents as direct measure of foraging success | REEM stomach contents data | Data available | Can be used in a spatial model to interpolate (examples: Arnaud Grüss et al. 2020; 2021; Ng et al. 2021); methods exist to fit with environmental | Data may require additional kriging or similar |

| Covariate | Source | Current status | Future direction | Data processing needed |
|---|---|---|---|---|
| | | | covariates using GAMs and GLMs | |

## Improve process and communication

Improving methodological approaches and clearly communicating them is a high priority. Review and input by the Council's SSC, Plan Teams, the stock assessment authors, and other stakeholders is an important part of the iterative EFH 5-year Review process. Expert peer-reviews, in particular, can help identify cases where changes are needed to account for species with lower quality data or low availability to the surveys where species data has been used to model and map EFH. Additionally, the EFH process involves communicating model results to a broad stakeholder audience and adapting models when appropriate based on feedback. For example, a species with poor model fits or low stock assessment author confidence in the EFH map might be evaluated using a different SDM, or certain data requirements might be identified early leading to that species being modeled differently. Each EFH 5-year Review is an opportunity to improve the process and communication.

We are proud of the process and communication improvements that we implemented during this EFH 5-year Review to improve coordination and collaboration between SDM EFH analysts and stock assessment authors. We have implemented SSC suggestions from 2021 about communicating methods and results, including providing descriptions of ensemble modeling methods and probability thresholds, clear data descriptions including data transformations and timeframes, and summaries of skill testing results. We (AKRO and AFSC) hosted a stock assessment author summit in January 2021 to discuss and co-develop the review process of the current and new EFH descriptions and maps. We set a timeline that worked for all parties and agreed on the content to be reviewed and the methods, which was well communicated and executed in an approachable process for the reviewers. In past EFH 5-year Reviews, current EFH descriptions and maps in the FMPs were provided to stock assessment authors with the new EFH

maps for review. In this EFH Review, as the SDM ensemble EFH methods represent a significant advancement over the 2017 SDM EFH approach, and expert peer-review is an important part of the iterative EFH 5-year Review process; we provided the stock assessment authors with the complete set of regional SDM ensemble EFH methods (3 regions) and species results chapters (118 chapters). Stock assessment authors are considered subject matter experts, whose input was used to ground-truth EFH information, including improving the modeling methodology in general and for their species. We recommend that agreement be reached at the beginning of next 5-year review regarding the process and scope for stock-assessment author review in a way that remains feasible for the EFH analytical team.

**Communicate confidence in EFH designations**

In 2021, the SSC recommended that analysts define thresholds for excluding or denoting areas where uncertainty is high (e.g., report the ratio of estimated response to uncertainty). This would allow scientists to communicate areas where confidence in the EFH designations was high vs. low. Propagating uncertainty through the existing EFH maps in this way is unclear and may lead to "patchy" maps that are more difficult to communicate with stakeholders and regional managers. Additionally, the coefficients of variation (CVs) from cross-validation reported in the present results largely track abundance predictions from SDMs, as areas with high abundance tend to have high uncertainty when abundance is Poisson-distributed. Future studies should evaluate uncertainty and find ways to communicate uncertainty in SDM predictions; determine where uncertainty in untrawled/untrawlable areas differs from that in trawled/trawlable areas, and evaluate how these designations might be successfully communicated and addressed in EFH descriptions.

### Develop thresholds for EFH mapping and test them

Another aspect where the EFH 5-year Review process and communication can be strengthened is the scientific guidance that informs the various thresholds applied to map EFH from SDMs and evaluate these EFH maps with the fishing effects model (SASI model; Smeltz et al. 2019) and subsequent analysis of stock level impacts by the stock assessment authors (Simpson et al. 2017). Conceptual frameworks should be considered in the future for developing, evaluating, and utilizing EFH descriptions and maps within the EFH Regulations (see above section "Increase Scope and Applicability of EFH Research"). We recommend forming a Work Group to develop and communicate scientific guidance on both of these aspects to the SSC prior to the start of the next EFH 5-year Review.

### Add more opportunities for communication

Monitoring research, process research, and model development should be coordinated in order to target knowledge gaps about the relationship between habitat, fishing, and fishery productivity. This coordination should occur across AFSC Divisions and include conversations with researchers who work outside the existing EFH areas in cases where species ranges are suspected to be shifting. Ongoing conversations with stakeholders about management priorities, risk tolerance, and tradeoffs will help frame process and modeling studies (Thorson et al. 2021). With consistent stakeholder involvement, simulation approaches such as management strategy evaluation (MSE; Smith 1994, Punt et al. 2016) can be used to compare the performance of different management strategies and data collection practices (like survey frequency) under various degrees of uncertainty, including process and model uncertainty.

## Streamline workflows and reproducibility

Further improving communication around data and code can be achieved with currently available tools. For the next EFH 5-year review, we recommend augmenting the existing review process with more best practices for open data science, sharing code with reviewers and collaborators, and creating more reproducible workflows to streamline the EFH process (e.g., Lowndes et al. 2017). These changes should include producing reproducible code, making covariate/raster data available through NCEI[21] ERDDAP[22] and AKFIN[23], and automating the generation of EFH reports and presentation slides using R Markdown or similar tools to streamline the creation of EFH products. Reproducible code practices should include the production of an R package for the EFH SDMs so that scientists with species distribution data can easily test model improvements and new data sources instead of waiting for EFH analysts to carry out these comparisons. When data or modeling approaches need to be modified for select species (first section of this chapter), they can be adjusted just for those species, while others are only updated with new data each EFH cycle. Tracking comments and changes to the models, making code available to stock assessment authors, and automating some of the map and report generation processes will improve transparency and speed up the generation of EFH products.

## Conclusions

We have identified several areas where Essential Fish Habitat research can be advanced in the coming EFH 5-year Review cycles (Table 61). Further work in these areas will identify better SDMs or SDM ensembles for defining EFH, especially for species with less available

[21] https://www.ncei.noaa.gov/
[22] https://coastwatch.pfeg.noaa.gov/erddap/index.html
[23] https://akfin.psmfc.org/

trawl data. Advancements in many of the areas we describe here are connected to other topics. For example, the development of approaches for quantifying and describing uncertainty in EFH maps (see the "Modeling" section) will also improve Process and Communication, providing a straightforward way of communicating uncertainty to stock assessment authors and the Council.

The studies recommended here will take longer than one EFH 5-year Review cycle, so some care should be taken to identify priorities for data collection, data setup, and model development. We identify next steps needed for projects involving new covariates in Table 60 and areas where cross-disciplinary collaboration will be especially helpful in Table 61. Cross-divisional collaborations will expand the suite of covariate data that can be incorporated into EFH models and provide a basis for ongoing discussions about ecosystem structure and function as they relate to EFH. Modeling advancements will provide ways to use existing data, account for processes that affect multiple life stages, and account for environmental drivers mechanistically. Finally, discussions with stakeholders and modelers can form a strong foundation for the design of simulation studies that assess the impacts of management decisions on EFH species.

Table 61. -- Summary table of future recommendations for EFH research to advance EFH component 1 descriptions and maps, and how EFH component 1 outputs are evaluated and applied to management.

| Area of research | Improvement/advancement | Taxa with potential EFH improvement |
|---|---|---|
| Prioritize and improve EFH for select species | Leverage existing species distribution data to expand spatial scope and improve predictions in existing EFH maps | Species where higher-quality EFH information is needed (current maps contradict expert experience; model fits are relatively low compared to other species modeled) |
| | Leverage environmental data | All (especially species where higher-quality EFH information is needed) |
| | Improve life history information with best available science | All (especially crab species) |
| | Expand and improve existing SDM EFH mapping to include species and life stages in the nearshore (e.g., at appropriate spatial resolutions) | Many EFH species and their prey that inhabit nearshore habitats |
| | Develop methodology for combining disparate datasets | Species where higher-quality EFH information is needed |
| | Develop process studies to inform EFH descriptions and maps (e.g., vital rates, movement, population dynamics) | All |
| | Consider diverse constituent models | Species where higher-quality EFH information is needed; especially those with EFH level 1 information only |
| Increase scope and applicability of EFH research | Describe prey species habitat (EFH component 7) | Most groundfish, especially those with diets more specialized on forage |
| | Expand to EFH Levels 3 and 4 | All |
| | Continue to advance and apply dynamic SDM methods in development to map and forecast shifts in EFH and spatial stock structure to improve climate-responsive approaches to EFH and EBFM | All |

| Area of research | Improvement/advancement | Taxa with potential EFH improvement |
|---|---|---|
| Improve process and communication | Communicate confidence in EFH designations/boundaries | All |
| | Develop thresholds for mapping EFH with SDMs and SDM EFH applied to the Fishing Effects analysis (e.g., thresholds applied), through research and an expert work group, and communicate this guidance to the SSC prior to the launch of the next EFH 5-year Review. | All |
| | Add more opportunities for communication | All |
| | Streamline workflows and reproducibility | All |

## ACKNOWLEDGMENTS

We thank Lyle Britt, Wayne Palsson, and Stan Kotwicki of the NMFS AFSC Groundfish Assessment Program for their strong support of this work. We wish to thank Gretchen Harrington, Kim Rand, Jim Thorson, and Molly Zaleski for their insightful reviews and important contributions. This work was greatly improved by the time and energy invested by all of the stock assessment authors and stock experts who contributed to the review of these documents. This project was funded by the AKRO/AFSC Essential Fish Habitat Research Funds.

## CITATIONS


Abookire, A. A. 2006. Reproductive biology, spawning season, and growth of female rex sole (*Glyptocephalus zachirus*) in the Gulf of Alaska. Fish. Bull., U.S. 104(3):350-359.

Abookire, A. A., and B. J. Macewicz. 2003. Latitudinal variation in reproductive biology and growth of female Dover sole (*Microstomus pacificus*) in the North Pacific, with emphasis on the Gulf of Alaska stock. J. Sea Res. 57:198-208.

Abookire, A. A., and K. M. Bailey. 2007. The distribution of life cycle stages of two deep-water pleuronectids, Dover sole (*Microstomus pacificus*) and rex sole (*Glyptocephalus zachirus*), at the northern extent of their range in the Gulf of Alaska. J. Sea Res. 50:187-197.

Alton, M. S., R. G. Bakkala, G. E. Walters, and P. T. Munro. 1988. Greenland turbot *Reinhardtius hippoglossoides* of the aastern Bering Sea and Aleutian Islands region. U.S. Dep. Commer., NOAA Tech. Rep. NMFS-71, 38 p.

Araujo, M. B., and M. New. 2007. Ensemble forecasting of species distributions. Trends Ecol. Evol. 22(1):42:47. https://doi.org/10.1016/j.tree.2006.09.010.

Bacheler, N. M., L. Ciannelli, K. M. Bailey, and J. T. Duffy-Anderson. 2010. Spatial and temporal patterns of walleye pollock (*Theragra chalcogramma*) spawning in the eastern Bering Sea inferred from egg and larval distributions. Fish. Oceanogr. 19(2):107-120.

Bailey, K. M. 2000. Shifting control of recruitment of walleye pollock *Theragra chalcogramma* after a major climatic and ecosystem change. Mar. Ecol. Prog. Ser. 198:215-224.

Bailey, K. M., A. A. Abookire, and J. T. Duffy-Anderson. 2008. Ocean transport paths for the early life history stages of offshore-spawning flatfishes: a case study in the Gulf of Alaska. Fish Fish. 9:44-66.

Balanov, A. A., V. V. Panchenko, and A. B. Savin. 2020. The First Record of a Spawning Ground of the Mud Skate *Bathyraja taranetzi* (Dolganov, 1983) and the Okhotsk Skate *B. violacea* (Suvorov, 1935) in Pacific waters off the Northern Kuril Islands. Russ. J. Mar. Biol. 46:501–505.

Barnes, C. L., A. H. Beaudreau, M. W. Dorn, K. K. Holsman, and F. J. Mueter. 2020. Development of a predation index to assess trophic stability in the Gulf of Alaska. Ecol. Appl. 30(7):e02141. doi: 10.1002/eap.2141.

Barnes C. L., J. T. Thorson, J. L. Pirtle, C. N. Rooper, E. A. Laman, K. K. Holsman, K. Y. Aydin, and T. E. Essington. *In prep*. Effects of model complexity on describing and forecasting species responses to changing climate. Ecography.

Barry, S. C., and A. H. Welsh 2002. Generalized additive modeling and zero inflated count data. Ecol. Model. 157:179-188.

Best, D. J., and D. E. Roberts. 1975. Algorithm AS 89: the upper tail probabilities of Spearman's rho. Appl. Stat. 24:377-379.

Boldt, J. L., T. W. Buckley, C. N. Rooper, and K. Aydin. 2012 Factors influencing cannibalism and abundance of walleye pollock (*Theragra chalcogramma*) on the eastern Bering Sea shelf, 1982-2006. Fish. Bull., U.S. 110(3):293−306.

Brewer, R.S. and B.L. Norcross. 2012. Long-term retention of internal elastomer tags in a wild population of North Pacific giant octopus (*Enteroctopus dofleini*), Fish. Res. 134-136: 17-20. https://doi.org/10.1016/j.fishres.2012.07.020

Brewer, R.S. 2016. Population biology and ecology of the North Pacific giant octopus in the eastern Bering Sea. Ph.D. thesis, Univ. Alaska Fairbanks, Fairbanks AK.

Brodeur, R. D. 2001. Habitat-specific distribution of Pacific ocean perch (*Sebastes alutus*) in Pribilof Canyon, Bering Sea. Continent. Shelf Res. 21:207-224.

Bryan, M. D., S. J. Barbeaux, J. Ianelli, S. Zador, and J. Hoff. 2020a. Assessment of Greenland turbot in the Bering Sea and Aleutian Islands, 96 p. ***In*** Stock Assessment and Fishery Evaluation Report for the Groundfish Resources of the Bering Sea/Aleutian Islands Regions. North Pacific Fishery Management Council 1007 West Third, Suite 400 Anchorage, AK 99501.

Bryan, M. D., K. Shotwell, S. Zador, and J. Ianelli. 2020b. Assessment of the Kamchatka flounder stock in the Bering sea/Aleutian islands, 91p. ***In*** Stock Assessment and Fishery Evaluation Report for the Groundfish Resources of the Bering Sea and Aleutian Islands. North Pacific Fishery Management Council 1007 West Third, Suite 400 Anchorage, AK 99501.

Bryan, D. R., S. F. McDermott, J. K. Nielsen, D. Fraser, and K. M. Rand. 2021. Seasonal migratory patterns of Pacific cod (*Gadus macrocephalus*) in the Aleutian Islands. Anim. Biotelemetry 9(1):24. https://doi.org/10.1186/s40317-021-00250-2

Buckley, T. W., A. Greig, and J. L. Boldt. 2009. Describing summer pelagic habitat over the continental shelf in the eastern Bering Sea, 1982-2006. U.S. Dep. Commer., NOAA Tech. Memo. NMFS-AFSC-196.

Canino, M. F., I. B. Spies, K. M. Cunningham, L. Hauser, and W. S. Grant. 2010. Multiple ice-age refugia in Pacific cod, *Gadus macrocephalus*, Mol. Ecol. 19:4339-4351.

Carlson, H. R., and R. R. Straty. 1981. Habitat and nursery grounds of Pacific rockfish, *Sebastes* spp., in rocky coastal areas of Southeastern Alaska. Mar. Fish. Rev. 43:13-19.

Ciannelli, L., R. D. Brodeur, and J. M. Napp. 2004. Foraging impact on zooplankton by age-0 walleye pollock (*Theragra chalcogramma*) around a front in the southeast Bering Sea. Mar. Biol. 144(3):515-526.

Ciannelli, L., P. Fauchald, K. S. Chan, V. N. Agostini, and G. E. Dingsør. 2008. Spatial fisheries ecology: recent progress and future prospects. J. Mar. Sys. 71(3-4):223-236.

Chilton, E. A. 2010. Maturity and growth of female dusky rockfish (*Sebastes variabilis*) in the central Gulf of Alaska. Fish. Bull., U.S. 108(1):70-78.

Clausen, D. M., and J. Heifetz. 2002. The northern rockfish, *Sebastes polyspinis*, in Alaska: Commercial fishery, distribution, and biology. Mar. Fish. Rev. 64:1-28.

Cochran, W. G. 1977. Sampling Techniques. 3rd ed. Wiley Series in Probability and Mathematical Statistics - Applied. John Wiley & Sons. N.Y., NY 428 p.

Conrath, C. L. 2017. Maturity, spawning omission, and reproductive complexity of deepwater rockfish. Trans. Am. Fish. Soc. 146:495-507.

Conrath, C. L. 2019. Reproductive potential of light dusky rockfish (*Sebastes variabilis*) and northern rockfish (*S. polyspinis*) in the Gulf of Alaska. Fish. Bull., U.S. 117:140-150.

Conrath, C. L., and M. E. Conners. 2014. Aspects of the reproductive biology of the North Pacific giant octopus (*Enteroctopus dofleini*) in the Gulf of Alaska. Fish. Bull., U.S. 112(4):253-260.

Cooper, D. W., K. R. Maslenikov, and D. R. Gunderson. 2007. Natural mortality rate, annual fecundity, and maturity at length for Greenland halibut (*Reinhardtius hippoglossoides*) from the northeastern Pacific Ocean. Fish. Bull., U.S. 105(2):296-304.

Cooper, D. W., S. F. McDermott, and J. N. Ianelli. 2010. Spatial and temporal variability in Atka mackerel female maturity at length and age. Mar. Coast. Fish. 2:329-338.

Copeman, L. A., B. J. Laurel, M. Spencer, and A. Sremba. 2017. Temperature impacts on lipid allocation among juvenile gadid species at the Pacific Arctic-Boreal interface: an experimental laboratory approach. Mar. Ecol. Prog. Ser. 566:183-198.

Cragg, J. G. 1971. Some statistical models for limited dependent variables with application to the demand for durable goods. Econometrica. 39:829-844.

Danielson, S., E. Curchitser, K. Hedstrom, T. Weingartner, and P. Stabeno. 2011. On ocean and sea ice modes of variability in the Bering Sea. J. Geophys. Res. 116: doi: 10.1029/2011JC007389.

Daly, B., C. Parada, T. Loher, S. Hinckley, A. J. Hermann, and D. Armstrong. 2020. Red king crab larval advection in Bristol Bay: Implications for recruitment variability. Fish. Oceanogr. 29:505– 525. https://doi.org/10.1111/fog.12492

Daly, B., C. Parada, T. Loher, S. Hinckley, A. J. Hermann, and D. Armstrong. 2020. Red king crab larval advection in Bristol Bay: Implications for recruitment variability. Fish. Oceanogr. 29:505– 525. https://doi.org/10.1111/fog.12492

Debenham, C., J. Moss, and R. Heintz. 2019. Ecology of age-0 arrowtooth flounder (*Atheresthes stomias*) inhabiting the Gulf of Alaska. Deep-Sea Res. II 165:140-149.

Diggle, P. J., and P. J. Ribeiro Jr. 2002. Bayesian inference in Gaussian model-based geostatistics. Geo. Environ. Model. 6(2):129-146.

Dolan, M. F. J., A. J. Grehan, J. C. Guinan, and C. Brown, C. 2008. Modelling the local distribution of cold-water corals in relation to bathymetric variables: Adding spatial context to deep-sea video data. Deep-Sea Res. P. I – Oceanogr. Res. Pap., 55(11), 1564-1579. https://doi.org/10.1016/j.dsr.2008.06.010.

Dolan, M. F. J., and V. L. Lucieer. 2014. Variation and Uncertainty in Bathymetric Slope Calculations Using Geographic Information Systems. Mar. Geodesy. 37(2): 187-219. https://doi.org/10.1080/01490419.2014.902888.

Doyle, M. J., C. Debenham, S. J. Barbeaux, T. W. Buckley, J. L. Pirtle, I. B. Spies, W. T. Stockhausen, S. K. Shotwell, M. T. Wilson, and D. W. Cooper. 2018. A full life history synthesis of arrowtooth flounder ecology in the Gulf of Alaska: Exposure and sensitivity to potential ecosystem change. J. Sea Res. 142:28-51. https://doi.org/10.1016/j.seares.2018.08.001

Doyle, M. J., S. L. Stromb, K. O. Coyle, A. J. Hermann, C. Ladd, A. C. Matarese, S. K. Shotwell, and R. R. Hopcroft. 2019. Early life history phenology among Gulf of Alaska fish species: Strategies, synchronies, and sensitivities. Deep-Sea Res. II 165:41-73.

Duchon, J. 1977. Splines minimizing rotation-invariant semi-norms in Solobev spaces, p. 85-100. ***In*** W. Shemp and K. Zeller (eds.), Construction Theory of Functions of Several Variables. Springer Verlag, Berlin.

Du Preez, C., and V. Tunnicliffe. 2011. Shortspine thornyhead and rockfish (Scorpaenidae) distribution in response to substratum, biogenic structures and trawling. Mar. Ecol. Prog. Ser. 425: 217-231. doi: 10.3354/meps09005.

Ebert, D. A. 2005. Reproductive biology of skates, *Bathyraja* (Ishiyama), along the eastern Bering Sea continental slope. J. Fish Biol. 66(3):618-649.

Ebert, D. A., W. D. Smith, D. L. Haas, S. M. Ainsley, and G. M. Cailliet. 2007. Life history and population dynamics of Alaskan skates: providing essential biological information for effective management of bycatch and target species. Final Report to the North Pacific Research Board, Project 510.

Egbert, G. D., and S. Y. Erofeeva. 2002. Efficient inverse modeling of barotropic ocean tides. J. Atmos. Ocean. Tech. 19(2):183-204. doi: 10.1175/1520-0426(2002)019.

Elith, J., S. J. Phillips, T. Hastie, M. Dudík, Y. E. Chee, and C. J. Yates. 2011. A statistical explanation of MaxEnt for ecologists. Divers. Distrib. 17:43-57.

Fissel, B., M. Dalton, B. Garber-Yonts, A. Haynie, S. Kasperski, J. Lee, D. Lew, C. Seung, K. Sparks, M. Szymkowiak, and S. Wise. 2020. Economic Status of the Groundfish Fisheries Off Alaska 2019, 284 p. ***In*** Stock Assessment and Fishery Evaluation Report for the Groundfish Fisheries of the Gulf of Alaska and Bering Sea/Aleutian Islands Area. North Pacific Fishery Management Council 1007 West Third, Suite 400 Anchorage, AK 99501.

Fithian, W., J. Elith, T. Hastie, and D. A. Keith. 2015. Bias correction in species distribution models: pooling survey and collection data for multiple species. Methods Ecol. Evol. 6:424-438. doi: 10.1111/2041-210X.12242.

Fisheries Leadership and Sustainability Forum. 2016. Regional EFH Profile: North Pacific. National Essential Fish Habitat Summit, 2016. https://www.fisheriesforum.org/our-work/special-projects/efh-summit/efh-profiles/.

Gharrett, A. J., A. P. Matala, E. L. Peterson, A. K. Gray, Z. Li, and J. Heifetz. 2005. Two genetically distinct rougheye rockfish sibling species differ phenotypically? Trans. Am. Fish. Soc. 135:792-800.

Gibson, G. A., W. T., Stockhausen, K. O. Coyle, S. Hinckley, C. Parada, A .J. Hermann, M. Doyle, and C. Ladd. 2019. An individual-based model for sablefish: Exploring the connectivity between potential spawning and nursery grounds in the Gulf of Alaska. Deep-Sea Res. Pt. II. 165:89-112.

Goethel, D. R., D. H. Hanselman, C. J., Rodgveller, K. H. Fenske, S. K. Shotwell, K. B. Echave, P. W. Malecha, K. A. Siwicke, and C. R. Lunsford. 2020. Assessment of the sablefish stock in Alaska, 257 p. ***In*** Stock assessment and fishery evaluation report for the groundfish resources of the GOA and BS/AI. North Pacific Fishery Management Council 1007 West Third, Suite 400 Anchorage, AK 99501.

Grüss, A., J. T. Thorson, G. Carroll, E. L. Ng, K. K. Holsman, K. Aydin, S. Kotwicki, H. N. Morzaria-Luna, C. H. Ainsworth, and K. A. Thompson. 2020. Spatio-temporal analyses of marine predator diets from data-rich and data-limited systems. Fish Fish. 21(4):718–739. https://doi.org/10.1111/faf.12457

Grüss, A., J. L. Pirtle, J. T. Thorson, M. R. Lindeberg, A. D. Neff, S. G. Lewis, and T. E. Essington. 2021a. Modeling nearshore fish habitats using Alaska as a regional case study. Fish. Res. 238. doi: 10.1016/j.fishres.2021.105905.

Grüss, A., J. T. Thorson, C. C. Stawitz, J. C. P. Reum, S. K. Rohan, and C. L. Barnes. 2021b. Synthesis of interannual variability in spatial demographic processes supports the strong influence of cold-pool extent on eastern Bering Sea walleye pollock (*Gadus chalcogrammus*). Prog. Oceanogr. 194:102569. https://doi.org/10.1016/j.pocean.2021.102569

Guisan, A., S. Weiss, and A. Weiss. 1999. GLM versus CCA spatial modeling of plant species distribution. Plant Ecol. 143:107–122.

Guisan, A., N. E. Zimmermann, J. Elith, C. H. Graham, S. Phillips, and A. T. Peterson. 2007. What matters for predicting the occurrences of trees: techniques, data, or species' characteristics? Ecol. Monogr. 77:615-630. https://doi.org/10.1890/06-1060.1.

Gunderson, D. R., D. A. Armstrong, Y. B. Shi, and R. A. McConnaughey. 1990. Patterns of estuarine use by juvenile English sole (*Parophrys vetulus*) and Dungeness crab (*Cancer magister*). Estuaries 13(1):59-71.

Haas, D. L., D. A. Ebert, and G. M. Cailliet. 2016. Comparative age and growth of the Aleutian skate, *Bathyraja aleutica*, from the eastern Bering Sea and Gulf of Alaska. Env. Biol. Fish. 99:813-828.

Hanselman, D. H., T. J. Quinn II, C. Lunsford, J. Heifetz, and D. M. Clausen. 2001. Spatial implications of adaptive cluster sampling on Gulf of Alaska rockfish, p 303-25. ***In*** Proceedings of the 17th Lowell-Wakefield Symposium: Spatial Processes and Management of Marine Populations, pp. 303-325. Univ. Alaska Sea Grant Program, Fairbanks, AK.

Hanselman, D. H., J. Heifetz, K. B. Echave, and S. C. Dressel. 2015. Move it or lose it: movement and mortality of sablefish tagged in Alaska. Can. J. Fish. Aquat. Sci. 72(2):238-251.

Hanselman, D. H., C. J. Rodgveller, K. H. Fenske, S. K. Shotwell, K. B. Echave, P. W. Malecha, C. R. Lunsford. 2019. Assessment of the sablefish stock in Alaska, 263 p. ***In*** Stock Assessment and Fishery Evaluation Report for the Groundfish Resources of the Gulf of Alaska. North Pacific Fishery Management Council 1007 West Third, Suite 400 Anchorage, AK 99501.

Hart, J. L. 1973. Pacific Fishes of Canada. Canadian Government Publishing Centre, Supply and Services Canada, Ottawa, Canada KIA OS9

Hastie, T. J., and R. J. Tibshirani. 1990. Generalized Additive Models. Monogr. Stat. Appl. Prob. 43. 338 p.

Hastie, T., R. J. Tibshirani, and J. H. Friedman. 2009. The Elements of Statistical Learning: Data Mining, Inference, and Prediction. Second edition. Springer, Berlin, Germany.

Hawley, J. H. 1931. Hydrographic Manual; U.S. Department of Commerce, U.S. Coast and Geodetic Survey, Special Publication No. 143; U.S. Government Printing Office: Washington, DC, USA.

Heifetz, J., and J. T. Fujioka. 1991. Movement dynamics of tagged sablefish in the northeastern Pacific. Fish. Res. 11:355-374.

Heifetz, J., B. L. Wing, R. Stone, P. Malecha, and D. Courtney. 2005. Corals of the Aleutian Islands. Fish. Oceanogr. 14(s1):131-138. doi: 10.1111/j.1365-2419.2005.00371.x.

Hinckley, S., W. Stockhausen, K. Coyle, B. Laurel, G. Gibson, C. Parada, A. Hermann, M. Doyle, and T. Hurst. 2019. Connectivity between spawning and nursery areas for Pacific cod (*Gadus macrocephalus*) in the Gulf of Alaska. Deep-Sea Res. Pt. II. 165:113-126.

Hoff, G. R. 2007. Reproduction of the Alaska skate (*Bathyraja parmifera*) with regard to nursery sites, embryo development and predation. Ph.D. dissertation, University of Washington, Seattle, WA.

Hoff, G. R. 2008. A nursery site of the Alaska skate (*Bathyraja parmifera*) in the eastern Bering Sea. Fish. Bull., U.S. 106(3):233-244.

Hoff, G. R. 2009. Embryo developmental events and the egg case of the Aleutian skate *Bathyraja aleutica* (Gilbert) and the Alaska skate *Bathyraja parmifera* (Bean). J. Fish. Biol. 74(3):438-501.

Horn, B. K. P. 1981. Hill shading and the reflectance map. Proc. IEEE. 69:14-47.

Hosmer, D. W., and S. Lemeshow. 2005. Assessing the Fit of the Model, pp. 143-202. ***In*** Applied Logistic Regression, Second Edition edn. John Wiley and Sons, Inc., Hoboken, NJ, USA, 07030.

Howell, K. L., R. Holt, I. P. Endrino, and H. Stewart. 2011. When the species is also a habitat: comparing the predictively modelled distributions of *Lophelia pertusa* and the reef habitat it forms. Biol. Conserv. 144: 2656–2665.

Hulson, P. J. F., D. H. Hanselman, C. R. Lunsford, and B. Fissel. 2017. Assessment of the Pacific ocean perch stock in the Gulf of Alaska, pp. 913-992. ***In*** Stock assessment and fishery evaluation report for the groundfish resources of the Gulf of Alaska. North Pacific Fishery Management Council 1007 West Third, Suite 400 Anchorage, AK 99501.

Ito, D. H. 1999. Assessing shortraker and rougheye rockfishes in the GOA: addressing a problem of habitat specificity and sampling capability. Ph.D. Dissertation, Univ. Washington, Seattle, WA. 205 p.

Johnson, S. W., M. L. Murphy, and D. J. Csepp. 2003. Distribution, habitat, and behavior of rockfishes, *Sebastes spp.*, in nearshore waters of southeastern Alaska: Observations from a remotely operated vehicle. Env. Biol. Fish. 66(3):259-270.

Johnson, S. W., A. D. Neff, J. F. Thedinga, M. R. Lindeberg, and J. M. Maselko. 2012. Atlas of nearshore fishes of Alaska: A synthesis of marine surveys from 1998 to 2011. U.S. Dep. Commer., NOAA Tech. Memo. NMFS-AFSC-239, 261 p.

Jones, D., C. D., Wilson, A. de Robertis, C. N. Rooper, T. C. Weber, and J. L. Butler. 2012. Evaluation of rockfish abundance in untrawlable habitat: combining acoustic and complementary sampling tools. Fish. Bull., U.S. 110:332-343.

Jorgensen, E.M. 2009. Field guide to squids and octopods of the eastern North Pacific and Bering Sea. Alaska Sea Grant Pub. No. SG-ED-65, 100 p.

Kastelle, C. R., D. K. Kimura, and S. R. Jay. 2000. Using 210Pb/226Ra disequilibrium to validate conventional ages in Scorpaenids (genera *Sebastes* and *Sebastolobus*). Fish. Res. 46(1-3):299-312.

Kastelle, C., T. Helser, T. TenBrink, C. Hutchinson, B. Goetz, C. Gburski, and I. Benson. 2020. Age validation of four rockfishes (genera Sebastes and Sebastolobus) with bomb-produced radiocarbon. Mar. Freshw. Res. 71(10):1355-1366.

Kendall, A. W., and A. C. Matarese. 1987. Biology of eggs, larvae, and epipelagic juveniles of sablefish, *Anoplopoma fimbria*, in relation to their potential use in management. Mar. Fish. Rev. 49:1-13.

Kotwicki, S., R.R. Lauth, K. Williams, and S. E. Goodman. 2017. Selectivity ratio: A useful tool for comparing size selectivity of multiple survey gears. Fish. Res. 191:76–86. https://doi.org/10.1016/j.fishres.2017.02.012.

Kotwicki, S., P. H. Ressler, J. N. Ianelli, A. E. Punt, and J.K. Horne 2018. Combining data from bottom-trawl and acoustic-trawl surveys to estimate an index of abundance for semipelagic species. Can. J. Fish. Aquat. Sci. 75:60–71. https://doi.org/10.1139/cjfas-2016-0362

Kramer, D. E., and V. M. O'Connell. 1988. A Guide to Northeast Pacific Rockfishes: Genera *Sebastes* and *Sebastolobus*. ***In*** Alaska Sea Grant Advisory Bulletin 25.

Krygier, E. E. and W. G. Pearcy. 1986. The role of estuarine and offshore nursery areas for young English sole, *Parophrys vetulus* Girard, of Oregon. Fish. Bull., U.S. 84(1):119-132.

Laman, E. A., S. Kotwicki, and C. N. Rooper. 2015. Correlating environmental and biogenic factors with abundance and distribution of Pacific ocean perch (*Sebastes alutus*) in the Aleutian Islands, Alaska. Fish. Bull., U.S. 113(3):270-289. doi:10.7755/FB.113.3.4.

Laman, E. A., C. N. Rooper, K. Turner, S. Rooney, D.W. Cooper, and M. Zimmermann. 2017. Model-based essential fish habitat definitions for Bering Sea groundfish species. U.S. Dep. Commer., NOAA Tech. Memo. NMFS-AFSC-357, 265 p.

Laman, E. A., C. N. Rooper, K. Turner, S. Rooney, D.W. Cooper, and M. Zimmermann. 2018. Using species distribution models to describe essential fish habitat in Alaska. Can. J. Fish. Aquat. Sci. https://doi.org/10.1139/cjfas-2017-0181.

Laurel, B. J., C. H. Ryer, B. Knoth, and A. W. Stoner. 2009. Temporal and ontogenetic shifts in habitat use of juvenile Pacific cod (*Gadus macrocephalus*). J. Exp. Mar. Biol. Ecol. 377(1):28-35.

Laurel, B. J., M. Spencer, P. Iseri, and L. A. Copeman. 2016. Temperature-dependent growth and behavior of juvenile Arctic cod (*Boreogadus saida*) and co-occurring North Pacific gadids. Polar Biol. 39:1127-1135. doi 10.1007/s00300-015-1761-5

Lauth, R. R., S. W. McEntire, and H. H. Zenger. 2007. Geographic Distribution, Depth Range, and Description of Atka Mackerel *Pleurogrammus monopterygius* Nesting Habitat in Alaska. AK Fish. Res. Bull. 12:165-186.

Legendre, P. and L. Legendre. 2012. Numerical Ecology, Volume 24 - 3rd Edition. Elsevier. https://www.elsevier.com/books/numerical-ecology/legendre/978-0-444-53868-0.

Loher, T., D. A. Armstrong, and B. G. Stevens. 2001. Growth of juvenile red king crab (*Paralithodes camtschaticus*) in Bristol Bay (Alaska) elucidated from field sampling and analysis of trawl-survey data. Fish. Bull. 99:572-587.

Long, W. C., K. M. Swiney, C. Harris, H. N. Page, and R. J. Foy. 2013. Effects of Ocean Acidification on Juvenile Red King Crab (*Paralithodes camtschaticus*) and Tanner crab (*Chionoecetes bairdi*) Growth, Condition, Calcification, and Survival. PLOS One 8: 10 p.

Love, M. S., M. Yoklavich, and L. Thorsteinson. 2002. The rockfishes of the Northeast Pacific. University of California Press, Berkeley and Los Angeles, CA. 404 p.

Lowe, S., J. Ianelli, W. Paulson, and B. Fissel. 2019. Assessment of the Atka mackerel stock in the Bering Sea and Aleutian Islands, 166 p. ***In*** Stock Assessment and Fishery Evaluation Report for the Groundfish Resources of the Bering sea and Aleutian islands. North Pacific Fishery Management Council 1007 West Third, Suite 400 Anchorage, AK 99501.

Lowndes, J. S. S., B. D. Best, C. Scarborough, J. C. Afflerbach, M. R. Frazier, C. C. O'Hara, N. Jiang, and B. S. Halpern. 2017. Our path to better science in less time using open data science tools. Nat. Ecol. Evol. 1:1–7. https://doi.org/10.1038/s41559-017-0160

Malecha, P. W., R. P. Stone, and J. Heifetz. 2005. Living substrate in Alaska: Distribution, abundance, and species associations, p. 289-299. ***In*** Barnes, P. W. and Thomas, J. P., eds. Benthic habitats and the effects of fishing. Amer. Fish. Soc., Symposium 41, Bethesda, Maryland.

Marliave, J., and W. Challenger. 2009. Monitoring and evaluating rockfish conservation areas in British Columbia. Can. J. Fish. Aquat. Sci. 66(6):995-1006. doi: 10.1139/F09-056.

Mason, J. C., R. J. Beamish, and G. A. McFarlane. 1983. Sexual maturity, fecundity, spawning, and early life history of sablefish (*Anoplopoma fimbria*) off the Pacific coast of Canada. Can. J. Fish. Aquat. Sci. 40: 2126-2134.

Matta, M. E., and D. R. Gunderson. 2007. Age, growth, maturity, and mortality of the Alaska skate, *Bathyraja parmifera*, in the eastern Bering Sea. Env. Biol. Fish. 80(2-3):309-323.

McCarthy, A., T. Honkalehto, N. Lauffenburger, and A. De Robertis. 2020. Results of the acoustic-trawl survey of walleye pollock (*Gadus chalcogrammus*) on the U.S. Bering Sea Shelf in June - August 2018 (DY1807). AFSC Processed Rep. 2020-07, 83 p. Alaska Fish. Sci. Cent., NOAA, Natl. Mar. Fish. Serv., 7600 Sand Point Way NE, Seattle WA 98115.

McCullagh, P., and J. A. Nelder. 1989. Generalized Linear Models (2nd edition), Chapman and Hall, London, UK. 511 p. ISBN 0-412-31760-5

McDermott, S. F., and S. A. Lowe. 1997. The reproductive cycle and sexual maturity of Atka mackerel, *Pleurogrammus monopterygius*, in Alaska waters. Fish. Bull., U.S. 95:321-333.

McGilliard, C. R., and W. Palsson. 2017. Assessment of the rex sole stock in the Gulf of Alaska, pp. 657-742. ***In*** Stock Assessment and Fishery Evaluation Report for the Groundfish Resources of the Gulf of Alaska. North Pacific Fishery Management Council 1007 West Third, Suite 400 Anchorage, AK 99501.

McGilliard, C. R., W. Palsson, A. Havron, and S. Zador. 2019. Assessment of the deepwater flatfish stock complex in the Gulf of Alaska, 82 p. ***In*** Stock Assessment and Fishery Evaluation Report for the Groundfish Resources of the Gulf of Alaska. North Pacific Fishery Management Council 1007 West Third, Suite 400 Anchorage, AK 99501.

McGilliard, C. R., J. Ianelli, A. E. Punt, T. Wilderbuer, D. Nichol, and R. Haehn. 2020. Assessment of the Northern Rock Sole Stock in the Bering Sea and Aleutian Islands, 74 p. ***In*** Stock assessment and Fishery Evaluation Report for the Groundfish Resources of the Bering Sea and Aleutian Islands. North Pacific Fishery Management Council 1007 West Third, Suite 400 Anchorage, AK 99501.

McGowan, D. W., J. K. Horne, J. T. Thorson, and M. Zimmermann. 2019. Influence of environmental factors on capelin distributions in the Gulf of Alaska, p. 238–254. ***In*** Understanding Ecosystem Processes in the Gulf of Alaska. Deep-Sea Res. Pt. II: Top. Studies Oceanogr. 165. https://doi.org/10.1016/j.dsr2.2017.11.018.

Mecklenburg, C. W., T. A. Mecklenburg, and L. K. Thorsteinson, L. K. 2002. Fishes of Alaska. American Fisheries Society: Bethesda, MD. 1037 p.

Mienis, F., H. C. de Stigter, M. White, G. Duineveld, H. de Haas, and T. C. E. van Weering. 2007. Hydrodynamic controls on cold-water coral growth and carbonate-mound development at the SW and SE Rockall Trough Margin, NE Atlantic Ocean. Deep Sea Res. P. I: Oceanogr. Res. Pap., 54(9), 1655-1674. https://doi.org/http://dx.doi.org/10.1016/j.dsr.2007.05.013.

Monnahan, C. C. 2020. Assessment of the other flatfish stock complex in the Bering Sea and Aleutian Islands, 22 p. ***In*** Stock Assessment and Fishery Evaluation Report for the Groundfish Resources of the Bering Sea/Aleutian Islands Regions. North Pacific Fishery Management Council 1007 West Third, Suite 400 Anchorage, AK 99501.

Monnahan, C. C., and R. Haehn. 2020. Assessment of the flathead sole-Bering flounder stock complex in the Bering Sea and Aleutian Islands, 91 p. ***In*** Stock Assessment and Fishery Evaluation Report for the Groundfish Resources of the Bering Sea and Aleutian Islands. North Pacific Fishery Management Council 1007 West Third, Suite 400 Anchorage, AK 99501.

Monnahan, C. C., J. T. Thorson, S. Kotwicki, N. Lauffenburger, J. N. Ianelli, and A. E. Punt. 2021. Incorporating vertical distribution in index standardization accounts for spatiotemporal availability to acoustic and bottom trawl gear for semi-pelagic species. ICES J. Mar. Sci. 78:1826–1839. https://doi.org/10.1093/icesjms/fsab085

Moser, H. G. 1996. The Early Stages of Fishes in the California Current Region. CalCOFI Atlas No. 33. Allen Press, Inc. Lawrence, Kansas. 1,505 p.

National Marine Fisheries Service (NMFS). 2005. Volume I: Final Environmental Impact Statement for Essential Fish Habitat Identification and Conservation in Alaska. https://repository.library.noaa.gov/view/noaa/17391.

Neidetcher, S. K., T. P. Hurst, L. Ciannelli, and E. A. Loggerwell. 2014. Spawning phenology and geography of Aleutian Islands and eastern Bering Sea Pacific cod (*Gadus macrocephalus*). Deep-Sea Res. II: Top. Studies Oceanogr. 109:204-214. http://cx.doi.org/10.1016/j.dsr2.2013.12.006i

Ng, E. L., J. J. Deroba, T. E. Essington, A. Grüss, B. E. Smith, and J. T. Thorson. 2021. Predator stomach contents can provide accurate indices of prey biomass. ICES J. Mar. Sci. 78(3):1146–1159. https://doi.org/10.1093/icesjms/fsab026

O'Leary, C. A., J. T. Thorson, J. N. Ianelli, and S. Kotwicki. 2020. Adapting to climate-driven distribution shifts using model-based indices and age composition from multiple surveys in the walleye pollock (*Gadus chalcogrammus*) stock assessment. Fish. Oceanogr. 29(6):541–557. https://doi.org/10.1111/fog.12494

O'Leary, C. A., S. Kotwicki, G. R. Hoff, J. T. Thorson, V. V. Kulik, J. N. Ianelli, R. R. Lauth, D. G. Nicol. J. Conner, and A. E. Punt. 2021. Estimating spatiotemporal availability of transboundary fishes to fishery-independent surveys. J. Appl. Ecol. doi:10.1111/1365-2664.13914.

Olson, A.P., C. E. Siddon, and G. L. Eckert. 2018. Spatial variability in size at maturity of golden king crab (*Lithodes aequispinus*) and implications for fisheries management. R. Soc. Open Science 5(3):171802.

Ormseth, O. A. 2020. Assessment of the skate stock complex in the Bering Sea and Aleutians Islands, 126 p. ***In*** Stock Assessment and Fishery Evaluation Report for the Groundfish Resources of the Bering Sea/Aleutian Islands Regions. North Pacific Fishery Management Council 1007 West Third, Suite 400 Anchorage, AK 99501.

Ormseth, O. A., M. E. Conners, K. Aydin, and C. Conrath. 2018. Assessment of the Octopus Stock Complex in the Bering Sea and Aleutian Islands, 136 p. ***In*** Stock Assessment and Fishery Evaluation Report for the Groundfish Resources of the Bering Sea/Aleutian Islands Regions. North Pacific Fishery Management Council 1007 West Third, Suite 400 Anchorage, AK 99501.

Orr, J. W., and A. C. Matarese. 2000. Revision of the genus Lepidopsetta Gill, 1862 (Teleostei: Pleuronectidae) based on larval and adult morphology, with a description of a new species from the North Pacific Ocean and Bering Sea. Fish. Bull., U.S. 98: 539-582.

Orr, J. W., and J. E. Blackburn. 2004. The dusky rockfishes (Teleostei: Scorpaeniformes) of the North Pacific Ocean: resurrection of *Sebastes variabilis* (Pallas, 1814) and a redescription of *Sebastes ciliatus* (Tilesius, 1813). Fish. Bull., U.S. 102(2):328-348.

Orr, J. W., and S. Hawkins. 2008. Species of the rougheye rockfish complex: resurrection of *Sebastes melanostictus* (Matsubara, 1934) and a redescription of *Sebastes aleutianus* (Jordan and Evermann, 1898) (Teleostei: Scorpaeniformes). Fish. Bull., U.S. 106:111-134.

Otto, R. S. and P. A. Cummiskey. 1985. Observations on the reproductive biology of golden king crab (*Lithodes aequispina*) in the Bering Sea and Aleutian Islands, pp. 123-135. ***In*** Proc. Int. King Crab Symp. University of Alaska, Fairbanks, AK.

Pardoe, I. 2012 Applied Regression Modeling, 2nd ed. John Wiley & Sons Inc, Hoboken, NJ, USA. 325 pp. DOI:10.1002/9781118345054.

Pearcy, W. G., M. J. Hosie, and S. L. Richardson. 1977. Distribution and duration of pelagic life of larvae of Dover sole, *Microstomus pacificus*; rex sole, *Glyptocephalus zachirus*; and petrale sole, *Eopsetta jordani*, in waters off Oregon. Fish. Bull., U.S. 75:173−183.

Pearson, K. E. and D. R. Gunderson. 2003. Reproductive biology and ecology of shortspine thornyhead rockfish, *Sebastolobus alascanus*, and longspine thornyhead rockfish, *S. altivelis*, from the northeastern Pacific Ocean. Env. Biol. Fish. 67(2):117-136.

Phillips, S. J., and M. Dudík. 2008. Modeling of species distributions with Maxent: New extensions and a comprehensive evaluation. Ecography 31(2):161–175. https://doi.org/10.1111/j.0906-7590.2008.5203.x

Phillips S. J., R. P. Anderson, and R. E. Schapire. 2006. Maximum entropy modeling of species geographic distributions. Ecol. Model. 190(3-4):231-59.

Phillips, S. J., R. P. Anderson, M. Dudík, R. E. Schapire, and M. E. Blair. 2017. Opening the black box: an open-source release of Maxent. Ecography 40:887-893.

Pirtle, J. L., T. C. Weber, C. D. Wilson, and C. N. Rooper. 2015. Assessment of trawlable and untrawlable seafloor using multibeam-derived metrics. Methods Oceanogr. 12:18–35.

Pirtle, J. L., S. K. Shotwell, M. Zimmermann, J. A. Reid, and N. Golden. 2019. Habitat suitability models for groundfish in the Gulf of Alaska. Deep-Sea Res. Pt. II. https://doi:10.1016/j.dsr2.2017.12.005.

Politou, C. Y., G. Tserpes, and J. Dokos. 2008. Identification of deepwater pink shrimp abundance distribution patterns and nursery grounds in the eastern Mediterranean by means of generalized additive modeling. Hydrobiol. 612(1):99-107. doi: 10.1007/s10750-008-9488-8.

Porter, S. M. 2005. Temporal and spatial distribution and abundance of flathead sole (*Hippoglossoides elassodon*) eggs and larvae in the western Gulf of Alaska. Fish. Bull., U.S. 103:648-658.

Potts, J., and J. Elith. 2006. Comparing species abundance models. Ecol. Model. 199:153-163.

Punt, A. E., D. S. Butterworth, C. L. de Moor, J. A. A. De Oliveira, and M. Haddon. 2016. Management strategy evaluation: best practices. Fish Fisher. 17:303–334. https://doi.org/10.1111/faf.12104

R Core Development Team. 2020. R: A Language and Environment for Statistical Computing. R Foundation for Statistical Computing. Vienna, Austria.

Richwine, K. A., K. R. Smith, and R. A. McConnaughey. 2018. Surficial sediments of the eastern Bering Sea continental shelf: EBSSED-2 database documentation. U.S. Dep. Commer., NOAA Tech. Memo. NMFS-AFSC-377, 48 p.

Rodgveller, C. J., K. B. Echave, P-J. F. Hulson, and K. M. Coutré. 2018. Age-at-maturity and fecundity of female sablefish sampled in December of 2011 and 2015 in the Gulf of Alaska. U.S. Dep. Commer., NOAA Tech. Memo. NMFS-AFSC-371, 31 p.

Rohan, S. K., S. Kotwicki, L. L. Britt, E. A. Laman, and K. Aydin. 2020. Deriving apparent optical properties from light measurements obtained using bottom-trawl-mounted archival tags. U.S. Dep. Commer., NOAA Tech. Memo. NMFS-AFSC-403, 91 p.

Rohan, S. K., S. Kotwicki, K. A. Kearney, J. A. Schulien, E. A. Laman, E. D. Cokelet, D. A. Beauchamp, L. L. Britt, K. Y. Aydin, and S. G. Zador. 2021. Using bottom trawls to monitor subsurface water clarity in marine ecosystems. Prog. Oceanogr. 194:102554. https://doi.org/10.1016/j.pocean.2021.102554

Rooney, S., E. A. Laman, C. N. Rooper, K. Turner, D. W. Cooper, and M. Zimmermann. 2018. Model-based essential fish habitat definitions for Gulf of Alaska groundfish species. U.S. Dep. Commer., NOAA Tech. Memo. NMFS-AFSC-373, 370 p.

Rooper, C. N. 2008. An ecological analysis of rockfish (*Sebastes* spp.) assemblages in the North Pacific Ocean along broad-scale environmental gradients. Fish. Bull., U.S. 106:1-11.

Rooper, C. N., J. L. Boldt, and M. Zimmermann. 2007. An assessment of juvenile Pacific ocean perch (*Sebastes alutus*) habitat use in a deepwater nursery. Estuar. Coastal Shelf Sci. 75:371-380.

Rooper, C. N., G. R. Hoff, and A. DeRobertis. 2010. Assessing habitat utilization and rockfish (*Sebastes* spp.) biomass on an isolated rocky ridge using acoustics and stereo image analysis. Can. J. Fish. Aquat. Sci. 67(10):1658-1670. doi: 10.1139/F10-088.

Rooper, C. N., Zimmermann, M., Prescott, M. M., and Hermann, A. J. 2014. Predictive models of coral and sponge distribution, abundance, and diversity in bottom trawl surveys of the Aleutian Islands, Alaska. Mar. Ecol. Prog. Ser. 503:157-176. doi: 10.3354/meps10710.

Rooper, C. N., M. F., Sigler, P. Goddard, P. Malecha, R. Towler, K. Williams, R. Wilborn, and M. Zimmermann. 2016. Validation and improvement of species distribution models for structure forming invertebrates in the eastern Bering Sea with an independent survey. Mar. Ecol. Prog. Ser. 551:117-130. doi: 10.3354/meps11703.

Rooper, C. N., R. Wilborn, P. Goddard, K. Williams, R. Towler, and G. R. Hoff. 2017a. Validation of deep-sea coral and sponge distribution models in the Aleutian Islands, Alaska. ICES J. Mar. Sci. 75(1):199-209.

Rooper, C. N., M. Zimmermann, and M. M. Prescott. 2017b. Comparison of modeling methods to predict spatial distribution of deep-sea coral and sponge in the Gulf of Alaska. Deep-Sea Res. Part I: Oceanogr. Res. Pap. 126:148-161. doi: 10.1016/j.dsr.2017.07.002.

Rooper C. N., I. Ortiz, A. J. Hermann, N. (E. A.) Laman, W. Cheng, K. Kearney, and K. Aydin. 2021. Predicted shifts of groundfish distribution in the eastern Bering Sea under climate change, with implications for fish populations and fisheries management. ICES J. Mar. Sci. doi: 10.1093/icesjms/fsaa215.

Rutecki, T. L., and E. R. Varosi. 1997. Distribution, age, and growth of juvenile sablefish, *Anoplopoma fimbria*, in Southeast Alaska, pp. 45-54. ***In*** Saunders, M., Wilkins, M. (Eds.), Biology and Management of Sablefish (*Anoplopoma fimbria*). U.S. Dep. Commer., NOAA Tech. Rep. NMFS-130.

Sasaki, T., D.H. Japan. In Hanselman, J. Heifetz, K.B. Echave, and S.C. Dressel. 1985. Studies on the 446 sablefish resources in the North Pacific Ocean. Far Seas Fish. Lab. Bull. 22 (2): 1-447.

Sampson, D. B., and S. M. Al-Jufaily. 1999. Geographic variation in the maturity and growth schedules of English sole along the U.S. West Coast. J. Fish Biol. 54:1–17. https://doi.org/10.1006/jfbi.1998.0841.

Scharf, H. R., X. Lu, P. J. Williams, and M. B. Hooten. Online Early (2019). Hierarchical approaches for flexible and interpretable binary regression models. arXiv preprint arXiv:1905.05242.

Schmidt, J., I. S. Evans, and J. Brinkmann. 2003. Comparison of polynomial models for land surface curvature calculation. Int. J. Geogr. Info. Sci. 17:797–814. https://doi.org/10.1080/1365881031000159605 8.

Shimada, A. M., and D. K. Kimura. 1994. Seasonal movements of Pacific cod, *Gadus macrocephalus*, in the eastern Bering Sea and adjacent waters based on tag-recapture data. Fish. Bull., U.S. 82: 800–816.

Shirley, T.C. and S. Zhou. 1997. Lecithotrophic development of the golden king crab *Lithodes aequispinus* (Anomura: Lithodidae). J. Crust. Biol. 17(2):207-216.

Shotwell, S. K., I. Spies, L. Britt, M. Bryan, D. H. Hanselman, D. G. Nichol, J. Hoff, W. Palsson, T. K. Wildebuer, and S. Zador. 2020a. Assessment of the arrowtooth flounder stock in the Eastern Bering Sea and Aleutian Islands, 88 p. ***In*** Stock assessment and fishery evaluation report for the groundfish resources of the BSAI. North Pacific Fishery Management Council 1007 West Third, Suite 400 Anchorage, AK 99501.

Shotwell, K. S., I. B. Spies, K. Echave, I. Ortiz, J. Sullivan, P. D. Spencer, and W. Palsson. 2020b. Assessment of the shortraker rockfish stock in the Bering Sea and Aleutian Islands, 40 p. ***In*** Stock Assessment and Fishery Evaluation Report for the Groundfish Resources of the Bering Sea/Aleutian Islands Regions. North Pacific Fishery Management Council 1007 West Third, Suite 400 Anchorage, AK 99501

Sinclair, E. H., D. S. Johnson, T. K. Zeppelin, and T. S. Gelatt. 2013. Decadal variation in the diet of western stock Steller sea lions (*Eumetopias jubatus*). U.S. Dep. Commer., NOAA Tech. Memo., NMFS-AFSC-248, 67 p.

Sibson, R. 1981. A Brief Description of Natural Neighbor Interpolation, Chapter 2 *In* V. Barnet (ed.), Interpolating Multivariate Data. John Wiley and Sons, Chichester, West Sussex, UK, PO19 8SQ.

Siddeek, M. S. M., J. Zheng, C. Siddon, B. Daly, M.J. Westphal, and L. Hulbert. Aleutian Islands Golden King Crab Stock Assessment, 129 p. ***In*** Stock Assessment and Fishery Evaluation Report for the king and tanner crab fisheries of the Bering Sea and Aleutian Islands Regions. North Pacific Fishery Management Council 1007 West Third, Suite 400 Anchorage, AK 99501.

Sigler, M. F., M. P. Eagleton, T. E. Helser, J. V. Olson, J. L. Pirtle, C. N. Rooper, S. C. Simpson, and R. P. Stone. 2017. Alaska Essential Fish Habitat Research Plan: A Research Plan for the National Marine Fisheries Service's Alaska Fisheries Science Center and Alaska Regional Office. AFSC Processed Rep. 2015-05, 22 p. Alaska Fish. Sci. Cent., NOAA, Natl. Mar. Fish. Serv., 7600 Sand Point Way NE, Seattle WA 98115.

Sigler, M. F., C. N. Rooper, G. R. Hoff, R. P. Stone, R. A. McConnaughey, and T. K. Wilderbuer. 2015. Faunal features of submarine canyons on the eastern Bering Sea slope. Mar. Ecol. Prog. Ser. 526:21-40.

Simpson, S. C., M. P. Eagleton, J. V. Olson, G. A. Harrington, and S. R. Kelly. 2017. Final Essential Fish Habitat (EFH) 5-year Review, Summary Report: 2010 through 2015. U.S. Dep. Commer., NOAA Tech. Memo. NMFS-F/AKR-15, 115p.

Siwicke, K. A., and K. Coutre. 2020. Periodic movements of Greenland turbot *Reinhardtius hippoglossoides* in the eastern Bering Sea and Aleutian Islands. Fish. Res. 229, 13 p.

Smith, A. D. M. 1994. Management strategy evaluation – the light on the hill, pp. 249-253. *In* D. Hancock (ed.), Population dynamics for fisheries management. Perth: Australian Society for Fish Biology.

Sohn, D., L. Ciannelli, J T. Duffy-Anderson. 2010. Distribution and drift pathways of Greenland halibut (*Reinhardtius hippoglossoides*) during early life stages in the eastern Bering Sea and Aleutian Islands. Fish. Oceanogr. 19:339-353.

Somerton, D. A., and R. S. Otto. 1986. Distribution and reproductive biology of the golden king crab, *Lithodes aequispina*, in the eastern Bering Sea. Fish. Bull., U.S. 84(3):571-584.

Spencer, P. D., and J. Ianelli. 2019. Assessment of the northern rockfish stock in the Bering Sea/Aleutian Islands, 76 p. ***In*** Stock Assessment and Fishery Evaluation Report for the Groundfish Resources of the Bering Sea and Aleutian Islands. North Pacific Fishery Management Council 1007 West Third, Suite 400 Anchorage, AK 99501.

Spencer, P. D., J. N. Ianelli, and W. Palsson. 2020. Assessment of the blackspotted and rougheye rockfish stock in the Bering Sea and Aleutian Islands, 102 p. ***In*** Stock Assessment and Fishery Evaluation Report for the Groundfish Resources of the Bering Sea/Aleutian Islands Regions. North Pacific Fishery Management Council 1007 West Third, Suite 400 Anchorage, AK 99501.

Spies, I. 2012. Landscape genetics reveals population subdivision in Bering Sea and Aleutian Islands Pacific cod. Trans. Am. Fish. Soc. 141:1557-1573.

Spies, I., R., G. G. Thompson, I. Ortiz, E. Siddon, and W. A. Palsson. 2020. Assessment of the Pacific cod stock in the Aleutian Islands, 41 p. ***In*** Stock assessment and fishery evaluation report for the groundfish resources of the Bering Sea and Aleutian Islands. North Pacific Fishery Management Council 1007 West Third, Suite 400 Anchorage, AK 99501.

Stabeno, P. J., J. D. Schumacher, and K. Ohtani. 1999. The physical oceanography of the Bering Sea, p. 1-59. ***In*** Loughlin T. R., and K. Ohtani (eds) Dynamics of the Bering Sea: A Summary of Physical, Chemical, and Biological Characteristics, and a Synopsis of Research on the Bering Sea, North Pacific Marine Science Organization (PICES), University of Alaska Sea Grant, AK-SG-99-03. Fairbanks, Alaska.

Stabeno, P. J., R. K. Reed, and J. M. Napp. 2002. Transport through Unimak Pass, Alaska. Deep-Sea Res. II 49:5919-5930.

Stahl, J.P. and G. H. Kruse. 2008. Spatial and temporal variability in size at maturity of walleye pollock in the eastern Bering Sea. Trans. Amer. Fish. Soc., 137(5):1543-1557.

Stark, J. W., and D. A. Somerton. 2002. Maturation, spawning and growth of rock soles off Kodiak Island in the Gulf of Alaska. J. Fish. Biol. 61:417-431.

Stark, J. W., 2007. Geographic and seasonal variations in maturation and growth of female Pacific cod (*Gadus macrocephalus*) in the Gulf of Alaska and Bering Sea. Fish. Bull., U.S. 105(3):396-407.

Stark, J. W. 2012a. Contrasting maturation and growth of northern rock sole in the eastern Bering Sea and Gulf of Alaska for the purpose of stock management. N. Amer. J. Fish. Manage. 32:93-99.

Stark, J. W. 2012b. Female maturity, reproductive potential, relative distribution, and growth compared between arrowtooth flounder (*Atheresthes stomias*) and Kamchatka flounder (*A. evermanni*) indicating concerns for management. J. Appl. Ichthyol. 28:226-230.

Stauffer, G. 2004. NOAA protocols for groundfish bottom trawl surveys of the Nation's fishery resources. U. S. Dep. Commer., NOAA Tech. Memo. NMFS-F/SPO-65, 205 p.

Stevenson, D. E., J. W. Orr, G. R. Hoff, and J. D. McEachran. 2007. Sharks, skates and ratfish of Alaska. Fairbanks, AK: Alaska Sea Grant, University of Alaska.

Stewart, I. J., and Hicks, A. C. 2018. Interannual stability from ensemble modelling. Can. J. Fish. Aquat. Sci. 75: 2109–2113.

Stone, R., H. Lehnert, and H. Reiswig. 2011. A guide to the deep-water sponges of the Aleutian Island archipelago. U.S. Dep. Commer., NOAA Professional Paper NMFS 12. Available from https://spo.nmfs.noaa.gov/content/guide-deepwater-sponges-aleutian-island-archipelago (accessed 29 August 2021).

Sullivan, J., I. Spies, P. Spencer, A. Kingham, T. Tenbrink, and W. Palsson. 2020. Assessment of the Other Rockfish stock complex in the Bering Sea/Aleutian Islands, 35 p. ***In*** Stock Assessment and Fishery Evaluation Report for the Groundfish Resources of the Bering Sea and Aleutian Islands. North Pacific Fishery Management Council 1007 West Third, Suite 400 Anchorage, AK 99501.

Tenbrink, T. T., and P. D. Spencer. 2013. Reproductive biology of Pacific ocean perch and northern rockfish in the Aleutian Islands. N. Amer. J. Fish. Manage. 33(2):373-383.

Tenbrink, T. T., and T. K. Wilderbuer. 2015. Updated maturity estimates for flatfishes (Pleuronectidae) in the eastern Bering Sea, with implications for fishery management. Mar. Coast. Fish. 7:474-482. https://doi.org/10.1080/19425120.2015.1091411

Tenbrink, T. T., and T. E. Helser. 2021. Reproductive biology, size, and age structure of harlequin rockfish: spatial analysis of life history traits. Mar. Coast. Fish. 13(5):463-477. https://doi.org/10.1002/mcf2.10172

Thompson, G. G., J. Conner, S. Kalei Shotwell, F. B. Fissel, T. Hurst, B. Laurel, L. Rogers, and E. Siddon. 2020. Assessment of the Pacific cod stock in the Eastern Bering Sea, 344 p. ***In*** Stock Assessment and Fishery Evaluation Report for the Groundfish Resources of the Bering Sea/Aleutian Islands Regions. North Pacific Fishery Management Council 1007 West Third, Suite 400 Anchorage, AK 99501.

Thorson, J. T., J. N. Ianelli, and S. Kotwicki. 2017. The relative influence of temperature and size-structure on fish distribution shifts: A case-study on walleye pollock in the Bering Sea. Fish Fish. 18(6):1073-1084.

Thorson, J. T. 2019. Measuring the impact of oceanographic indices on species distribution shifts: The spatially varying effect of cold-pool extent in the eastern Bering Sea. Limnol. Oceanogr. 64(6):2632–2645. https://doi.org/10.1002/lno.11238

Thorson, J. T., C. F. Adams, E. N. Brooks, L. B. Eisner, D. G. Kimmel, C. N. Legault, L. A. Rogers, and E. M. Yasumiishi. 2020a. Seasonal and interannual variation in spatio-temporal models for index standardization and phenology studies. ICES J. Mar. Sci. 77:1879–1892. https://doi.org/10.1093/icesjms/fsaa074

Thorson, J. T., W. Cheng, A. J. Hermann, J. N. Ianelli, M. A. Litzow, C. A. O'Leary, and G. Thompson. 2020b. Empirical orthogonal function regression: Linking population biology to spatial varying environmental conditions using climate projections. Global Change Biol., 26(8):4638–4649. https://doi.org/10.1111/gcb.15149

Thorson, J. T., A. J. Hermann, K. Siwicke, and M. Zimmermann. 2021. Grand challenge for habitat science: Stage-structured responses, nonlocal drivers, and mechanistic associations among habitat variables affecting fishery productivity. ICES J. Mar. Sci. 78(6):1956–1968. https://doi.org/10.1093/icesjms/fsaa236

Tribuzio, C. A., and K. B. Echave. 2019. Assessment of the other rockfish stock complex in the Gulf of Alaska. ***In*** Stock Assessment and Fishery Evaluation Report for the Groundfish Resources of the Gulf of Alaska. North Pacific Fishery Management Council 1007 West Third, Suite 400 Anchorage, AK 99501.

Turner, K., C. N. Rooper, E. A. Laman, S. Rooney, C. W. Cooper, D. W., and M. Zimmermann. 2017. Model-based essential fish habitat definitions for Aleutian Islands groundfish species. U.S. Dep. Commer., NOAA Tech. Memo. NMFS-AFSC-360, 239 p.

Venables W. N., and B. D. Ripley. 2002. Modern Applied Statistics with S. Fourth Edition. Springer Science+Business Media, New York, N.Y.

von Szalay, P. G., and N. W. Raring. 2018. Data Report: 2017 Gulf of Alaska bottom trawl survey. U.S. Dep. Commer., NOAA Tech. Memo. NMFS-AFSC-374, 260 p.

von Szalay, P. G., and N. W. Raring. 2020. Data Report: 2018 Aleutian Islands bottom trawl survey. U.S. Dep. Commer., NOAA Tech. Memo. NMFS-AFSC-409, 175 p.

Wakabayashi, K., R. G. Bakkala, and M. S. Alton. 1985. Methods of the Japan demersal trawl surveys, p. 7-29. ***In*** R. G. Bakkala and K. Wakabayashi (Editors), Results of cooperative Japan groundfish investigations in the Bering Sea during May-August 1979. Int. N. Pac. Fish. Comm. Bull. 44.

Walbridge, S., N. Slocum, M. Pobuda, and D. J. Wright. 2018. Unified geomorphological analysis workflows with Benthic Terrain Modeler. Geosci. 8:94. Version 3.0 is available at: http://github.com/EsriOceans/btm.

Walters, G. E., and T. K. Wilderbuer. 2000. Decreasing length at age in a rapidly expanding population of northern rock sole in the eastern Bering Sea and its effect on management advice. J. Sea Res. 44:17-26.

Watson, D. F., and G. M. Philip. 1985. A refinement of inverse distance weighted interpolation. Geo-processing 2(4):315-327.

Weinberg, K. L., and S. Kotwicki. 2008. Factors influencing net width and sea floor contact of a survey bottom trawl. Fish. Res. 93:265-279.

Weiss, A. D. 2001. Topographic Positions and Landforms Analysis (Conference Poster). Proceedings of the 21st Annual ESRI User Conference. San Diego, CA, July 9-13.

Wilson, M. F. J., B. O'Connell, C. Brown, J. C. Guinan, and A. J. Grehan. 2007. Multiscale terrain analysis of multibeam bathymetry data for habitat mapping on the continental slope. Mar. Geodesy 30:3–35.

Wing, B. L. 1997. Distribution of sablefish, *Anoplopoma fimbria*, larvae in the Eastern Gulf of Alaska, p. 13-26. ***In*** M. Saunders and M. Wilkins (eds.), Proceedings of the International Symposium on the Biology and Management of Sablefish. U.S. Dep . Commer., NOAA Tech. Rep. 130.

Wood, S.N. (2003) Thin plate regression splines. J. R. Statist. Soc. B 65(1):95-114.

Wood, S.N. 2011. Fast stable restricted maximum likelihood and marginal likelihood estimation of semiparametric generalized linear models. Journal of the Royal Stat. Soc. (B) 73(1):3-36.

Wood, S. N. 2017. Generalized Additive Models: An Introduction with R, Second Edition. CRC Press, Taylor & Francis Group. 476 p.

Wright, D. J., M. Pendleton, J. Boulware, S. Walbridge, B. Gerlt, D. Eslinger, D. Sampson, et al. 2012. ArcGIS Benthic Terrain Modeler (BTM), v. 3.0, Environmental Systems Research Institute, NOAA Coastal Services Center, Massachusetts Office of Coastal Zone Management. Available at: ⟨http://esriurl.com/5754⟩.

Yang, M. S. 2007. Food Habits and Diet Overlap of Seven Skate Species in the Aleutian Islands. U.S. Dep. Commer., NOAA Tech. Memo. NMFS-AFSC-177: 57 p.

Yang, M. S., and P. A. Livingston. 1986. Food habits and diet overlap of two congeneric species, *Atheresthes stomias* and *Atheresthes evermanni*, in the eastern Bering Sea. Fish. Bull., U.S. 82:615-623.

Yeung, C., and D. W. Cooper, 2020. Contrasting the variability in spatial distribution of two juvenile flatfishes in relation to thermal stanzas in the eastern Bering Sea. ICES J. Mar. Sci. 77(3):953-963.

Zar, J. H. 1984. Biostatistical Analysis, 2nd Ed., Simon and Schuster Company, New Jersey, USA. 717 p.

Zevenbergen, L. W., and Thorne, C. R. 1987. Quantitative analysis of land surface topography. Earth Surface Processes and Landforms, 12: 47–56.

Zheng, J., and M. S. M. Siddeek. 2019. Bristol Bay red king crab stock assessment in Fall 2019, 204 p. ***In*** Stock Assessment and Fishery Evaluation Report for the king and tanner crab fisheries of the Bering Sea and Aleutian Islands Regions. North Pacific Fishery Management Council 1007 West Third, Suite 400 Anchorage, AK 99501.

Zimmermann, M., and J. L. Benson. 2013. Smooth sheets: How to work with them in a GIS to derive bathymetry, features and substrates. U.S. Dep. Commer., NOAA Tech. Memo. NMFS-AFSC-249, 52 p.

Zimmermann, M., M. M. Prescott, and C. N. Rooper. 2013. Smooth Sheet Bathymetry of the Aleutian Islands. U.S. Dep. Commer., NOAA Tech. Memo. NMFS-AFSC-250, 43 p.

Zimmerman, M., and P. Goddard. 1996. Biology and distribution of arrowtooth, *Athersthes stomias*, and Kamchatka, *A. evermanni*, flounders in Alaskan waters. Fish. Bull., U.S. 94: 358-370.

Zimmermann, M., M. M. Prescott, and P. J. Haeussler. 2019. Bathymetry and Geomorphology of Shelikof Strait and the Western Gulf of Alaska. Geosci. 9:409. https://doi.org/10.3390/geosciences9100409.

Zuur, A. F., E. N., Ieno, N. J. Walker, A. A. Saveliev, and G. M. Smith. 2009. Mixed Effects Models and Extensions in Ecology with R. Springer Science+Business Media, LLC. New York, N.Y.

U.S. Secretary of Commerce
Gina M. Raimondo

Under Secretary of Commerce for Oceans and Atmosphere
Dr. Richard W. Spinrad

Assistant Administrator, National Marine Fisheries Service. Also serving as Acting Assistant Secretary of Commerce for Oceans and Atmosphere, and Deputy NOAA Administrator
Janet Coit

December 2022

www.nmfs.noaa.gov

OFFICIAL BUSINESS

National Marine Fisheries Service
Alaska Fisheries Science Center
7600 Sand Point Way N.E.
Seattle, WA 98115-6349